QUANTIFYING STRUCTURAL IRREGULARITY EFFECTS FOR SIMPLE SEISMIC DESIGN

By

Vinod Kota Sadashiva

A THESIS SUBMITTED IN PARTIAL FULFILMENT OF THE REQUIREMENTS FOR THE DEGREE OF DOCTOR OF PHILOSOPHY

in

THE DEPARTMENT OF CIVIL AND NATURAL RESOURCES ENGINEERING

UC
UNIVERSITY OF CANTERBURY
Te Whare Wānanga o Waitaha
CHRISTCHURCH NEW ZEALAND

UNIVERSITY OF CANTERBURY
CHRISTCHURCH, NEW ZEALAND

2010

ABSTRACT

This study was initiated to quantify the effect of different degrees of irregularity on structures designed for earthquake using simplified analysis. The types of irregularity considered were:

(a) Vertical Irregularity

- Mass
- Stiffness -Strength

(b) Horizontal (Plan) Irregularity

- Diaphragm Flexibility

Simple models were used to allow many analyses to be conducted in a relatively short time. For vertical irregularity studies, simple shear-type structures were designed according to the New Zealand design Standard, NZS1170.5, firstly as regular structures, and then they were redesigned as irregular structures to the same target drift. Both regular and irregular structures were then subjected to a suite of records, and vertical irregularity effects evaluated from the difference in response. For the flexible diaphragm effect study, simple models of structures were developed with: (a) a rigid diaphragm assumption; and (b) a flexible diaphragm assumption. Flexible diaphragm effects were evaluated by conducting time-history analyses and comparing the responses of structures with rigid and flexible diaphragms. A mechanics based approach was developed to quantify flexible diaphragm effects, which was shown to produce consistent results with those from time-history analyses.

Relationships between the *degree of irregularity* and the *change in behaviour* were developed. This information facilitates designers and plan checkers to rapidly evaluate the likely effect of irregularity on structures. It provides guidance as to: (a)

when the effect of structural irregularity can be ignored, and (b) the change in demands for different degrees of structural irregularity. The relations developed also provide a rigorous technical basis for future regularity provisions in the NZS1170.5 and other world-wide seismic design codes.

ACKNOWLEDGMENTS

The research work described in this thesis was part of a project titled, "*Building Regularity for Simplified Modelling*", funded by the New Zealand Earthquake Commission (EQC). I wish to thank the EQC for providing me with the financial support to carry out my PhD study.

I would like to express my sincere gratitude to my supervisor, Assoc. Prof. Gregory MacRae, who has given me invaluable support and advice through out my post-graduate study at the University of Canterbury. I have learnt a lot from him; not just in technical aspects, but also in various other forms. He has been a great source of inspiration to me for which I am grateful to him.

I wish to thank various people within the department who have helped me in many ways during my studies: Dr. Bruce Deam, Assoc. Prof. Richard Fenwick, Prof. Athol Carr and other academic staff are all thanked for their constructive criticism and support with the project. My thanks and appreciation goes to the department for providing me with additional scholarships and encouragement to present the research outcomes at various technical conferences. With regards to this, I want to thank Assoc. Prof. Roger Nokes, Assoc. Prof. Misko Cubrinovski and Mr. Alan Jolliffe. My thanks are extended to Mr. Brandon Hutchison and Mr. Joost for providing me with several computers that were necessary to conduct numerous analyses. I also want to thank Ms. Elizabeth Ackermann for her help managing administrative tasks during my PhD study.

I owe my acknowledgements to former students, Mr. Cedric Maunoury and Mr. Mathew Spooner, for their help in my research work.

I would like to thank my past and present officemates for providing great friendship and support in the last four years. They are: Min Ho Chey, Koichi Sugioka, David Yeoh, Mohammad Ashtiani, Colin Whittaker, Amir Khanlou, and Jose Golondrino. My thanks also go to several other friends of mine here at the University of Canterbury. To name a few of them: Brian Peng, Frederico Ferreira, Aline Lang, Brendon Bradley, Wen Yuen Kam, Manoocher Ardalany, Miharu Yamamoto, Masoud Moghaddasi, Umut Akguzel, Yati, Basil Daniel, Alejandro Amaris. It has been a pleasure working along with all these people.

I want to thank Prof. Raghunath and Prof. Ranganath from BMS College of Engineering, Bangalore, India, for all their help in my past. They have supported me in many ways, for which I will always be grateful to them.

Heartfelt thanks to my brothers, sister-in-laws, my nephew and niece, for providing me with lots of encouragement and love. My appreciation and thanks to my wife, Shantha, who has been my all-time friend since we first met during our under-graduate studies. I am very lucky to have her along as a fellow PhD student in the department.

My acknowledgements are not complete without mentioning my parents, to whom I dedicate this thesis. Without their blessings, love and encouragement, I could not have reached this stage of my life. Thank you.

TABLE OF CONTENTS

LIST OF TABLES

LIST OF FIGURES

GLOSSARY OF ABBREVIATIONS

CISDR	Constant Interstorey Drift Ratio model
CS	Constant Stiffness
CS-CSTG	Constant Stiffness and Constant Strength model
CS-VSTG	Constant Stiffness and Varying Strength model
DDR	Ductility Demand Ratio
DISDR	Design (target) Interstorey Drift Ratio
EDP	Engineering Demand Parameter
EDTHA	Elastic Dynamic Time History Analysis
EOM	Equation of Motion
ES	Equivalent Static method
IDTHA	Inelastic Dynamic Time History Analysis
IRR	Irregular Response Ratio
ISDR	Interstorey Drift Ratio
ISRD	Initial Stiffness Rayleigh Damping
LFR	Lateral Force Resisting system
MDOF	Multi-Degree-of-Freedom
MR	Mass Ratio
SB	Shear Beam
SDOF	Single-Degree-of-Freedom
SFB	Shear-Flexural Beam
SMF	Stiffness Modification Factor
TASRD	Tangent Stiffness Rayleigh Damping with Total Equation of Motion
TSRD	Tangent Stiffness Rayleigh Damping with Incremental Equation of Motion
VLFR	Vertical Lateral Force Resisting system

1. INTRODUCTION

1.1 Motivation

As part of structural design, members in buildings are selected and detailed such that the expected demands, such as forces or displacements, on a structure are less than the capacity of the structure to resist those forces and displacements. However, to obtain these forces or displacements, structural analysis is required considering the loading applied to the building from its weight, its use, and other factors such as wind, or shaking of the ground in the case of earthquake.

The sophistication of the structural analysis affects both the detail of the analysis results and the design fee. Simple methods (e.g., Equivalent Static method) may provide a reasonable representation of the likely seismic behaviour to enable rapid assessment of the expected building performance. They may also be used in the initial stages of the design process of sophisticated structures. More complex methods, such as inelastic dynamic time history analysis provide more information about the response, but take more time and computational cost to perform properly.

Since most modern seismic design codes were first drafted there have been significant advances in both modelling software and computing power. However, even with these advances, full inelastic dynamic time-history analysis of 3-D structural models that include diaphragm flexibility, statistical variations in element behaviour, etc. are currently not conducted for the majority of structures in New Zealand. Simple analysis methods and simple models are likely to be the major techniques used for some time yet.

Engineers need conceptually simple methods for the following reasons:

(1) to design full structures

(2) to enable a rapid check of likely building performance

(3) to preliminary size members before some more sophisticated studies are undertaken.

Simple analysis methods have been developed from studies carried out on structures with different structural forms, structural materials, and heights which have been idealized as being regular (e.g., Lee and Foutch [1], Chopra [2]). However, no real structure is perfectly *regular* as a result of accidental or intentional non-uniform mass, stiffness, strength, structural form, or a combination of these in the horizontal or vertical directions as shown in Figure 1-1. Also structures with a high *degree of irregularity* have the possibility of behaving significantly differently from that of a *nominally regular structure*. This different behaviour may result in larger demands and less safe irregular structures, and in some cases; structures may even collapse (Arnold and Reitherman [3], Paulay and Priestley [4]).

In order to prevent the possible underestimation of actual demands, and to produce safer structures, world-wide codes (e.g., NZS 1170.5 [5], IBC [6], Eurocode 8 [7]) provide limitations on the maximum degree of irregularity for structures designed according to simple analysis methods. Many present design codes classify some of the structural irregularities shown in Figure 1-1 into two categories: (a) Vertical irregularities (b) Plan irregularities.

Regularity limits are set in the codes for the above two types of irregularities. Such limits are intended to dictate the type and sophistication of the analysis method to be used for structures. For example, according to NZS 1170.5 [5], if a structure with a

fundamental natural period less than 2s does not satisfy the code regularity limits in Table 1-1, the Equivalent Static method is not permitted. If the same structure is vertically irregular based on Table 1-1(a), but satisfies plan irregularity conditions in Table 1-1(b), a 2-D Modal Response Spectrum method can be adopted. For the same structure, if it is classified as "torsionally sensitive" from Table 1-1(b), then a 3-D analysis has to be conducted. On the other hand, if a structure does not satisfy the regularity limits in Table 1-1, but has its total height less than 10m, or if its fundamental natural period is less than 2s, the structure can be analysed using the Equivalent Static method. It should be mentioned here that many regularity limits in NZS 1170.5 are similar to the regularity conditions in other design codes. As an example, Table 1-2 shows the regularity limits specified by the IBC [6].

While the code regularity limits provide some insight on the likely undesired effects due to the presence of irregularities, these limits were developed by consensus, rather than being based on quantitative data. For example, the SEAOC blue book [8], from which irregularity provisions in many worldwide codes are adopted, states that:

"Extensive engineering experience and judgment are required to quantify irregularities and provide guidance for special analysis. As yet, there is no complete prescription for all special analysis considerations for irregularities", (Cl. 104.5.1);

and

".. irregularities create great uncertainties in the ability of the structure to meet the design objectives of [the code] … These Requirements are intended only to make designers aware of the existence and potential detrimental effects of irregularities, and to provide minimum requirements for their accommodation…. The various ratios and related criteria stated to define irregularity in Tables 104-4 and 104-5 [in code]

have been assigned by judgement based on the interpretation of past earthquake damage effects and design experience…the guidelines given for the assessment of irregularities are qualitative in nature and must be interpreted with sound engineering judgement…", (Cl. 104.5.3).

Several studies (e.g., [9-16]) have been conducted in the past explaining the behaviour of irregular structures. However, such studies have not been conducted particularly to quantify the variation in response associated with a particular degree of irregularity so the validity of the irregularity limits, or the variation in response due to structures meeting these limits, is not known.

There is therefore a need to address the above issue. This thesis seeks to develop rational criteria for irregularity based on the change in response for a particular level of irregularity. The particular types of irregularity considered include:

(a) Vertical Mass Irregularity

(b) Vertical Stiffness-Strength Irregularity for structures with constant interstorey heights

(c) Vertical Stiffness-Strength Irregularity for structures with different interstorey heights

(d) Horizontal diaphragm flexibility which affects the structural behaviour

1.2 Organisation of the Thesis

The thesis is laid out primarily in terms of papers, as these have been written as the work has progressed. Because of this, there is some unavoidable repetition of background material in the following chapters. Conference papers and poster

presentations have also been made from this study. A complete list of conference contributions is provided in Table 1-3.

Chapter 2. Mass Irregularity

Paper: Sadashiva VK, MacRae GA, Deam BL. Determination of structural irregularity limits – mass irregularity example. *Bulletin of the New Zealand Society for Earthquake Engineering* 2009; **42**(4): 288-301.

Chapter 3. Stiffness-Strength Irregularity (Uniform Storey Height)

Paper: Sadashiva VK, MacRae GA, Deam BL. Seismic response of structures with coupled vertical stiffness-strength irregularities. *Earthquake Engineering and Structural Dynamics* 2011. DOI: 10.1002/eqe.1121.

Chapter 4. Stiffness-Strength Irregularity (Variable Storey Height)

Paper: Sadashiva VK, MacRae GA, Deam BL. Effects of coupled vertical stiffness-strength irregularity due to modified interstorey height. *Bulletin of the New Zealand Society for Earthquake Engineering* 2011; **44**(1): 31-44.

Chapter 5. Diaphragm Flexibility

Paper: Sadashiva VK, MacRae GA, Deam BL. Quantifying the seismic response of structures with flexible diaphragms. *Earthquake Engineering and Structural Dynamics* 2011. (under review, Manuscript ID: *EQE-10-0224.R1*).

Chapter 6. Summary of Recommendations

Chapter 7. Opportunities for Further Work

In addition, a series of appendices describe detailed information and computations which are too specific for the papers, but are useful background to the work conducted.

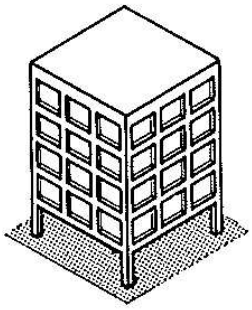

(1) "Soft" lower levels

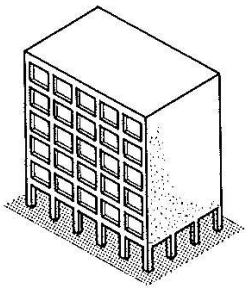

(2) Opening in Shear Walls

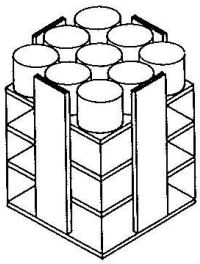

(3) Difference in floor mass

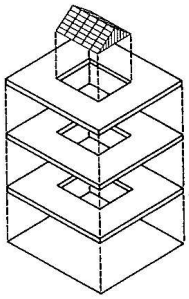

(4) Openings in diaphragms or difference in diaphragm systems

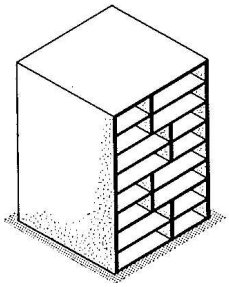

(5) Interruption of vertical-resisting elements

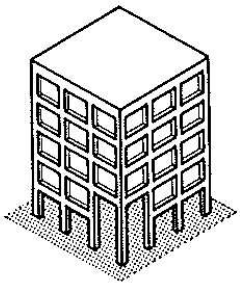

(6) Interruption of beams

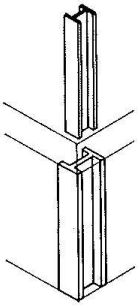

(7) Abrupt changes in member sizes

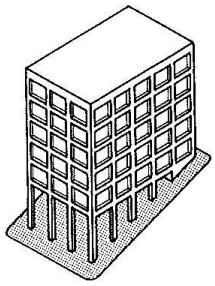

(8) Buildings on hillsides

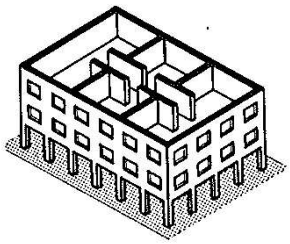

(9) Different lateral force resisting systems in different storeys

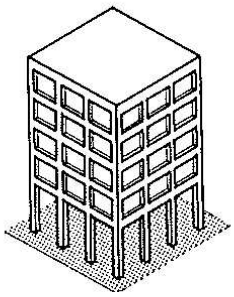

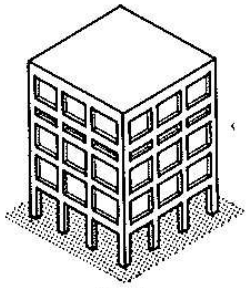

(10) A storey height being higher or lower than adjacent storey height

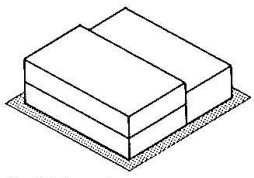

(11) Split levels

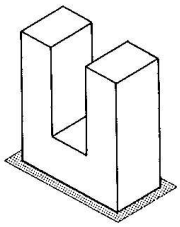

(12) Multiple towers

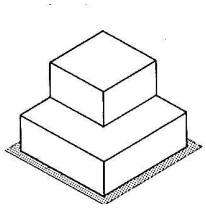

(13) Set-backs

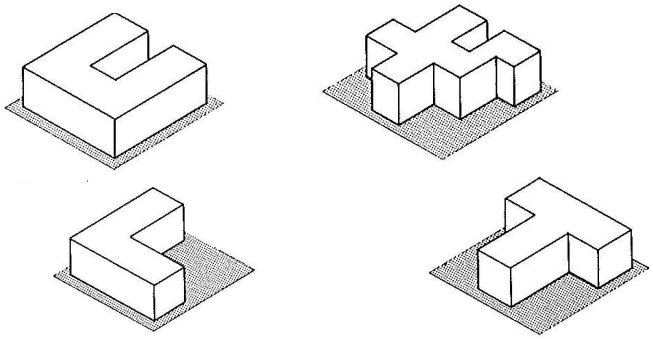

(14) Buildings with different plan types (L, T, U etc. shapes)

Figure 1-1: Examples of some common irregularities in structures.

Table 1-1: NZS 1170.5 criteria's for structural irregularity

(a) Vertical Irregularities (Cl. 4.5.1)

1. *Weight (mass) irregularity* – Weight irregularity shall be considered to exist where the weight, W_i, of any storey is more than 150% of the weight of an adjacent storey. A roof that is lighter than the floor below need not be considered.

2. *Vertical stiffness irregularity* – Vertical stiffness irregularity shall be considered to exist when the lateral stiffness of the primary structure in a storey is less than 70% of the stiffness of any adjacent storey, or less than 80% of the average stiffness of the three storeys above or below.

3. *Discontinuity in capacity (weak storey)* – A weak storey is one in which the storey shear strength is less than 90% that in the storey above. The storey shear strength is the total strength of all vertical seismic-resisting elements of the primary structure sharing the storey shear for the direction under consideration.

4. *Vertical geometric irregularity* – Vertical geometric irregularity shall be considered to exist where the sum of the horizontal dimensions of the vertical elements of the primary structure in the direction under consideration in any storey is more than 130% of that in an adjacent storey.

(b) Plan Irregularities (Cl. 4.5.2)

1. *Horizontal offsets of columns in moment-resisting frames* – Horizontal plan irregularity shall be considered to exist where, in the direction under consideration, in-plane or out-of-plane offsets of columns at any floor level are present where either:

   (a) The average of the absolute values of the tangent of the offset angle:

$$\frac{\sum^{N_c}\left|\frac{a_j}{b_j}\right|}{N_c} > 0.1 \qquad (1\text{-}1)$$

   Where:

   a_j = the horizontal offset at column j;

   b_j = the vertical distance between the base of the upper column and the top of

the lower column *j*;

N_c = the total number of columns at the level under consideration.

(b) For any single column j, the tangent of the offset angle:

$$\frac{a_j}{b_j} > 0.4 \qquad (1\text{-}2)$$

2. *Out-of-plane offsets of lateral force resisting walls* – Horizontal plan irregularity shall be considered to exist in lateral force resisting walls where out-of-plane offsets occur that conform to Equations 1-1 or 1-2.

3. *Torsional sensitivity* – Horizontal plan irregularity resulting from torsional sensitivity shall be considered to exist when the ratio γ exceeds 1.4 when calculated as follows.

   The ratio γ_i for each level, *i*, according to the following equation is determined independently for each orthogonal direction:

$$\gamma_i = \frac{d_{\max}}{d_{av}} \qquad (1\text{-}3)$$

   Where:

   d_{av} = the average of the displacements at the extreme points of the structure at level *i* produced by the actions above this level;

   d_{max} = the maximum storey displacement at the extreme points of the structure at level *i* in the direction of the earthquake induced by the equivalent static actions acting at distances ± 0.10 times the plan dimension of the structure, *b*, from the centres of mass at each floor;

   γ = the maximum of all values of γ_i in both orthogonal directions.

Note: One storey penthouses or roofs with a weight less than 10% of the level below shall not be considered when applying the criteria's in Clause 4.5.

Table 1-2: IBC 2003 criteria's for structural irregularity

(a) Vertical Irregularities (Cl. 1616.5.1.2)

	IRREGULARITY TYPE AND DESCRIPTION	REFERENCE SECTION	SEISMIC DESIGN CATEGORY[a] APPLICATION
1a	Stiffness Irregularity—Soft Story A soft story is one in which the lateral stiffness is less than 70 percent of that in the story above or less than 80 percent of the average stiffness of the three stories above.	9.5.2.5.1 of ASCE 7	D, E, and F
1b	Stiffness Irregularity—Extreme Soft Story An extreme soft story is one in which the lateral stiffness is less than 60 percent of that in the story above or less than 70 percent of the average stiffness of the three stories above.	1620.5.1 9.5.2.5.1 of ASCE 7	E and F D, E and F
2	Weight (Mass) Irregularity Mass irregularity shall be considered to exist where the effective mass of any story is more than 150 percent of the effective mass of an adjacent story. A roof that is lighter than the floor below need not be considered.	9.5.2.5.1 of ASCE 7	D, E and F
3	Vertical Geometric Irregularity Vertical geometric irregularity shall be considered to exist where the horizontal dimension of the lateral-force-resisting system in any story is more than 130 percent of that in an adjacent story.	9.5.2.5.1 of ASCE 7	D, E and F
4	In-plane Discontinuity in Vertical Lateral-Force-Resisting Elements An in-plane offset of the lateral-force-resisting elements greater than the length of those elements or a reduction in stiffness of the resisting element in the story below.	1620.4.1 9.5.2.5.1 of ASCE 7 1620.2.9	D, E and F D, E and F B, C, D, E and F
5	Discontinuity in Capacity—Weak Story A weak story is one in which the story lateral strength is less than 80 percent of that in the story above. The story strength is the total strength of seismic-resisting elements sharing the story shear for the direction under consideration.	1620.2.3 9.5.2.5.1 of ASCE 7 1620.5.1	B, C, D, E and F D, E and F E and F

a. Seismic design category is determined in accordance with Section 1616.

(b) Plan Irregularities (Cl. 1616.5.1.1)

	IRREGULARITY TYPE AND DESCRIPTION	REFERENCE SECTION	SEISMIC DESIGN CATEGORY[a] APPLICATION
1a	Torsional Irregularity—to be considered when diaphragms are not flexible as determined in Section 1602.1.1 Torsional irregularity shall be considered to exist when the maximum story drift, computed including accidental torsion, at one end of the structure transverse to an axis is more than 1.2 times the average of the story drifts at the two ends of the structure.	9.5.5.5.2 of ASCE 7 1620.4.1 9.5.2.5.1 of ASCE 7 9.5.5.7.1 of ASCE 7	C, D, E and F D, E and F D, E and F C, D, E and F
1b	Extreme Torsional Irregularity—to be considered when diaphragms are not flexible as determined in Section 1602.1. Extreme torsional irregularity shall be considered to exist when the maximum story drift, computed and including accidental torsion, at one end of the structure transverse to an axis is more than 1.4 times the average of the story drifts at the two ends of the structure.	9.5.5.5.2 of ASCE 7 1620.4.1 1620.5.1 9.5.2.5.1 of ASCE 7 9.5.5.7.1 of ASCE 7	C, D, E and F D E and F D, E and F C, D, E and F
2	Reentrant Corners Plan configurations of a structure and its lateral-force-resisting system contain reentrant corners where both projections of the structure beyond a reentrant corner are greater than 15 percent of the plan dimension of the structure in the given direction.	1620.4.1	D, E and F
3	Diaphragm Discontinuity Diaphragms with abrupt discontinuities or variations in stiffness, including those having cutout or open areas greater than 50 percent of the gross enclosed diaphragm area, or changes in effective diaphragm stiffness of more than 50 percent from one story to the next.	1620.4.1	D, E and F
4	Out-of-Plane Offsets Discontinuities in a lateral-force-resistance path, such as out-of-plane offsets of the vertical elements.	1620.4.1 9.5.2.5.1 of ASCE 7 1620.2.9	D, E and F D, E and F B, C, D, E and F
5	Nonparallel Systems The vertical lateral-force-resisting elements are not parallel to or symmetric about the major orthogonal axes of the lateral-force-resisting system.	1620.3.2	C, D, E and F

a. Seismic design category is determined in accordance with Section 1616.

Table 1-3: Conference contributions from this structural irregularity study

1. Sadashiva VK, MacRae GA, Deam BL. A mechanics based approach to quantify diaphragm flexibility effects. *9th Pacific Conference on Earthquake Engineering (9PCEE)*, Auckland, 14th – 16th April 2011. Paper No. 114.
2. Sadashiva VK, MacRae GA, Deam BL. Building regularity provisions for seismic design of structures. *14th European Conference on Earthquake Engineering (14ECEE)*, Ohrid, Macedonia, 30th Aug – 3rd Sep 2010. Paper No. 1351.
3. Sadashiva VK, MacRae GA, Deam BL. Seismic response of structures with coupled vertical stiffness-strength variations. *14th European Conference on Earthquake Engineering (14ECEE)*, Ohrid, Macedonia, 30th Aug – 3rd Sep 2010. Paper No. 1352.
4. Sadashiva VK, MacRae GA, Deam BL. Simple methods to evaluate structural irregularities effects. *New Zealand Society of Earthquake Engineering (NZSEE) Conference*, Wellington, New Zealand, 26th - 28th March 2010. Paper No. 12.
5. Sadashiva VK, MacRae GA, Deam BL. Irregularity limits for structures with coupled vertical stiffness-strength variations. *New Zealand Society of Earthquake Engineering (NZSEE) Conference*, Wellington, New Zealand, 26th - 28th March 2010. Poster presentation.
6. Sadashiva VK, MacRae GA, Deam BL. Determination of irregularity limits. *The 14th World Conference on Earthquake Engineering (14WCEE)*, Beijing, China, 12th - 17th October 2008. Paper ID. 05-01-0513.
7. Sadashiva VK, MacRae GA, Deam BL, Fenwick RC. Determination of acceptable structural irregularity limits for the use of simplified seismic design methods. *New Zealand Society of Earthquake Engineering (NZSEE) Conference*, Wairakei, New Zealand, 11th - 13th April 2008. Paper No. 14.
8. Sadashiva VK, MacRae GA, Deam BL. Evaluation of vertical mass irregularity on the seismic performance of nine storey buildings. *8th Pacific Conference on Earthquake Engineering (8PCEE)*, Singapore, 5th - 7th December 2007. Paper No. 43.
9. Sadashiva VK, MacRae GA, Deam BL. Vertical mass irregularity effects on the seismic performance of shear buildings. *New Zealand Society of Earthquake Engineering (NZSEE) Conference*, Palmerston North, New Zealand, 30th March – 1st April 2007. Paper No. 59 & Poster presentation.

1.3 References

[1] Lee K, Foutch DA. Seismic Performance Evaluation of Pre-Northridge Steel Frame Buildings with Brittle Connections. *Journal of Structural Engineering* 2002; **128**(4): 546-555.

[2] Chopra AK. Dynamics of structures: Theory and Applications to Earthquake Engineering. New Jersey: Prentice Hall, 2000; 844 pp.

[3] Arnold C, Reitherman R. *Building configuration and seismic design.* John Wiley & Sons, New York, 1982, 296pp.

[4] Paulay T, Priestley MJN. 1992. *Seismic design of reinforced concrete and masonry buildings.* John Wiley & Sons, New York, 1992, 744pp.

[5] SNZ. NZS 1170.5 Supp 1:2004, Structural Design Actions. Part 5: Earthquake actions – New Zealand – commentary. Standards New Zealand, Wellington, 2004.

[6] IBC. International Building Code. International Code Council (ICC), Whittier, CA, 2003.

[7] CEN. EN 1998-1. Eurocode 8. Design of structures for earthquake resistance – Part 1: General Rules, Seismic Actions and Rules for Buildings, European Committee for Standardization, 2004.

[8] SEAOC. Recommended lateral force requirements and commentary. Seventh Edition, Seismology Committee, Structural Engineers Association of California, 1999.

[9] Valmundsson EV, Nau JM. Seismic response of building frames with vertical structural irregularities. *Journal of Structural Engineering* 1997; **123**(1): 30-41.

[10] Al-Ali AAK, Krawinkler H. Effects of vertical irregularities on seismic behaviour of building structures. Report No. 130, Department of Civil and Environmental Engineering, Stanford University, San Francisco, 1998.

[11] Fragiadakis M, Vamvatsikos D, Monolis P. Evaluation of the influence of vertical irregularities on the seismic performance of a nine-storey steel frame.

Journal of Earthquake Engineering and Structural Dynamics 2006; **35**(12): 1489-1509.

[12] Tremblay R, Poncet L. Seismic performance of concentrically braced steel frames in multistory buildings with mass irregularity. *Journal of Structural Engineering* 2005; **131**(9): 1363-1375.

[13] De Stefano M, Pintucchi B. EAEE task group (TG) 8: Seismic behaviour of irregular and complex structures: Progress since 2002. *First European Conference on Earthquake Engineering and Seismology* 2006. Paper No: 1443.

[14] Chopra AK, Goel GK. A modal push over analysis procedure to estimate seismic demands for unsymmetric-plan buildings". *Journal of Earthquake Engineering & Structural Dynamics* 2004; **33**(8): 903-927.

[15] Panahshahi N, Reinhorn AM, Kunnath SK. Seismic response of a 1:6 reinforced concrete scale-model structure with flexible floor diaphragms. *ACI Structural Journal* 1991; **88(3)**:615-624.

[16] Tremblay R, Stiemer SF. Seismic behavior of single-storey steel structures with a flexible roof diaphragm. *Canadian Journal of Civil Engineering* 1996; **23**(1):49-62.

2. DETERMINATION OF STRUCTURAL IRREGULARITY LIMITS – MASS IRREGULARITY EXAMPLE

2.1 Overview

Structures may be irregular due to non-uniform distributions of mass, stiffness, strength or due to their structural form. For regular structures, simple analysis techniques such as the Equivalent Static Method have been calibrated against advanced analysis methods, such as the Inelastic Dynamic Time-History Analysis. Most worldwide codes allow simple analysis techniques to be used only for structures which satisfy regularity limits. Currently, such limits are based on engineering judgement and lack proper calibration. This paper describes a simple and efficient method for quantifying irregularity limits. The method is illustrated on 3, 5, 9 and 15 storey models of shear-type structures, assumed to be located in Wellington, Christchurch and Auckland. They were designed in accordance with the Equivalent Static Method of NZS 1170.5. Regular structures were defined to have constant mass at every floor level and were either designed to produce constant interstorey drift ratio at all the floors simultaneously or to have a uniform stiffness distribution over their height. Design structural ductility factors of 1, 2, 4 and 6, and target (design) interstorey drift ratios ranging between 0.5% and 3% were used in this study. Inelastic dynamic time-history analysis was carried out by subjecting these structures to a suite of code design level earthquake records. Irregular structures were created with floor masses of magnitude 1.5, 2.5, 3.5 and 5 times the regular floor mass. These increased masses were considered separately at the first floor level, mid-height and at

the roof. The irregular structures were designed for the same drifts as the regular structures.

The effect of increased mass at the top or bottom of the structure tended to increase the median peak drift demands compared to regular structures for the record suite considered. When the increased mass was present at the mid-height, the structures generally tended to produce lesser drift demands than the corresponding regular structures. A simple equation was developed to estimate the increase in interstorey drift due to mass irregularity. This can be used to set irregularity limits.

2.2 Introduction

Current earthquake codes define structural configuration as either regular or irregular in terms of size and shape of the building, arrangement of the structural and non-structural elements within the structure, distribution of mass in the building etc. A regular structure can be envisaged to have uniformly distributed mass, stiffness, strength and structural form. When one or more of these properties is non-uniformly distributed, either individually or in combination with other properties in any direction, the structure is referred to as being irregular.

Structural irregularity may occur for many reasons. Some irregularities are *architecturally planned*. Examples of these are:

- A factory with heavy machinery, or an educational institution with a library at one floor level that leads to irregular distribution of mass as shown in Figure 2-1(a);
- A residential building having a car park in the basement producing a flexible first storey as shown in Figure 2-1(b);

- A shopping complex with setbacks to accommodate boundary offset requirements as shown in the plan of Figure 2-1(c);
- Buildings with flexible, rigid or no diaphragms at a floor level, or structural plan having different lateral load resisting systems (resulting in torsion) as shown in the plan of Figure 2-1(d).

A structure can also be irregular because of unplanned effects, which are referred to as *aleatoric uncertainties*. These include rearrangement of loadings, as well as material strength and stiffness variations.

For the above reasons, structures are never perfectly regular and hence the designers routinely need to evaluate the likely degree of irregularity and the effect of this irregularity on a structure during an earthquake.

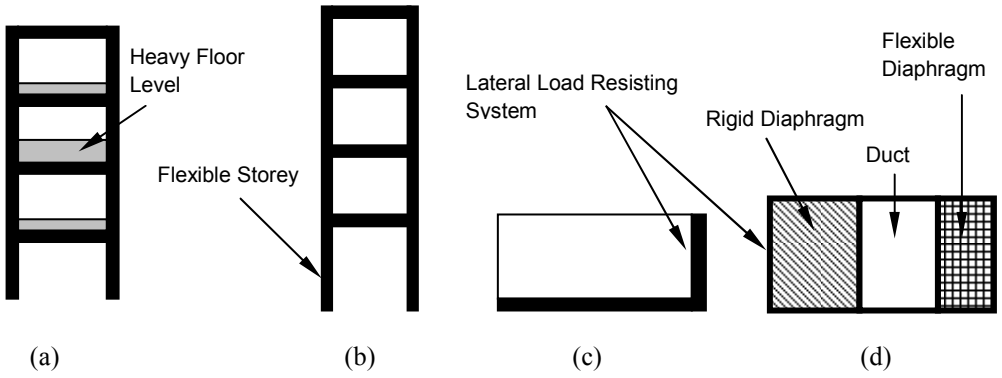

Figure 2-1: Examples of vertical and horizontal structural irregularities.

Structural demand estimates are dependent on the analysis method. For example, the most costly 3-D *Inelastic Dynamic Time-History Analysis* (**IDTHA**) method with appropriate modelling can consider most irregularities, but it takes significant time to build, verify and analyse the model for a suite of ground motion records. Aleatory uncertainties may be considered by modelling the statistical variation in structural

properties as well as that of the ground motions. Also, analysis methods such as the *Equivalent Static* (**ES**) Method, defined in the New Zealand seismic design Standard NZS 1170.5 (SNZ 2004); the Modal Response Spectrum Method; and the Pushover Method are simplified methods which have been calibrated against the IDTHA for regular structures. However, such calibrations have not always been carried out for structures with significant irregularity. Appropriate calibration is required for each analysis method to ensure that they estimate a realistic value of likely demand.

The ability to estimate structural demands is also dependent on the structural model. For example, 2-D analysis is generally not able to adequately represent the response of significantly irregular 3-D structures. Similarly, floor diaphragms may need to be modelled to adequately represent the behaviour.

Due to the above reasons, designers need simple methods that are effective in quantifying the irregularities in structures. Having this as the focal objective, this paper aims to answer the following questions:

1. What are the current NZS 1170.5 recommendations for structural irregularities, and where do they come from?
2. Does the past research on mass irregularity justify the current NZS 1170.5 mass irregularity requirements?
3. Can a simple and effective method be developed to quantify the effects of irregularities for structures designed for New Zealand?
4. Can a suite of shear-type structures having a range of structural irregularity be developed?

5. Is it possible to model these structures which can represent realistic behaviour well?
6. Do damping assumptions significantly affect irregularity effects on shear-type structures?
7. Does the NZS 1170.5 ES method predict the displacement response of structures well?
8. What are the effects of magnitude and floor level of mass irregularity on the drift demands?
9. What degree of irregularity corresponds to what change in response?

2.3 NZS 1170.5 Current Consideration for Irregularity

The simple ES method (including structural actions and displacement amplification due to P-Delta effects) has been used to design many New Zealand structures. NZS 1170.5 permits the ES method to be used to design:

- any structure less than 10 m high;
- any structure having a fundamental translational period of less than 0.4s;
- any structure with a fundamental translational period of up to 2.0s if certain regularity requirements are satisfied.

If the structure does not meet the above requirements, then a more sophisticated and therefore expensive analysis method needs to be employed.

NZS 1170.5, similar to many other worldwide codes, defines limits for different types of irregularities, and these limits form the basis for applying the ES method. For example, structures are considered to have mass irregularity when the seismic weight,

W_i, in any storey is more than 150% of the seismic weight of either adjacent storey. Such a limit of 1.5 for mass irregularity and other limits for other types of irregularities have been specified from engineering judgment rather than from rigorous quantitative analysis. For example, the SEAOC blue book (1999), with recommendations similar to that in NZS 1170.5, states that:

".. irregularities create great uncertainties in the ability of the structure to meet the design objectives of [the code] ... These Requirements are intended only to make designers aware of the existence and potential detrimental effects of irregularities, and to provide minimum requirements for their accommodation….", (C104.5.3),

and

"Extensive engineering experience and judgment are required to quantify irregularities and provide guidance for special analysis. As yet, there is no complete prescription for ... irregularities" (C104.5.1).

From the above quotes, it is evident that there is a need to quantify regularity limits so that the structures can be designed to have a consistent level of reliability for each type of irregularity and for each analysis or modelling method. This aim is consistent with probabilistic multi-objective *performance based earthquake engineering*.

2.4 Previous Research on Mass Irregularity

Researchers evaluating the effects of irregularities have mainly focussed on plan irregularities due to non-uniform distribution of mass, strength and stiffness in the horizontal direction (e.g., Chopra and Goel (2004), Aziminejad and Moghadam (2005), Fajfar *et al.* (2006)). Studies that have investigated vertical irregularity effects have given insight into the behaviour of structures with vertical irregularities, but they

have not developed general methods for quantifying acceptable irregularity limits. A brief summary of works related to vertical mass irregularity is presented below.

Valmundsson and Nau (1997) investigated the appropriateness of provisions for considering different irregularities as laid out in the 1994 *Uniform Building Code*. They considered 2-D building frames with heights of 5, 10 and 20 storeys, assuming the beams to be stiffer than the columns. For each structure height, uniform structures were defined to have a constant mass of 35 Mg at all the floor levels, and the storey stiffnesses were calculated to give a set of 6 desired fundamental periods. The maximum calculated drifts from the lateral design forces for the regular structures with the target period were found to lie within the UBC limit. Mass irregularities at three floor levels in the elevation of structures were then applied by means of mass ratios (ratio of modified mass of the irregular structure to the mass of uniform structure at a floor level) ranging between 0.1 and 5, and the responses were calculated for design ductility's of 1, 2, 6 and 10 considering four earthquake records. The increase in ductility demand was found to be not greater than 20% for a mass ratio of 1.5 and mass discontinuity was most critical when located on lower floors. Mass irregularity was found to be the least important of the irregularity effects considered.

Al-Ali and Krawinkler (1998) assessed the effects of vertical irregularities by evaluating the roof drift demands and the distribution of storey demands over the height of the structure. This was obtained by conducting elastic and inelastic dynamic analyses on 2-D single-bay 10-storey generic structures, assuming a column hinge model. A base structure was defined to have a uniform distribution of mass over the height. The stiffness distribution that resulted in a straight-line first mode shape was

tuned to produce a first mode period of 3s when designed according to the Modal Superposition technique. Structures with mass irregularities were created by changing the mass distribution of the base model and keeping the same stiffness distribution as the base model. Mass ratios between 0.25 and 4 were chosen and applied either at one floor or in a series of floors, and the stiffness distribution was tuned until the structures had a fundamental period of 3.0s. Dynamic analyses were then conducted on each structure by subjecting them to a suite of 15 ground motion records. *P*-Delta effects were not considered and Rayleigh damping was used to obtain a damping ratio of 5% for the first and fourth modes. It was found that mass irregularities had a relatively small effect on elastic and inelastic storey shear and storey drift demands. It was also shown that mass increase at the top had a larger effect on roof and storey drifts than when increased mass was applied at the mid-height or at the lower floors. Again it was concluded that mass irregularity effects were less than other types of vertical irregularities.

Fragiadakis *et al.* (2006) carried out incremental dynamic analyses on a realistic nine storey steel frame to evaluate the effect of irregularities for each performance level, from serviceability to global collapse. A mass ratio of 2 was applied at a series of floors over the selected frame and the effects of mass irregularity were evaluated. It was found that the influence of mass irregularity on interstorey drifts was comparable to the influence of stiffness irregularity.

Although the above researchers and few others (e.g., Chintanapakdee and Chopra (2004), Tremblay and Poncet (2005)) have given useful insights into the topic of vertical irregularities and their effects on structural response, these studies are not carried out with a design perspective. It may be seen that in many of the cases

described above, an appropriate comparison was not conducted. That is, regular and irregular structures were not generally designed for the same *engineering demand parameter* (**EDP**). For example, irregular structures were sometimes designed to have the same period as the regular structures. This is problematic because it is possible that the design drifts of the irregular structure with the same period may be different from that of the regular structure. They may even violate the code drift requirements. Furthermore, the structures with greater design drifts would be expected to have greater drift demands in the dynamic analysis. A more meaningful comparison is obtained if both regular and irregular structures are designed to the same EDP. Earlier studies are also limited to specific structural type/height and there is a lack of information on the appropriateness of the limit of 150% imposed on mass irregularity. Also, the above studies may not be relevant for structures designed according to NZ code analysis procedures which have some differences from overseas methods.

2.5 Simple Methodology for Evaluating Vertical Irregularity Effects

Recognising the need to provide rational basis for structural irregularity limits and to have a consistent meaningful comparison between regular and irregular structures designed according to the NZ code, the following simple methodology is proposed:

1. Define an EDP that characterises structural damage. Peak interstorey drift ratio over all the storeys has been used as the EDP to assess the vertical irregularity effects in this paper.

2. Choose a set of target (design) interstorey drifts that span the range of values that could be used by the designers (e.g., from 0.5% to 3%). Then for each target interstorey drift:

   a) Design a regular structure using the ES method to the target interstorey drift.

   b) Introduce an irregularity into the structure and use the ES method to design this new structure to the same target interstorey drift.

   c) Conduct IDTHA on each structure with each earthquake record and obtain the peak interstorey drift ratio over all the floor levels. The median peak interstorey drift ratio is then obtained for all the records in the suite.

   d) Evaluate the performance for all of the ground motion records as either (i) the difference between the median peak interstorey drifts of the two structures or (ii) the probability that the demand for the irregular building is greater than the demand for the regular building. Only the median peak interstorey drift ratio was considered in this paper.

3. The performance distributions for the chosen degrees of irregularity and target interstorey drift ratio may then be used to characterise the effect of both of these variables and select appropriate limits.

2.6 Structural Forms Considered & Definition of Regular Structures

Simple one-dimensional models of 3, 5, 9 and 15 storey shear-type structures were considered. These models are adequate for determination of overall structural response (Cruz and Chopra, 1986) and reduce the computational effort.

There is no specification for the distributions of stiffness and strength within structures designed using the NZS 1170.5 ES method. Therefore, two classes of building having constant mass at every floor level were chosen to represent the two extremes of design choice for stiffness that defined the base (regular) structures (Paulay and Priestley (1992)). It is expected that the configuration of realistic frames would fall between these two extreme design models and hence the results serve as bounds. One class of building was designed for all the storeys to have a *constant interstorey drift ratio* (**CISDR**) and the other class was designed for all the storeys to have a *constant stiffness* (**CS**) with the target interstorey drift ratio at the first storey. These two models and their deflection profiles are shown in Figure 2-2. In the design, storey stiffnesses were iterated until the critical storey/storeys had the *design* (target) *interstorey drift ratio* (**DISDR**). For the CISDR model, at the end of iteration a constant strength to stiffness ratio was established at each floor level, so the shear strength provided at each level was the minimum required to resist the equivalent static design forces. But for the CS design model all the storeys had a *constant stiffness*, and the strength distribution over the height was either:

1. The minimum required to resist the design forces from the ES method, thus having a varying strength distribution (CS-VSTG) or
2. Every floor level was provided with a constant strength as required to resist the design force at the first floor (CS-CSTG). This stiffness-strength configuration ensured that every floor level had a constant strength to stiffness ratio.

Likely storey strength to scaled stiffness ratios for realistic structures were determined based on approximate empirical relations (Priestley *et al.* 2007) giving

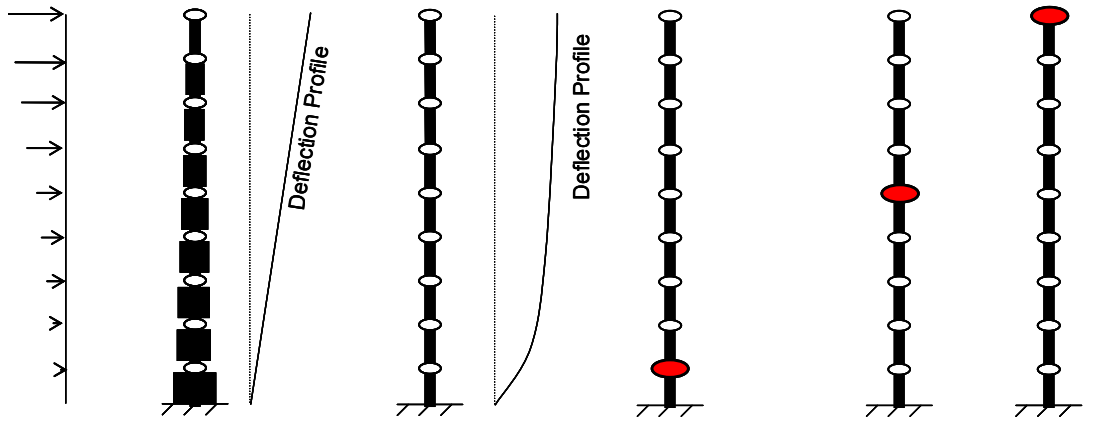

(a) Forces (b) CISDR Model (c) CS Model (d) Level 1 Mass Increased (e) Level 5 Mass Incr. (f) Level 9 Mass Incr.

Figure 2-2: Deformed shape for different structural configurations and mass irregularity.

yield drift ratios for different types of lateral force resisting systems. Here, stiffness used was the storey stiffnesses multiplied by the interstorey height, thereby resulting in dimensionless storey strength to stiffness ratios. Based on this, lower and upper limits of storey strength to scaled stiffness ratios of 0.3% and 3% were set (Appendix A, Sadashiva 2010), and structures with storey strength to scaled stiffness ratios outside this range were eliminated from this study.

2.7 Design Approach: NZS 1170.5 Equivalent Static Method

All the structures were designed according to the NZS 1170.5 ES method. Appendix B explains the steps involved in NZS 1170.5 ES method. In this appendix, examples of CISDR and CS design using the NZS 1170.5 ES method are shown. Section B.3 of Appendix B provides the Matlab [18] codes that were developed to apply the ES method.

The design parameters and assumptions used in this study were:

- Site sub-class chosen - A;
- Shortest distance from the site to the nearest fault, $D = 0$;
- Return period factor, $R_u = 1$;
- Zone hazard factor, Z = 0.4 (Wellington), 0.22 (Christchurch) and 0.13 (Auckland);
- Structural ductility factor, $\mu = 1, 2, 4$ and 6;
- Structural performance factor, S_p, for the appropriate μ value;
- Period calculation – Eigenvalue analysis ignoring *P*-Delta effects.

After calculation of the design base shear without consideration of *P*-Delta effects, *V*, *P*-Delta effects were considered according to *Section 6.5.4.2-Method B* of NZS1170.5 to obtain the additional structural actions and displacements. The horizontal design action coefficient, C_d, used for determining the design base shear is given by Equation (2-3) (*Cl. 5.2.1.1, NZS 1170.5*).

$$C_d(T_1) = \frac{C(T_1)\,S_p}{k_\mu} \tag{2-1}$$

$$C_{d,\min} = \max\begin{cases}(Z/20+0.02)\,R_u \\ 0.03\,R_u\end{cases} \tag{2-2}$$

$$C_d = \max\left\{C_d(T_1), C_{d,\min}\right\} \tag{2-3}$$

As an example, for a structure in a zone with hazard factor of 0.4 (e.g., Wellington), Figure 2-3 shows coefficient C_d (calculated according to Equation (2-1)) plotted

against fundamental period for ductility factors of 1, 2, 4 and 6. The solid line shows the minimum value of this coefficient, $C_{d,\min}$, calculated according to Equation (2-2).

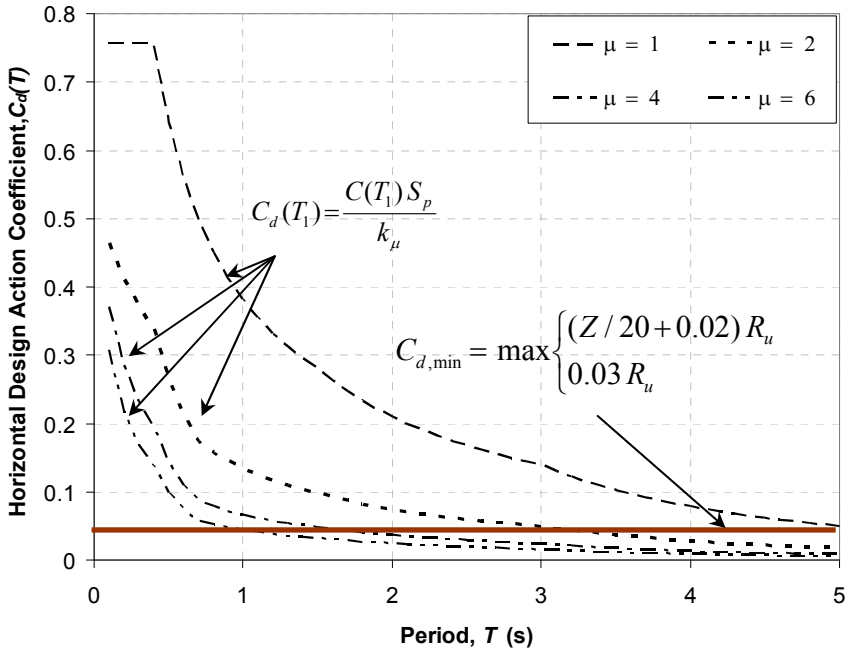

Figure 2-3: Variation of horizontal design action coefficient with fundamental period for a zone with hazard factor of 0.4.

According to Figure 2-3, when long period structures are designed with a design ductility factor, the base shear may be governed by Equation (2-2) which is the horizontal line in Figure 2-3. These structures have an effective ductility factor lower than the design ductility factor. For example, in Figure 2-3, for structures designed to have ductility factor of 2 and with periods more than 3.4s, the coefficient C_d is governed by Equation (2-2), and the effective ductility factor is less than 2. For this reason, structures having base shear governed by Equation (2-2) were eliminated from this study. Many structures designed for Auckland and Christchurch were controlled by this criterion. So, only results obtained for Wellington are shown in this paper.

2.8 Incorporation of Mass Irregularity

A structure with mass irregularity was obtained in the following way. The mass of one floor of a regular structure was modified at a time by means of a mass ratio. Here, mass ratio is defined as the ratio of the modified mass in the new irregular structure, to that of the regular structure. Four mass ratios of 1.5, 2.5, 3.5 and 5 were used. These were applied separately at the first floor level, mid-height and at the roof. This is illustrated in Figures 2-2(d) to 2-2(f) for the 9 storey structures. Each time the mass was increased, the structures were redesigned according to the method explained in the earlier section until the critical floor/floors had the target interstorey drift ratio. It should however be noted that the natural periods and base shears of the irregular structures were slightly different from those of the regular structures because their stiffness distribution was adjusted to produce the same specified design interstorey drift as the corresponding CISDR and CS regular structures.

2.9 Structural Modelling and Analysis

To investigate the effects of structural modelling on interstorey drift demands, each frame was modelled in two ways. Frames were initially modelled as a vertical *shear beam* (**SB**), assuming that the columns develop a point of contraflexure at the mid-height of each storey under the earthquake loading (Tagawa *et al.* 2004). Secondly, each frame was modelled as a combination of vertical *shear* beam and a vertical *flexural beam* (representing all of the continuous columns in the structure) that is pinned at the base. This model is labelled as **SFB**, and is shown in Figure 2-4. The shear beams had a bilinear hysteresis loop with a bilinear factor of 1 %. Here, the

choice of 1% for the bilinear factor was based on a sensitivity study conducted in Appendix C.

Previous studies (MacRae *et al.* 2004, Tagawa *et al.* 2006) have shown that the SFB model can represent frame behaviour well. A parameter defined as continuous column stiffness ratio α_{cci} (MacRae *et al.* 2004), representing the stiffness of flexural beam relative to the shear beam at the i^{th} floor level is computed using Equation (2-4).

$$\alpha_{cci} = \frac{E I_i}{H_i^3 K_{oi}} \tag{2-4}$$

where α_{cci} = continuous column stiffness ratio at floor level, i;

E = elastic modulus;

I_i = moment of inertia at the i^{th} floor level;

H_i = storey height of the i^{th} floor level; and

K_{oi} = initial lateral stiffness of the i^{th} floor level.

It is shown (Tagawa 2005) that when parameter $\alpha_{cci} = 0$, the structure behaves like a shear structure in which each storey behaves as an independent *single-degree-of-*

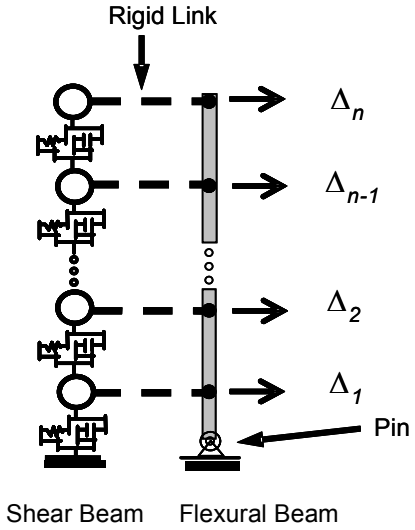

Figure 2-4: Combined vertical Shear and Flexural Beam (SFB model).

freedom (**SDOF**) system. For structures with low post-elastic stiffness, this can result in large interstorey drift concentrations due to soft storey mechanisms. Tagawa has also shown that for real frames, α_{cci} varies between 0.13 and 1.58, and the variation in response between these values was small. Hence, for this study a continuous column stiffness ratio of 0.5 at any floor level was assumed, and the additional moment of inertia at each floor level was calculated from Equation (2-4).

2.9.1 Choice of Damping Model for Time-History Analysis

A common damping model available in most of the time-history programs (e.g., SAP 2000, ETABS, RUAUMOKO, OpenSees etc.) for linear and non-linear analysis of *multi-degree-of-freedom* (**MDOF**) systems is the Rayleigh damping model, shown in Figure 2-5. This type of damping model has structural damping matrix, [*C*], given as the summation of mass and stiffness proportional damping models. Here, the mass damping matrix is given as the product of the proportionality constant, a_o and the mass matrix, [*M*], and the stiffness damping matrix is given as the product of proportionality constant, b_o and the stiffness matrix, [*K*].

To investigate the effects of different damping models on the responses of regular and irregular structures, three of the Rayleigh damping models available in RUAUMOKO (Carr 2004) time-history program were used. A brief explanation of these damping models is given below.

(a) Initial Stiffness Rayleigh Damping (ISRD): This type of Rayleigh damping is commonly used by the researchers conducting linear or non-linear dynamic time-history analysis. The structural damping matrix is formed considering the elastic stiffness matrix, [K_0], the mass matrix, [*M*], and the proportionality constants based

on the elastic frequency, a_o and b_o. The computed damping matrix remains constant

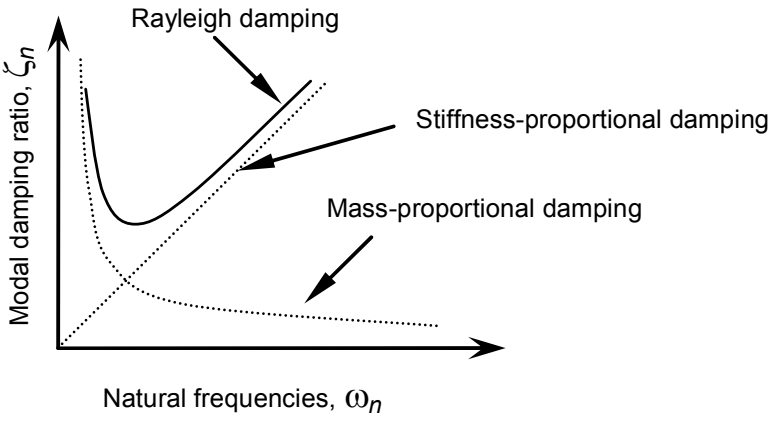

Figure 2-5: Variation of modal damping ratio with natural frequency.

throughout the analysis, and the damping forces, F_{damp} , at time *t,* are obtained as a product of the damping matrix and the current velocity, $\dot{u}$, as given by Equation (2-5).

$$\{F_{damp}(t)\} = [a_0[M] + b_0[K_0]]\{\dot{u}(t)\} \qquad (2\text{-}5)$$

During non-linear analysis the structure softens by yielding. This results in a decrease in the tangent structural stiffness and instantaneous natural frequencies. Therefore the damping matrix, which is based on the initial stiffness and initial elastic frequencies, causes a higher damping ratio in the yielding structure which may be unrealistic (Otani 1981).

(b) Tangent Stiffness Rayleigh Damping with Incremental Equation of Motion (TSRD): This is a modified version of initial stiffness Rayleigh damping, and it considers the nonlinearity effects. It uses Newmark's formation of the *Equation of Motion* (**EOM**) in terms of incremental equilibrium. In this case, as the structure yields and stiffness reduces, the tangent stiffness matrix, $[K_t]$ is utilised to compute

the damping matrix at each time-step. The damping forces are adjusted in each time-step with the increment of damping forces being product of the tangent damping matrix and the incremental velocities in the structure, $\Delta\dot{u}$. The incremental damping forces are then added to the damping forces existing in the structure at the beginning of time-step to give damping forces at the end of time-step, as in Equation (2-6).

$$\{F_{damp}(t+\Delta t)\} = \{F_{damp}(t)\} + [a_0[M] + b_0[K_t]]\{\Delta\dot{u}\} \quad (2\text{-}6)$$

Since the tangent damping matrix is obtained from the tangent stiffness matrix, using the incremental solution to the EOM, at the end of earthquake when the velocity of the structure goes to zero, the damping forces do not necessarily go to zero, thus may result in unrealistic residual damping forces and displacements.

(c) Tangent Stiffness Rayleigh Damping with Total Equation of Motion (TASRD): This is a modified version of tangent stiffness Rayleigh damping using the absolute form of the EOM. The damping forces at a time-step, given by Equation (2-7), are computed as the product of tangent damping matrix (obtained from tangent stiffness matrix) and the instantaneous velocities of the structure.

$$\{F_{damp}(t)\} = [a_0[M] + b_0[K_t]]\{\dot{u}\} \quad (2\text{-}7)$$

This damping model has the properties that: (a) damping forces go to zero at the end of excitation; and (b) damping is appropriate while the structure is elastic.

In addition to careful choice of appropriate damping model, the two modes chosen to apply the user specified damping ratio should be carefully chosen in the analysis. Crisp (1980) has shown that improper selection of modes for applying the damping ratios could lead to high levels of viscous damping in higher modes of free vibration of a structure. Thus for all the analyses, the first mode and the mode corresponding to

the number of storeys in the structure were nominated as the two modes with 5% of critical damping (Carr 2004).

2.9.2 Selection and Scaling of Earthquake Ground Motions for Time-History Analysis

Many works at the Pacific Earthquake Engineering Research Centre, and at other places, are aimed at addressing issues with ground motions selection and scaling methods for dynamic analysis. For example, Baker (2006 & 2007) has shown that random ground motion record selection can produce unrealistic scaling and increase the scatter of absolute responses. He also suggests that the records matching the shape of the uniform hazard spectrum may incorrectly evaluate the response at different periods. A recent study by Chase *et al*. (2011) has shown that relative values from suites of records are relatively invariant It is expected that the record selection and scaling will have less influence on the relative responses used in this study than on the absolute responses. Hence, the 20 SAC (SEAOC-ATC-CUREE) earthquake ground motion records (tabulated in Table 2-1) for Los Angeles, with probabilities of exceedance of 10% in 50 years, were used for the ground motion suite. Here, the acceleration time histories were originally derived from historical recordings or from physical simulations and have been modified (through scaling in the frequency domain) to match their mean response spectrum with the 1997 *National Earthquake Hazards Reduction Program* design spectrum. Figure D-1 (Appendix D) shows the acceleration time histories of the earthquake records used for dynamic analysis.

The New Zealand design Standard, NZS1170.5, requires the ground motion records to be scaled before conducting time-history analysis. A procedure to scale earthquake records is given in *Cl. 5.5.2* of NZS 1170.5. It requires each record to be scaled by a

record scale factor, k_1, so as to match the target spectra over a period range of interest ($0.4T_1 – 1.3T_1$ with T_1 not to be less than 0.4s). Here, the target spectrum is the design spectrum appropriate for the site and limit state of the structure under consideration. Each record, within the family of records, is then scaled by the family scale factor, k_2 which is applied to ensure that the energy content of at least one record in the family exceeds that of the design spectrum over the target period range. The Standard has about 15 steps making it quite complex. Also, the code scaling approach can result in the target spectral acceleration to be less than that expected for an elastically responding structure. Therefore, a simpler scaling method, as adopted by previous researchers (e.g., Shome *et al*., 1998; Iervolino and Cornell, 2005; Luco and Bazzurro, 2007), has been used to scale each of the selected 20 SAC records. It consists of the following three steps:

(a) Target Spectral Acceleration: The target spectral acceleration, $S_{a,des}$ (g), is equal to the elastic site hazard spectrum for horizontal loading, $C(T_1)$, calculated according to *Clause* 3.1 of NZS 1170.5:2004 (see Equation B-3). Here, structural ductility factor, μ, and structural performance factor, S_p, are taken equal to unity.

(b) Record Unscaled Spectral Acceleration ($S_{a,i}$)*:* Calculate the spectral acceleration of each earthquake record, i, at the fundamental natural period of the structure, T_1.

(c) Scaling Records: Scale the magnitude of each i^{th} record by a scale factor, $SF_i = S_{a,des}/ S_{a,i}$. Here, the scaled records will have the same spectral acceleration at the fundamental natural period of the structure.

Section D.2 of Appendix D explains the steps used to obtain response spectra for each of the selected records, and Section E.3.1 of Appendix E shows a Matlab [18] code developed to calculate the record scale factors.

Table 2-1: Ground motion suite used for time-history analysis

SAC Name	Earthquake Record	Moment Magnitude	PGA (g)
LA01	Imperial Valley, 1940, El Centro	6.9	0.461
LA02	Imperial Valley, 1940, El Centro	6.9	0.676
LA03	Imperial Valley, 1979, Array #05	6.5	0.393
LA04	Imperial Valley, 1979, Array #05	6.5	0.488
LA05	Imperial Valley, 1979, Array #06	6.5	0.301
LA06	Imperial Valley, 1979, Array #06	6.5	0.234
LA07	Landers, 1992, Barstow	7.3	0.421
LA08	Landers, 1992, Barstow	7.3	0.426
LA09	Landers, 1992, Yermo	7.3	0.52
LA10	Landers, 1992, Yermo	7.3	0.360
LA11	Loma Prieta, 1989, Gilroy	7	0.665
LA12	Loma Prieta, 1989, Gilroy	7	0.970
LA13	Northridge, 1994, Newhall	6.7	0.678
LA14	Northridge, 1994, Newhall	6.7	0.657
LA15	Northridge, 1994, Rinaldi RS	6.7	0.533
LA16	Northridge, 1994, Rinaldi RS	6.7	0.580
LA17	Northridge, 1994, Sylmar	6.7	0.570
LA18	Northridge, 1994, Sylmar	6.7	0.817
LA19	North Palm Springs, 1986	6	1.02
LA20	North Palm Springs, 1986	6	0.987

2.9.3 Inelastic Time-History Analysis and Interpretation of Results

The RUAUMOKO computer program [5] was used to carry out all the *inelastic dynamic time-history analyses* (**IDTHA**). Here, in order to conduct many analyses in a relatively short time, the batch mode option available within the program was used. The creation of RUAUMOKO input files required for each parametric analysis, executing the program, and post-processing the output from RUAUMOKO result files, was all automated systematically using Matlab [18]. Appendix E provides the Matlab codes that were developed for RUAUMOKO automation.

In RUAUMOKO, two time-history integration schemes are available: (a) *Central Difference* method and (b) *Newmark Constant Average Acceleration* method. A brief description of these two numerical methods is given below from Chopra [8].

(a) *Central Difference* method – it is based on finite difference expressions of velocity and acceleration. The time-stepping Central Difference method is a conditionally stable explicit numerical procedure that leads to bounded solutions if the time-step (Δt) is shorter than some stability limit. This method is considered to be stable, if $\Delta t/T_n < 1/\pi$, where T_n is the shortest natural period of the structure. The above stability limit is necessary to avoid obtaining meaningless results, in the presence of numerical round-off errors, as a result of a large time-step length. This effect on the results, due to improper time-step size, will be more pronounced for structures having significant higher mode contributions to the total response. In addition to meeting the stability requirement, adequate accuracy in the numerical results should be ensured by taking the time-step less than $0.5T_n$ [5], or less than $0.1T_n$ [8]. A choice of time-step size based on the above accuracy

requirements will also satisfy the stability requirements. Although the Central Difference method may be easily adapted for solving the nonlinear equation of motions at time *i*, this method is uneconomical for most framed structures subjected to earthquake loadings, and hence it is not recommended [5]. A more commonly adopted time-history integration scheme for analysing multi-storey frame buildings is explained next.

(b) *Newmark Constant Average Acceleration* method – it is based on the assumption that the variation of acceleration over a time-step is constant, equal to the average acceleration. The time-stepping Newmark Constant Average Acceleration method is an unconditionally stable implicit numerical procedure that leads to bounded solutions regardless of the time-step size. Here, although the length of the time-step is not limited by stability considerations, in order to obtain accurate representation of the excitation and response, the time-step size should be small enough such that using a smaller time-step does not significantly change the response. It is recommended that the time-step length should be less than 0.1 times the period of the highest mode of free vibration that contributes significantly to the response of the structure, but often Δt = 0.01s is found satisfactory for multi-storey structures [5]. In this study, a time-step size of Δt = 0.001s was found to be more than sufficient in producing converging results. Therefore, this time-step size of 0.001s was used for all time-history analyses using the Newmark Constant Average Acceleration method.

The peak *interstorey drift ratio* (**ISDR**) within the structure, when subjected to each of the 20 earthquake records, was obtained. It was assumed that the distribution of

peak ISDR is lognormal (Cornell *et al.* 2002), so the median and dispersion were calculated as per Equations (2-8) and (2-9).

$$\hat{x} = e^{\left(\frac{1}{n}\sum_{i=1}^{n}\ln(x_i)\right)} \tag{2-8}$$

$$\sigma_{\ln x} = \sqrt{\frac{1}{(n-1)}\sum_{i=1}^{n}\left(\ln x_i - \ln \hat{x}\right)^2} \tag{2-9}$$

where x_i = peak interstorey drift ratio due to i^{th} record; and

n = total number of earthquake records considered.

It should be noted that the label "Median interstorey drift ratio" on all the response plots in the following sections refers to the median peak interstorey drift ratio.

2.9.4 Comparison between SB and SFB Models

Median peak interstorey drift ratios obtained for 3, 9, 15 and 20 storey CISDR and CS-VSTG models, modelled as shear (**SB**) and shear-flexural vertical beams (**SFB**) were compared for each of the design interstorey drift ratios.

Figure 2-6(a) shows that when 3 and 9 storey regular CISDR structures are modelled as SB, there is significant increase in the median peak ISDR for all the design interstorey drift ratios compared to the corresponding SFB models. The median peak ISDR was on average 40% and 90% more than those obtained when the 3 and 9 storey structures were modelled as SFB respectively. For CS-VSTG regular structures, Figure 2-6(b) shows that the average increase in median peak ISDR for 3 and 9 storey structures modelled as SB is 53% and 94%, respectively. It was also observed that these average increases in drift increased with the structure's height for both the design models. Since neglecting the effect of column continuity can result in

a likelihood of a soft-storey mechanism and high interstorey drift which would not be expected in realistic structures which have continuous columns over their height, the SFB model was used for all further analyses.

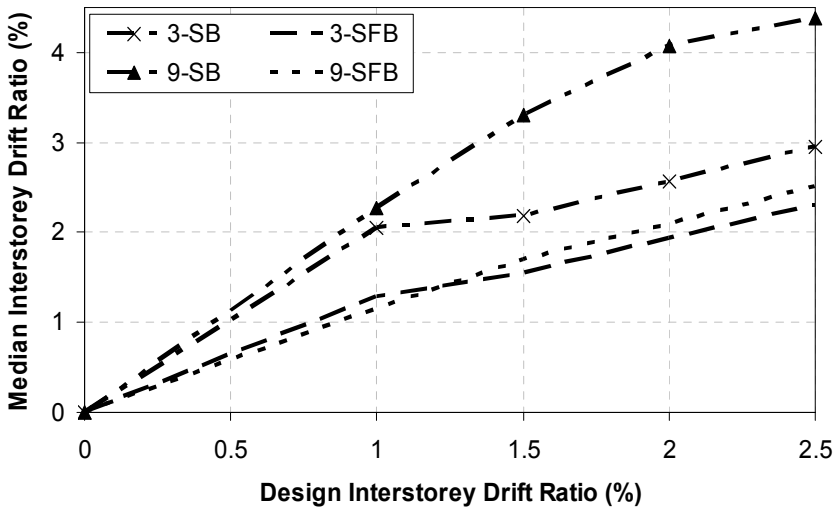

(a) CISDR Design Model

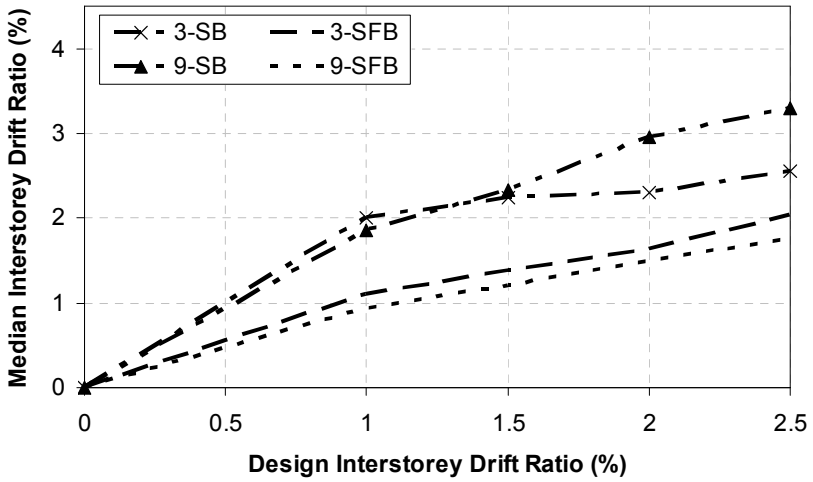

(b) CS-VSTG Design Model

Figure 2-6: Comparison between SB and SFB models for regular CISDR and CS-VSTG design models ($\mu = 4$, $Z = 0.4$).

2.9.5 Comparison between Damping Models

The effect of damping model on median peak ISDR for 3 and 9 storey structures designed for a ductility of 4 in Wellington was investigated. The three types of Rayleigh damping models explained in the earlier section were considered for this sensitivity study.

Figures 2-7(a) and 2-7(b) show median peak ISDR for regular 3 and 9 storey CISDR design models respectively. Due to yielding of the structure and structural stiffness reducing, the TASRD produced on average 2% and 0.7% more median peak ISDR than the Initial Stiffness Rayleigh damping model for 3 and 9 storey structures respectively. The figures also show that there is no significant difference in drift due to TSRD and TASRD damping assumptions.

In the case of regular CS-VSTG design models, the TASRD damping assumption produced on average 2.9% and 0.6% more drift than the Initial Stiffness Rayleigh damping model for 3 and 9 storey structures respectively. Again there was no apparent difference in drift demands observed due to TSRD and TASRD damping models.

The choice of damping model is likely to be even less important when comparing the relative responses of the regular and the irregular structures. If it is not stated otherwise explicitly below, the Tangent Stiffness Rayleigh Damping model with total equation of motion (TASRD) was used for all other analyses in this paper.

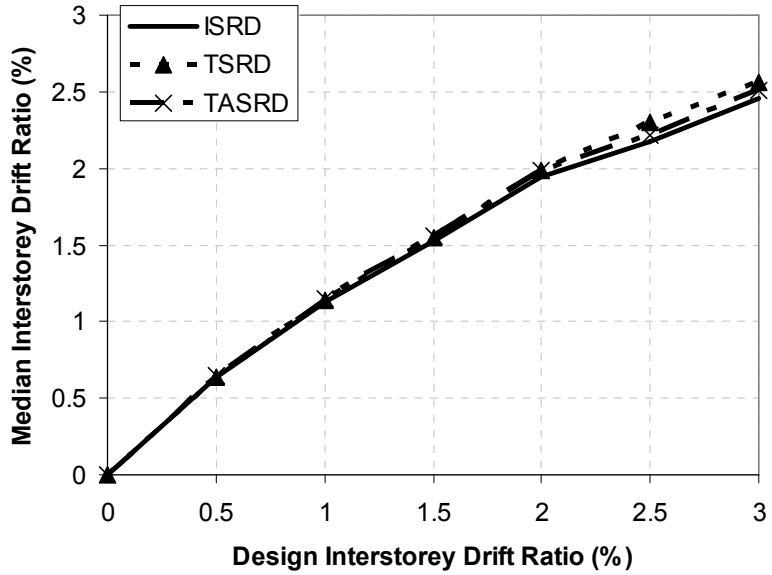

(a) Number of Storeys: 3

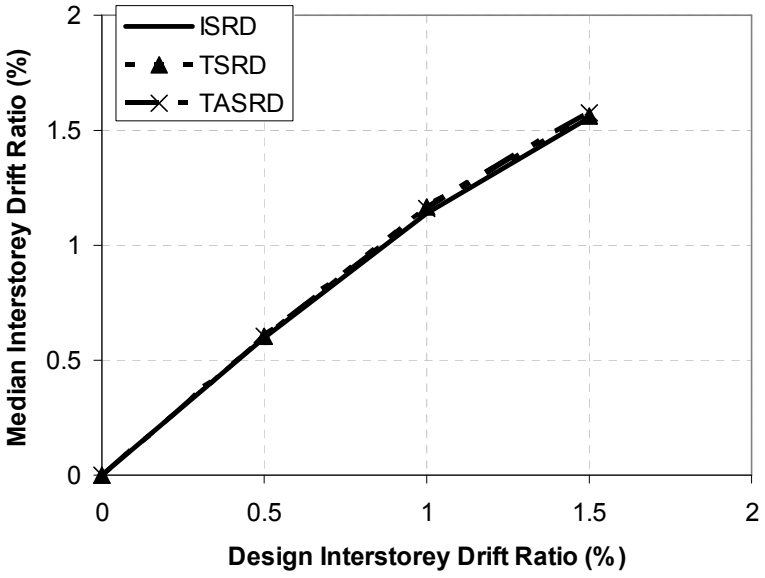

(b) Number of Storeys: 9

Figure 2-7: Comparison of median peak ISDR due to different damping models – regular CISDR design models ($\mu = 4$, $Z = 0.4$).

2.9.6 Comparison between IDTHA and Code Responses

The NZ 1170.5 ES method is based on the assumption that the peak design interstorey drifts are comparable to those predicted using inelastic dynamic time-history analysis. If this assumption is true, the median peak interstorey drift ratio for the earthquake record suite will be close to the design interstorey drift ratio. The following plots show comparison between IDTHA and code responses for regular CISDR and CS-VSTG structures designed for structural ductility factors (μ) of 1 and 2. The corresponding response comparison plots for μ = 4 and 6 are provided in Appendix L.1.

Figures 2-8(a) and 2-8(b) show the differences between the code and IDTHA responses for regular CISDR models designed for a structural ductility factor of 1 and 2 respectively. Figure 2-8(a) shows that when structures were designed for μ = 1, the drift demands for 5 storey structures nearly matched the code drift prediction. It can be seen that the ES method under-predicts the median peak ISDR for taller structures, and for shorter structures the median responses are over-predicted. For structures designed for a ductility factor of 2, Figure 2-8(b) shows that the ES method non-conservatively estimates the median peak ISDR for all DISDR values irrespective of the structure height. Design interstorey drift ratios for the 15 storey structure are not more than 1.5% because $C_{d,min}$ from Equation (2-2) controls. When μ was increased to 6, the ES method provided slightly non-conservative estimates of the interstorey drift ratio for DISDR < 2%. Results for higher DISDR values were not obtained because of $C_{d,min}$.

For regular CS-VSTG structures designed for $\mu = 1$, the ES method over-estimates the median peak ISDR for all the DISDR considered in this study as shown in Figure 2-9(a). Figure 2-9(b) shows that for any structure height designed for $\mu = 2$, the median drifts closely matched the code prediction for DISDR < 1.5%. Again when μ was increased to 6, it was seen that the code over-estimates the drift demands for DISDR > 1.5%.

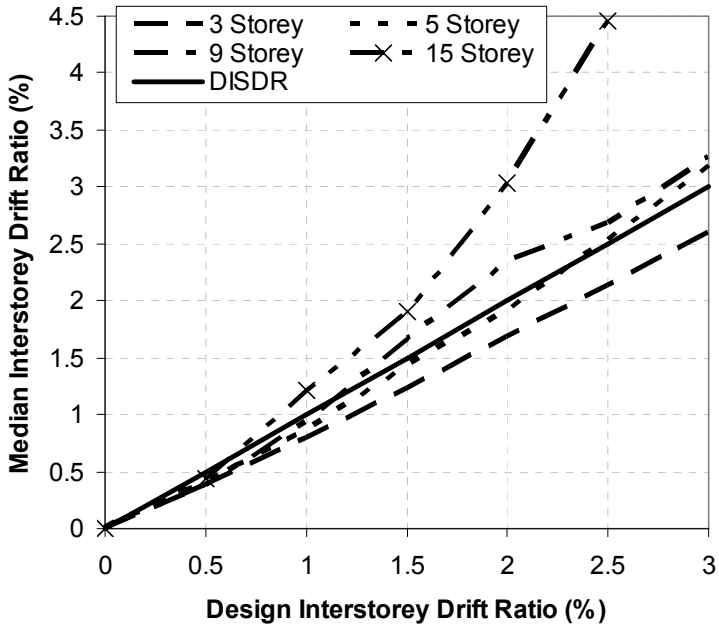

(a) Structural Ductility Factor, $\mu = 1$

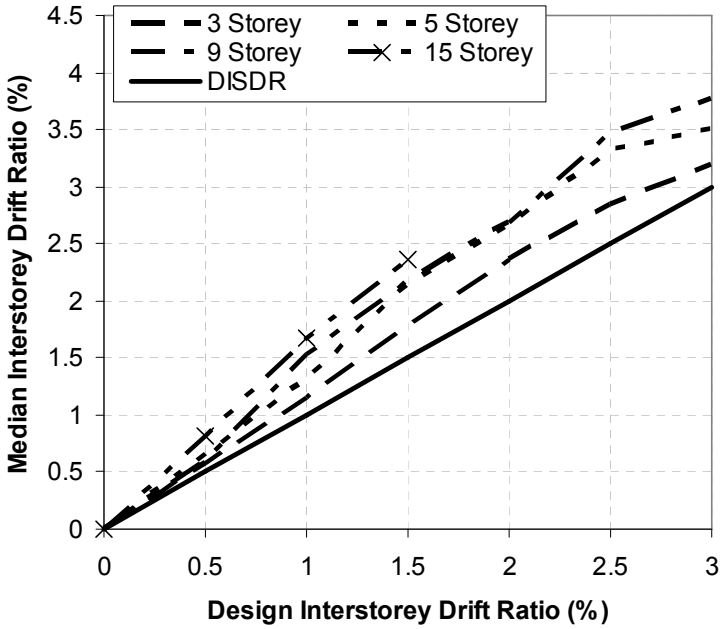

(b) Structural Ductility Factor, $\mu = 2$

Figure 2-8: Comparison between actual and code response for regular CISDR models.

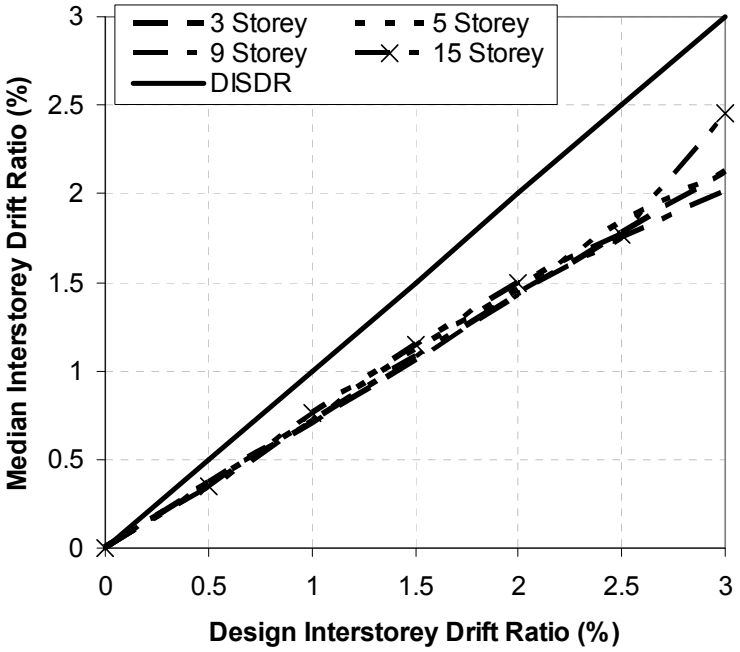

(a) Structural Ductility Factor, μ = 1

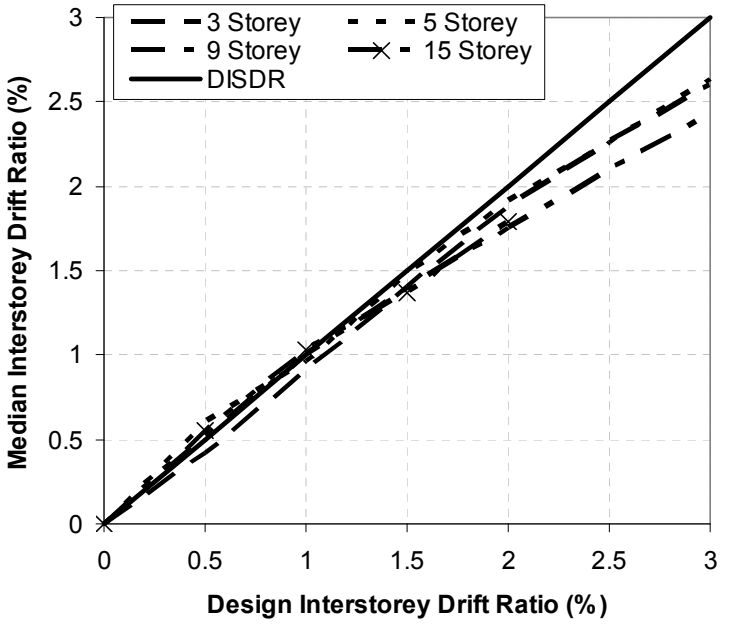

(b) Structural Ductility Factor, μ = 2

Figure 2-9: Comparison between actual and code response for regular CS-VSTG models.

2.9.7 Effect of Magnitude and Floor Level of Mass Irregularity

3, 5, 9 and 15 storey structures having mass irregularity were designed for three cities (Wellington, Christchurch and Auckland) considering four structural ductility factors (1, 2, 4 and 6). Four mass ratios of 1.5, 2.5, 3.5 and 5 times the floor mass at the corresponding floor level of regular structure, were adopted in this study. The chosen mass ratios were placed separately at the first floor level, mid-height and at the topmost floor level. All the structures were modelled as a combination of vertical shear and flexural beams. Tangent stiffness Rayleigh damping based on the total equilibrium (TASRD) was used and inelastic time-history analyses were carried out to obtain peak interstorey drift responses. Median peak ISDR responses from irregular structures were then compared with those corresponding to regular structures to estimate the increase in drift demand for each of the design interstorey drift ratios.

For brevity, only results for Wellington structures designed for a ductility factor of 2 are presented in the following plots to show the effect of mass irregularity. The ductility of 2 was chosen because the Wellington structures designed to this level are not generally governed by Equation (2-2); so many data points are available. The response plots for Wellington structures designed for structural ductility factors of 4 and 6 are provided in Appendix L.2. The response plot labels in the following figures have the format "N-L(Q)", where N refers to the number of storeys in the structure, L refers to the floor level of the irregularity and Q defines the magnitude of irregularity (mass ratio).

Note: As mentioned earlier, many designs for structures in Auckland and Christchurch were eliminated because of not satisfying the conditions specified in

Sections 2.6 and 2.7. Appendix F shows some examples of limited results obtained for structures in these two relatively less seismic active regions.

Figure 2-10 shows the effect of magnitude and floor level of mass irregularity on the median peak ISDR for CISDR design models. For all structure heights, the maximum increase in median peak ISDR due to a mass ratio of 1.5 at the first and topmost floor level relative to that of regular structures is less than 9% and 6% respectively. For many design interstorey drift ratios, it can be seen that the regular structures produced slightly higher drift demands than when the mass ratio of 1.5 was applied at the mid-height of all structures. The maximum increase in median peak ISDR at this height over the regular structure was less than 2%. The mass ratio was increased from 1.5 to a maximum of 5 at the three chosen floor levels. When the increased mass was present at the top or bottom floor levels, it tended to produce higher drift demands than for regular structures. For taller structures the mass ratio at the mid-height produced lower median peak ISDR than those from regular structures. Maximum increases in median peak ISDR of 20% and 25% were observed due to any mass irregularity present at the first and the topmost floor level respectively. The increase in drift demands due to increased mass at the mid-height was less than 6%.

The effect of mass irregularities' magnitude and floor level on median peak ISDR for CS-VSTG design models is shown in Figure 2-11. It is seen that when a mass ratio of 1.5 is applied at the topmost floor level, it produces a maximum of 8% increase in drift demand due to irregularity considering all the structure heights. A mass ratio of 1.5 at the first floor level or at the mid-height of all the structures generally tends to produce lesser drift demands than regular structures. When the mass ratio is increased from 1.5 to a maximum of 5, the maximum increase in median peak ISDR due to any

mass ratio was found to be less than 6% and 19% for increased mass at the first floor level and the mid-height of structures respectively, and 56% for mass ratio at the topmost floor level. Again, the drift demands over those from regular structures tended to decrease for higher DISDR when any mass ratio was applied at the first floor level or at the mid-height.

Figure 2-12 shows the effect of mass ratio and floor level on the CS-CSTG model, designed for structural ductility factor of 2. For a mass ratio of 1.5, Figure 2-12 (a) shows that the maximum increase in median peak ISDR is produced when the increased mass is present at the topmost floor level for all structure heights. When the mass ratio was increased to 5, the maximum increase in median peak ISDR is shown in Figure 2-12 (d) to be 40%, obtained from 3 storey structure having the increased mass at the roof. Figure 2-12 also shows that the effect of mass irregularity decreases as the structure height increases, irrespective of the magnitude of mass irregularity. It can also be seen that for many cases, the increased mass at the first floor level tended to produce lesser median peak ISDR than the regular structure.

Note: The response plots in Figures 2-10, 2-11 and 2-12 are based on median peak ISDR of regular and irregular structures. The effect of magnitude and floor level of mass irregularity considering 16^{th} and 84^{th} percentile peak ISDR results is presented in Figure L-8 (Appendix L.3).

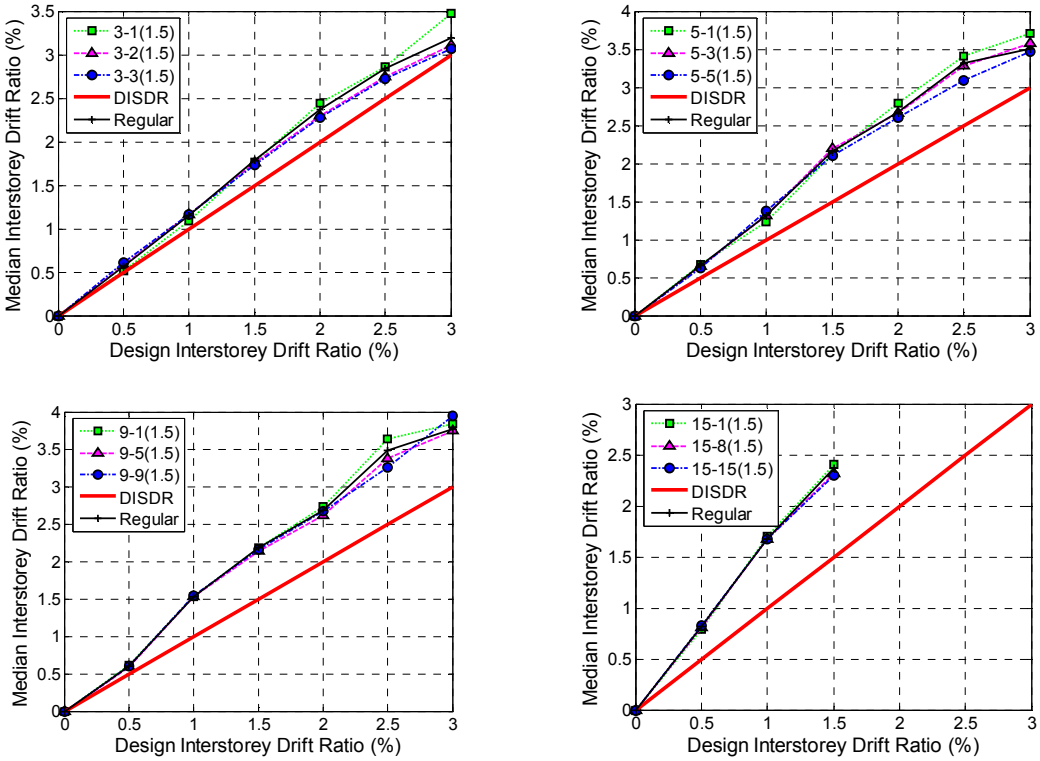

(1) Mass Ratio: 1.5

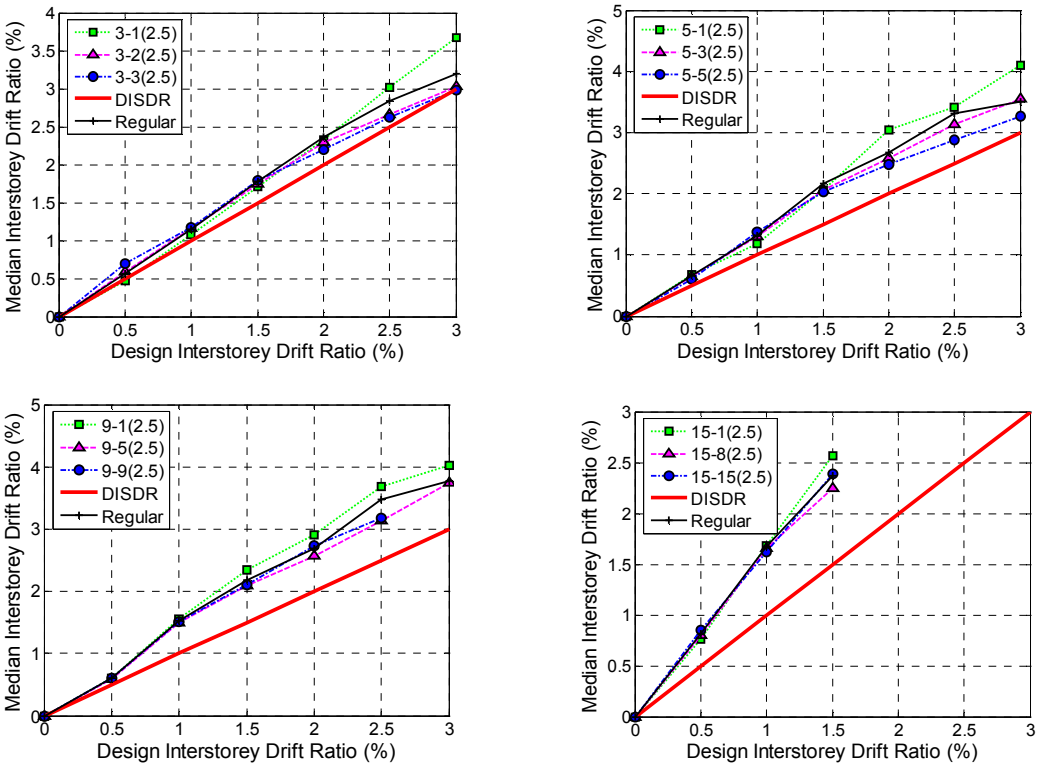

(2) Mass Ratio: 2.5

Figure 2-10(a): Effect of magnitude and floor level of mass irregularity for CISDR model ($\mu = 2$, $Z = 0.4$) – Mass Ratios: 1.5 & 2.5.

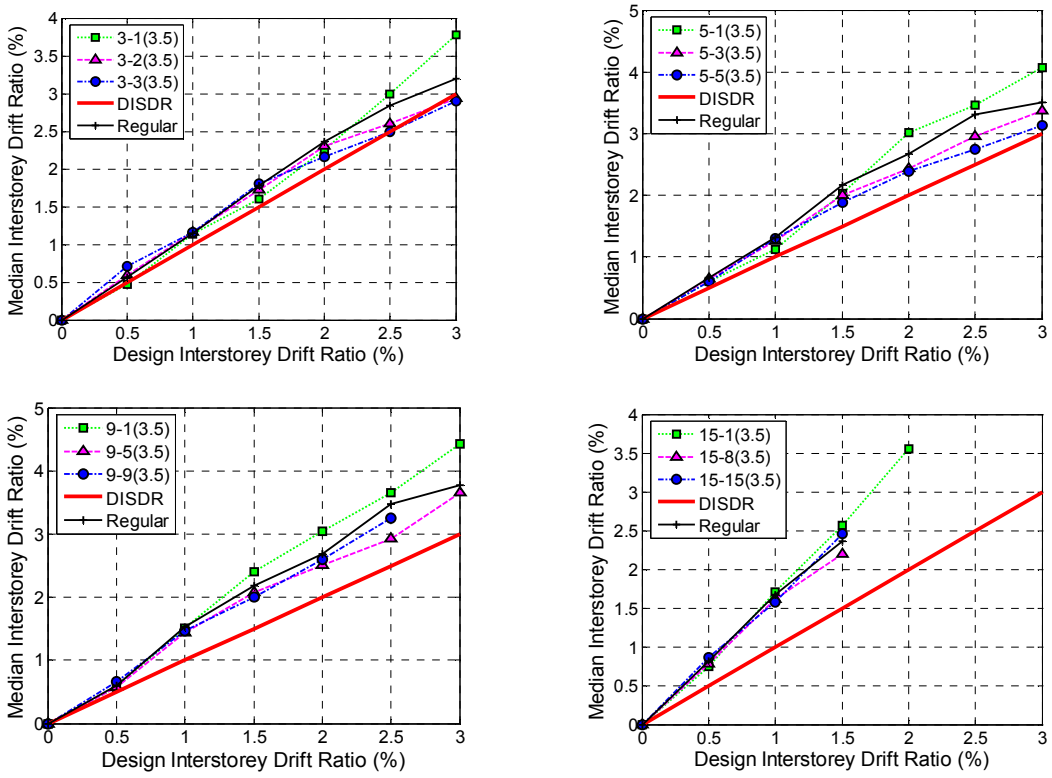

(1) Mass Ratio: 3.5

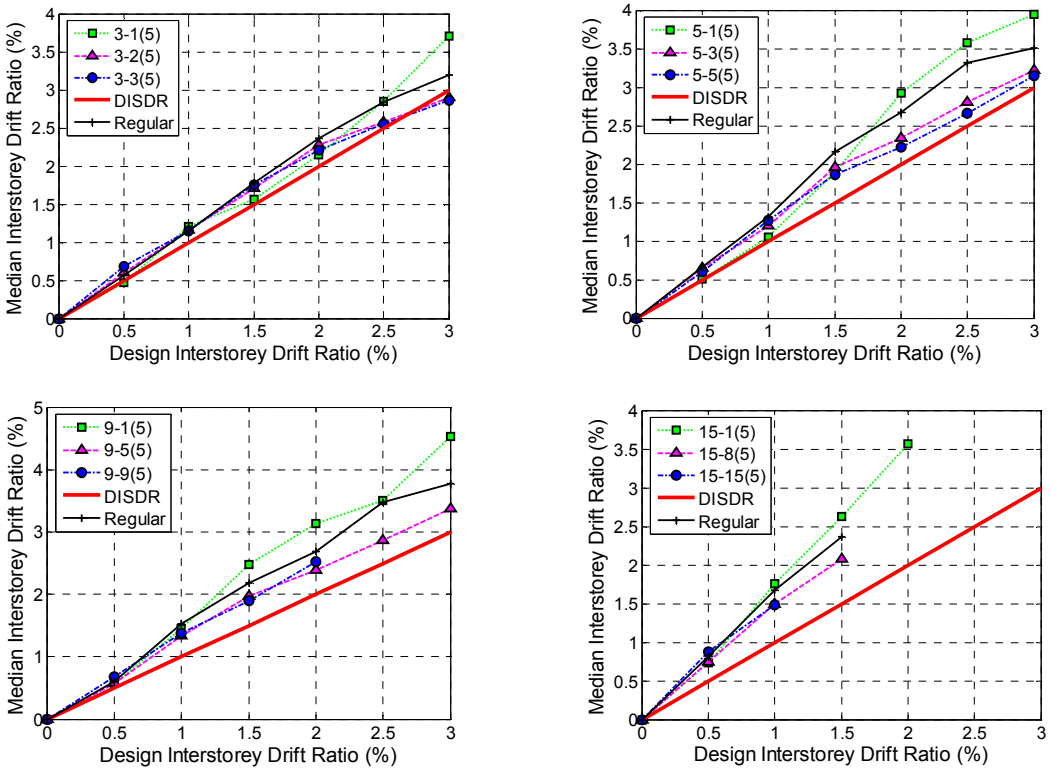

(2) Mass Ratio: 5

Figure 2-10(b): Effect of magnitude and floor level of mass irregularity for CISDR model ($\mu = 2$, $Z = 0.4$) – Mass Ratios: 3.5 & 5.

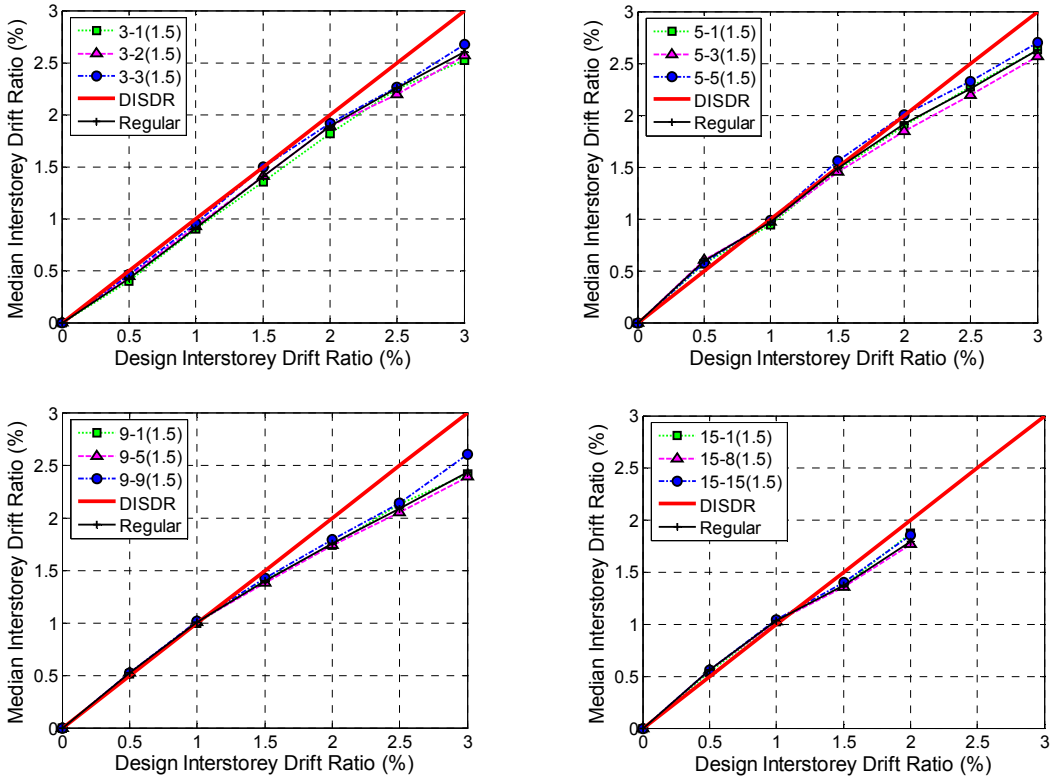

(1) Mass Ratio: 1.5

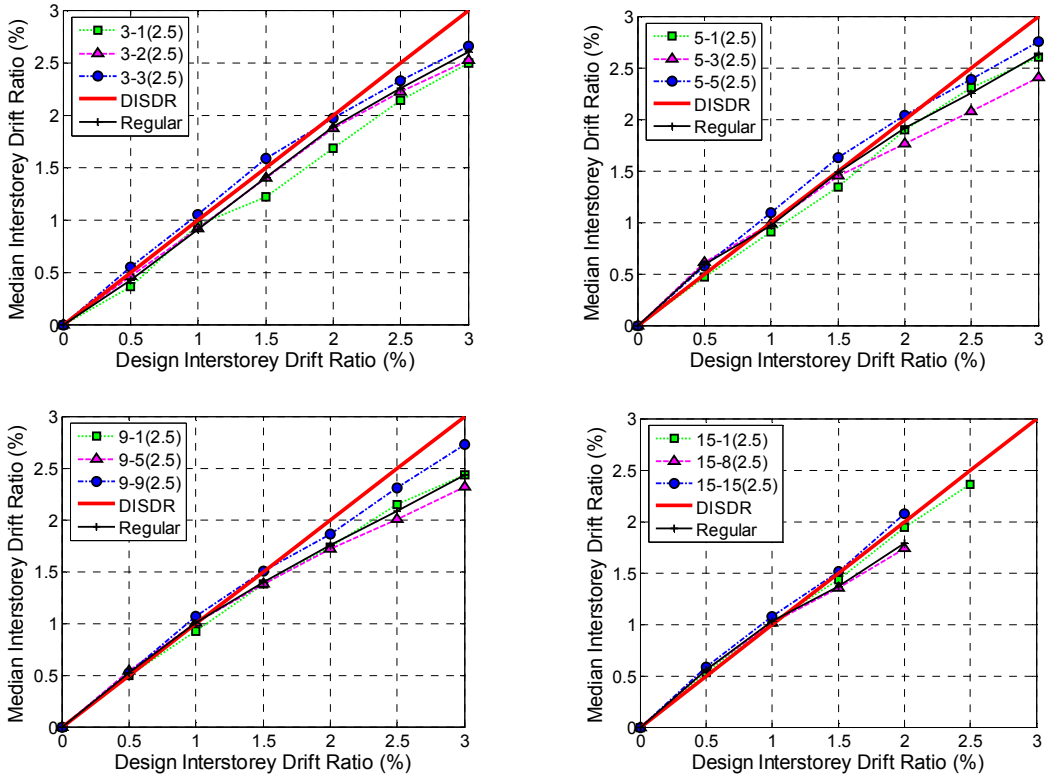

(2) Mass Ratio: 2.5

Figure 2-11(a): Effect of magnitude and floor level of mass irregularity for CS-VSTG model ($\mu = 2$, $Z = 0.4$) – Mass Ratios: 1.5 & 2.5.

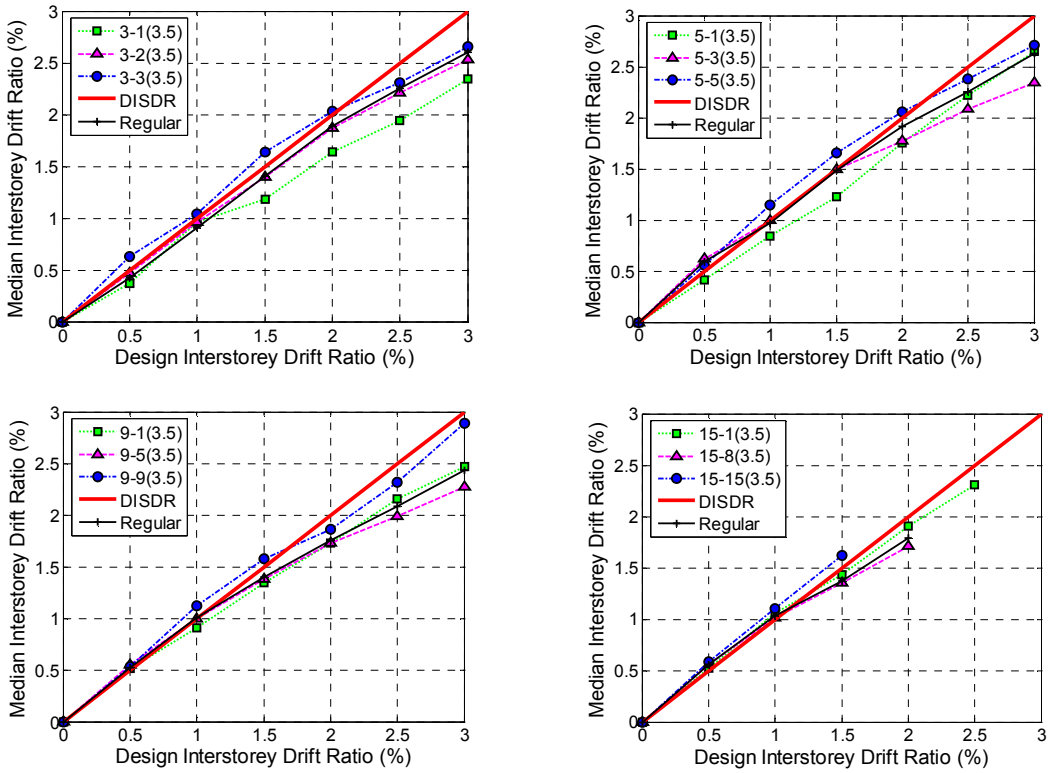

(1) Mass Ratio: 3.5

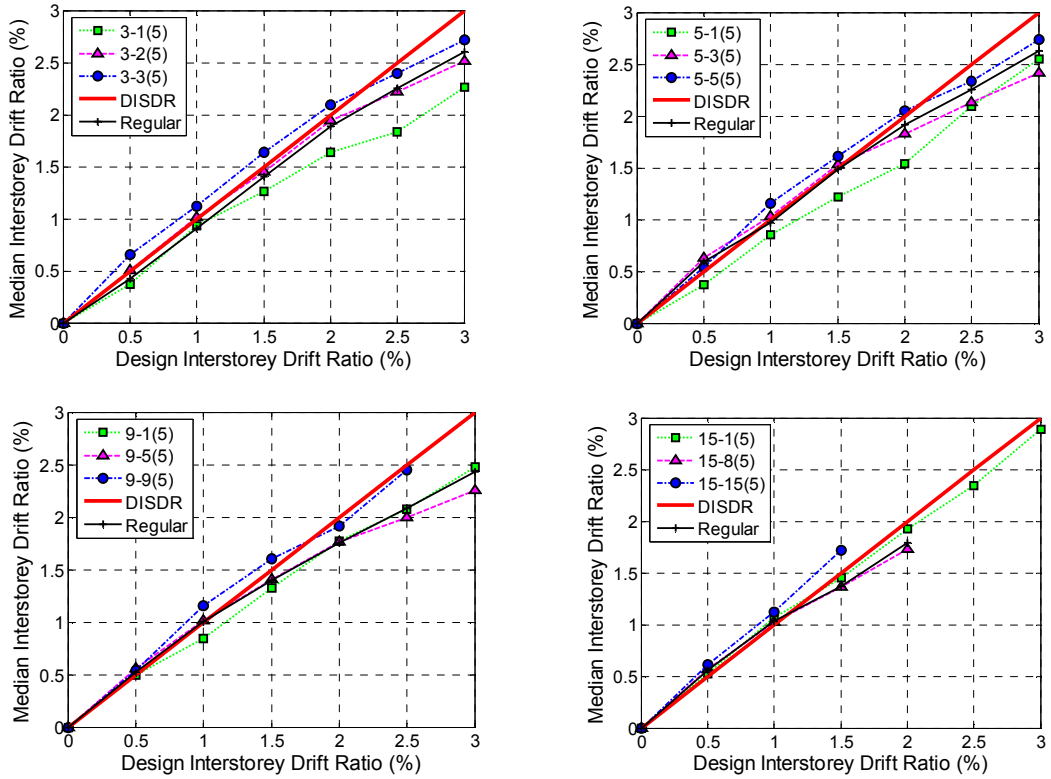

(2) Mass Ratio: 5

Figure 2-11(b): Effect of magnitude and floor level of mass irregularity for CS-VSTG model ($\mu = 2$, $Z = 0.4$) – Mass Ratios: 3.5 & 5.

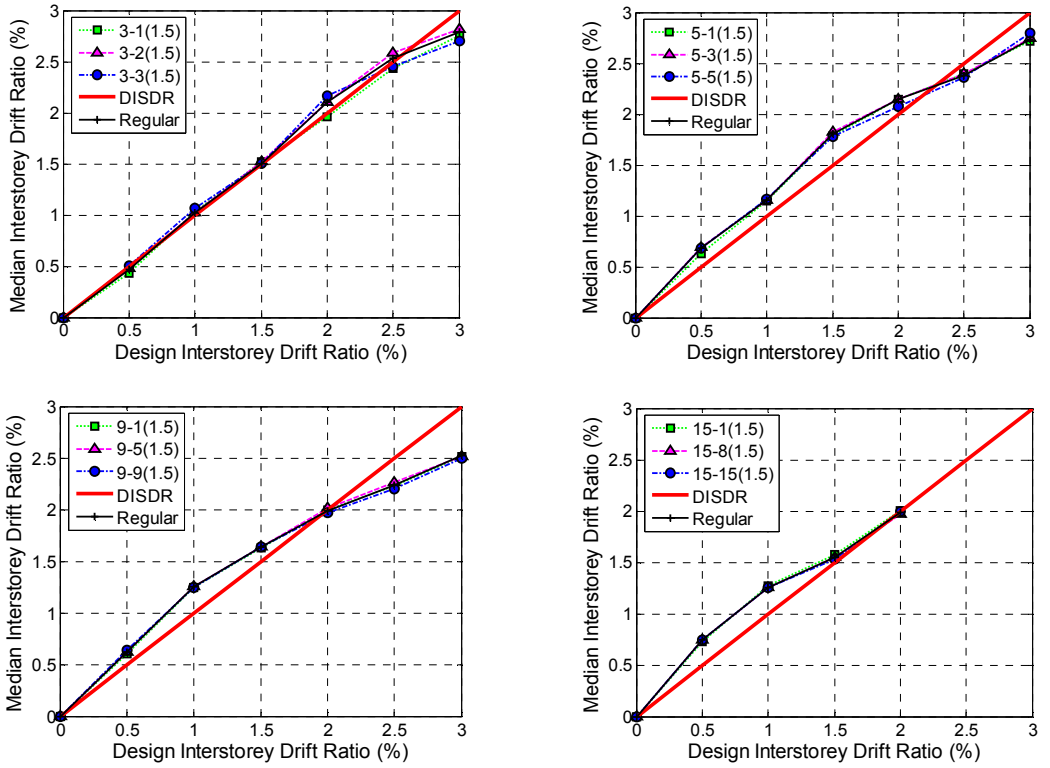

(1) Mass Ratio: 1.5

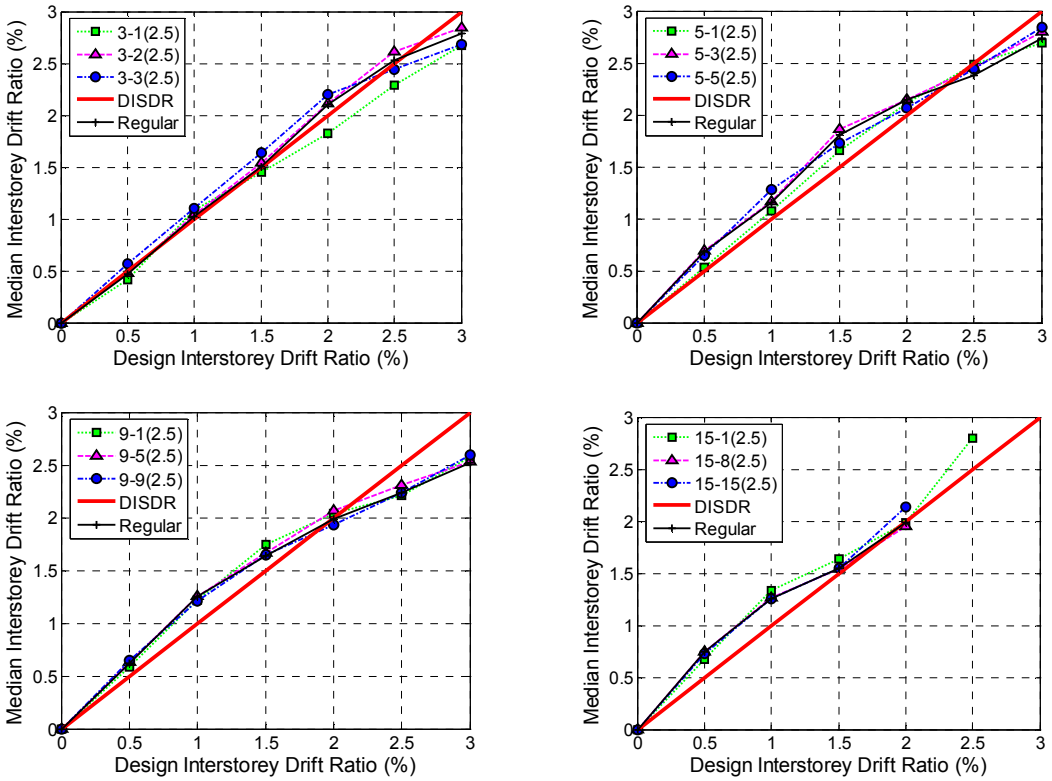

(2) Mass Ratio: 2.5

Figure 2-12(a): Effect of magnitude and floor level of mass irregularity for CS-CSTG model ($\mu = 2$, $Z = 0.4$) – Mass Ratios: 1.5 & 2.5.

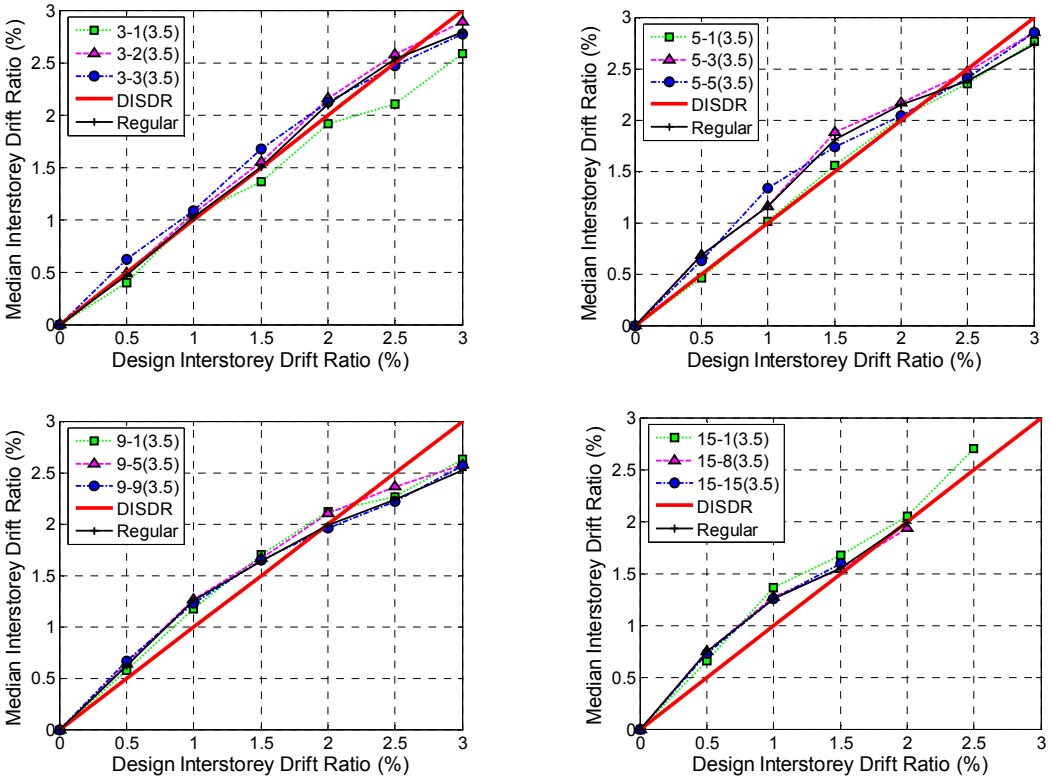

(1) Mass Ratio: 3.5

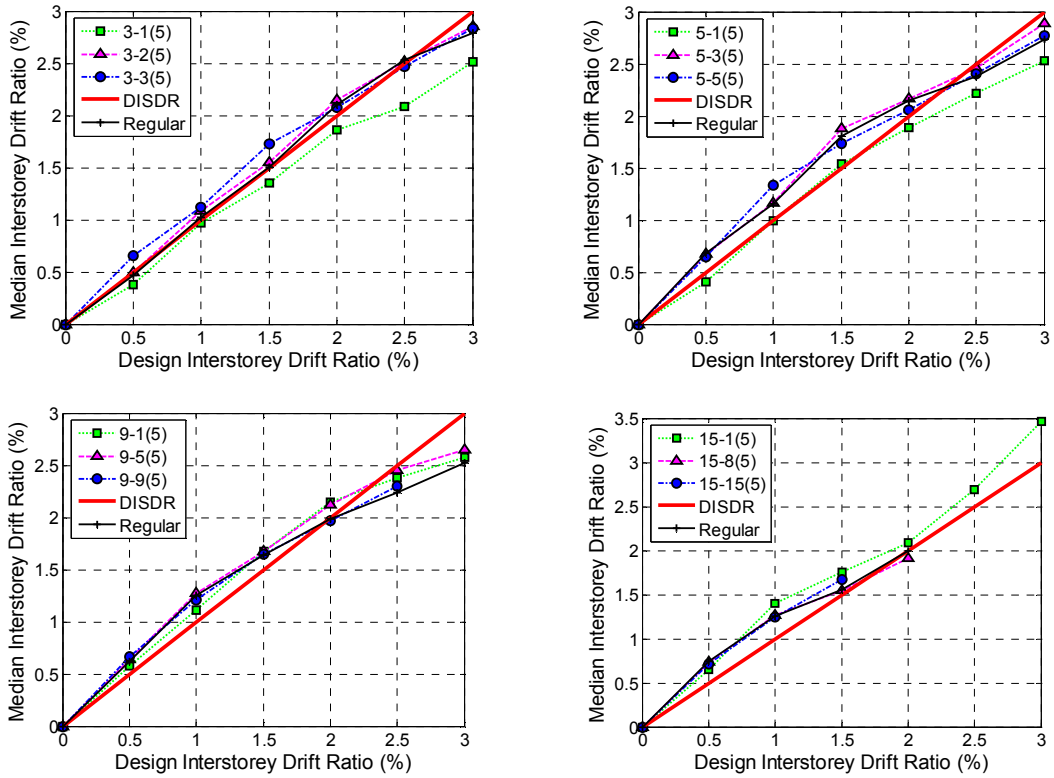

(2) Mass Ratio: 5

Figure 2-12(b): Effect of magnitude and floor level of mass irregularity for CS-CSTG model ($\mu = 2$, $Z = 0.4$) – Mass Ratios: 3.5 & 5.

2.10 Determination of Mass Irregularity Limit

The following steps were used to compute the relationship between the increase in median peak interstorey drift ratio, $ISDR_{incr}$, due to irregularity and mass ratio:

Step 1. For a combination of structural form, structural ductility factor, design interstorey drift ratio, structure height, and the floor level of mass irregularity, the median peak ISDR for the regular structure, $ISDR_R$, is computed from the results of the structure to the suite of records. In a similar way, the median of peak interstorey drift ratio for the irregular structure, $ISDR_I$, is obtained. Thus, the increase in median peak ISDR due to irregularity, $ISDR_{incr}$, is calculated by Equation (2-10).

$$ISDR_{incr} = \left(\frac{ISDR_I}{ISDR_R} - 1 \right) * 100 \ (\%) \qquad (2\text{-}10)$$

Step 2. Step 1 is repeated for all the combinations of structural form, structural ductility factor, design interstorey drift ratio, structure height, floor level of mass irregularity, and mass ratio.

Step 3. For each mass ratio, find the maximum value of $ISDR_{incr}$, $ISDR_{max\_incr.}$

Figure 2-13 shows $ISDR_{max\_incr}$ plotted against mass ratio for structures with specified structural ductility factors. Generally the structures with the greatest increase in drift due to irregularity were the CS models as shown in Figure 2-13. However, those with the greatest absolute drifts were the CISDR models as shown in Figures 2-10 to 2-12.

Equation (2-11) has been developed to estimate the increase in seismic demand due to irregularity for any structure. The relationship between *IRR* and mass ratio is shown in Figure 2-13. Here, *IRR* is generally a conservative estimate of $ISDR_{max\_incr}$ because

it is based on the most critical structural form, structure height, structural ductility factor, design interstorey drift ratio and floor level of irregularity.

$$IRR\,(\%) = 15\,(MR - 1) \qquad (2\text{-}11)$$

where *IRR* is the Irregular response greater than regular response; and *MR* is the Mass Ratio.

Equation (2-11) may be used for design. For example, if it were decided that the mass irregularity should produce less than 15% additional interstorey drift, then Figure 2-14 shows that the mass ratio needs to be less than 2. The figure also shows that the code mass ratio of 1.5 corresponds to an increase in median peak ISDR of up to approximately 7.5%.

Note: While Equation 2-11 provides an estimate of *IRR* for $MR > 1$, a similar irregular response ratio equation can be developed for $MR < 1$. The effect of reduced floor masses on seismic response of structures, and the development of *IRR* equation for $MR < 1$, is explained in Appendix G.

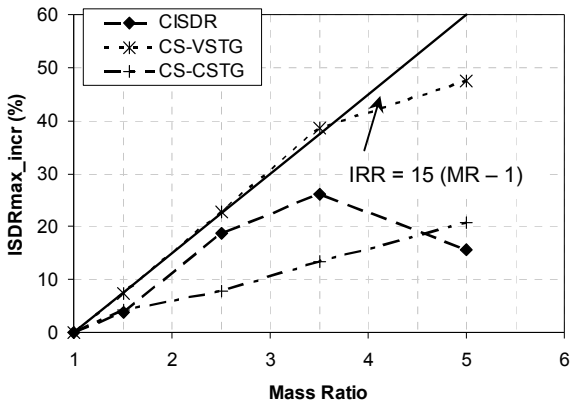

(a) Structural Ductility Factor, μ = 1

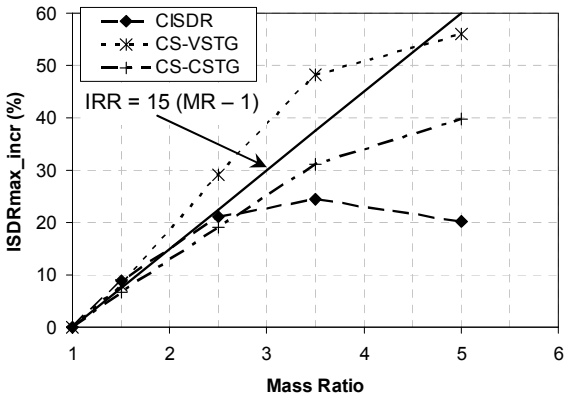

(b) Structural Ductility Factor, μ = 2

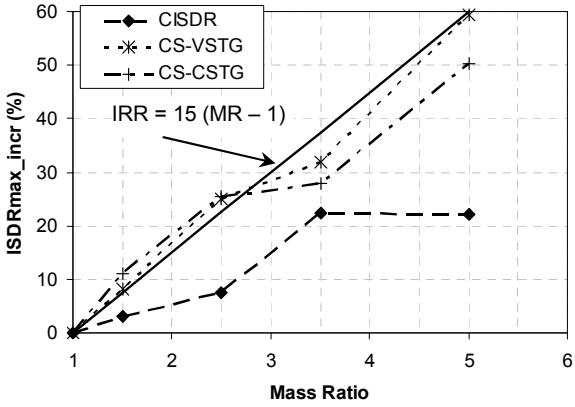

(c) Structural Ductility Factor, μ = 4

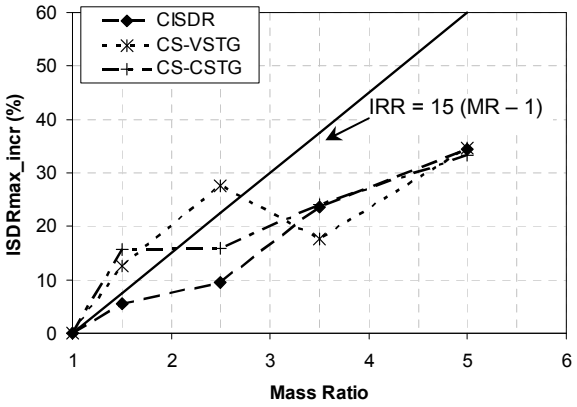

(d) Structural Ductility Factor, μ = 6

Figure 2-13: Increase in median peak ISDR due to mass irregularities in structures designed for different structural ductility factors.

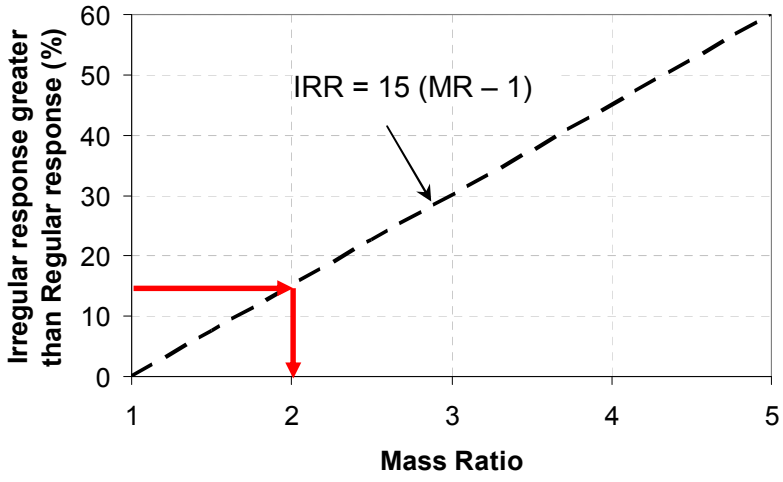

Figure 2-14: Determination of mass irregularity limit

2.11 Summary

This study on structural irregularity effects can be summarised as below:

1. Current regularity provisions in NZS 1170.5 are based on overseas irregularity recommendations. They are based on engineering judgement and lack rational justification;

2. Past research on vertical irregularities effects does not justify the appropriateness of regularity limits slated in NZS 1170.5. A better and more meaningful comparison is obtained if structures designed to a target drift are compared with the actual drift demand rather than tuning the structures to have the same period. Also, earlier works may not be appropriate for structures designed for New Zealand;

3. A method to quantify vertical irregularity effects was proposed for all irregularity types. This method was applied to evaluate the effects of mass irregularity on simple shear-type structures with 3, 5, 9 and 15 storey heights, assumed to be located in Wellington, Christchurch and Auckland, and designed for a range of structural ductility factors;

4. Regular structures were defined to have a constant floor mass at every floor level using the NZ 1170.5 Equivalent Static method. The structures were either designed to have constant interstorey drift ratios at all the floors simultaneously (CISDR), or to have a uniform stiffness distribution over the height of structure (CS). Various target interstorey drift ratios were considered. The CISDR models had constant strength to stiffness ratios at all floor levels. Two CS models were considered. One had storey shear strengths matching the design shears at every floor level (CS-

VSTG). The other had constant shear strength over all the floor levels (CS-CSTG). The shear strength in this case matched the design shear in the first floor level of the frame. Irregular structures were created with floor masses of magnitude 1.5, 2.5, 3.5 and 5 times the regular floor mass. These increased masses were considered separately at the first floor level, mid-height, and at the roof. The irregular structures were designed in exactly the same way as the regular structures with the same target drifts. All the structures were then analysed using inelastic dynamic time-history analysis to obtain the change in the median peak interstorey drift demand due to mass irregularity;

5. The structures were modelled as a combination of vertical shear and flexural beam elements (SFB). The flexural beam, modelling the effect of all continuous columns in the structure, has been shown to represent 2-D frame behaviour well;

6. The choice of the type of Rayleigh damping model for the inelastic time-history analysis was shown to be not significant for assessing irregularity effects. This is because the absolute drifts were not sensitive to the damping model. Furthermore, when comparing both the regular and irregular structure response, it is the relative rather than the absolute response which is important. This difference is likely to be less than for the absolute response;

7. Median peak interstorey drift ratio estimates due to NZS 1170.5 ES method was found to be generally non-conservative for CISDR designs, and conservative for CS designs;

8. The drift demands were sensitive to both the magnitude and floor level of the mass irregularity. Increased mass, when present at either the first floor level or at the roof, produced higher drift demands than when located at the mid-height;

9. A simple equation was developed to provide a general conservative estimate of the increase in drift demand due to mass irregularity. The current code requirement of a maximum mass ratio of 1.5 corresponds to an increase in median response of approximately 7.5% according to this equation.

2.12 Acknowledgements

The authors would like to thank the New Zealand Earthquake Commission (www.eqc.govt.nz) for their financial assistance to undertake this research. The authors would also like to thank Prof. Richard Fenwick for his critical comments on the methodology developed for this work.

2.13 References

[1] Al-Ali AAK, Krawinkler H. Effects of vertical irregularities on seismic behaviour of building structures. Report No. 130, Department of Civil and Environmental Engineering, Stanford University, San Francisco, 1998.

[2] Aziminejad A, Moghadam AS. Performance of asymmetric single story buildings based on different configuration of centre of mass, rigidity and resistance. *4th European Workshop on the Seismic Behaviour of Irregular and Complex Structures*, 2005, Thessaloniki, CD ROM proceedings.

[3] Baker JW. Spectral shape, epsilon and record selection. *Journal of Earthquake Engineering & Structural Dynamics* 2006; **35**(9): 1077-1095.

[4] Baker JW. Measuring bias in structural response caused by ground motion scaling. *8th Pacific Conference on Earthquake Engineering*, Singapore, 2007, Paper No. 56, CD ROM proceedings.

[5] Carr AJ. Ruaumoko 2D – Inelastic dynamic analysis. Department of Civil and Natural Resources Engineering, University of Canterbury, Christchurch, New Zealand, 2004.

[6] Chase JG, Rodgers GW, Corman S, MacRae GA. Development and spectral analysis of an advanced control law for semi-active resettable devices. *9th Pacific Conference on Earthquake Engineering*, Auckland, 2011, Paper No. 135, CD ROM proceedings.

[7] Chintanapakdee C, Chopra AK. Seismic response of vertically irregular frames: Response history and modal pushover analyses. *Journal of Structural Engineering* 2004; **130**(8): 1177-1185.

[8] Chopra AK. Dynamics of structures: Theory and Applications to Earthquake Engineering. New Jersey: Prentice Hall, 2000; 844.

[9] Chopra AK, Goel GK. A modal push over analysis procedure to estimate seismic demands for unsymmetric-plan buildings. *Journal of Earthquake Engineering & Structural Dynamics* 2004; **33**(8): 903-927.

[10] Cornell CA, Fatemeh JF, Hamburger RO, Foutch DA. Probabilistic basis for 2000 SAC FEMA steel moment frame guidelines. *Journal of Structural Engineering* 2002; **128**(4): 526-533.

[11] Crisp DJ. Damping models for inelastic structures. M.E. Report, Department of Civil and Natural Resources Engineering, University of Canterbury, Christchurch, New Zealand, 1980.

[12] Cruz EF, Chopra AK. Elastic earthquake response of building frames. *Journal of Structural Engineering* 1986; **112**(3): 443-459.

[13] Fajfar P, Marusic D, Perus I. The N2 method for asymmetric buildings. *First European Conference on Earthquake Engineering and Seismology*, Geneva, Switzerland, 2006, Paper No. 539, CD ROM proceedings.

[14] Fragiadakis M, Vamvatsikos D, Monolis P. Evaluation of the influence of vertical irregularities on the seismic performance of a nine-storey steel frame. *Journal of Earthquake Engineering and Structural Dynamics* 2006; **35**(12): 1489-1509.

[15] Iervolino I, Cornell CA. Record selection for non-linear seismic analysis of structures. *Earthquake Spectra* 2005; **21**(3): 685-713.

[16] Luco N, Bazzurro P. Does amplitude scaling of ground motion records result in biased non-linear structural drift responses? *Journal of Earthquake Engineering and Structural Dynamics* 2007. DOI: 10.1002/eqe.695.

[17] MacRae GA, Kimura Y, Roeder CW. Effect of column stiffness on braced frame seismic behaviour. *Journal of Structural Engineering* 2004; **130**(3): 381-391.

[18] MATLAB 7.9 (R2009b). The Maths Works, Inc.: Natick, MA, 2009.

[19] Otani S. Hysteretic models of reinforced concrete for earthquake response analysis. *Journal of the Faculty of Engineering* 1981; University of Tokyo. **XXXVI**(2): 407-441.

[20] Paulay T, Priestley MJN. Seismic design of reinforced concrete and masonry buildings. *John Wiley & Sons, Inc.*, 1992; 744pp.

[21] Priestley MJN, Calvi GM, Kowalsky MJ. Displacement-based seismic design of structures. *IUSS Press*, Pavia, Italy, 2007; 721pp.

[22] Sadashiva VK. Quantifying structural irregularity effects for simple seismic design. Ph.D. Thesis (in preparation), Department of Civil and Natural Resources Engineering, University of Canterbury, Christchurch, New Zealand, 2010.

[23] SEAOC. Recommended lateral force requirements and commentary. Seventh Edition, Seismology Committee, Structural Engineers Association of California, 1999.

[24] Shome N, Cornell CA, Bazzurro P, Carballo JE. Earthquakes, records, and nonlinear responses. *Earthquake Spectra* 1998; **14**(3): 245-272.

[25] SNZ. NZS 1170.5 Supp 1:2004, Structural Design Actions. Part 5: Earthquake actions – New Zealand – commentary. Standards New Zealand, Wellington, 2004.

[26] Tagawa H, MacRae G, Lowes L. Evaluations of 1D simple structural models for 2D steel frame structures. *13th World Conference on Earthquake Engineering*, Vancouver, B.C., Canada, 2004.

[27] Tagawa H. Towards an understanding of 3D structural behaviour - Stability & Reliability. Ph.D. dissertation, University of Washington, Seattle, 2005.

[28] Tagawa H, MacRae GA, Lowes LN. Evaluation of simplification of 2D moment frame to 1D MDOF coupled shear-flexural-beam model. *Journal of Structural & Constructional Engineering* 2006; Transactions of AIG, No. 609.

[29] Tremblay R, Poncet L. Seismic performance of concentrically braced steel frames in multistory buildings with mass irregularity. *Journal of Structural Engineering* 2005; **131**(9): 1363-1375.

[30] Valmundsson EV, Nau JM. Seismic response of building frames with vertical structural irregularities. *Journal of Structural Engineering* 1997; **123**(1): 30-41.

3. SEISMIC RESPONSE OF STRUCTURES WITH COUPLED VERTICAL STIFFNESS-STRENGTH IRREGULARITIES

3.1 Overview

The present New Zealand seismic design standard, NZS 1170.5, restricts the use of the Equivalent Static analysis method to structures satisfying structural regularity limits. These regularity limits are based on engineering judgement and lack quantitative justification. One common irregularity is that of a change in vertical stiffness over the building height. This stiffness irregularity is almost always associated with a change in vertical strength over the building height. For this reason, the effect of various realistic combinations of stiffness-strength irregularity in shear-type buildings is evaluated to quantify regularity limits.

Structures analysed had 3, 5, 9 and 15 storeys, and were designed for the region of Wellington. Both regular and irregular structures were designed in accordance with the Equivalent Static method of NZS 1170.5. The irregular structures were created by modifying specific storey lateral stiffnesses from that of the regular structure. Strengths at these storeys were also modified to ensure realistic relationships between stiffness and strength. The modified structures were then redesigned until the target interstorey drift ratio was achieved at the critical storey. Design structural ductility factors of 1, 2, 3, 4 and 6, and target (design) interstorey drift ratios ranging between 0.5% and 3%, were used in this study. Inelastic dynamic time-history analysis was conducted to compare the maximum interstorey drift ratio demands of the regular and irregular structures. Simple equations were developed to estimate possible variations

in demand due to vertical stiffness-strength irregularity applied at critical locations in structures.

3.2 Introduction

Current earthquake codes define structures to be irregular based on the relative differences in storey properties. A structure is often said to be "regular" if it has uniform structural properties or a uniform variation in properties in all the directions. Conversely, a structure is termed as "irregular" if it has a non-uniform distribution of structural properties, either individually or in combination, in any axis of the structure. Structural regularity is broadly classified into two types; (a) *architecturally planned* and (b) *architecturally unplanned*. Architecturally planned structures are designed to be irregular, while architecturally unplanned structures are irregular due to rearrangement of loadings, as well as material strength and stiffness variations.

Vertical stiffness and strength irregularity, which is the focus of this paper, occurs due to numerous reasons. Some of the common causes are:

- Differences in interstorey height at a particular storey as compared to adjacent storey;
- Modification of member properties, member sizes, material, at a storey;
- Vertical discontinuities of structural members at a particular storey;
- Lack of infill material or an open storey at a storey.

This paper addresses the effects of vertical stiffness-strength irregularities on structures having a constant interstorey height by finding answers to the following questions:

1. How does the current NZ seismic standard, NZS 1170.5 [1], restrict the use of simple methods to analyse structures with stiffness-strength irregularity?
2. What past research on stiffness-strength irregularity has been conducted?
3. What stiffness-strength coupling is likely in realistic structures?
4. Which storey/storeys are most sensitive to a decrease in storey stiffness and strength?
5. How do responses change due to an increase in storey stiffness-strength?
6. What level of increase in response due to stiffness-strength irregularity does the current NZ seismic standard correspond to?

3.3 NZS 1170.5 Stiffness-Strength Irregularity Limits

Approximations to the exact response of a structure under the design level excitation may be obtained by carrying out numerous 3-D *inelastic dynamic time history analyses* (**IDTHA**) considering all relevant effects and using the best information available. Factors that should be considered include foundation effects, floor diaphragm effects, and the likely variation of earthquake demand and structural capacity.

In general, this type of "approximate analysis" is too complex for design, so engineers commonly use simpler, and hence more approximate, analysis methods [2]. These methods are calibrated based on the response of regular structures. However, for irregular structures, some approximate analysis methods are not permitted to be used. Many worldwide codes (e.g., FEMA 450 [3], IBC [4], Eurocode 8 [5]) define structures to be irregular if they do not meet code specified "regularity limits".

A common simple analysis method, such as the NZS 1170.5 *Equivalent Static* (**ES**) method, is not permitted to be used for designing a structure if: (a) the height of the structure is more than 10m; (b) the fundamental natural period of the structure computed by a code equation is more than 0.4s; and (c) the regularity limits are not satisfied. NZS 1170.5, like many other worldwide codes, specifies individual regularity limits for structures with mass, stiffness, strength and plan irregularities that restrict the use of ES method. These irregularity limits are set to make designers aware of the existence of irregularities and the ill effects they produce when a structure has irregularities. However, they are based on engineering judgement and lack theoretical justification [6].

Stiffness-strength irregularities, the effects of which are investigated in this study, exist according to *Cl. 4.5.1*, NZS 1170.5, when:

- The lateral stiffness of a storey is less than 70% of the stiffness of any adjacent storey, or less than 80% of the average stiffness of the three storeys above or below in the structure.
- The shear strength of a storey is less than 90% of that in the storey above.

Although separate irregularity limits are defined for stiffness and strength irregularity above, in most practical scenarios, stiffness and strength vary together. For example, when cross-sectional properties are changed at a storey, the stiffness and strength at that storey both change. Hence, in this paper, stiffness and strength irregularities are combined and their effects on seismic demands are evaluated.

3.4 Previous Research on Vertical Stiffness-Strength Irregularity

Valmundsson and Nau [7] evaluated stiffness-strength limits for 5, 10, and 20 storey buildings designed according to the equivalent static method of the 1994 Uniform Building Code with strong beams and weak columns. Regular structures had a uniform stiffness distribution over the building height. This stiffness distribution was changed to achieve a series of 6 target fundamental periods for each structural height. Irregular structures were obtained by modifying the structure in the following ways. Firstly, the first storey stiffness was modified by different amounts and the resulting stiffness distribution was scaled until specified periods were obtained. The strength distribution was held constant as that in the regular structure. They described demands in terms of peak storey *ductility demand ratio* (**DDR**) which is the ratio of the peak storey ductility demand for the irregular structure to the peak storey design ductility for the regular structure. For each level of design ductility, the DRR was less than unity, and it decreased with greater design ductility demand. This decrease in DDR corresponds to greater first storey drifts because the yield drift had increased due to the reduced stiffness and the constant strength. Secondly, the first storey strength was reduced and stiffness was held constant. The DDR increased by up to 7 times for a strength reduction of 50%. This is expected for a frame with a soft storey mechanism (e.g., MacRae *et al.* [8]). The first storey ductility increased with greater design ductility. Thirdly, the stiffness and strength at the first storey were reduced proportionally. Here, the DDR was lower than for strength irregularity alone due to the large yield displacements as was seen for stiffness variations alone. The study concluded that for a structure to be recognised as being “regular”, the first storey should be stronger than the storey above it.

Al-Ali and Krawinkler [9] studied the effects of vertical irregularities on height-wise variations of seismic demands by conducting elastic and inelastic dynamic analyses using 15 records on 2-D single-bay 10-storey generic structures. The columns were made weaker than the beams, allowing for a soft-storey mechanism. Responses of structures with stiffness or/and strength irregularity were compared with the response of a reference structure that had a uniform distribution of mass over the height and an associated stiffness distribution that resulted in a straight-line first mode shape. Storey stiffnesses were tuned to produce a first mode period of 3s. Irregularity was introduced in a number of ways: (i) The stiffnesses were modified in two ways. For one set, stiffnesses at the first storey or at the mid-height of reference structures were multiplied by 0.1, 0.25 and 0.5. For the second set, storey stiffnesses of the lower half of each reference structure were multiplied by factors of 2, 4 and 10. The stiffness distributions for all the cases were then tuned until the irregular structures had a fundamental period of 3s. Since stiffness irregularities change the distribution of elastic storey shear demands, storey strengths for each of the cases with stiffness irregularities were tuned to their own elastic storey shear distribution obtained from SRSS analyses using the 1997 National Earthquake Hazard Reduction Program spectrum reduced by strength reduction factors of 3 and 6. Storey drift demands rather than the DDR [7] were the parameter used. They were found to increase in the storey with reduced stiffness and decrease in most of the other storeys. Roof drift demands were less sensitive to the presence of stiffness irregularity. (ii) Effects of strength irregularities *alone* were studied. The strength of a specific storey (or storeys) was increased to 2 times the strength of the same storey in the reference base structure. The stiffness and mass distributions were kept the same as for the base case.

This effectively resulted in some weaker storeys. The maximum drifts were more than 6 times that of the reference structure in some cases where there was only one weak storey. (iii) Combined stiffness and strength irregularity was also considered. It was limited to cases where the storey stiffness and strength was changed by two times that from the base case. It was applied separately at the first storey, the mid-height, or in the lower half of structure. The stiffness-strength distribution at the other storeys was kept the same as for their individual irregularity cases. Cases with combined stiffness-strength irregularity generally gave the same trends in response as the strength irregularity cases, but with a larger magnitude.

Chintanapakdee and Chopra [10] performed a similar study to [9]. The significant difference was that they used a beam hinge model, which discouraged soft-storey mechanisms. They compared the seismic demands for vertically irregular and regular frames of 12 storey frames subject to a set of 15 earthquake records. Behaviour observed was similar to that of [9] except that the peak drift did not concentrate solely in the flexible/weak storey. It also occurred in the neighbouring storeys due to the effect of column continuity in the strong column weak beam frame.

Fragiadakis *et al.* [11] studied irregularity due to stiffness, strength and also their combined effects under different intensities of shaking. The base structure was a realistic nine storey steel frame with a higher basement than other storeys. It had a fundamental period of 2.25s, and it was designed for a Los Angeles site. Stiffness and/or strength irregularities were considered by multiplying the base cases' stiffness and strength by factors of 0.5 and 2. These factors were applied at various locations over the height of the structure. The authors adopted the Incremental Dynamic Analysis method. At each scaling level, the maximum interstorey drift ratio, θ_{max}, was

obtained. In order to compare the performance of the modified versus the base case, a continuum of limit states was defined, each at a given value of θ_{max} , spanning all the structural response range from elasticity to global dynamic instability. The distribution of peak interstorey demands over the height of irregular structures, normalised by that due to the base case was found for each irregularity case. In the stiffness irregularity studies, they found that a storey with reduced stiffness sometimes decreased the drift demand depending on the intensity of shaking. Also the position of maximum demand was not always at the location of irregularity. The strength irregularity studies generally showed similar behaviour. They stated that for combined stiffness and strength irregularity, the change in drift demand distribution was approximately equal to that obtained by adding both the stiffness and strength irregularity results. Irregularities were also introduced at multiple storeys simultaneously. The influence of multi-storey modifications was quantitatively shown as added effects of corresponding single-storey influences.

It may be seen that a number of interesting investigations have been undertaken to show how vertical stiffness/strength irregularity has affected the response of structures. This study builds on these previous works, and seeks to extend them by considering the variation due to vertical stiffness-strength irregularity on a range of realistic structures to obtain a relationship between the amount of irregularity and the change in response for these structures.

3.5 Evaluating Vertical Coupled Stiffness-Strength Irregularity Effects

3.5.1 Definition of Regular Structures

A simple method to determine vertical irregularity limits was developed for structures having vertical mass irregularities [2]. A similar approach is used in the present study for vertical coupled stiffness-strength irregularities as follows. Simple models of shear-type structures of 3, 5, 9 and 15 storeys, having a uniform mass at every floor, and with equal storey heights of 4m were adopted for this parametric study.

Each regular structure was assumed to be located in Wellington, and was designed according to the NZ 1170.5 ES method considering a set of structural ductility factors of 1, 2, 3, 4, and 6. Additional actions and displacements due to P-delta effects were also calculated according to the code method. A complete description on the design approach adopted in this study is explained in [2].

In order to have appropriate comparisons between regular and irregular structures, each regular design model was provided with storey strengths such that a constant strength to stiffness ratio was maintained at all the storeys. Two classes of regular structures were defined. The models are: (a) *Constant Interstorey Drift Ratio* (**CISDR**) model. These structures have a decreasing stiffness distribution over the height, as shown in Figure 3-1(c). Iteration was carried out until all storeys simultaneously achieved the *design* (target) *interstorey drift ratio* (**DISDR**). The shear strength provided at each storey was the minimum required to resist the equivalent static design forces, as shown in Figure 3-1(d), and (b) *Constant Stiffness* and *Constant Strength* (**CS-CSTG**) model. These structures have a uniform stiffness

distribution over the height, as shown in Figure 3-1(g). Iteration was conducted until the first storey achieved the target interstorey drift ratio. For this design model, the minimum shear strength required to resist the design force at the first storey was provided at all the storeys, thus producing a constant strength to stiffness ratio at all

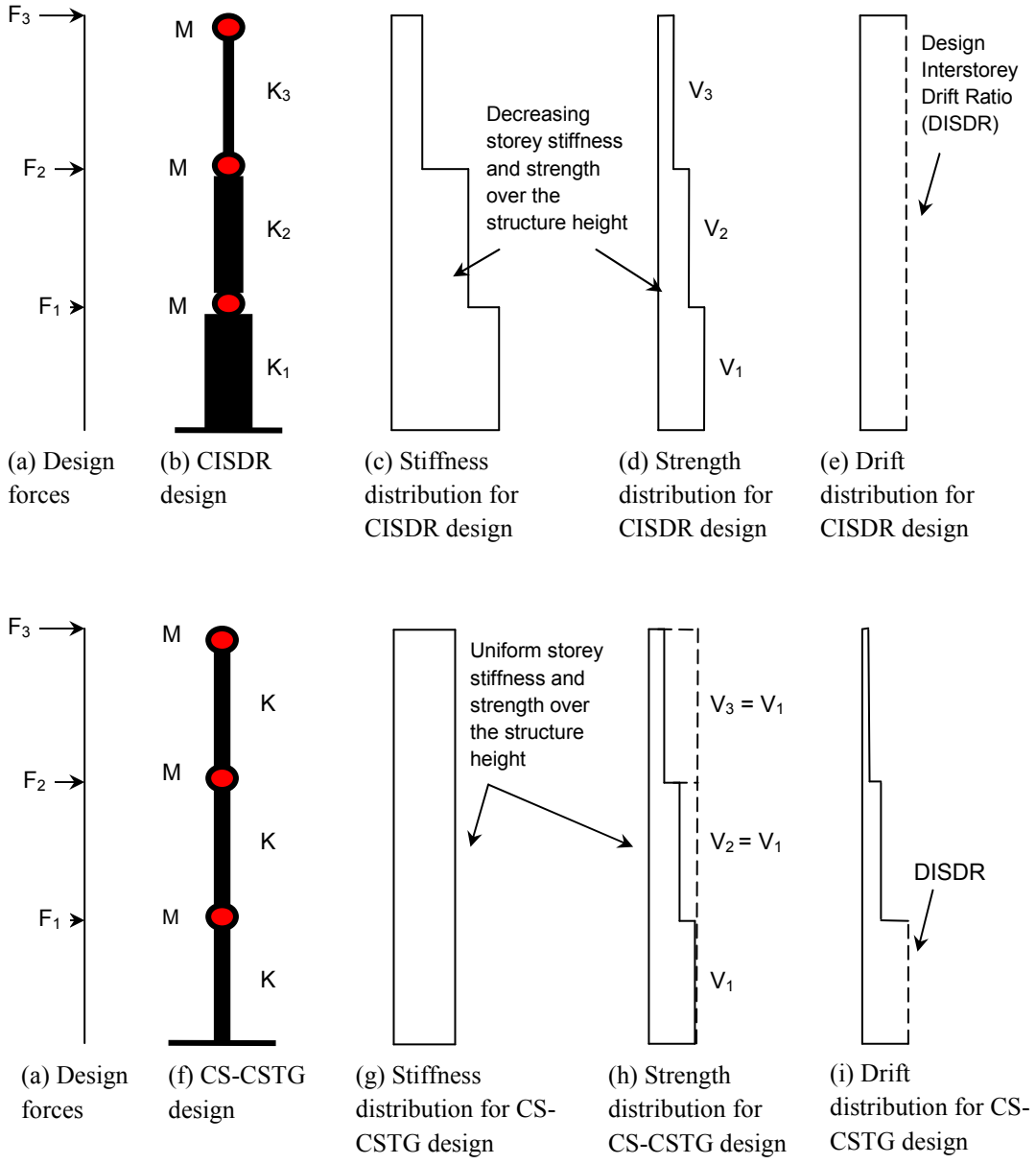

Figure 3-1: Structural configurations defining regular structures.

the storeys. The strength distribution for this model is shown in Figure 3-1(h). Although these two configurations may not necessasarily reflect the variation of properties in actual buildings, they define the bounds for the likely properties of realistic structures.

Unrealistic structures were avoided in this study by eliminating structures having:

- Strength to scaled stiffness ratios outside the range of 0.3% - 3%. This limit was set based on the likely storey strength to scaled stiffness ratios for realistic structures, determined based on simple and approximate empirical relations (Priestley *et al.* [12]) giving yield drift ratios for different types of *lateral force resisting* (**LFR**) systems.

- A horizontal design action coefficient, C_d, governed by Equation (3-2) (*Cl. 5.2.1.1, NZS 1170.5*). This was to avoid long period structures which have an effective ductility lower than the chosen design ductility factor. For example, Figure 3-2 shows that for structures designed to have a ductility factor of 2, and with fundamental period more than 3.4s, the coefficient C_d is governed by Equation (3-2) (solid line). Since this type of structure would need to be designed for strength greater than that associated with a ductility factor of 2, the effective design ductility factor would have been less than 2.

$$C_d(T_1) = \frac{C(T_1)\,S_p}{k_\mu} \tag{3-1}$$

$$C_{d,\min} = \max\begin{cases}(Z/20+0.02)\,R_u\\ 0.03\,R_u\end{cases} \tag{3-2}$$

$$C_d = \max\left\{C_d(T_1), C_{d,\min}\right\} \tag{3-3}$$

where $C(T_1)$ = the ordinate of the elastic site hazard spectrum;

S_p = the structural performance factor;

k_μ = the inelastic spectrum scaling factor;

Z = the hazard (zone) factor; and

R_u = the return period factor for the ultimate limit state.

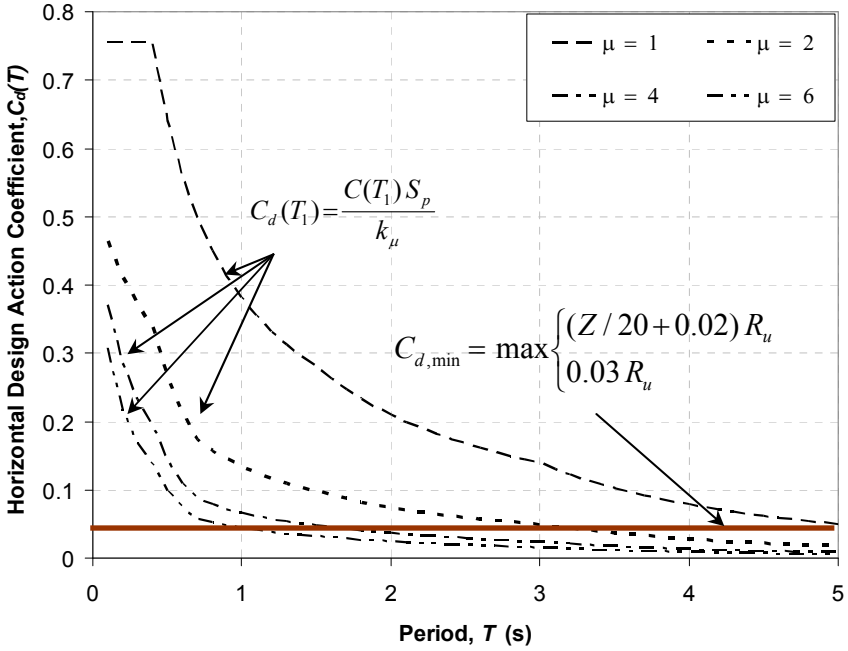

Figure 3-2: Variation of horizontal design action coefficient with fundamental period for a zone with hazard factor of 0.4.

3.5.2 Storey Stiffness-Strength Relationships

In most practical scenarios, a change in stiffness of an actual structure is accompanied by a change in strength. Therefore, studying stiffness irregularity alone, or strength irregularity alone, while being interesting, is not necessarily realistic. Stiffness-strength relationships for structures of uniform height are evaluated in Table 3-1 for a number of LFR systems. In Table 3-1a, the modified lateral stiffness at a chosen

storey for irregularity, K_m, irrespective of the LFR system, is given as the product of the stiffness modification factor, α_k, and the initial lateral stiffness at the chosen storey, K_o. The modified storey strength provided at the chosen storey, V_m, for braced frames and shear wall type of LFR systems (Cases a & b in Table 3-1b), is given as the product of strength modification factor, α_v, and the initial storey strength, V_o, provided for the storey. Here, $\alpha_v = \alpha_k$, and the factor α_k is approximated from the stiffnesses of the members using the approach in Figure 3-1. However, in case of moment frames (Cases c & d in Table 3-1b), the storey strength does not vary proportionally with the storey stiffness at the modified storey. That is, the strength modification factor, $\alpha_v = \sqrt{\alpha_k}$ for these cases. The derivation for this is given in Table 3-1, and all symbols are defined in the nomenclature.

Two groups of structures were considered based on the relations between storey stiffness and strength, as shown in Table 3-2. Group A represents braced frame and shear wall types of LFR systems having strength varying proportionally with stiffness, and Group B represents stiffness-strength coupling relation for moment frames. In order to investigate the sensitivity of magnitude of irregularities on seismic demands, a range of stiffness-strength modification factor pairs, as tabulated in Table 3-2, covering cases of storey stiffness and strength increased or reduced, were used.

Table 3-1a: Modified storey stiffness due to modified member properties.

Lateral-force-resisting (LFR) system	Modified storey stiffness, K_m
(a) ***Braced Frame*** 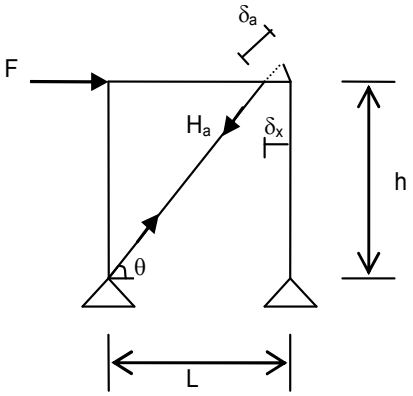 Stiffness, $K = \frac{A_a\ E}{\sqrt{L^2 + h^2}}$	$\frac{K_m}{K_o} = \left(\frac{A_{am}\ E}{\sqrt{L^2 + h^2}}\right) * \left(\frac{\sqrt{L^2 + h^2}}{A_{ao}\ E}\right)$ $K_m = \left(\frac{A_{am}}{A_{ao}}\right) * K_o$ $K_m = \alpha_k * K_o$
(b) ***Non-buckling Steel Shear Wall*** 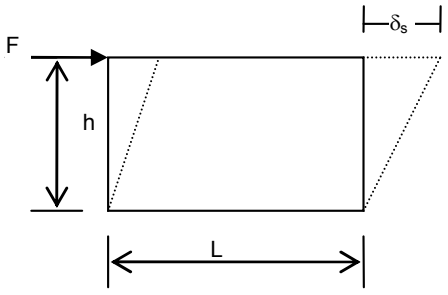 Stiffness, $K = \frac{G\ A_s}{h}$	$\frac{K_m}{K_o} = \left(\frac{G\ A_{sm}}{h}\right) * \left(\frac{h}{G\ A_{so}}\right)$ $K_m = \left(\frac{A_{sm}}{A_{so}}\right) * K_o$ $K_m = \alpha_k * K_o$

(c) ***Moment Frame (strong column weak beam mechanism)***

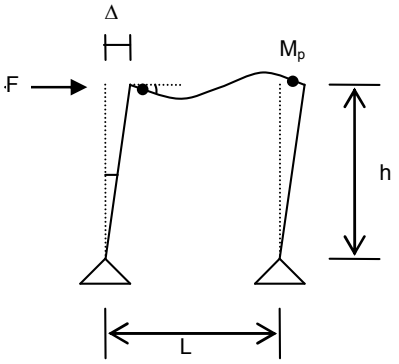

Stiffness, $K = \frac{6EI}{Lh^2}$

$$\frac{K_m}{K_o} = \left(\frac{6EI_m}{Lh^2}\right) * \left(\frac{Lh^2}{6EI_o}\right)$$

$$K_m = \left(\frac{I_m}{I_o}\right) * K_o$$

$$K_m = \left(\frac{d_m}{d_o}\right)^2 * K_o$$

$$K_m = \alpha_k * K_o$$

(d) ***Moment Frame (strong beam weak column mechanism)***

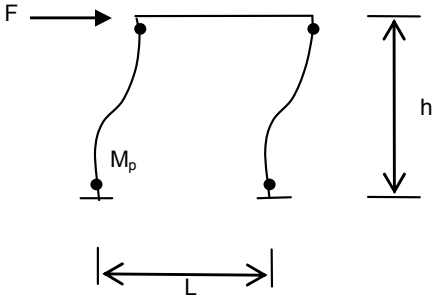

Stiffness, $K = \frac{12EI}{h^3}$

$$\frac{K_m}{K_o} = \left(\frac{12EI_m}{h^3}\right) * \left(\frac{h^3}{12EI_o}\right)$$

$$K_m = \left(\frac{I_m}{I_o}\right) * K_o$$

$$K_m = \left(\frac{d_m}{d_o}\right)^2 * K_o$$

$$K_m = \alpha_k * K_o$$

Table 3-1b: Modified storey strength due to modified member properties.

Lateral-force-resisting (LFR) system	Modified storey strength, V_m
(a) ***Braced Frame*** 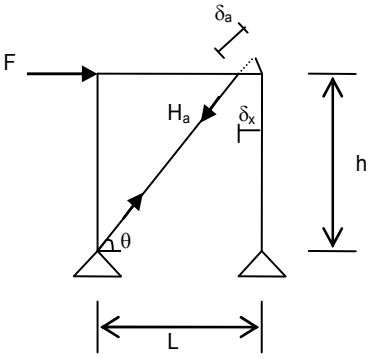 Strength, $V = \frac{A_a \sigma_y L}{\sqrt{L^2 + h^2}}$	$\frac{V}{K h} = \left(\frac{A_a \sigma_y L}{\sqrt{L^2 + h^2}}\right) * \left(\frac{\sqrt{L^2 + h^2}}{A_a E}\right) * \frac{1}{h}$ $= \frac{\varepsilon_y L}{h}$ $\frac{\left(V_m / K_m h\right)}{\left(V_o / K_o h\right)} = \left(\frac{\varepsilon_y L}{h}\right) * \left(\frac{h}{\varepsilon_y L}\right)$ $V_m = \left(\frac{K_m}{K_o}\right) * V_o$ $V_m = \alpha_v * V_o$ where $\alpha_v = \alpha_k$
(b) ***Non-buckling Steel Shear Wall*** 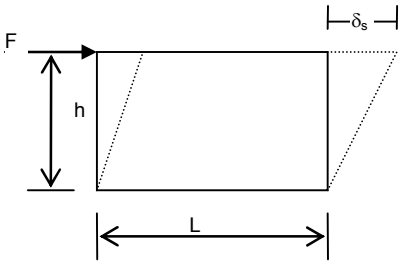 Strength, $V = \frac{A_s \sigma_y}{\sqrt{3}}$	$\frac{V}{K h} = \left(\frac{A_s \sigma_y}{\sqrt{3}}\right) * \left(\frac{h}{G A_s}\right) * \frac{1}{h} = \frac{\sigma_y}{G\sqrt{3}}$ $\frac{\left(V_m / K_m h\right)}{\left(V_o / K_o h\right)} = \left(\frac{\sigma_y}{G\sqrt{3}}\right) * \left(\frac{G\sqrt{3}}{\sigma_y}\right)$ $V_m = \left(\frac{K_m}{K_o}\right) * V_o$ $V_m = \alpha_v * V_o$ where $\alpha_v = \alpha_k$

(c) ***Moment Frame (strong column weak beam mechanism)***

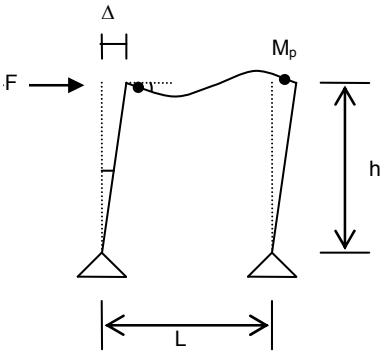

Strength, $V = \frac{M_p}{h}$

$$\frac{V}{Kh} = \left(\frac{M_p}{h}\right) * \left(\frac{Lh^2}{6EI}\right) * \frac{1}{h}$$

$$= \left(\frac{M_p}{EI}\right) * \frac{L}{6} = \left(\frac{2\varepsilon_y}{d}\right) * \frac{L}{6}$$

$$\frac{\left(V_m / K_m h\right)}{\left(V_o / K_o h\right)} = \left(\frac{d_o}{d_m}\right)$$

$$V_m = \left(\frac{K_m}{K_o}\right) * \left(\frac{d_o}{d_m}\right) * V_o = \left(\frac{d_m}{d_o}\right) * V_o$$

$V_m = \alpha_v * V_o$ where $\alpha_v = \sqrt{\alpha_k}$

(d) ***Moment Frame (strong beam weak column mechanism)***

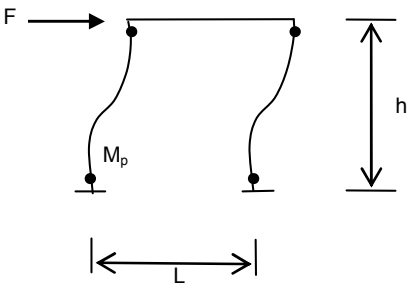

Strength, $V = \frac{2M_p}{h}$

$$\frac{V}{Kh} = \left(\frac{2M_p}{h}\right) * \left(\frac{h^3}{12EI}\right) * \frac{1}{h}$$

$$= \left(\frac{2\varepsilon_y}{d}\right) * \frac{h}{6}$$

$$\frac{\left(V_m / K_m h\right)}{\left(V_o / K_o h\right)} = \left(\frac{d_o}{d_m}\right)$$

$$V_m = \left(\frac{K_m}{K_o}\right) * \left(\frac{d_o}{d_m}\right) * V_o = \left(\frac{d_m}{d_o}\right) * V_o$$

$V_m = \alpha_v * V_o$ where $\alpha_v = \sqrt{\alpha_k}$

Table 3-2: Cases defining structures with coupled vertical stiffness-strength irregularities

Case:	Group A	Group B
(a) Increased Stiffness (α_k, α_v)	(1.2, 1.2), (1.5, 1.5), (2, 2)	(1.2, 1.095), (1.5, 1.224), (2, 1.414)
(b) Reduced Stiffness (α_k, α_v)	(0.5, 0.5), (0.6, 0.6), (0.7, 0.7), (0.8, 0.8), (0.9, 0.9)	(0.5, 0.707), (0.7, 0.836), (0.9, 0.948)

3.5.3 Applying Coupled Stiffness and Strength Irregularities

The effect of coupled stiffness-strength irregularity over the height of the structures was investigated by applying the irregularities separately at the first storey, the mid-height storey, and at the topmost storey of the regular structures. This was done by introducing the stiffness modification factor at the chosen regular storey, and then redesigning the modified structure until the target interstorey drift ratio is achieved at the critical storey. For example, as shown in Figure 3-3, consider a regular 3 storey CS-CSTG structure designed to have a uniform stiffness distribution resulting in a design interstorey drift ratio (DISDR) of 1% at the first storey. If it is intended to have a reduced stiffness at the third storey, the corresponding storey stiffness of the regular structure is reduced by means of stiffness modification factor, α_k, by an amount of say, 0.5. Upon making this change to storey stiffness, the critical storey would no longer have the chosen DISDR. In order to compare the responses of regular and irregular structures, all storey stiffnesses are then uniformly scaled by a scaling factor, λ. The irregular structure is redesigned until the selected λ resulted in

DISDR at the critical storey. Since all storey stiffnesses are uniformly scaled, at the end of iteration, the irregular structure would still have the same stiffness irregularity, α_k, at the chosen storey. This is the third storey in Figure 3-3. However, the relative storey stiffnesses at other storeys remain unchanged and equal the corresponding storey stiffnesses of regular structure.

In order to have a meaningful comparison between regular and irregular structures, the strength to stiffness ratios at all the storeys other than the irregular storey were kept the same. Therefore, the shear strength provided over the height of irregular structures was different from the strength demand. Here, the modified strength at the chosen storey for irregularity was provided according to Equation (3-4), which considers the λ factor. The strengths at other storeys were provided as the product of λ factor and the corresponding regular storey strength. The actual ductility obtained considering the other specifications was different from the target ductility implying that the final drifts were not identical to those obtained with the target ductility. However, the difference in ductility and drifts was always less than 1.2%, and it was generally much smaller than this value. It was considered that this was not enough to significantly affect the results.

$$V_m = \lambda \alpha_v V_o \tag{3-4}$$

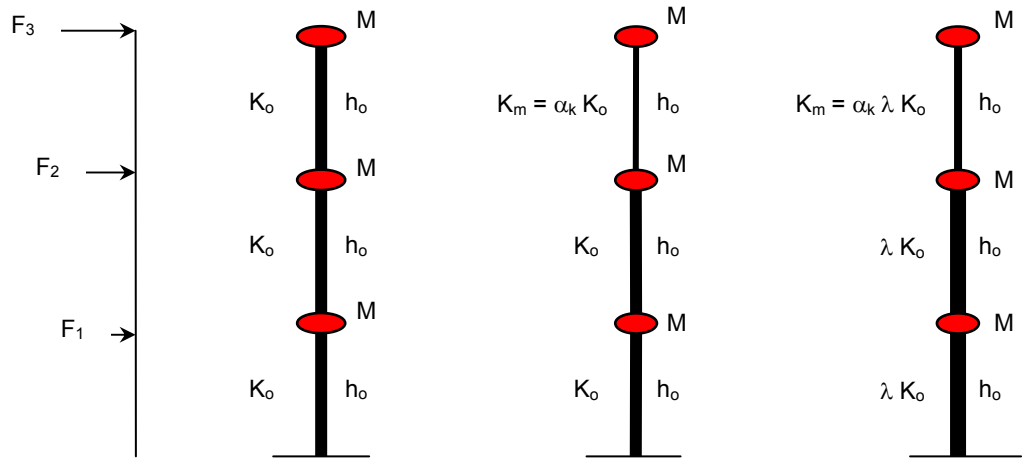

(a) Design forces

(b) Regular CS-CSTG design with DISDR at first storey

(c) Introducing stiffness modification at third storey

(d) Irregular structure with DISDR at critical storey

Figure 3-3: Stiffness irregularity due to change in member property for CS-CSTG design.

3.5.4 Structural Modelling and Analysis

Earlier studies (e.g., [8], Tagawa *et al*. [13]) on structural modelling have shown that the frames modelled as a combination of vertical *shear beam* and a vertical *flexural* beam (labelled as **SFB** in Figure 3-4) can represent the behaviour of real structures well. The flexural beam represents all continuous columns throughout the whole structure. If the flexural beam is not considered, unrealistically high drift concentrations may occur [2]. The flexural beam stiffness ratio, α_{cc}, in an actual structure tends to be between 0.13 and 1.58. In fact, the drift demands around this value are not sensitive to a change in α_{cc}. Therefore, a continuous column stiffness ratio of 0.5 at all storeys was used in all the analyses. *EI* was computed for the flexural beam from the equation in Figure 3-4. The shear beams had a bilinear hysteresis loop with a bilinear factor of 1 %.

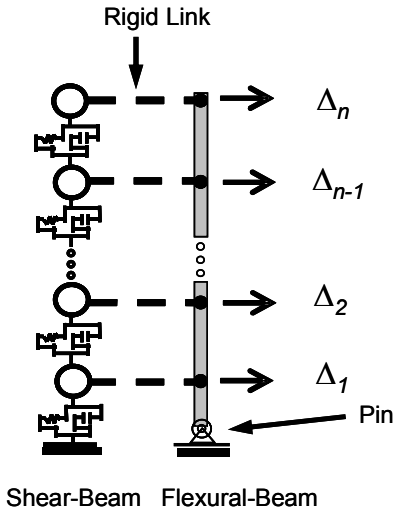

$$\alpha_{cci} = \frac{E I_i}{H_i^{\,3} K_{oi}}$$

where α_{cci} = continuous column stiffness ratio at level, i;
E = elastic modulus;
I_i = moment of inertia at the i^{th} level;
H_i = storey height of the i^{th} level; and
K_{oi} = lateral initial stiffness of the i^{th} level.

Figure 3-4: Combined vertical Shear and Flexural Beam (SFB model).

Rayleigh damping is commonly used to represent damping effects within multi-degree-of-freedom structures. There are many ways in which Rayleigh damping can be applied. A recent study [2] shows that the differences in drift responses due to three types of Rayleigh damping models available in RUAUMOKO (Carr [14]) were minimal. Tangent stiffness proportional Rayleigh damping model that uses the absolute form of equation of motion was used for all the IDTHA described in this paper. In order to avoid super-critical damping or negative damping, the first mode and the mode corresponding to the number of storeys in the structure [14] were nominated as the two modes with 5% of critical damping.

The computer program, RUAUMOKO, was used to carry out all the inelastic dynamic time-history analyses. Here, the dynamic equation of equilibrium is integrated by the unconditionally stable implicit Newmark Constant Average Acceleration method (Newmark parameters, $\gamma = 0.5$ and $\beta = 0.25$) [15]. A time-step size of 0.001s was used for all the time-history analyses. For the ground motion suite, a set of 20 SAC (SEAOC-ATC-CUREE) earthquake ground motion records

developed for Los Angeles, with probabilities of exceedance of 10% in 50 years, was used [2]. Response spectra were developed for each of the selected records, and the records were scaled to the NZS 1170.5 elastic design level spectral acceleration values for the period calculated in the city chosen. Here, both the structural ductility factor and the structural performance factor were unity.

3.5.4.1 Interpretation of Inelastic Dynamic Time-History Analysis Results

The *peak interstorey drift ratio* (**ISDR**) at every storey, and within the structure, when subjected to each of the 20 earthquake records, was obtained. It was assumed that the distribution of ISDR is lognormal [16], so the median results were calculated.

3.5.4.2 Comparison between Regular and Irregular Structures

The change in median peak ISDR, due to the presence of coupled stiffness-strength irregularity, has been used to show the effects of irregularity in the following section. For brevity, representative results obtained for structures designed for a structural ductility factor of 3 have only been shown in Figures 3-5 through 3-8. As explained earlier, structures having unrealistic strength to scaled stiffness ratios and/or having the base shear governed by the code lower limit were eliminated from this study. Hence, some of the following response plots show limited data points.

3.5.4.2.1 Effect of magnitude and storey of coupled vertical stiffness-strength irregularity for Group A structures

(a) Reduced storey stiffness-strength -

For CISDR designs, the median peak ISDR obtained for both the regular and irregular structures with stiffness-strength *reduced* in a storey, are plotted against DISDR in Figure 3-5(a). The Figure 3-5(a1) shows the behaviour for α_k of 0.5. This implies that the chosen storey for irregularity has 50% of the stiffness in the neighbouring storeys. The storey strength was also modified by the same amount. When the irregularity is applied at the first storey, higher median peak ISDR than for the regular structure, is obtained for taller structures designed for DISDR < 2%. A maximum of 77% and 40% increase in median peak drift demand over the regular structure is observed for 9 and 15 storey structures respectively, designed for DISDR = 0.5%, and with α_k of 0.5 at the first storey. For 3 and 5 storey structures, this increase in demand is respectively 16% and 4.5%, both obtained for DISDR = 1%. When coupled stiffness-strength irregularity of 0.5 is introduced at the mid-height of all the structures, the median peak drift demands are lesser than those for regular structures for all DISDR. Taller structures, designed for DISDR > 1%, produced higher drifts than the regular structure when the stiffness and strength of the topmost storey was reduced by 0.5. The maximum increase in median peak ISDR due to irregularity at the roof from all the DISDR is 15%, 41%, 56% and 52% for 3, 5, 9 and 15 storeys respectively. As expected, when the stiffness modification ratio is increased from 0.5 to 0.9 at a storey, the differences in responses between the regular and irregular structures are reduced. Irregularities at the topmost storey tended to produce higher drifts than at the other two positions, and the maximum increase in median peak ISDR over the regular structures from all the structure heights, are 42%, 23%, 10% and 1.2% for α_k = 0.6, 0.7, 0.8 and 0.9, respectively.

Response comparison between the regular and irregular structures for CS-CSTG design is shown in Figure 3-5(b). Irregular structures, created by reducing the first storey stiffness and strength, produced the largest change in median peak ISDR, compared to the other two irregular positions for all structure heights considered in this study. For α_k = 0.5 at the first storey, the median peak ISDR increases with the structure height, as shown in Figure 3-5(b). The maximum increase in drift demand over the regular structures is found to be 30%, 33%, 48% and 83% for 3, 5, 9 and 15 storey structures respectively. Similar to the CISDR design, irregularity at the mid-height, produced drifts lesser than the regular structure for all the structures. For all structural heights, the structures having a reduced stiffness-strength topmost storey, has median peak ISDR closely matching with the corresponding drift response of the regular structure for most of the DISDR values. The influence of stiffness modification factor on the responses reduces as the factor α_k is increased from 0.5 up to 0.9. The maximum increase in median peak ISDR due to irregularity at the first storey, obtained from all structural heights, was 45%, 29%, 23% and 13% for α_k = 0.6, 0.7, 0.8 and 0.9 respectively.

(b) Increased storey stiffness-strength -

Figure 3-6(a) shows the median peak ISDR response plots for the regular and irregular CISDR structures having stiffness-strength *increased* at a chosen storey. 3 storey irregular structures created using α_k = 1.2 at any irregularity location, produced smaller drifts than the regular structures. For taller structures with this α_k at the mid-height, a maximum increase in median peak ISDR of 2.6% and 1.6% was found for 9 and 15 storey structures respectively. Irregularity at the roof produced drifts less than

those for the regular structures for all the structural heights and DISDR. Differences in responses between the regular and irregular structures increased with an increase in the factor α_k, as shown in Figure 3-6(a). As α_k was increased from 1.2 to 2, the coupled stiffness-strength irregularity introduced at the first storey for 3 & 5 storey structures, and for the 15 storey structure it was the mid-height that generally produced higher median peak ISDR. In case of 9 storey structures, irregularities at both these storeys tended to giver higher drift demands, as shown. The maximum increase in median peak ISDR for 3, 5, 9 and 15 storey structures was 15%, 24%, 12% and 4.5% respectively.

The effect of a storey having its stiffness-strength *increased* for CS-CSTG designs is shown in Figure 3-6(b). Five, 9 and 15 storey structures with the first storey stiffness-strength increased by $\alpha_k = 1.2$, performed better than the regular structures. However, in case of a 3 storey structure having the same magnitude of irregularity and located at the same storey, a maximum increase in ISDR of 26% is obtained for DISDR = 0.5%. As α_k was increased up to 2, irregularity at the first storey helped the performance of the irregular structures compared to the regular structures irrespective of the structure height. Similar to the CS-CSTG design with reduced stiffness, the irregularity at the topmost storey has drift demands closely matching with the corresponding drifts of the regular structures for many DISDR. However, in case of irregularity at the mid-height, which was generally seen to perform better than the regular structures for CS-CSTG design with a reduced stiffness, is in this case of increased stiffness, has produced a maximum increase in median peak ISDR of 25% from a 3 storey structure designed for DISDR = 1%. As the structure height

increased, the increase in median peak ISDR due to α_k = 2 at mid-height storey decreased.

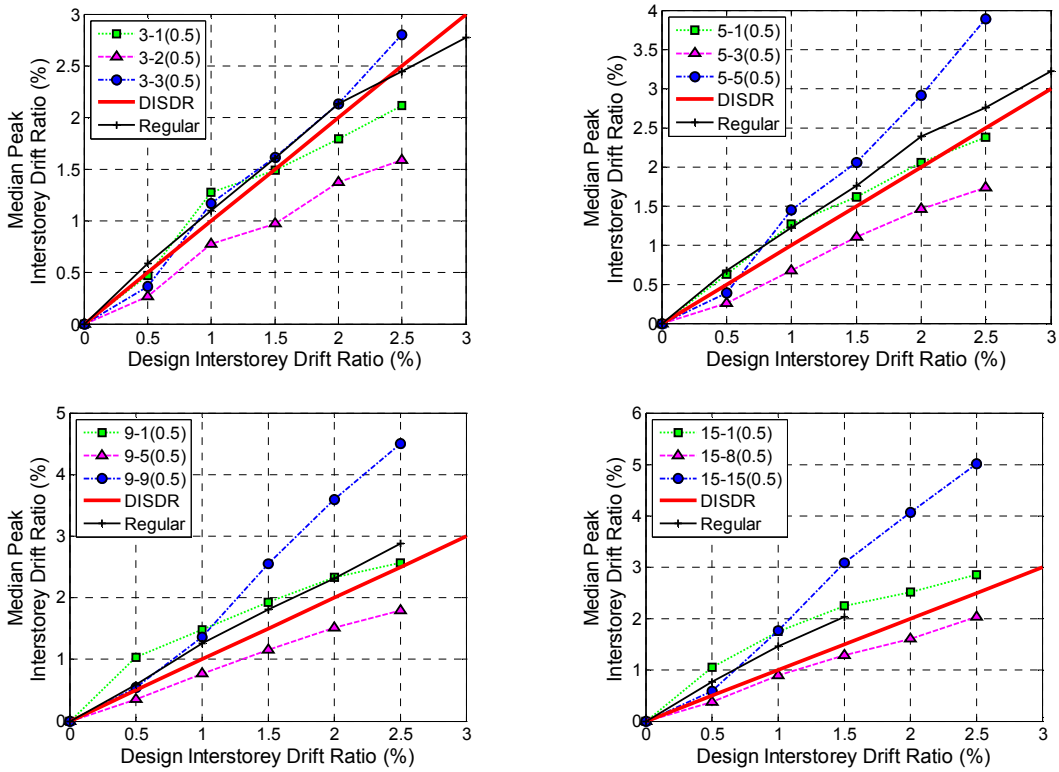

(1) $\alpha_k = 0.5$ & $\alpha_v = 0.5$

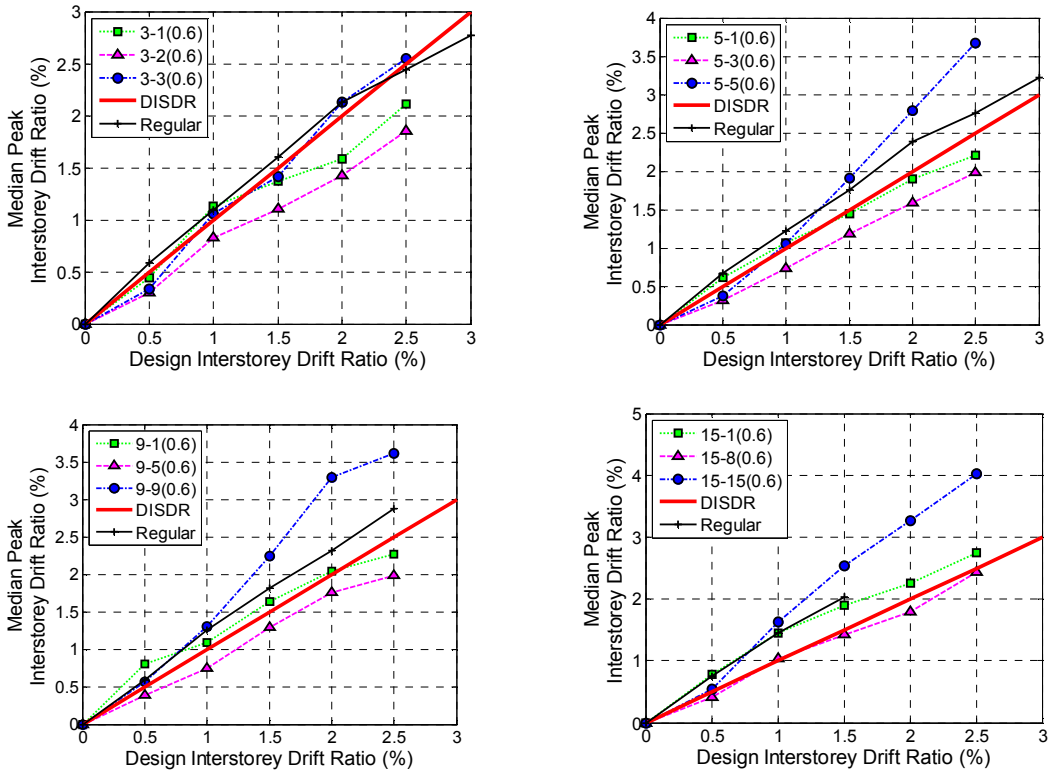

(2) $\alpha_k = 0.6$ & $\alpha_v = 0.6$

Figure 3-5(a): Effect of storey stiffness-strength reduction for Group A structures – CISDR design ($\mu = 3$, $Z = 0.4$): (1) $\alpha_k = 0.5$ & $\alpha_v = 0.5$; and (2) $\alpha_k = 0.6$ & $\alpha_v = 0.6$

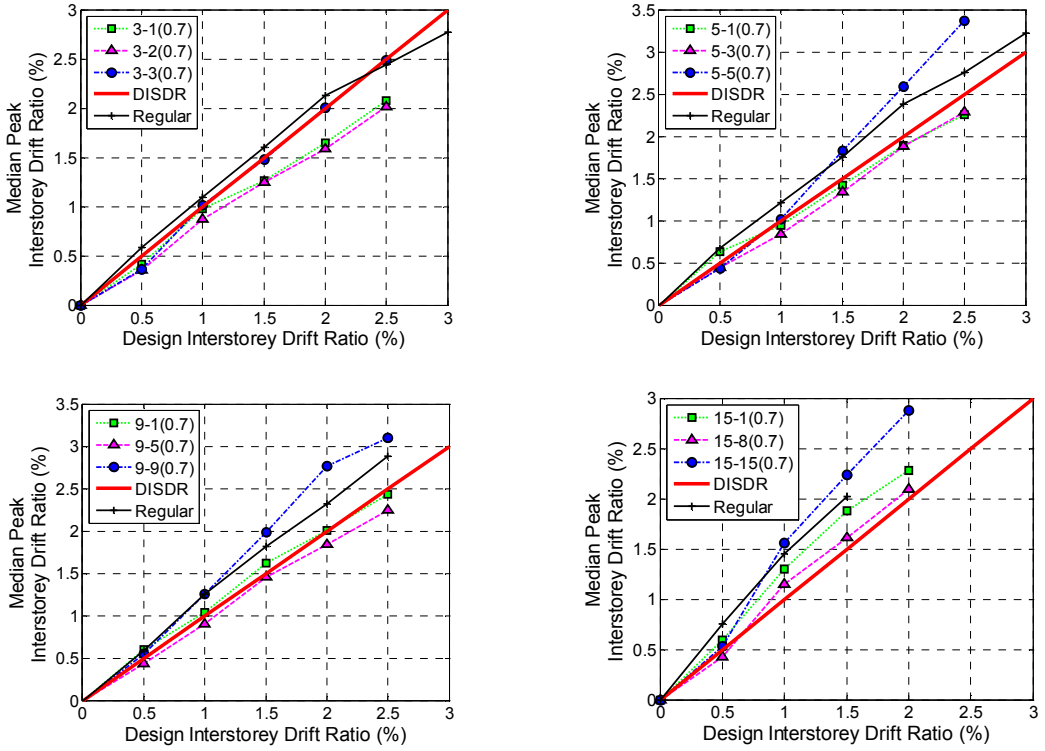

(3) $\alpha_k = 0.7$ & $\alpha_v = 0.7$

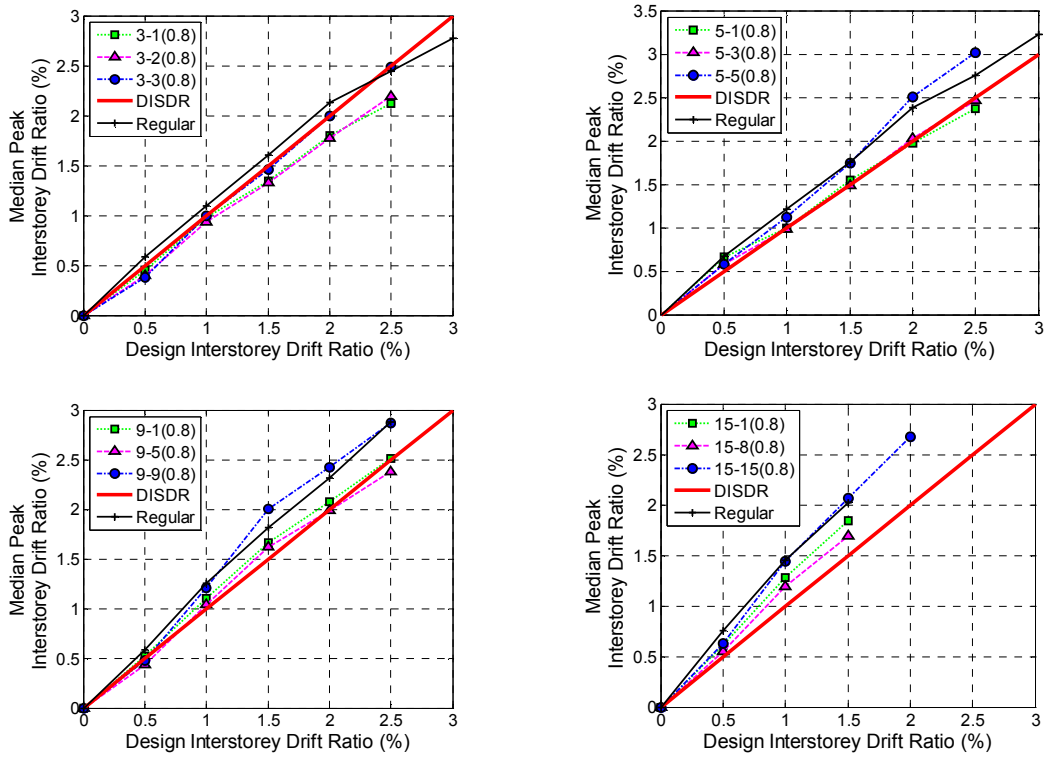

(4) $\alpha_k = 0.8$ & $\alpha_v = 0.8$

Figure 3-5(a): Effect of storey stiffness-strength reduction for Group A structures – CISDR design ($\mu = 3$, $Z = 0.4$): (3) $\alpha_k = 0.7$ & $\alpha_v = 0.7$; and (4) $\alpha_k = 0.8$ & $\alpha_v = 0.8$

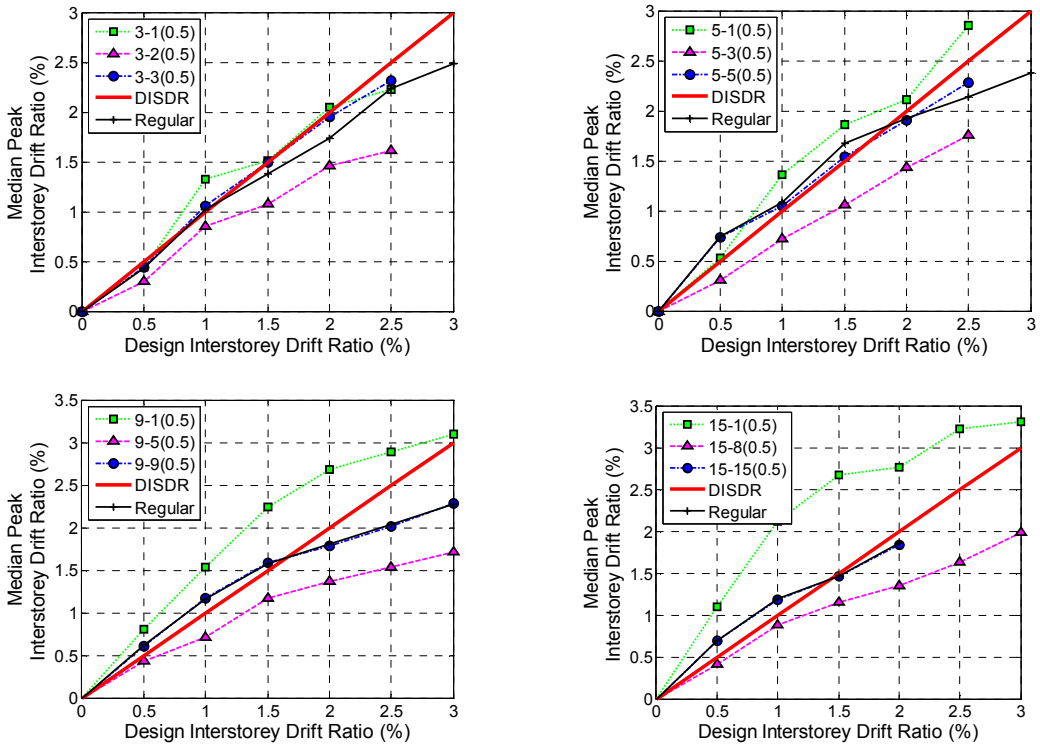

(1) $\alpha_k = 0.5$ & $\alpha_v = 0.5$

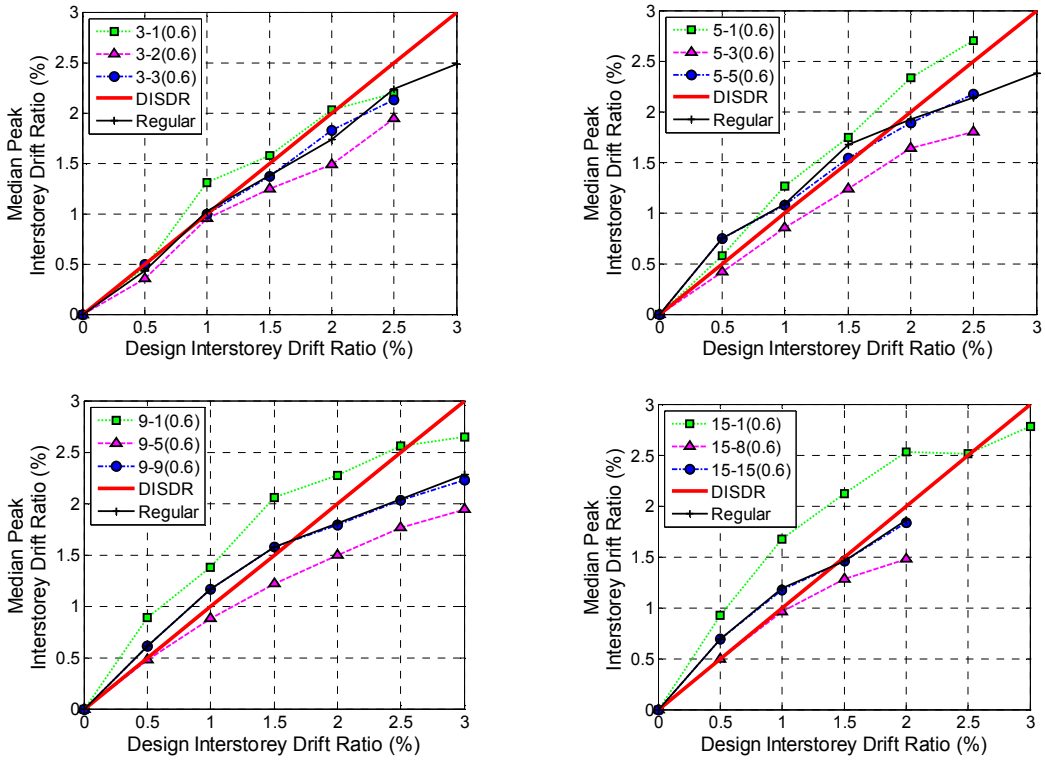

(2) $\alpha_k = 0.6$ & $\alpha_v = 0.6$

Figure 3-5(b): Effect of storey stiffness-strength reduction for Group A structures – CS-CSTG design ($\mu = 3$, $Z = 0.4$): (1) $\alpha_k = 0.5$ & $\alpha_v = 0.5$; and (2) $\alpha_k = 0.6$ & $\alpha_v = 0.6$

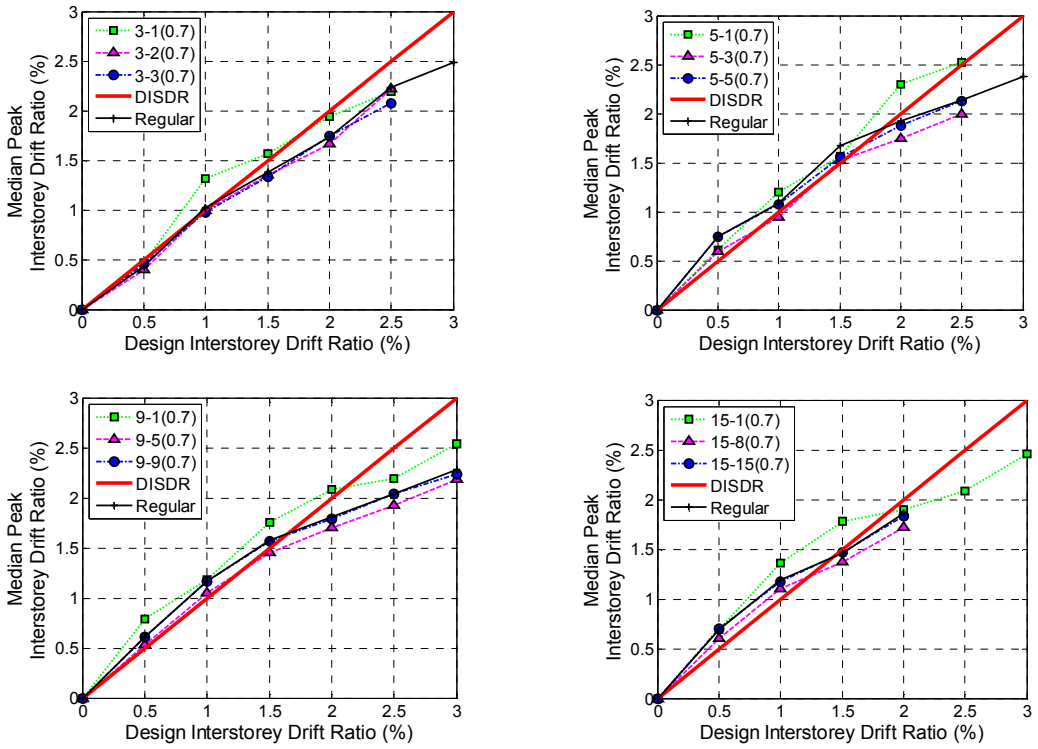

(3) $\alpha_k = 0.7$ & $\alpha_v = 0.7$

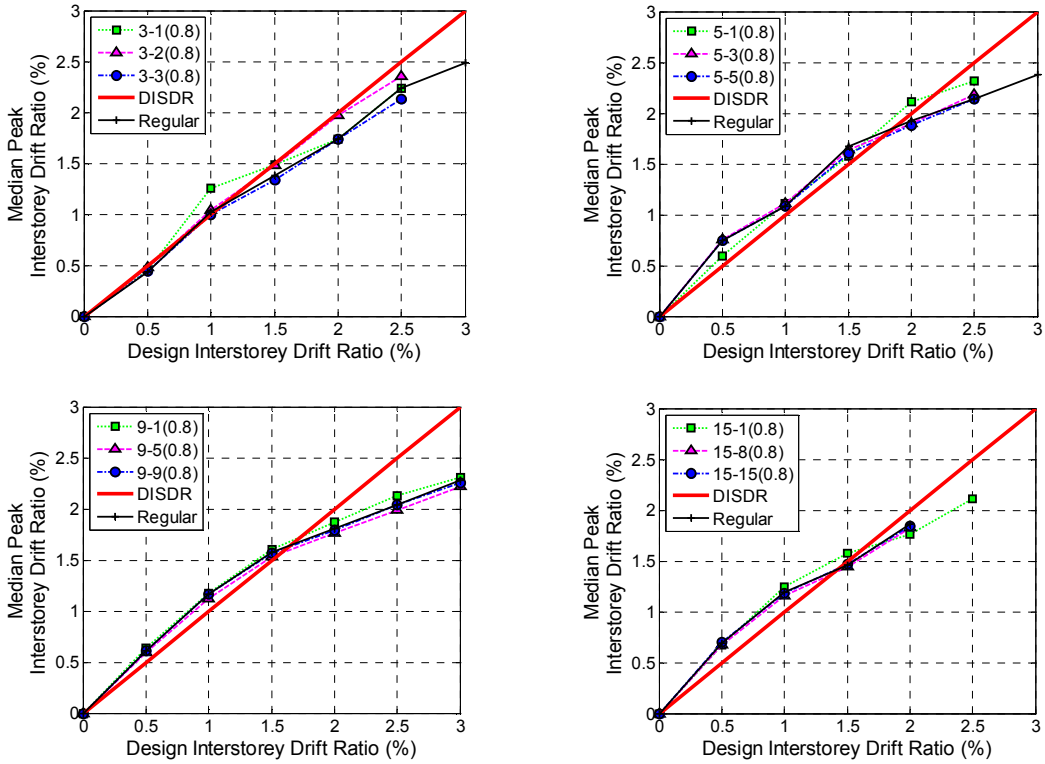

(4) $\alpha_k = 0.8$ & $\alpha_v = 0.8$

Figure 3-5(b): Effect of storey stiffness-strength reduction for Group A structures – CS-CSTG design ($\mu = 3$, $Z = 0.4$): (3) $\alpha_k = 0.7$ & $\alpha_v = 0.7$; and (4) $\alpha_k = 0.8$ & $\alpha_v = 0.8$

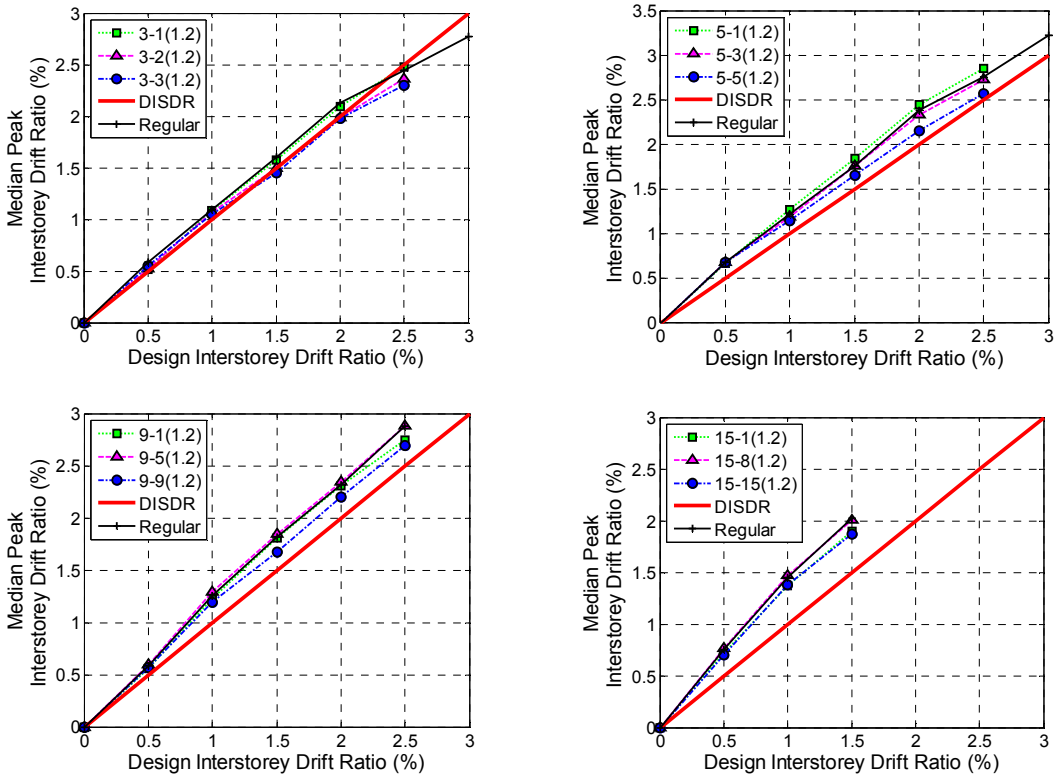

(1) $\alpha_k = 1.2$ & $\alpha_v = 1.2$

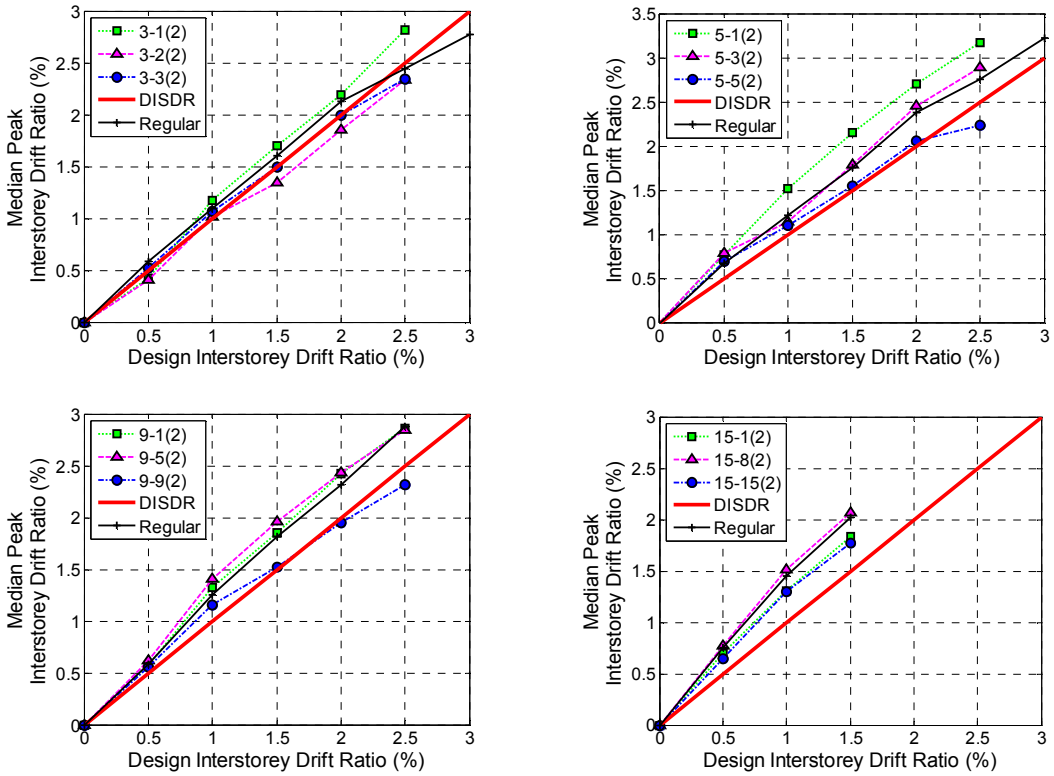

(2) $\alpha_k = 2$ & $\alpha_v = 2$

Figure 3-6(a): Effect of storey stiffness-strength increased for Group A structures – CISDR design ($\mu = 3$, $Z = 0.4$) : (1) $\alpha_k = 1.2$ & $\alpha_v = 1.2$; and (2) $\alpha_k = 2$ & $\alpha_v = 2$

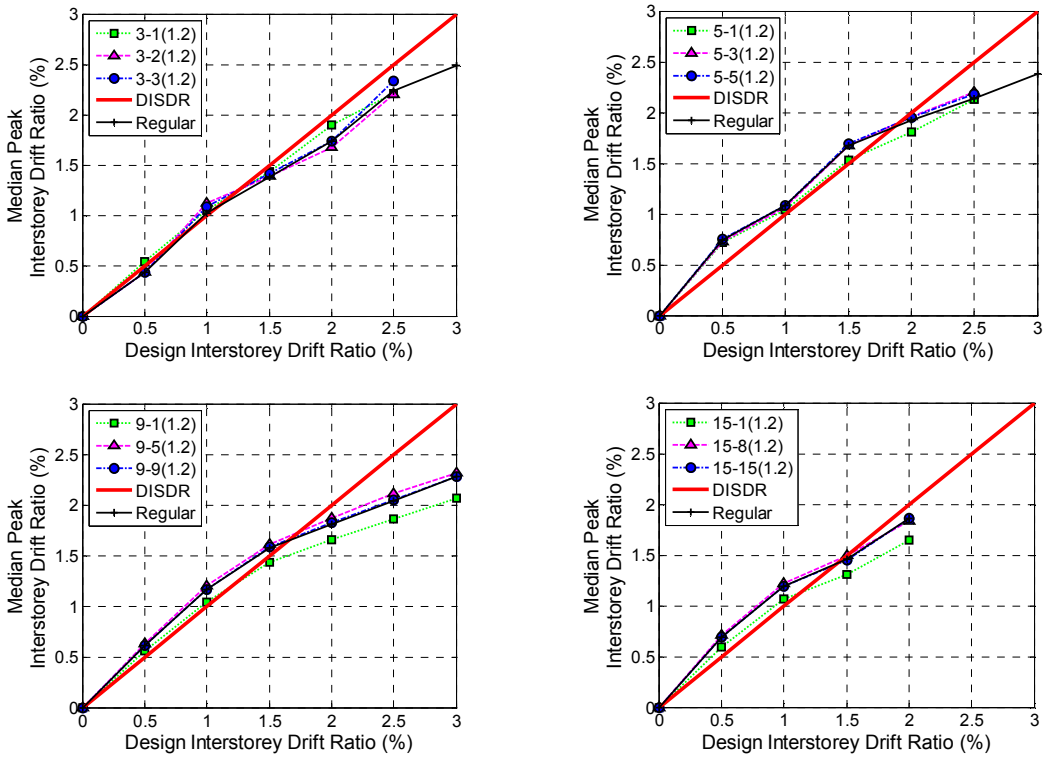

(1) $\alpha_k = 1.2$ & $\alpha_v = 1.2$

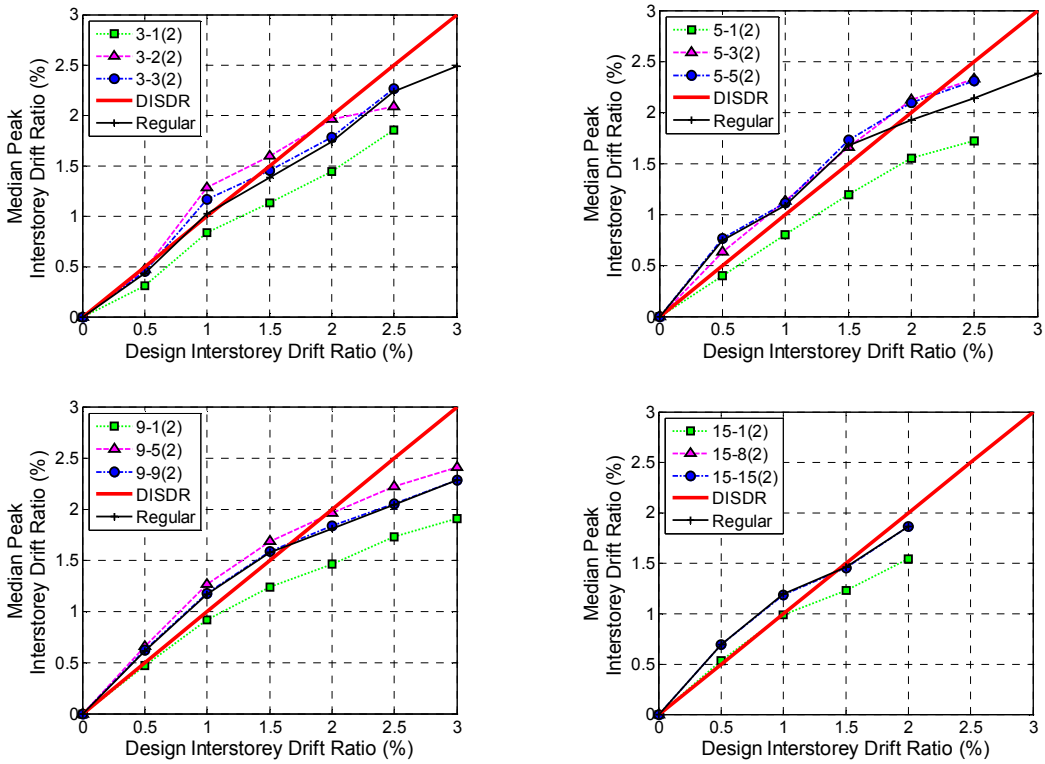

(2) $\alpha_k = 2$ & $\alpha_v = 2$

Figure 3-6(b): Effect of storey stiffness-strength increased for Group A structures – CS-CSTG design ($\mu = 3$, $Z = 0.4$): (1) $\alpha_k = 1.2$ & $\alpha_v = 1.2$; and (2) $\alpha_k = 2$ & $\alpha_v = 2$

3.5.4.2.2 Effect of magnitude and storey of coupled vertical stiffness-strength irregularity for Group B structures

(a) Reduced storey stiffness-strength -

The responses of irregular 3, 9 and 15 storey Group B structures with a reduced storey stiffness and strength are presented in Figure 3-7. For CISDR designs, Figure 3-7(a) shows that the irregular structures have lesser median peak ISDR than the corresponding regular structures. For α_k = 0.5 and α_v = 0.707 at the first storey, mid-height and at the roof, the respective average reductions in median peak ISDR were 42%, 56% and 53%. These reductions in drifts reduced with an increase in α_k and α_v, as seen in Figure 3-7(a). Figure 3-7(b) shows drift comparison between CS-CSTG regular and structures with a reduced storey stiffness-strength. For α_k = 0.5 and α_v = 0.707 at the first storey and at the mid-height, the median peak ISDR decreased due to irregularity by an average of 29% and 42% respectively. For the same amount of irregularity at the roof, generally the median peak ISDR closely matched with the corresponding drift of regular structures. A maximum of 3.5% increase in median peak ISDR was obtained for this irregularity at the roof. Similar trend in responses were observed for α_k = 0.7 and α_v = 0.836.

(b) Increased storey stiffness-strength -

Figures 3-8(a) and 3-8(b) respectively show the median peak ISDR plotted against DISDR for CISDR and CS-CSTG structures with increased stiffness-strength at each of the three chosen storeys. For α_k = 1.5 and α_v = 1.224, the median peak drifts generally reduced due to the presence of irregularity. A maximum increase in median peak ISDR of 2% was obtained due to an increased storey stiffness-strength at the

mid-height of a 15 storey structure. When α_k was increased to 2, Figure 3-8(a) shows that the 3 storey regular structures had lesser drifts than the corresponding irregular structures. For taller structures, and with the irregularity at the mid-height, the median peak ISDR slightly increased over the regular structures. The average increase due to irregularity at this storey was 4%. In case of CS-CSTG designs with $\alpha_k = 1.5$ and $\alpha_v = 1.224$, it is the roof with irregularity for short period structures, and irregularity at the mid-height for taller structures, that has produced increased drifts. Figure 3-8(b) shows similar trends in responses for $\alpha_k = 2$ and $\alpha_v = 1.414$.

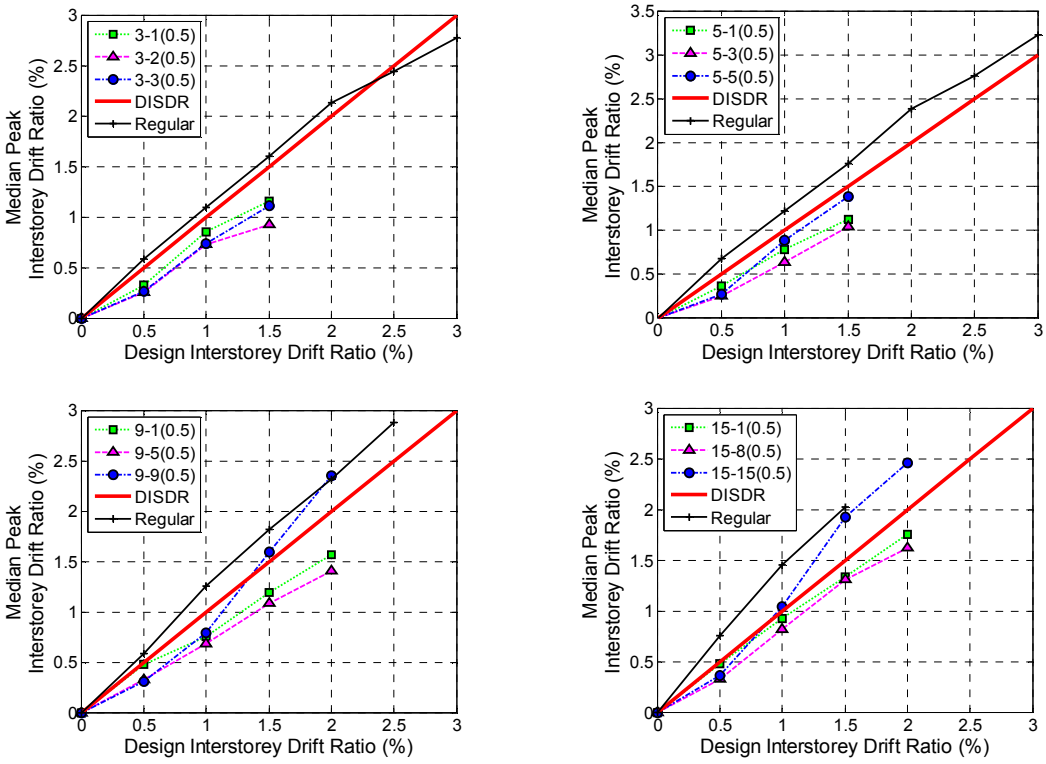

(1) $\alpha_k = 0.5$ & $\alpha_v = 0.707$

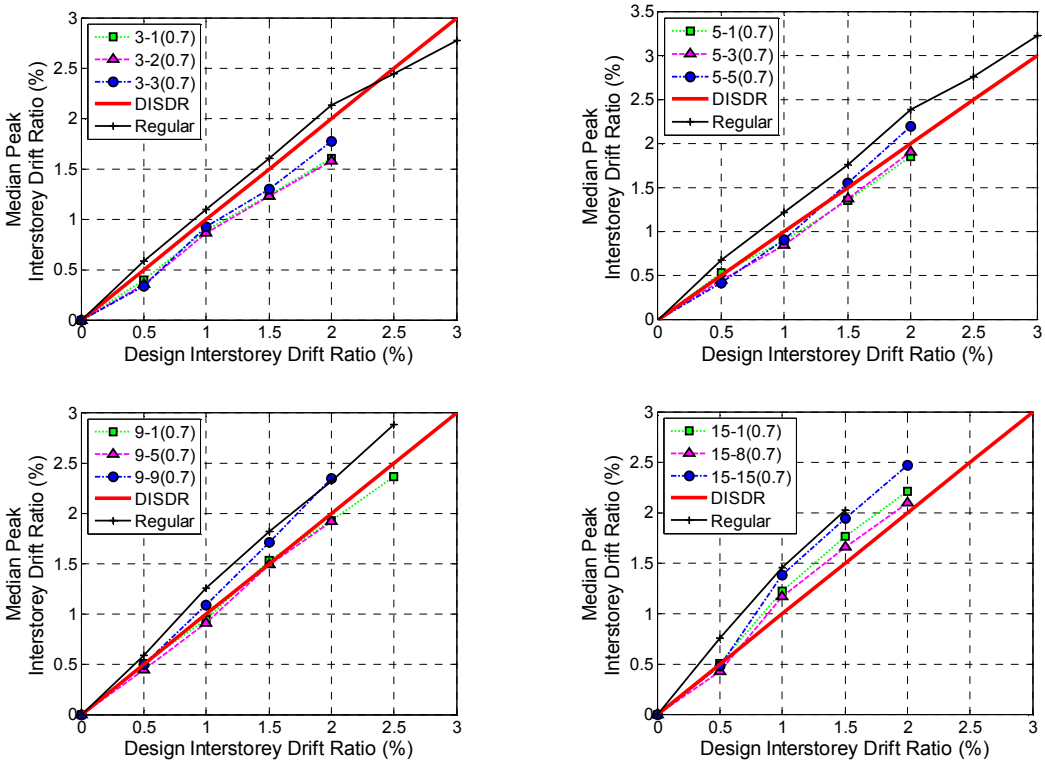

(2) $\alpha_k = 0.7$ & $\alpha_v = 0.836$

Figure 3-7(a): Effect of storey stiffness-strength reduction for Group B structures – CISDR design ($\mu = 3$, $Z = 0.4$): (1) $\alpha_k = 0.5$ & $\alpha_v = 0.707$; and (2) $\alpha_k = 0.7$ & $\alpha_v = 0.836$

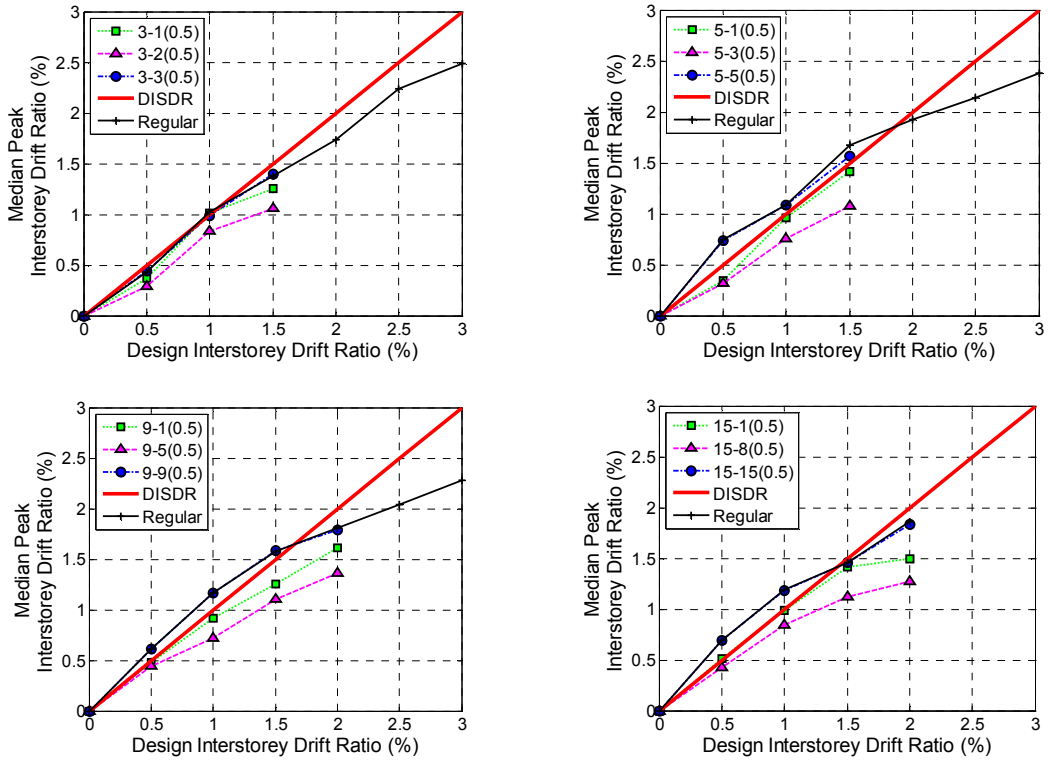

(1) $\alpha_k = 0.5$ & $\alpha_v = 0.707$

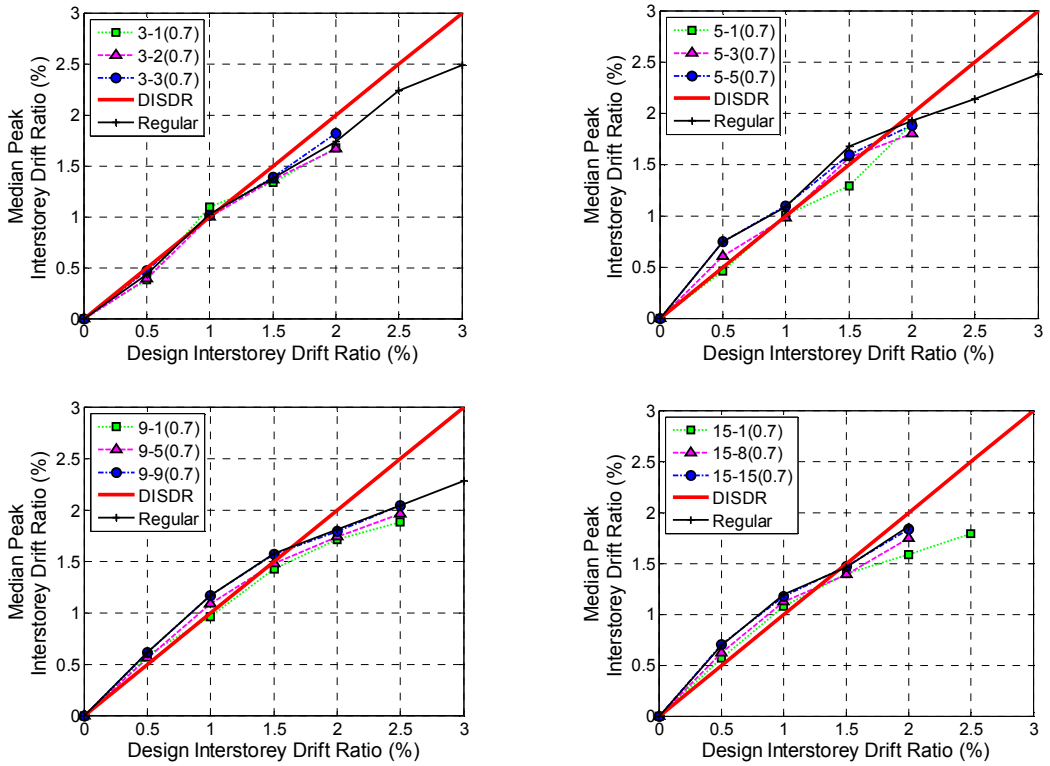

(2) $\alpha_k = 0.7$ & $\alpha_v = 0.836$

Figure 3-7(b): Effect of storey stiffness-strength reduction for Group B structures – CS-CSTG design ($\mu = 3$, $Z = 0.4$): (1) $\alpha_k = 0.5$ & $\alpha_v = 0.707$; and (2) $\alpha_k = 0.7$ & $\alpha_v = 0.836$

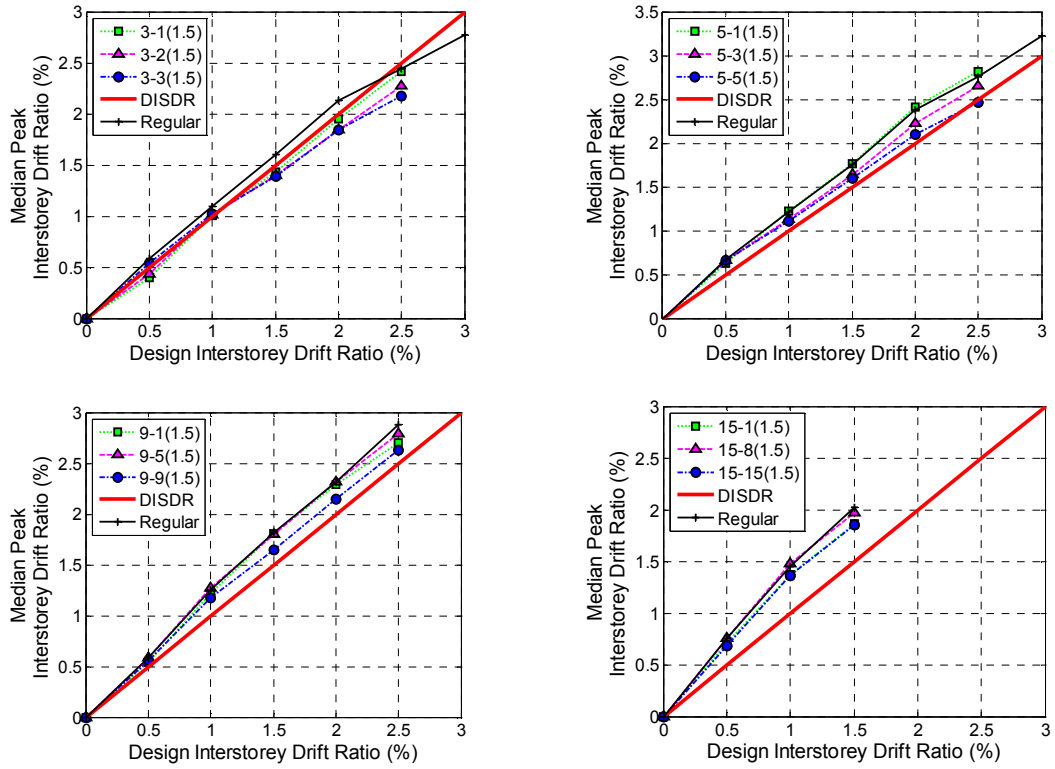

(1) $\alpha_k = 1.5$ & $\alpha_v = 1.224$

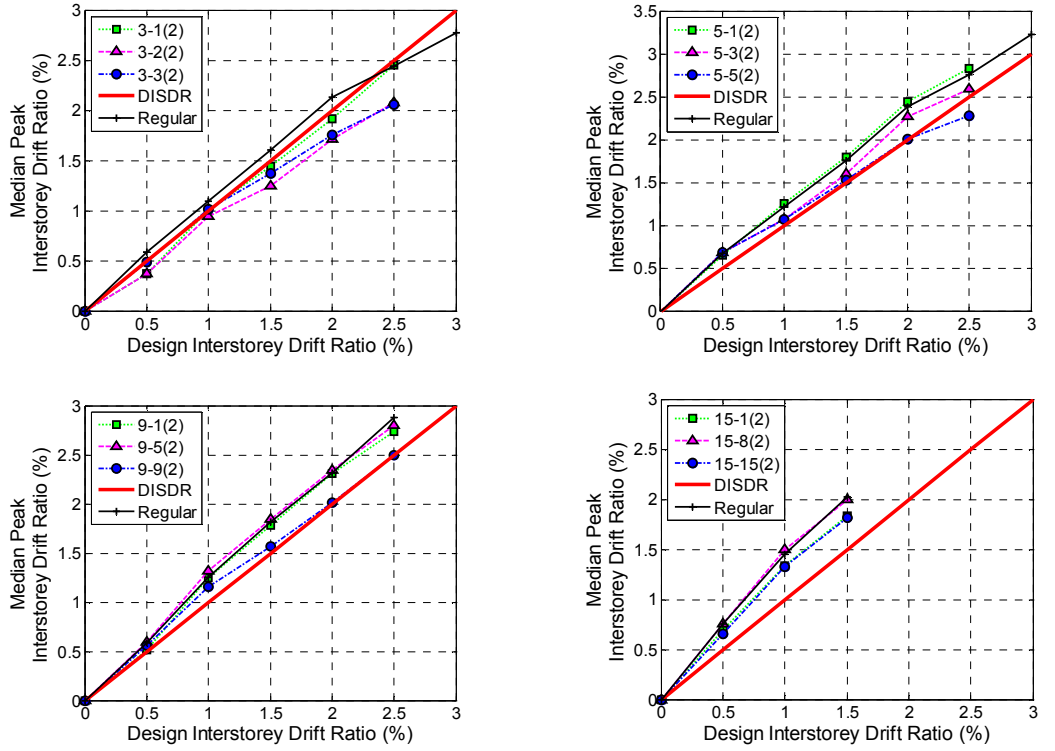

(2) $\alpha_k = 2$ & $\alpha_v = 1.414$

Figure 3-8(a): Effect of storey stiffness-strength increased for Group B structures – CISDR design ($\mu = 3$, $Z = 0.4$): (1) $\alpha_k = 1.5$ & $\alpha_v = 1.224$; and (2) $\alpha_k = 2$ & $\alpha_v = 1.414$

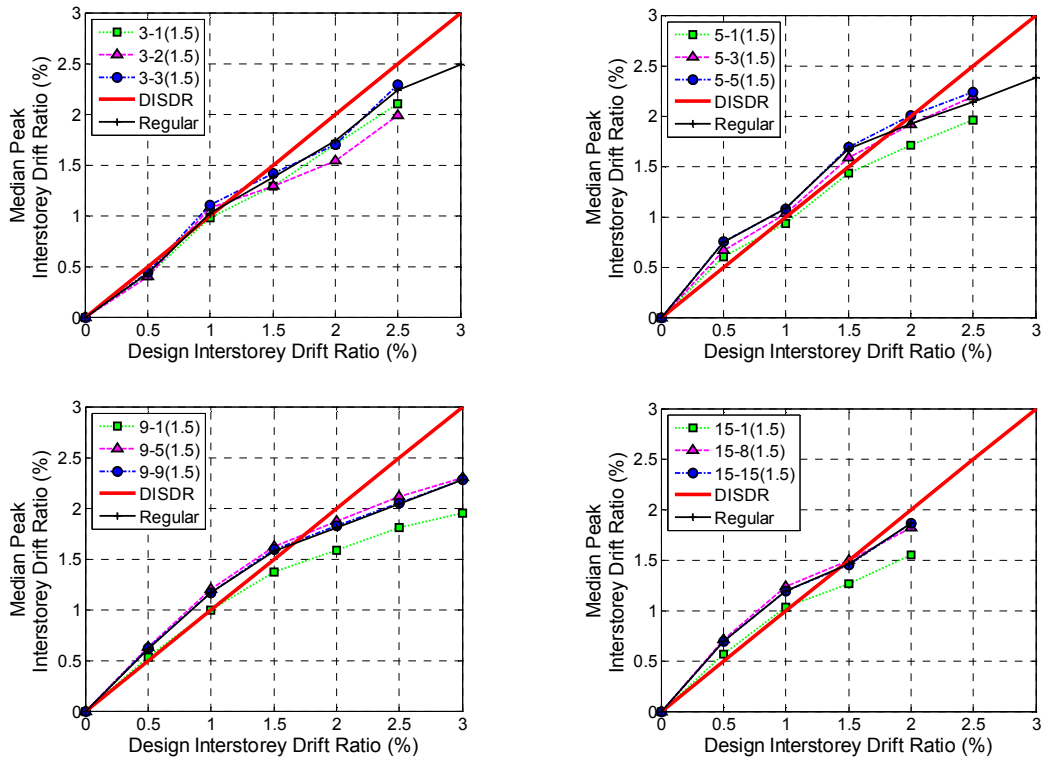

(1) $\alpha_k = 1.5$ & $\alpha_v = 1.224$

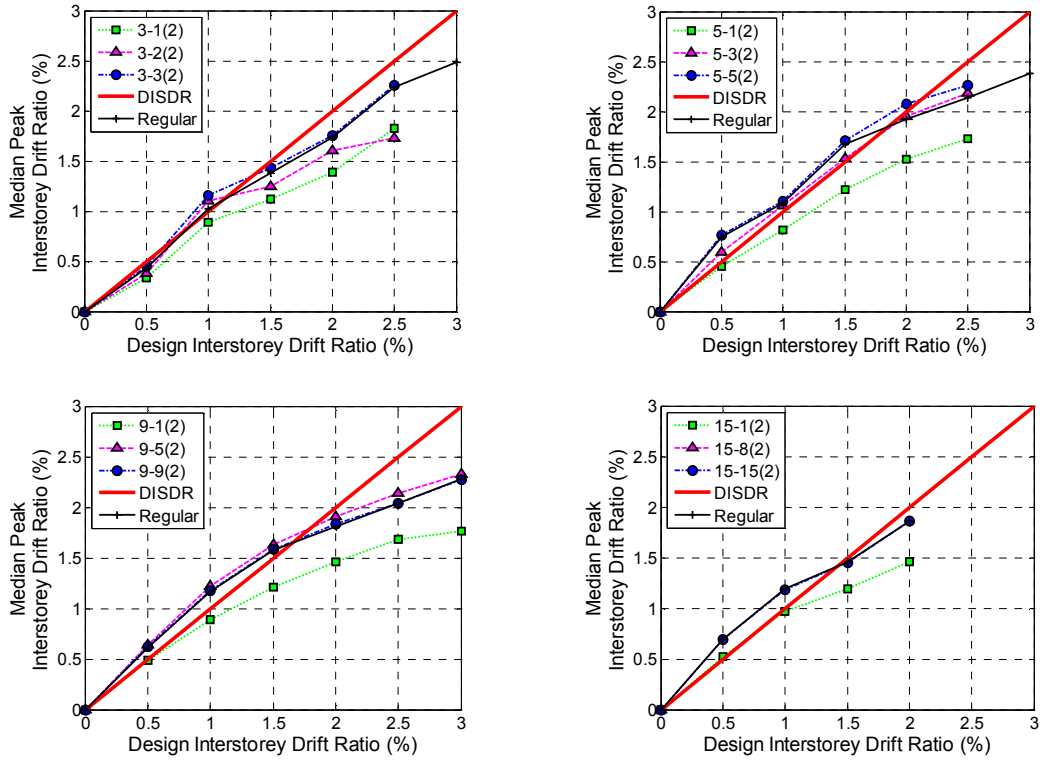

(2) $\alpha_k = 2$ & $\alpha_v = 1.414$

Figure 3-8(b): Effect of storey stiffness-strength increased for Group B structures – CS-CSTG design ($\mu = 3$, $Z = 0.4$): (1) $\alpha_k = 1.5$ & $\alpha_v = 1.224$; and (2) $\alpha_k = 2$ & $\alpha_v = 1.414$

3.6 Determination of Coupled Stiffness-Strength Irregularity Limit

The following steps were used to compute the relationship between the *increase* in *median peak interstorey drift ratio*, $ISDR_{incr}$, for different magnitudes of irregularity:

Step 1. For a combination of structural form, structural ductility factor, design interstorey drift ratio, structure height, and the storey of stiffness-strength irregularity, the median peak ISDR for the regular structure, $ISDR_R$, is computed from the results of the structure to the suite of records. In a similar way, the median of peak interstorey drift ratio for the irregular structure, $ISDR_I$, is obtained. Thus, the increase in median peak ISDR due to irregularity, $ISDR_{incr}$, is calculated by Equation (3-5).

$$ISDR_{incr} = \left(\frac{ISDR_I}{ISDR_R} - 1 \right) * 100 \ (\%) \qquad (3\text{-}5)$$

Step 2. Step 1 is repeated for all the combinations of structural form, structural ductility factor, design interstorey drift ratio, structure height, storey of stiffness-strength irregularity, and magnitude of irregularity.

Step 3. For each magnitude of irregularity, the *maximum* value of $ISDR_{incr}$, $ISDR_{max\_incr}$ is found.

The maximum increase in the median peak ISDR obtained from Step 3, $ISDR_{max\_incr}$, due to coupled stiffness-strength irregularities for Group A and Group B structures, designed for structural ductility factors of 1, 2, 3, 4 and 6 are shown in Figures 3-9(a) and 3-9(b) respectively. The data points in the figures are due to the responses of the critical structures. For example, in Figure 3-9(b), for the CS-CSTG Group B model designed for $\mu = 4$ and α_k = 0.7, $ISDR_{max\_incr}$ = 12.8%. This particular example is

governed by a 3 storey structure with DISDR = 1% and stiffness-strength irregularity at the first storey. Similarly, for the same CS-CSTG design with $\mu = 4$ and $\alpha_k = 0.5$, the figure shows $ISDR_{max\_incr} = 6.7\%$, obtained from a 3 storey structure with DISDR = 2% and stiffness-strength irregularity at the topmost storey. The reason for the decrease in response due to increasing irregularity corresponding to α_k changing from 0.7 to 0.5 for Group B structures was investigated. It was not due to structures with some irregularities being removed from the analyses according to the exclusion criteria in Section 3.5. It seems to be due to the approach used to obtain $ISDR_{max\_incr}$ for each magnitude of irregularity.

The increase in the median peak ISDR due to a reduced stiffness-strength at a storey was larger than that due to increased stiffness-strength for Group A structures. As seen in Figure 3-9, Group A structures, representing the uniformly varying stiffness and strength relation, generally produced higher increase in response than the Group B structures. Also, the figures show that generally the structures designed to have a uniform distribution of stiffness and strength (CS-CSTG) have greater increases in median peak ISDR due to coupled stiffness-strength irregularities than do structures designed to produce equal storey drifts (CISDR). However, the response plots of CISDR and CS-CSTG irregular structures have shown that the former type of structure, in many cases, produced larger median peak ISDR than the CS-CSTG structures. Similar observations were seen in the study of mass irregularity effects [2].

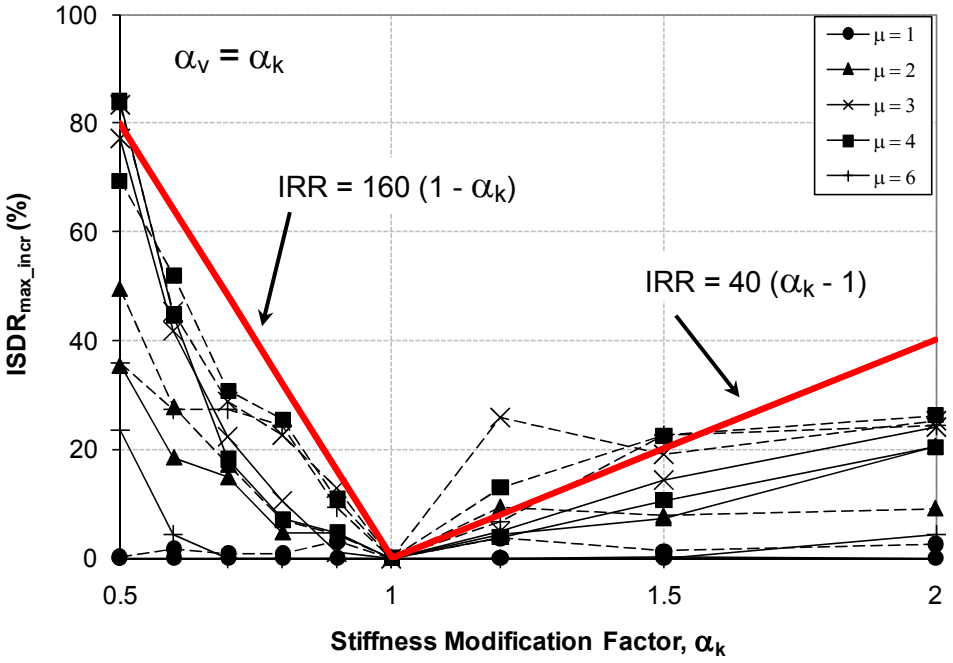

(a) Group A Structures

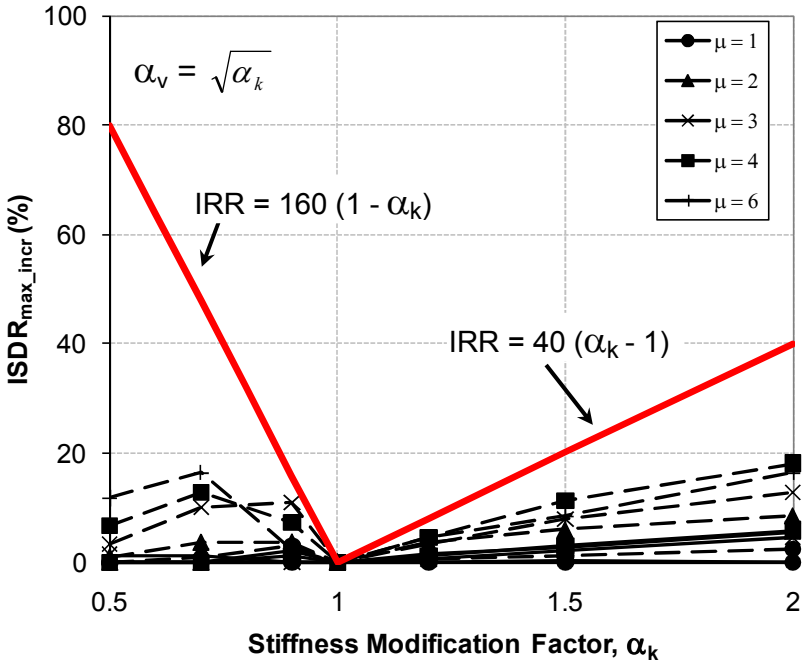

(b) Group B Structures

Figure 3-9: Maximum increase in median peak ISDR due to coupled stiffness-strength irregularities.

(CISDR —— CS-CSTG - - - - -)

Equations (3-6) and (3-7) can be developed empirically to estimate the likely change in response due to irregularity for critical structures. These are based on Group A structures. They are more conservative for Group B structures and for those with irregularity at the non-critical storeys.

$$IRR(\%) = 160\left(1-\alpha_k\right) \;\; with\ \alpha_k < 1 \qquad (3\text{-}6)$$

$$IRR(\%) = 40\left(\alpha_k - 1\right) \;\; with\ \alpha_k > 1 \qquad (3\text{-}7)$$

Here, *IRR* is the *irregular response ratio* which specifies how much the irregular response is greater than the regular response; and α_k is the stiffness modification factor.

These two equations can then be used to estimate the likely increase in the response due to coupled stiffness-strength irregularity. For example, according to Figure 3-10, if it is not intended to have responses change more than 20% due to coupled stiffness-strength irregularity, then the storey stiffness-strength can be modified by an amount between 0.875 and 1.5. The NZS 1170.5 states stiffness and strength regularity limits of 0.7 and 0.9 respectively. Therefore for critical structures which have the same stiffness and strength variation (i.e. Group A structures), the likely increase in median peak ISDR is 15% due to the strength regularity limit of 0.9. For structures in which the stiffness variation follows the square of the strength variation (i.e. Group B structures), the maximum code strength regularity limit of 0.9 corresponds to α_k = 0.81. This implies a variation of 30% from Figure 3-10.

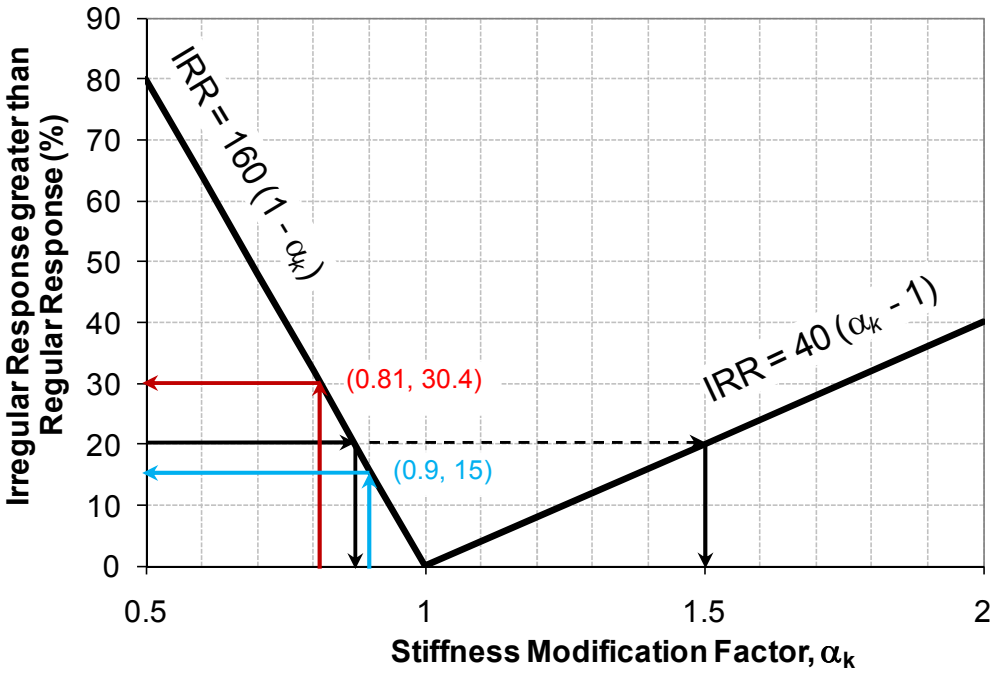

Figure 3-10: Determination of coupled stiffness-strength irregularity limit

3.7 Conclusions

Coupled vertical stiffness-strength irregularity effects were evaluated on the seismic response of structures in this paper. Realistic regular structures, represented by shear-type structures of 3, 5, 9 and 15 storeys, having equal storey height, assumed to be in Wellington, and having a constant floor mass at every floor level were designed for a range of structural ductility factors of 1, 2, 3, 4 and 6, according to the New Zealand Standard Equivalent Static (ES) method. The stiffness distribution over the height was chosen to either give the design (target) interstorey drift ratios (DISDR) at all storeys simultaneously, or to have a uniform stiffness distribution that produced the DISDR at the first storey. Storey strengths were provided such that every storey had a constant strength to stiffness ratio. Irregular structures were created by modifying the storey stiffness-strength of the base structure at a storey and redesigning the structure until the critical storey achieved the target DISDR. The change in the median peak

interstorey drift ratios (ISDR) due to irregularity obtained from inelastic dynamic time-history analysis was then used to quantify the effects of coupled stiffness-strength irregularity. It was shown that:

1. Simple analysis methods, such as the NZS 1170.5 Equivalent Static method, are not allowed to be used for the design of structures if the structure is irregular. Irregularity is defined in codes for structures where the structural parameters violate "regularity limits". Current code regularity limits are based on engineering judgement and do not have a systematic quantitative justification. As a result, the variation in response due to irregularity is not clear.

2. A number of studies have been conducted on vertical stiffness and strength irregularity and they provide valuable insight into the structural behaviour. However, previous studies have not always compared structures with the same design demand parameter or considered realistic strength to stiffness ratios. Also, studies have not been conducted to evaluate the code regularity limits.

3. Realistic correlations between storey stiffness and strength due to modifications in member properties for a few common lateral force resisting systems were determined. The storey stiffness and strength were varied realistically either proportionally by the same amount (Group A structures) or with the strength varied less than the stiffness (Group B structures). A range of stiffness and strength modification factors were selected to investigate the effects of irregularities. For the same stiffness modification, the increase in drift demands due to Group B structures which had a lower strength change, was generally less than the Group A structures, which had equal stiffness and strength variations.

4. For most of the cases, the median peak ISDR due to constant interstorey drift ratio (CISDR) designs were found to be higher than those due to constant stiffness and constant strength (CS-CSTG) designs, but the percentage increase in median peak ISDR due to irregularities from CS-CSTG designs were found to be larger than those with CISDR configuration. Irregular structures with correlations between stiffness and strength for Group A CISDR configurations, and reduced stiffness-strength at the topmost storey produced larger median peak ISDR than for irregularity at the first storey. Stiffness-strength reduced at the mid-height storey generally made irregular structures perform better than the regular ones. For Group A CS-CSTG designs, median peak ISDR increased due to irregularity at the first storey. Stiffness-strength reduction at the topmost storey was insignificant, and the irregularity at the mid-height storey produced demands less than those of the regular structures.

5. In a contrast to the stiffness-strength reduction case, Group A structures with CISDR and CS-CSTG configurations generally resulted in increased median peak ISDR when the coupled properties at the mid-height storey were increased rather than at the other two irregular storeys.

6. Simple equations to rapidly estimate the likely increase in median peak ISDR due to coupled stiffness-strength irregularity were developed. These equations are generally conservative as they were developed for critical structures. From those equations, it is seen that the present NZS 1170.5 “regularity limits” for braced and moment framed structures with maximum code irregularities correspond to a increase in median peak ISDR of 15% and 30% respectively for critical structures.

3.8 Acknowledgements

The authors gratefully acknowledge the support for this work provided by the New Zealand Earthquake commission (www.eqc.govt.nz).

3.9 References

[1] SNZ. NZS 1170.5 Supp 1:2004, Structural Design Actions. Part 5: Earthquake actions – New Zealand – Commentary, Standards New Zealand, Wellington, 2004.

[2] Sadashiva VK, MacRae GA, Deam BL. Determination of structural irregularity limits – mass irregularity example. *Bulletin of the New Zealand Society for Earthquake Engineering* 2009; **42**(4): 288-301.

[3] FEMA 450. National Earthquake Hazards Reduction Program recommended provisions for seismic regulations for new buildings and other structures. Prepared by the Building Seismic Safety council, National Institute of building sciences, Washington, D.C., 2003.

[4] IBC. International Building Code. International Code Council (ICC), Whittier, CA, 2003.

[5] CEN. EN 1998-1. Eurocode 8. Design of structures for earthquake resistance – Part 1: General Rules, Seismic Actions and Rules for Buildings, European Committee for Standardization, 2004.

[6] SEAOC. Recommended Lateral Force Requirements and Commentary. Seismology Committee, Structural Engineers Association of California, 1999, Seventh Edition.

[7] Valmundsson EV, Nau JM. Seismic response of building frames with vertical structural irregularities. *Journal of Structural Engineering* 1997; **123**(1): 30-41.

[8] MacRae GA, Kimura Y, Roeder CW. Effect of column stiffness on braced frame seismic behaviour. *Journal of Structural Engineering* 2004; **130**(3): 381-391.

[9] Al-Ali AAK, Krawinkler H. Effects of vertical irregularities on seismic behaviour of building structures. Report No. 130, Department of Civil and Environmental Engineering, Stanford University, San Francisco, 1998.

[10] Chintanapakdee C, Chopra AK. Seismic response of vertically irregular frames: Response history and modal pushover analyses. *Journal of Structural Engineering* 2004; **130**(8): 1177-1185.

[11] Fragiadakis M, Vamvatsikos D, Papadrakakis M. Evaluation of the influence of vertical irregularities on the seismic performance of a nine-storey steel frame. *Earthquake Engineering and Structural Dynamics* 2006; **35**(12): 1489-1509. DOI: 10.1002/eqe.591.

[12] Priestley MJN, Calvi GM, Kowalsky MJ. Displacement-based seismic design of structures. *IUSS Press*, Pavia, Italy, 2007; 721pp.

[13] Tagawa H, MacRae GA, Lowes LN. Evaluation of simplification of 2D moment frame to 1D MDOF coupled shear-flexural-beam model. *Journal of Structural & Constructional Engineering* 2006; Transactions of AIG, No. 609.

[14] Carr AJ. Ruaumoko 2D – Inelastic dynamic analysis. Department of Civil Engineering, University of Canterbury, Christchurch, 2004.

[15] Chopra AK. Dynamics of structures: Theory and Applications to Earthquake Engineering. New Jersey: Prentice Hall, 2000; 844.

[16] Cornell CA, Jalayer F, Hamburger RO, Foutch DA. Probabilistic basis for 2000 SAC FEMA steel moment frame guidelines. *Journal of Structural Engineering* 2002; **128**(4): 526-533.

Nomenclature for Table 3-1

A_a = *cross*-sectional area of the bracing member

A_{am} = *modified* cross-sectional area of the bracing member

A_s = cross-sectional shear area

A_{sm} = modified cross-sectional shear area

d_o = initial overall depth of the member section

d_m = modified overall depth of the member section

E = modulus of elasticity

G = shear modulus of elasticity

h = interstorey height

I_o = initial moment of inertia of the member section

I_m = modified moment of inertia of the member section

K = lateral stiffness of the structure

K_o = initial lateral stiffness of the structure

K_m = modified lateral stiffness of the structure due to modified member property

L = span length of the frame or wall

M_p = section plastic moment

V = lateral strength of the structure

V_o = initial lateral strength of the structure

V_m = modified lateral strength of the structure

α_k = stiffness modification factor

α_v = strength modification factor

ε_y = yield strain of the material

σ_y = yield stress of the material

4. EFFECTS OF COUPLED VERTICAL STIFFNESS-STRENGTH IRREGULARITY DUE TO MODIFIED INTERSTOREY HEIGHT

4.1 Overview

Structures may have vertical stiffness or strength irregularity for many reasons. In many practical cases, a change in storey stiffness, results in a change in strength at the same storey. In this paper, the effect of a change in interstorey height is quantified. In order to do this, relationships between storey stiffness and strength resulting due to a modified interstorey height for a few common lateral force resisting systems was considered. It was applied to simple shear-type structures of 3, 5, 9 and 15 storeys, assumed to be located in Wellington. All structures were considered to have a constant mass at every floor level. Both regular and irregular structures were designed in accordance with the Equivalent Static method of the current New Zealand seismic design Standard, NZS 1170.5. Regular structures were designed to either (i) produce a constant target interstorey drift ratio at all the storeys simultaneously or (ii) to have uniform stiffness distribution over the height of the structure, with the target interstorey drift ratio at the first storey. An "interstorey height ratio" was defined as the ratio of modified to initial interstorey height, and applied separately at the first storey, mid-height storey and at the topmost storey by amounts between 0.5 and 3. The modified structures were then redesigned until the target interstorey drift ratio was achieved at the critical storey/storeys. Design structural ductility factors of 1, 2, 3, 4 and 6, and target (design) interstorey drift ratios ranging between 0.5% and 3%, were used in this study. Inelastic dynamic time-history analysis was carried out by

subjecting these structures to code design level earthquake records, and the maximum interstorey drift ratio demands due to each record were used to compare the responses of regular and irregular structures.

It was found that structural types in which only the storey stiffness was modified due to a change in the interstorey height produced the maximum increase in drift demands rather than structural forms with other stiffness-strength coupling cases. Shorter structures having an increased first storey height, and taller structures with an increased middle storey height generally produced greater interstorey drift demands than regular structures. For cases of increased storey stiffness due to decreased storey heights, the shorter structures with a decreased middle storey height resulted in higher median peak ISDR due to irregularity. A simple equation describing the maximum increase in response due to modifications to a storey height was developed. The equation was used along with the realistic correlations between storey stiffness and strength to obtain the governing code regularity limit.

4.2 Introduction

No real structure is perfectly regular. While some structures are planned to be architecturally irregular, other structures may be irregular due to unplanned effects. One of the common types of irregularity is the stiffness and strength irregularity over the height of the structures. This irregularity generally exists in buildings due to:

- Difference in interstorey height at a particular storey as compared to adjacent storey, as shown in Figure 4-1(b);
- Modification of member properties, member sizes, material, at a storey, as shown in Figure 4-1(c);

- Vertical discontinuities of structural members at a particular storey, as shown in Figure 4-1(c); or
- Lack of infill material or open storey, as shown in Figure 4-1(d).

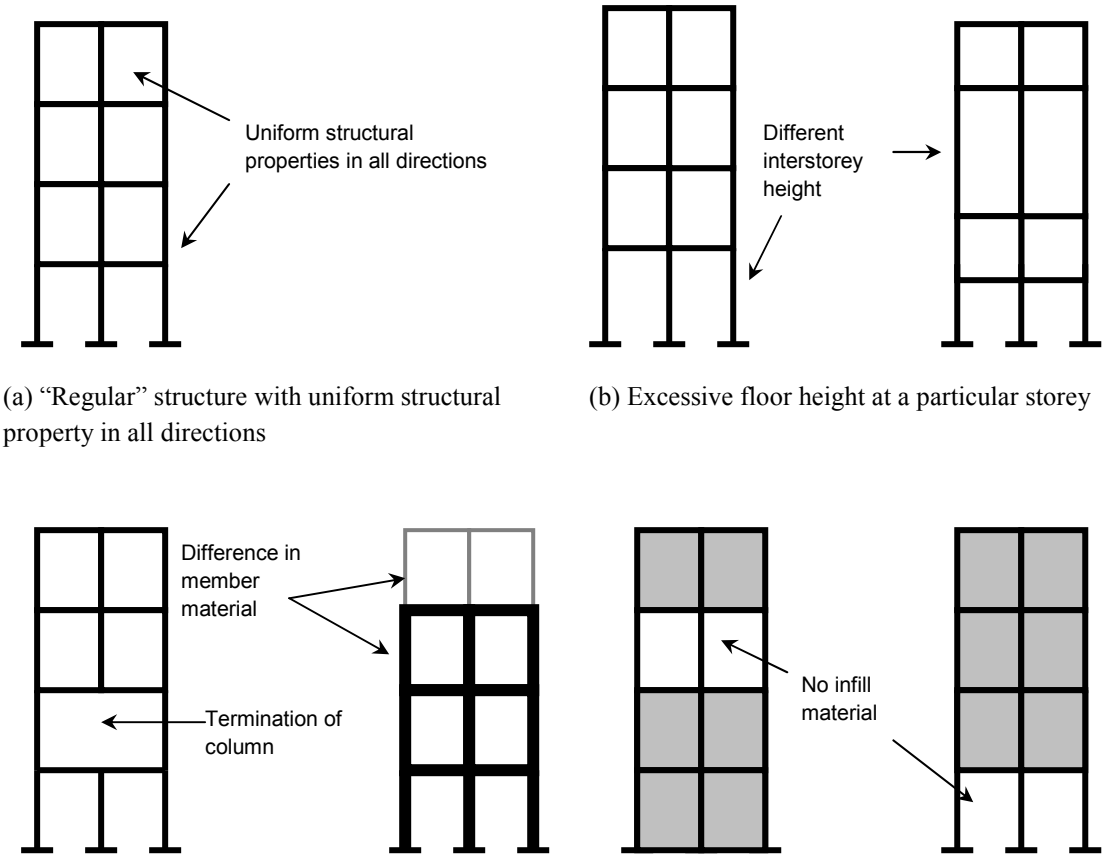

(a) "Regular" structure with uniform structural property in all directions

(b) Excessive floor height at a particular storey

(c) Vertical discontinuity at a floor level or adjacent levels with dissimilar structural materials

(d) Lack of infill material at a storey

Figure 4-1: Examples of vertical stiffness-strength irregularities.

Many world-wide earthquake codes define structures to be irregular based on the relative differences in storey structural properties. Regularity limits are set in codes, which determine the analysis method permitted to be used. Such regularity limits are based on heuristic thinking and lack rational justification (Sadashiva *et al.* 2009). For

example, the present New Zealand seismic Standard, NZS 1170.5 (*Cl. 4.5.1*, SNZ 2004), defines stiffness and strength irregularities to exist in buildings if:

- The lateral stiffness of a storey is less than 70% of the stiffness of any adjacent storey, or less than 80% of the average stiffness of the three storeys above or below in the structure.
- The shear strength at a storey is less than 90% that in the storey above.

Although separate irregularity limits are defined for stiffness and strength irregularity, in many practical scenarios, a change in the storey stiffness is usually accompanied by a change in the storey strength. For example, when cross-sectional property is changed at a storey, stiffness and strength at that storey are modified together.

Research on the effects of plan irregularity (e.g., Rutenberg (2002), Chopra and Goel (2004), De Stefano and Pintucchi (2006)) has received more attention than the vertical irregularity effects. Earlier studies on the influence of vertical stiffness and strength irregularity on the performance of structures have been summarised by Sadashiva *et al.* (2010). It includes studies by Valmundsson and Nau (1997), Al-Ali and Krawinkler (1998) and Fragiadakis *et al.* (2006). These previous works neither provide simple methods to determine regularity limits nor justify the suitability of the code regularity limits. The methods used in their designs may result in structures which do not meet the code criteria and they may have unrealistic strength-to-stiffness distribution. An effective methodology to determine vertical regularity limits was developed and applied on shear-type structures to evaluate the effects of vertical mass irregularity (Sadashiva *et al.* 2009). A study on the effects of coupled vertical stiffness-strength irregularity due to a change in member properties on realistic code-

complying structures was conducted (Sadashiva *et al.* 2010) using the same method. The method involved using the NZS 1170.5 *Equivalent Static* (**ES**) method to design both the regular and irregular structures to the same target drift, and comparing the actual drift demands from inelastic dynamic time-history analyses. Simple conservative equations, relating the magnitude of irregularity and the increase in drift demands due to irregularity were derived that could be used in the design. In this paper, the methodology is applied on structures having vertical stiffness-strength irregularity due to a change in interstorey height, and their coupled effects are evaluated. Other member properties are assumed to remain unchanged and equal that of regular structures. The study answers the following questions:

1. What stiffness-strength coupling is likely in realistic structures due to a modified storey height?
2. Which storey/storeys are sensitive to a reduced stiffness only/and strength change due to a taller storey?
3. How do the responses differ when a storey's height is decreased compared to other storeys?
4. How can we estimate the likely increase in response due to stiffness-strength irregularity caused by a modified interstorey height?

4.3 Structural Configuration for Regular Structures

Simple models of shear-type structures of 3, 5, 9 and 15 storeys, having uniform mass at every floor, and with equal storey height of 4m, were used to define the regular (base) structures. Each regular structure was assumed to be located in Wellington, and

was designed according to the NZ 1170.5 ES method. All the structures were designed for structural ductility factors of 1, 2, 3, 4 and 6. A complete description on the design approach adopted in this study is explained in Sadashiva *et al.* (2009).

In order to have an appropriate comparison between regular and irregular structures, each regular design model was provided with storey strengths such that a constant strength to stiffness ratio was maintained at all the storeys. Any structure having its storey strength to scaled stiffness ratio outside the range of 0.3% - 3% was eliminated from this study. Also, structures having the horizontal design action coefficient, $C_d(T_1)$, governed by the lower limit (*Equation 5.2(2) - Cl. 5.2.1.1*, NZS 1170.5) were ignored [11].

Two classes of regular structures were assumed to define the bounds within which the realistic structures are assumed to have their configuration. The two model types are shown in Figure 4-2. The structures were provided with:

(a) Decreasing stiffness distribution over the height, with iterations carried out until all storeys simultaneously achieved the *design* (target) *interstorey drift ratio* (**DISDR**). Henceforth, this design model is referred as **CISDR** for *constant interstorey drift ratio*. Since a constant strength to stiffness ratio was obtained for CISDR design models at the end of iteration, the shear strength provided at each storey was the minimum required to resist the equivalent static design forces.

(b) Uniform stiffness distribution up the height, with iterations conducted until the first storey (critical) achieved the target interstorey drift ratio. The minimum shear strength required to resist the design force at the first storey was provided for all storeys, thus producing a constant strength to stiffness ratio at all the storeys.

Henceforth, this design model will be referred as **CS-CSTG** for *constant stiffness* and *constant strength*.

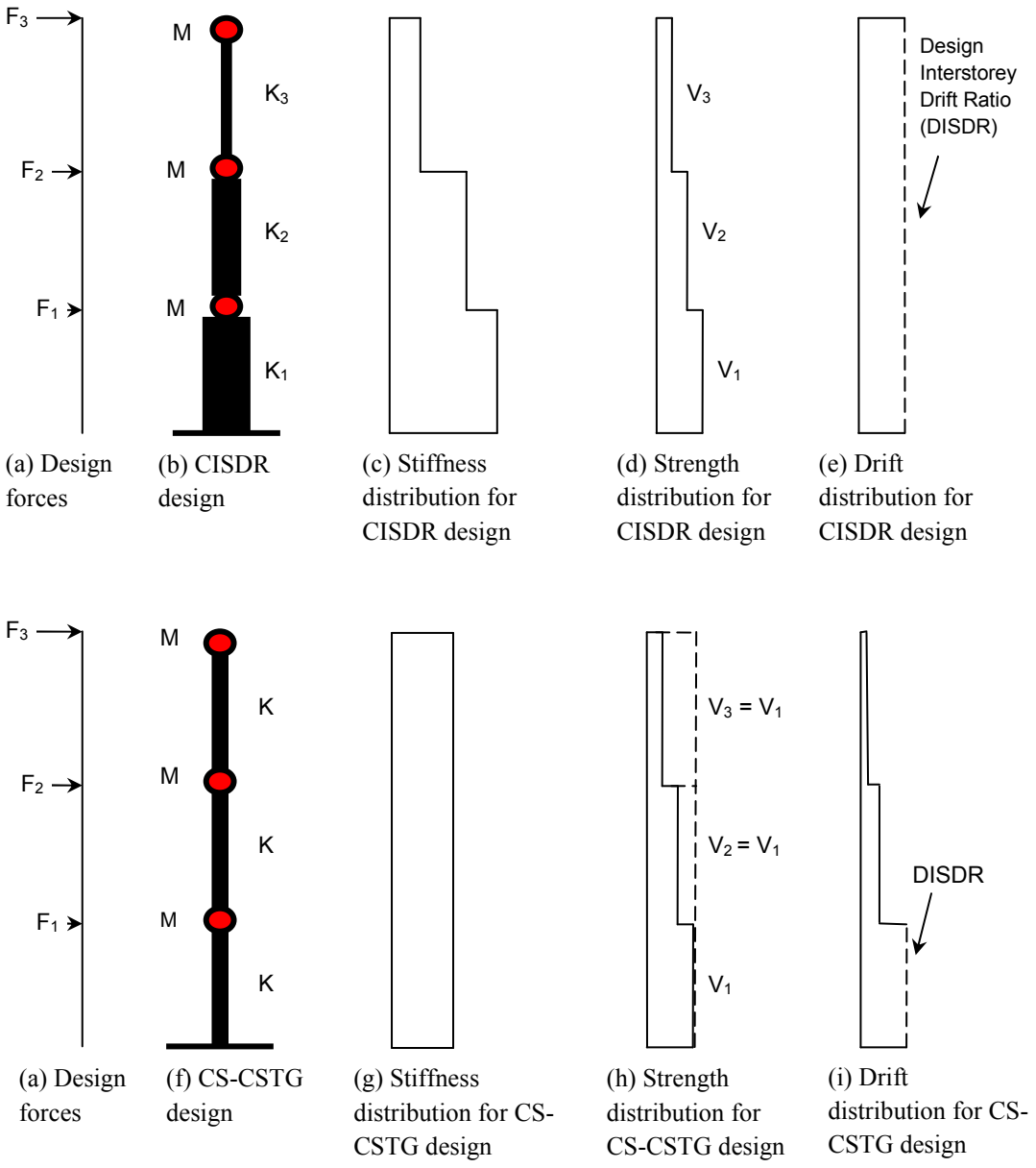

Figure 4-2: Structural configurations defining regular structures.

4.4 Correlations between Storey Stiffness and Strength Due to Modification to a Storey Height

A change in interstorey height from h_o to h_m results in a change in storey stiffness. Relationships between the storey stiffness and strength due to a modified interstorey height can be obtained for various types of *lateral-force-resisting* (**LFR**) systems, as given in Table 4-1. Here, the modified lateral stiffness at a chosen storey, $\boldsymbol{K_{hm}}$, is given by Equation (4-1) as the product of the *stiffness modification factor* corresponding to the LFR system, $\boldsymbol{\beta_{k\text{-}LFR}}$, and the initial lateral stiffness at the chosen storey, $\boldsymbol{K_o}$. The corresponding storey strength may remain unchanged, as for a non-buckling steel shear wall, or vary proportionally with stiffness, as for a braced frame, or vary by differing amounts, as for moment frames. Hence, similar to Equation (4-1), the modified storey strength, $\boldsymbol{V_{hm}}$, at the storey with modified interstorey height, is given by Equation (4-2) as the product of *strength modification factor* corresponding to the LFR system, $\boldsymbol{\beta_{v\text{-}LFR}}$, and the initial storey strength provided for the storey, $\boldsymbol{V_o}$. Thus, a total of four groups with the above correlations between storey stiffness and strength are formed that define the types of irregular structures that are used in this paper to evaluate their coupled effects. In Equations (4-1) and (4-2), the modification factors are functions of the parameter *interstorey height ratio*, $\boldsymbol{h_{rat}}$, which is defined by Equation (4-3) as the ratio of modified interstorey height, $\boldsymbol{h_m}$, to the initial interstorey height, $\boldsymbol{h_o}$.

$$K_{hm} = \beta_{k-LFR} * K_o \tag{4-1}$$

$$V_{hm} = \beta_{v-LFR} * V_o \tag{4-2}$$

$$h_{rat} = \left(\frac{h_m}{h_o} \right) \tag{4-3}$$

The sensitivity of the magnitude of coupled stiffness-strength irregularities on the response of structures were investigated by choosing a set of h_{rat} that resulted in cases of stiffness reduction or enhancement at the storey with the modified interstorey height. For each h_{rat}, the stiffness and strength modification factors were calculated and applied to obtain the modified properties. The modification factors used in this study, calculated for each group and for the set of h_{rat}, are tabulated in Table 4-2. The ratio of $\beta_{v\text{-}LFR}$ to $\beta_{k\text{-}LFR}$ ranges from unity to h^2_{rat} depending on the system. For the values of h_{rat} chosen in this paper, this ratio of modification factors range between 0.25 and 9.

Table 4-1a: Modified storey stiffness due to modified interstorey height

Lateral-force-resisting (LFR) system	Modified storey stiffness, K_{hm}
(a) ***Non-buckling Steel Shear Wall – Group 1*** 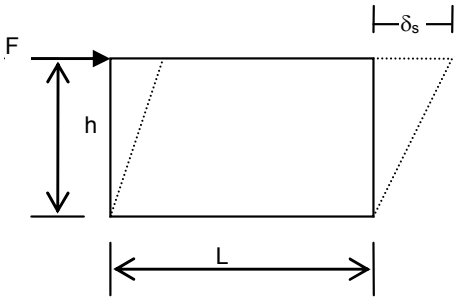 Stiffness, $K = \frac{G A_s}{h}$	$\frac{K_{hm}}{K_o} = \left(\frac{G A_s}{h_m}\right) * \left(\frac{h_o}{G A_s}\right)$ $K_{hm} = \left(\frac{h_o}{h_m}\right) * K_o$ $K_{hm} = \left(\frac{1}{h_{rat}}\right) * K_o$ $K_{hm} = \beta_{k-1} * K_o$
(b) ***Moment Frame (strong column weak beam mechanism) – Group 2*** 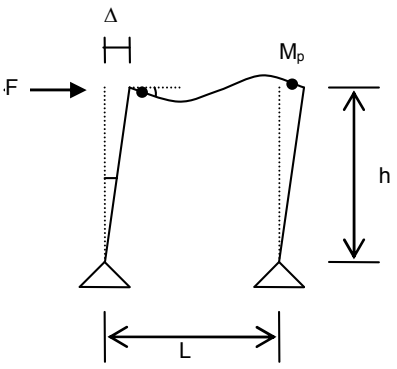 Stiffness, $K = \frac{6 E I}{L h^2}$	$\frac{K_{hm}}{K_o} = \left(\frac{6 E I}{L h_m^{\,2}}\right) * \left(\frac{L h_o^{\,2}}{6 E I}\right)$ $K_{hm} = \left(\frac{h_o}{h_m}\right)^2 * K_o$ $K_{hm} = \left(\frac{1}{h_{rat}}\right)^2 * K_o$ $K_{hm} = \beta_{k-2} * K_o$

(c) ***Moment Frame (strong beam weak column mechanism) – Group 3***

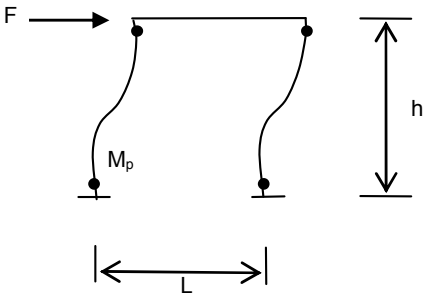

Stiffness, $K = \dfrac{12\,E\,I}{h^3}$

$$\frac{K_{hm}}{K_o} = \left(\frac{12\,E\,I}{h_m{}^3}\right) * \left(\frac{h_o{}^3}{12\,E\,I}\right)$$

$$K_{hm} = \left(\frac{h_o}{h_m}\right)^3 * K_o$$

$$K_{hm} = \left(\frac{1}{h_{rat}}\right)^3 * K_o$$

$$K_{hm} = \beta_{k-3} * K_o$$

(d) ***Braced Frame – Group 4***

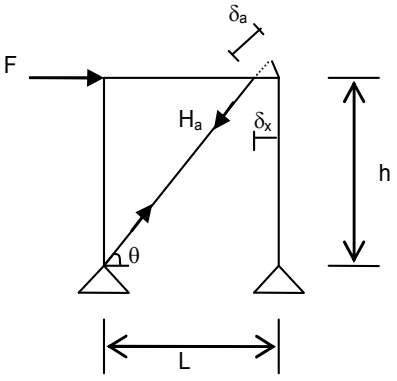

Stiffness, $K = \dfrac{A_a\ E}{\sqrt{L^2 + h^2}}$

$$\frac{K_{hm}}{K_o} = \left(\frac{A_a\ E}{\sqrt{L^2 + h_m{}^2}}\right) * \left(\frac{\sqrt{L^2 + h_o{}^2}}{A_a\ E}\right)$$

$$K_{hm} = \left(\frac{\sqrt{L^2 + h_o{}^2}}{\sqrt{L^2 + h_m{}^2}}\right) * K_o$$

$$K_{hm} = \left(\frac{\sqrt{L^2 + h_o{}^2}}{\sqrt{L^2 + \left(h_{rat} * h_o\right)^2}}\right) * K_o$$

$$K_{hm} = \beta_{k-4} * K_o$$

Table 4-1b: Modified storey strength due to modified interstorey height

Lateral-force-resisting (LFR) system	Modified storey strength, V_{hm}
(a) ***Non-buckling Steel Shear Wall – Group 1*** 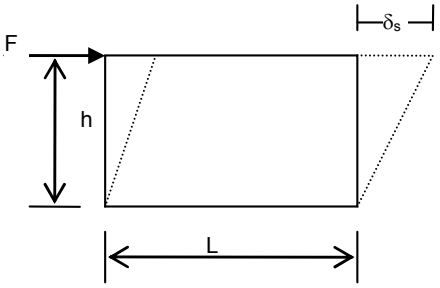 Strength, $V = \frac{A_s \sigma_y}{\sqrt{3}}$	$\frac{\left(V_{hm} / K_{hm}\, h_m\right)}{\left(V_o / K_o\, h_o\right)} = \left(\frac{\sigma_y}{G\sqrt{3}}\right) * \left(\frac{G\sqrt{3}}{\sigma_y}\right)$ $V_{hm} = \left(\frac{K_{hm}}{K_o}\right) * \left(\frac{h_m}{h_o}\right) * V_o$ $V_{hm} = V_o$ $V_{hm} = \beta_{v-1} * V_o$
(b) ***Moment Frame (strong column weak beam mechanism) – Group 2*** 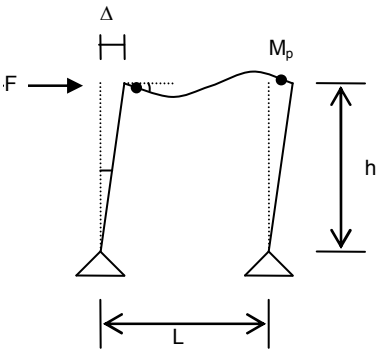 Strength, $V = \frac{M_p}{h}$	$\frac{\left(V_{hm} / K_{hm}\, h_m\right)}{\left(V_o / K_o\, h_o\right)} = 1$ $V_{hm} = \left(\frac{K_{hm}}{K_o}\right) * \left(\frac{h_m}{h_o}\right) * V_o$ $= \left(\frac{h_o}{h_m}\right)^2 * \left(\frac{h_m}{h_o}\right) * V_o$ $V_{hm} = \left(\frac{1}{h_{rat}}\right) * V_o$ $V_{hm} = \beta_{v-2} * V_o$

(c) ***Moment Frame (strong beam weak column mechanism) – Group 3***

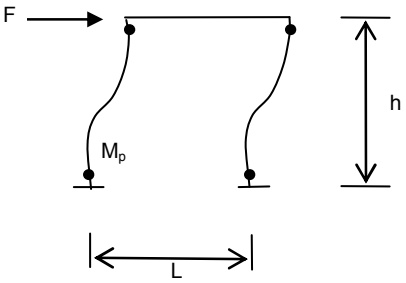

Strength, $V = \dfrac{2 M_p}{h}$

$$\frac{\left(V_{hm} / K_{hm}\, h_m\right)}{\left(V_o / K_o\, h_o\right)} = \left(\frac{h_m}{h_o}\right)$$

$$V_{hm} = \left(\frac{K_{hm}}{K_o}\right) * \left(\frac{h_m}{h_o}\right)^2 * V_o$$

$$= \left(\frac{h_o}{h_m}\right)^3 * \left(\frac{h_m}{h_o}\right)^2 * V_o$$

$$V_{hm} = \left(\frac{1}{h_{rat}}\right) * V_o$$

$$V_{hm} = \beta_{v-3} * V_o$$

(d) ***Braced Frame – Group 4***

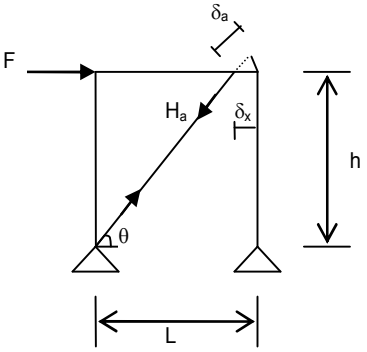

Strength, $V = \dfrac{A_a\, \sigma_y\, L}{\sqrt{L^2 + h^2}}$

$$\frac{\left(V_{hm} / K_{hm}\, h_m\right)}{\left(V_o / K_o\, h_o\right)} = \left(\frac{\varepsilon_y\, L}{h_m}\right) * \left(\frac{h_o}{\varepsilon_y\, L}\right)$$

$$V_{hm} = \left(\frac{K_{hm}}{K_o}\right) * V_o$$

$$V_{hm} = \left(\frac{\sqrt{L^2 + {h_o}^2}}{\sqrt{L^2 + \left(h_{rat} * h_o\right)^2}}\right) * V_o$$

$$V_{hm} = \beta_{v-4} * V_o$$

Table 4-2a: Stiffness modification factors due to modified interstorey height.

Group	Stiffness modification factor, β_k	Interstorey height ratio, h_{rat}							
		0.5	**0.75**	**1.25**	**1.5**	**1.75**	**2**	**2.5**	**3**
1	$\left(\frac{1}{h_{rat}}\right)$	2	1.33	0.8	0.67	0.57	0.5	0.4	0.33
2	$\left(\frac{1}{h_{rat}}\right)^2$	4	1.78	0.64	0.44	0.327	0.25	0.16	0.11
3	$\left(\frac{1}{h_{rat}}\right)^3$	8	2.37	0.512	0.3	0.187	0.125	0.064	0.036
4	$\left(\frac{\sqrt{L^2+h_o^{\,2}}}{\sqrt{L^2+\left(h_{rat} * h_o\right)^2}}\right)$	1.14	1.07	0.92	0.85	0.782	0.72	0.62	0.54

Table 4-2b: Strength modification factors due to modified interstorey height.

Group	Strength modification factor, β_v	Interstorey height ratio, h_{rat}							
		0.5	**0.75**	**1.25**	**1.5**	**1.75**	**2**	**2.5**	**3**
1	1	1	1	1	1	1	1	1	1
2	$\left(\frac{1}{h_{rat}}\right)$	2	1.33	0.8	0.67	0.57	0.5	0.4	0.33
3	$\left(\frac{1}{h_{rat}}\right)$	2	1.33	0.8	0.67	0.57	0.5	0.4	0.33
4	$\left(\frac{\sqrt{L^2+h_o^{\,2}}}{\sqrt{L^2+\left(h_{rat} * h_o\right)^2}}\right)$	1.14	1.07	0.92	0.85	0.78	0.72	0.62	0.54

4.5 Applying Coupled Stiffness and Strength Irregularities

The effect of coupled stiffness-strength over the height of the structures was conducted by applying the irregularities separately at the first storey, mid-height storey and at the topmost storey of regular structures. This was done by modifying the interstorey height by h_{rat} at the chosen storey for irregularity. The resulting storey stiffness and strength were obtained for structures with the range of stiffness and strength modification factors according to Table 4-1 for the particular h_{rat}. The modified structure was then redesigned until the target interstorey drift ratio was achieved at the critical storey/storeys. For example, as shown in Figure 4-3, consider a regular 3 storey CS-CSTG structure having stiffness distribution resulting in a target interstorey drift ratio (DISDR) of 1% at the first storey. If it is intended to have a taller third storey, the third storey height is modified by h_{rat}. This change in storey height will result in corresponding storey stiffness to be modified. Therefore, the stiffness at that storey is multiplied by stiffness modification factor, β_k, by an amount corresponding to h_{rat} and the group of LFR system (see Tables 4-1a and 4-2a). Upon making this change in storey stiffness, the critical storey would no longer have the chosen DISDR. Therefore, all storey stiffnesses are then uniformly scaled by a scaling factor, λ, and the irregular structure is redesigned until the chosen DISDR is achieved at the critical storey/storeys. Since all storey stiffnesses are uniformly scaled, at the end of iteration, the irregular structure would still maintain the applied β_k at the chosen storey, which is third storey in this example. However, the relative storey stiffnesses at other storeys remain unchanged. To have a meaningful comparison between regular and irregular structures, the strength to stiffness ratios at all the storeys other than the irregular storey were kept the same. Therefore, the shear

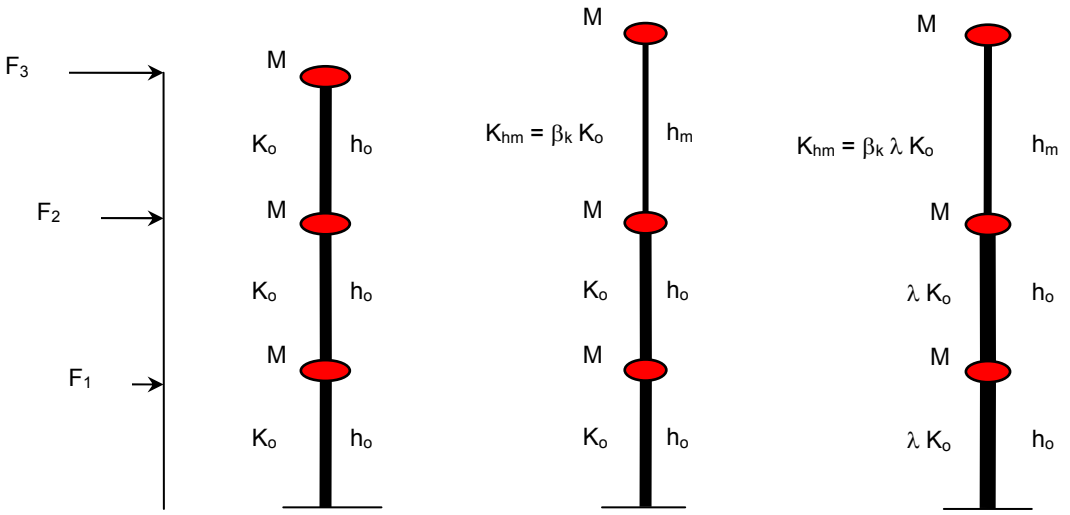

(a) Design forces

(b) Regular CS-CSTG design with DISDR at first storey

(c) Introducing stiffness modification at third storey

(d) Irregular structure with DISDR at critical storey

Figure 4-3: Stiffness irregularity introduced by modifying the interstorey height for CS-CSTG design.

strengths provided over the height of irregular structures were different from the strength demand. Here, the modified strength at the chosen storey for irregularity was provided according to Equation (4-2), and multiplied by the λ factor. In Equation (4-2), $\beta_{v\text{-}LFR}$ is the strength modification factor having a value corresponding to h_{rat} and the group of LFR system (see Tables 4-1b and 4-2b). The strengths at other storeys were provided as the product of λ factor and the corresponding regular storey strength.

Note: The modified structure design ductility from this process was different from the target design ductility implying that the final drifts were not identical to those obtained with the target ductility. However, the difference in ductility and drifts was always less than 1.2%, and it was generally much smaller than this value. It was considered that this was not enough to significantly affect the results.

4.6 Structural Modelling and Analysis

Shear type models represented all the vertical lateral force resisting systems in Table 4.1. All the structures were modelled as a combination of vertical shear and a vertical flexural beam. The flexural column, which represents all of the continuous columns in the structure, is necessary to be included, without which high drift concentrations can be expected (e.g., MacRae *et al*. 2004, Tagawa *et al*. 2004, Tagawa *et al*. 2006, Sadashiva *et al.* (2009)). The stiffness of the flexural beam relative to the shear beam at the i^{th} floor level was computed using Equation (2-4), using a continuous column stiffness ratio, α_{cci} (MacRae *et al.* 2004), of 0.5 for all the storeys. It should be mentioned here that in actual structures α_{cci} tends to be between 0.13 and 1.58; however, the drift demands around this value are not sensitive to a change in α_{cci} (Tagawa 2005). Therefore the choice of $\alpha_{cci} = 0.5$ for all the storeys was assumed to be appropriate for this study.

Rayleigh damping has commonly been adopted to represent damping effects within multi-degree-of-freedom structures for several decades. A sensitivity study by Sadashiva *et al.* (2009) on the effects of different types of Rayleigh damping model show that the differences in drift responses due to three types of Rayleigh damping models available in RUAUMOKO (Carr 2004) time-history program were minimal. However, the tangent stiffness proportional Rayleigh damping model that uses the absolute form of equation of motion was considered to be more appropriate than other types of Rayleigh damping, to be used in IDTHA. Such a damping model that considers the non-linearity effects of structures, also assures that the damping forces go to zero at the end of excitation, and hence it has been used for all IDTHA

conducted in this work. In order to avoid super-critical damping or negative damping, the first mode and the mode corresponding to number of storeys in the structure (Carr 2004) were nominated as the two modes with 5% of critical damping. The RUAUMOKO computer program was used to carry out all the IDTHA considering a post elastic stiffness (bilinear) factor of 1%. For the time-history analyses, the Newmark Constant Average Acceleration integration scheme, with a time-step of 0.001s, was used.

A set of 20 SAC (SEAOC-ATC-CUREE) earthquake ground motion records for Los Angeles, with probabilities of exceedance of 10% in 50 years, were used for the ground motion suite. Response spectra were developed for each of the selected records and the accelerations within each record were scaled so that the single-degree-of-freedom elastic response matched the NZS 1170.5 design acceleration considering a structural ductility factor and a structural performance factor of unity [11].

4.6.1 Interpretation of Inelastic Dynamic Time-History Analysis Results

The peak *interstorey drift ratio* (**ISDR**) from all the storeys within the structure, from any earthquake record, was obtained. This was obtained for each of the 20 records used. Here, the distribution of ISDR was assumed to follow a lognormal distribution (Cornell *et al*. 2002), so the median results, calculated according to Equation (4-4), were used for response comparison.

$$\hat{x} = e^{\left(\frac{1}{n}\sum_{i=1}^{n}\ln(x_i)\right)} \qquad (4\text{-}4)$$

where x_i = peak interstorey drift ratio due to i^{th} record; and

n = total number of earthquake records considered.

4.6.2 Comparison between Regular And Irregular Structures – Effect Of Magnitude and Location of Modified Interstorey Height Ratio

The median peak interstorey drift ratio (ISDR) obtained for each irregular structure was compared with the corresponding median peak ISDR of the regular structure. The change in median peak ISDR due to the presence of coupled stiffness-strength irregularity was used to show the effects of irregularity. The response plot labels in the following figures have the format "N-L (Q)", where N refers to the number of storeys in the structure, L refers to the location (storey) of h_{rat}, and Q defines the magnitude of interstorey height ratio, h_{rat}. As explained earlier, structures having unrealistic storey strength to scaled stiffness ratios and/or having the base shear governed by the code lower limit, were eliminated from this study. Hence, many designs for Group 2-4 structures, and some of the response plots in Figures 4-4 and 4-5 for Group 1 structures, were eliminated due to these two conditions imposed in the design.

4.6.2.1 Effect of Increased Interstorey Height and Reduced Storey Stiffness

The response plots for Group 1 CISDR and CS-CSTG designs are shown in Figures 4-4(a) and 4-4(b) respectively for cases of *increase* in interstorey height.

Figure 4-4(a) shows that for all DISDR when the first storey of 3 storey structures and the mid-height storey of taller structures were increased by h_{rat} of 1.5, the median peak ISDR increased relative to that for the corresponding regular structure. The

maximum median peak ISDR increase due to this magnitude of h_{rat} at the first storey was 28%, 0.6%, 1.5% and 1.7% respectively for 3, 5, 9 and 15 storey structures. An increased storey height at the middle storey increased the median peak ISDR by 10% for 3 storey structures and about 6% for 9 and 15 storey structures. For all DISDR, a taller storey at the topmost storey for all structures produced lesser drifts than for the regular structures. On average, the decrease in median peak ISDR due to irregularity at the roof was 7%, 6%, 4% and 3% for 3, 5, 9 and 15 storey structures respectively. As the interstorey height ratio was increased from 1.5 to a maximum of 3, the same response trends were seen for all structural heights.

Figure 4-4(b) shows that for Group 1 CS-CSTG designs, an increase in the first storey height by h_{rat} = 1.5, produced a maximum increase in median peak ISDR of 37% for 3 storey structures, whereas for other structures, the median peak ISDR decreased due to this h_{rat} by upto 4%. The increase in storey height of the topmost storey rather than the mid-height storey was most significant for 3 storey structures with DISDR = 0.5%, producing a maximum of 16% increase in the median peak ISDR over the regular structure, and for taller structures this increase in median peak ISDR was less than 2.5% for the same h_{rat} and DISDR. The responses of CS-CSTG designs were more sensitive to an increase in h_{rat} than CISDR designs. For h_{rat} = 3, the maximum median peak ISDR due to an increased storey height at the first storey for 3 storey structures was 40%, and for taller structures with this h_{rat} of 3 at the first storey, the responses closely matched with those of corresponding regular structures. The effects of an increased storey height by h_{rat} = 3 at the mid-height was more significant than due to irregularity at the topmost storey, producing respectively a maximum increase in median peak ISDR of 26%, 13% and 4% for 3, 9 and 15 storey irregular structures.

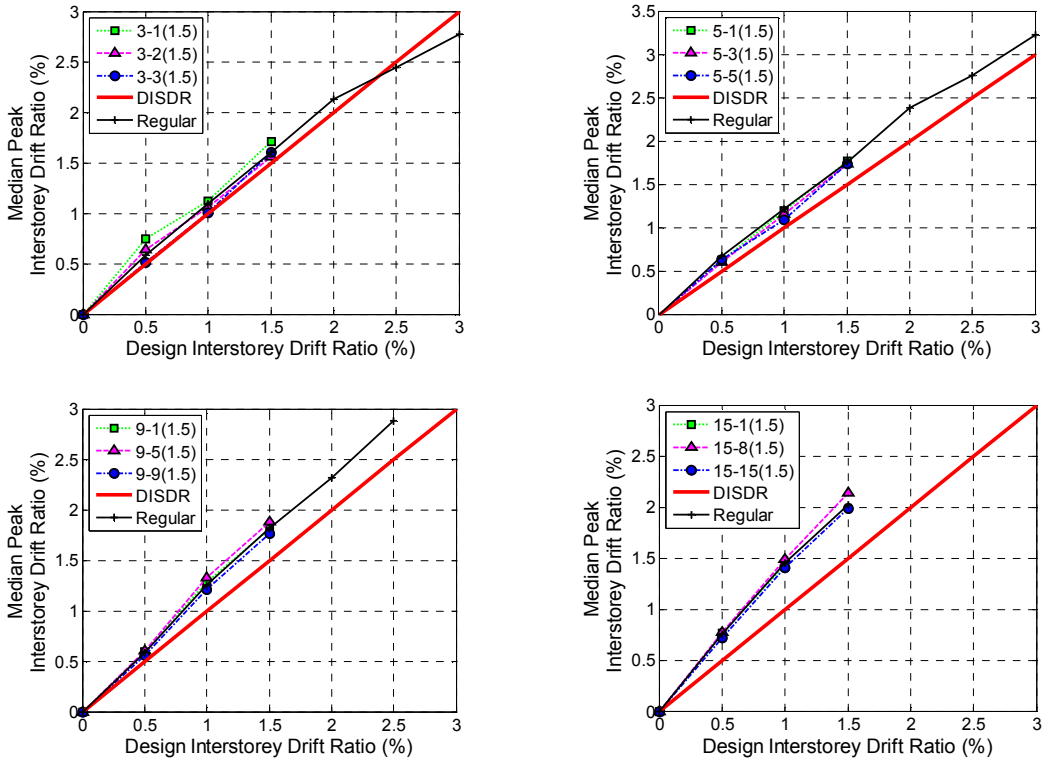

(1) $h_{rat} = 1.5$

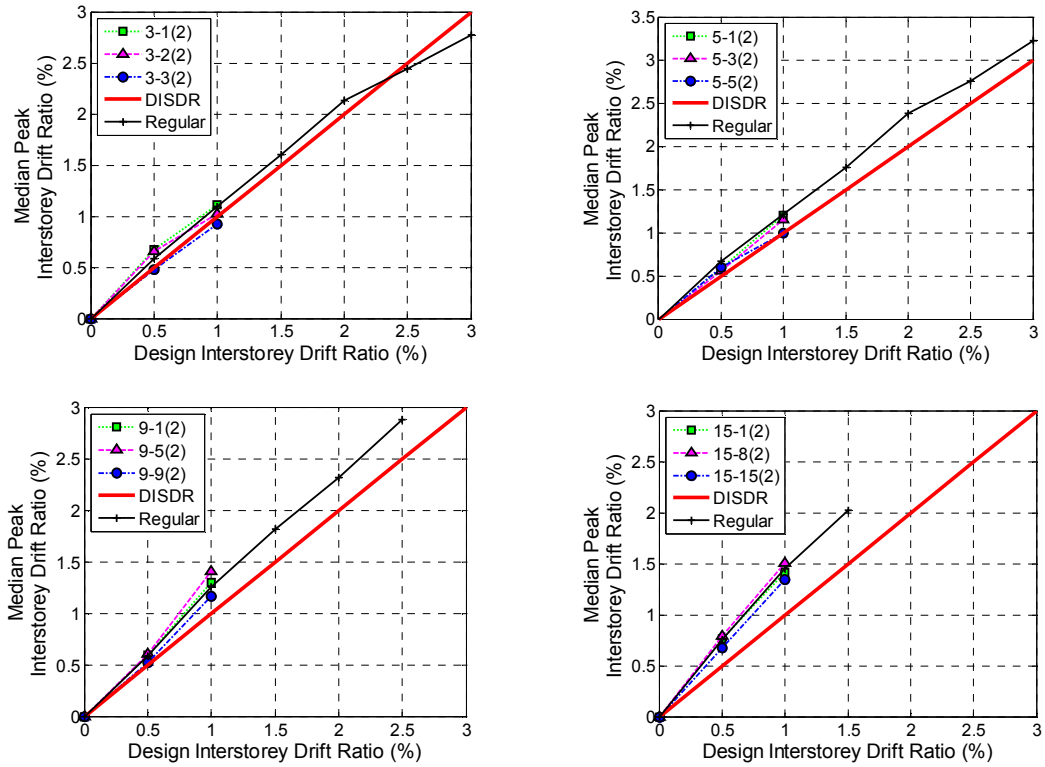

(2) $h_{rat} = 2$

Figure 4-4(a): Effect of increased interstorey height for Group 1 structures - CISDR design ($\mu = 3$, $Z = 0.4$): (1) $h_{rat} = 1.5$; and (2) $h_{rat} = 2$

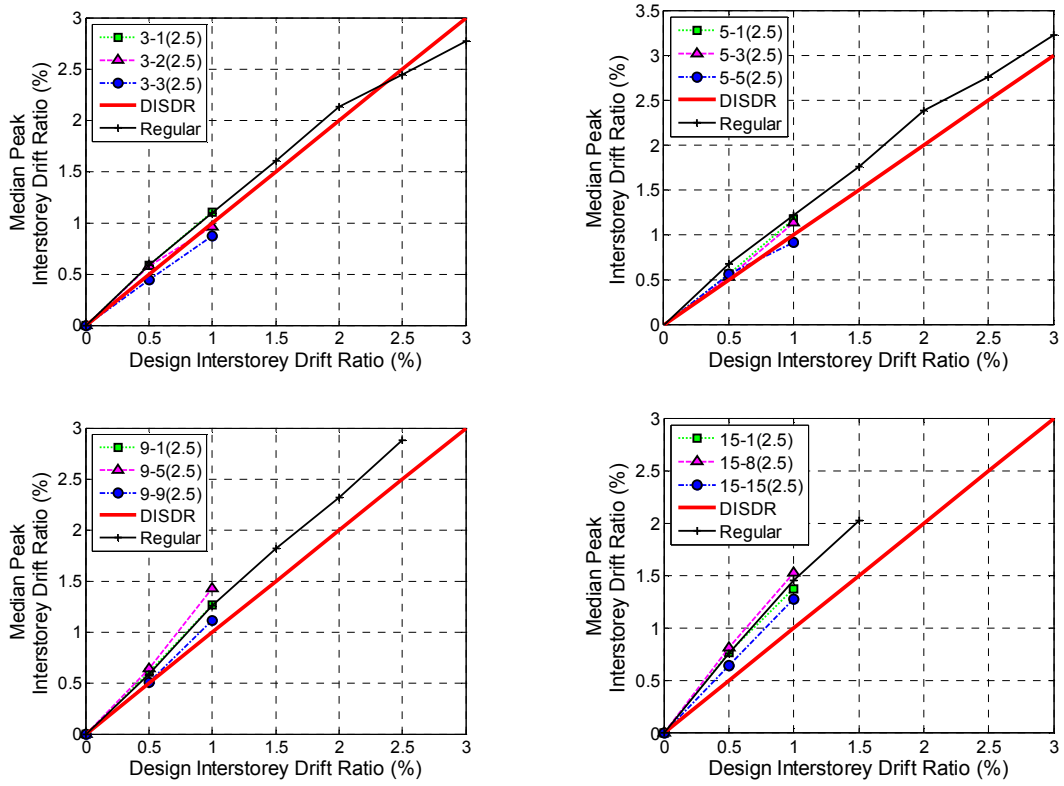

(3) $h_{rat} = 2.5$

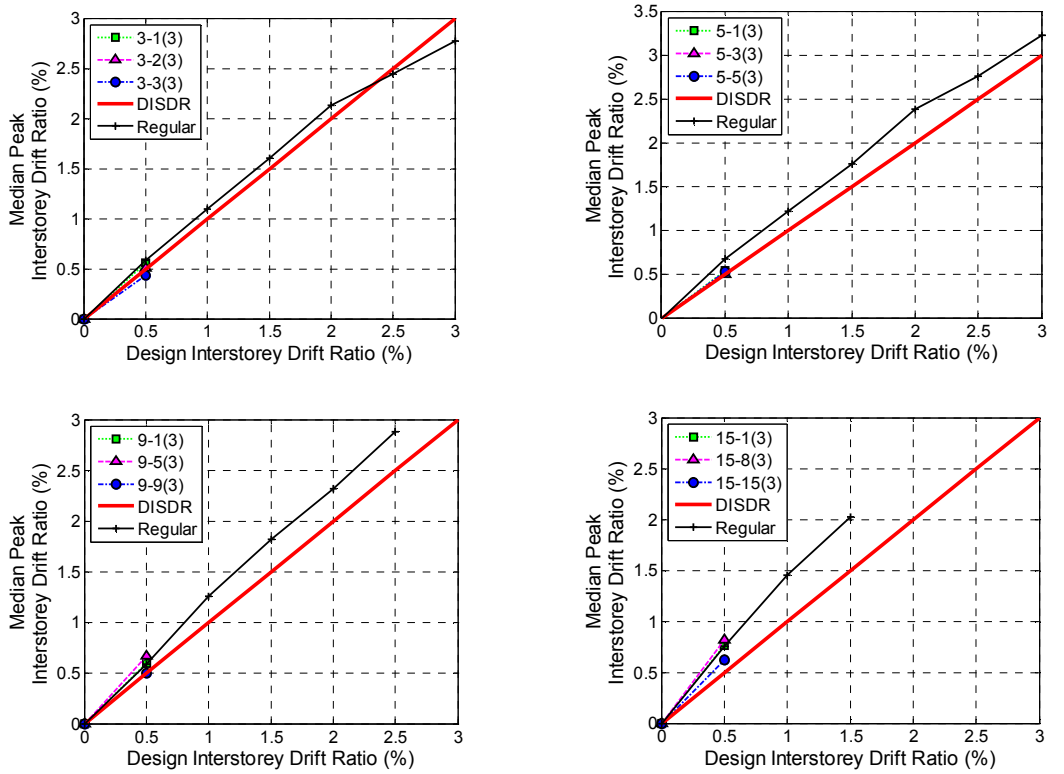

(4) $h_{rat} = 3$

Figure 4-4(a): Effect of increased interstorey height for Group 1 structures - CISDR design ($\mu = 3$, $Z = 0.4$): (3) $h_{rat} = 2.5$; and (4) $h_{rat} = 3$

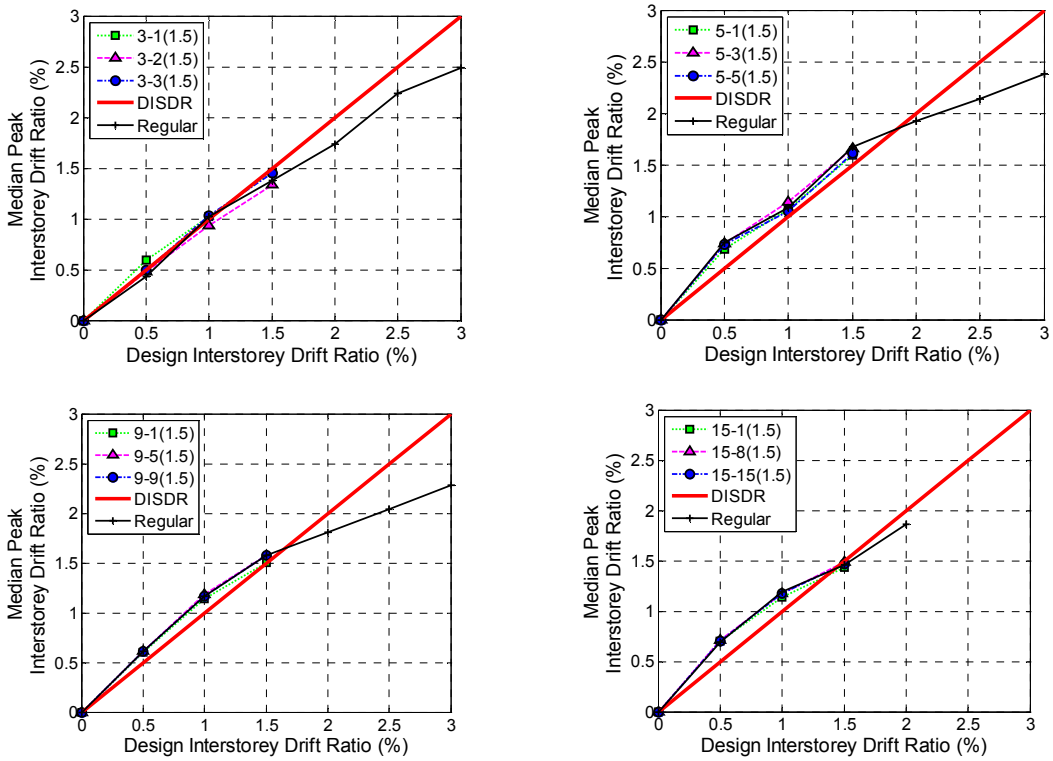

(1) $h_{rat} = 1.5$

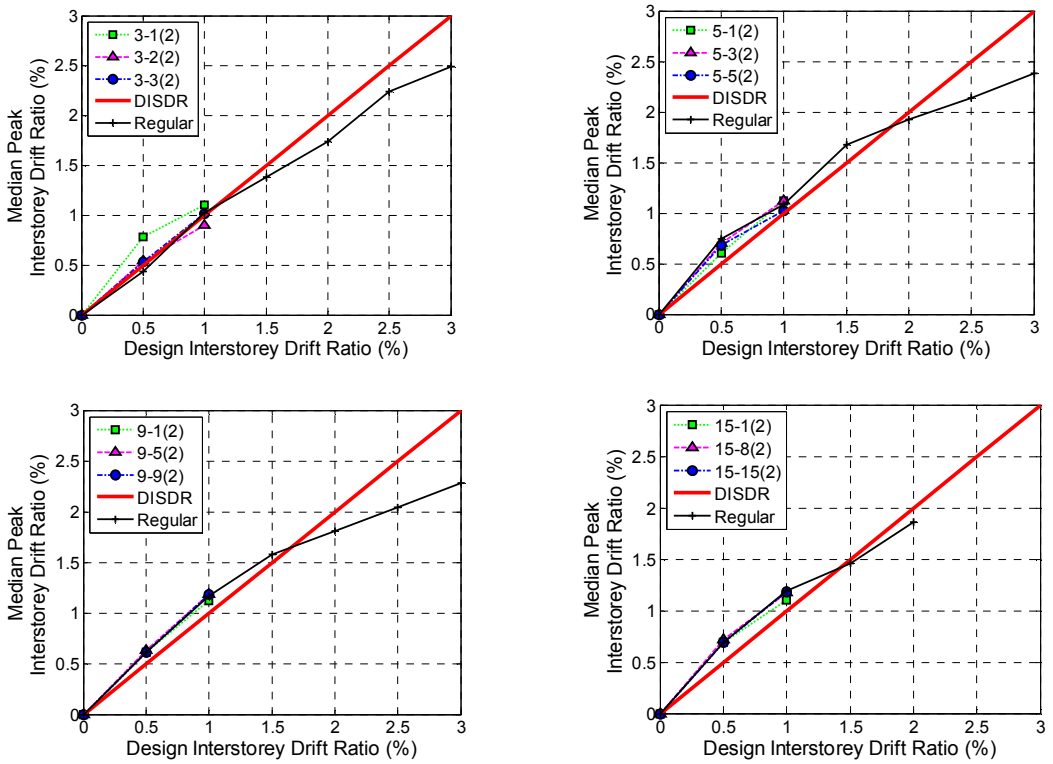

(2) $h_{rat} = 2$

Figure 4-4(b): Effect of increased interstorey height for Group 1 structures – CS-CSTG design ($\mu = 3$, $Z = 0.4$): (1) $h_{rat} = 1.5$; and (2) $h_{rat} = 2$

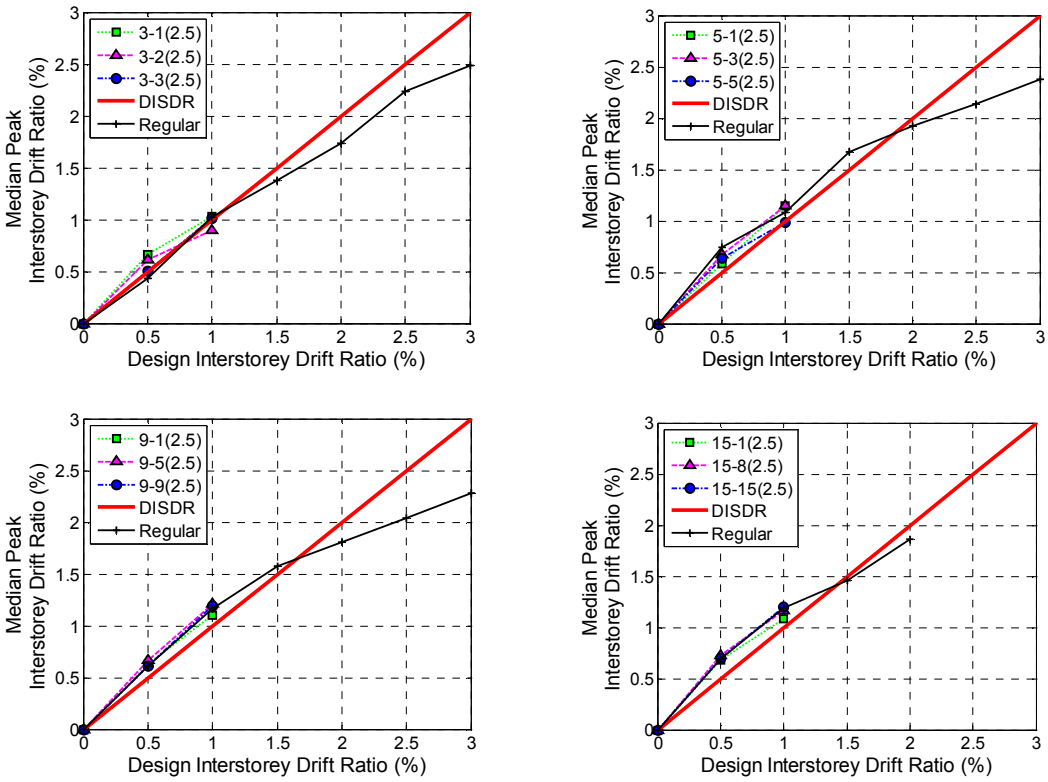

(3) $h_{rat} = 2.5$

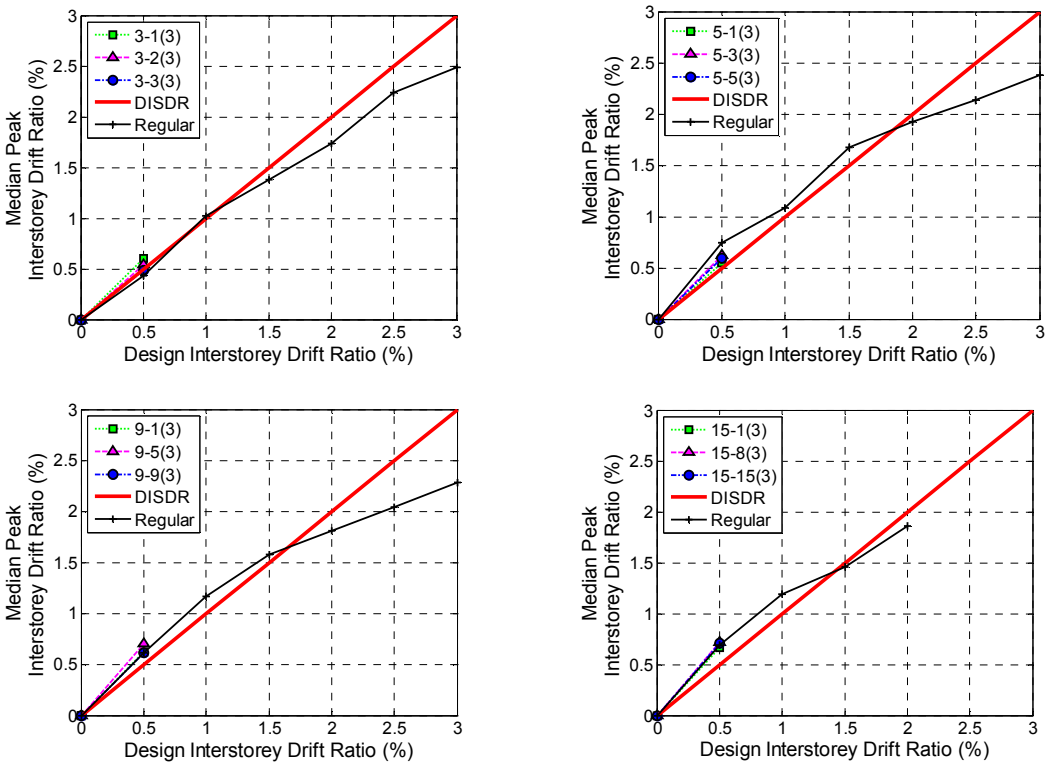

(4) $h_{rat} = 3$

Figure 4-4(b): Effect of increased interstorey height for Group 1 structures – CS-CSTG design ($\mu = 3$, $Z = 0.4$): (3) $h_{rat} = 2.5$; and (4) $h_{rat} = 3$

4.6.2.2 Effect of Decreased Interstorey Height and Increased Storey Stiffness

The effect of *decreased* interstorey height for Group 1 CISDR designs is shown in Figure 4-5(a). For h_{rat} = 0.75 at the first storey of any structure height, the regular structures generally have median peak ISDR higher than the irregular ones. It is the decreased storey height of the mid-height level for 3 storey structures, and the topmost storey for 9 and 15 storey high structures that has produced increased drifts over the regular structure. In case of 5 storey structures, irregularity at mid-height and topmost storey has resulted in increased drift demands. For h_{rat} = 0.75 at the mid-height of 3 and 5 storey structures, a maximum increase in median peak ISDR of 7% and 3% respectively was observed. There was an average decrease of 3% for taller structures with this magnitude of h_{rat} at the mid-height storey. The maximum increases in median peak ISDR due to a shorter topmost storey decreased with the structure height, and were 6%, 4%, 3% and 2% respectively for 3, 5, 9 and 15 storey irregular structures. The above effects also occurred for h_{rat} = 0.5, however with slightly higher magnitude.

In case of Group 1 CS-CSTG designs, as seen in Figure 4-5(b), the mid-height of 3 storey structure and the first storey of other structures with h_{rat} = 0.75, produces higher drift demands due to irregularity than the other two storeys chosen for irregularity. A maximum increase in median peak ISDR due to this h_{rat} at the first storey for 3 storey structures was 17%, and its magnitude decreased with the structure height. Here, increases in median peak ISDR of up to 10%, 5% and 3%, due to h_{rat} = 0.75 at the first storey of 5, 9 and 15 storey structures were respectively obtained. For h_{rat} = 0.75 at the mid-height storey, the increase in median peak ISDR was 22% for 3

storey structures, and less than 2% for 5, 9 and 15 storey irregular structures. Effects of irregularity at the topmost storey were insignificant for all structure heights, and the responses closely matched with the responses of the regular structures. Again, the above observations were generally the same when h_{rat} was decreased from 0.75 to 0.5.

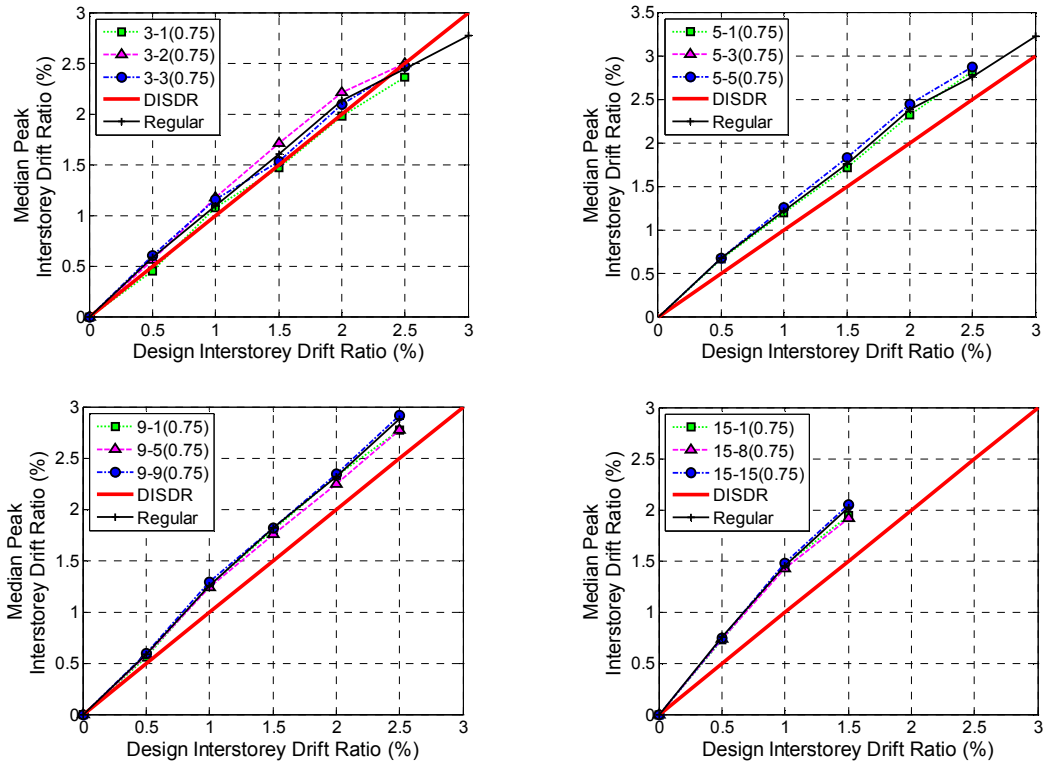

(a) CISDR Design - $h_{rat} = 0.75$

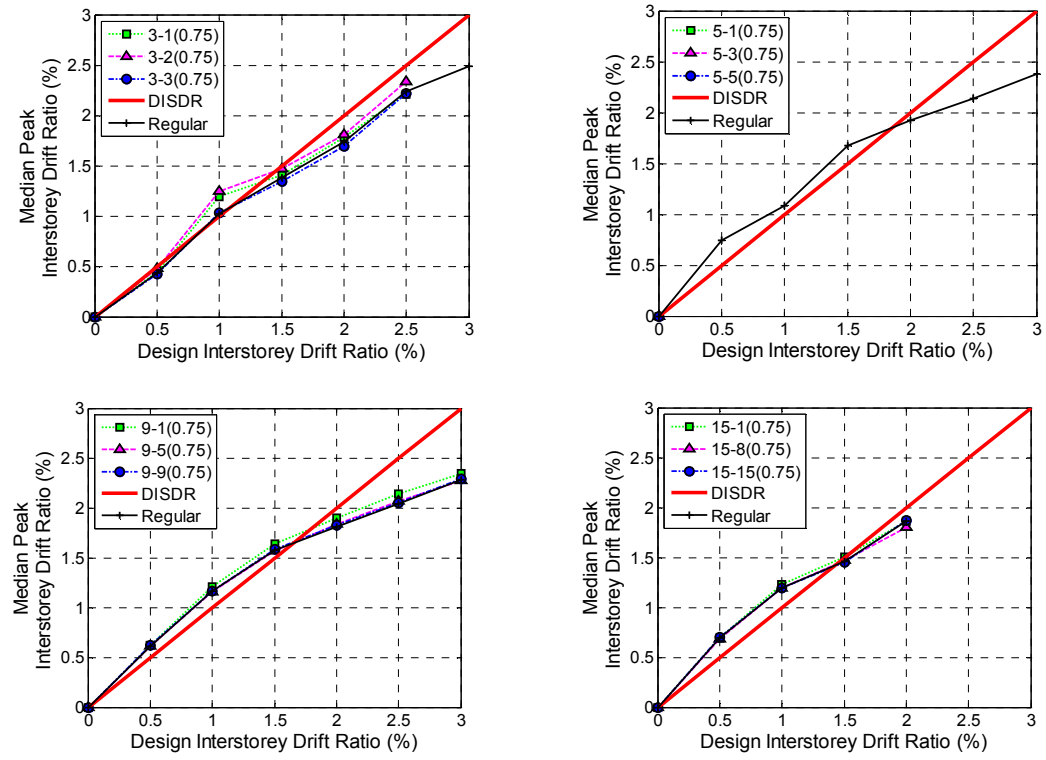

(b) CS-CSTG Design - $h_{rat} = 0.75$

Figure 4-5: Effect of decreased interstorey height for Group 1 CISDR and CS-CSTG structures ($\mu = 3$, $Z = 0.4$).

4.7 Determination of Allowable Interstorey Height Ratio

The relationship between *increase* in *median peak interstorey drift ratio*, $\boldsymbol{ISDR_{incr}}$, due to irregularity and magnitude of irregularity, was computed as below:

Step 1. For a combination of structural form, structural ductility factor, design interstorey drift ratio, structure height, and the storey with stiffness-strength irregularity, the median peak ISDR for the regular structure, $\boldsymbol{ISDR_R}$, and for the irregular structure, $\boldsymbol{ISDR_I}$, is computed from the results of the structure to the suite of records. The increase in median peak ISDR due to irregularity, $ISDR_{incr}$, is calculated by Equation (4-6).

$$ISDR_{incr} = \left(\frac{ISDR_I}{ISDR_R} - 1 \right) * 100 \ (\%) \qquad (4\text{-}6)$$

Step 2. Step 1 is repeated for all the combinations of structural form, structural ductility factor, design interstorey drift ratio, structure height, storey with stiffness-strength irregularity, and magnitude of irregularity.

Step 3. For each magnitude of irregularity, find the *maximum* value of $ISDR_{incr}$. This is labelled as $\boldsymbol{ISDR_{max\_incr}}$.

For example, Group 1 CS-CSTG structures having h_{rat} = 2 and μ = 3, produce $ISDR_{max\_incr}$ = 81.4% as shown in Figure 4-6(a). This maximum value of $ISDR_{incr}$ is obtained from a three storey structure with its first storey height modified and designed for DISDR = 0.5%. For this example, Figure 4-4(b) shows that the median peak ISDR for the regular structure, $ISDR_R$, is equal to 0.43%, and the median peak ISDR for the irregular structure, $ISDR_I$, is equal to 0.78%.

Figure 4-6 shows $ISDR_{max\_incr}$ plotted against interstorey height ratio, h_{rat}, for all the coupled stiffness-strength irregularity cases considered in this study. The figure shows that the group of structures having only storey stiffness modified due to a change in storey height produces higher increases in response due to irregularity than other groups. The figure also shows that generally the structures designed to have a uniform distribution of stiffness and strength (CS-CSTG), have greater increases in median peak ISDR due to h_{rat} than the structures designed to produce equal storey drifts (CISDR). However, the absolute responses of CISDR designs are greater than the CS-CSTG designs, as seen in Figures 4-4 and 4-5. This observation is consistent with the findings in studies of mass irregularity (Sadashiva *et al.* 2009) and coupled stiffness-strength irregularity due to modified member properties (Sadashiva *et al.* 2010).

Equation (4-7) is a simple equation that gives a measure of the likely increase in drift response due to modifications to a storey height. This equation is based on Group 1 structures, and it is very conservative for Group 2-4 structures and for those with irregularity at the non-critical storeys, as shown in Figure 4-6.

$$IRR = \left|100\left(h_{rat} - 1\right)\right| \% \qquad (4\text{-}7)$$

where ***IRR*** is the *irregular response ratio* which specifies how much the irregular response is greater than the regular response; and h_{rat} is the interstorey height ratio.

According to Figure 4-7, if it is not intended to have responses to be more than 20% due to change to a storey height, then the modified storey height cannot be less than 0.85, or more than 1.2 times the regular storey height. Equation (4-7) can also be used to calculate *IRR* values due to respective NZS 1170.5 stiffness and strength regularity

limits of 0.7 and 0.9. This is done by using the relation between stiffness-strength modification factors and h_{rat}, shown in Figure 4-6, and applying in Equation (4-7). The evaluated *IRR* values due to code stiffness and strength regularity limits are shown in Table 4-3. The governing code regularity limit for each group of structure is also shown in the table by the corresponding *IRR* values in bold.

It should be noted here that; while Equation (4-7) provides *IRR* for a given h_{rat}, alternative *IRR* expressions can be developed using the coupled stiffness-strength relations. Appendix H shows the development of *IRR* equations as a function of stiffness modification factor.

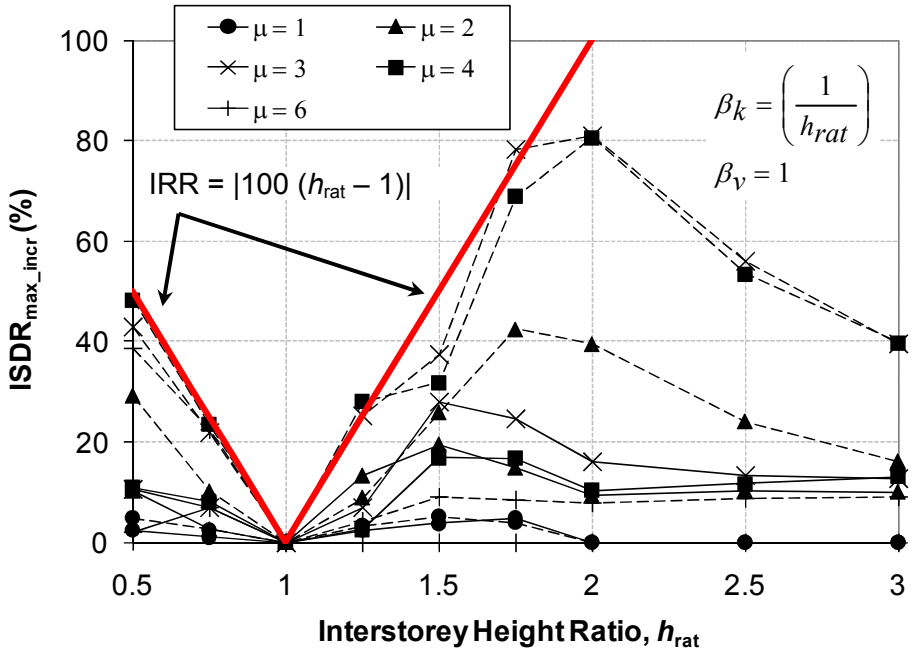

(1) Group 1

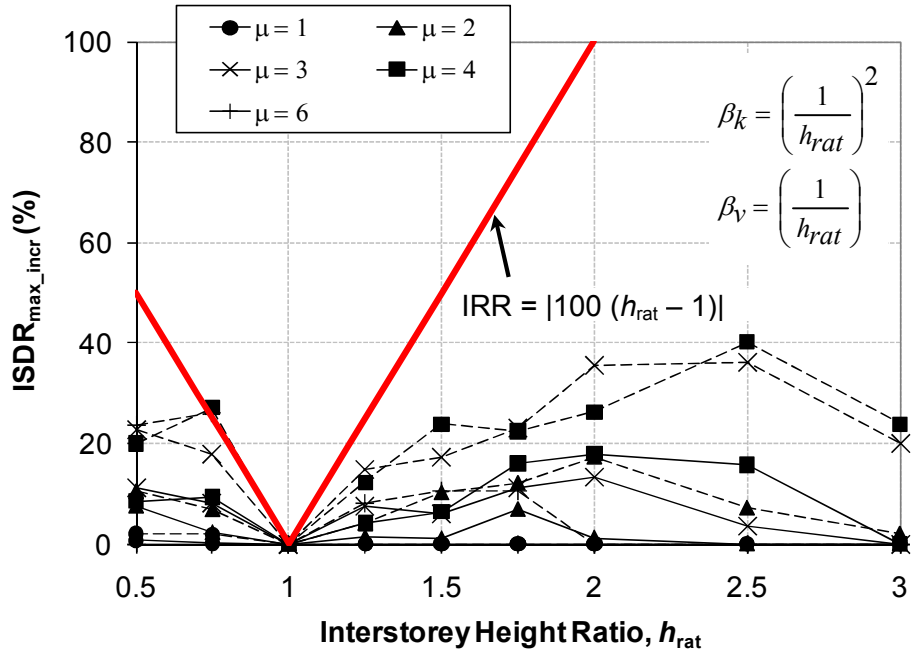

(2) Group 2

Figure 4-6(a): Maximum increase in median peak ISDR due to modified interstorey height – Group 1 and Group 2 structures.

(CISDR —— CS-CSTG - - - - -)

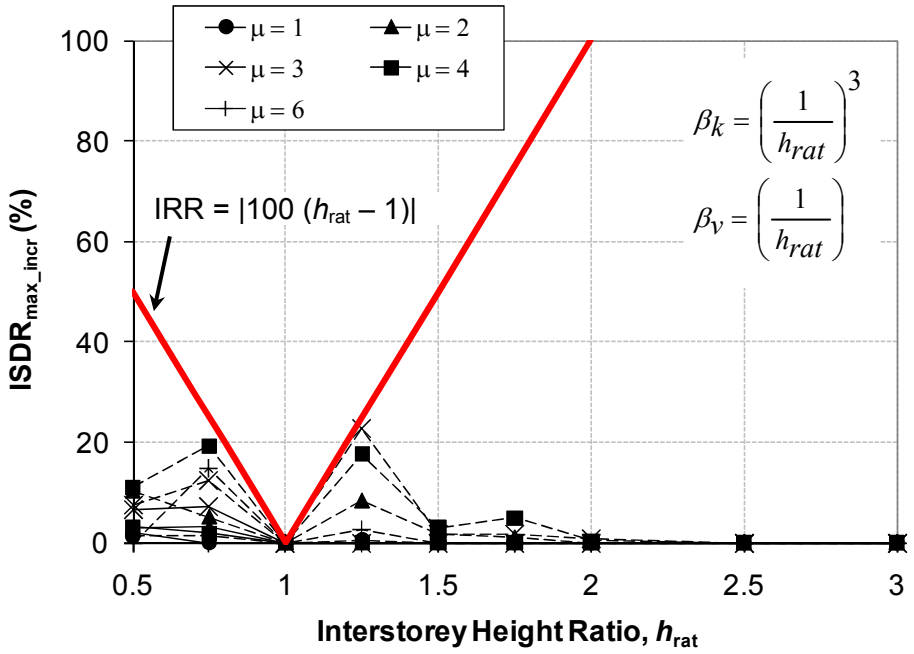

(1) Group 3

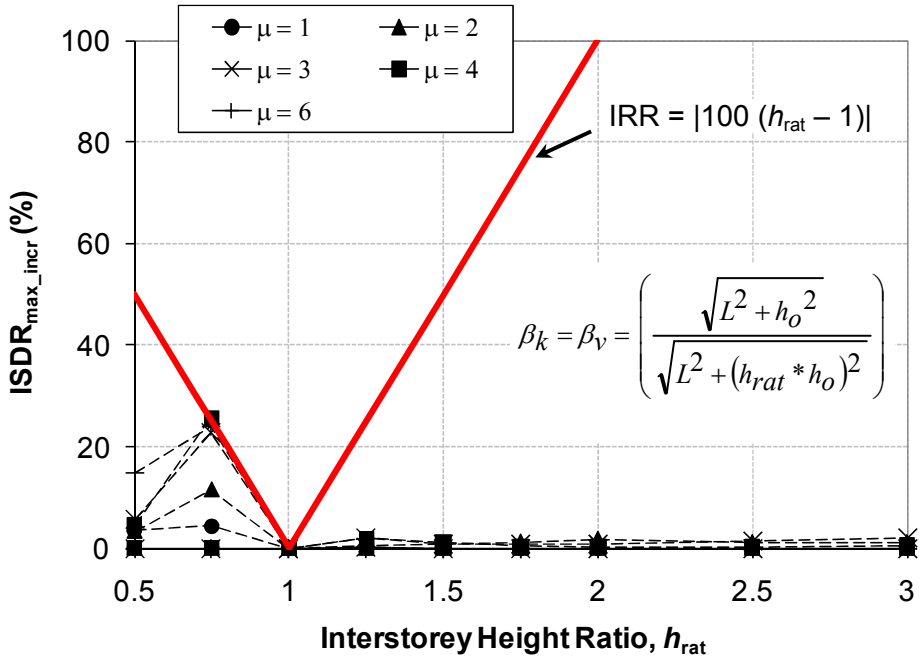

(2) Group 4

Figure 4-6(b): Maximum increase in median peak ISDR due to modified interstorey height – Group 3 and Group 4 structures.

(CISDR —— CS-CSTG - - - - -)

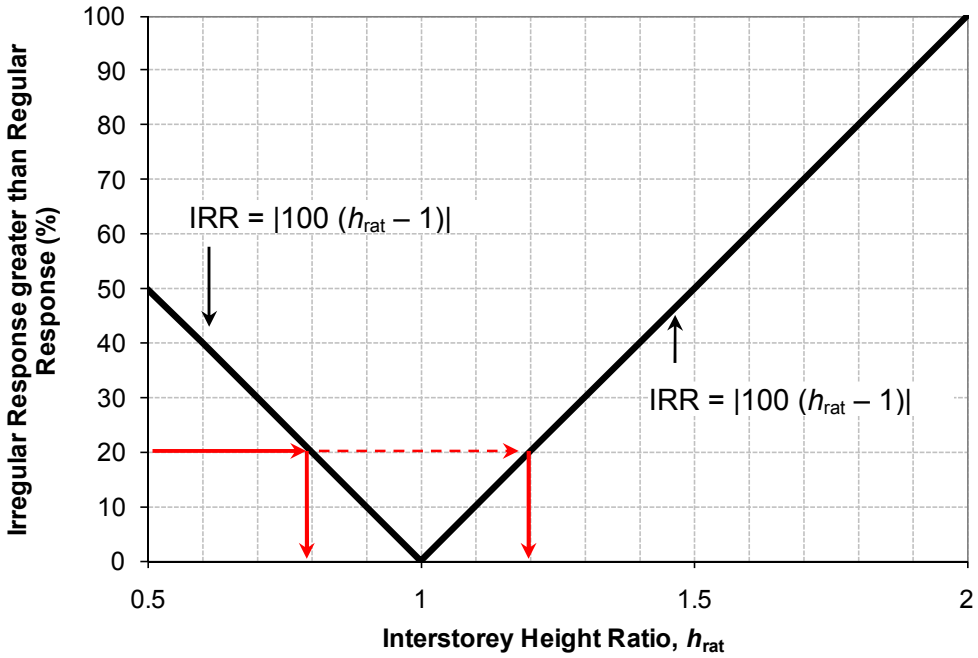

Figure 4-7: Determination of allowable interstorey height ratio

Table 4-3: Irregular Response Ratio (IRR) (%) due to NZS 1170.5 stiffness and strength regularity limits

Group	1	2	3	4
$\beta_k = 0.7$	**42.85**	19.52	12.62	109.3
$\beta_v = 0.9$	----	**11.11**	**11.11**	**32.72**

4.8 Conclusions

The effects of coupled vertical stiffness-strength irregularities caused in structures due to a modified interstorey height were evaluated and presented in this paper. Regular structures, represented by shear-type structures of 3, 5, 9 and 15 storeys having equal storey height, assumed to be in Wellington and having a constant floor mass at every floor level, were designed for a range of structural ductility factors of 1, 2, 3, 4 and 6 according to the NZS 1170.5 Equivalent Static method. The stiffness distribution over the height was either provided such that it resulted in design (target) interstorey drift ratios (DISDR) at all storeys simultaneously or a uniform stiffness distribution that produced DISDR at the first storey was provided. The strength distribution over the height was provided such that the strength to stiffness ratio at each storey was constant. An "interstorey height ratio" was defined as the ratio of modified to initial interstorey height, and applied separately at the first storey, mid-height storey and at the topmost storey. This generally corresponded to a modification of the storey stiffness and strength. The modified structures were then redesigned until the critical storey/storeys achieved the target DISDR. The change in the median peak interstorey drift ratio (ISDR), due to coupled stiffness-strength irregularities, obtained from inelastic dynamic time-history analysis were then used to explain the effects of coupled stiffness-strength irregularity. The conclusions derived from this study can be summarised as below:

1. Realistic correlations between storey stiffness and strength due to modifications to a storey height for a few common lateral force resisting systems were determined. A range of interstorey height ratios that produced cases of stiffness-strength

reduction or enhancement were selected to investigate the effects of the magnitude of irregularities;

2. The group of structures having only the storey stiffness modified due to a change to a storey height (Group 1 structures), produced the maximum adverse effects of irregularity. For this group with CISDR or CS-CSTG configuration, a taller first storey for short period structures, and a taller mid-height storey for taller structures, was found to produce median peak ISDR greater than the regular structures. The increase in median peak ISDR due to irregularity generally reduced with the structure height;

3. For Group 1 structures, the effects of a short storey were less than those due to a taller storey in the structure. A shorter mid-height storey of short period CISDR and CS-CSTG designs generally tended to produce higher increases in median peak ISDR due to irregularity than other irregularity positions and structure heights; and

4. A simple equation that can estimate the likely increase in response due to a modified interstorey height was developed. Similar equations can be easily developed for different types of engineering demand parameters and used in design. The equation was also used along with the realistic correlations between storey stiffness and strength to obtain the governing code regularity limit.

4.9 Acknowledgements

This research work is a part of the New Zealand Earthquake commission (EQC) project titled, "*Building Regularity for Simplified Modelling"*. The authors are

thankful to EQC (www.eqc.govt.nz) for their financial assistance to undertake this study.

4.10 References

[1] Al-Ali AAK, Krawinkler H. Effects of vertical irregularities on seismic behaviour of building structures. Report No. 130, Department of Civil and Environmental Engineering, Stanford University, San Francisco, 1998.

[2] Carr AJ. Ruaumoko 2D – Inelastic dynamic analysis program. Department of Civil Engineering, University of Canterbury, Christchurch, 2004.

[3] Chintanapakdee C, Chopra AK. Seismic response of vertically irregular frames: Response history and modal pushover analyses. *Journal of Structural Engineering* 2004; **130**(8): 1177-1185.

[4] Chopra AK, Goel GK. A modal push over analysis procedure to estimate seismic demands for unsymmetric-plan buildings. *Earthquake Engineering & Structural Dynamics* 2004; **33**(8): 903-927.

[5] Cornell CA, Fatemeh JF, Hamburger RO, Foutch DA. Probabilistic basis for 2000 SAC FEMA steel moment frame guidelines. *Journal of Structural Engineering* 2002; **128**(4): 526-533.

[6] De Stefano M, Pintucchi B. EAEE task group (TG) 8: Seismic behaviour of irregular and complex structures: Progress since 2002. *First European Conference on Earthquake Engineering and Seismology*, 2006. Paper No: 1443.

[7] MacRae GA, Kimura Y, Roeder CW. Effect of column stiffness on braced frame seismic behaviour. *Journal of Structural Engineering* 2004; **130**(3): 381-391.

[8] Fragiadakis M, Vamvatsikos D, Monolis P. Evaluation of the influence of vertical irregularities on the seismic performance of a nine-storey steel frame. *Earthquake Engineering and Structural Dynamics* 2006; **35**(12): 1489-1509.

[9] Priestley MJN, Calvi GM, Kowalsky MJ. Displacement-based seismic design of structures. *IUSS Press*, Pavia, Italy, 2007; 721pp.

[10] Rutenberg A. EAEE task group (TG) 8: Seismic behaviour of irregular and complex structures: Progress since 1998. *12th European Conference on Earthquake Engineering*, 2002. Paper No: 832.

[11] Sadashiva VK, MacRae GA, Deam BL. Determination of structural irregularity limits – mass irregularity example. *Bulletin of the New Zealand Society for Earthquake Engineering* 2009; **42**(4): 288-301.

[12] Sadashiva VK, MacRae GA, Deam BL. Seismic response of structures with coupled vertical stiffness-strength irregularities. *Earthquake Engineering and Structural Dynamics* 2011. DOI: 10.1002/eqe.1121.

[13] SNZ. NZS 1170.5 Supp 1:2004, Structural Design Actions. Part 5: Earthquake actions – New Zealand – Commentary, Standards New Zealand, Wellington, 2004.

[14] SEAOC. Recommended Lateral Force Requirements and Commentary. Seismology Committee, Structural Engineers Association of California, 1999, Seventh Edition.

[15] Tagawa H, MacRae G, Lowes L. Evaluations of 1D simple structural models for 2D steel frame structures. *13th World Conference on Earthquake Engineering*, Vancouver, B.C., Canada, 2004.

[16] Tagawa H. Towards an understanding of 3D structural behaviour - Stability & Reliability. Ph.D. dissertation, University of Washington, Seattle, 2005.

[17] Tagawa H, MacRae GA, Lowes LN. Evaluation of simplification of 2D moment frame to 1D MDOF coupled shear-flexural-beam model. *Journal of Structural & Constructional Engineering* 2006; Transactions of AIG, No. 609.

[18] Valmundsson EV, Nau JM. Seismic response of building frames with vertical structural irregularities. *Journal of Structural Engineering* 1997; **123**(1): 30-41.

Nomenclature for Table 4-1

A_a = *cross*-sectional area of the bracing member

A_{am} = *modified* cross-sectional area of the bracing member

A_s = cross-sectional shear area

A_{sm} = modified cross-sectional shear area

d_o = initial overall depth of the member section

d_m = modified overall depth of the member section

E = modulus of elasticity

G = shear modulus of elasticity

h = interstorey height

I_o = initial moment of inertia of the member section

I_m = modified moment of inertia of the member section

K = lateral stiffness of the structure

K_o = initial lateral stiffness of the structure

K_m = modified lateral stiffness of the structure due to modified member property

L = span length of the frame or wall

M_p = section plastic moment

V = lateral strength of the structure

V_o = initial lateral strength of the structure

V_m = modified lateral strength of the structure

α_k = stiffness modification factor

α_v = strength modification factor

ε_y = yield strain of the material

σ_y = yield stress of the material

5. QUANTIFYING THE SEISMIC RESPONSE OF STRUCTURES WITH FLEXIBLE DIAPHRAGMS

5.1 Overview

Floor diaphragm in-plane stiffness affects building response to horizontal ground accelerations. This paper describes a series of elastic and inelastic time history analyses of symmetric structures with different deformation types, configurations and heights to quantify these effects. It is shown that displacements of single storey elastically responding structures tend to be most significantly affected by diaphragm flexibility. Analyses of these structures were cross-verified by a closed-form mechanics-based formulation developed to describe the response. Simple relationships were proposed to allow designers to conservatively estimate the increase in in-plane diaphragm displacement resulting from diaphragm flexibility.

5.2 Introduction

Floor and roof diaphragms are generally provided primarily to carry out-of-plane vertical gravity loads in the structure. However, for them to function reliably, they must resist lateral forces (such as wind and earthquake) and transfer them dependably to the *vertical lateral force resisting* (**VLFR**) elements (such as walls and frames) within a structure.

Diaphragm flexibility is generally quantified in terms of the diaphragm displacement, δ_d, relative to displacement of the VLFR elements, δ_w, due to a lateral uniformly distributed load along the diaphragm. The floor diaphragm in-plane stiffness affects the building response in the following ways:

a) Increased diaphragm flexibility changes the demands on the whole structure. That is, it increases the structural period and this affects the forces entering the structures thereby changing the force demands and displacements of the elements.

b) It changes the distribution of forces between the VLFR elements.

For example, a structure with a diaphragm with very high lateral stiffness which exhibits no torsional response has an in-plane translation that is nearly identical along the length of the diaphragm. In this case, the diaphragm distributes forces to the VLFR elements in proportion to their relative rigidities. However, for a more flexible diaphragm, more force is likely to be carried on the VLFR elements with a greater tributary area.

The New Zealand seismic Standard, NZS 1170.5 [1] Clause 6.1.4.1 specifies that: "*where diaphragms are not rigid compared to the vertical elements of the vertical action resisting system, the model should include representation of the diaphragm's flexibility*". Since no structure is perfectly rigid, it would seem that diaphragm flexibility must always be explicitly considered. However, the Standard proceeds to define "rigid" and "flexible" structures. These are illustrated in Figure 5-1. Here, a diaphragm is classified as "flexible" when the computed maximum in-plane deflection of the diaphragm itself under the lateral load is more than two times the average storey drift of the associated storey. For a diaphragm that has a maximum lateral deformation less than or equal to two times the average storey drift, many design codes define the diaphragm as "rigid" (e.g., NZS 1170.5 [1], IBC [2], FEMA 450 [3]). A slightly different diaphragm classification is provided by Eurocode 8 [4]. It specifies that a diaphragm is "rigid", if, when it is modelled with it's actual in-plane flexibility, its horizontal displacements nowhere exceeds those resulting from the

rigid diaphragm assumption by more than 10% of the corresponding absolute horizontal displacements.

While the above limits are simple for design, they lack rational justification. There is no referenced set of studies stating where these limits come from and structures with diaphragm flexibilities either side of the code limit are unlikely to have the significantly different responses stated in the codes. It is also unclear how seismic demands would vary for different levels of diaphragm flexibility.

When a structure with a flexible diaphragm is considered to have a rigid diaphragm, the period will be underestimated. For structures with periods on the descending branch of the spectral acceleration – period plot, this may result in some structural base shears being slightly overestimated. This is conservative. However, the actual displacement will be greater than that predicted. This is most likely to increase the possibility of the structural pounding with other structures. It will also affect the

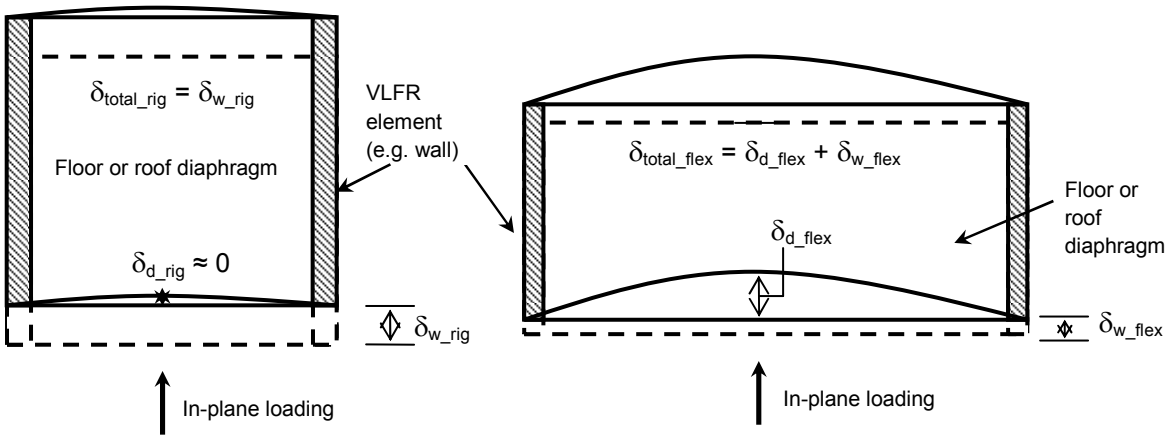

(a) Rigid diaphragm (b) Flexible diaphragm

Figure 5-1: Typical diaphragm behaviour under in-plane loading (structure in plan view).

distribution of forces between VLFR elements, which may be critical if they, or the elements they are connected to, do not possess sufficient strength or ductility.

It may be seen from the above discussion that there is a need to quantify the effect of different amounts of diaphragm flexibility on the structural response so that designers can be aware of the likely impact of their decisions. This paper addresses this need for simple symmetric structures which are not subjected to torsion.

The paper has been organized in the following way. The first section provides a review of previous research on diaphragm flexibility effects. This is followed by a step-by-step procedure developed to quantify diaphragm flexibility effects. Consequent sections describe how the methodology was applied on simple structures to evaluate the effects of in-plane diaphragm flexibilities when subjected to a suite of ground motion records. Simple single storey elastic models, models with yielding bracing elements, models with different configurations, and multi-storey structural models, are all considered. The final section describes how simple mathematical models can be developed to describe diaphragm flexibility effects.

5.2.1 Previous Research on Diaphragm Flexibility Effects

Evidence of damage due to flexible diaphragms in past earthquakes (e.g., Jain and Mandal [5], Barron and Hueste [6]) has attracted many researchers to work on this topic. A summary of analytical studies, followed by limited experimental studies, is provided below.

Jain and Jennings [7] developed simple analytical models of single span one storey and multi-storeys structures with flexible diaphragms supported by end walls. Their study showed that the dynamic response of structures was dominated by floor

flexibility. This was explained by the large displacement of the diaphragm at the mid-span with respect to the displacement of the two ends of the diaphragm. Initial symmetric modes of vibration were shown to have the most contribution to the total base shear, while the asymmetric modes contributed nothing.

Kunnath *et al.* [8] studied the seismic response of multi-spanned one storey and multi-storeyed RC buildings with flexible diaphragms. They showed that both elastic and inelastic flexible diaphragms caused floor displacements and middle frame base shears greater than those from buildings with rigid diaphragms. The fundamental natural period was shown to increase due to diaphragm flexibility. These effects increased with an increase of the number of spans and a decrease of the number of storeys.

Saffarini and Qudaimat [9] examined the appropriateness of the rigid diaphragm assumption for RC multistorey structures with flexible diaphragms. For a symmetrical one-bay by four-bay structure with only shear walls, the ratio of wall shears to the total base shear was calculated. It was shown that as the number of storeys was increased, the ratio of wall shears for flexible and rigid diaphragm assumptions closely matched. The effect of diaphragm flexibility was shown to be relatively insignificant when the structure had more than 4 storeys. It was reported that for structures having only moment-resisting frames, the slabs generally behaved as rigid slabs. However, when shear walls were used along with the frames in symmetric multi-storey buildings, considerable errors in column shears due to rigid diaphragm assumption were reported. The error in the first floor deflection was shown to be more significant compared to that in other storeys. This error decreased for buildings with more storeys. In the case of asymmetrically arranged walls and

framed multi-storey structures, the wall shears errors increased. The effect of diaphragm flexibility was also explained by using other parameters (e.g., openings in slab, floor plan aspect ratio etc.). A similar study, with similar findings, was conducted by Ju and Lin [10].

Tremblay and Stiemer [11] conducted inelastic dynamic time-history analyses on single storey steel-framed structures with uniform rectangular shaped flexible diaphragms. Inelastic action took place in the bracing bents, while the diaphragms oscillated about the deformed position of the vertical bracing. Therefore, they recommended that only the portion of total drift contributed by the bracing elements be multiplied by the force reduction factor while using the code method for calculating the peak horizontal storey drift. It was shown that the structures mainly responded in the fundamental mode from all the analyses. The fundamental natural period of the structures increased due to diaphragm flexibility, and the computed fundamental periods were higher than those calculated according to 1990 National Building Code of Canada. This means that design forces are likely to be over-estimated, which is conservative. Comparison of responses obtained from inelastic dynamic time-history analyses and static analyses were made and a dynamic amplification factor was recommended for static roof deformations and diaphragm bending moments. The dynamic magnification, presumably resulting from dynamic magnification effects, was 2.3. Also, the diaphragm shear was close to the capacity design value, or sometimes even greater than it, over most of the diaphragm length. The under-prediction of fundamental period calculation by code empirical methods for structures with flexible diaphragms is also shown by Tena-Colunga and Abrams [12].

Fleischman *et al.* [13 & 14] carried out a modal examination and time-history analyses on three and six storey structures with long-floor spans and perimeter lateral systems (shear wall or frame). Diaphragm flexibility was varied by reducing the long floor-span length while holding a constant floor width. Fundamental natural period increased with increasing diaphragm flexibility. They reported that a critical level of diaphragm flexibility exists when the mass tributary to the lateral-system and the reminder of the diaphragm mass act independently. Only a small reduction in maximum drift was obtained by keeping the diaphragms elastic, and the major force demands occurred in the elastic diaphragm case, while the maximum deformation demands occurred in the inelastic diaphragm case at the lower floor levels. They proposed very detailed design recommendations for perimeter VLFR structures with flexible diaphragms in high seismic regions based on the analyses of structures of these heights.

Lee et al. [15] described the effects of diaphragm flexibility by conducting inelastic dynamic time-history analyses on analytical models of 3 to 6 storey high structures supported by end shear walls. Diaphragm flexibility was represented by varying the floor plan aspect ratio and effective stiffness factor (defined as the ratio of estimated stiffness accounting for diaphragm connectors to gross diaphragm stiffness). The mean peak total diaphragm displacement and the interstorey drifts were shown to increase with an increase in aspect ratio for all structures. They showed that for each aspect ratio considered, the peak overall displacement of floors including wall deformations generally increased with the structural height, and the first storey rather than other storeys had higher interstorey drifts for all structures considered. A method based on a lumped mass model for the diaphragms was proposed to predict peak

interstorey drifts in medium height structures with flexible diaphragms. Here, the lumped mass model considered quarter of total diaphragm mass lumped at each end support, while the remaining half of the total diaphragm mass was lumped at the centre of the diaphragm. The interstorey drift estimates using their proposed method differed between 7% and 34% when compared to the interstorey drifts from dynamic analyses.

Very few experimental studies have been conducted to investigate the effects of diaphragm flexibility. Panahshahi *et al.* [16, 17] carried out shake table tests on one-sixth scale models of single storey four-span RC buildings. They described the changes in force distribution due to yielding of the shear walls and the diaphragm. For example, the percentage of lateral force carried by the flexible frames increased from 4.6% to 20.4% of the total base shear in one case due to inelastic cycles of diaphragm loading. A comparison with stiff diaphragms was not performed.

Tremblay *et al.* [18] built a scaled model of a one-storey steel structure with a flexible rectangular diaphragm supported by vertical bracing of *tension-only* diagonal members along four exterior walls. The structure was designed according to Canadian Codes and tested by applying ground motion parallel to the short walls. The actual fundamental natural period of the structure increased due to diaphragm flexibility, and it was shown to be higher than the period obtained by code method. The measured responses (e.g., peak in-plane roof deformation, diaphragm shear force) were reported to be more than responses due to uniformly distributed static loading condition.

5.2.2 Modelling Techniques

Several modelling techniques have been used by previous researchers to analyse structures with flexible diaphragms. The three-dimensional diaphragm has generally been modelled using surface elements such as shell, membrane, plate elements ([6], [9], [10], [12]) or beam elements ([7], [11], [15]). While beam-column elements are a common choice for the frames ([8], [10], [13]), the shear walls have been modelled using surface elements ([6], [10], [12]) or beam-column elements [15]. Other alternatives for VLFR components include use of spring or truss elements [11]. A three-dimensional finite element analysis may capture the real structural behaviour well [19], but this technique is computationally more expensive. The additional complexity also involves more input data preparation and interpretation time. Additionally, difficulties arise in accurately defining the connections between the diaphragm and it's bracing VLFR elements. Such a sophisticated modelling method may seldom be used for day-to-day designs. The need for simple modelling assumptions has also been emphasized by other researchers (e.g., [5]). In fact, regardless of the modelling method, many previous works outlined in this paper showed similar behaviour (e.g., sensitivity of diaphragm flexibility effect to aspect ratios, structure height etc.).

5.3 Structures Considered and Analysis Methodology

5.3.1 Structures Analysed

Symmetric structures with a high diaphragm length-to-width ratio are modelled. The number of storeys considered was 1, 2, 3 and 5. Both structures with one-span and equal two-spans are considered. Figures 5-2(a) and 5-2(c) show examples of typical

structures analysed. Note that although VLFR elements in the figures are illustrated as shear walls, they could be any combination of frame and/or wall components.

5.3.2 Structural Modelling

All structures are modelled and analysed in this paper using SAP2000 [20]. SAP2000 can either be executed in a *GUI* mode, or a batch mode process can be set. Due to the large number of analyses involved in this study, the batch mode option was chosen, and all the analyses were systematically automated using Matlab [21]. The extraction of results from SAP2000 was also carried out using Matlab. Appendix I provides information on automating SAP2000.

The structures are assumed to have a rigid foundation; therefore the soil-foundation interaction and foundation flexibility effects are ignored. Diaphragms are represented using beam elements. In this study, shear and rotary inertia effects are neglected, an assumption which is reasonable, especially for analysis of lower modes of vibration of beams with large aspect ratios (e.g., [7], [22], [23]). For example, Humar has shown that for a beam having its length equal to 10 times the depth of its cross-section, the percentage reduction in frequency caused by ignoring combined effect of shear deformation and rotary inertia is less than 2% and 12.5% respectively for the first and the third mode of vibration. Even if it is considered, results are similar for diaphragms with all shear deformations and all flexural deformations [24]. For example, Figure J-6 [Appendix J.5 in 25] shows minimal difference in peak displacement response obtained due to the above extreme diaphragm modelling. The VLFR elements, assumed as shear walls, are modelled as linear springs for elastic analyses. For two-span structures, the effect of structural configuration on seismic

demands was investigated by assuming the connection at the mid-span to be either a "pin" or a "built-in". Here, the first configuration can be regarded as a form of tributary area model, while the latter configuration defines a continuous diaphragm along the entire diaphragm span. For all structures, beams were provided with high axial stiffness. Figures 5-2(b) and 5-2(d) show the analytical modelling methods used in this paper.

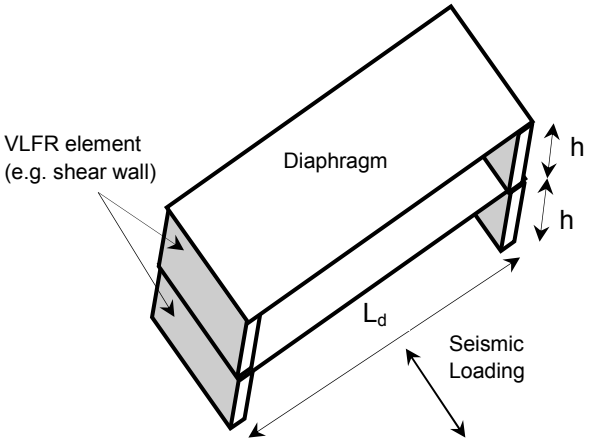

(a) Schematic of single-span two storey structure

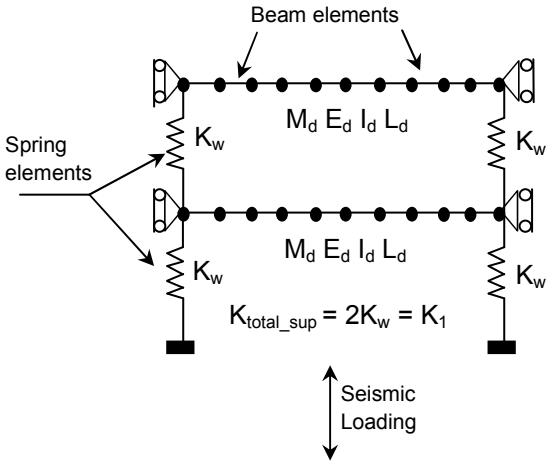

(b) Analytical model of single-span two storey structure (plan view)

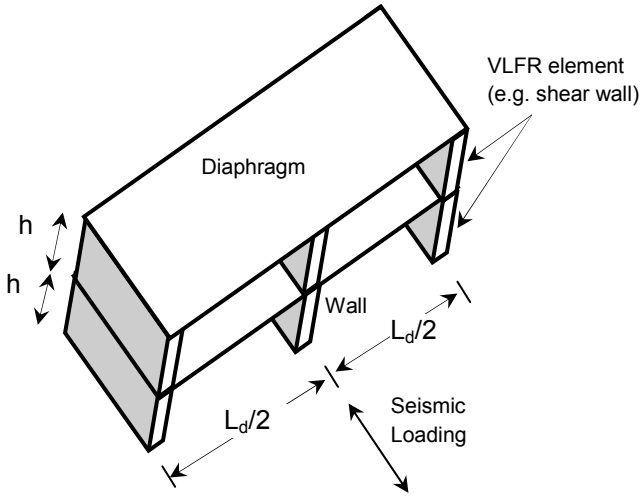

(c) Schematic of equal two-spans two storey structure

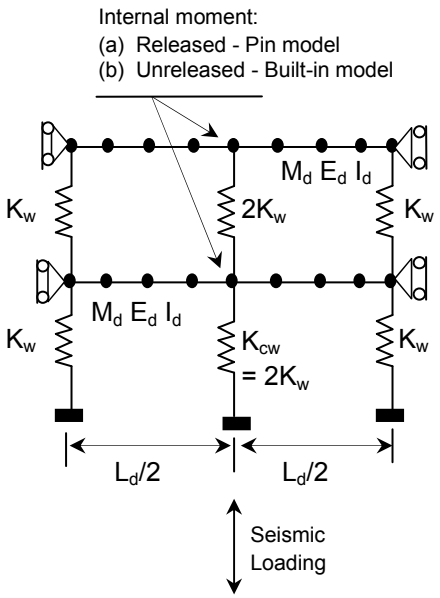

(d) Analytical model of equal two-spans two storey structure (plan view)

Figure 5-2: Example of structural configurations and structural modelling used in this paper.

5.3.3 Incorporating Diaphragm Flexibility

In this paper, a rigid diaphragm is assumed to have negligible deformations compared to that of bracing elements (see Figure 5-1(a)), and therefore, the total in-plane displacement of a structure with a rigid diaphragm, δ_{total_rig}, equals the in-plane displacement of the wall alone, δ_{w_rig}. For a structure with a flexible diaphragm, as shown in Figure 5-1(b), the total in-plane displacement of the structure, δ_{total_flex}, can be calculated as the summation of wall in-plane displacement, δ_{w_flex}, and the lateral displacement of the flexible diaphragm, δ_{d_flex}.

A common measure of diaphragm flexibility used in many codes is the maximum diaphragm displacement alone divided by the average bracing element displacement due to in-plane loading [1-3]. This can be expressed by Equation (5-1), where γ_s is defined as the *static flexibility ratio*, having a value of zero for rigid diaphragms and greater than zero for flexible diaphragms. In this paper, a range of γ_s values ($0 < \gamma_s \leq 5$) are used.

$$\gamma_s = \frac{\delta_{d\_flex}}{\delta_{w\_flex}} \tag{5-1}$$

5.3.4 Analysis Methodology

A step-by-step procedure to evaluate diaphragm flexibility effects on the structures is provided below. There are 3 main steps - structural design of rigid diaphragm structures, analysis of rigid diaphragm structures, and analysis of flexible diaphragm structures. For illustration purposes, the two storey structures shown in Figure 5-2 are considered.

A. *Structural Design of Rigid Diaphragm Structures (bench-mark case)*:

(a) A fundamental natural period of the structure with rigid diaphragms, T_{rig}, is selected.

Note: (1) A range of T_{rig}, covering structures with short periods through long period structures are considered in this study. (2) In order to design multi-storey structures of a given period, a trial and error method can be used to determine the stiffness of the different storeys within the structural analysis program. Instead of this, it was decided to use a first principles approach using Matlab [21] as described below.

(b) Assuming a total weight of each diaphragm, W_d, of unity, the total diaphragm mass, M_{d_i}, is computed at every i^{th} storey. Other storey masses (e.g., mass of supporting walls) are assumed to be negligible compared to the diaphragm mass and are therefore neglected for simplicity. The structural mass matrix, M, is given by Equation (5-2).

$$M = \begin{bmatrix} M_d & 0 \\ 0 & M_d \end{bmatrix} \tag{5-2}$$

(c) The total lateral stiffness of the supports at every i^{th} storey, $K_{total\_\sup_i}$ ($=\sum K_{w_i}$), is assumed to be constant, thus resulting in the structural stiffness matrix, K, given by Equation (5-3).

$$K = \begin{bmatrix} 2K_{total\_\sup} & -K_{total\_\sup} \\ -K_{total\_\sup} & K_{total\_\sup} \end{bmatrix} \tag{5-3}$$

The rows in the above matrices in Equations (5-2) and (5-3) relate to the horizontal degrees of freedom in the first and the second floor respectively.

(d) Iterate on $K_{total\_\sup_i}$ until the target T_{rig} from eigenvalue analysis is achieved.

B. *Structural Modelling and Analysis of Rigid Diaphragm Structures*:

(a) Each spring at the i^{th} storey is provided with lateral stiffness corresponding to the number of supporting walls in the following way.

i. For diaphragms supported by two end walls, the lateral stiffness of each wall at i^{th} storey, K_{w_i}, is given by Equation (5-4a).

$$K_{w_i} = \frac{K_{total\_\sup_i}}{2} \qquad (5\text{-}4a)$$

ii. For diaphragms supported by two end walls and one central wall, the total support stiffness is divided between the supporting walls according to Equations (5-4b) and (5-4c), where CSK_f is defined as the central support stiffness factor. A value of $CSK_f = 2$ was found to produce the most change in response due to diaphragm flexibility [Appendix J.3 in 25], therefore this value of $CSK_f = 2$ is used in this paper.

$$K_{w_i} = \frac{K_{total\_\sup_i}}{2 + CSK_f} \quad \text{(for each end wall)} \qquad (5\text{-}4b)$$

$$K_{cw_i} = CSK_f \; K_{w_i} \quad \text{(for central wall)} \qquad (5\text{-}4c)$$

The diaphragms are provided with a very high stiffness for this rigid diaphragm case. Here, in order to obtain the moment of inertia of the rigid diaphragm, I_{d_rigid}, the value of I_{d_rigid} is increased until the fundamental natural period from modal analysis converges to the target value, T_{rig}.

(b) Conduct dynamic time-history analyses by subjecting the structure to a suite of earthquake ground motions. The modal time-history analysis option available within SAP2000 was used over the direct-integration time-history analysis, due to its higher efficiency and accuracy in performing the analysis ([20], Marjanishvili and Agnew [26], Wilson [27]). A constant damping of 5% of critical damping for all the modes is considered. In this paper, 20 SAC (SEAOC-ATC-CUREE) LA records with probabilities of exceedance of 10% in 50 years [28] are used for all the dynamic analyses. Figure 5-3 shows the response spectra for the record suite.

Note: Appendix K provides a brief note on the time-history analysis options available in SAP2000 to conduct elastic and inelastic dynamic time-history analysis.

(c) Obtain peak values of following response parameters at every storey due to each earthquake record.

1. In-plane displacement of the end wall, $\delta_{w\_rig_i}$
2. Total in-plane displacement at diaphragm mid-span, $\delta_{total\_rig_i}$
3. Interstorey drift (from end walls), $ISD_{w\_rig_i}$
4. End wall shear force, $V_{w\_rig_i}$
5. Diaphragm bending moment at mid-span, $M_{d\_rig_i}$

For rigid diaphragms on end walls and a central wall, the diaphragm forces and displacements are obtained at quarter span (L_d/4). In addition to the above, the following parameters are also calculated.

6. Relative displacement between the end wall and the mid-span wall, $RD\_W_{rig_i}$
7. Middle-wall shear force, $V_{w\_rig_i}$

8. Interstorey drift (from mid-span walls), $ISD_{cw\_rig_i}$

The maximum for each of the above demand parameters, from all the storeys are also calculated.

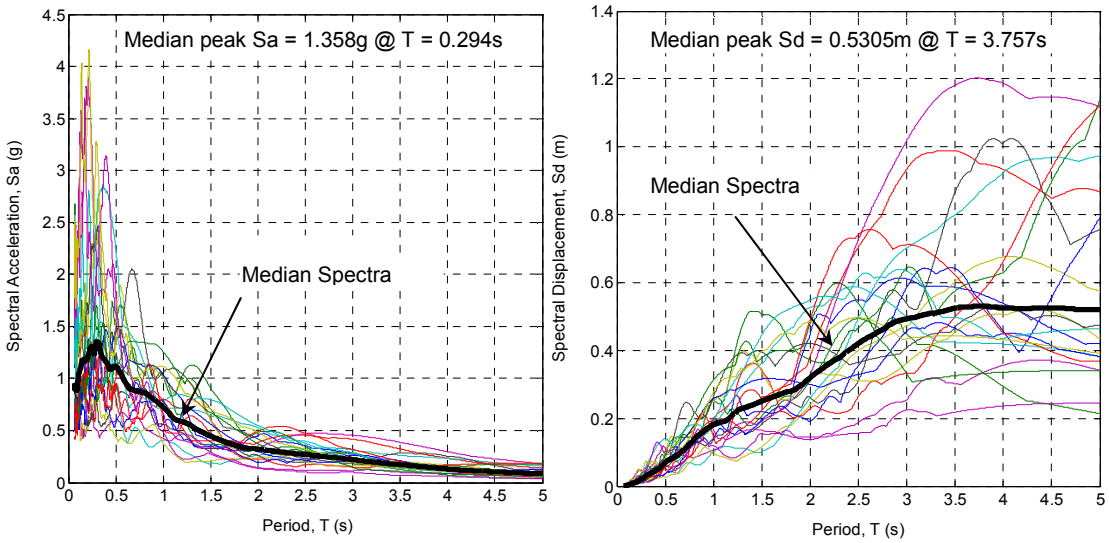

(a) Acceleration spectrum (b) Displacement spectrum

Figure 5-3: Response spectra for the 20 SAC LA 10in50 ground motion records used in this paper ($\zeta = 0.05$).

C. <u>*Structural Modelling and Analysis of Flexible Diaphragm Structures*</u>:

For each selected static flexibility ratio, γ_{s_j}, carry out the following steps:

(1) Calculate the stiffness of supports and diaphragms –

(a) *Stiffness of supports*:

The total lateral support stiffness required to achieve the target T_{rig}, as previously obtained for the rigid diaphragm case, $K_{total\_sup_i}$, and the calculated wall stiffnesses (Equations (5-4a) to (5-4c)), are again used.

(b) *Stiffness of diaphragms*:

Equation (5-1) is rearranged to obtain Equation (5-5a). The diaphragm stiffness at every level is then computed as a function of static flexibility ratio using Equation (5-5b).

$$\left(W_{d_i} \Big/ \sum K_{w_i} \right) = \frac{\left(W_{d\,i} \Big/ K_{d\_flex_i} \right)}{\gamma_{s_j}} \tag{5-5a}$$

$$K_{d\_flex_i} = \frac{K_{total\_\sup_i}}{\gamma_{s_j}} \tag{5-5b}$$

Assuming a realistic value for the diaphragm modulus of elasticity, E_d, calculate the flexible diaphragm moment of inertia, I_{d_flex}:

i. For diaphragms simply supported by end supports, the mid-span flexural deflection under a uniform distributed load, $\overline{w}_d$, is given by Equation (5-6a).

$$\delta_{d\max} = \frac{5\overline{w}_d L_d^4}{384\, E_d\, I_{d\_flex}} \tag{5-6a}$$

ii. For diaphragms supported by two end walls and one wall at the mid-span, the quarter-span flexural deflection due to $\overline{w}_d$ is given by Equation (5-6b).

$$\delta_{d\max} = \frac{\overline{w}_d \left(L_d \Big/ 2 \right)^4}{192\, E_d\, I_{d\_flex}} \tag{5-6b}$$

The moment of inertia for all flexible diaphragms is provided according to Equation (5-7).

$$I_{d\_flex_i} = K_{d\_flex_i} \frac{5L_d^3}{384\,E_d} \qquad \text{(for single-span case)} \qquad (5\text{-}7a)$$

$$I_{d\_flex_i} = K_{d\_flex_i} \frac{\left(L_d/2\right)^3}{192\,E_d} \qquad \text{(for equal two-span case)} \qquad (5\text{-}7b)$$

(2) Structural modelling and analysis –

(a) Model the structure in a similar way described for the rigid diaphragm structure. This time though, the diaphragm flexibility is included to obtain the fundamental natural period of the structure with a flexible diaphragm, T_{flex_j} .

(b) Conduct dynamic time-history analysis using the suite of 20 SAC records and obtain peak values of response parameters at every i^{th} storey, and from all storeys, due to each record. Here, in addition to similar demand parameters as described for the rigid diaphragm structure (subscript "rigid" is replaced by "flex"), the following maximum storey demands are also obtained at either $L_d/2$ (single span case) or at $L_d/4$ (equal two-span case) :

1. Relative drift between the diaphragm and the end support, $\delta_{d\_flex_i}$. This gives the displacement of the diaphragm alone.
2. Total in-plane displacement, $\delta_{total\_flex_i}$
3. Interstorey drift due to total in-plane displacement, $ISD_{total\_flex_i}$

Note – Henceforth in this paper, diaphragm mid-span refers to diaphragm node at either $L_d/2$ (for single span models) or $L_d/4$ (for equal two-span models).

(3) Evaluate diaphragm flexibility effects –

Non-dimensional demand parameters are used to describe the effect of diaphragm flexibility. For example, the change in total in-plane displacement at mid-span for a single span structure due to γ_{s_j} is given by Equation (5-8a). Additionally, fundamental natural period ratio, T_{ratio}, and dynamic flexibility ratio, γ_{d_j}, are calculated respectively according to Equations (5-8b) and (5-8c).

$$\delta_{total\_ratio_i} = \frac{\delta_{total\_flex_i}}{\delta_{total\_rig_i}} \tag{5-8a}$$

$$T_{ratio_j} = \frac{T_{flex_j}}{T_{rig}} \tag{5-8b}$$

$$\gamma_{D_i} = \frac{\delta_{d\_flex_i}}{ISD_{w\_flex_i}} \tag{5-8c}$$

In the above, the ratios of demand parameters correspond to each earthquake record. Therefore, the median responses for the record suite can be calculated according to Equation (5-9) [29, 30].

$$\hat{x} = e^{\left(\frac{1}{n}\sum_{i=1}^{n}\ln(x_i)\right)} \tag{5-9}$$

All the above steps (A to C) are repeated for the range of T_{rig} selected.

5.4 Evaluating Diaphragm Flexibility Effects

5.4.1 Diaphragm Flexibility Effect on Fundamental Natural Period of Structures

The variation of T_{ratio} with diaphragm flexibility ratio is shown in Figure 5-4. In this and later figures, "nbs" refers to the number of storeys in the structure, "2WM" is used for structural models supported by two end walls, and structures with end supports and a central wall, having a mid-span pinned connection is represented by "3WM-Pinned".

The figure shows that T_{ratio} is not sensitive to the chosen T_{rig}. Increases to the natural period due to flexible diaphragm are observed in all structural types; with higher increases for equal two-span structures than for the single span structures because of the different I_{d_flex} and configuration. Figure 5-4 shows that T_{ratio} increases with increasing flexibility ratio, and that this effect reduces with increasing structural height. Similar effect of diaphragm flexibility on the natural periods can be found in the literature (e.g., [8], [6]).

From Figure 5-4, a rigid diaphragm code assumption for structures with flexible diaphragms will underestimate the fundamental natural period of the structure. This can result in an overestimate of design base shears [12] and an underestimate of displacements. For example, according to Figure 5-4(a), the fundamental natural period of a single span one storey structure (2WM) with γ_s = 2.5, is 1.68 times that due to a rigid diaphragm assumption for the same structure. According to NZS 1170.5 [1] for the region of Wellington; for T_{rig} greater than 0.35s, the over-estimation of design base shear due to rigid diaphragm assumption can be as much as

30% [Appendix J.4 in 25]. Ignoring diaphragm flexibility may therefore result in uneconomical design forces.

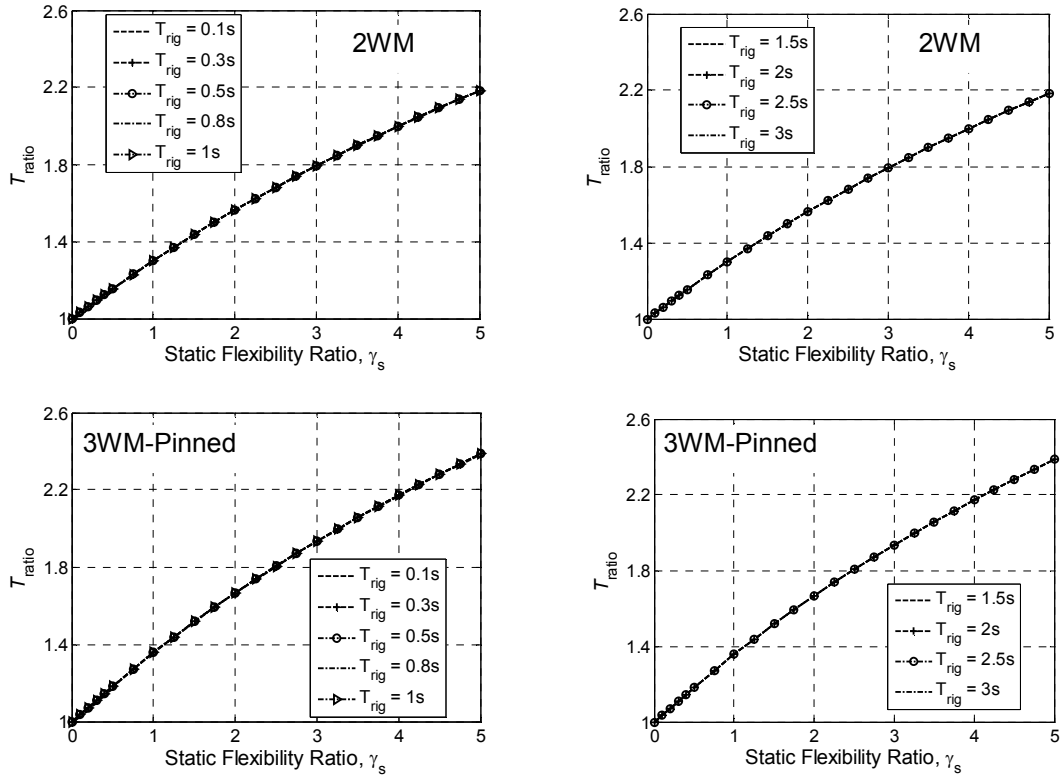

(a) Number of Storeys = 1

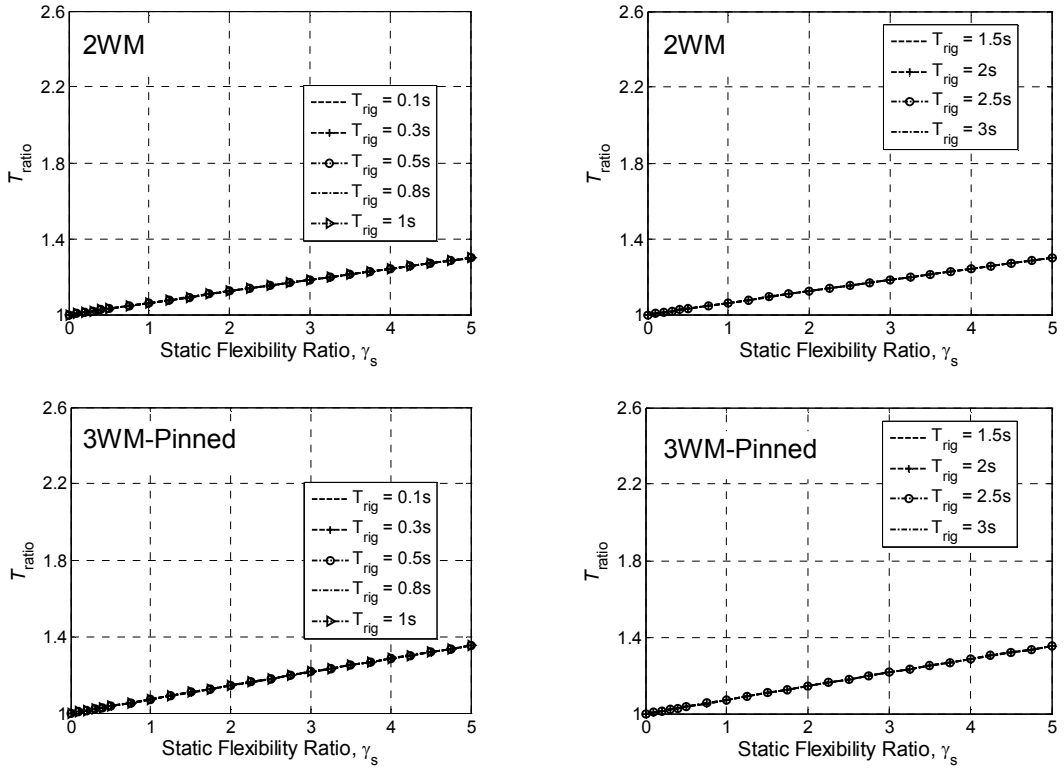

(b) Number of Storeys = 3

Figure 5-4: Change in structural fundamental natural period due to diaphragm flexibility.

5.4.2 Elastic Dynamic Time-History Analyses (EDTHA)

Peak in-plane deformations

Figure 5-5 shows the variation of end support median peak interstorey drifts, ISD_{w_flex}, with diaphragm flexibility ratio, γ_s. The interstorey drifts decrease with increasing γ_s, except perhaps for the structures with T_{rig} = 0.1s. For all structures, interstorey drifts are higher for long period structures than for short periods. The figure shows that single storey structures have higher ISD_{w_flex} than multi-storey structures with the same T_{rig}. For multi-storey structures, ISD_{w_flex} increases with decreasing structural height, making the first storey critical. This can be expected for structures having equal storey stiffness at all the storeys [28]. Figures 5-5(b) and 5-5(c) show that both 3WM-Pinned and 3WM-Built-in models, where the diaphragm is built into the central support, had nearly the same drift demands; however, the 3WM-Pinned configuration generally produced slightly higher demands. The figures also show that single-span structures have demands close to those from 3WM-Pinned structures. Similar observations were also seen for median peak $ISD_{\mathrm{w\_flex}}$ obtained at diaphragm mid-span and at other support nodes.

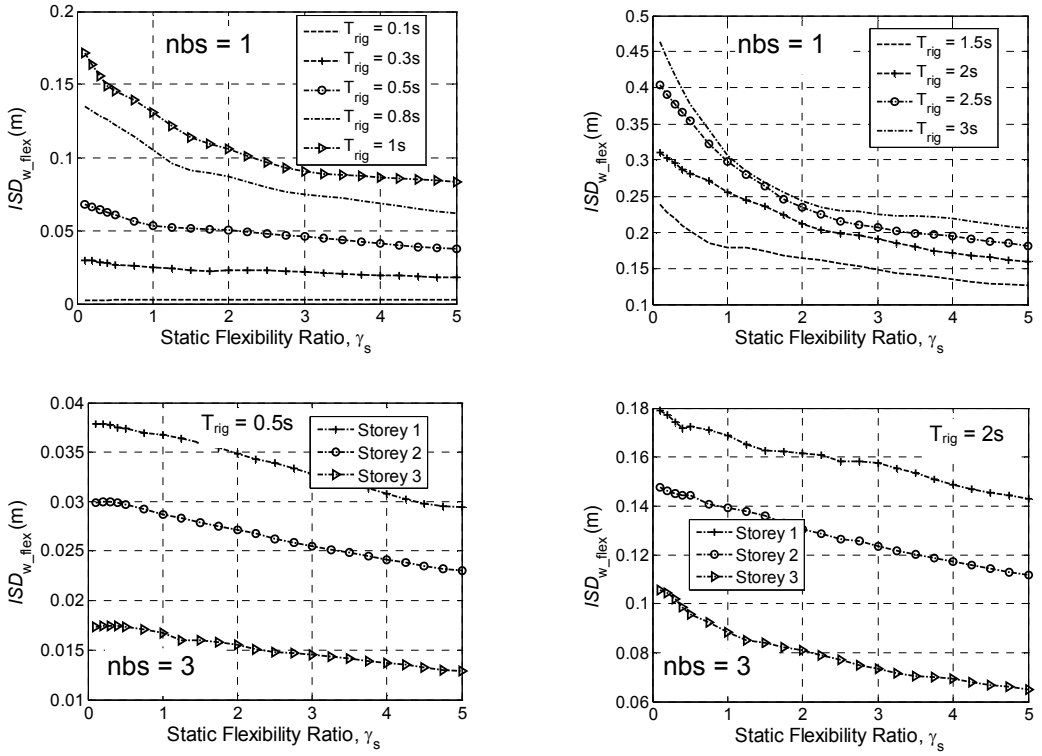

(a) 2WM

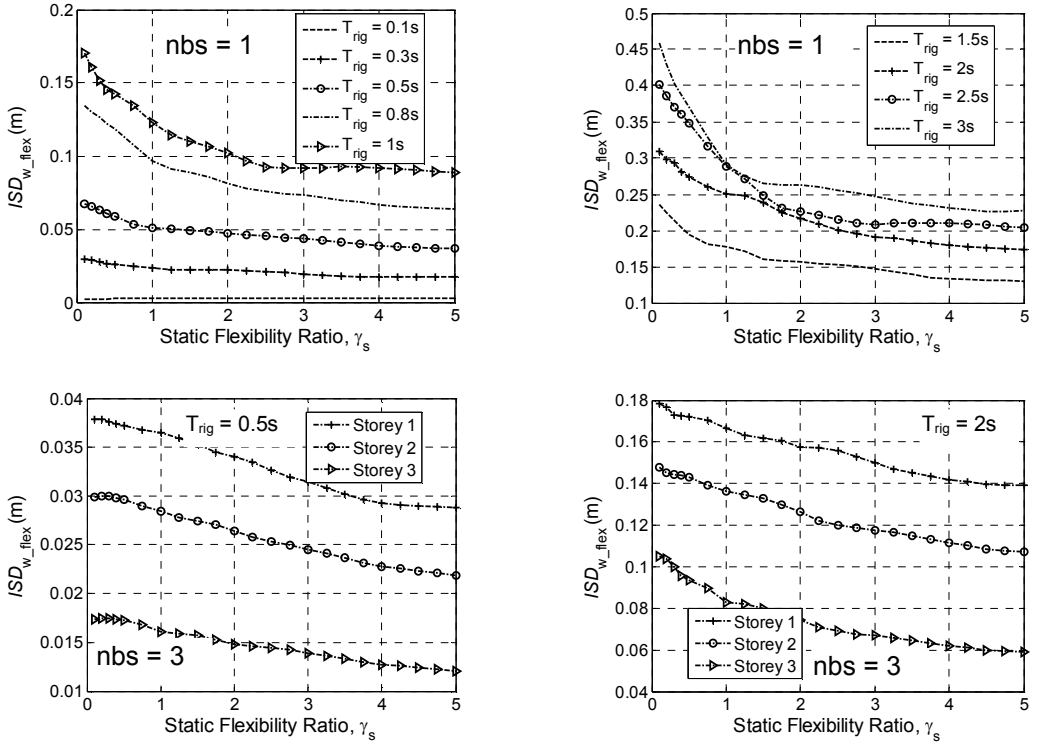

(b) 3WM-Pinned

Figure 5-5: Typical variation of end support median peak interstorey drifts with diaphragm flexibility ratio: (a) 2WM; and (b) 3WM-Pinned structures.

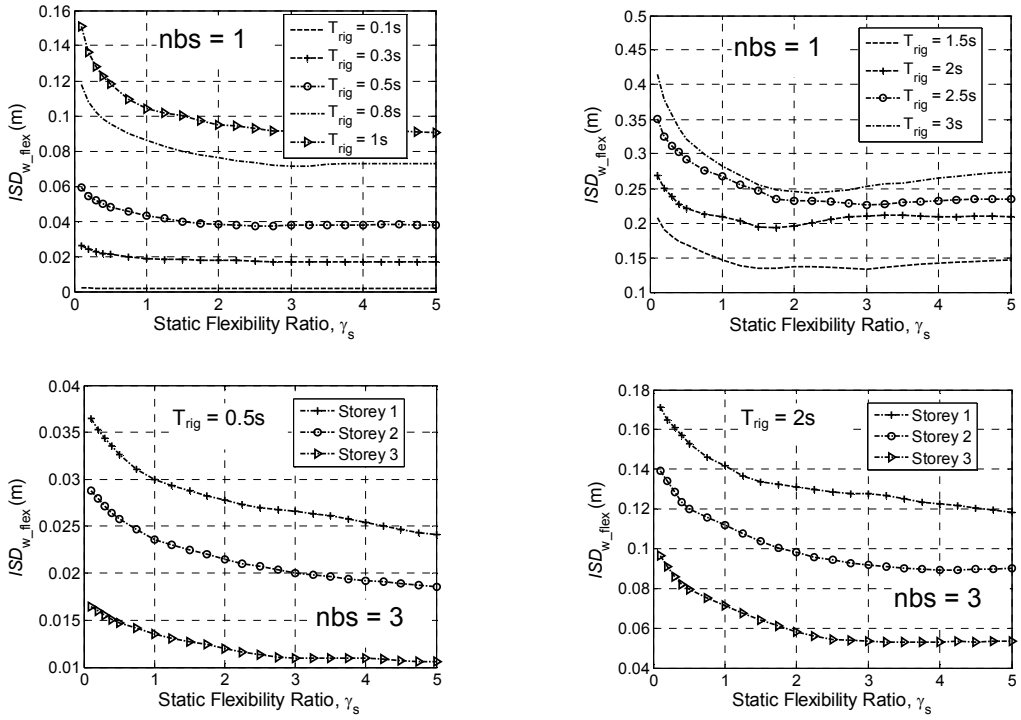

(c) 3WM-Built-in

Figure 5-5: Typical variation of end support median peak interstorey drifts with diaphragm flexibility ratio: (c) 3WM-Built-in structure.

Representative results of median peak relative drifts between the diaphragm and the end supports are shown in Figure 5-6. It shows that; with increasing T_{rig} and γ_s, the in-plane diaphragm displacements increase. The in-plane diaphragm displacements of multi-storey structures are less sensitive to diaphragm flexibility than one storey structures, and the diaphragm displacements increase with increasing storeys. Figure 5-6 shows that the diaphragm in-plane displacements of single span and 3WM-Pinned structures closely match, and they generally have slightly higher diaphragm displacements than those of 3WM-Built-in structures. The above trends in responses were also observed for other demand parameters such as the total in-plane displacements at diaphragm mid-span, the support displacements, the relative drifts between the end supports and the central support (for 3WM-Built-in case), and the diaphragm bending moments.

Figure 5-7 shows the increase in total mid-span displacement due to different diaphragm flexibility ratios. It shows that irrespective of the structural configuration and height, the ratio δ_{total_ratio} increases with γ_s. The figure shows that this diaphragm flexibility effect tends to be higher for short period structures, with the highest increases in total mid-span displacement obtained for T_{rig} = 0.1s. This observation is more prominent for the one storey structures that are critical compared to the multi-storey structures.

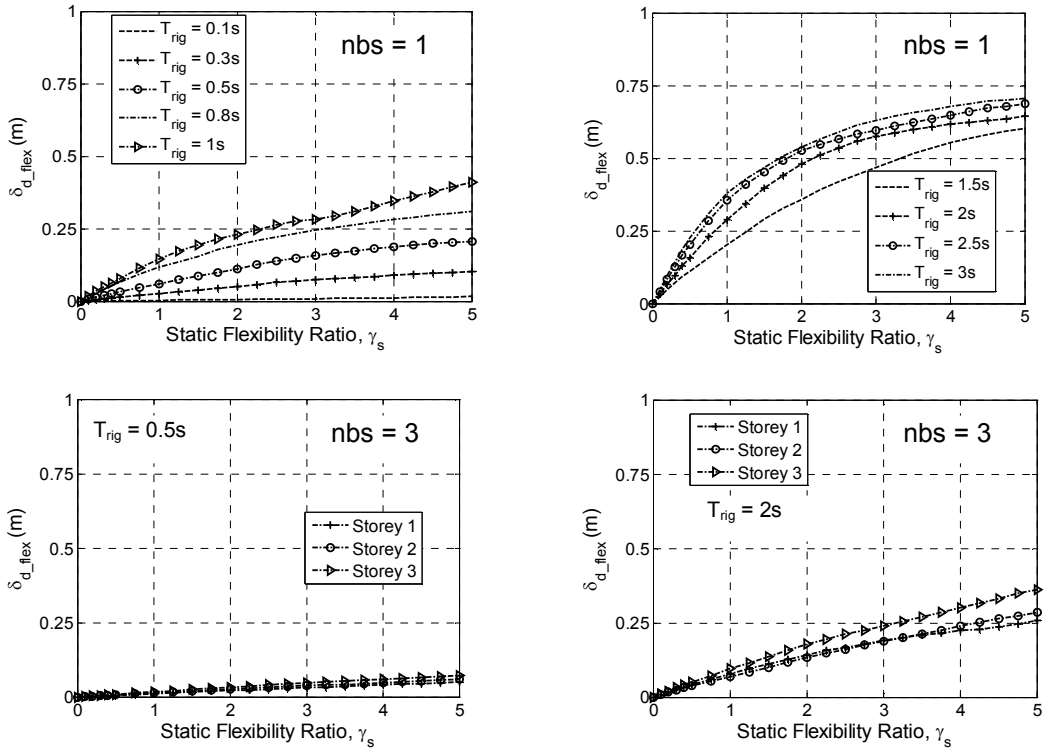

(a) 2WM

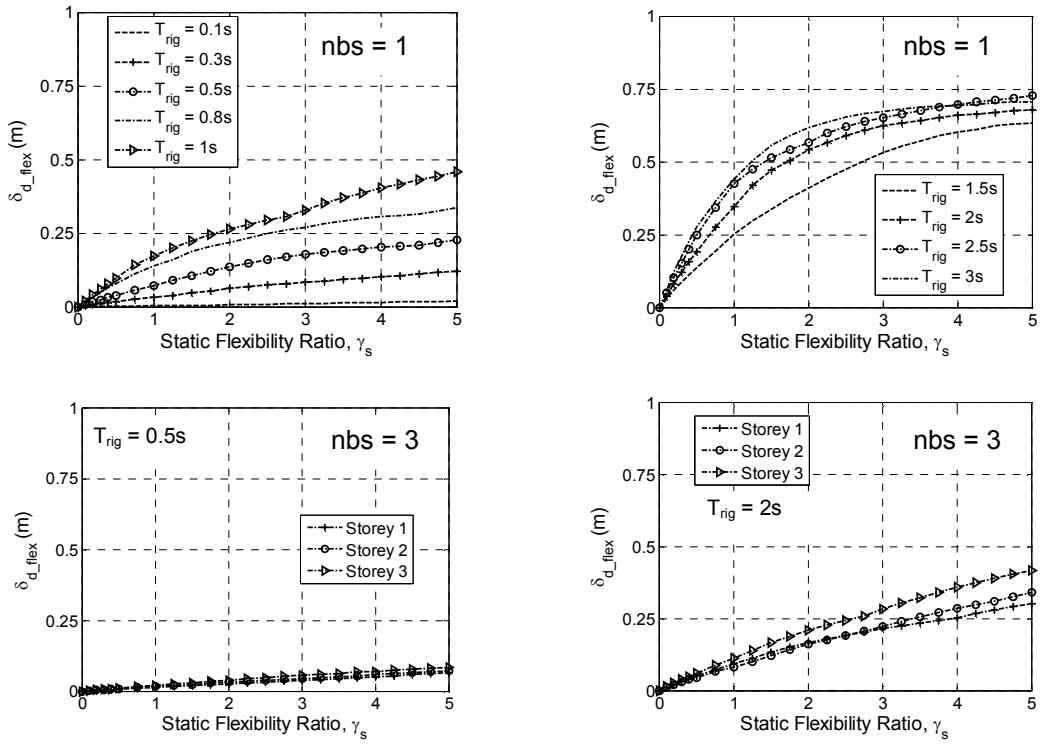

(b) 3WM-Pinned

Figure 5-6: Typical variation of median peak diaphragm in-plane displacement with diaphragm flexibility ratio: (a) 2WM; and (b) 3WM-Pinned structures.

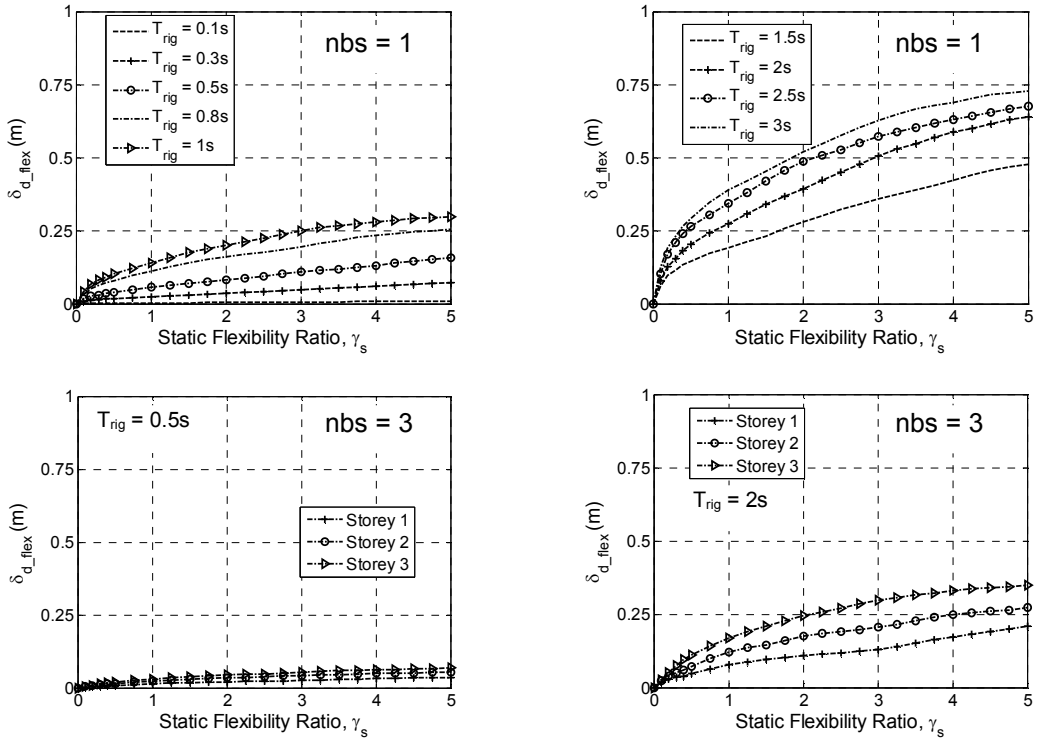

(c) 3WM-Built-in

Figure 5-6: Typical variation of median peak diaphragm in-plane displacement with diaphragm flexibility ratio: (c) 3WM-Built-in structure.

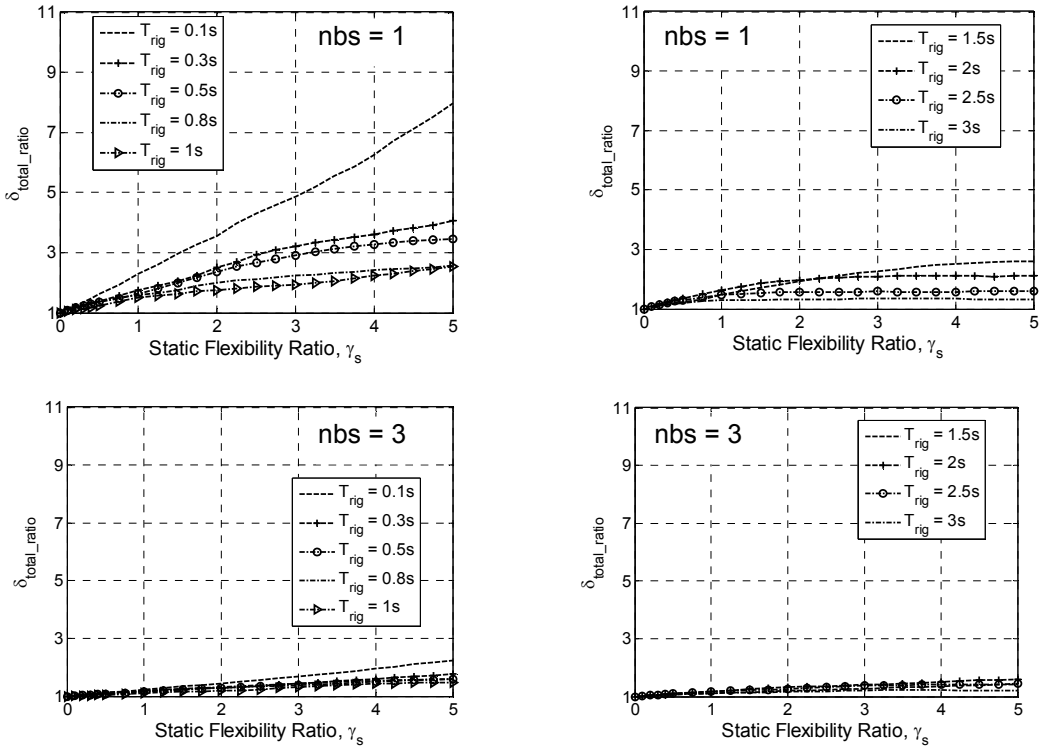

(a) 2WM

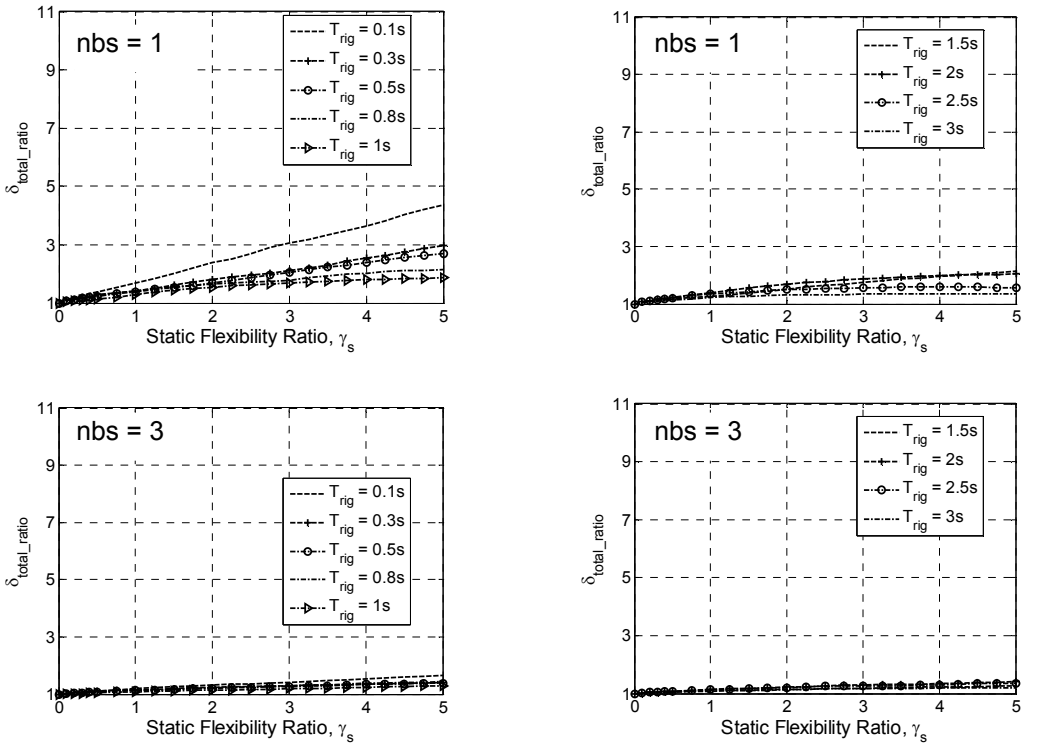

(b) 3WM-Built-in

Figure 5-7: Effect of diaphragm flexibility on median peak total in-plane displacements at diaphragm mid-span

The effect of diaphragm flexibility on median peak diaphragm mid-span bending moments is shown in Figure 5-8. For 2WM structures with T_{rig} > 0.1s, the mid-span diaphragm bending moments due to flexible diaphragms are less than those due to rigid diaphragms. However, for T_{rig} = 0.1s, Figure 5-8(a) shows that the ratio M_{d_ratio} increases with γ_s. In case of 3WM-Built-in structures, the ratio M_{d_ratio} generally decreases with γ_s, with M_{d_ratio} being always less than 1 as shown in Figure 5-8(b).

The change to median peak wall shear forces due to diaphragm flexibility is represented by V_{w_ratio} in Figure 5-9. The response plots show similar trends as observed for diaphragm mid-span bending moments. This can be expected; because the support shear forces arising from the ground motion are the diaphragm end reactions and therefore define the diaphragm bending moments. This also implies that the shear force is not affected significantly by higher modes of vibration.

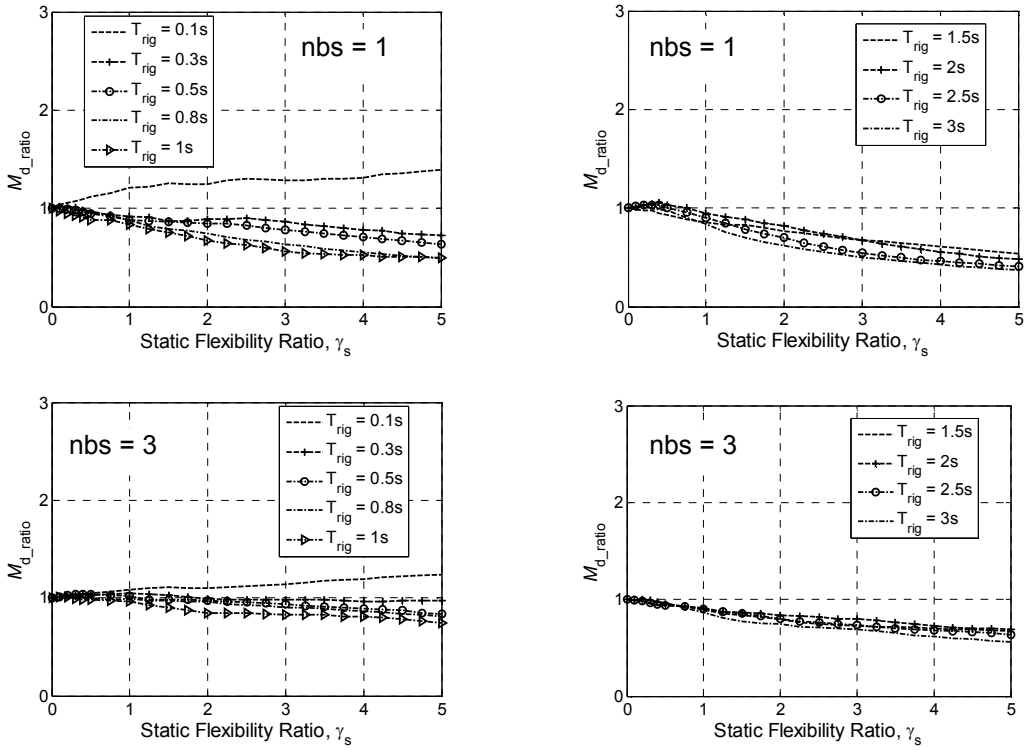

(a) 2WM

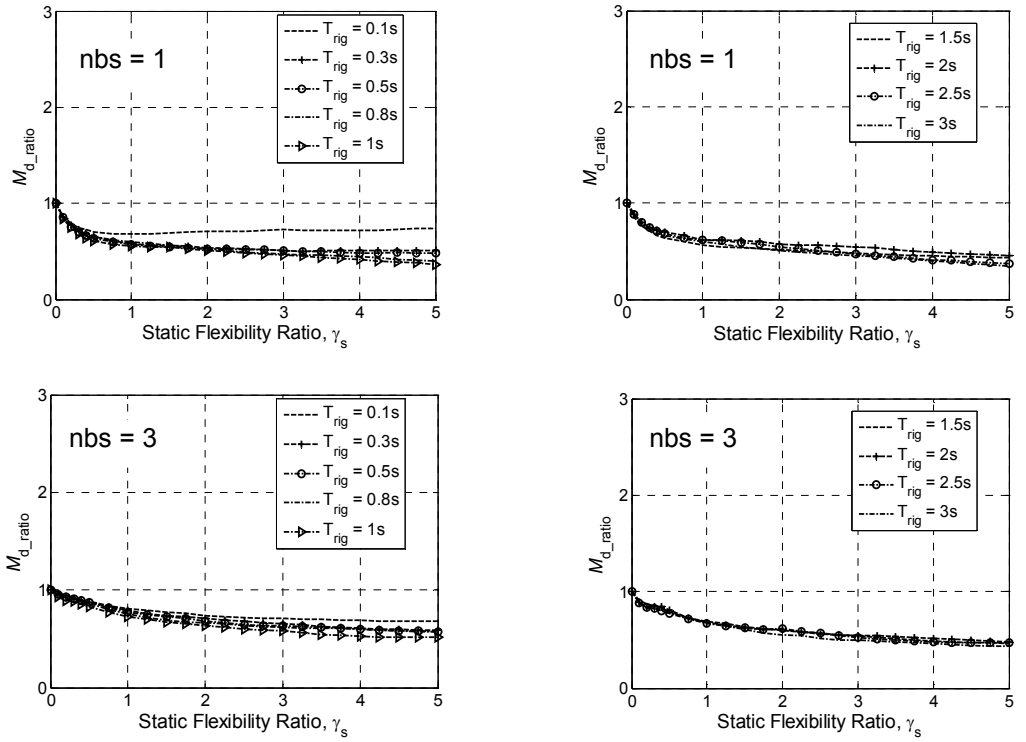

(b) 3WM-Built-in

Figure 5-8: Effect of diaphragm flexibility on median peak bending moment at diaphragm mid-span.

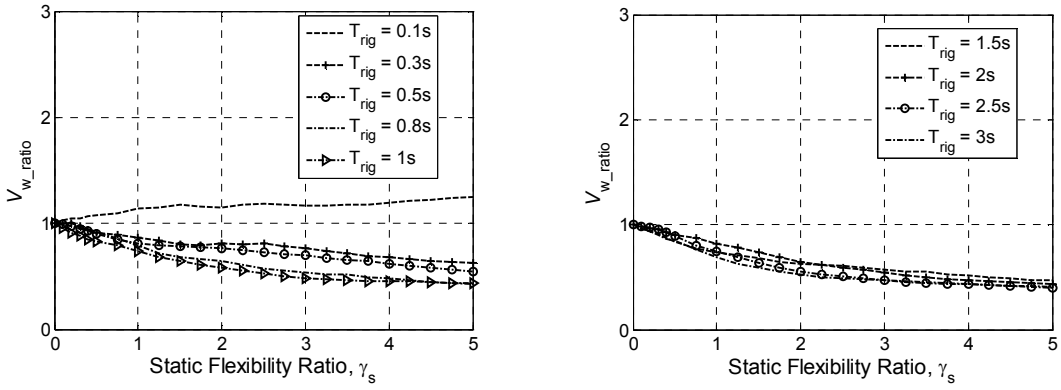

(a) 2WM

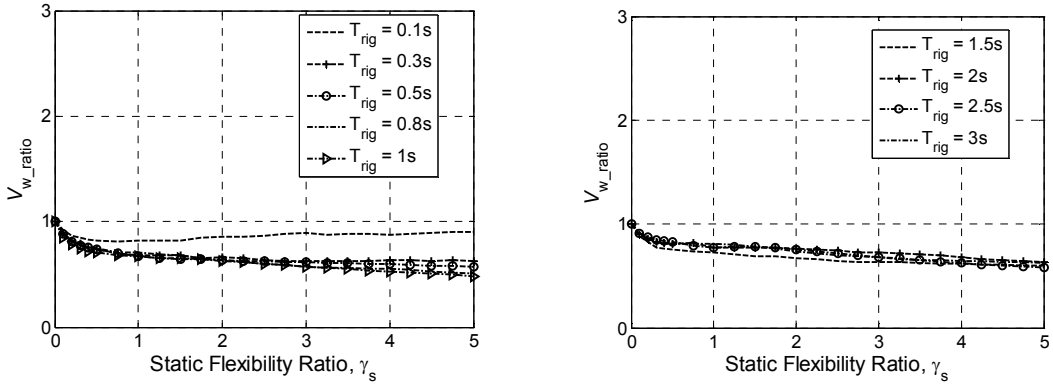

(b) 3WM-Built-in

Figure 5-9: Change in median peak end support shear due to diaphragm flexibility for one storey structures.

The above response plots showed that diaphragm flexibility effects on seismic demands are higher for short period structures than for medium or long period structures. This relationship between T_{rig} and demand can be related to the increase in structural fundamental period arising from additional diaphragm flexibility, which is in turn defined by the acceleration response spectrum. Figure 5-3(a) shows the median acceleration response spectrum for the suite of 20 ground motion records used in this paper. For structures with a period less than the T = 0.29s peak, the fundamental natural period of the structure increases from T_{rig} to T_{flex} due to diaphragm flexibility, thereby increasing the spectral acceleration and force according to Figure 5-3(a). Conversely, the figure shows that for structures with periods greater

than 0.29s, the increase in period from T_{rig} to T_{flex} due to diaphragm flexibility tends to decrease the spectral acceleration and force. Similarly, the differences in peak displacement demands between structures with rigid and flexible diaphragms can be related to the change in the spectral displacement due to shifting period in Figure 5-3(b).

The above observation of reducing diaphragm flexibility effects with increasing structure height is also consistent with previous studies ([8], [9], [6]). It should be noted that other multi-storey structures considered in this study had similar trends in responses to that described above for 3 storey structures. Here, the diaphragm flexibility effects were higher for 2 storey structures, and lower for 5 storey structures, than for the described 3 storey structures. Since the single storey structures were most affected due to diaphragm flexibility, the reminder of this paper only refers to these. Also, since the 2WM and the 3WM-Pinned structures had similar responses and the 3WM-Built-in structures were least affected by diaphragm flexibility, only 2WM structures are considered henceforth.

Dynamic flexibility ratio

The dynamic flexibility ratio, γ_D, defined by Equation (5-8c), is plotted against static flexibility ratio in Figure 5-10 for one storey 2WM structures. For one storey structures, γ_D was computed as the peak value of diaphragm displacement, δ_{d_flex}, divided by the peak value of wall displacement, δ_{w_flex}. These displacements do not necessarily occur at the same time due to higher mode effects. For short period structures, γ_D is almost equal to γ_s. For long period structures with $\gamma_s > 3$, higher mode effects are likely to be more significant and the dynamic flexibility ratios vary from γ_s.

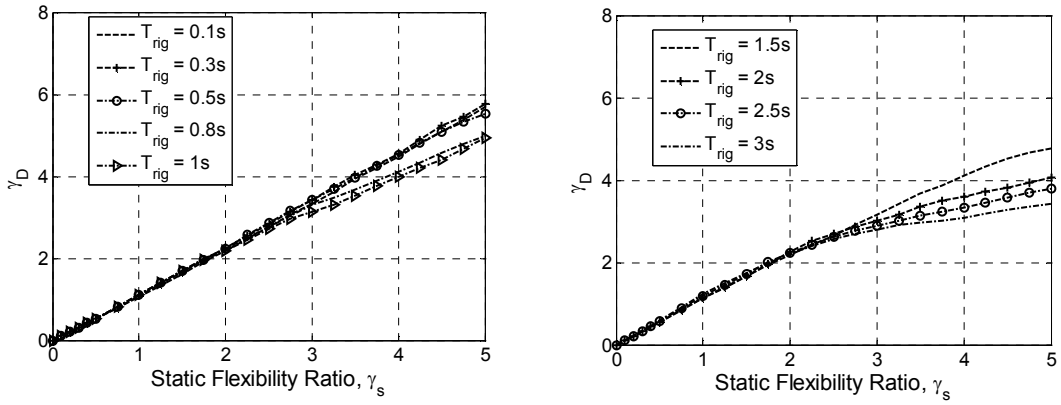

Figure 5-10: Median dynamic flexibility ratio for one storey 2WM structures.

5.4.3 Inelastic Dynamic Time-History Analyses (IDTHA)

The effect of VLFR element inelasticity on one storey structures with flexible diaphragms is investigated. The nonlinear modal time-history analysis (see Appendix K) option in SAP2000 is used here. This time-history analysis method is also called as Fast Nonlinear Analysis, and it is highly efficient for analysing structures with limited nonlinearities [20]. A constant damping of 5% of critical damping for all the modes is again considered.

The VLFR elements, represented as walls in this paper, are modelled using non-linear link elements, and the diaphragms are once again modelled as beam elements. For the hysteretic behaviour of the VLFR elements, the ratio of post-yield stiffness to elastic stiffness was set to 0.001 for all IDTHA described below. The wall yield strength, F_y, is provided according to Equation (5-10), where $F_{elastic}$ is the maximum elastic wall shear force obtained from EDTHA for each earthquake record, and R is the lateral force reduction factor. A range of R values (1, 1.5, 2, 3 and 4) are considered, and effects of end support inelasticity and diaphragm flexibility are evaluated by applying the proposed methodology on 2WM structures.

$$F_y = \frac{F_{elastic}}{R} \quad (5\text{-}10)$$

Figure 5-11 shows the change in seismic demands due to diaphragm flexibility for each lateral force reduction factor. It should be noted that the demand ratios obtained for R = 1 were identical to the demand ratios from EDTHA in Figures 5-7 to 5-9, and therefore the response plots for R = 1 have been omitted below. The median peak total mid-span diaphragm displacements, δ_{total_ratio}, increase with increasing diaphragm flexibility for all ductility levels as shown in Figure 5-11(a). However, this diaphragm effect on total diaphragm displacements reduces with increasing bracing wall inelasticity. In all cases, short period structures had higher increases in displacement than medium-long period structures. While the above findings are based on responses from symmetrical structures, similar trends in behaviour can be expected for irregular structures [31]. A comparison of Figures 5-7(a) and 5-11(a) clearly shows that δ_{total_ratio} obtained from elastic structures are higher than due to inelastic structures for all T_{rig}.

The change in the diaphragm mid-span bending moment due to diaphragm flexibility is shown in Figure 5-11(b). For T_{rig} = 0.1s, the diaphragm bending moment ratio, M_{d_ratio}, increases with γ_s. The figure shows that this increase in diaphragm bending moment due to diaphragm flexibility increases with the lateral force reduction factor, thus producing a maximum of M_{d_ratio} = 2.3 for R = 4. This is consistent with the dynamic amplification factor of 2.3 for diaphragm bending moment proposed by Tremblay and Stiemer [11]. For T_{rig} > 0.1s, the mid-span diaphragm bending moments increase up to γ_s = 0.5 (approximately), and for γ_s > 0.5, it decreases. This value of γ_s = 0.5 may be similar to that for many actual structures. This diaphragm

flexibility effect on diaphragm bending moment increases with bracing wall inelasticity. The figure also shows that $M_{d\_ratio} > 1$ can be expected even for long period inelastic structures (e.g., T_{rig} = 3s) having high diaphragm flexibilities (e.g., $\gamma_s < 4$ for $R = 4$). For the critical T_{rig} = 0.1s one storey structures, Figures 5-8(a) and 5-11(b) show that the elastic structures underestimate the increase in mid-span diaphragm moment due to diaphragm flexibility and end support inelasticity. A similar conclusion can be made by comparing Figures 5-9(a) and 5-11(c) for the change in end wall shear ratio, with the elastic structures having slightly lesser V_{w_ratio} than those from the inelastic structures. It should be mentioned here that; while the maximum shear forces always occurred at the diaphragm ends for elastic structures, in case of inelastic structures, the maximum shear force did not always occur at the diaphragm ends. A similar observation can be found in the literature [11].

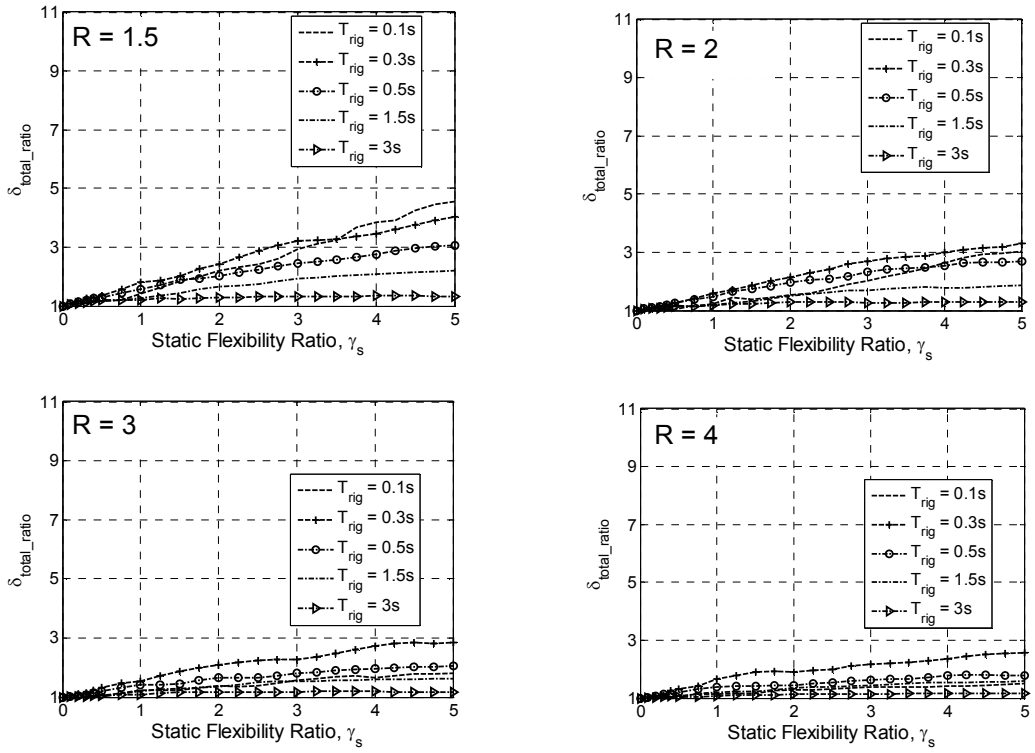

(a) Total in-plane diaphragm mid-span displacement ratio, δ_{total_ratio}

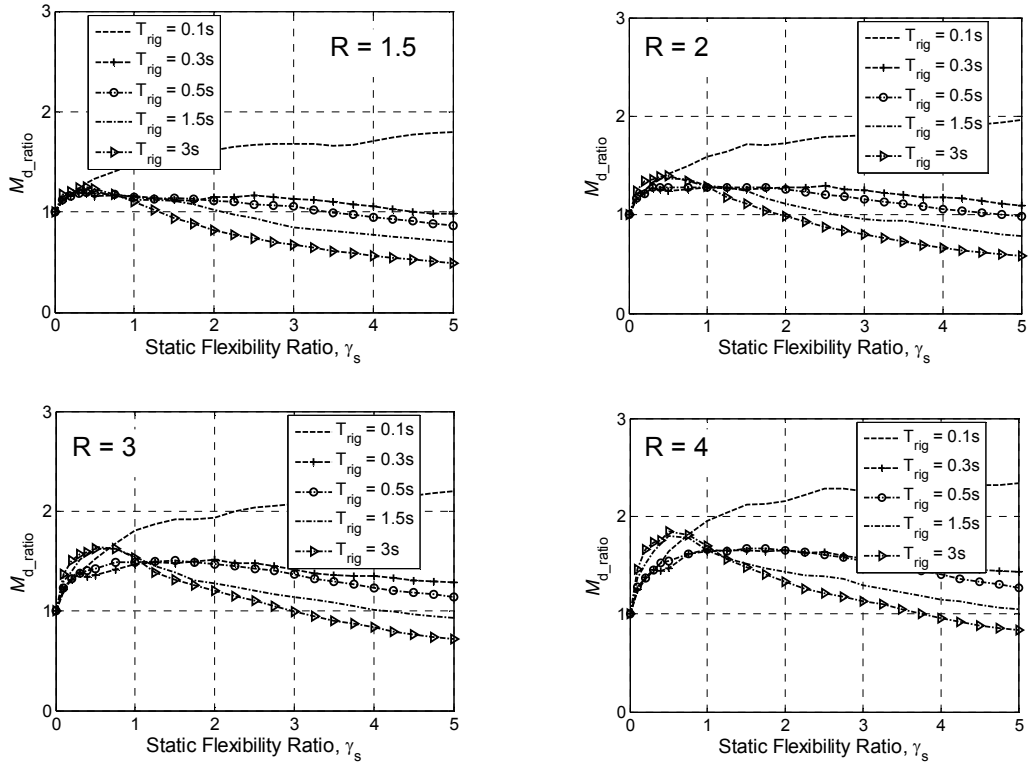

(b) Diaphragm mid-span bending moment ratio, M_{d_ratio}

Figure 5-11: Effect of end support inelasticity and diaphragm flexibility on median peak seismic demands for one storey 2WM structures: (a) δ_{total_ratio} ; and (b) M_{d_ratio}.

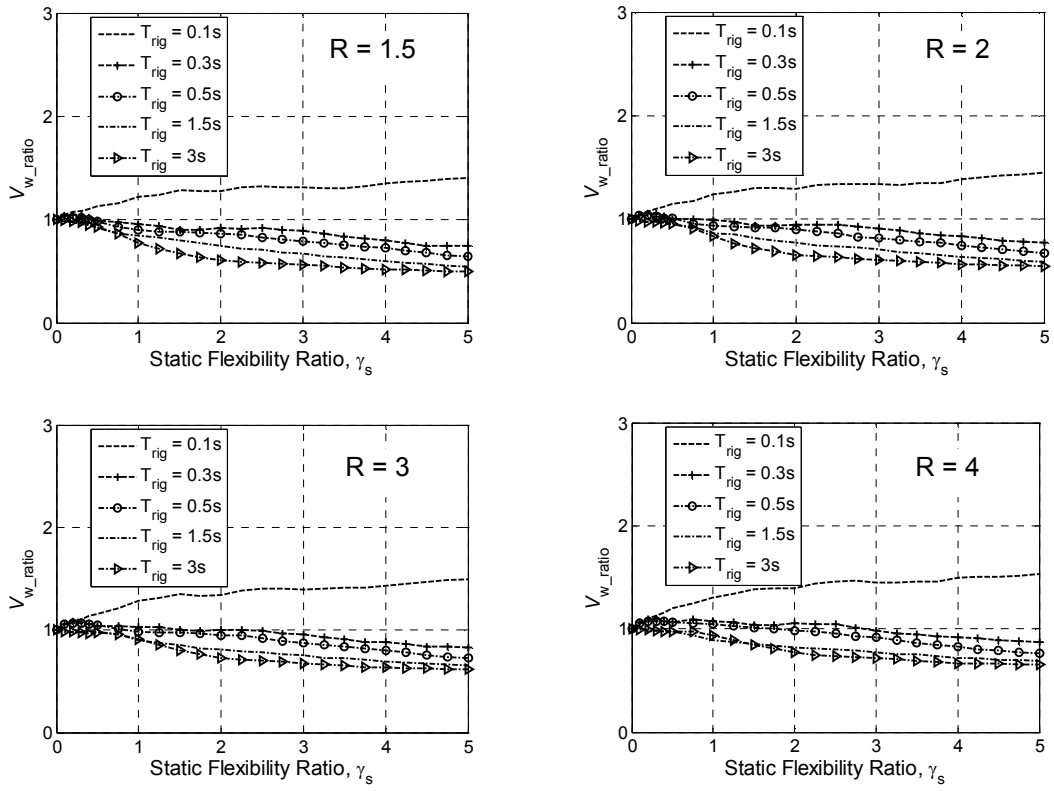

(c) End support shear ratio, $V_{\text{w\_ratio}}$

Figure 5-11: Effect of end support inelasticity and diaphragm flexibility on median peak seismic demands for one storey 2WM structures: (c) V_{w_ratio}.

5.5 Development of Simple Assessment Procedure of Displacement Response

The following procedure was developed to assess the peak displacement of flexible diaphragm model. It involves: (a) estimating the increase in fundamental natural period of the structure and (b) a method to quantify the increase in diaphragm mid-span total displacements through response spectra analyses for different degrees of diaphragm flexibilities.

5.5.1 Modelling Floor Alone As a Stiffness and Mass

The continuous diaphragm in Figure 5-12(a) is modelled as a simply supported beam, where the total diaphragm mass, M_d (= m_d * L_d), can then be lumped at infinite nodal

points along the length of the beam, as shown in Figure 5-12(b). Chopra [19] has shown that fundamental natural period and mode shape for a continuous beam are given by Equations (5-11a) and (5-11b) respectively.

$$T_{1d\_MDOF} = \sqrt{\frac{4\,m_d L_d^4}{E_d I_d\,\pi^2}} \tag{5-11a}$$

$$\phi_1(x) = Sin\left(\frac{\pi x}{L_d}\right) \tag{5-11b}$$

The maximum first mode peak deflection of the MDOF diaphragm occurs at the mid-span of the beam, given by Equation (5-12). Here, Γ_1 is the first mode participation factor, and S_{d1} is the spectral displacement. For this simply supported MDOF diaphragm, the first mode total base shear, V_{1b_MDOF}, can be derived [Appendix J.1 in 25] to produce Equation (5-13).

$$\delta_{d1\max} = \phi_1(L/2) * \Gamma_1 * S_{d1} = \left(\frac{4}{\pi}\right) * S_{d1} \tag{5-12}$$

$$V_{1b\_MDOF}(t) = \left(\frac{8\pi^2 E_d I_d}{L_d^3}\right) * S_{d1} \tag{5-13}$$

The MDOF flexible diaphragm shown in Figure 5-12(a) can be represented by an equivalent *single-degree-of-freedom* (**SDOF**) system shown in Figure 5-12(b). The conditions to be satisfied for this idealisation are:

(1) The fundamental natural period of both the SDOF and MDOF diaphragm systems should be the same; and

(2) The base shear of the SDOF system should be the same as the first mode base shear in the MDOF system.

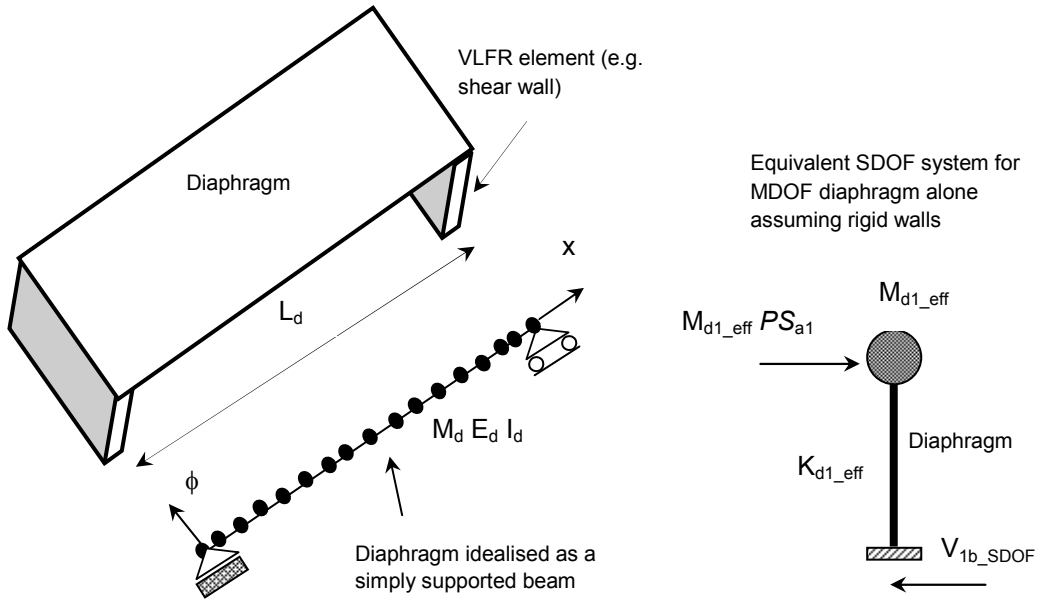

(a) Schematic of single-span one storey structure

(b) Lumped mass model of MDOF flexible diaphragm with rigid supports (in plan)

Figure 5-12: Mathematical model for single-span one storey structure (not to scale).

In order to satisfy the above first condition, the equivalent SDOF system should have an effective modal mass and stiffness for the diaphragm. The effective first mode diaphragm modal mass, M_{d1_eff}, for the SDOF system is given by Equation (5-14) as the product of the first mode participation factor and the generalised excitation, L_1^*.

$$M_{d1\_eff} = \Gamma_1 \; L_1^* = \left(\frac{4}{\pi}\right)\left(\frac{2\,m_d\,L_d}{\pi}\right) \qquad (5\text{-}14)$$

Since the fundamental natural period of the MDOF diaphragm, T_{1d_MDOF}, should be equal to the natural period of an equivalent SDOF diaphragm, T_{1d_SDOF}, Equations (5-11a) and (5-14) can be used to obtain the effective first mode diaphragm modal stiffness, K_{d1_eff}, given by Equation (5-15).

$$K_{d1\_eff} = \frac{8\pi^2 E_d I_d}{L_d^3} \tag{5-15}$$

From Figure 5-12(b), the total base shear of the SDOF system, V_{1b_SDOF}, is given as the product of the effective first mode diaphragm modal mass and the first mode pseudo-acceleration of the SDOF system, PS_{a1}. Approximating PS_{a1} by the product of the first mode spectral displacement and the square of the fundamental natural frequency, V_{1b_SDOF} can be derived to produce Equation (5-16c), which is identical to Equation (5-13) for the MDOF diaphragm.

$$V_{1b\_SDOF}(t) = M_{d1\_eff} * \omega_{d\_SDOF}^2 * S_{d1} \tag{5-16a}$$

$$= M_{d1\_eff} * \left(\frac{K_{d1\_eff}}{M_{d1\_eff}} \right) * S_{d1} \tag{5-16b}$$

$$= \left(\frac{8\pi^2 E_d I_d}{L_d^3} \right) * S_{d1} \tag{5-16c}$$

Since both the conditions specified above are satisfied, the MDOF diaphragm can be conveniently converted into an equivalent SDOF system.

5.5.2 Modelling One Storey Structure as 2DOF System

The lumped mass model explained above for the diaphragm is now used to model the one storey structure in Figure 5-12(a). The structure with a rigid diaphragm can be easily modelled as shown in Figure 5-13(a), and the structure with a flexible diaphragm can be approximated by a lumped mass model shown in Figure 5-13(b). In Figure 5-13, the support masses have been assumed to be negligible compared to the diaphragm mass, and hence they are ignored in the formulation of structural mass matrix.

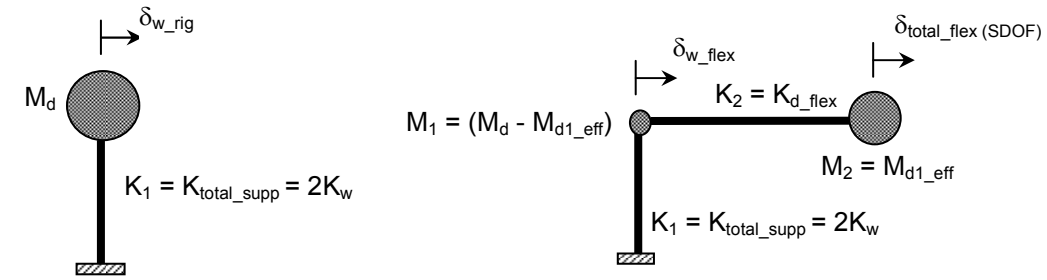

(a) Rigid diaphragm case (b) Flexible diaphragm case

Figure 5-13: Lumped mass models for one storey structure (not to scale).

The following step-by-step procedure was used to estimate the likely increase in the structural fundamental natural period and the total diaphragm mid-span displacement due to diaphragm flexibility.

A. <u>*Rigid Diaphragm Structure (bench-mark case)*</u>:

(1) Select a fundamental natural period of the structure with a rigid diaphragm, T_{rig}.

(2) Calculate the total lateral stiffness of supports, K_{total_sup}, using Equation (5-17).

$$K_{total\_sup} = M_d \left(\frac{2\pi}{T_{rig}} \right)^2 \qquad (5\text{-}17)$$

(3) Conduct *Response Spectra Analysis* for each earthquake record and obtain the peak in-plane displacement of the end wall, δ_{w_rig} (= $S_d(T_{rig})$). The displacement response spectrum for the 20 SAC records shown in Figure 5-3(b) is used in this paper.

(4) For this rigid diaphragm case, the in-plane displacement along the diaphragm length is assumed to be constant, and therefore, the total in-plane displacement at diaphragm mid-span, δ_{total_rig}, equals δ_{w_rig}.

B. *Flexible Diaphragm Structure*:

For each selected static flexibility ratio, γ_{s_j} and T_{rig}, carry out the following steps:

(1) Calculate the lateral stiffness of flexible diaphragm, K_{d_flex}, according to Equation (5-18b). For a certain force F on the structure, Equation (5-1) is used in the formulation of K_{d_flex} as shown below.

$$\gamma_s = \frac{\left(\frac{4}{\pi}\right)\delta_{d\_flex(SDOF)}}{\delta_{w\_flex}} = \frac{\left(\frac{4}{\pi}\right)\left(\frac{8F}{\pi^2 K_{d\_flex}}\right)}{\left(\frac{F}{K_{total\_sup}}\right)} \qquad (5\text{-}18a)$$

$$K_{d\_flex} = \frac{32 K_{total\_sup}}{\pi^3 \gamma_s} \qquad (5\text{-}18b)$$

The total lateral stiffness of the supports is provided according to Equation (5-17).

Note: A fuller development of Equation (5-18a) can be found in Appendix J.6 [25].

(2) Lump the total diaphragm mass as shown in Figure 5-13(b). Here, the effective first mode diaphragm modal mass is lumped at the centre of the flexible diaphragm and the remaining mass from the total diaphragm mass is lumped equally at the two ends of the diaphragm.

(3) Formulate the equation of motion (**EOM**) using the above structural properties and solve the EOM to obtain the dynamic properties. Equations (5-19) and (5-20) can be respectively used to determine natural frequencies and mode shapes

for both degrees-of-freedom shown in Figure 5-13(b), where $k = 1$ for mode 1 and $k = 2$ for mode 2. Alternatively, external programs (e.g., [21]) can be used.

$$\omega_{n_k}^2 = \frac{1}{2}\left(\frac{K_1 + K_2}{M_1} + \frac{K_2}{M_2}\right) \pm \frac{1}{2}\left[\left(\frac{K_1 + K_2}{M_1} + \frac{K_2}{M_2}\right)^2 - \left(\frac{4\,K_1\,K_2}{M_1 M_2}\right)\right]^{1/2} \quad (5\text{-}19)$$

$$\phi_k = \left\{\begin{pmatrix} 1 \\ \dfrac{K_2}{K_2 - M_2\,\omega_{n_k}^2} \end{pmatrix}\right\} \quad (5\text{-}20)$$

(4) Calculate the generalised properties and participation factors for each k^{th} mode of vibration [19].

(5) Obtain participatory displacement magnitude of each mode, *k*.

$$q_k = \Gamma_k\, S_d(T_{flex_k}) \quad (5\text{-}21)$$

(6) Compute displacement for each mode, *k*. Since the contribution of the second mode is negligible, only the first mode is considered, and δ_{w_flex} and $\delta_{total\_flex(SDOF)}$ are obtained.

$$\{u_k\} = \{\phi_k\}\, q_k \quad (5\text{-}22)$$

(7) For each earthquake record, calculate δ_{total_ratio} according to Equation (5-23) [Appendix J.2 in 25].

$$\delta_{total\_ratio} = \frac{\delta_{total\_flex}}{\delta_{total\_rig}} = \left[\frac{4 + 4\gamma_{s_j}}{\pi\gamma_{s_j} + 4}\right]\left(\frac{\delta_{total\_flex(SDOF)}}{\delta_{w\_rig}}\right) \quad (5\text{-}23)$$

(8) Calculate the median δ_{total_ratio} for the record suite using Equation (5-9).

Calculate the increase in fundamental natural period of the structure, T_{ratio}, similar to Equation (5-8b). However, the periods obtained for the structures, represented

by the simplified lumped mass approximation shown in Figure 5-13, are used for estimating T_{ratio}.

5.5.3 Verification of Simple Method

Figure 5-14 shows the comparison of T_{ratio} obtained from analyses results due to simplified analytical model and SAP modelling. Although the analytical method described above was specific for the one storey structure, a similar method was used to calculate the increase in fundamental natural period of multi-storey structures due to diaphragm flexibility. This is represented by the 3 storey structures in Figure 5-

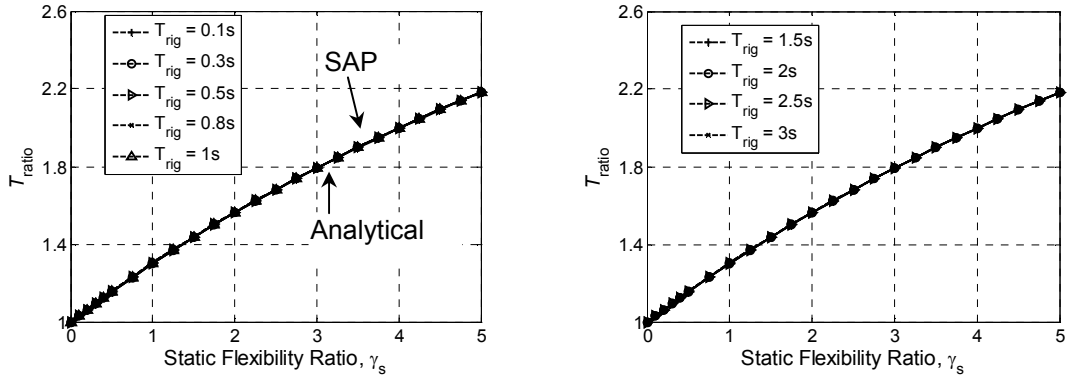

(a) Number of Storeys = 1

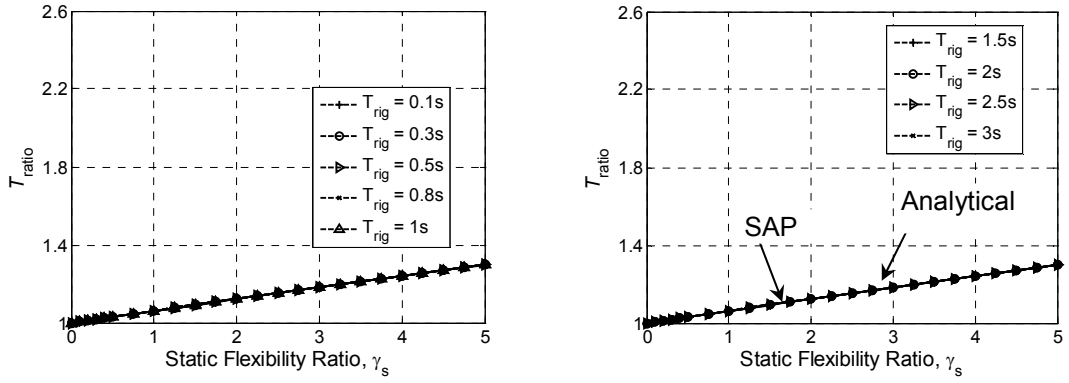

(b) Number of Storeys = 3

Figure 5-14: Comparison of T_{ratio} obtained from SAP and simplified analytical model.

(SAP —— Analytical ------)

14(b). The figure shows that for any structural height, the simple analytical model has T_{ratio} matching with T_{ratio} obtained from SAP results.

For a given structural height, it can be seen from Figures 5-4 and 5-14 that the variation of T_{ratio} with γ_s is not sensitive to T_{rig}. Therefore, based on Figure 5-15, Equation (5-24) is developed empirically to estimate the fundamental natural period of a structure with flexible diaphragms, T_{flex}. In Equation (5-24), a_{T_nbs} is a period coefficient whose value depends on the structural height, calculated using Equation (5-25).

$$T_{flex} = \left(1+\gamma_s\, a_{T\_nbs}\right) T_{rig} \tag{5-24}$$

$$a_{T\_nbs} = 0.57\, e^{-0.78*nbs} \tag{5-25}$$

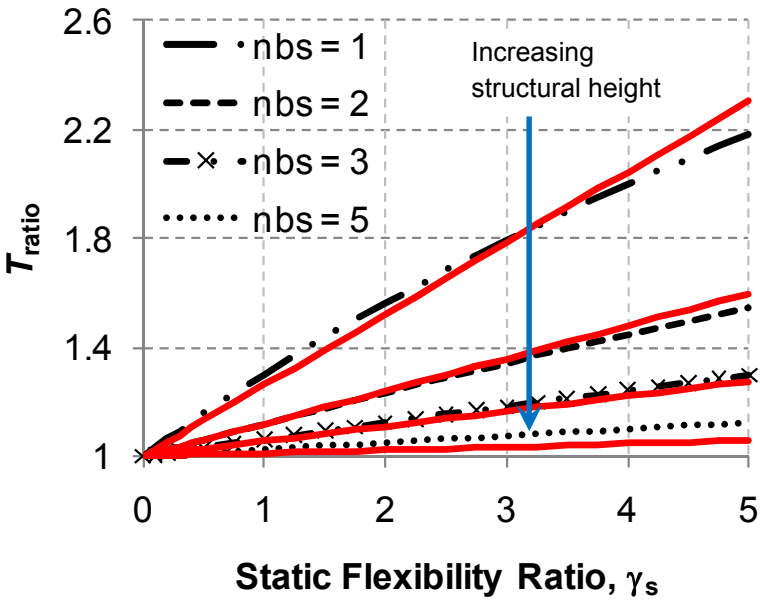

Figure 5-15: Increase in fundamental natural period due to diaphragm flexibility.

The variation of T_{ratio} with γ_s, according to Equation (5-24) is shown by red solid lines in Figure 5-15. Here, although the approximate equation can be slightly non-conservative for the non-critical 5 storey structures, the figure shows that the equation can be effectively used for estimating the increase in period for critical shorter structures.

In Figure 5-16, the non-dimensional demand parameter, δ_{total_ratio}, obtained due to elastic dynamic time-history analyses of one storey 2WM structures, are compared against δ_{total_ratio} calculated by applying the methodology described above for one storey simplified analytical model. Here, the period was estimated through Equation (5-19), rather than using Equation (5-24). Figure 5-16 clearly shows that the simplified method can be effectively used to describe the effects of diaphragm flexibility. The figure also confirms that the structural response is mainly dominated by the fundamental mode of vibration for the type of structures analysed in this paper, a conclusion in agreement with previous researchers (e.g., [11]).

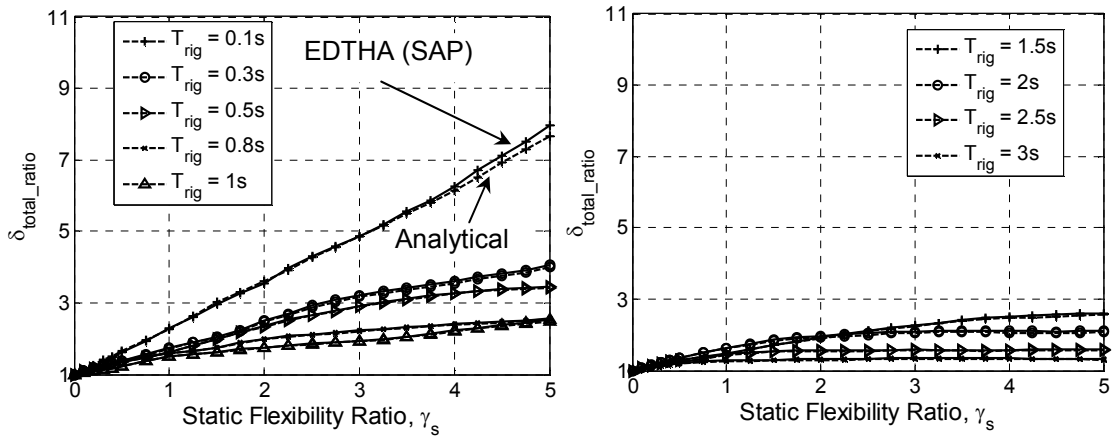

Figure 5-16: Comparison of δ_{total_ratio} obtained from EDTHA (SAP) and simplified analytical model methodology for one storey structures.

(SAP ——— Analytical - - - - - -)

5.6 Conclusions

In many practical designs, the roof or floor systems that connect the vertical lateral force resisting elements are assumed to behave as rigid diaphragms. For designers, determining whether or not a diaphragm is rigid or not is a matter of simply following the limits set in world-wide design codes that define when a diaphragm should be treated as being rigid or flexible. Unfortunately, the methods by which current code determine whether a diaphragm should be treated as rigid or not lack a robust quantitative basis and no guidance is provided regarding the likely change in response for different levels of diaphragm flexibility. While code limits simplify the structural analysis, a rigid diaphragm assumption for a structure with some diaphragm flexibility may result in conservatively designed structures and/or unsafe structures during a seismic event. A series of analyses were conducted to quantify diaphragm flexibility effects on symmetrical structures. The major findings from this study are given below.

1. A brief review of previous studies on diaphragm flexibility effects was provided. This included analytical studies and experimental studies related to diaphragm flexibility. Although different approaches were used, they showed that there was an increase in the structural period with diaphragm flexibility, and generally diaphragm flexibility effects decreased in structures with greater numbers of storeys.

2. A methodology to quantify diaphragm flexibility effects was developed and applied to symmetrical structures with different deformation types, different vertical lateral force resiting element configurations, and different structural heights.

3. The fundamental natural period of structures with flexible diaphragms was always greater than those with rigid diaphragms. The structural natural period increased with increasing amount of diaphragm flexibility. However, this increase to period was not sensitive to the period of rigid diaphragm structure. The rate of increase of structural natural period due to diaphragm flexibility decreased with increasing structural height.

4. In-plane diaphragm displacements of elastic structures with flexible diaphragms increased with diaphragm flexibility while forces generally decreased. This is consistent with the response spectra shape. One storey elastic structures were most affected by diaphragm flexibility.

5. Single span structures, and the two-span structures with a central pin connection, had nearly the same change in response due to diaphragm flexibility. However, the two span structures with a built-in mid-span connection generally were least affected.

6. Some yielding structures with flexible diaphragms had greater mid-span diaphragm bending moments and support shears than did structures with rigid diaphragms.

7. The single-storey continuous diaphragm and walls were modelled as a 2DOF system governed by first mode response. This approximation allowed the peak displacement to be captured well.

5.7 Acknowledgements

The authors gratefully acknowledge the financial support for this work provided by the New Zealand Earthquake commission (www.eqc.govt.nz).

5.8 References

[1] SNZ. NZS 1170.5 Supp 1:2004, Structural Design Actions. Part 5: Earthquake actions New Zealand – Commentary, Standards New Zealand, Wellington, 2004.

[2] IBC. International Building Code. International Code Council (ICC), Whittier, CA, 2003.

[3] FEMA 450. National Earthquake Hazards Reduction Program recommended provisions for seismic regulations for new buildings and other structures. Prepared by the Building Seismic Safety council, National Institute of building sciences, Washington, D.C., 2003.

[4] CEN. EN 1998-1. Eurocode 8. Design of structures for earthquake resistance – Part 1: General Rules, Seismic Actions and Rules for Buildings, European Committee for Standardization, 2004.

[5] Jain SK and Mandal UK. Dynamics of buildings with V-shaped plan. *Journal of Engineering Mechanics* 1992; **118**(6):1093-1112.

[6] Barron JM, Hueste MBD. Diaphragm effects in rectangular reinforced concrete buildings. *ACI Structural Journal* 2004; **101**(5):615-624.

[7] Jain SK, Jennings PC. Analytical models for low-rise buildings with flexible floor diaphragms. *Journal of Earthquake Engineering and Structural Dynamics* 1985; **13**(2):225-241.

[8] Kunnath SK, Panahshahi N, Reinhorn AM. Seismic response of RC buildings with inelastic floor diaphragms. *Journal of Structural Engineering* 1991; **117**(4):1218-1237.

[9] Saffarini HS, Qudaimat MM. In-plane floor deformations in RC structures. *Journal of Structural Engineering* 1992; **118**(11):3089-3102.

[10] Ju SH, Lin MC. Comparison of building analyses assuming rigid or flexible floors. *Journal of Earthquake Engineering and Structural Dynamics* 1999; **125**(1):25-31.

[11] Tremblay R, Stiemer SF. Seismic behavior of single-storey steel structures with a flexible roof diaphragm. *Canadian Journal of Civil Engineering* 1996; **23**(1):49-62.

[12] Tena-Colunga A, Abrams DP. Seismic behaviour of structures with flexible diaphragms (ASCE). *Journal of Structural Engineering* 1996; **122**:439-445.

[13] Fleischman RB, Farrow KT. Dynamic behavior of perimeter lateral-system structures with flexible diaphragms. *Journal of Earthquake Engineering and Structural Dynamics* 2001; **30**(5):745-763.

[14] Fleischman RB, Farrow KT, Eastman K. Seismic performance of perimeter lateral system structures with highly flexible diaphragms. *Earthquake Spectra* 2002; **18**:251-286.

[15] Lee HJ, Aschheim MA, Kuchma D. Interstorey drift estimates for low-rise diaphragm structures. *Journal of Engineering Structures* 2007; **29**:1375-1397.

[16] Panahshahi N, Reinhorn AM, Kunnath SK. Seismic response of a 1:6 reinforced concrete scale-model structure with flexible floor diaphragms. *ACI Structural Journal* 1991; **88**(3):615-624.

[17] Panahshahi N, Reinhorn AM, Kunnath SK. Earthquake simulation study of a one- sixth scale model RC building with flexible floor diaphragms. *Fifth U.S. National Conference on Earthquake Engineering* 1994; pp 641-650.

[18] Tremblay R, Berair T, Filiatrault A. Experimental behaviour of low-rise steel buildings with flexible roof diaphragms. *12th World Conference on Earthquake Engineering* 2000. Paper No. 2567.

[19] Chopra AK. Dynamics of structures: Theory and Applications to Earthquake Engineering. New Jersey: Prentice Hall, 2000; 844 pp.

[20] CSI. Computers and Structures Inc. SAP2000 Advanced 11.0.8. Static and Dynamic Finite Element Analysis of Structures, Berkeley, 2007.

[21] MATLAB 7.9 (R2009b). The Maths Works, Inc.: Natick, MA, 2009.

[22] Han SM, Benaroya H, Wei T. Dynamics of transversely vibrating beams using four engineering theories. *Journal of Sound and Vibration* 1999; **225**(5): 935-988.

[23] Humar JL. Dynamics of Structures. Lisse, Netherlands; Exton, PA: A.A. Balkema Publishers, 2002.

[24] Spooner MS. Quantifying the dynamic response of flexible floor diaphragms. Third Professional Year Project, Department of Civil and Natural Resources Engineering, University of Canterbury, Christchurch, 2008.

[25] Sadashiva VK. Quantifying structural irregularity effects for simple seismic design. Ph.D thesis (to be published), Department of Civil and Natural Resources Engineering, University of Canterbury, Christchurch, 2010.

[26] Marjanishvili S, Agnew E. Comparison of various procedures for progressive collapse analysis. *Journal of Performance of Constructed Facilities* 2006. **20** (4): 365-374.

[27] Wilson EL. Three-dimensional static and dynamic analysis of structures, 3rd Edition, *Computers and Structures*, Inc., Berkeley, California, 2002.

[28] Sadashiva VK, MacRae GA, Deam BL. Determination of structural irregularity limits – mass irregularity example. *Bulletin of the New Zealand Society for Earthquake Engineering* 2009; **42**(4): 288-301.

[29] Cornell CA, Fatemeh JF, Hamburger RO, Foutch DA. Probabilistic basis for 2000 SAC FEMA steel moment frame guidelines. *Journal of Structural Engineering* 2002. **128**(4): 526-533.

[30] Luco N. Probabilistic seismic demand analysis, SMRF connection fractures, and near-source effects. Ph.D. Dissertation, Department of Civil and Environmental Engineering, Stanford University, Stanford, CA, 2002.

[31] De-La-Colina J. In-plane floor flexibility effects on torsionally unbalanced systems. *Journal of Earthquake Engineering and Structural Dynamics* 1999; **28**(12):1705-1715.

6. SUMMARY OF RECOMMENDATIONS

It was recognised in this thesis that there was a need to quantify the code regularity limits. With this as the focal objective, the influence of different types of irregularities on the seismic response of structures was studied. Simple methodologies were developed and applied on conceptually simple models to explain the change in the response due to different degrees of irregularities. Relationships linking the degree of irregularity and the change in seismic demand were developed. These relationships are generally conservative as they relate to the median demand increase over a suite of records for a critical location of irregularity in a critical structure. As such, they are suitable for code implementation. Specific conclusions for each of the irregularity investigated is described in the preceding chapters, this Chapter describes a summary of recommendations based on the outcomes of the study. A note to the engineers, explaining how the information from this study can be useful to the engineering community, is also provided here.

6.1 Relationships between Irregularity and Increased Drift

The equations below give an estimate of the likely median increase in interstorey drift demand for critical structures with the irregularity at the critical location. This information should give designers a better understanding of the influence of irregularity and more confidence in their designs.

(1) ***Mass irregularity***

$$ISD_I = ISD_R \times \left[1 + 0.5(1 - MR)\right] \quad \text{for } MR < 1.0 \qquad \text{(6-1a)}$$

$$ISD_I = ISD_R \times \left[1 + 0.15(MR - 1)\right] \quad \text{for } MR > 1.0 \qquad \text{(6-1b)}$$

where; ISD_I is the peak interstorey drift demand of the irregular structure, ISD_R is the peak interstorey drift demand of the regular structure, and MR is the mass ratio at one storey relative to that of a neighbouring storey.

(2) ***Stiffness-strength irregularity (constant interstorey height)***

$$ISD_I = ISD_R \times \left[1+1.6(1-SMF)\right] \quad \text{for } SMF < 1.0 \qquad \text{(6-2a)}$$

$$ISD_I = ISD_R \times \left[1+0.4(SMF-1)\right] \quad \text{for } SMF > 1.0 \qquad \text{(6-2b)}$$

where; SMF is the stiffness modification factor, which is defined as the stiffness of one storey relative to that of the neighbouring storey.

The above two equations are based on the responses of the structures having storey stiffness and strength varying by the same amount (SMF).

(3) ***Stiffness-strength irregularity (changing interstorey height)***

$$ISD_I = ISD_R \times \left[1+\left(\left|h_{rat}-1\right|\right)\right] \qquad \text{(6-3)}$$

where; h_{rat} is the interstorey height ratio, which is defined as the ratio of modified interstorey height to the initial interstorey height.

Equation (6-4) provides an estimate of the irregular structure drift demand in terms of the stiffness modification factor (SMF).

$$ISD_I = ISD_R \times \left[1+1.6(1-SMF)\right] \quad \text{for } SMF < 1.0 \qquad \text{(6-4a)}$$

$$ISD_I = ISD_R \times \left[1+0.5(SMF-1)\right] \quad \text{for } SMF > 1.0 \qquad \text{(6-4b)}$$

The above Equations (6-3) and (6-4) are based on the responses of the structures having only the storey stiffness modified due to a change in the storey height.

(4) ***Diaphragm flexibility effects***

Forces are not generally increased due to diaphragm flexibility. However, displacements are. The increase in peak in-plane displacement due to diaphragm flexibility can be obtained by:

$$D_{FD} = D_{RD} \times (1+1.35\ \gamma_s) \quad \text{for } T_{rig} \leq 0.5\text{s} \qquad \text{(6-5a)}$$

$$D_{FD} = D_{RD} \times (1+0.5\ \gamma_s) \quad \text{for } T_{rig} > 0.5\text{s} \qquad \text{(6-5b)}$$

The above equations are based on the responses of one storey structures which were the most affected by diaphragm flexibility. Here, D_{FD} is the peak in-plane displacement of the structure considering diaphragm flexibility, D_{RD} is the peak in-plane displacement of the same structure ignoring diaphragm flexibility (rigid diaphragm assumption), γ_s is the static flexibility ratio (Equation (5-1)), and T_{rig} is the natural period of the structure with a rigid diaphragm assumption.

6.2 Irregularity Limits Based On A 10% Increase in Drift

If irregularity limits are desired, then a specified level of drift increase should be specified. This can be developed for any strength increase. In the example below, a 10% increase in the drift is considered with the equations in Section 6.1 above.

(1) ***Mass irregularity***

(a) *Acceptable irregularity* –

The mass ratio, *MR*, must lie between -20% and +67% of the regular floor mass.

(b) *Current code provision implication* –

This compares with the current allowable mass increase by 50% in Clause 4.5.1.1 of NZS1170.5. This increase in mass value by 50%, corresponds to a change in response of 1.075 times, for a structure designed to show the most effect of

increased mass irregularity with the irregularity at the critical level according to the equation in Section 6.1.

(2) ***Stiffness-strength irregularity (constant storey height)***

(a) *Acceptable irregularity* –

The stiffness modification factor, *SMF*, for a change in the properties of one storey relative to the other storeys, must lie in the range of -6.25% to +25% that of the storey above.

(b) *Current code provision implication* –

NZS1170.5 currently considers strength and stiffness irregularity separately.

The stiffness of a storey is not permitted to be less than 70% of an adjacent story in Clause 4.5.1.2 of NZS1170.5. This corresponds to a decrease to storey stiffness by 30%.

In NZS1170.5, the storey strength is not permitted to be any less than 90% of the strength of the storey above (Clause 4.5.1.3). This corresponds to a decrease to storey strength by 10%.

Based on this, for structures in which stiffness and strength are proportional at each level, NZS1170.5 limits on strength control, and the expected change in response is expected to be 1.16 times for a critical structure according to the equation in Section 6.1.

(3) ***Stiffness-strength irregularity (changing storey height)***

(a) *Acceptable irregularity* –

According to Section 6.1, a storey height can be modified by any h_{rat} having a magnitude between 0.9 and 1.1.

(b) *Current code provision implication –*

NZS 1170.5 currently does not imply any restriction on the allowable interstorey height modification.

(4) ***Diaphragm Flexibility Effects***

(a) *Acceptable irregularity –*

For a 10% increase in displacement due to diaphragm flexibility, γ_s has to be less than 0.075 for $T_{rig} \leq 0.5$s, and for $T_{rig} > 0.5$s, γ_s has to be less than 0.2.

(b) *Current code provision implication –*

NZS 1170.5 recommends $\gamma_s < 2$ for diaphragms to be considered stiff. This corresponds to the peak in-plane displacement of a short period structure ($T_{rig} \leq$ 0.5s) with a flexible diaphragm, to be 3.7 times that due to a rigid diaphragm assumption for the same structure according to Section 6.1. This displacement increase will however be considerably less for other one storey structures ($T_{rig} >$ 0.5s) or multi-storey structures.

It should be noted that a number of assumptions were made with respect to the equations and values given above. Some subjective assessments were also made. Before using these equations, readers should familiarize themselves with these assumptions, as described in the appropriate chapter.

6.3 A Note to Engineers – How Can This Work Be Used?

The work was conducted to provide engineers with:

(1) a rational basis for regularity limits for design

(2) an understanding of the sensitivity of drift response to the magnitude of an irregularity

(1) Rational Basis for Irregularity Limits for Design

It is possible to specify an acceptable variation in response, and then, using the relationships in Section 6.1, determine the acceptable level of irregularity. This has been done for a 10% variation in response as shown in Section 6.2, but other levels of variation can also be selected.

The use of a consistent variation for all irregularity types, results in consistent recommendations for code irregularity limits to suggest the engineer as to what type of analysis should be used for design.

The consistent and rational approach developed above will be promoted for incorporation into the NZ loadings standard "NZS1170.5 – Structural Design Actions – Earthquake Actions – New Zealand", based on discussion with engineers about an acceptable level of variation.

(2) Sensitivity of Behaviour to Irregularity

The variation in response as a function of the magnitude of irregularity, as specified in Section 6.1, is useful for designers to:

(a) Perform a rapid preliminary design of a structure with irregularity.

(b) Tell the client whether the structure can be built with an irregularity modification at a client-engineer meeting. That is, the information developed from this study can be used on structures with obvious irregularities to be made regular (and therefore have a more predictable and desirable response) by making other compensating changes in the structure. This will help mitigate irregularity effects during the preliminary design.

(c) Perform a rapid check of structures which have been designed with more complex analysis methods.

(d) Better consider the required capacity. In probabilistic performance based earthquake engineering, or in code development, the variation in response due to irregularity may be used to provide better estimates of the likely demands on elements of actual structures. This knowledge is important in determining the required capacity of a member.

(e) Develop more confidence in their designs because they are aware of the likely variation in response to the amount of irregularity.

7. OPPORTUNITIES FOR FURTHER WORK

As with any study, there are further opportunities for investigation to improve and refine knowledge. Some activities, but not limited to the below, can be conducted.

7.1 Structures with Other Types of Vertical and Plan Irregularities

The work explained in this thesis is limited to certain types of vertical and plan irregularities. Other types of irregularities exist in structures as shown in Figure 1-1. The code regularity limits for such irregularities that are not considered in this study require proper justification.

7.2 Structures with a Combination of Different Types of Irregularities

The work conducted in this study evaluates the effect of one type of irregularity at a time, except when strength and stiffness irregularities were considered where there is an obvious correlation between these two types of irregularity. It is possible that a structure can have a combination of different types of irregularities shown in Figure 1-1. For example, a structure can have a heavier floor at one level, and the storey supporting that floor may have a taller storey height that produces a stiffness-strength irregularity. Additional complexity may also exist in the structure due to an irregular plan shape, thus resulting in torsional irregularity. Other combinations of irregularity are also possible. In such cases, structures with multiple irregularities may perform worse than those described here. Studies on these topics are open.

7.3 Structures with Irregularities at Multiple Locations

While the structures analysed in this study considered irregularity at one location at a time, there are possibilities that several floor/storeys within a structure can have irregularities. Again, this could either be due to the existence of the same type of irregularity at multiple locations, or there could be further complications due to several irregularity combinations at various locations. Studies on the above aspects of irregularities can be challenging.

7.4 Evaluate Structures Other Than Simple Structures

For simplicity, all structures considered for vertical irregularity studies in this thesis were idealised as shear-type of structures. For diaphragm flexibility study, no specific structure was considered, and simple modelling technique was adopted. It would be useful to perform a more advanced study of structures which consist of other types of structural systems. For example; structural walls, which perform in a flexural mode, rather than in a shear mode, can have different response change due to irregularity than those described in this thesis. Such wall structures have behaved exceptionally well in the past [1].

7.5 Structures Designed Using Other Analysis Methods

The work conducted in this study indicates that the Equivalent Static method is reasonably robust, but there is a change in response for some structures with different amounts of irregularity. Other more sophisticated methods, such as the linear dynamic methods, or non-linear pushover methods, are likely to be more accurate and less sensitive to inelasticity. However, the criteria for the static procedure are not severe, so it is likely that results from other methods will be even less severe. For this

reason, the likely incremental change in response equations is unlikely to have a significant effect on the design. This should, however, be confirmed by further studies.

7.6 Other Factors

The conclusions and recommendations derived from this study are limited to the several assumptions identified in the included Chapters. Examples of these assumptions and their implications include: (a) The developed regularity recommendations were based on response of critical structures. The proposed equations may therefore be conservative for other non-critical structures and with other structural configurations; (b) Structures were assumed to be resting on strong rock; therefore, sensitivity studies on the effect of soil type on the change in the response due to irregularity will be interesting; (c) Peak interstorey drift ratio was the chosen engineering demand parameter (EDP) to evaluate vertical irregularity effects. The developed methodology can also be used to consider other types of EDP's (e.g., peak bending moments and shear forces in beams and slabs etc. [2]), and accordingly regularity equations can be formulated; (d) A set of 20 earthquake records was used for all dynamic time-history analyses explained in this thesis. Recent studies (e.g., Pacific Earthquake Engineering Research Centre [3]) have shown that use of randomly selected earthquake records may result in biased results. It was stated in this study that; since regular and irregular structures are subjected to the same set of records, there is likely to be no significant effect of earthquake record selection method on the developed regularity recommendations. Although this assumption may seem reasonable, further studies are required to show that the regularity provisions are independent of the method used to select the earthquake records. Similarly,

implications on relative responses, due to alternative modelling assumptions (e.g., damping models, hysteresis rules etc.) that are not considered in this study, should not be significant. However, proper justification is necessary. (e) The regularity recommendations in this thesis are based on the median responses of structures. Similar regularity recommendations can be developed for other levels of confidence limits using the dispersion and median results.

7.7 References

[1] Fintel H. Performance of buildings with shear walls in earthquakes of the last thirty years. *Journal of Precast/Prestressed Concrete Institute (PCI)* 1995; **40**(3): 62-80.

[2] ATC-58 Project Task Report (Phase 2, Task 2.3) prepared by ATC-58 Nonstructural Performance Products team. Engineering demand parameters for structural framing systems, Applied Technology Council, California. www.atcouncil.org/pdfs/atc582t22.pdf

[3] Pacific Earthquake Engineering Research Centre (PEER). Ground motion selection and modification program (GMSM).

peer.berkeley.edu/gmsm/Mission.html

APPENDIX A: YIELD DRIFT RATIO LIMITS

A.1 Approximate Yield Drift Ratios for Frame Buildings

In Chapters 2 to 4, one of the two conditions set was to eliminate structures that had unlikely strength to scaled stiffness ratios. Likely storey strength to scaled stiffness ratios for realistic structures were determined based on empirical relations giving yield drift ratios for some common frame buildings (Priestley *et al.* [1]). Here, stiffness used was the storey stiffnesses multiplied by the interstorey height, thereby resulting in dimensionless storey strength to stiffness ratios. The approximate yield drift ratio relations are shown in Table A-1. Here, values in Table A-2 were assumed for parameters defined in Table A-1, and the possible ranges of yield drift ratios were calculated as shown in Table A-1 and Figure A-1. Based on Figure A-1, lower and upper limits of storey strength to scaled stiffness ratios of 0.3% and 3% were set, and structures with storey strength to scaled stiffness ratios outside this range were eliminated from analyses described in Chapters 2 to 4.

Table A-1: Approximate yield drift ratios for different frame buildings.

Lateral force resisting system	**Yield drift ratio**	**Minimum (%)**	**Maximum (%)**
1. Reinforced Concrete Frame 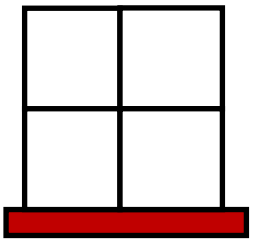	$\theta_y = 0.5\,\varepsilon_y \left(\frac{L_b}{h_b}\right)$ *The average ratio of drift ratios obtained through experiment to theory is 1.03 with a standard deviation of 0.16.*	**0.1825** Experimental: **0.188**	**3.95** Experimental: **4.06**
2. Hybrid Frame System 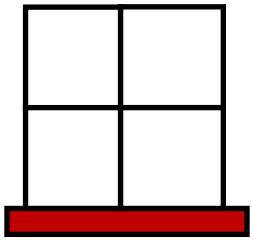	*The yield drift of hybrid frames is approximately 40-50% of RC frames.*	**0.167**	**1.5**
3. Structural Steel frame 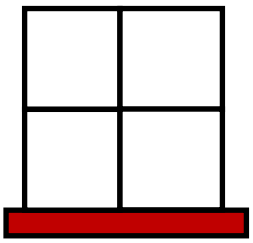	$\theta_y = 0.65\,\varepsilon_y \left(\frac{L_b}{h_b}\right)$ where, $h_b = 2.2\left(\frac{I}{Z_P}\right)$ $\frac{I}{Z_P}$ is essentially constant for a given W- group of steel beams [2], with the values as shown in Table A-3.	**0.209**	**3.2**

4. Concentric Braced Steel Frame 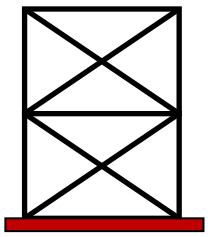	$\theta_y = \varepsilon_y \left(\frac{L_{bay}}{H_s} \right)$	**0.046**	**0.79**

where: h_b = overall beam section depth

H_s = storey height

L_b = beam span between column centrelines

L_{bay} = length of the frame bay

ε_y = yield strain of steel

Table A-2: Properties assumed to obtain Figure A-1

Lateral force resisting system	Parameter	Minimum	Maximum
1. Reinforced Concrete Frame/ Hybrid Frame	L_b	2500 mm	7500 mm
	h_b	250 mm	750 mm
	ε_y	1.095×10^{-3}	2.632×10^{-3}
2. Structural Steel Frame	L_b	2500 mm	7500 mm
	h_b	400 mm	850 mm
	ε_y	1.095×10^{-3}	2.632×10^{-3}
3. Concentric Braced Frame	L_{bay}	2500 mm	7500 mm
	H_s	2500 mm	6000 mm
	ε_y	1.095×10^{-3}	2.632×10^{-3}

Table A-3: $\frac{Z_p}{I}$ ***values for ASCE beam section groups [2]***

W- Shape Group	$\frac{Z_p}{I}$ (in^{-1})	$\frac{Z_p}{I}$ (m^{-1})
W 14	0.14	5.52
W 16	0.136	5.36
W 18	0.119	4.67
W 21	0.103	4.04
W 24	0.087	3.44
W 27	0.077	3.04
W 30	0.066	2.58
W 33	0.072	2.82

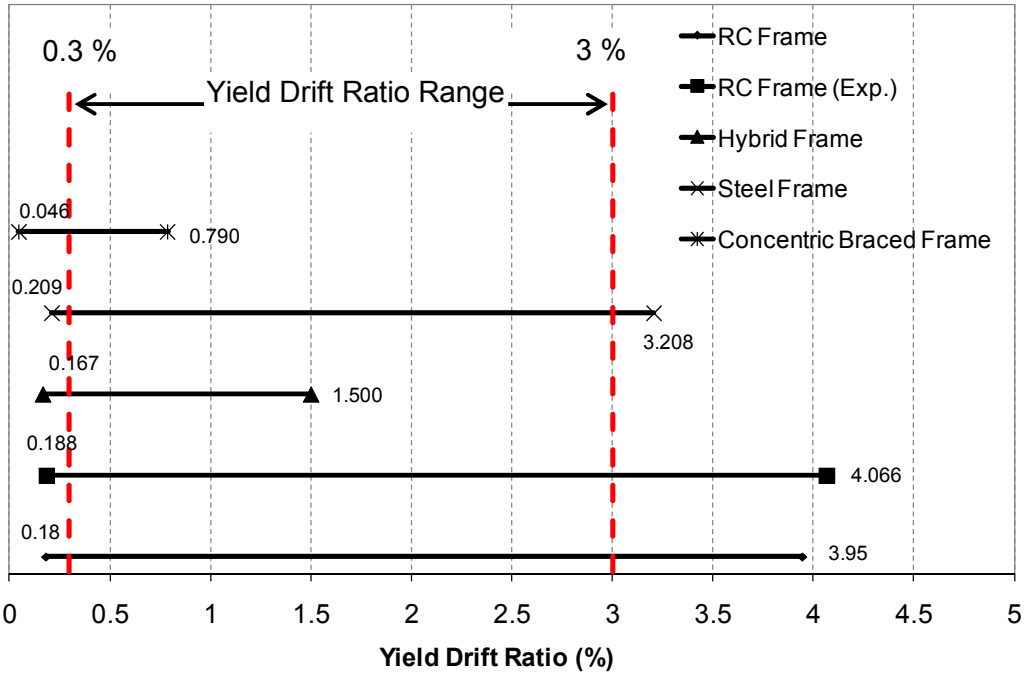

Figure A-1: Yield drift ratios for some frame buildings.

A.2 References

[1] Priestley MJN, Calvi GM, Kowalsky MJ. Displacement-based seismic design of structures. *IUSS Press*, Pavia, Italy, 2007; 721pp.

[2] Sullivan TJ, Priestley MJN, Calvi GM. Seismic design of frame-wall structures. ROSE Research Report No. 2006/02, *IUSS Press*, Pavia, Italy, 2006; 333pp.

APPENDIX B: NZS 1170.5 EQUIVALENT STATIC METHOD EXAMPLES

B.1 NZS 1170.5 Equivalent Static Method

The New Zealand seismic Standard, NZS 1170.5 [1], like other international seismic building codes (e.g., IBC [2]), require that structures be designed to resist specified static lateral forces related to the properties of the structure and the seismicity of the region. Here, several empirical relations are provided, including methods to calculate the structural base shear and the distribution of lateral forces over the structure height. In addition, many modification factors are employed in this procedure to obtain a reasonable approximation of the actual structural response. A brief description of the steps involved in the NZS 1170.5 Equivalent Static (ES) method is given below.

1. Determination of horizontal seismic base shear

The horizontal seismic shear, V, acting at the base of the structure in the direction under consideration, shall be calculated according to Clause 6.2.1.2, as given by Equation (B-1).

$$V = C_d(T_1)W_t \qquad \text{(B-1)}$$

where; $C_d(T_1)$ is the horizontal design action coefficient as given below, from Clause 5.2.1.1 for the ultimate limit state, and W_t is the seismic weight of the structure as defined in Clause 4.2.

$$C_d(T_1) = \max\begin{cases} \dfrac{C(T_1)\,S_p}{k_\mu} \\ (Z/20 + 0.02)\,R_u \\ 0.03\,R_u \end{cases} \qquad \text{(B-2)}$$

In Equation (B-2):

$C(T_1)$ = the ordinate of the elastic site hazard spectrum determined from Clause 3.1.1, given by Equation (B-3).

T_1 = the largest translational period in the direction under consideration. The fundamental period of the structure can be calculated using Rayleigh's method given in Clause 4.1.2.1, or by eigenvalue analysis (used by most computer programs).

S_p = the structural performance factor to represent a balance between risk and economical considerations, determined by Clause 4.4. For ultimate limit state, this factor shall be taken as 0.7 except where $1.0 < \mu < 2.0$, then $S_p = (1.3 - 0.3\mu)$.

k_μ = the ductility reduction factor for lateral force from Clause 5.2.1.1. For example, k_μ is calculated according to Equation (B-6) for site subsoil Class A (Strong Rock), where T_1 shall not be taken less than 0.4s.

Z = the hazard factor determined from Clause 3.1.4. It is taken equal to 0.13, 0.22 and 0.4 for Auckland, Christchurch and Wellington respectively.

R_u = the return period factor for the ultimate limit state, to consider for return periods other than 500 years. It is determined according to Clause 3.1.5, and is

taken as equal to 1.0 when the annual probability of the design event for safety is 1/500. The product of Z and R_u shall however be not taken greater than 0.7 according to Clause 3.1.1.

$$C(T) = C_h(T)\, Z\, R\, N(T, D) \qquad \text{(B-3)}$$

In Equation (B-3), $C_h(T)$ is the spectral shape factor determined from Clause 3.1.2, also obtained from Figure B-1 for the ES method, and $N(T, D)$ is the near-fault factor determined from Clause 3.1.6. For annual probability of exceedance less than 1/250, the near-fault factor is calculated by Equation (B-4), where $N_{max}(T)$ is the maximum near-fault factor linearly interpolated for period T from Table B-1, and D is the shortest distance (in km) from the site to the nearest fault listed in Table 3.6 of NZS 1170.5.

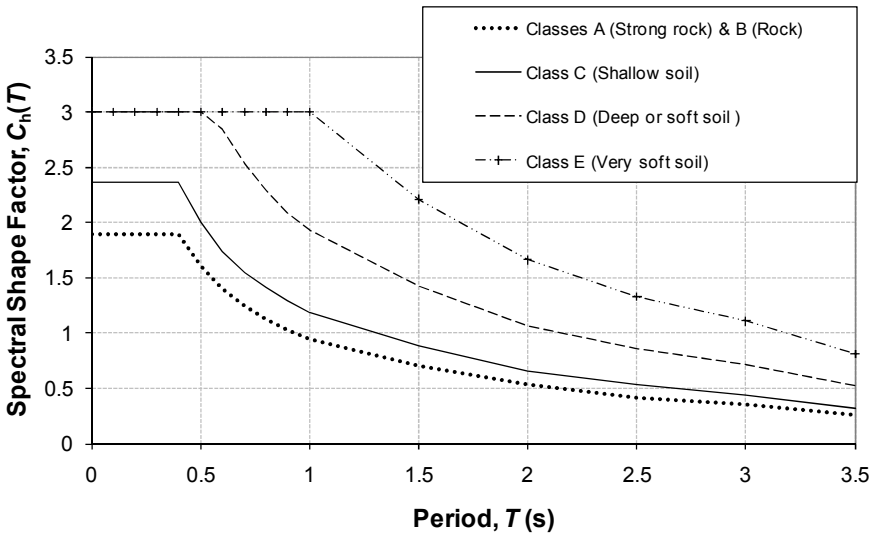

Figure B-1: NZS 1170.5 spectral shape factor for Equivalent Static method.

$$N(T,D) = \begin{cases} N_{\max}(T) & D \le 2 \text{ km} \\ 1+(N_{\max}(T)-1)\dfrac{20-D}{18} & 2 \text{ km} < D \le 20 \text{ km} \\ 1.0 & D > 20 \text{ km} \end{cases} \quad \text{(B-4)}$$

Table B-1: NZS 1170.5 Maximum near-fault factors

T (s)	≤ 1.5	2	3	4	≥ 5
$N_{max}(T)$	1.0	1.12	1.36	1.60	1.72

$$k_\mu = \begin{cases} \mu & \text{for } T_1 \ge 0.7\text{s} \\ \dfrac{(\mu-1)T_1}{0.7}+1 & \text{for } T_1 < 0.7\text{s} \end{cases} \quad \text{(B-5)}$$

2. Distribution of the lateral seismic force over structure height

The total base shear V calculated from Equation (B-1) is distributed over the height of the structure as a force at each level, F_i, determined from Clause 6.2.1.3, given by Equation (B-6). Here, $F_t = 0.08V$ at the top level and zero elsewhere. This additional force at the top of the building is to compensate for the higher mode effects in the upper few storeys.

$$F_i = F_t + 0.92V\left(\frac{W_i h_{ib}}{\sum_{i=1}^{n}(W_i h_{ib})}\right) \quad \text{(B-6)}$$

where; W_i is the seismic weight at level i, h_{ib} is the height of level i above the base of the structure, and n is the number of levels in the structure.

3. Consideration of *P*-Delta effects

NZS 1170.5 provides two methods to consider the *P*-Delta effects, and it permits either of the methods to be used. Method A in Clause 6.5.4.1 is a simple method in which the lateral forces are simply scaled up. This method can, however, result in conservative answers [1]. A second method (Method B in Clause 6.5.4.2) is a more complex procedure, but it is expected to produce less conservative results than Method A. This alternative *P*-Delta analysis method is, however, more difficult to apply due to its complication involved in the below steps.

Step 1. Analyse the structure using the ES method and obtain the envelope of lateral elastic displacements of the centre of the mass neglecting the *P*-Delta effects.

Step 2. The horizontal displacements found in Step 1 are scaled according to Clause 7.2.1.1 to predict the horizontal displacement allowing for inelastic deformation.

Step 3. Assuming that the seismic weight at each level is concentrated at its centre, calculate the actions induced by these weights being displaced through the displacements found in Step 2. Find the additional displacements due to these above actions.

Step 4. The structural actions obtained from Step 3 are multiplied by a factor β that makes allowance for ductility. This β factor is calculated according to Equation (B-7), but in no case β be taken less than 1.0. In Equation (B-7), K_{TS} is a factor that makes an allowance for the period and the foundation sub-soil type. For site sub-soil Class A, K_{TS} factor is calculated using Equation (B-8).

$$\beta = \begin{cases} 2\mu K_{TS} / 3.5 & \text{for } \mu \le 3.5 \\ 2K_{TS} & \text{for } \mu > 3.5 \end{cases} \qquad \text{(B-7)}$$

$$K_{TS} = \begin{cases} 1.0 & \text{for } T_1 < 2.0 \\ \dfrac{(6.0 - T_1)}{4} & \text{for } 2.0 \le T_1 \le 4.0 \\ 0.5 & \text{for } T_1 > 4.0 \end{cases} \qquad \text{(B-8)}$$

Step 5. The structural actions found in Step 1 are added to the corresponding values from Step 4 to give the required design actions.

Step 6. Multiply the additional displacements from Step 3 with the β factor and add these to the corresponding lateral displacements due to the ES forces. The resultant displacements are then scaled as required by Clause 7.2.1.1 to give the resultant deflection profile for the structure including *P*-Delta actions.

4. Modifications to storey displacements and interstorey drift

The following modifications are done to the calculated deformations –

(a) The magnitudes of the deflections due to the ES design forces are multiplied by a deflection scale factor, k_d, given in Clause 6.2.3. This modification to the deflections is applied because; in the actual response, the modes have contributions in different directions, thus reducing the actual response. Multiplying by the scale factors in Table B-2 reduces the difference in deflections due to the ES method and the modal response spectrum method.

Table B-2: NZS 1170.5 Deflection scale factor, k_d.

No. of storeys	1	2	3	4	5	≥ 6
k_d	1.0	0.97	0.94	0.91	0.88	0.85

(b) The elastic deflections from design level forces, which may be close to the yield deflections, are multiplied by the structural ductility factor, μ, according to Clause 7.2.1.1 to obtain the likely inelastic deflections. The Clause 7.2.1.1 also states that

sidesway mechanisms should also be considered. However, "sidesway mechanism" is not defined appropriately in the code, and it is not clear if a total frame sidesway mechanism, as well as a storey mechanism should be considered. Therefore, the elastic deflections are only multiplied by the structural ductility factor to get the inelastic deflections.

(c) Elastic based methods such as the ES method may underestimate the critical inter-storey deflections as compared to the deflections predicted from time-history analysis. A drift modification factor, k_{dm}, is thus introduced in Clause 7.3.1.1 to make allowance for this difference in the inter-storey deflection calculation. The value of this factor is chosen from Table B-3. Clause 7.3.1.1 also states that "*when computing P-Delta effects…., the interstorey deflection between adjacent levels shall be the unmodified maximum value found from the deflection profile*". This is a confusing statement; because it is unclear as to what modification is being considered, or what deflection profile is considered. Therefore, the k_{dm} factor is applied to the resultant deflection profile including the *P*-Delta effects.

Table B-3: NZS 1170.5 Drift modification factor, k_{dm}.

Structure height, H (m)	$H < 15$	$15 \leq H \leq 30$	$H > 30$
$\boldsymbol{k_{dm}}$	1.2	$1.2 + 0.02(H - 15)$	1.5

B.2 Application of NZS 1170.5 Equivalent Static Method

The NZS 1170.5 Equivalent Static method explained in the previous section was used for all the designs in vertical irregularity studies described in this thesis. Matlab [3] codes were developed to carry out all the steps involved in the designs. Section B.3 provides sample Matlab codes developed for designing the regular Constant Interstorey Drift Ratio (CISDR) models and Constant Stiffness (CS) models. The codes also show the iteration steps involved in achieving the target interstorey drift ratio. One example of application of the ES method to a regular shear-type of structure is provided below for both the design models. Prior to the examples, a note on shear-type idealization is given.

Note on Shear-type building:

A shear-type of structure may be defined as a structure in which there is no rotation of a horizontal section at the floor levels and that the deflected building will have many of the features of a cantilever beam that is deflected by shear forces alone [4]. While idealising shear-type of structures, it is assumed that: (a) the total mass distributed throughout the building is concentrated at the floor levels; (b) the beams and floor systems are infinitely rigid as compared to the columns; and (c) the deformation of the structure is independent of the axial forces present in the columns, and that the axial deformations of the beams are neglected. These above assumptions transform a complex structure with an infinite number of degrees-of-freedom due to the distributed mass, into a idealized structure that has only as many degrees-of-freedom as it has lumped masses at the floor levels. For example, a three storey structure modelled as a shear-type of structure shown in Figure B-2(a), will have three degrees-of-freedom, equal to the three horizontal displacements at the corresponding floor

levels (y_1, y_2 and y_3). The second assumption implies that the joints between the girders and the columns are fixed against rotation, and according to the third assumption above, the rigid beams and diaphragms remain horizontal during motion.

A building with a number of bays is often represented by an equivalent shear-type of structure with a single bay. This shear building can be further idealised into a single column as shown in Figure B-2(b). Here, it is assumed that only horizontal displacements of the lumped floor masses (m_1, m_2 and m_3) are possible. Another alternative to represent the shear building is to use an equivalent multi mass-spring

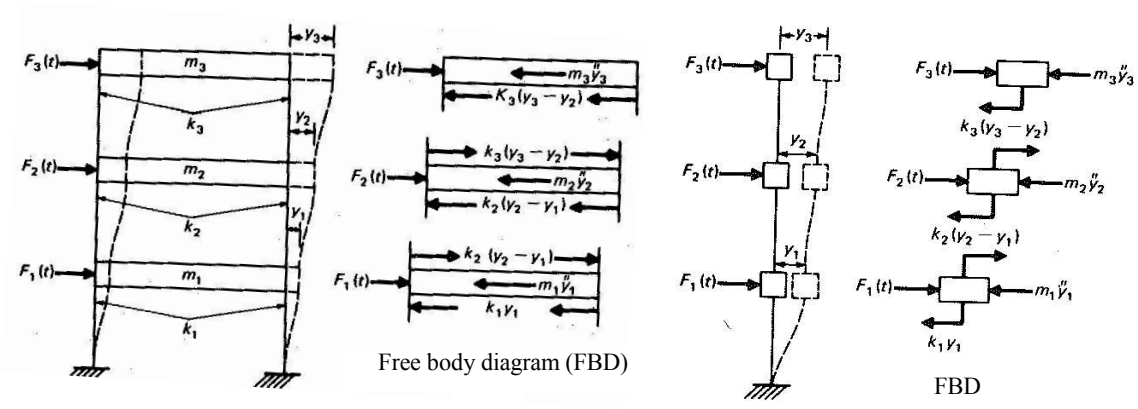

(a) Single Bay Model (b) Single Column Model

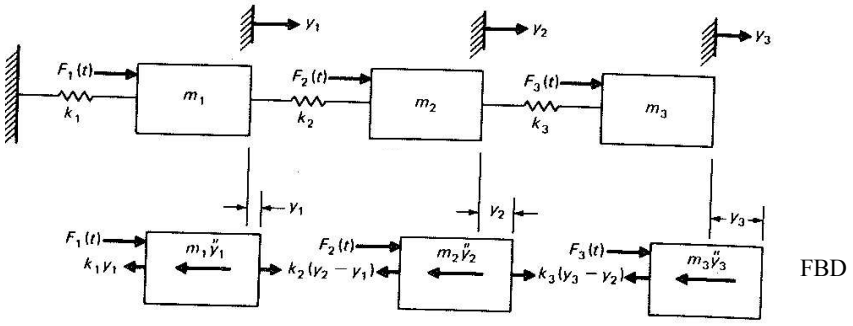

(c) Multi Mass-Spring Model

Figure B-2: Representation of shear-type of buildings, from [4].

model as shown in Figure B-2(c). In Figure B-2, the stiffness coefficient or spring constant k_i shown between any two consecutive masses is the force required to produce a relative unit displacement of the two adjacent floor levels. For a storey of height h and a column with modulus of elasticity E and second moment of area I_c, the lateral stiffness of a column with two ends fixed against rotation, implied by the shear building, is $12EI_c/h^3$. Therefore, the lateral stiffness of storey i, is given by Equation (B-9) as the summation of the lateral stiffness of all columns in that storey.

$$k_i = \sum_{columns} \frac{12\,EI_c}{h_i^3} \tag{B-9}$$

B.2.1 Example of Constant Interstorey Drift Ratio (CISDR) Design Model

For simplicity, a three storey shear-type of structure is considered here. The structure is assumed to have equal storey heights of 4m, and the mass ratio between the floors is kept constant. The following are the design parameters adopted for the structure.

- Location of the structure = Wellington ($Z = 0.4$)
- Structural ductility factor, $\mu = 4$
- Site subsoil class chosen = *Class A* (Strong rock)
- Shortest distance from the site to the nearest fault, $D = 0$
- Return period factor, $R_u = 1$
- Structural performance factor, $S_p = 0.7$
- Design (target) Interstorey Drift Ratio (DISDR) = 2%

As explained in Chapter 2, for a CISDR design, the storey stiffnesses are iterated until all the storeys achieve the same design (target) interstorey drift ratio (DISDR). Column (4) in Table B-4 shows the required storey stiffnesses for this CISDR design example. The following are the additional parameters calculated to obtain the values in Table B-4.

1. *Determination of fundamental natural period of the structure, T_1.*

The fundamental natural period of the structure is calculated according to NZS 1170.5 Rayleigh method, given by Equation (B-10). Columns (12) and (13) from Table B-4 are used in Equation (B-10) to obtain T_1 = 1.378s. Eigenvalue analysis also provides the same value of T_1.

$$T_1 = 2\pi \sqrt{\frac{\sum_{i=1}^{n} W_i \delta_i^2}{g \sum_{i=1}^{n} F_i \delta_i}} \qquad \text{(B-10)}$$

where; W_i = the seismic weight at level i

F_i = the displacing force acting at level i

g = acceleration due to gravity

δ_i = the horizontal displacement of the centre of mass at level i

n = number of levels in a structure

2. *Elastic site hazard spectrum, $C(T_1)$.*

Substituting the following values for parameters defined in Equation (B-3), gives the elastic site hazard spectrum, $C(T_1)$ = 0.2992.

$C_h(T_1)$ = 0.748 (from Figure B-1)

$Z R_u$ = 0.4 (< 0.7, according to Clause 3.1.1)

$N(T_1, D)$ = 1 (from Equation (B-4) and Table B-1)

3. *Horizontal design action coefficient, $C_d(T_1)$.*

From Equation (B-2), the horizontal design action coefficient, $C_d(T_1)$ = 0.0523. Here, the inelastic spectrum scaling factor, k_μ, is equal to 4 from Equation (B-5).

4. *Horizontal seismic base shear, V*.

The horizontal seismic shear, V, acting at the base of the structure is given by Equation (B-1) as the product of the horizontal design action coefficient, $C_d(T_1)$, and the seismic weight of the structure, W_t. Substituting $C_d(T_1)$ = 0.0523 and W_t = 29.43 N (from Column (6) in Table B-4), Equation (B-1) gives V as equal to 1.54 N.

5. *Equivalent static horizontal force at each level, F_i*.

The equivalent static horizontal force, F_i at each level i in Column (8) of Table B-4, is calculated from Equation (B-6).

6. *Other steps – Consideration of P-Delta effects, modifications to storey displacements and interstorey drift*.

The remaining steps involved in the NZS 1170.5 ES method explained earlier are self-explanatory in Table B-4. This includes calculation of additional actions and displacements due to *P*-Delta effects and modifications applied to the storey displacements and interstorey drifts as shown in Table B-4. Column (26) in Table B-4 shows that all the storeys of this CISDR model have achieved the same target interstorey drift ratio (DISDR) of 2%. The following are the values used for other parameters in Table B-4.

β = 2 (from Equation (B-7))

k_d = 0.94 (from Table B-2)

k_{dm} = 1.2 (from Table B-3)

Table B-4: NZS 1170.5 ES method for CISDR design

(1) Level, i	(2) h_i (m)	(3) h_{ib} (m)	(4) K_i (N/m)	(5) M_i (kg)	(6) W_i (= M_i g) (N)
3	4	12	61.8	1	9.81
2	4	8	101.9	1	9.81
1	4	4	127.1	1	9.81
Σ					29.43

Table B-4: NZS 1170.5 ES method for CISDR design (contd.)

Level, i	(7) W_i h_{ib} (N-m)	(8) F_i ($\times 10^{-2}$ N)	(9) V_{eq} ($\times 10^{-2}$ N)	(10) $\Delta\delta_i = V_{eq,i}/K_i$ ($\times 10^{-2}$ m)	(11) δ_i ($\times 10^{-2}$ m)
3	117.72	83.17	83.17	1.345	3.837
2	78.48	47.23	130.40	1.280	2.491
1	39.24	23.62	154.02	1.211	1.211
Σ	235.44	154.02			

Table B-4: NZS 1170.5 ES method for CISDR design (contd.)

Level, i	(12) W_i δ_i^2 ($\times 10^{-2}$ N-m^2)	(13) F_i δ_i ($\times 10^{-2}$ N-m)	(14) δ_i μ k_d ($\times 10^{-2}$ m)	(15) $\Delta\delta_{m,i}$ ($\times 10^{-2}$ m)	(16) $V_{P\text{-}D,i}$ = W_i i $\Delta\delta_{im}/h_i$ ($\times 10^{-2}$ N)
3	1.444	3.191	14.429	5.060	12.410
2	0.609	1.176	9.369	4.812	23.607
1	0.144	0.286	4.556	4.556	33.524
Σ	2.197	4.653			

Table B-4: NZS 1170.5 ES method for CISDR design (contd.)

Level, i	(17) $(V_{P\text{-}D,i+1} - V_{P\text{-}D,i})$ $(\times 10^{-2}$ N)	(18) $F_{P\text{-}D,i} = (17) \times \beta$ $(\times 10^{-2}$ N)	(19) $\Delta\delta_{P\text{-}D,i} = V_{P\text{-}D,i}/K_i$ $(\times 10^{-2}$ m)	(20) $\delta_{P\text{-}D,i}$ $(\times 10^{-2}$ m)
3	12.410	24.820	0.2008	0.6963
2	11.197	22.394	0.2317	0.4954
1	9.917	19.834	0.2637	0.2637
Σ				

Table B-4: NZS 1170.5 ES method for CISDR design (contd.)

Level, i	(21) $F_{final,i}$ $= (8) + (18)$ $(\times 10^{-2}$ N)	(22) $V_{final,i}$ $= (9) + (16) \times \beta$ $(\times 10^{-2}$ N)	(23) $\delta_{final,i}$ $= (\delta_i k_d + \delta_{P\text{-}D,i}\,\beta) \times \mu$ $(\times 10^{-2}$ m)
3	107.991	107.991	20.000
2	69.627	177.618	13.333
1	43.451	221.069	6.667
Σ	221.069		

Table B-4: NZS 1170.5 ES method for CISDR design (contd.)

Level, i	(24) $(\delta_{final,i} - \delta_{final,i-1})$ $(\times 10^{-2}$ m)	(25) $\Delta\delta_{final,i} = (24) \times k_{dm}$ $(\times 10^{-2}$ m)	(26) $ISDR_i = (\Delta\delta_{final,i}/h_i) \times 100$ (%)
3	6.667	8.00	2.00
2	6.667	8.00	2.00
1	6.667	8.00	2.00

B.2.2 Example of Constant Stiffness (CS) Design Model

The three storey building used to describe the NZ ES method for CISDR design, is once again used for this example of a Constant Stiffness (CS) model. As the name suggests, the structure has a constant stiffness distribution over the height. The design assumptions for this CS model are taken the same as that used for the CISDR model. The fundamental natural period of the structure is found to be 1.20s using the Rayleigh's method or Eigenvalue analysis. The steps explained for the CISDR design are once again followed for this example, and the corresponding values in Table B-5 are calculated accordingly. For this design model with a uniform distribution of stiffness at all the storeys, the first storey has the maximum interstorey drift ratio of 2% (target interstorey drift ratio) as seen in Column (26) of Table B-5.

Table B-5: NZS 1170.5 ES method for CS design

(1) Level, i	(2) h_i (m)	(3) h_{ib} (m)	(4) K_i (N/m)	(5) M_i (kg)	(6) W_i (= M_i g) (N)
3	4	12	137.33	1	9.81
2	4	8	137.33	1	9.81
1	4	4	137.33	1	9.81
Σ					29.43

Table B-5: NZS 1170.5 ES method for CS design (contd.)

Level, i	(7) W_i h_{ib} (N-m)	(8) F_i ($\times 10^{-2}$ N)	(9) V_{eq} ($\times 10^{-2}$ N)	(10) $\Delta\delta_i = V_{eq,i}/K_i$ ($\times 10^{-2}$ m)	(11) δ_i ($\times 10^{-2}$ m)
3	117.72	92.04	92.04	0.6701	2.9620
2	78.48	52.27	144.30	1.0507	2.2918
1	39.24	26.13	170.44	1.2410	1.2410
Σ	235.44	170.44			

Table B-5: NZS 1170.5 ES method for CS design (contd.)

Level, i	(12) W_i δ_i^2 ($\times 10^{-2}$ N-m^2)	(13) F_i δ_i ($\times 10^{-2}$ N-m)	(14) δ_i μ k_d ($\times 10^{-2}$ m)	(15) $\Delta\delta_{m,i}$ ($\times 10^{-2}$ m)	(16) $V_{P\text{-}D,i}$ = W_i i $\Delta\delta_{im}/h_i$ ($\times 10^{-2}$ N)
3	0.8606	2.726	11.137	2.519	6.179
2	0.5152	1.197	8.617	3.950	19.379
1	0.1510	0.324	4.666	4.666	34.333
Σ	1.5270	4.248			

Table B-5: NZS 1170.5 ES method for CS design (contd.)

Level, i	(17) $(V_{P\text{-}D,i+1} - V_{P\text{-}D,i})$ $(\times 10^{-2}$ N)	(18) $F_{P\text{-}D,i} = (17) \times \beta$ $(\times 10^{-2}$ N)	(19) $\Delta\delta_{P\text{-}D,i} = V_{P\text{-}D,i}/K_i$ $(\times 10^{-2}$ m)	(20) $\delta_{P\text{-}D,i}$ $(\times 10^{-2}$ m)
3	6.179	12.359	0.0450	0.4361
2	13.199	26.398	0.1411	0.3911
1	14.953	29.907	0.2500	0.2500
Σ				

Table B-5: NZS 1170.5 ES method for CS design (contd.)

Level, i	(21) $F_{final,i}$ $= (8) + (18)$ $(\times 10^{-2}$ N)	(22) $V_{final,i}$ $= (9) + (16) \times \beta$ $(\times 10^{-2}$ N)	(23) $\delta_{final,i}$ $= (\delta_i k_d + \delta_{P\text{-}D,i}\,\beta) \times \mu$ $(\times 10^{-2}$ m)
3	104.396	104.396	14.626
2	78.665	183.062	11.746
1	56.041	239.103	6.666
Σ	239.103		

Table B-5: NZS 1170.5 ES method for CS design (contd.)

Level, i	(24) $(\delta_{final,i} - \delta_{final,i-1})$ $(\times 10^{-2}$ m)	(25) $\Delta\delta_{final,i} = (24) \times k_{dm}$ $(\times 10^{-2}$ m)	(26) $ISDR_i = (\Delta\delta_{final,i}/h_i) \times 100$ (%)
3	2.880	3.456	0.864
2	5.080	6.096	1.524
1	6.666	8.000	2.00

B.3 Sample Matlab Codes For Vertical Irregularity Studies

B.3.1 Regular Constant Interstorey Drift Ratio (CISDR) Design Using NZS 1170.5 ES Method

```
function [hfl wfl K Vfinal T ISDR Cdt1 Cdt2]=
CISDR_Design_fn(nbs,h,mass,tr,R,mu)

%==========================================================================
% CISDR_Design_fn carries out the design for regular CISDR design model
%according to NZS 1170.5 Equivalent Static (ES) method.
% Inputs:
% nbs  : Number of storeys in the structure
% h    : Interstorey height (m)
% mass : Mass at one floor level (kg)
% tr   : Target (design) interstorey drift ratio (%)
% R    : Return period factor (Clause 3.1.5)
% mu   : Structural ductility factor
% Outputs:
% hfl  : Storey heights between floors (m)
% wfl  : Weight at every floor level (N)
% K    : Lateral stiffnesses of the storeys (N/m)
% Vfinal     : Final storey shears (incl. P-Delta effects) (N)
% T    : Fundamental natural period of the structure (s)
% ISDR : Final interstorey drift ratios
% Cdt1 : Upper limit of NZS 1170.5 horizontal design action coefficient
% Cdt2 : Lower limit of NZS 1170.5 horizontal design action coefficient
% Notes: Please also refer to NZS 1170.5. The coefficients Cdt1 and Cdt2 are
%required to check if the design is acceptable according to the restrictions
%imposed in Section 2.6. This check and the strength to scaled stiffness
ratio %checks have to be done before carrying out time-history analyses.
%==========================================================================
% Author - Vinod K. Sadashiva (vinod.sadashiva@pg.canterbury.ac.nz)
% Date - January 2007
%==========================================================================


%============================== START OF FUNCTION ==========================


%Storey heights between floor levels (m).
h_fl=[];
for i=1:nbs
    h_fl(i)=h;
end
```

```
hfl=h_fl;

%Height of each floor from the ground level (m).
hfg=cumsum(hfl);

%Target interstorey drift ratios.
t_ratio=[];
for i=1:nbs
    t_ratio(i)=(tr/100);
end
tratio=t_ratio;

%Mass at every floor (kg).
m_fl=[];
for i=1:nbs
    m_fl(i)=mass;
end
mfl=m_fl;

%Mass matrix (kg).
m_mat=[];
for i=1:nbs
    m_mat(i,i)=mfl(i);
end
mmat=m_mat;

%Weight of each floor (N).
wfl=mfl*9.81;

%Total seismic weight of the structure (N).
wfl_g=cumsum(wfl);
wst=wfl_g(nbs);

%Product of weight and height of each floor from G.L. (N-m)
wh=wfl.*hfg;
wh_st=cumsum(wh);
whst=wh_st(nbs);     %Total

%Lateral stiffness of each storey (N/m).
kiter=[];
for i=1:nbs
```

```
    kiter(i)=1;     %Initial assumption
end

%Calculation of deflection scale factor, kd (Table 6.1 in NZS 1170.5).
if (nbs==1)
    kd=1;
elseif (nbs==2)
    kd=0.97;
elseif (nbs==3)
    kd=0.94;
elseif (nbs==4)
    kd=0.91;
elseif (nbs==5)
    kd=0.88;
else
    kd=0.85;
end

%Calculation of drift modification factor, kdm (Table 1.1 in NZS 1170.5).
tsh=hfg(nbs);    %Total height of the structure, in m.
if (tsh<15)
    kdm=1.2;
elseif (tsh>=15&tsh<=30)
    kdm=1.2+0.02*(tsh-15);
else
    kdm=1.5;
end

check=1;
tol=1e-6;
cpt=0;
%********************** Iteration begins from here ***********************
while ((check>tol)&(cpt<5000))
    cpt=cpt+1;
    K=kiter;

    %Formation of structural stiffness matrix (N/m).
    k_mat=[];
    for i=1:(nbs-1)
        k_mat(i,i)=K(i)+K(i+1);
        k_mat(i,i+1)=-K(i+1);
```

```
    k_mat(i+1,i)=-K(i+1);
end
k_mat(nbs,nbs)=K(nbs);
kmat=k_mat;

%Calculation of fundamental natural period of the structure (s).
e_value=eig(kmat,mmat);
evalue=sqrt(e_value);
omega=min(evalue);   %fundamental natural circular frequency in rad/sec.
funda_freq=omega/(2*pi); %fundamental natural frequency in Hz or cps.
T=(1/funda_freq);        %fundamental natural period in s.

%Call the function to calculate the horizontal design action coefficient
[Cdt Cdt1 Cdt2]=NZS11705_CdT_fn(T,R,mu);

%Calculation of horizontal seismic base shear, N (Clause 6.2.1.2).
Vb=Cdt*wst;

%Equivalent static horizontal force at each level, N (Clause 6.2.1.3)
%floor level in N (clause 6.2.1.3)).
F_eq=[];
for i=1:(nbs-1)
    F_eq(i)=0.92*Vb*(wh(i)/whst);
end
F_eq(nbs)=(0.08*Vb)+0.92*Vb*(wh(nbs)/whst);
Feq=F_eq;

Feq_tot=cumsum(Feq);
Feq_base=Feq_tot(nbs);  %Total force acting at the base, N (=Vb).

%Shear force at each level (N).
veq1=fliplr(Feq);
veq2=cumsum(veq1);
Veq=fliplr(veq2);

%Interstorey drift at every storey, m (without P-Delta effects).
del_di=(Veq./K);

%Displacement of each floor, m (Clause 6.5.4.2 - Step 1).
dieqsm=cumsum(del_di);
```

```
%Modified floor displacements, m (Clause 6.2.3 & 6.5.4.2 - Step 2).
m_dieqsm=(kd*mu*dieqsm);

%Ultimate storey inter-storey drifts, m (without P-Delta effects).
udel_d_i=[];
for i=2:nbs
    udel_d_i(i)=m_dieqsm(i)-m_dieqsm(i-1);
end
udel_d_i(1)=m_dieqsm(1);
udel_di=udel_d_i;

%P-Delta storey shears, N (Clause 6.5.4.2, Step 3).
w_pd1=fliplr(wfl);
w_pd2=cumsum(w_pd1);
w_pd=fliplr(w_pd2);
Vpd=((w_pd.*udel_di)./hfl);

%P-Delta forces, N (Clause 6.5.4.2, Step 3).
F_pd=[];
for i=1:(nbs-1)
    F_pd(i)=Vpd(i)-Vpd(i+1);
end
F_pd(nbs)=Vpd(nbs);
Fpd=F_pd;

%P-Delta interstorey drifts, m (Clause 6.5.4.2, Step 3).
del_dipd=(Vpd./K);

%P-Delta displacements, m (Clause 6.5.4.2, Step 3).
dipd=cumsum(del_dipd);

%Calculation of beta factor used in Step 4 of Clause 6.5.4.2
if (T<2)
    kbeta=1;
elseif (T>=2&T<=4)
    kbeta=(6-T)/4;
else
    kbeta=0.5;
end
if (mu<=3.5)
    beta=max((2*mu*kbeta)/3.5,1);
```

```
    else
        beta=max(2*kbeta,1);
    end

    %Final force at each level (incl. P-Delta effects), N -(Clause 6.5.4.2,
    %Step 5).
    Ffinal=(Feq+Fpd*beta);

    %Final shear force at each level, N (incl. P-Delta effects).
    Vfinal=(Veq+Vpd*beta);

    %Final floor displacements (incl. P-Delta effects), m -(Clause 6.5.4.2,
    %Steps 5 & 6).
    Difinal=mu*(kd*dieqsm+dipd*beta);

    %Final interstorey drifts, m (Clause 6.5.4.2, Steps 5 & 6).
    deld_final=[];
    for i=2:nbs
        deld_final(i)=kdm*(Difinal(i)-Difinal(i-1));
    end
    deld_final(1)=kdm*(Difinal(1));
    Deldifinal=deld_final;

    %Interstorey drift ratios.
    ISDR=(Deldifinal./hfl);

    %Error calculator.
    Delratio=((tratio-ISDR)./tratio);
    abdelratio=abs(Delratio);
    check=max(abdelratio);

    %Adjusting storey stiffnesses.
    for i=1:nbs
        kiter(i)=K(i)*(ISDR(i)/tratio(i));
    end
end
%********************** Iteration ends here ********************************

%================================ END OF FUNCTION ==========================
```

B.3.2 Regular Constant Stiffness (CS) Design Using NZS 1170.5 ES Method

```
function [hfl wfl K Vfinal T ISDR Cdt1 Cdt2]=
CS_Design_fn(nbs,h,mass,tr,R,mu)
%=========================================================================
% CS_Design_fn carries out the design for regular CS design model according
%to NZS 1170.5 Equivalent Static (ES) method.
% Inputs:
% nbs  : Number of storeys in the structure
% h    : Interstorey height (m)
% mass : Mass at one floor level (kg)
% tr   : Target (design) interstorey drift ratio (%)
% R    : Return period factor (Clause 3.1.5)
% mu   : Structural ductility factor
% Outputs:
% hfl  : Storey heights between floors (m)
% wfl  : Weight at every floor level (N)
% K    : Lateral stiffnesses of the storeys (N/m)
% Vfinal     : Final storey shears (incl. P-Delta effects) (N)
% T    : Fundamental natural period of the structure (s)
% ISDR : Final interstorey drift ratios
% Cdt1 : Upper limit of NZS 1170.5 horizontal design action coefficient
% Cdt2 : Lower limit of NZS 1170.5 horizontal design action coefficient
% Notes: Please also refer to NZS 1170.5. The storey strengths provided for
%CS models will either be constant strength (CSTG) or varying strength
%(VSTG) configuration described in Section 2.6. The coefficients Cdt1 and
%Cdt2 are required to check if the design is acceptable according to the
%restrictions imposed in Section 2.6. This check and the strength to scaled
%stiffness ratio checks have to be done before carrying out time-history
%analyses.
%=========================================================================
% Author – Vinod K. Sadashiva (vinod.sadashiva@pg.canterbury.ac.nz)
% Date – January 2007
%=========================================================================


%============================== START OF FUNCTION ==========================


%Storey heights between floor levels (m).
h_fl=[];
for i=1:nbs
    h_fl(i)=h;
end
```

```
hfl=h_fl;

%Height of each floor from the ground level (m).
hfg=cumsum(hfl);

%Target interstorey drift ratios.
t_ratio=[];
for i=1:nbs
    t_ratio(i)=(tr/100);
end
tratio=t_ratio;

%Mass at every floor (kg).
m_fl=[];
for i=1:nbs
    m_fl(i)=mass;
end
mfl=m_fl;

%Mass matrix (kg).
m_mat=[];
for i=1:nbs
    m_mat(i,i)=mfl(i);
end
mmat=m_mat;

%Weight of each floor (N).
wfl=mfl*9.81;

%Total seismic weight of the structure (N).
wfl_g=cumsum(wfl);
wst=wfl_g(nbs);

%Product of weight and height of each floor from G.L. (N-m)
wh=wfl.*hfg;
wh_st=cumsum(wh);
whst=wh_st(nbs);     %Total

%Lateral stiffness of each storey (N/m).
kiter=1;     %Initial assumption
```

```
%Calculation of deflection scale factor, kd (Table 6.1 in NZS 1170.5,
%2004).
if (nbs==1)
    kd=1;
elseif (nbs==2)
    kd=0.97;
elseif (nbs==3)
    kd=0.94;
elseif (nbs==4)
    kd=0.91;
elseif (nbs==5)
    kd=0.88;
else
    kd=0.85;
end

%Calculation of drift modification factor, kdm (Table 1.1 in NZS 1170.5,
%2004).
tsh=hfg(nbs);    %Total height of the structure, in m.
if (tsh<15)
    kdm=1.2;
elseif (tsh>=15&tsh<=30)
    kdm=1.2+0.02*(tsh-15);
else
    kdm=1.5;
end

check=1;
tol=1e-6;
cpt=0;
%********************* Iteration begins from here **********************
while ((check>tol)&(cpt<5000))
    cpt=cpt+1;
    K=kiter;

    %Formation of structural stiffness matrix (N/m).
    k_mat=[];
    for i=1:(nbs-1)
        k_mat(i,i)=2*K;
        k_mat(i,i+1)=-K;
        k_mat(i+1,i)=-K;
```

```
end
k_mat(nbs,nbs)=K;
kmat=k_mat;

%Calculation of fundamental natural period of the structure (s).
e_value=eig(kmat,mmat);
evalue=sqrt(e_value);
omega=min(evalue);   %fundamental natural circular frequency in rad/sec.
funda_freq=omega/(2*pi); %fundamental natural frequency in Hz or cps.
T=(1/funda_freq);        %fundamental natural period in s.

%Call the function to calculate the horizontal design action coefficient
[Cdt Cdt1 Cdt2]=NZS11705_CdT_fn(T,R,mu);

%Calculation of horizontal seismic base shear, N (Clause 6.2.1.2).
Vb=Cdt*wst;

%Equivalent static horizontal force at each level, N (Clause 6.2.1.3)
%floor level in N (clause 6.2.1.3)).
F_eq=[];
for i=1:(nbs-1)
    F_eq(i)=0.92*Vb*(wh(i)/whst);
end
F_eq(nbs)=(0.08*Vb)+0.92*Vb*(wh(nbs)/whst);
Feq=F_eq;

Feq_tot=cumsum(Feq);
Feq_base=Feq_tot(nbs);  %Total force acting at the base, N (=Vb).

%Shear force at each level (N).
veq1=fliplr(Feq);
veq2=cumsum(veq1);
Veq=fliplr(veq2);

%Interstorey drift at every storey, m (without P-Delta effects).
del_di=(Veq/K);

%Displacement of each floor, m (Clause 6.5.4.2 - Step 1).
dieqsm=cumsum(del_di);

%Modified floor displacements, m (Clause 6.2.3 & 6.5.4.2 - Step 2).
```

```
m_dieqsm=(kd*mu*dieqsm);

%Ultimate storey inter-storey drifts, m (without P-Delta effects).
udel_d_i=[];
for i=2:nbs
    udel_d_i(i)=m_dieqsm(i)-m_dieqsm(i-1);
end
udel_d_i(1)=m_dieqsm(1);
udel_di=udel_d_i;

%P-Delta storey shears, N (Clause 6.5.4.2, Step 3).
w_pd1=fliplr(wfl);
w_pd2=cumsum(w_pd1);
w_pd=fliplr(w_pd2);
Vpd=((w_pd.*udel_di)./hfl);

%P-Delta forces, N (Clause 6.5.4.2, Step 3).
F_pd=[];
for i=1:(nbs-1)
    F_pd(i)=Vpd(i)-Vpd(i+1);
end
F_pd(nbs)=Vpd(nbs);
Fpd=F_pd;

%P-Delta interstorey drifts, m (Clause 6.5.4.2, Step 3).
del_dipd=(Vpd/K);

%P-Delta displacements, m (Clause 6.5.4.2, Step 3).
dipd=cumsum(del_dipd);

%Calculation of beta factor used in Step 4 of Clause 6.5.4.2
if (T<2)
    kbeta=1;
elseif (T>=2&T<=4)
    kbeta=(6-T)/4;
else
    kbeta=0.5;
end
if (mu<=3.5)
    beta=max((2*mu*kbeta)/3.5,1);
else
```

```
        beta=max(2*kbeta,1);
    end

    %Final force at each level (incl. P-Delta effects), N - (Clause 6.5.4.2,
    %Step 5).
    Ffinal=(Feq+Fpd*beta);

    %Final shear force at each level, N (incl. P-Delta effects).
    Vfinal=(Veq+Vpd*beta);

    %Final floor displacements (incl. P-Delta effects), m - (Clause 6.5.4.2,
    %Steps 5 & 6).
    Difinal=mu*(kd*dieqsm+dipd*beta);

    %Final interstorey drifts, m (Clause 6.5.4.2, Steps 5 & 6).
    deld_final=[];
    for i=2:nbs
        deld_final(i)=kdm*(Difinal(i)-Difinal(i-1));
    end
    deld_final(1)=kdm*(Difinal(1));
    Deldifinal=deld_final;

    %Interstorey drift ratios.
    ISDR=(Deldifinal./hfl);

    %Error calculator.
    Delratio=((tratio-ISDR)./tratio);
    abdelratio=abs(Delratio);
    check=abdelratio(1);

    %Adjusting storey stiffnesses.
    kiter=K*(ISDR(1)/tratio(1));
end
%********************** Iteration ends here ***********************
K=K*ones(1,nbs);        %Final storey stiffnesses.

%================================ END OF FUNCTION ==========================
```

B.3.3 Function to Calculate NZS 1170.5 Horizontal Design Action Coefficient

```
function [Cdt Cdt1 Cdt2] = NZS11705_CdT_fn(T,R,mu)
%==========================================================================
% NZS11705_CdT_fn calculates the NZS 1170.5 (2004) horizontal design action
%coefficient for the Equivalent Static (ES) method. It follows the Clause
%5.2.1.1. This function is called by CISDR_Design_fn and CS_Design_fn
%functions.
% Inputs:
% T    : Fundamental natural period of the structure (s)
% R    : Return period factor (Clause 3.1.5)
% mu   : Structural ductility factor
% Outputs:
% Cdt  : Horizontal design action coefficient
% Cdt1 : Upper limit of horizontal design action coefficient
% Cdt2 : Lower limit of horizontal design action coefficient
% Notes: Please also refer to NZS 1170.5. The following code considers soil
%class type A (rock) and for a region with zone hazard factor, Z = 0.4 (e.g.
%Wellington). For other soil types or regions, the following code has to be
%appropriately modified according to NZS 1170.5.
%==========================================================================
% Author - Vinod K. Sadashiva (vinod.sadashiva@pg.canterbury.ac.nz)
% Date - January 2007
%==========================================================================

%============================== START OF FUNCTION ==========================

%Hazard Factor (Clause 3.1.4).
Z=0.4;  %e.g. Wellington

%Calculation of Spectral Shape Factor for Soil Class A (Table 3.1 in
%NZS1170.5, 2004).
if (T<=0.4)
    Cht=1.89;
elseif (T<=1.5)
    Cht=(1.6*(0.5/T)^0.75);
elseif (T<=3)
    Cht=(1.05/T);
else
    Cht=3.15/(T^2);
end
```

```
%Calculation of Near-fault factor (Clause 3.1.6.1).
if (R<=0.75)
    Ntd=1;
elseif (T<=1.5)
    Ntd=1;
%Calculation of Maximum near-fault factor (Table 3.7 in NZS1170.5, 2004).
elseif (T<=2)
    Ntd=(1+0.12*(T-1.5)/0.5);
elseif (T<=3)
    Ntd=(1.12+0.24*(T-2));
elseif (T<=4)
    Ntd=(1.36+0.24*(T-3));
elseif (T<5)
    Ntd=(1.6+0.12*(T-4));
else
    Ntd=1.72;
end

%Elastic site hazard spectrum for horizontal loading (Clause 3.1.1).
Ct=Cht*Ntd*min(0.7,Z*R);

%Calculation of Horizontal design action coefficient (Clause 5.2.1.1).
%Calculation of inelastic spectrum scaling factor:
if (T>=0.7)
    kmu=mu;
else
    kmu=((mu-1)*max(T,0.4)/0.7)+1;
end
%Calculation of Structural performance factor (Clause 4.4).
if (mu>=1&mu<=2)
    Sp=(1.3-0.3*mu);
else
    Sp=0.7;
end
%Horizontal design action coefficient.
Cdt1=(Ct*Sp)/kmu;   %Equation 5.2(1) in NZS 1170.5.
Cdt2=max(((Z/20)+0.02)*R,0.03*R);   %Equation 5.2(2) in NZS 1170.5.
Cdt=max(Cdt1,Cdt2);

%================================ END OF FUNCTION ========================
```

B.4 References

[1] SNZ. NZS 1170.5 Supp 1:2004, Structural Design Actions. Part 5: Earthquake actions – New Zealand – commentary. Standards New Zealand, Wellington, 2004.

[2] IBC. International Building Code. International Code Council (ICC), Whittier, CA, 2003.

[3] MATLAB 7.9 (R2009b). The Maths Works, Inc.: Natick, MA, 2009.

[4] Paz M. Structural dynamics: theory and computation – Third Edition. *Van Nostrand Reinhold*, New York, 1985; 626pp.

APPENDIX C: CHOICE OF BILINEAR FACTOR

C.1 Elasto-Plastic and Bi-Linear Hysteresis Models

One of the important steps involved prior to conducting an inelastic dynamic time-history analysis is defining the hysteresis model for structural members. That is, the force-deformation relationship of members observed in a laboratory test must be idealised into an analytical moment-curvature hysteresis model. At the initial development stage of the nonlinear dynamic analysis, an elastic-perfectly plastic hysteresis model (elasto-plastic) was used, intended for perfectly elasto-plastic materials. The elasto-plastic approximation to the actual force-deformation curve under initial loading is shown in Figure C-1, where the areas under the two curves are the same at the selected value of the maximum displacement, d_m [1]. Here, the area enclosed by the hysteresis curves is a measure of the energy dissipated.

Figure C-2(a) shows a typical cycle of loading, unloading and reloading for an elasto-plastic system. The primary curve in this figure consists of a bi-linear relationship, which also defines member stiffness during loading, unloading and reloading. Accordingly, the elastic slope represents the initial stiffness, K_o, of the member prior to yielding. Yielding begins when the force reaches F_y, the yield strength. At this yield load, the

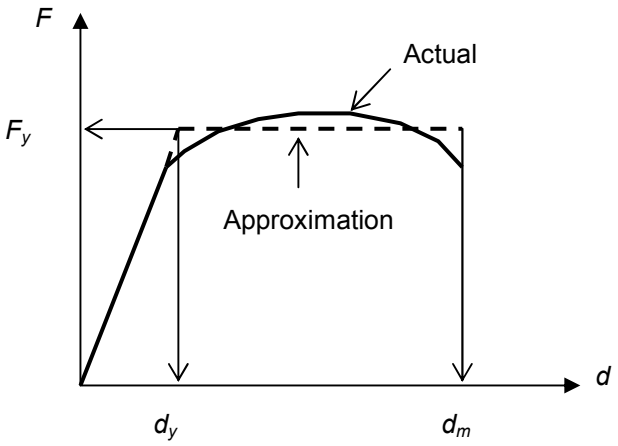

Figure C-1: Actual and approximation of force-deformation curve during initial loading.

member is assumed to have zero stiffness (i.e. yielding takes place at constant F_y force) until unloading begins. Both, unloading from a point of maximum deformation, and reloading from a point of minimum deformation, takes place along a parallel path to the initial elastic branch, with the same initial stiffness being used. It can thus be defined by only three rules, defining the regime of stiffness changes for loading and load reversal [2].

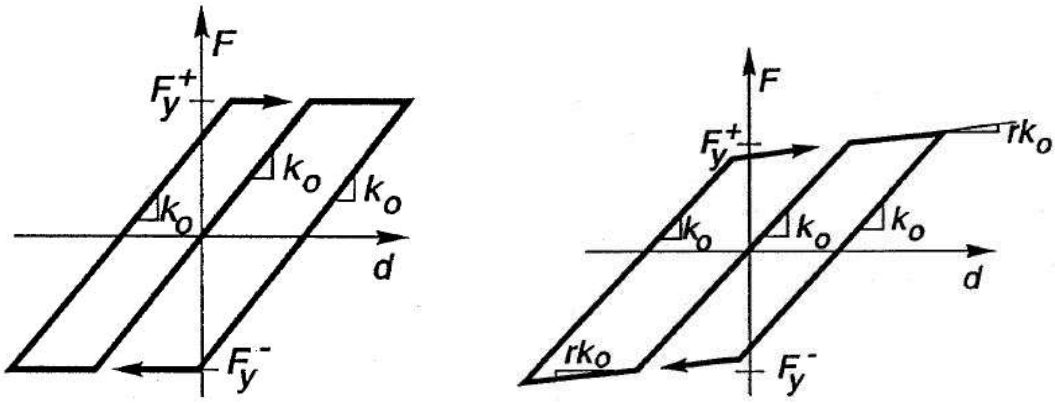

(a) Elasto-plastic hysteresis (b) Bi-linear hysteresis

Figure C-2: Commonly used hysteretic models for inelastic dynamic time-history analysis.

Another commonly used hysteresis model in inelastic analysis is the Bi-linear hysteresis model shown in Figure C-2(b). The primary curve of this model also consists of two segments as in the Elasto-Plastic model. It has a finite positive slope that is assigned to the stiffness after yielding to simulate the strain hardening characteristics of the structural member. The unloading stiffness after yielding is equal to the initial elastic stiffness. The post-yield stiffness, $r \times k_0$, in Figure C-2(b), is the effect of the strain hardening, and is usually expressed as a fraction, r, of the initial stiffness, K_0.

Although the above two hysteresis models do not represent the degradation of unloading and reloading stiffnesses due to inelastic deformation, and they may not be fully appropriate for a refined nonlinear analysis of a structure [3], these two models have been widely used because of the simplicity and reasonable approximation they offer.

C.2 Choice of Bi-Linear Factor for Vertical Irregularity Studies

The Bi-linear hysteresis model has been used for all inelastic dynamic time-history analyses (IDTHA) described in this thesis. This hysteresis model requires specifying the post-yield bi-linear factor, *r*, in the time-history analysis program, Ruaumoko [4]. The sensitivity of the bi-linear factor, *r*, on the peak drift demand, was investigated for structures described in Chapter 2. Three bi-linear factors (*r*): 1%, 5% and 10%, were used for this sensitivity study. For each bi-linear factor, both regular and mass irregular structures were subjected to the suite of earthquake ground motion, and peak interstorey drift ratio (ISDR) from all the storeys was obtained, as explained in Chapter 2. The median peak ISDR was calculated for the suite of records for comparison. Representative results showing the variation of median peak ISDR due to the three bi-linear factors are shown in Figures C-3 through C-5. The figures show that; irrespective of structural configuration, structural height, and regularity condition, higher median peak ISDR are obtained with decreasing bi-linear factor. This is consistent with dynamic stability considerations (MacRae *et al*. [5-7]). However, since the methodology developed in this thesis involves calculating the change in response due to irregularity, the results shows that the difference in responses due to different bi-linear factors is unlikely to have major implications on

the final regularity recommendations. Therefore, a bi-linear factor of 1% has been used for all vertical irregularity studies in this thesis.

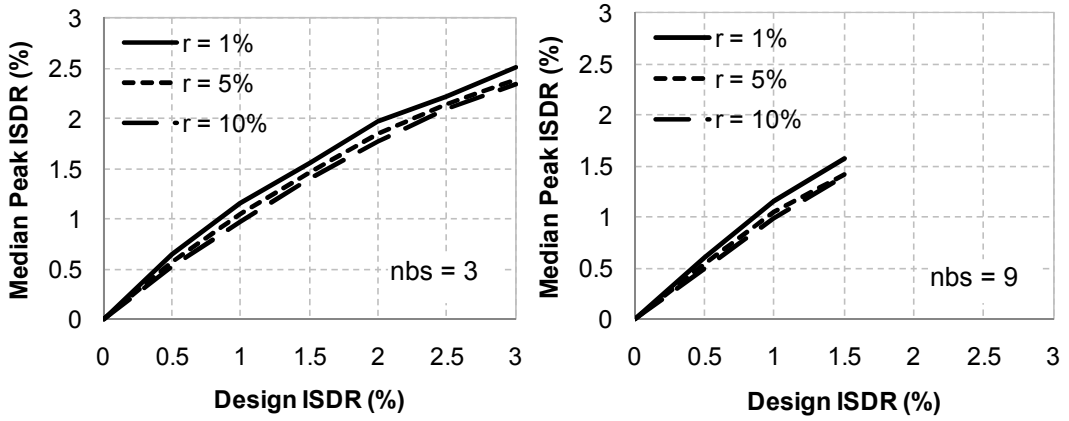

(a) Regular structures

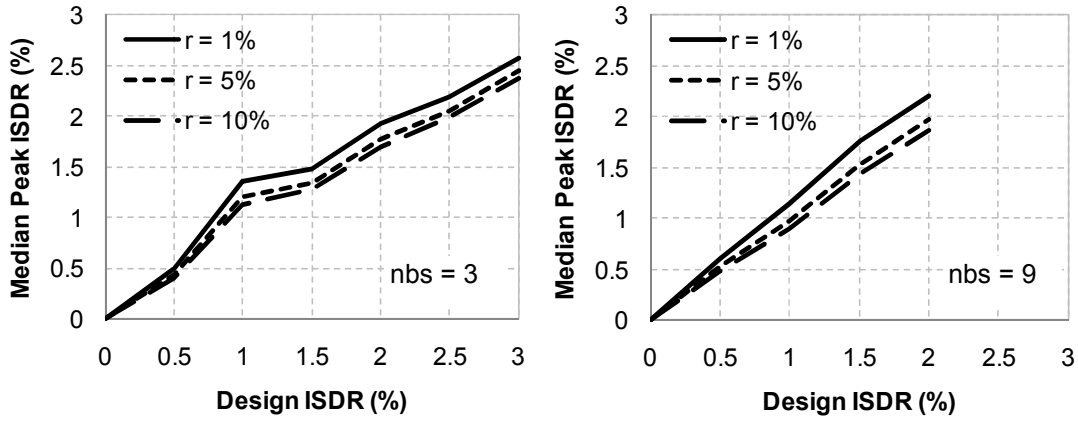

(b) Irregular structures with Mass Ratio = 5 at first floor

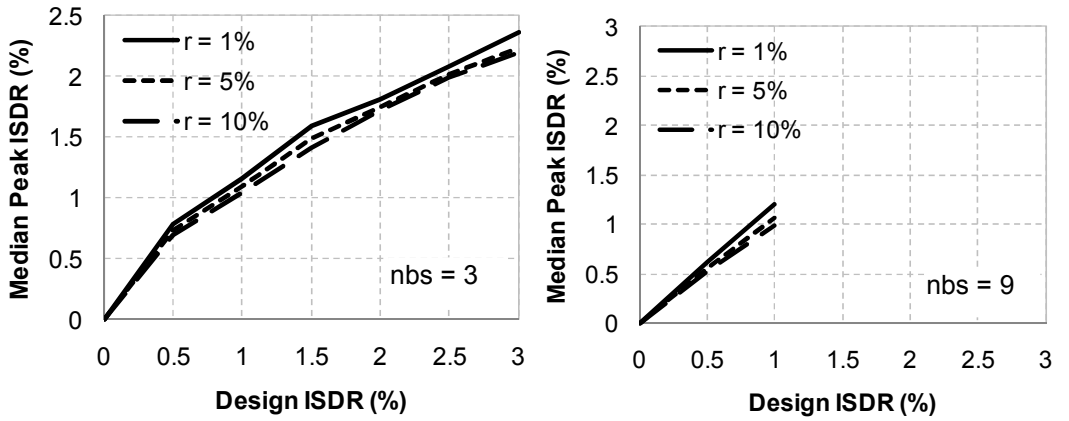

(c) Irregular structures with Mass Ratio = 5 at roof

Figure C-3: Sensitivity of choice of bilinear factor on median peak ISDR for 3 and 9 storey CISDR design models ($\mu = 4$, $Z = 0.4$).

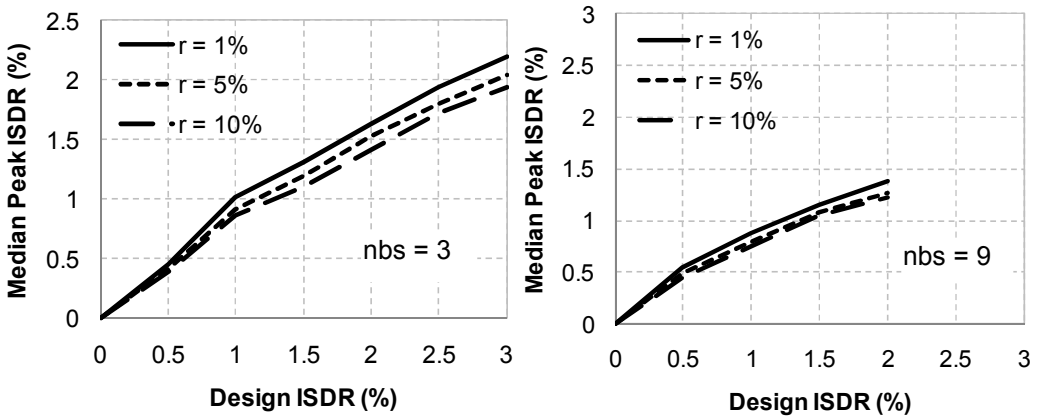

(a) Regular structures

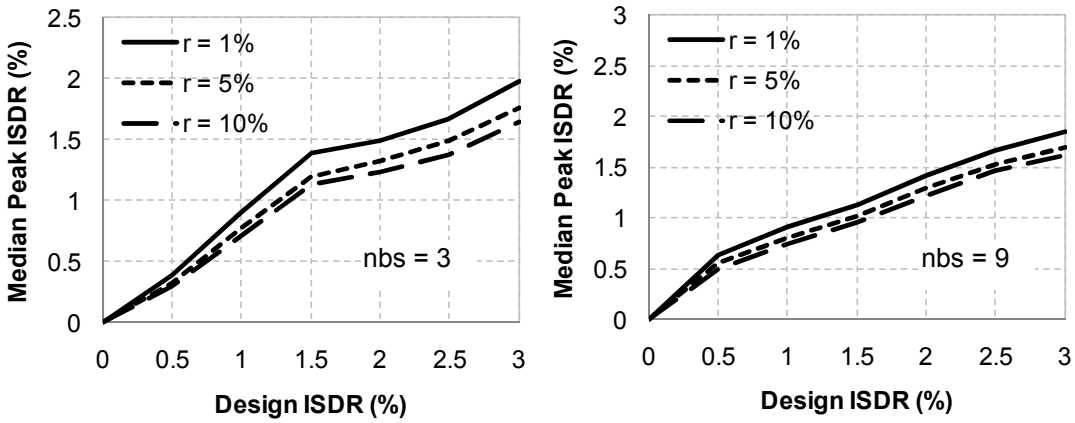

(b) Irregular structures with Mass Ratio = 5 at first floor

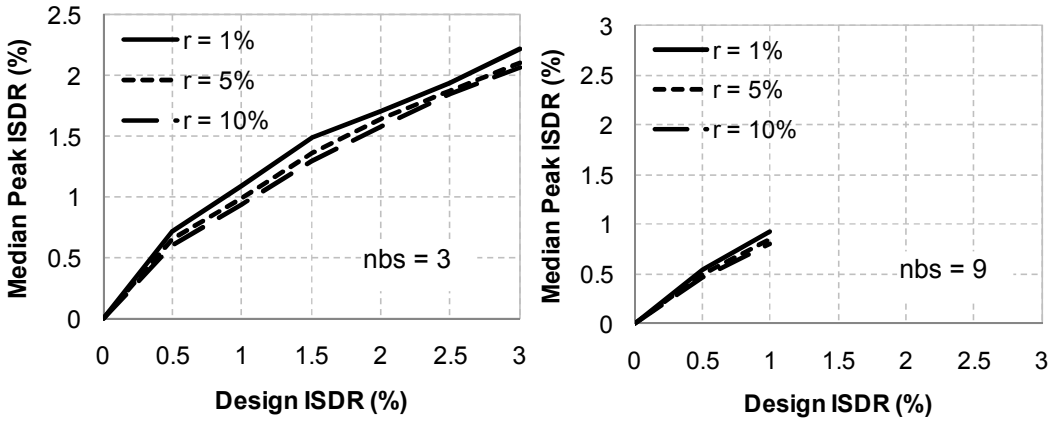

(c) Irregular structures with Mass Ratio = 5 at roof

Figure C-4: Sensitivity of choice of bilinear factor on median peak ISDR for 3 and 9 storey CS-VSTG design models ($\mu = 4$, $Z = 0.4$).

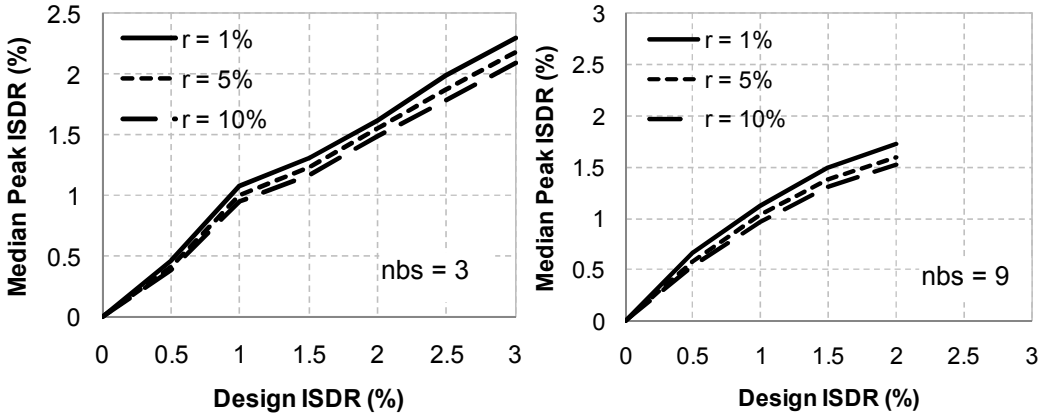

(a) Regular structures

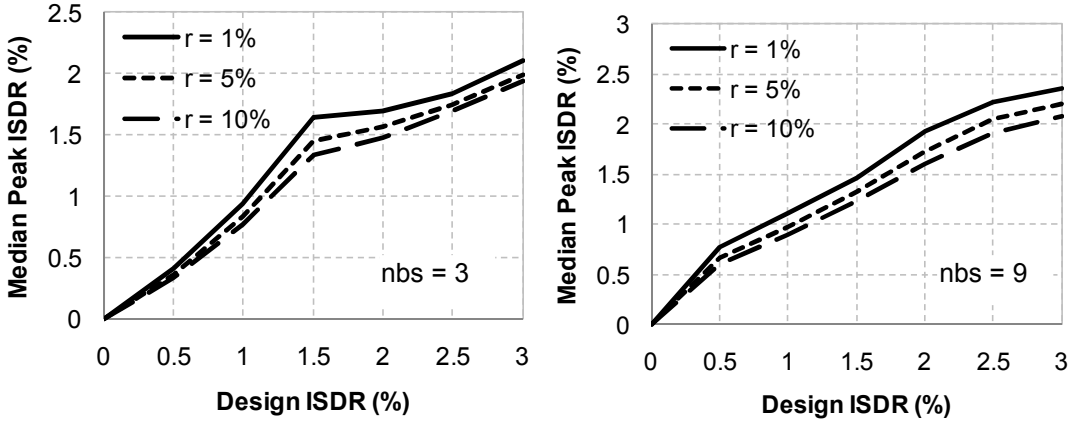

(b) Irregular structures with Mass Ratio = 5 at first floor

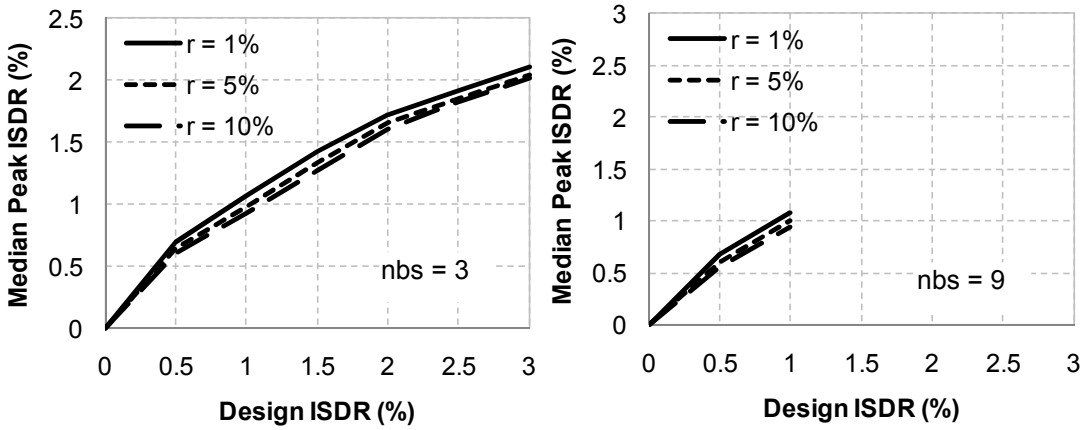

(c) Irregular structures with Mass Ratio = 5 at roof

Figure C-5: Sensitivity of choice of bilinear factor on median peak ISDR for 3 and 9 storey CS-USTG design models ($\mu = 4$, $Z = 0.4$).

C.3 References

[1] Chopra AK. Dynamics of structures: Theory and Applications to Earthquake Engineering. New Jersey: Prentice Hall, 2000; 844 pp.

[2] Saiidi M. Hysteresis models for reinforced concrete. *Journal of Structural Division* 1982; **116**(ST5):1077-1087.

[3] Otani S. Hysteretic models of reinforced concrete for earthquake response analysis. *Journal of the Faculty of Engineering* 1981; University of Tokyo. **XXXVI**(2): 407-441.

[4] Carr AJ. Ruaumoko 2D – Inelastic dynamic analysis. Department of Civil and Natural Resources Engineering, University of Canterbury, Christchurch, New Zealand, 2004.

[5] MacRae GA, Kawashima K. The seismic response of bilinear oscillators using Japanese earthquake records. Public Works Research Institute, Vol. 30, Ministry of Construction, Japan, 1993.

[6] MacRae GA. *P*-delta effects on single-degree-of-freedom structures in earthquakes. *Earthquake Spectra* 1994; **10**(3): 539-568.

[7] MacRae GA, Kawashima K. Post-earthquake residual displacements of bilinear oscillators. *Journal of Earthquake Engineering & Structural Dynamics* 1997; **26**: 701-716.

APPENDIX D: GROUND MOTION RECORDS USED FOR DYNAMIC ANALYSIS

D.1 Acceleration Time-Histories

The set of 20 ground motion records used in this thesis (see Table 2-1) are part of suites of ground motion records developed for analyses of model buildings located in various sites across the United States of America [1]. The acceleration time histories are originally derived from historical recordings or from physical simulations and have been modified to match their mean response spectrum with the 1997 *National Earthquake Hazards Reduction Program* design spectrum, modified from soil type of S_B (rock) – S_C (very dense soil and soft rock) to soil type S_D (stiff soil) and having a hazard according to the 1997 *United States Geological Survey* (USGS) maps. It was mentioned in Section 2.7 that for all the locations (i.e. Wellington, Christchurch and Auckland) considered in this study, structures were assumed to be resting on rock (Soil Type A according to NZS 1170.5). While some studies (e.g., [2]) have shown that random selection of earthquake ground motion records for dynamic analysis can result in unrealistic scaling and increase the scatter of absolute responses, it can be expected that relative values from suites of records can be relatively invariant, as shown by Chase *et al*. [3].

The acceleration time histories of the 20 Los Angeles (LA) 10in50 earthquake records used for dynamic analysis described in this thesis are shown in Figure D-1.

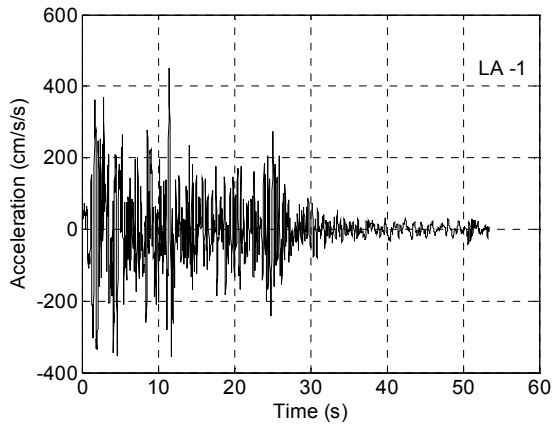
LA -1
Acceleration (cm/s/s)
Time (s)

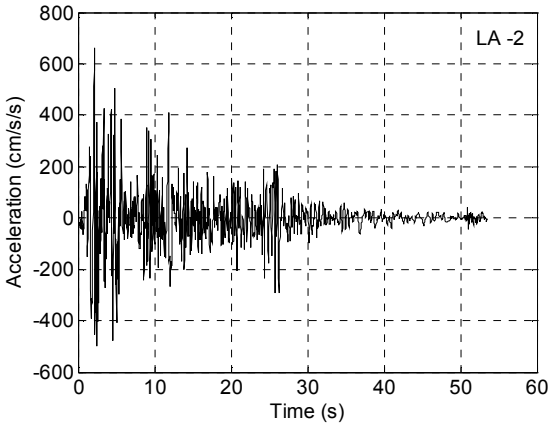
LA -2
Acceleration (cm/s/s)
Time (s)

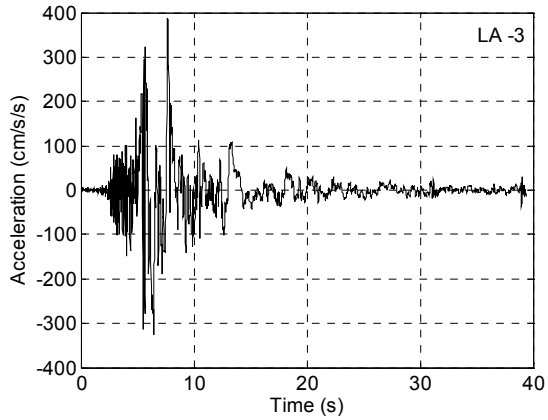
LA -3
Acceleration (cm/s/s)
Time (s)

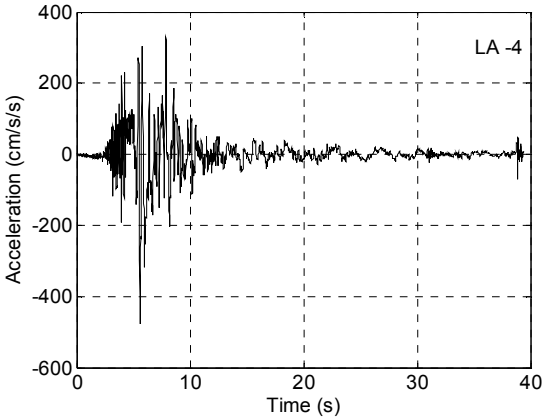
LA -4
Acceleration (cm/s/s)
Time (s)

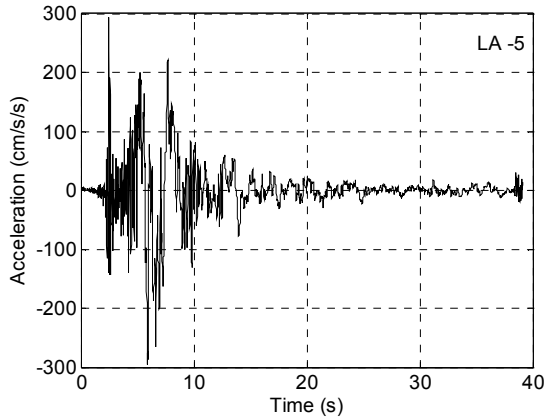
LA -5
Acceleration (cm/s/s)
Time (s)

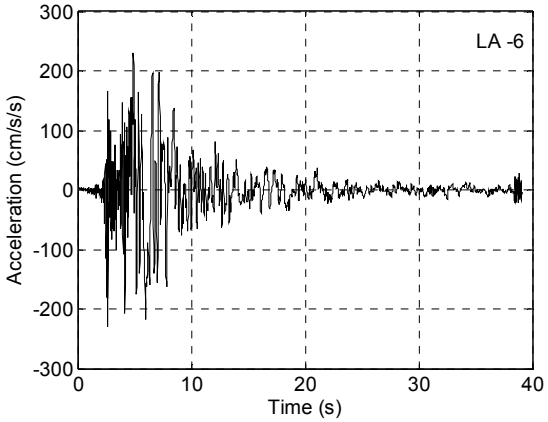
LA -6
Acceleration (cm/s/s)
Time (s)

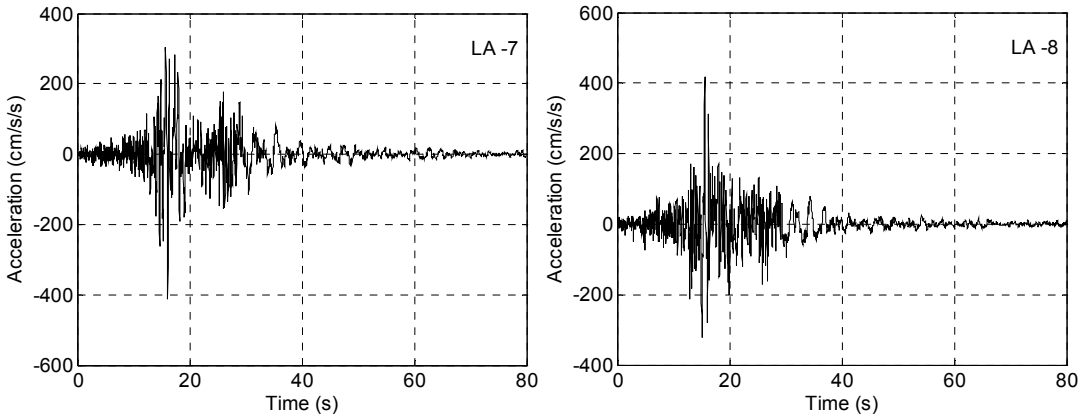
LA -7
LA -8
Acceleration (cm/s/s)
Time (s)

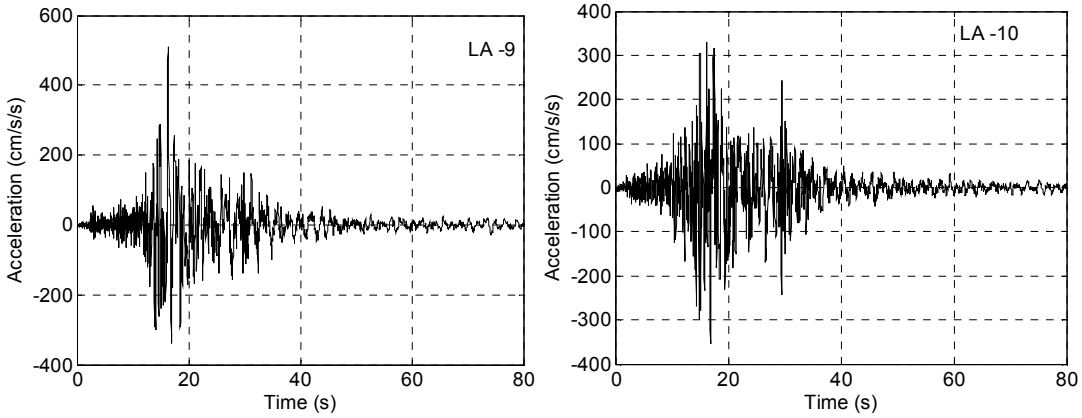
LA -9
LA -10
Acceleration (cm/s/s)
Time (s)

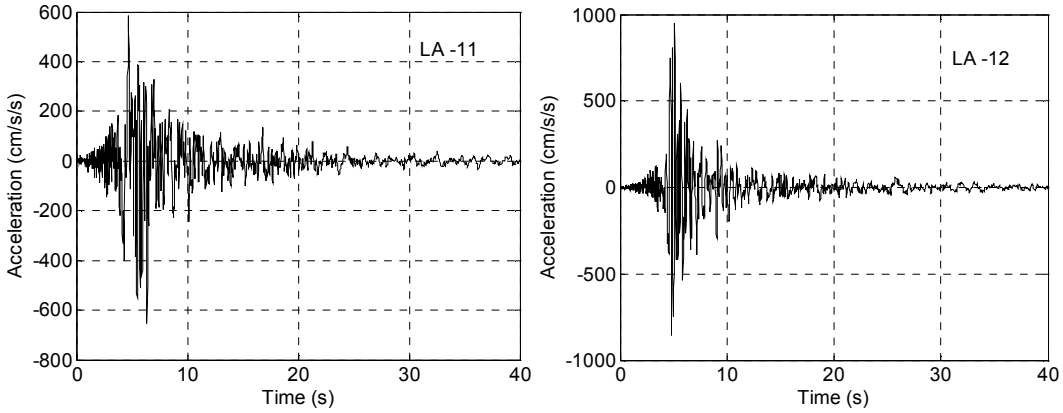
LA -11
LA -12
Acceleration (cm/s/s)
Time (s)

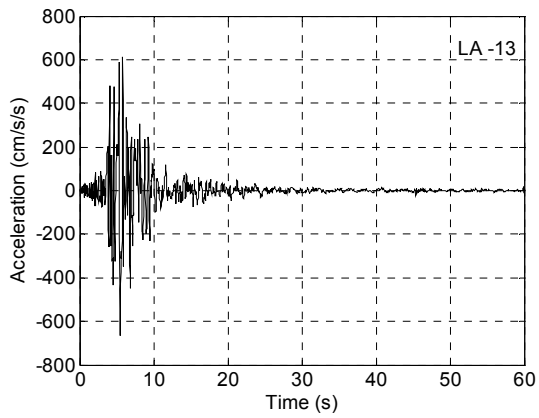
LA -13
Acceleration (cm/s/s)
Time (s)

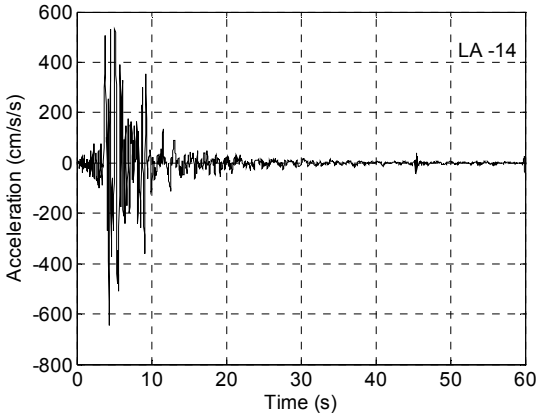
LA -14
Acceleration (cm/s/s)
Time (s)

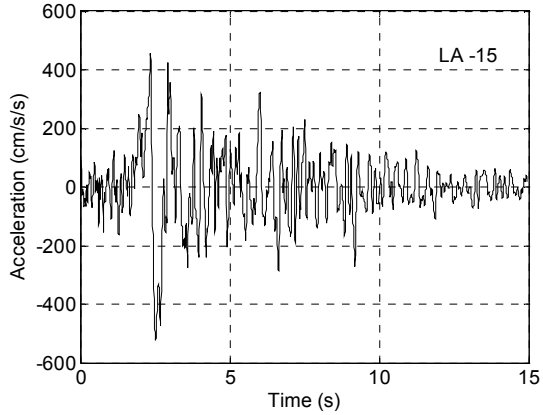
LA -15
Acceleration (cm/s/s)
Time (s)

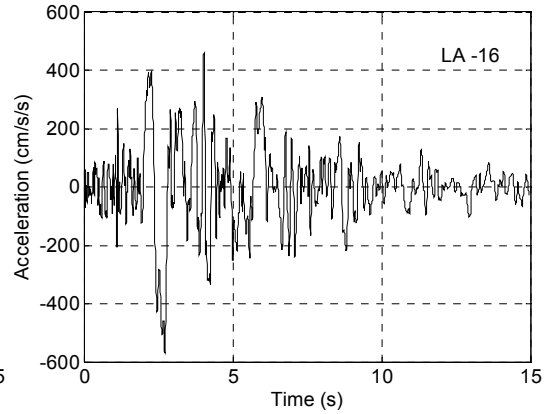
LA -16
Acceleration (cm/s/s)
Time (s)

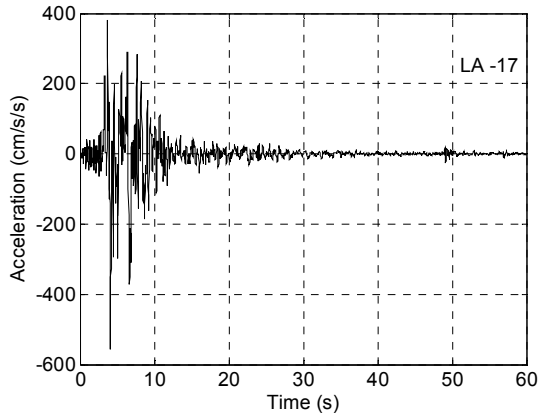
LA -17
Acceleration (cm/s/s)
Time (s)

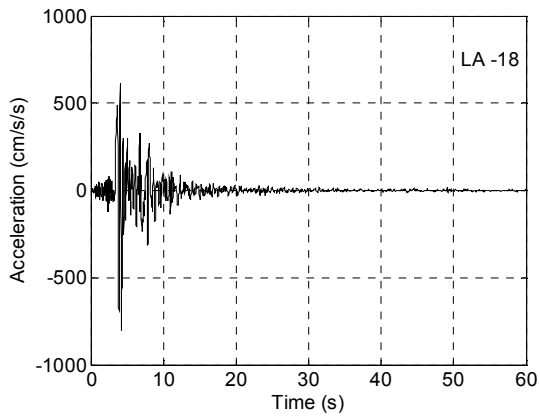
LA -18
Acceleration (cm/s/s)
Time (s)

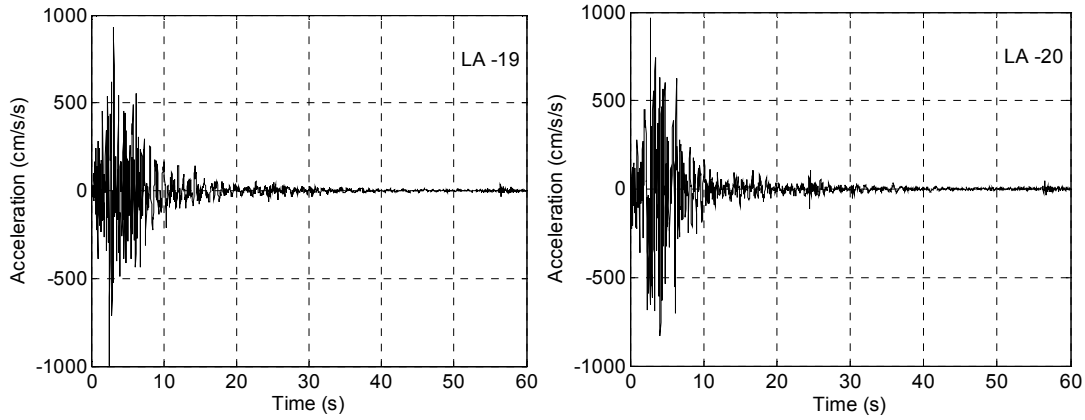

Figure D-1: Acceleration time-histories of the 20 SAC LA 10in50 earthquake ground motion records.

D.2 Response Spectrum

The dynamic response spectrums for single degree-of-freedom elastic systems were computed for the selected earthquake records. A step-by-step Central Difference numerical method [4] was used to compute the peak response quantities for each earthquake record considering a damping ratio, ζ, of 5%. The steps involved in this method (Table D-1) were implemented in Matlab [5], and the response spectra values were calculated. Here, a time-step size of $\Delta t = 0.001$s produced consistent results, and therefore this value of Δt was used for calculations in Table D-1. Figures D-2 and D-3 show the acceleration and displacement response spectrum for the record suite used in this work. Also, the median (50th percentile), the 16th percentile, and the 84th percentile of the acceleration and displacement response spectrum for the record suite, were calculated respectively according to Equations (D-1) to (D-3) (Luco [6]). The corresponding response spectra plots are shown in Figure D-4.

$$\hat{x} = e^{\left(\frac{1}{n}\sum_{i=1}^{n}\ln(x_i)\right)} \qquad \text{(D-1)}$$

$$1 + sigma\,level = \hat{x} \,/\, \exp\left[\sqrt{\frac{1}{(n-1)}\sum_{i=1}^{n}\left(\ln x_i - \ln \hat{x}\right)^2}\right] \qquad \text{(D-2)}$$

$$1 - sigma\,level = \hat{x} \cdot \exp\left[\sqrt{\frac{1}{(n-1)}\sum_{i=1}^{n}\left(\ln x_i - \ln \hat{x}\right)^2}\right] \qquad \text{(D-3)}$$

where x_i = response quantity due to i^{th} record; and

n = total number of earthquake records considered, equal to 20 in this thesis.

Table D-1: Calculation of response spectra values using Central Difference method

1.0 *Initial calculations*

1.1 $\ddot{u}_0 = \dfrac{p_0 - c\dot{u}_0 - ku_0}{m}$.

1.2 $u_{-1} = u_0 - \Delta t\dot{u}_0 + \dfrac{(\Delta t)^2}{2}\ddot{u}_0$.

1.3 $\hat{k} = \dfrac{m}{(\Delta t)^2} + \dfrac{c}{2\Delta t}$.

1.4 $a = \dfrac{m}{(\Delta t)^2} - \dfrac{c}{2\Delta t}$.

1.5 $b = k - \dfrac{2m}{(\Delta t)^2}$.

2.0 *Calculations for time step i*

2.1 $\hat{p}_i = p_i - au_{i-1} - bu_i$.

2.2 $u_{i+1} = \dfrac{\hat{p}_i}{\hat{k}}$.

2.3 If required: $\dot{u}_i = \dfrac{u_{i+1} - u_{i-1}}{2\Delta t}$; $\ddot{u}_i = \dfrac{u_{i+1} - 2u_i + u_{i-1}}{(\Delta t)^2}$.

3.0 *Repetition for the next time step*

Replace i by $i + 1$ and repeat steps 2.1, 2.2, and 2.3 for the next time step.

m = lumped mass of SDOF system, c = damping coefficient, k = lateral stiffness of the SDOF system, p_i = applied force at time i = -m $\ddot{u}_{gi}$, $\ddot{u}_{gi}$ = ground acceleration at time i, $\ddot{u}_i$ = acceleration at time i, $\mathring{u}_i$ = velocity at time i, u_i = displacement at time i, Δt = time step ($\leq 0.1T_1$). Note: Computed response values are relative to the ground. Spectral acceleration, $Sa(T) = |\ddot{u} + \ddot{u}_g|_{\max}$, Spectral displacement, $S_d(T) = |u|_{\max}$.

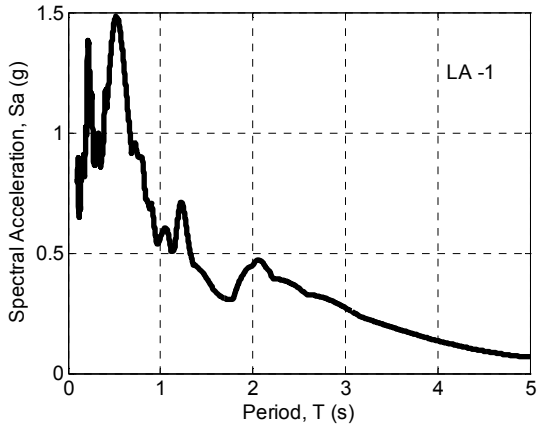
LA -1
Spectral Acceleration, Sa (g)
Period, T (s)

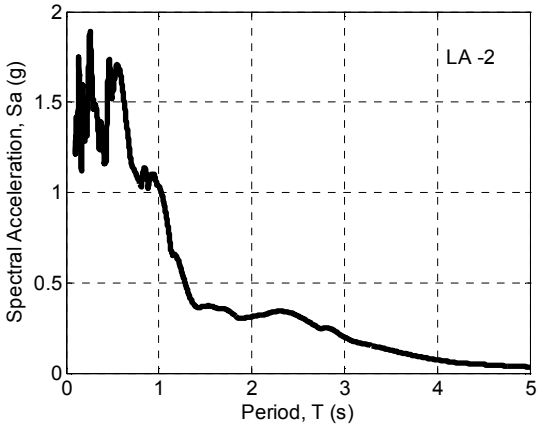
LA -2
Spectral Acceleration, Sa (g)
Period, T (s)

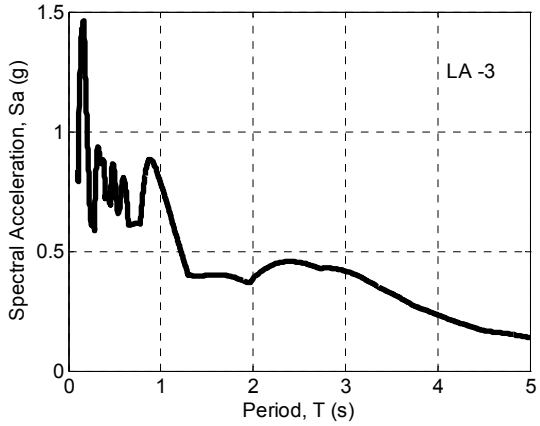
LA -3
Spectral Acceleration, Sa (g)
Period, T (s)

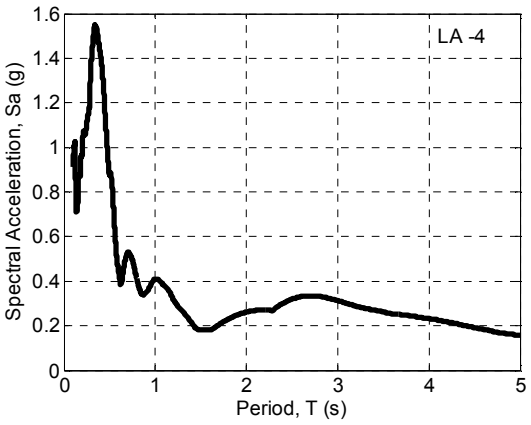
LA -4
Spectral Acceleration, Sa (g)
Period, T (s)

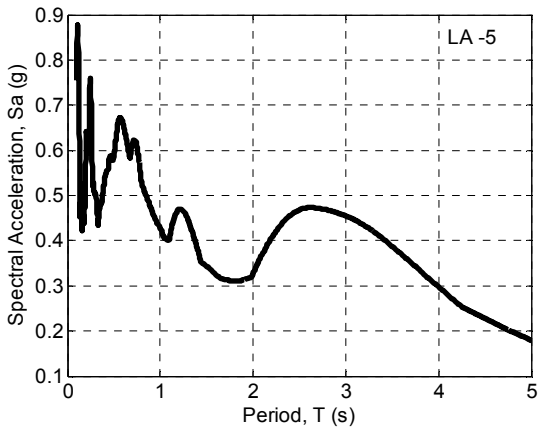
LA -5
Spectral Acceleration, Sa (g)
Period, T (s)

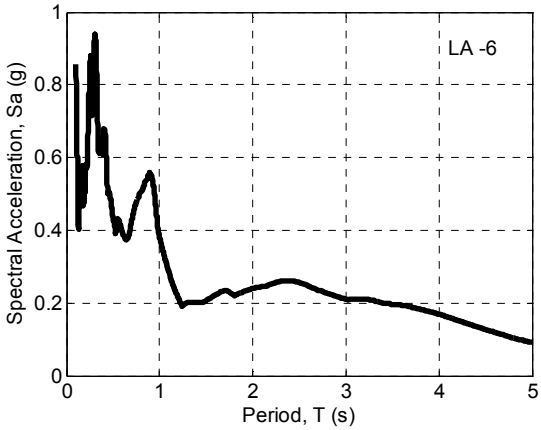
LA -6
Spectral Acceleration, Sa (g)
Period, T (s)

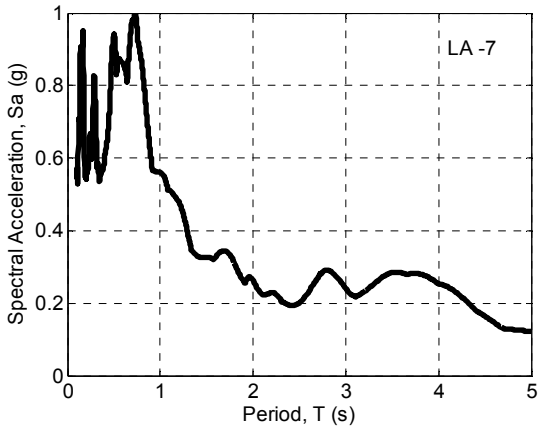
LA -7
Spectral Acceleration, Sa (g)
Period, T (s)

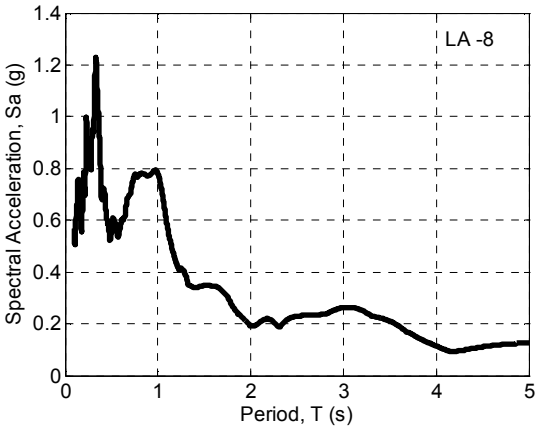
LA -8
Spectral Acceleration, Sa (g)
Period, T (s)

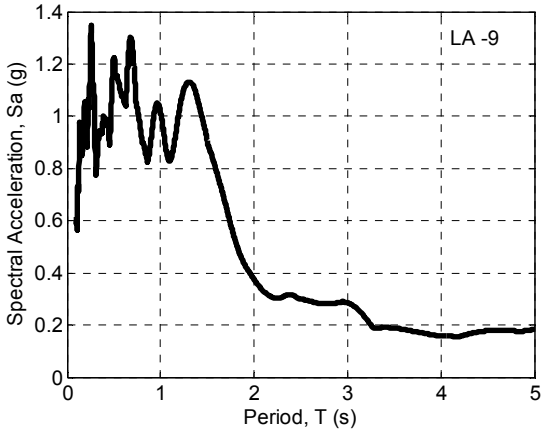
LA -9
Spectral Acceleration, Sa (g)
Period, T (s)

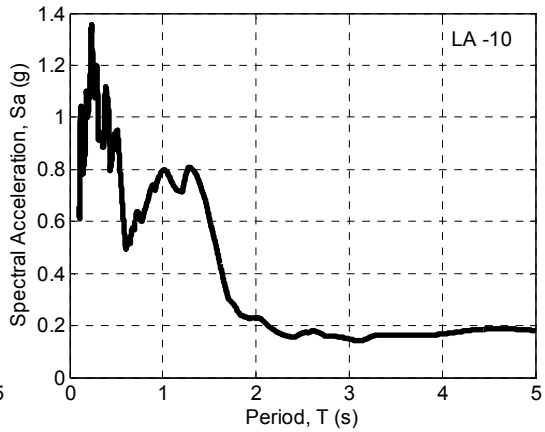
LA -10
Spectral Acceleration, Sa (g)
Period, T (s)

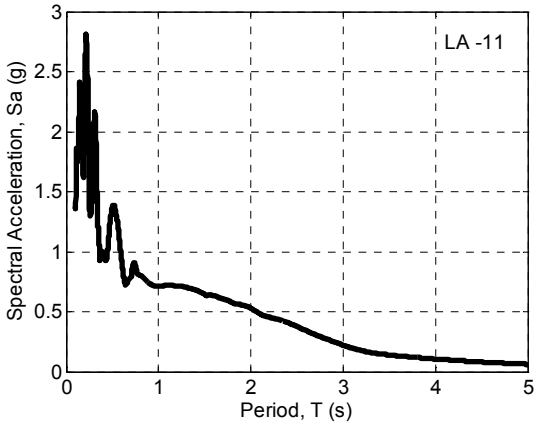
LA -11
Spectral Acceleration, Sa (g)
Period, T (s)

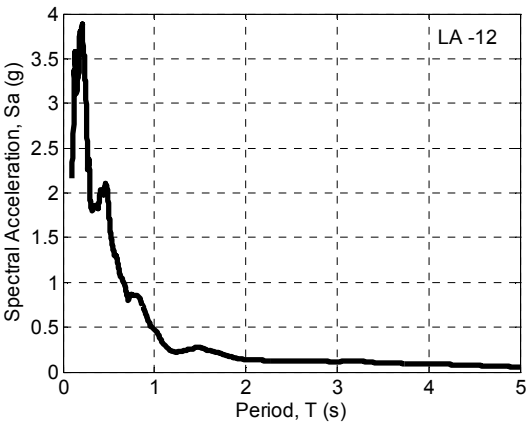
LA -12
Spectral Acceleration, Sa (g)
Period, T (s)

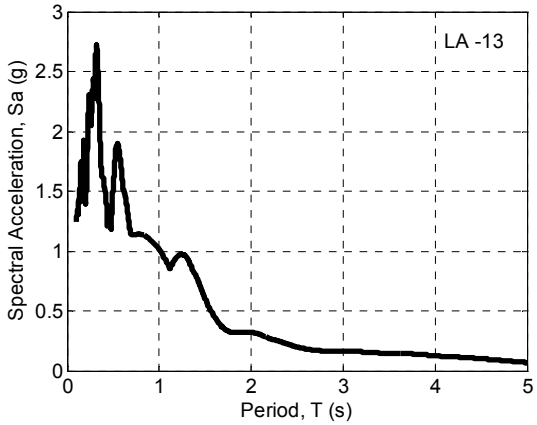
LA -13
Spectral Acceleration, Sa (g)
Period, T (s)

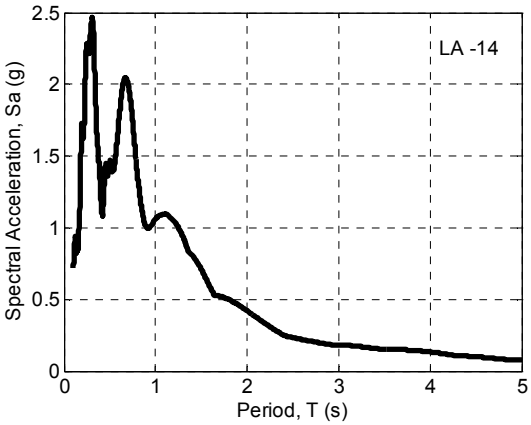
LA -14
Spectral Acceleration, Sa (g)
Period, T (s)

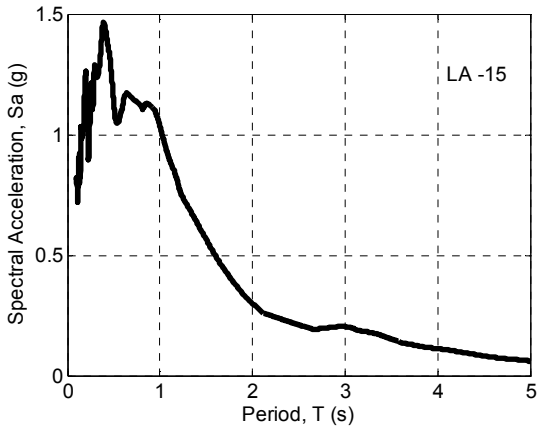
LA -15
Spectral Acceleration, Sa (g)
Period, T (s)

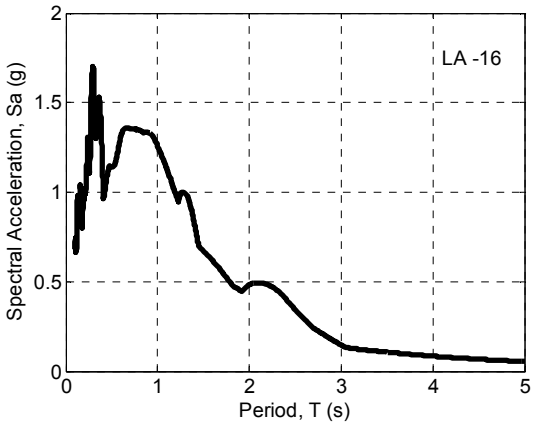
LA -16
Spectral Acceleration, Sa (g)
Period, T (s)

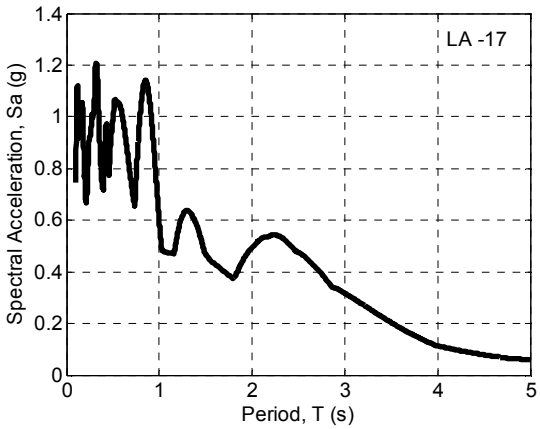
LA -17
Spectral Acceleration, Sa (g)
Period, T (s)

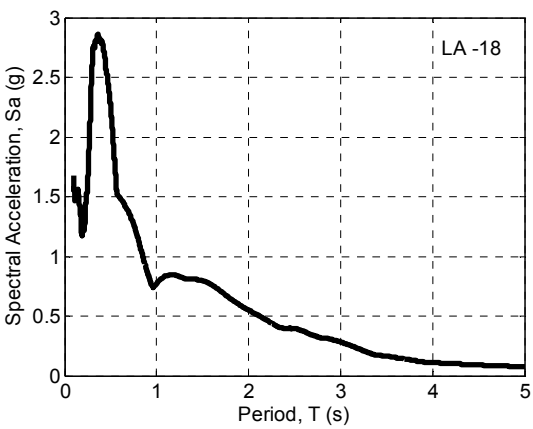
LA -18
Spectral Acceleration, Sa (g)
Period, T (s)

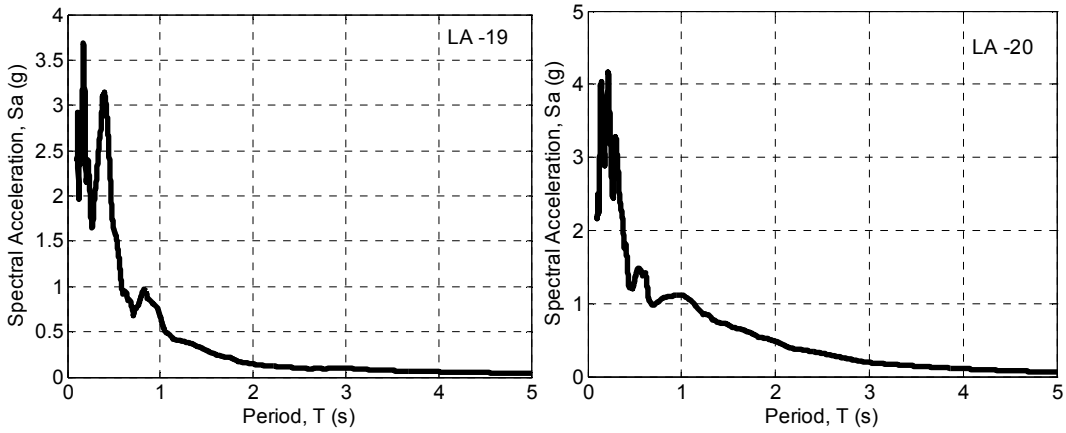

Figure D-2: Acceleration response spectra for the 20 SAC LA 10in50 earthquake ground motion records ($\zeta = 0.05$).

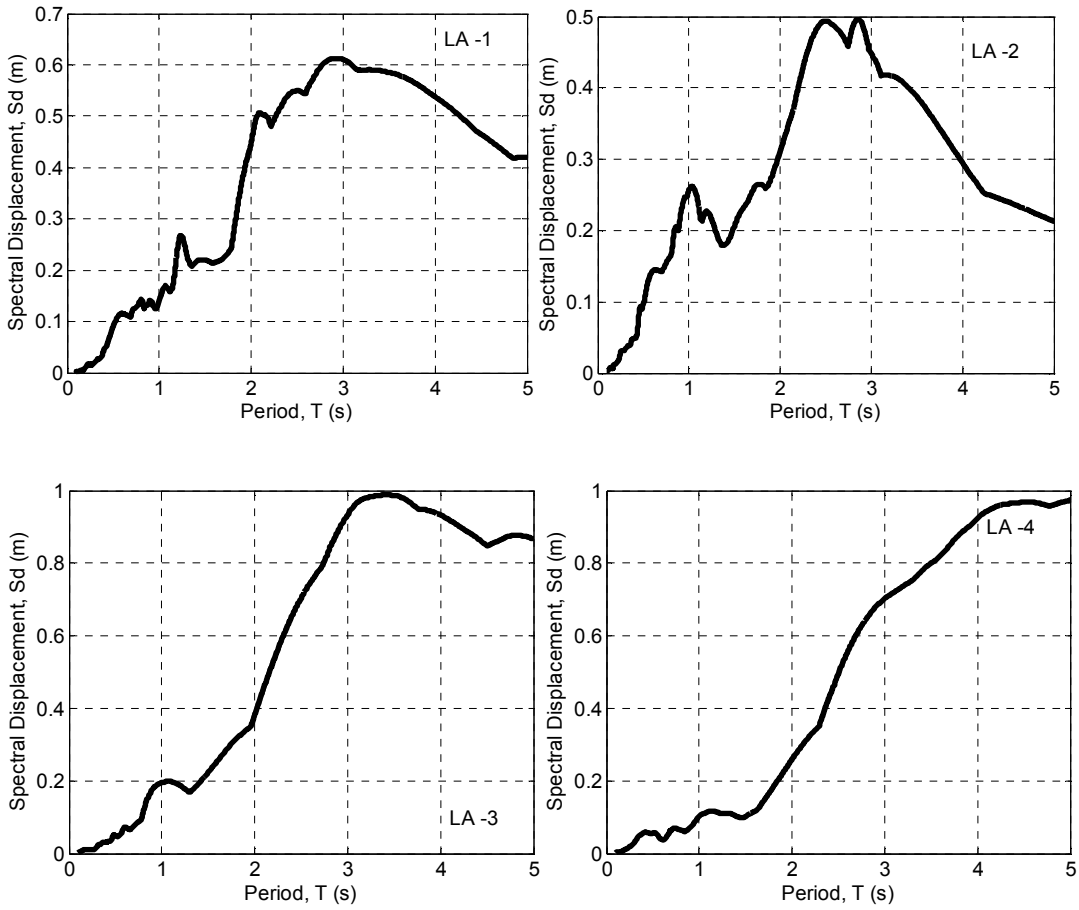

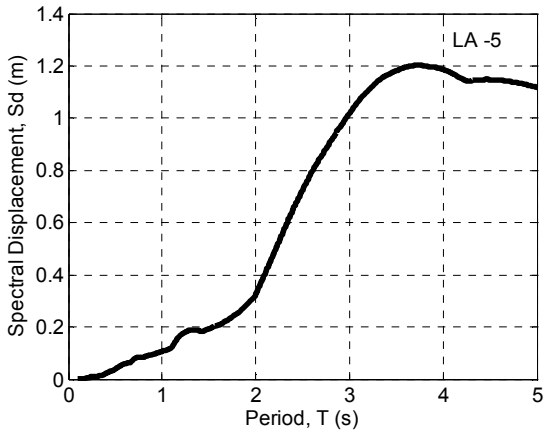
LA -5
Spectral Displacement, Sd (m)
Period, T (s)

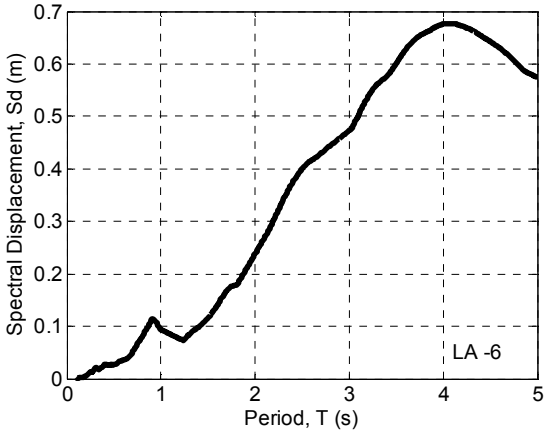
LA -6
Spectral Displacement, Sd (m)
Period, T (s)

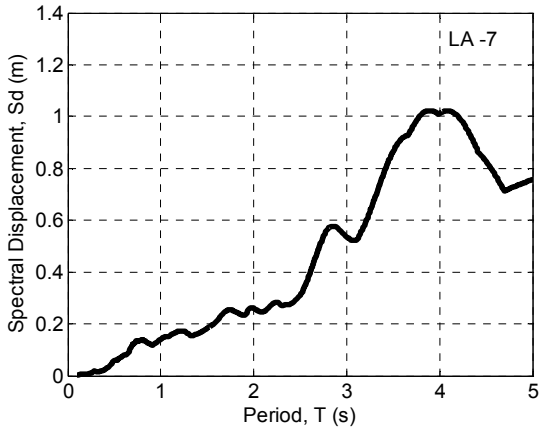
LA -7
Spectral Displacement, Sd (m)
Period, T (s)

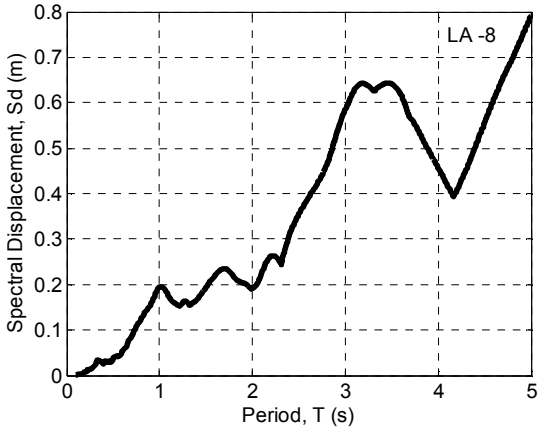
LA -8
Spectral Displacement, Sd (m)
Period, T (s)

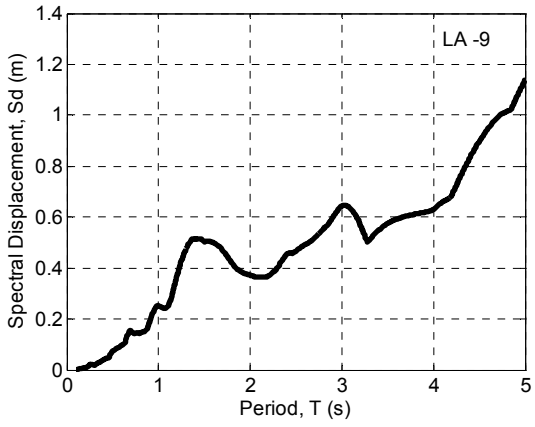
LA -9
Spectral Displacement, Sd (m)
Period, T (s)

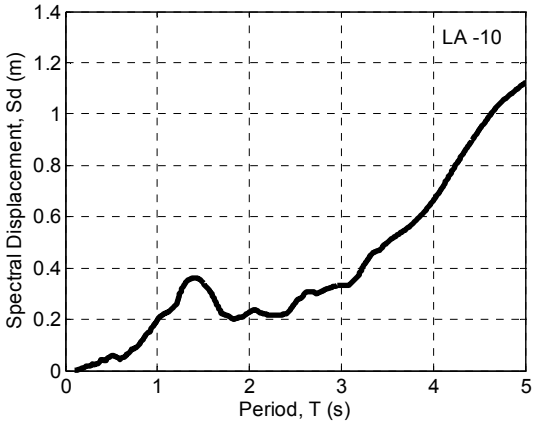
LA -10
Spectral Displacement, Sd (m)
Period, T (s)

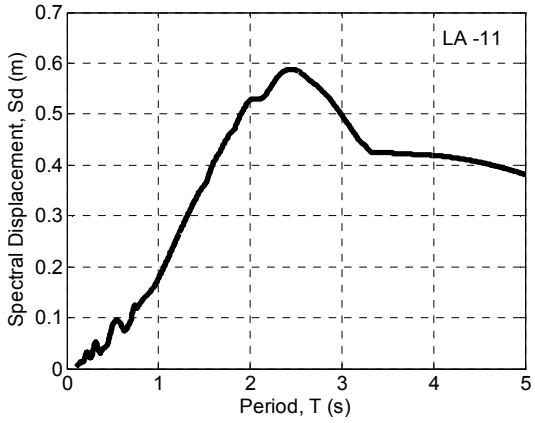
LA -11
Spectral Displacement, Sd (m)
Period, T (s)

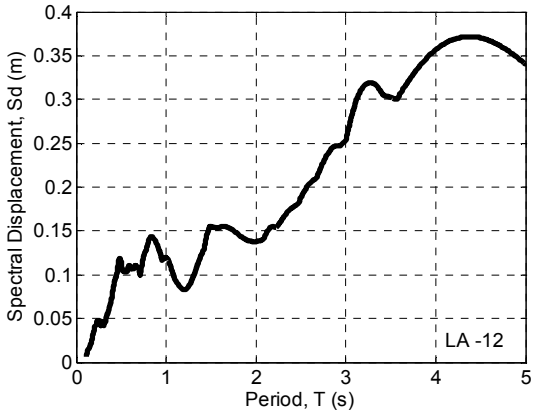
LA -12
Spectral Displacement, Sd (m)
Period, T (s)

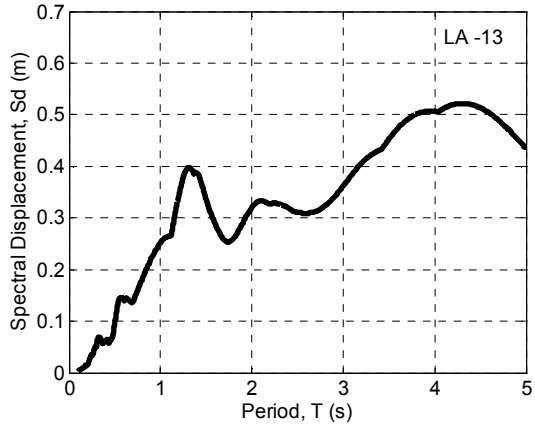
LA -13
Spectral Displacement, Sd (m)
Period, T (s)

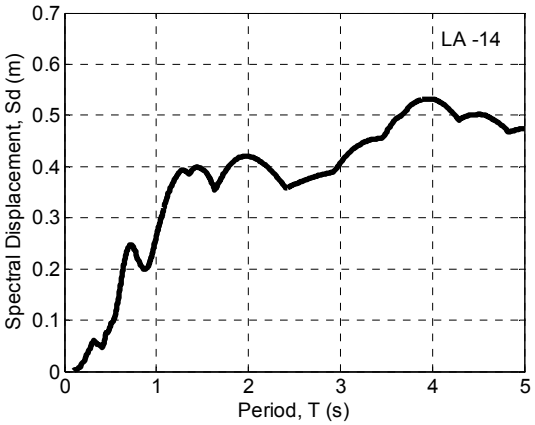
LA -14
Spectral Displacement, Sd (m)
Period, T (s)

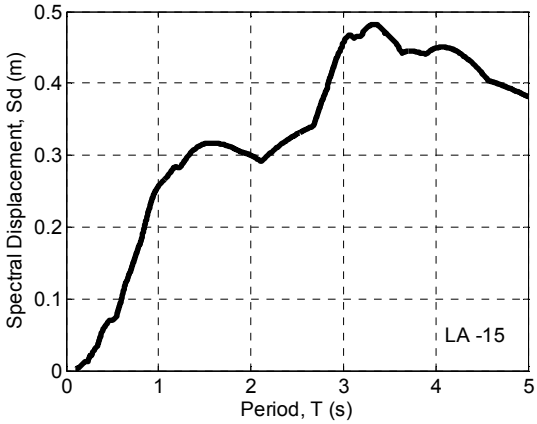
LA -15
Spectral Displacement, Sd (m)
Period, T (s)

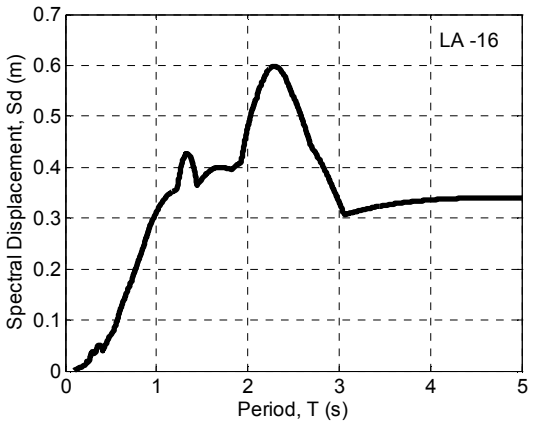
LA -16
Spectral Displacement, Sd (m)
Period, T (s)

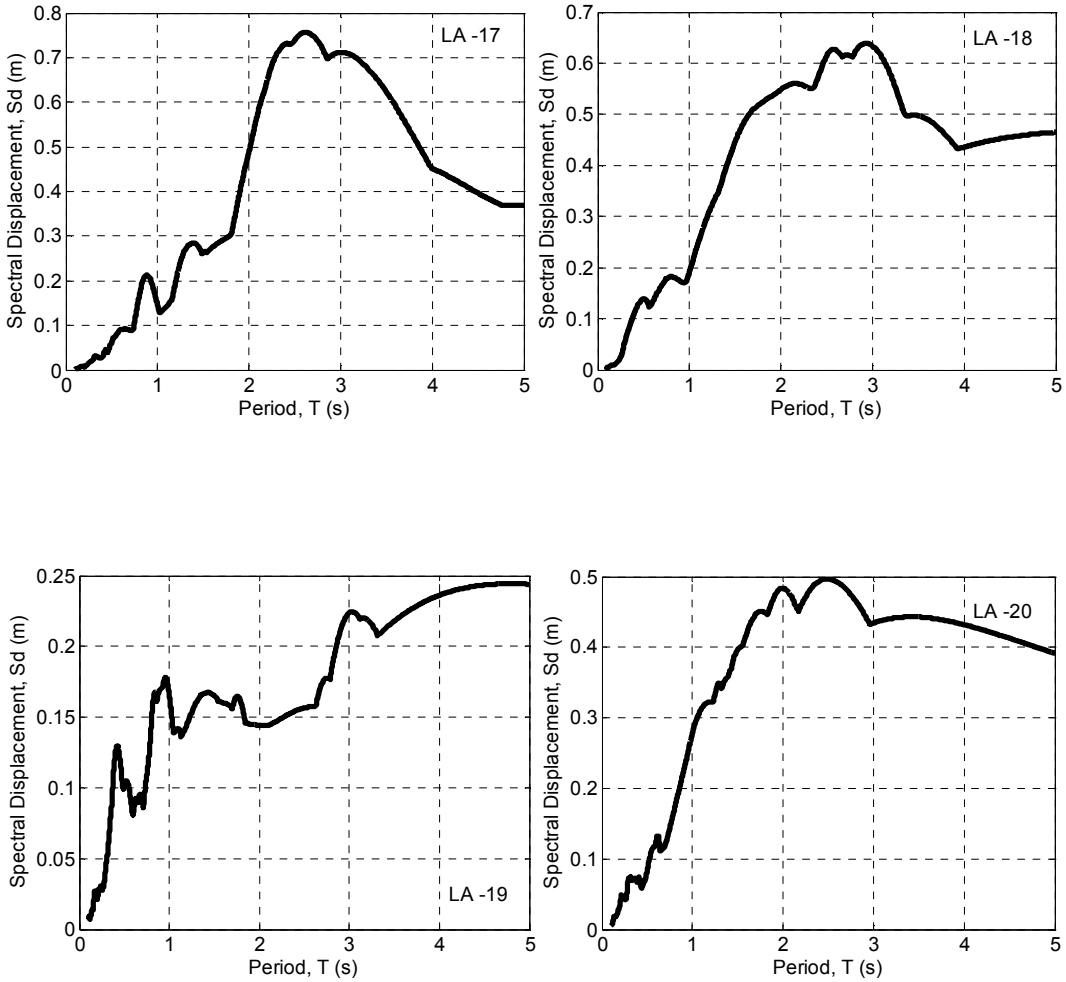

Figure D-3: Displacement response spectra for the 20 SAC LA 10in50 earthquake ground motion records ($\zeta = 0.05$).

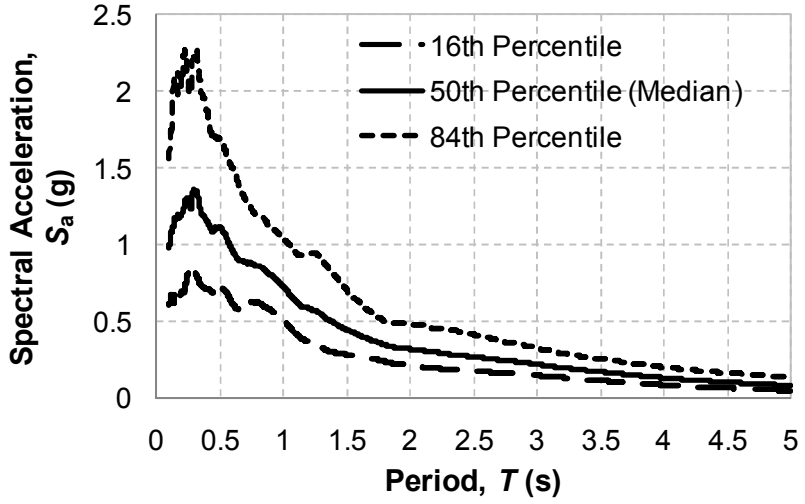

(a) Acceleration Response Spectra

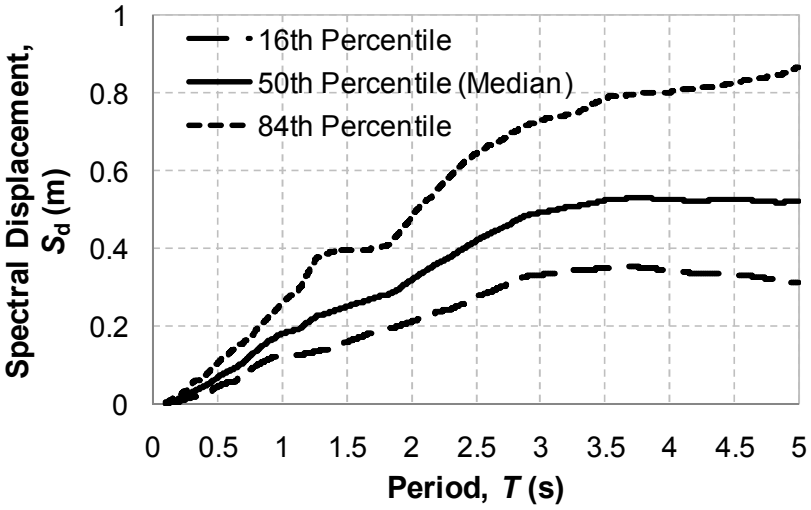

(b) Displacement Response Spectra

Figure D-4: Statistics of response spectra for the 20 SAC LA 10in50 earthquake ground motion records ($\zeta = 0.05$).

D.3 References

[1] Suites of earthquake ground motions for analysis of steel moment frame structures. http://nisee.berkeley.edu/data/strong_motion/sacsteel/ground_motions.html

[2] Baker JW. Measuring bias in structural response caused by ground motion scaling. *8th Pacific Conference on Earthquake Engineering*, Singapore, 2007, Paper No. 56, CD ROM proceedings.

[3] Chase JG, Rodgers GW, Corman S, MacRae GA. Development and spectral analysis of an advanced control law for semi-active resettable devices. *9th Pacific Conference on Earthquake Engineering*, Auckland, 2011, Paper No. 135, CD ROM proceedings.

[4] Chopra AK. Dynamics of structures: Theory and Applications to Earthquake Engineering. New Jersey: Prentice Hall, 2000; 844.

[5] MATLAB 7.9 (R2009b). The Maths Works, Inc.: Natick, MA, 2009.

[6] Luco N. Probabilistic seismic demand analysis, SMRF connection fractures, and near-source effects. Ph.D. Dissertation, Department of Civil and Environmental Engineering, Stanford University, Stanford, CA, 2002.

APPENDIX E: MATLAB CODES FOR RUAUMOKO

E.1 Overview

Ruaumoko [1] is a structural engineering program developed by Prof. Athol Carr at the University of Canterbury, Christchurch, New Zealand. The program is specifically designed to undertake elastic and inelastic dynamic analysis of structures subjected to earthquake and other dynamic loadings. Ruaumoko has been used in this thesis to carry out all time-history analyses described for vertical irregularity studies. The program has the facility to run the analysis in an interactive mode or in a batch mode. Therefore, to minimise the time required to run the analyses; the batch mode option was used. The creation of Ruaumoko input files required for each parametric analysis, executing Ruaumoko, and post-processing the output from Ruaumoko result files, was carried out systematically using Matlab [2]. This appendix provides sample Matlab codes written to: (a) generate Ruaumoko input files; (b) run Ruaumoko in a batch mode; and (c) obtain analyses results from Ruaumoko output file. Prior to these codes, information on the parameters used in the Ruaumoko input file is provided from the Ruaumoko user manual.

E.2 Ruaumoko Parameter Definitions

The analysis data for the structure is described by the following sequence of input lines or card images.

1. *Description of the Analysis*

Description of the structure (up to 79 alphanumeric characters)

2. *Principal Analysis Options*

Name Tag	Value	Description
IPANAL	2	Dynamic Time-history analysis using Newmark Constant Average Acceleration method (Newmark parameters, $\gamma = 0.5$ and $\beta = 0.25$)
IFMT	0	Binary post-processor file with extension .RES
IPLAS	1	In-elastic Time-history Analysis
IPCONM	0	Lumped mass matrix used in Time-history
ICTYPE	6	Rayleigh Damping with Tangent damping matrix as Secant damping matrix
IPVERT	0	X-direction earthquake only
INLGEO	2	P-Delta effects included
IPNF	0	Modal analysis is carried out after the static analysis (normal case)
IZERO	0	All zero output is omitted
ORTHO	0	Mode shape orthogonality check not carried out
IMODE	0	Householder QR eigenvalue algorithm used (default)

3. *Frame Control Parameters*

Name Tag	Value	Description
NNP	TBC*	Number of nodal points in the structure
NMEM	TBC*	Number of members in the structure
NTYPE	TBC*	Number of different cross-section in the section table
M	TBC*	Number of mode-shapes required to be printed in the modal analysis
MODE1	1	The mode number at which the first damping ratio is applied
MODE2	TBC*	The mode number at which the second damping ratio is applied
GRAV	9.81	The acceleration of gravity
C1	5	The percentage of critical damping at mode MODE1
C2	5	The percentage of critical damping at mode MODE2
DT	0.001	The time-step (s)
TIME	TBC*	The length of time-history to be run

FACTOR	TBC*	A scale factor applied to the time-history input (default = 1.0)

TBC* = To Be Calculated

4. *Output Intervals and Plotting Control Parameters*

Name Tag	Value	Description
KP	0	Time-history output suppressed
KPA	0	Post-processor DYNAPLOT output suppressed
KPLOT	10	Plastic hinges plotted every k time-steps
JOUT	0	Not used any longer, supply 0
DSTORT	1	Not used any longer, supply 1
DFACT	1	Displacement multiplying scale factor for on-screen graphics (≥ 1)
XMAX	0.1	Maximum X displacement for use in the on-screen graphics
YMAX	0.1	Maximum Y displacement for use in the on-screen graphics
NLEVEL	TBC*	Number of levels for computed inter-storey (i.e. no. of storeys +1)
NUP	2	Vertical axis for inter-storey drifts (1=X axis, 2=Y axis)
IRESID	1	Residual displacements and forces output at end of time-history output
KDUMP	0	Mass and Stiffness matrices output suppressed

TBC* = To Be Calculated

5. *Iteration Control and Wave Velocities*

Name Tag	Value	Description
MAXIT	10	Maximum number of cycles of Newton-Raphson iteration per Time-step
MAXCIT	0	Maximum number of cycles of iteration/solution step for damping models (for ICTYPE = 6, use 0)
FTEST	0.0001	Norm of the out-of-balance force vector relative to the incremental force vector for the Newton-Raphson or damping iteration. The value is the square of the iteration tolerance required (i.e. 0.0001 implies a tolerance of 1% in the residual vector
WAVEX	0	Wave velocity of propagation in the X-direction (if 0.0 taken as infinite)

WAVEY	0	Wave velocity of propagation in the Y-direction (if 0.0 taken as infinite)
THETA	0	Angle of Earthquake X and Y direction to structure X and Y directions degrees (default = 0)
DXMAX	0	X displacement to terminate analysis
DYMAX	0	Y displacement to terminate analysis
D	0	Travelling wave dispersion factor (0.0 implies no dispersion)
OMEGA	0	Earthquake characteristic frequency (rad/s) used for dispersion
F	0	Scale factor for dispersion

6. *Nodal Point Input (one input line with the word NODES starting in column 1)*

Name Tag	Value	Description
IOUT	0	Output control flag (IOUT = 0; if required, the results will be sent to both the output file and written to the DYNAPLOT file)
N	TBC*	Nodal point number
X(N)	TBC*	X-coordinate of node N
Y(N)	TBC*	Y-coordinate of node N
NF1	0	x-displacement is unconstrained
	1	x-displacement is zero (i.e. fixed)
NF2	0	y-displacement is unconstrained
	1	y-displacement is zero (i.e. fixed)
NF3	0	z-rotation is unconstrained
	1	z-rotation is zero (i.e. fixed)
KUP1	0	No coupling of the X-displacement degree-of-freedom
	J	X-displacement of this node is coupled to that of node *J*
KUP2	0	No coupling of the Y-displacement degree-of-freedom
	J	Y-displacement of this node is coupled to that of node *J*
KUP3	0	No coupling of the Z-rotation degree-of-freedom
	J	Z-rotation of this node is coupled to that of node *J*

TBC* = To Be Calculated

7. *Interstorey Drift Input (only if NLEVEL is greater than 2)*

Name Tag	Value	Description
DRIFT	-	Interstorey drifts are the differences in the storey displacements
N1	TBC*	Nodal point number at ground floor, or first level, of the structure
N2	TBC*	Nodal point number at the second level of the structure
….	TBC*	Nodal point numbers at intermediate levels of the structure
Ntop	TBC*	Nodal point at the top level of the structure

TBC* = To Be Calculated

8. *Member Topology or Geometry (one input line with the word ELEMENTS starting in column1)*

Name Tag	Value	Description
N	TBC*	Member number
MT	TBC*	Member type number, refers to the member properties that follows
NODE1	TBC*	Nodal point number at end 1 of the member
NODE2	TBC*	Nodal point number at end 2 of the member
NODE3	TBC*	Inner nodal point at end 1 of the member (if NODE3 is zero or blank, it is reset to equal to NODE1)
NODE4	TBC*	Inner nodal point at end 2 of the member (if NODE4 is zero or blank, it is reset to equal to NODE2)

TBC* = To Be Calculated

9. *Member Property Tables (one input line with the word PROPS starting in column 1) and Section Property Information*

Name Tag	Value	Description
N	TBC*	Section number
MTYPE	F	Beam or Beam-Column (Frame) member. The frame member type covers the beam and beam-column members. A beam member is a general three dimensional member which may use almost any of the hysteresis rules governing the behaviour of the plastic hinges that may form at each end of the member. A beam member may also have a bi-linear axial load - axial displacement hysteresis. However,

		there is no interaction between the axial yield states and those associated with the moment-curvature yield states. A beam-column member differs from a beam member in that the axial force in the member affects the current yield moments at each end or the member. The inelastic behaviour of the frame members follow the concept of Giberson one-component model (Sharpe [3]) which has a plastic hinge possible at one or both ends of the elastic central length of the member.
LABEL	-	Maximum 30 character label for section

TBC* = To Be Calculated

10. *Basic Section Properties*

Name Tag	Value	Description
IPIN	0	Member built-in to joint (use 1 for end 1, 2 for end 2, and 3 for both ends, pinned internally to the joint)
ICOND	0	No initial loads applied
IHYST	2	Bi-linear hysteresis rule
ILOS	0	No strength degradation
IDAMG	0	No damage indices computed
ICOL	0	Column ductilities computed at balance point of axial force (default)
IGA	0	Shear deformation is elastic (default) (only option if ITYPE = 7)

11. *Elastic Section Properties*

Name Tag	Value	Description
E	2.1E+11	Elastic (Young's) Modulus of member material (N/m^2)
G	8.1E+10	Shear Modulus of member material (N/m^2)
A	TBC*	Cross-sectional area of the member section
AS	TBC*	Effective shear area of the member section (if 0, then shear deformations in the section are suppressed)
I	TBC*	Moment of inertia (2^{nd} Moment of Area) of section
WGT	0	Weight/(unit length) of the member
END1	0	Length of rigid end-block at end 1 of member

END2	0	Length of rigid end-block at end 2 of member
FJ1	0	Joint flexibility at end 1 (rad/unit moment)
FJ2	0	Joint flexibility at end 2

TBC* = To Be Calculated

12. *Member Bi-linear Factors and Hinge Properties (only if IHYST ≠0)*

Name Tag	Value	Description
RA	0.01	Bi-linear factor (or Ramberg-Osgood *r*) - Axial
RF	0.01	Bi-linear factor (or Ramberg-Osgood *r*) - Flexure
H1	TBC*	Plastic hinge length at end 1
H2	TBC*	Plastic hinge length at end 1

TBC* = To Be Calculated

13. *Yield Interaction Surface at End 1 of Member*

Name Tag	Value	Description
PYC	TBC*	Axial compressive yield force (< 0.0)
PB	TBC*	Axial compression force at B (< 0.0)
MB	TBC*	Yield moment at B (> 0.0)
MO	TBC*	Yield moment at P=0.0 (> 0.0)
PC	TBC*	Axial tension force at C (> 0.0)
MC	TBC*	Yield moment at C (> 0.0)
PYT	TBC*	Axial tension yield force (> 0.0)
IEND	0	End 2 of the member has the same yield surface

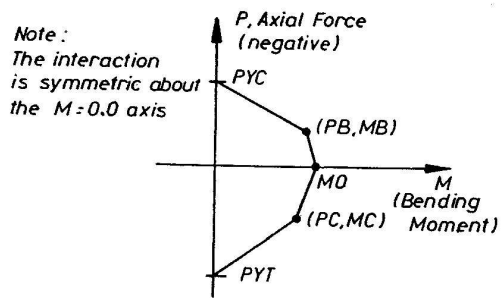

TBC* = To Be Calculated

14. *Lumped Weights at the Nodes*

Name Tag	Value	Description
INTERP	0	Omitted Nodes have no point weight
N	TBC*	Nodal point number
WX	TBC*	Lumped nodal weight acting in the X direction
WY	TBC*	Lumped nodal weight acting in the Y direction
WM	TBC*	Lumped nodal weight acting in rotation at node

TBC* = To Be Calculated

15. *External (static) Nodal Loads (one input line with the word LOADS starting in column 1)*

Name Tag	Value	Description
N	TBC*	Nodal point number
FX	0	Static load at node N in the X direction
FY	0	Static load at node N in the Y direction
FM	0	Static moment at node N about the Z axis

TBC* = To Be Calculated

16. *Earthquake Input Control Parameters (one input line with the word EQUAKE staring in column 1)*

Name Tag	Value	Description
FILE	-	Name of the file where excitation is to be found (maximum of 60 characters)
IBERG	3	Excitation in FREE Format (one point per line)
ISTART	1	The number of the first line of the excitation that is to be used
DELTAT	TBC*	Excitation data interval
ASCALE	981	1/(Scale factor) for the record (if records are in cm/s/s, ASCALE=981 to bring the records to units of the acceleration of gravity)
END	-1	Any missing part of the record is padded with zero values
VEL	0	Initial ground velocity (default = 0)
DIS	0	Initial ground displacement (default = 0)

TSCALE	1	Time scale for the record – the times implied in the record are effectively divided by TSCALE (default = 1)

TBC* = To Be Calculated

E.3 Sample Matlab Code for Generating Ruaumoko Input File

```
function ROMKO_INPfl_fn(nbs,hfl,wfl,K,V,eqfilelink,EQdur,DELTAT,Slfactor)

%=========================================================================
% ROMKO_INPfl_fn creates the Ruaumoko input file for a regular structure.
% Inputs:
% nbs  : Number of storeys in the structure
% hfl  : Storey heights between floors (m)
% wfl  : Weight at every floor level (N)
% K    : Storey lateral stiffness (N/m)
% V    : Storey strengths (N) (according to Section 2.6)
% eqfilelink : Link to the directory containing the earthquake file
% EQdur      : Duration of the earthquake (s)
% DELTAT     : Excitation data interval (s)
% Slfactor   : Scale factor applied to the time-history input
% Notes: Please also refer to the Ruaumoko manual for complete description
%of the parameters involved. Checks on the designs explained in Sections 2.6
%and 2.7 have to be carried out before conducting time-history analyses. The
%above last three input information can be obtained using EQ_ScaleFact_fn
%function, provided at the end of this function.
%=========================================================================
% Author – Vinod K. Sadashiva (vinod.sadashiva@pg.canterbury.ac.nz)
% Date – January 2007
%=========================================================================


%============================== START OF FUNCTION ==========================


% Ruaumoko input file name.
filename = 'ROMKO.txt';


% Description of the analysis.
dlmwrite(filename,'Regular Structure','delimiter','','newline','pc');


% Principal analysis options.
% [IPANAL,IFMT,IPLAS,IPCONM,ICTYPE,IPVERT,INLGEO,IPNF,IZERO,ORTHO,IMODE]
dlmwrite(filename,' ','-append','delimiter','','newline','pc');
line2=[2,0,1,0,6,0,2,0,0,0,0];
```

```
dlmwrite(filename,line2,'-append','delimiter',' ','newline','pc');

% Frame control parameters.
% [NNP,NMEM,NTYPE,M,MODE1,MODE2,GRAV,C1,C2,DT,TIME,FACTOR]
line3=[(nbs+1)*2,(nbs*2),(nbs*2),nbs,1,nbs,9.81,5,5,0.001,EQdur,Slfactor];
dlmwrite(filename,line3,'-append','delimiter',' ','newline','pc');

% Output intervals and plotting control parameters.
% [KP,KPA,KPLOT,JOUT,DSTORT,DFACT,XMAX,YMAX,NLEVEL,NUP,IRESID,KDUMP]
line4=[0,0,10,0,1,1,0.1,0.1,(nbs+1),2,1,0];
dlmwrite(filename,line4,'-append','delimiter',' ','newline','pc');

% Iteration control and wave velocities.
% [MAXIT,MAXCIT,FTEST,WAVEX,WAVEY,THETA,DXMAX,DYMAX,D,OMEGA,F]
line5=[10,0,0.0001,0,0,0,0,0,0,0,0];
dlmwrite(filename,line5,'-append','delimiter',' ','newline','pc');

% Nodal point input.
dlmwrite(filename,' ','-append','delimiter','','newline','pc');
dlmwrite(filename,'NODES 1','-append','delimiter','','newline','pc');
% Node information.
nodenum=[];
xnode=[];
ynode1=[];
uxnode=[];
uynode=[];
uznode=[];
kup1=[];
kup2=[];
kup3=[];
nodeflag=[];
H=hfl;
h=H(1);       % Height of one regular floor, in m.
for i=1:(nbs+1)
    nodenum(i)=i;
    xnode(i)=0;
    ynode1=[ynode1,i*h];
    uxnode(i)=0;
    uynode(i)=0;
    uznode(i)=1;
    kup1(i)=0;
```

```
    kup2(i)=0;
    kup3(i)=0;
    nodeflag(i)=1;
end
Ynode=(ynode1-h);
uxnode(1)=1;
uynode(1)=1;
for i=(nbs+2):(nbs*2+2)
    nodenum(i)=i;
    xnode(i)=1;
    uxnode(i)=0;
    uynode(i)=0;
    uznode(i)=0;
    kup1(i)=(i+1)-(nbs+2);
    kup2(i)=0;
    kup3(i)=0;
    nodeflag(i)=1;
end
uxnode(nbs+2)=1;
uynode(nbs+2)=1;
kup1(nbs+2)=0;
ynode=[Ynode,Ynode];
% [N,X(N),Y(N),NF1,NF2,NF3,KUP1,KUP2,KUP3,IOUT]
line6b=[nodenum',xnode',ynode',uxnode',uynode',uznode',kup1',kup2',kup3',nod
eflag'];
dlmwrite(filename,line6b,'-append','delimiter','\t','newline','pc')

% Interstorey drift input.
dlmwrite(filename,' ','-append','delimiter','','newline','pc');
dlmwrite(filename,'DRIFT','-append','delimiter','','newline','pc');
nodedrift=[]; % N1, N2…Ntop
for i=1:((nbs+1)*2)
    nodedrift(i)=i;
end
dlmwrite(filename,nodedrift,'-append','delimiter',' ','newline','pc');

% Member topology or geometry.
dlmwrite(filename,' ','-append','delimiter',' ','newline','pc');
dlmwrite(filename,'ELEMENTS 1','-append','delimiter','','newline','pc');
% Element information.
memnum=[];
memtype=[];
```

```
memnode1=[];
memnode2=[];
memnode3=[];
memnode4=[];
memflag=[];
for i=1:nbs
    memnum(i)=i;
    memtype(i)=i;
    memnode1(i)=i;
    memnode2(i)=(i+1);
    memnode3(i)=0;
    memnode4(i)=0;
    memflag(i)=1;
end

for i=(nbs+1):(nbs*2)
    memnum(i)=i;
    memtype(i)=i;
    memnode1(i)=(i+1);
    memnode2(i)=(i+2);
    memnode3(i)=0;
    memnode4(i)=0;
    memflag(i)=1;
end
% [N,MT,NODE1,NODE2,NODE3,NODE4,IOUT]
line8b=[memnum',memtype',memnode1',memnode2',memnode3',memnode4',memflag'];
dlmwrite(filename,line8b,'-append','delimiter','\t','newline','pc');

% Member property tables.
dlmwrite(filename,' ','-append','delimiter','','newline','pc');
dlmwrite(filename,'PROPS','-append','delimiter','','newline','pc');
%Section property information:
for i=1:nbs
    secno=int2str(i);
    line9b=[secno ,' FRAME '];
    dlmwrite(filename,line9b,'-append','delimiter','','newline','pc');
    % [ITYPE,IPIN,ICOND,IHYST,ILOS,IDAMG,ICOL,IGA]
    line9c=[3,0,0,2,0,0,0,0];
    dlmwrite(filename,line9c,'-append','delimiter',' ','newline','pc');
    % [E,G,A,AS,I,WGT,END1,END2,FJ1,FJ2]
    I1=(K(i)*H(i)^3)/(12*(2.1E+11));
```

```
    line9d=[2.1E+11,8.1E+10,1,1,I1,0,0,0,0,0];
    dlmwrite(filename,line9d,'-append','delimiter',' ','newline','pc');
    % [RA,RF,H1,H2]
    %Reference for H1 and H2 - Tagawa [4].
    line9e=[0.01,0.01,((H(i)/2)/3),((H(i)/2)/3)];
    dlmwrite(filename,line9e,'-append','delimiter',' ','newline','pc');
    % [PYC,PB,MB,MO,PC,MC,PYT,IEND]
    line9f=[-1E+10,-1E+10,1E+10,((H(i)*V(i))/2),1E+10,1E+10,1E+10,0];
    dlmwrite(filename,line9f,'-append','delimiter',' ','newline','pc');
    dlmwrite(filename,' ','-append','delimiter','','newline','pc');
end
for i=(nbs+1):(nbs*2)
    secno=int2str(i);
    line9b=[secno ,' FRAME '];
    dlmwrite(filename,line9b,'-append','delimiter','','newline','pc');
    % [ITYPE,IPIN,ICOND,IHYST,ILOS,IDAMG,ICOL,IGA]
    line9c=[3,0,0,2,0,0,0,0];
    dlmwrite(filename,line9c,'-append','delimiter',' ','newline','pc');
    % [E,G,A,AS,I,WGT,END1,END2,FJ1,FJ2]
    I2=(K((i-nbs))*H((i-nbs))^3*0.5)/(2.1E+11);
    line9d=[2.1E+11,8.1E+10,1,1,I2,0,0,0,0,0];
    dlmwrite(filename,line9d,'-append','delimiter',' ','newline','pc');
    % [RA,RF,H1,H2]
    line9e=[0.01,0.01,((H(i-nbs)/2)/3),((H(i-nbs)/2)/3)];
    dlmwrite(filename,line9e,'-append','delimiter',' ','newline','pc');
    % [PYC,PB,MB,MO,PC,MC,PYT,IEND]
    line9f=[-1E+10,-1E+10,1E+10,((H((i-nbs))*V((i-
    nbs))/2)),1E+10,1E+10,1E+10,0];
    dlmwrite(filename,line9f,'-append','delimiter',' ','newline','pc');
    dlmwrite(filename,' ','-append','delimiter','','newline','pc');
end

% Lumped weights at the nodes.
dlmwrite(filename,'WEIGHTS 0','-append','delimiter','','newline','pc');
nlumpwt(1,1)=1;
nlumpwt(1,2:4)=0;
for i=1:nbs
    nlumpwt(i+1,1)=(i+1);
    nlumpwt(i+1,2:3)=(wfl(i))/2;
    nlumpwt(i+1,4)=0.01;
end
nlumpwt((nbs+2),1)=(nbs+2);
```

```
nlumpwt((nbs+2),2:4)=0;
for i=(nbs+3):(nbs*2+2)
    nlumpwt(i,1)=i;
    nlumpwt(i,2:3)=(wfl((i-(nbs+2)))/2);
    nlumpwt(i,4)=0.01;
end
% [N,WX,WY,WM]
dlmwrite(filename,nlumpwt,'-append','delimiter','\t','newline','pc');

% External (static) nodal loads.
dlmwrite(filename,' ','-append','delimiter','','newline','pc');
dlmwrite(filename,'LOADS','-append','delimiter','','newline','pc');
for i=1:(nbs*2+2)
    nload(i)=i;
end
sloads=zeros((nbs*2+2),3);
% [N,FX,FY,FM]
line11b=[nload',sloads];
dlmwrite(filename,line11b,'-append','delimiter','\t','newline','pc');

% Earthquake input control parameters.
dlmwrite(filename,' ','-append','delimiter','','newline','pc');
exctname='EQUAKE ';
line12a=[exctname,eqfilelink];
dlmwrite(filename,line12a,'-append','delimiter','','newline','pc');
% [IBERG,ISTART,DELTAT,ASCALE,END,VEL,DIS,TSCALE]
line12b=[3,1,DELTAT,981,-1,0,0,1];
dlmwrite(filename,line12b,'-append','delimiter',' ','newline','pc');

%================================ END OF FUNCTION ==========================
```

E.3.1 Matlab Function to Calculate Earthquake Record Scale Factor

```
function [EQdur DELTAT Slfactor] = EQ_ScaleFact_fn(Ct_mu1,T,EQFlName)

%=========================================================================
% EQ_ScaleFact_fn calculates the earthquake record scale factor.
% Inputs:
% Ct_mu1      : NZS 1170.5 Elastic site hazard spectrum for horizontal
               loading (Clause 3.1.1 with μ = 1, Sp = 1)
% T           : Fundamental natural period of the structure (s)
% EQFlName    : Earthquake record file name
% Outputs:
% EQdur       : Duration of the earthquake (s)
% DELTAT      : Excitation data interval (s)
% Slfactor    : Scale factor applied to the time-history input
% Notes: The central difference numerical method in Table D-1 is used for
%creating this code. A damping ratio of 5%, and a time-step size of 0.001s,
%is assumed for all calculations here. The above outputs are used in the
%function: ROMKO_INPfl_fn. The input parameter, Ct_mu1, can be obtained
%through the function NZS11705_CdT_fn (provided in Section B.3.3) with the
%appropriate defined parameters.
%=========================================================================
% Author – Vinod K. Sadashiva (vinod.sadashiva@pg.canterbury.ac.nz)
% Date – January 2007
%=========================================================================

%============================== START OF FUNCTION ==========================

Sadesign=Ct_mu1;
alldata=xlsread(EQFlName);
timesp=alldata(:,2);            %Time steps column in the Eq. file.
DELTAT=timesp(2)-timesp(1);     %Record time interval (s).
EQdur=timesp(size(timesp,1));   %Earthquake duration (s).
gaccln=alldata(:,3)/100;        %Accln. column in the Eq. file (m/s2).
tmstep=0.001;                   %Time-step for Central Diff. method (s).
Melast=1;                       %Lumped mass of the SDOF system (kg).
Kelast=((2*pi)/T)^2*Melast;     %Lateral stiffness of SDOF system (N/m).
dcoeff=(5/100)*2*(sqrt(Kelast*Melast)); %Damping co-efficient (N-s/m).

%Calculation of Unscaled spectral acceleration.
kstar=((Melast/(tmstep)^2)+(dcoeff/(2*tmstep)));     %Step 1.3 in Table D-1.
aconst=((Melast/(tmstep)^2)-(dcoeff/(2*tmstep)));    %Step 1.4 in Table D-1.
bconst=(Kelast-((2*Melast)/(tmstep)^2));             %Step 1.5 in Table D-1.
mug=-Melast*gaccln;
```

```
%Creation of the first 2 rows of the table.
total=numel(mug);
ua=[0;0];
ub=0;
pa=mug(1)-aconst*ua(1)-bconst*ub;
uc=pa/kstar;
ub(2)=uc(1);
pa(2)=mug(2)-aconst*ua(2)-bconst*ub(2);
uc(2)=pa(2)/kstar;
ub=ub';
pa=pa';
uc=uc';
%Creation of the remaining rows of the table.
for i=3:total
    ua(i)=uc(i-2);
    ub(i)=uc(i-1);
    pa(i)=mug(i)-aconst*ua(i)-bconst*ub(i);
    uc(i)=pa(i)/kstar;
end
relataccln=((uc-2*ub+ua)/(tmstep)^2);   %Relative acceleration.
totalaccln=(relataccln+gaccln);         %Total acceleration.
Saunscaled=(max(abs(totalaccln)))/9.81; %Unscaled Spectral Accln. (g).

%Record Scale Factor.
Slfactor=(Sadesign/Saunscaled);         %References [5, 6].

%================================ END OF FUNCTION ==========================
```

E.3.2 Example of Ruaumoko Input File Generated

Sample Ruaumoko input file generated for a three storey regular CISDR design model -

```
REGULAR CISDR-MODEL

2 0 1 0 6 0 2 0 0 0 0
8 6 6 3 1 3 9.81 5 5 0.001 53.48 0.66761
0 0 10 0 1 1 0.1 0.1 4 2 1 0
10 0 0.0001 0 0 0 0 0 0 0 0

NODES 1
```

```
1       0       0       1       1       1       0       0       0       1
2       0       4       0       0       1       0       0       0       1
3       0       8       0       0       1       0       0       0       1
4       0       12      0       0       1       0       0       0       1
5       1       0       1       1       0       0       0       0       1
6       1       4       0       0       0       2       0       0       1
7       1       8       0       0       0       3       0       0       1
8       1       12      0       0       0       4       0       0       1

DRIFT
1 2 3 4 5 6 7 8

ELEMENTS 1
1       1       1       2       0       0       1
2       2       2       3       0       0       1
3       3       3       4       0       0       1
4       4       5       6       0       0       1
5       5       6       7       0       0       1
6       6       7       8       0       0       1

PROPS
1 FRAME
3 0 0 2 0 0 0 0
2.1e+011 8.1e+010 1 1 3.2279e-009 0 0 0 0 0
0.01 0.01 0.66667 0.66667
-1e+010 -1e+010 1e+010 4.4214 1e+010 1e+010 1e+010 0

2 FRAME
3 0 0 2 0 0 0 0
2.1e+011 8.1e+010 1 1 2.5873e-009 0 0 0 0 0
0.01 0.01 0.66667 0.66667
-1e+010 -1e+010 1e+010 3.5524 1e+010 1e+010 1e+010 0

3 FRAME
3 0 0 2 0 0 0 0
2.1e+011 8.1e+010 1 1 1.5695e-009 0 0 0 0 0
0.01 0.01 0.66667 0.66667
-1e+010 -1e+010 1e+010 2.1598 1e+010 1e+010 1e+010 0

4 FRAME
3 0 0 2 0 0 0 0
```

```
2.1e+011 8.1e+010 1 1 1.9367e-008 0 0 0 0 0
0.01 0.01 0.66667 0.66667
-1e+010 -1e+010 1e+010 4.4214 1e+010 1e+010 1e+010 0

5 FRAME
3 0 0 2 0 0 0 0
2.1e+011 8.1e+010 1 1 1.5524e-008 0 0 0 0 0
0.01 0.01 0.66667 0.66667
-1e+010 -1e+010 1e+010 3.5524 1e+010 1e+010 1e+010 0

6 FRAME
3 0 0 2 0 0 0 0
2.1e+011 8.1e+010 1 1 9.4173e-009 0 0 0 0 0
0.01 0.01 0.66667 0.66667
-1e+010 -1e+010 1e+010 2.1598 1e+010 1e+010 1e+010 0

WEIGHTS 0
1      0      0      0
2      4.905  0.01   0.01
3      4.905  0.01   0.01
4      4.905  0.01   0.01
5      0      0      0
6      4.905  0.01   0.01
7      4.905  0.01   0.01
8      4.905  0.01   0.01

LOADS
1      0      0      0
2      0      0      0
3      0      0      0
4      0      0      0
5      0      0      0
6      0      0      0
7      0      0      0
8      0      0      0

EQUAKE Eqfiles/la1.eqf
3 1 0.02 981 -1 0 0 1
```

E.4 Matlab Script for Running Ruaumoko in a Batch Mode

```
%=========================================================================

%Notes: This script is used to analyse a structure using Ruaumoko. The
%following script can be modified and used within loops when parametric
%analyses are to be conducted involving structures subjected to many
%earthquakes. This script assumes that the design of structures have been
%carried out prior to using Ruaumoko.

%=========================================================================

% Author - Vinod K. Sadashiva (vinod.sadashiva@pg.canterbury.ac.nz)

% Date - January 2007

%=========================================================================


%============================== START OF SCRIPT ==========================


dos('erase ROMKO'); %Erase old Ruaumoko file before executing a new one

% Calling function ROMKO_INPfl_fn to create Ruaumoko input file. It requires
%the corresponding input variables to be prior defined.

ROMKO_INPfl_fn(nbs,hfl,wfl,K,V,eqfilelink,EQdur,DELTAT,Slfactor);

%Running Ruaumoko in a batch mode.

dos('Ruaumoko2N ROMKO ROMKO.txt');


%=============================== END OF SCRIPT ==========================
```

E.5 Matlab Function for Obtaining Peak ISDR from Ruaumoko Output File

```
function RMK_ISDR_MAX = ROMKOOut_Puller_fn(nbs,hfl)

%=========================================================================

% ROMKOOut_Puller_fn pulls out peak interstorey drift ratio (ISDR) from all
%the storeys from Ruaumoko output file.

% Inputs:

% nbs  : Number of storeys in the structure

% hfl  : Storey heights between floors (m)

% Output:

% RMK_ISDR_MAX : Peak interstorey drift ratio from all the storeys

% Notes: Extra care needs to be taken while using this code. This is
%because; a newer version of Ruaumoko may give output in a different format.
%In such a case, this code may need to be modified accordingly. Trial checks
%are recommended before automating this code.

%=========================================================================

% Author - Vinod K. Sadashiva (vinod.sadashiva@pg.canterbury.ac.nz)
```

```
% Date - January 2007
%=========================================================================

%============================== START OF FUNCTION ==========================

%"One" counts in Ruaumoko output file.
if (nbs<=6)
    a=12;
elseif (nbs<=9)
    a=13;
elseif (nbs<=15)
    a=15;
else
    a=16;   %for nbs>15. Check this!
end

H=hfl;
fid = fopen('ROMKO','r');
cpt1=0;
DFO=[];
cl=0;
while (1)
    cl=cl+1;
    tline = fgetl(fid);
    if (~ischar(tline))
        break
    elseif (size(tline)==0)
    elseif (strcmp(tline(1),'1')==1)
        if (cpt1==a)
            for i=1:5
                tline=fgetl(fid);
            end
            cptline=0;
            while (strcmp(tline(1),'0')<1)
                Hi=H(cptline+1);
                DrP=tline(19:27);
                DrN=tline(51:60);
                DFO(2*cptline+1)=str2num(DrP)/Hi; %ISDR (positive envelope)
                DFO(2*cptline+2)=str2num(DrN)/Hi; %ISDR (negative envelope)
                tline=fgetl(fid);
                cptline=cptline+1;
```

```
            end;
            DFO(2*cptline+1)=max(abs(DFO(1:(2*cptline))));
            RMK_ISDR_MAX=DFO(2*cptline+1);
            return
        else
            cpt1=cpt1+1;
        end
    end
end

%============================== END OF FUNCTION =========================
```

E.6 References

[1] Carr AJ. Ruaumoko 2D – Inelastic dynamic analysis. Department of Civil and Natural Resources Engineering, University of Canterbury, Christchurch, New Zealand, 2004.

[2] MATLAB 7.9 (R2009b). The Maths Works, Inc.: Natick, MA, 2009.

[3] Sharpe RD. The seismic response of inelastic structures. PhD Thesis, Department of Civil Engineering, University of Canterbury, Christchurch, New Zealand, 1974.

[4] Tagawa H. Seismic response of 3-D steel frames with bi-directional columns. Masters thesis, Department of Civil Engineering, University of Washington, Seattle, 1999.

[5] Iervolino I, Cornell CA. Record selection for nonlinear seismic analysis of structures. *Earthquake Spectra* 2005; **21**(3):685-713.

[6] Shome N, Cornell CA, Bazzurro P, Carballo JE. Earthquakes, records, and nonlinear responses. *Earthquake Spectra* 1998; **14**(3):469-500.

APPENDIX F: MASS IRREGULARITY EFFECTS FOR STRUCTURES IN LESS SEISMICALLY ACTIVE REGIONS

The effect of magnitude and floor level of mass irregularity was investigated in Chapter 2. A range of mass ratios were considered and applied separately at the first floor, the mid-height floor and at the roof of 3, 5, 9 and 15 storey structures. The structures were assumed to be located in: (a) Wellington (high seismic active region, with NZS 1170.5 zone hazard factor, Z = 0.4); (b) Christchurch (medium seismic active region, with Z = 0.22); and (c) Auckland (low seismic active region, with Z = 0.13). As part of the design process explained in Chapter 2, structures that had their design action coefficients (used for base shear calculation) equal to the lower limit (Equation 5.2(2) in NZS 1170.5), and therefore unable to achieve the target ductility, were not considered for analyses. Additionally, structures that had storey strength to scaled stiffness ratios outside the range of 0.3% and 3% were eliminated. Many designs for structures located in Auckland and Christchurch were governed by either one, or both of the above set conditions. This resulted in insufficient data points for describing the responses of irregular structures. For example, Figures F-1 and F-2 show the effect of location and magnitude of mass ratios for 3 and 9 storey structures in Auckland and Christchurch respectively. The figures show very limited data points, and therefore, only structures assumed to be in the high seismically active region (Wellington, with Z = 0.4) were considered to quantify vertical irregularity effects.

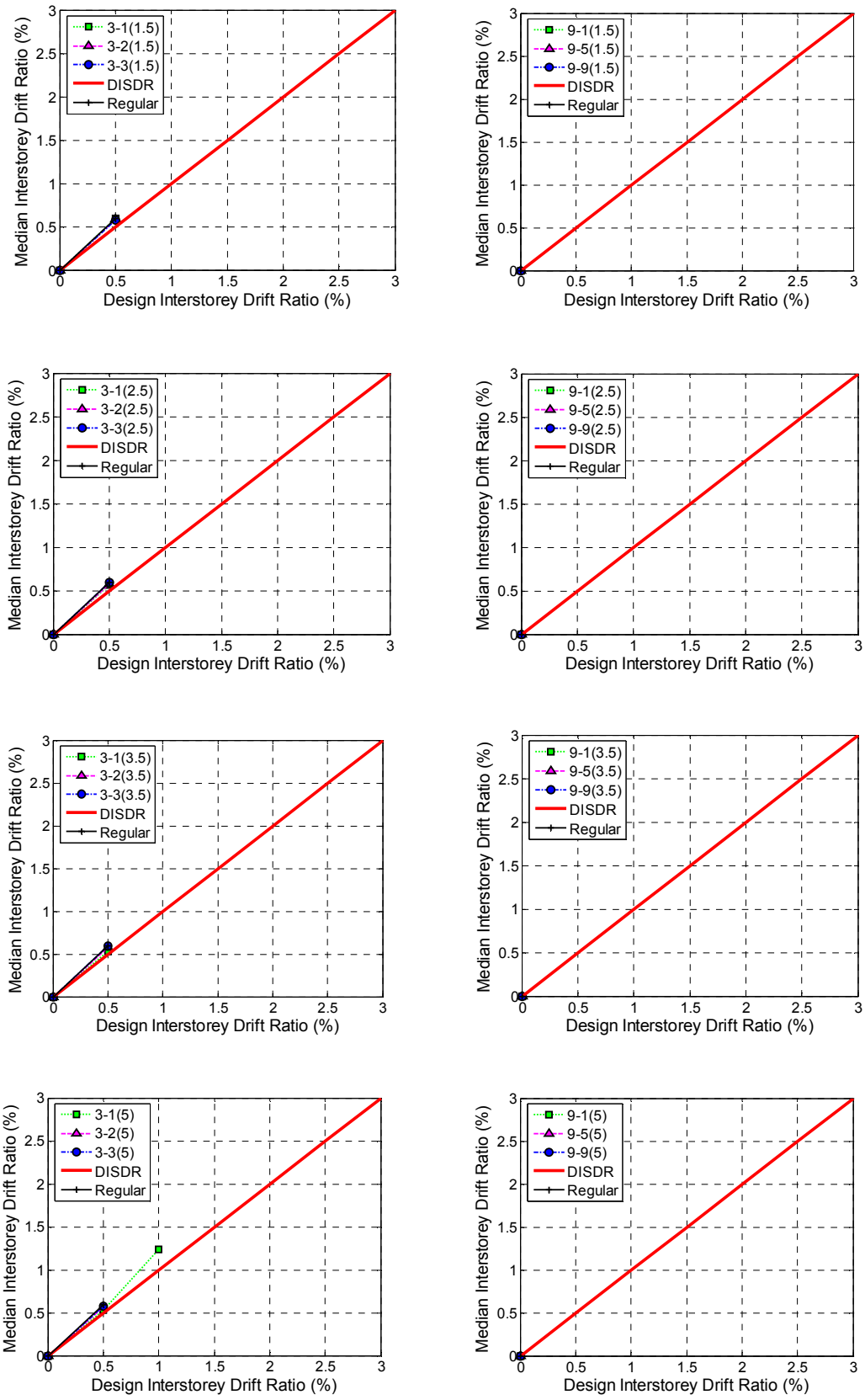

Figure F-1(a): Effect of magnitude and floor level of mass irregularity for 3 and 9 storey CISDR model ($\mu = 2$, $Z = 0.13$) – Mass Ratios: 1.5, 2.5, 3.5 & 5.

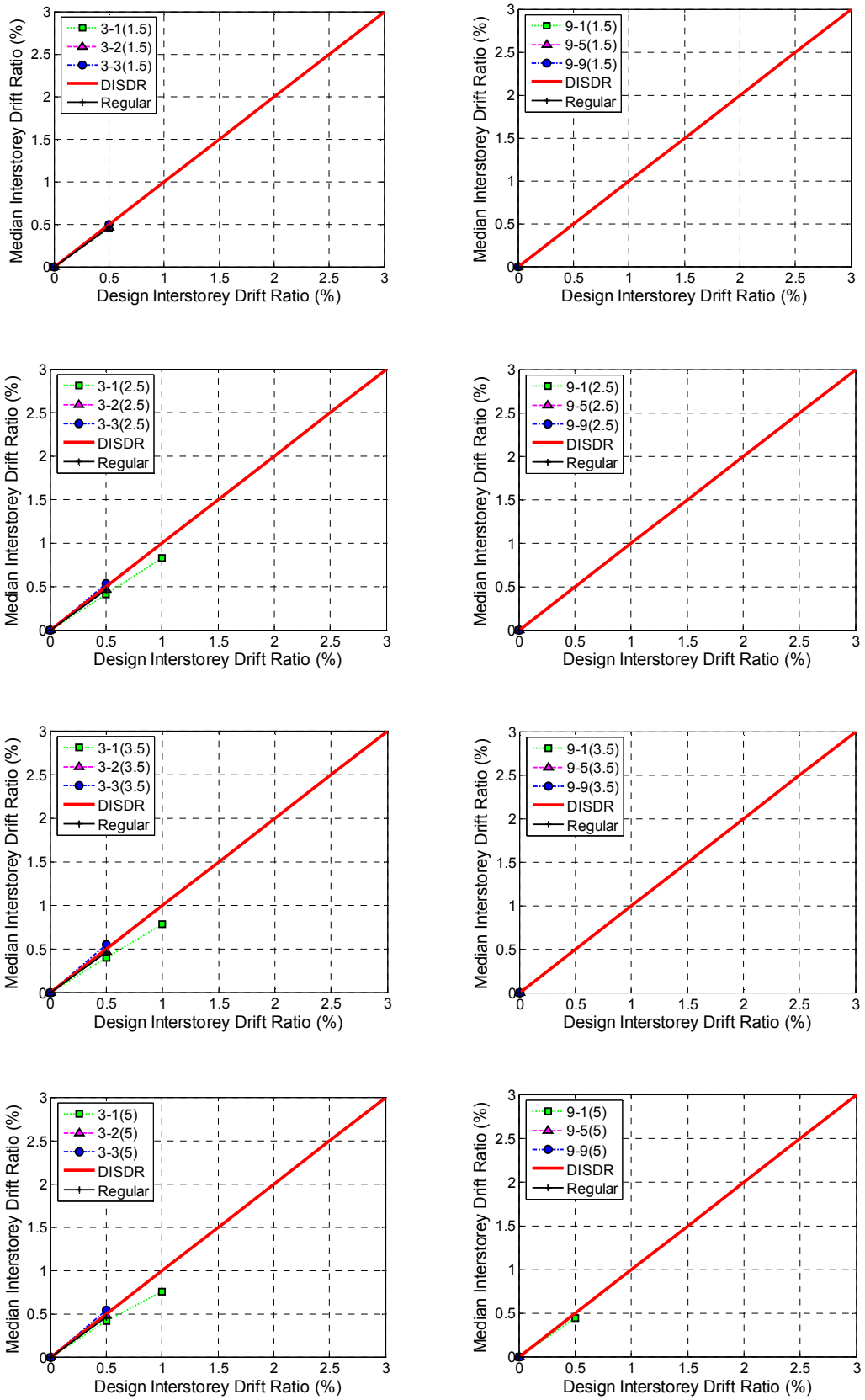

Figure F-1(b): Effect of magnitude and floor level of mass irregularity for 3 and 9 storey CS-VSTG model ($\mu = 2$, $Z = 0.13$) – Mass Ratios: 1.5, 2.5, 3.5 & 5.

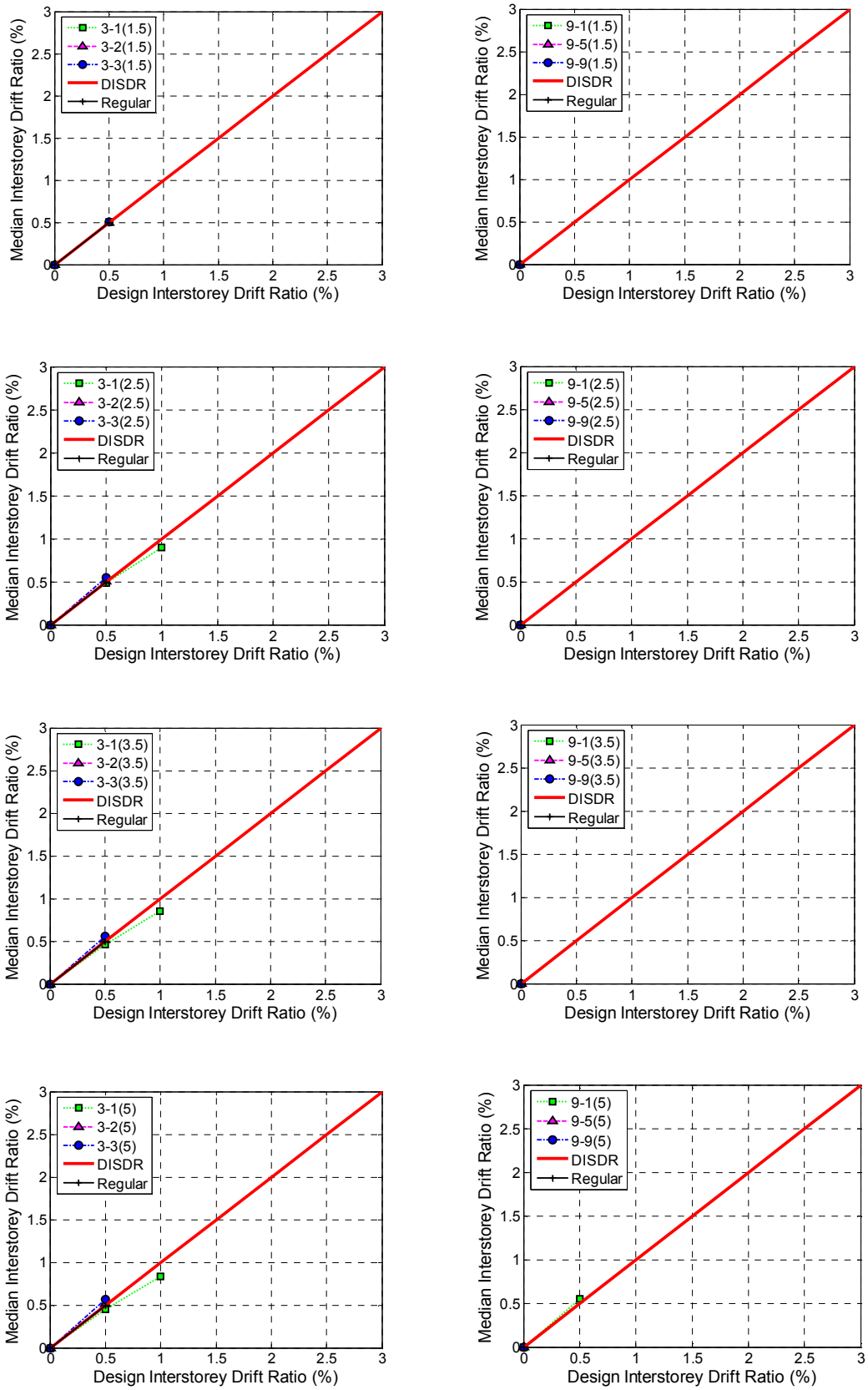

Figure F-1(c): Effect of magnitude and floor level of mass irregularity for 3 and 9 storey CS-CSTG model ($\mu = 2$, $Z = 0.13$) – Mass Ratios: 1.5, 2.5, 3.5 & 5.

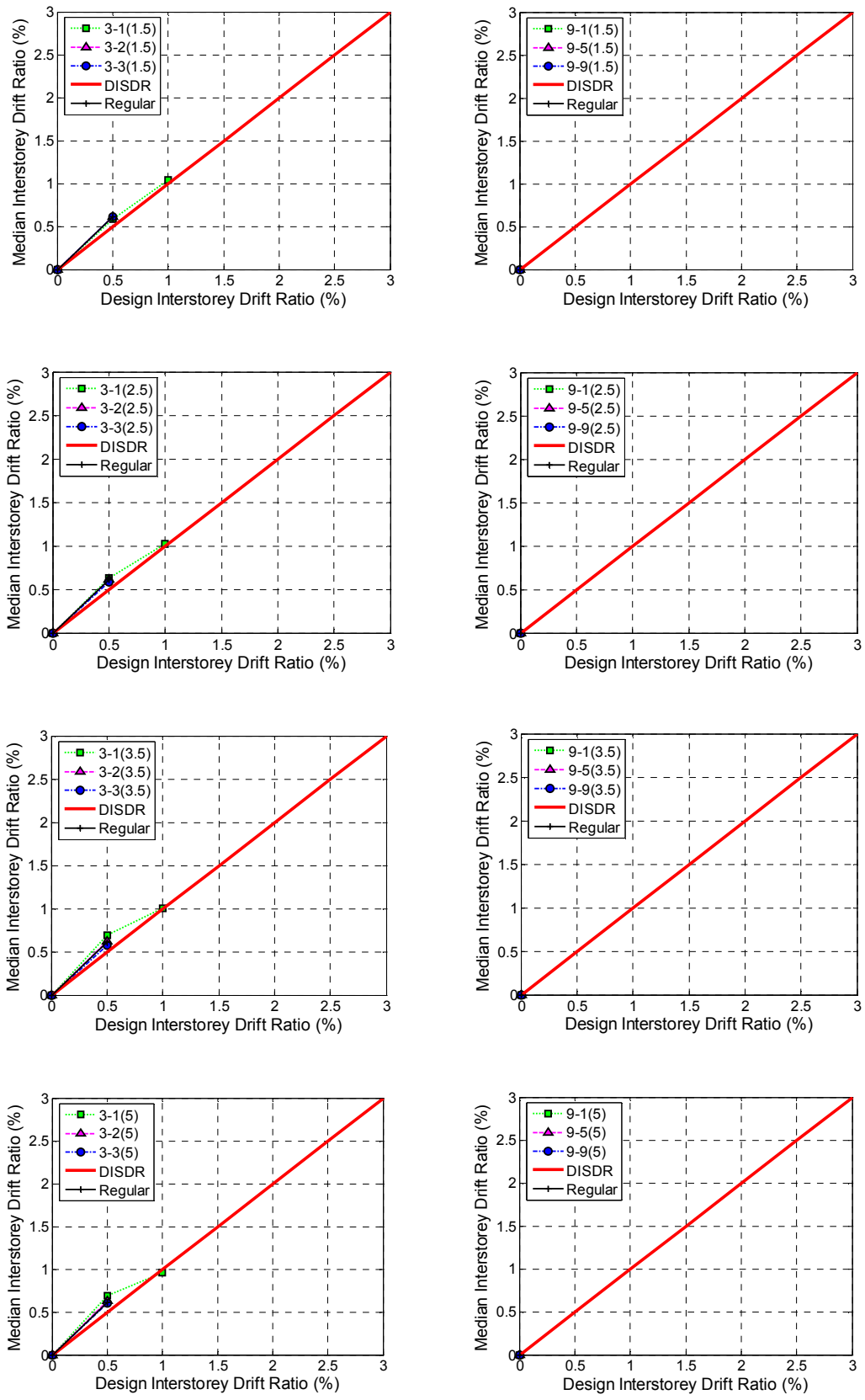

Figure F-2(a): Effect of magnitude and floor level of mass irregularity for 3 and 9 storey CISDR model ($\mu = 2$, $Z = 0.22$) – Mass Ratios: 1.5, 2.5, 3.5 & 5.

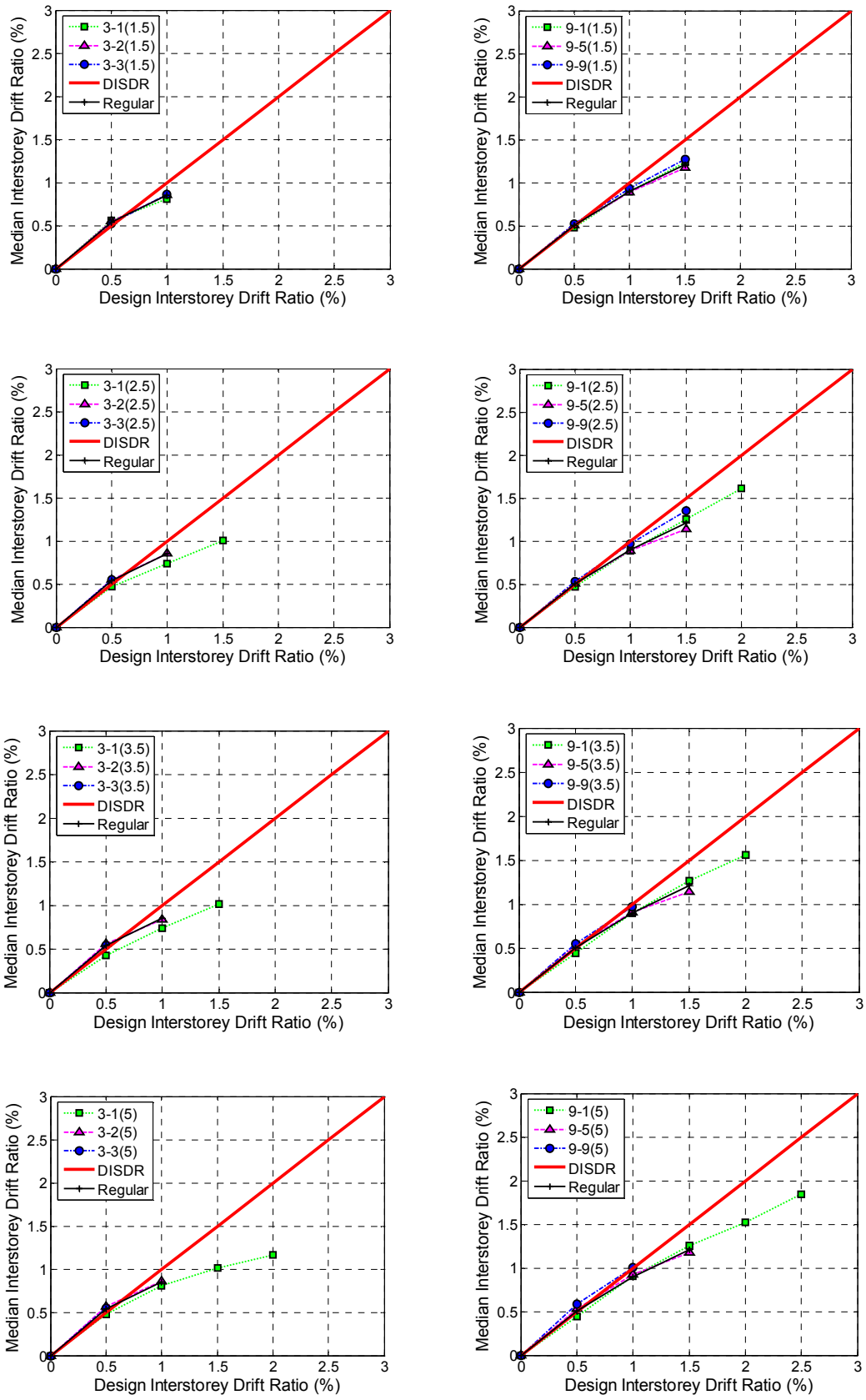

Figure F-2(b): Effect of magnitude and floor level of mass irregularity for 3 and 9 storey CS-VSTG model ($\mu = 2$, $Z = 0.22$) – Mass Ratios: 1.5, 2.5, 3.5 & 5.

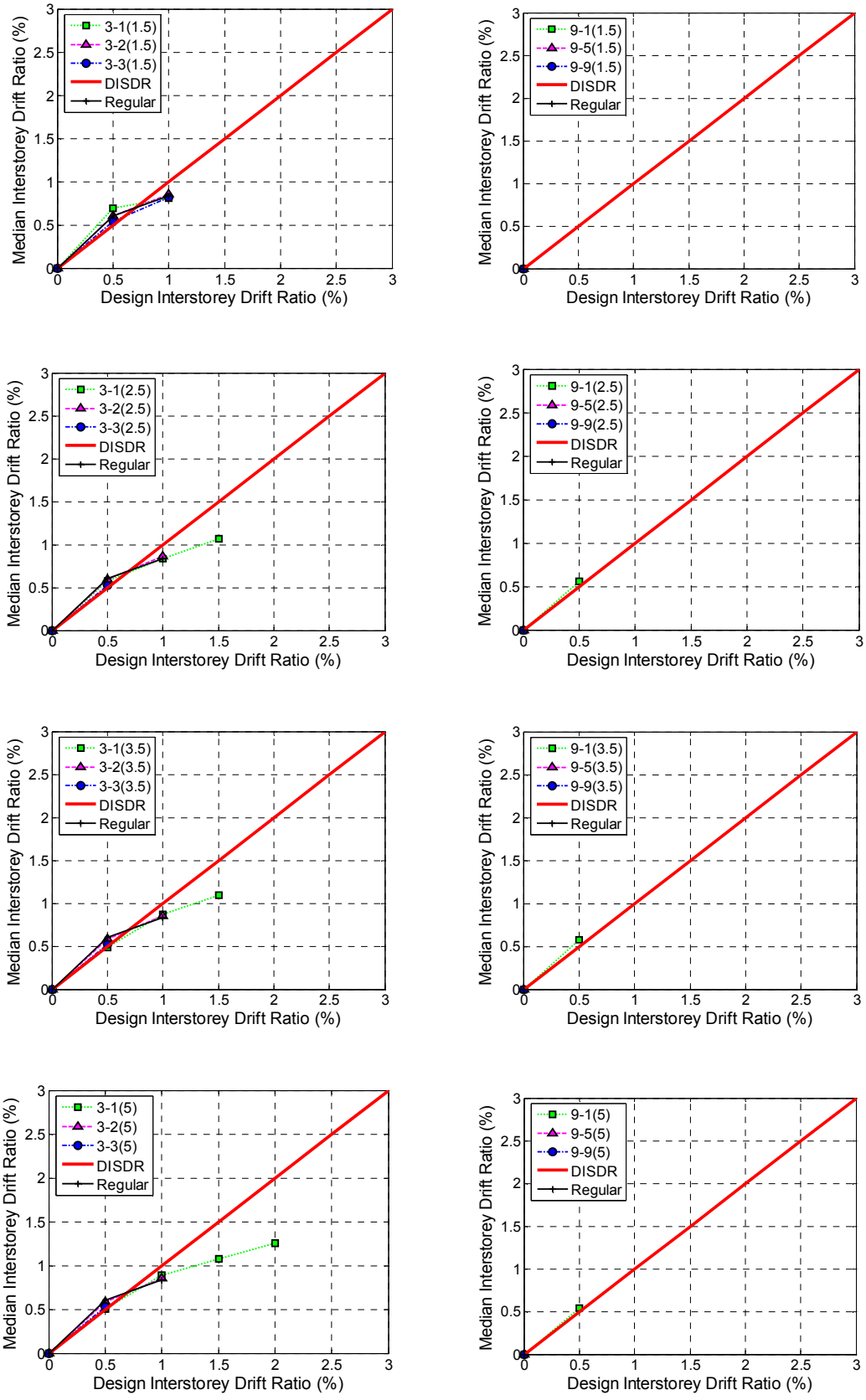

Figure F-2(c): Effect of magnitude and floor level of mass irregularity for 3 and 9 storey CS-CSTG model ($\mu = 2$, $Z = 0.22$) – Mass Ratios: 1.5, 2.5, 3.5 & 5.

APPENDIX G: EFFECT OF REDUCED FLOOR MASS ON SEISMIC RESPONSE

G.1 Effect of Magnitude and Floor Level of Reduced Floor Mass

The effect of increased floor mass on seismic response of structures was explained in Chapter 2. In the following section, the effect of magnitude and floor level of reduced floor mass is investigated for 3, 5, 9 and 15 storey high shear-type structures, assumed to be located in Wellington. Four mass ratios (MR) of 0.75, 0.5, 0.25 and 0.1 times the floor mass at the corresponding floor level of regular structure, was used. These reduced mass were separately applied at the first floor, mid-height floor and roof, and the seismic response of regular and irregular structures were compared to explain the effect of reduced floor mass. Structural modelling and analyses methodology explained in Chapter 2 is once again followed here for obtaining the results in Figures G-1 through G-4.

Representative results from this study are shown in Figures G-1 through G-3. Here, the median peak interstorey drift ratios (ISDR) for regular and irregular design models, designed for a structural ductility factor of 2, are plotted against the design interstorey drift ratios (DISDR).

Figure G-1 shows the effect of magnitude and floor level of reduced floor mass on median peak ISDR for CISDR design model. For MR = 0.75 at the roof for 3 and 5 storey structures, and this reduced floor mass at the first floor of 9 and 15 storey structures, produced higher median peak ISDR than from regular structures. There is less effect on median peak ISDR due to this mass ratio of 0.75 at the mid-height floor for all structural heights. The maximum increase in median peak ISDR due to this

mass ratio is less than 5%, obtained from a three storey structure. As the magnitude of the mass ratio was reduced, the short period structures generally had responses similar to the regular structures, and the taller structures produced increased drift demands due to irregularity. For a mass ratio of 0.1 at the first floor, Figure G-1(b) shows that the maximum increase in median peak ISDR from all DISDR is 29%, 10%, 2% and 6% for 3, 5, 9 and 15 storey structures respectively. While this mass ratio of 0.1 at the mid-height floor of 3 and 5 storey structures helped the irregular structures perform better than the respective regular structures, 9 storey structures with MR = 0.1 at the mid-height produced increased drift demands for all DISDR. The maximum increase to median peak ISDR due to this magnitude of mass ratio at the mid-height floor is 8%. All structures have produced lesser drift demands than those from regular structures for MR = 0.1 at the roof.

The effect of magnitude and location of reduced floor mass for CS-VSTG design models is shown in Figure G-2. Short period structures are affected more than the taller structures for mass ratio of 0.75 at the first floor. The maximum increase in median peak ISDR due to this mass ratio is 8% for 3 storey structures and it is less than 2% for other structures. For the same mass ratio of 0.75 at the mid-height floor, the maximum increase in median peak ISDR is always less than 2.5%, and when this mass ratio is present at the roof, the irregular structures have performed better than the regular structures. The effect of reduced floor mass on drift demands increases with reducing floor mass ratio as shown in Figure G-2. For the least MR = 0.1 at the first floor, all structures have produced higher drift demands than the regular structures. Here, a maximum increase to median peak ISDR of 46%, 11%, 6% and 5% is obtained for 3, 5, 9 and 15 storey structures respectively. The figure shows that

MR = 0.1 at the mid-height floor has little effect on the response of 3 storey irregular structures. However, for other structural heights, this mass ratio has produced median peak ISDR greater than those from regular structures, producing a maximum increase to median peak ISDR of less than 5.3% from all DISDR. The figure also shows that when mass ratio of 0.1 is present at the roof, the median peak ISDR of the regular, as well as the irregular structures, is generally the same.

Figure G-3 shows the effect of reduced floor mass on response of CS-CSTG design models. The figure shows that mass irregularity effects on the drift demands increase with reducing mass ratio. The median peak ISDR is more sensitive to irregularity at the first floor rather than at the mid-height or at the roof. A reduced first floor mass, irrespective of the magnitude of the mass ratio and the structural height, has resulted in higher median peak ISDR than those from regular structures. For all mass ratios and the three irregular floor levels, the increase to median peak ISDR reduces with increasing structural height.

G.2 Irregular Response Ratio (IRR) Equation for Reduced Floor Mass

A conservative equation (Equation (2-11)) describing the likely increase to median peak ISDR, due to mass ratios greater than 1, was developed in Section 2.10. A similar equation can be developed for estimating the likely increase in median peak ISDR due to mass ratios less than 1. The steps outlined in Section 2.10 is used here to produce Figure G-4. Here, $ISDR_{max\_incr}$ is the maximum increase to median peak interstorey drift ratio due to each mass ratio (MR) considered in this thesis. Based on Figure G-4, Equation (G-1) is proposed to calculate Irregular Response Ratio (IRR) for $MR < 1$. According to Equations G-1 and 2-11, if IRR has to be less than 15%,

then a storey can have its floor mass between 0.7 and 2 times the floor mass at other storeys.

$$IRR = 50(1 - MR) \qquad \text{(G-1)}$$

where IRR is the Irregular response greater than regular response; and MR is the Mass Ratio.

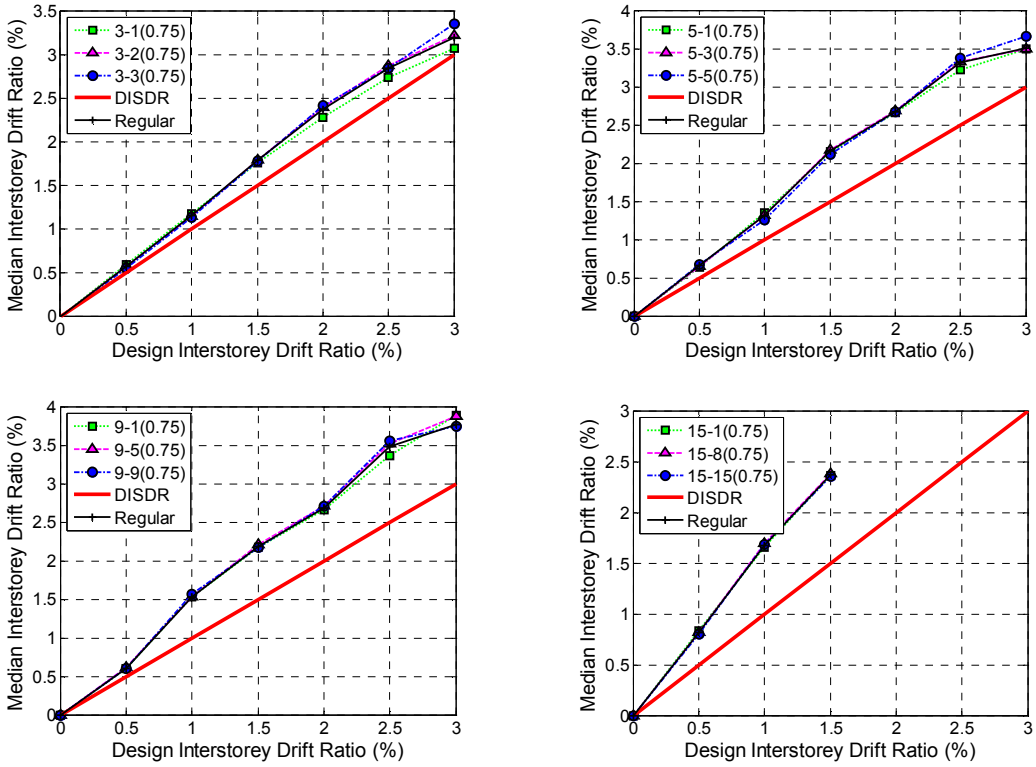

(1) Mass Ratio: 0.75

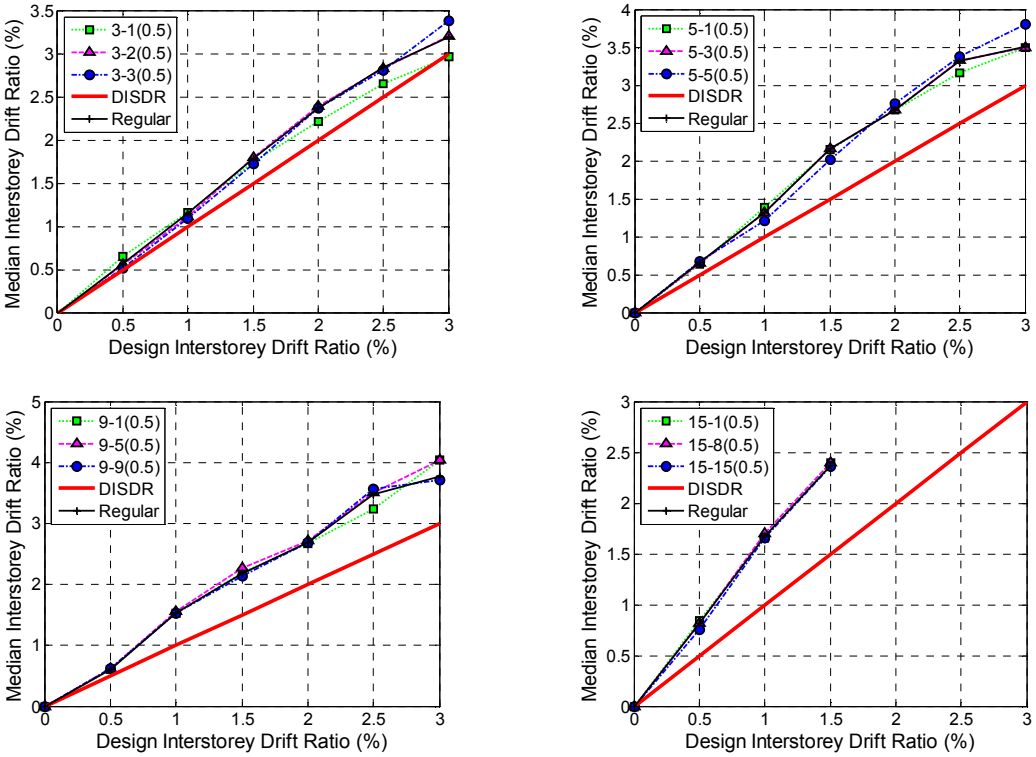

(2) Mass Ratio: 0.5

Figure G-1(a): Effect of magnitude and floor level of reduced floor mass for CISDR model ($\mu = 2$, $Z = 0.4$) – Mass Ratios: 0.75 & 0.5.

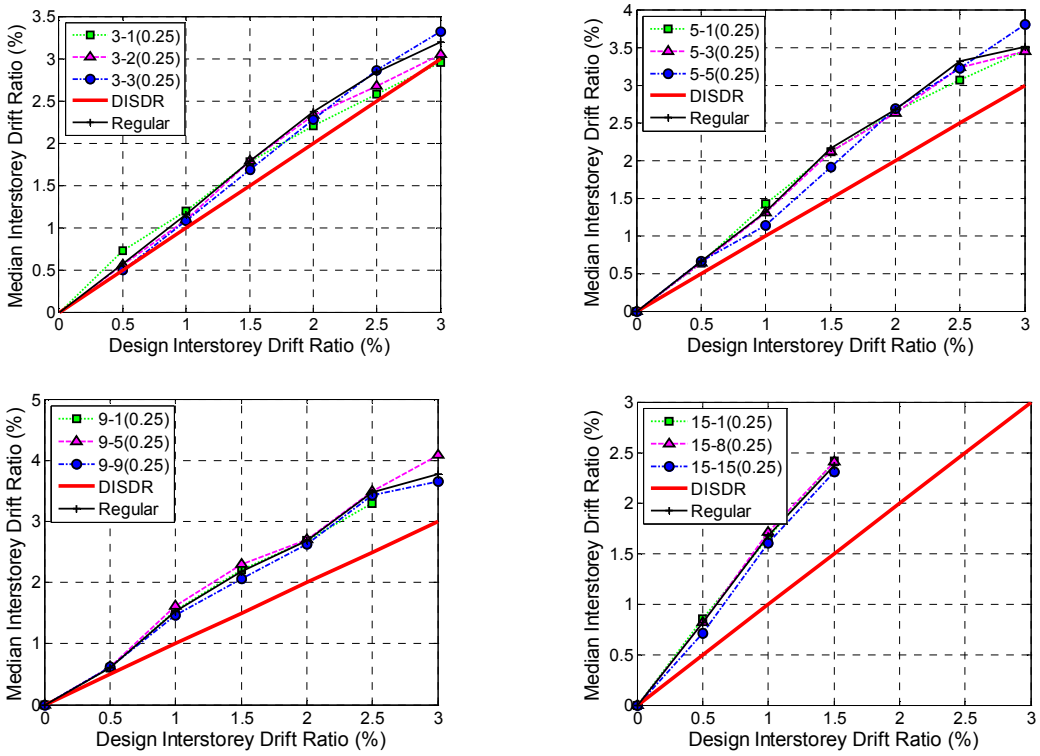

(3) Mass Ratio: 0.25

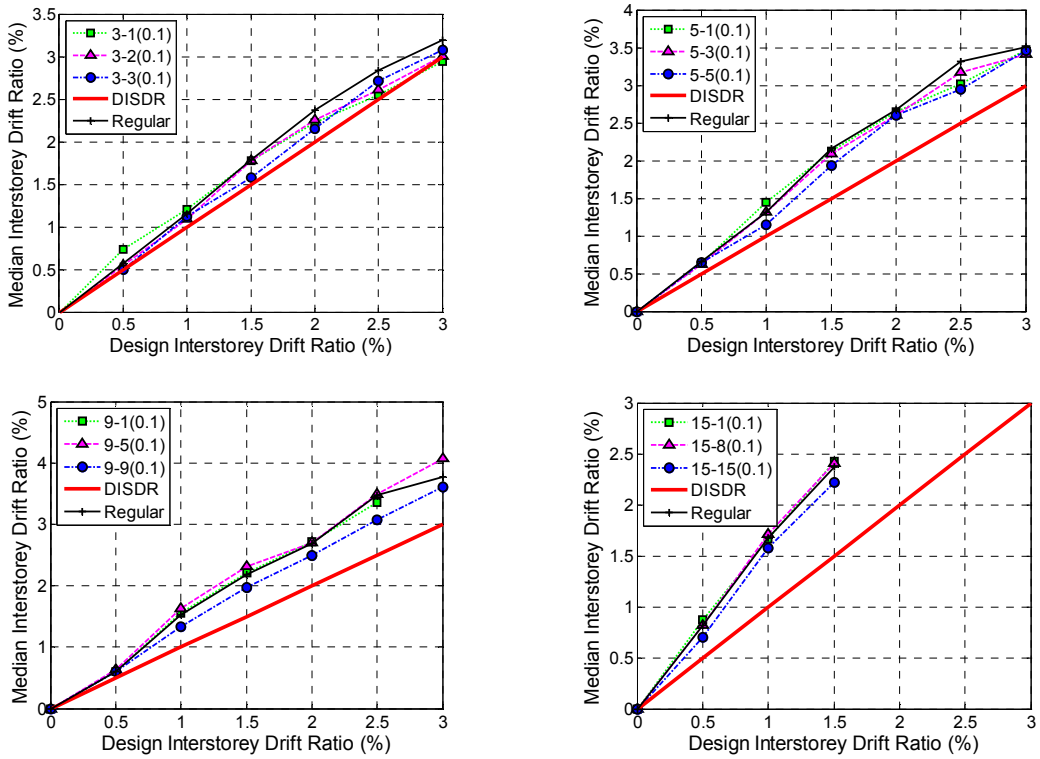

(4) Mass Ratio: 0.1

Figure G-1(b): Effect of magnitude and floor level of reduced floor mass for CISDR model ($\mu = 2$, $Z = 0.4$) – Mass Ratios: 0.25 & 0.1.

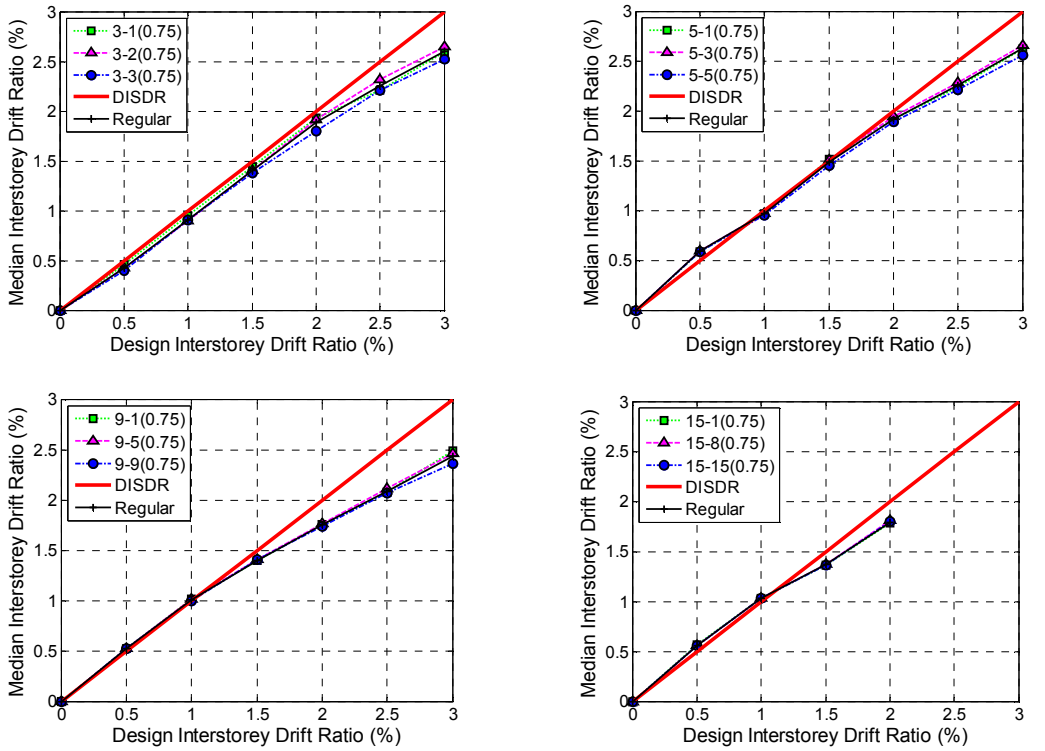

(1) Mass Ratio: 0.75

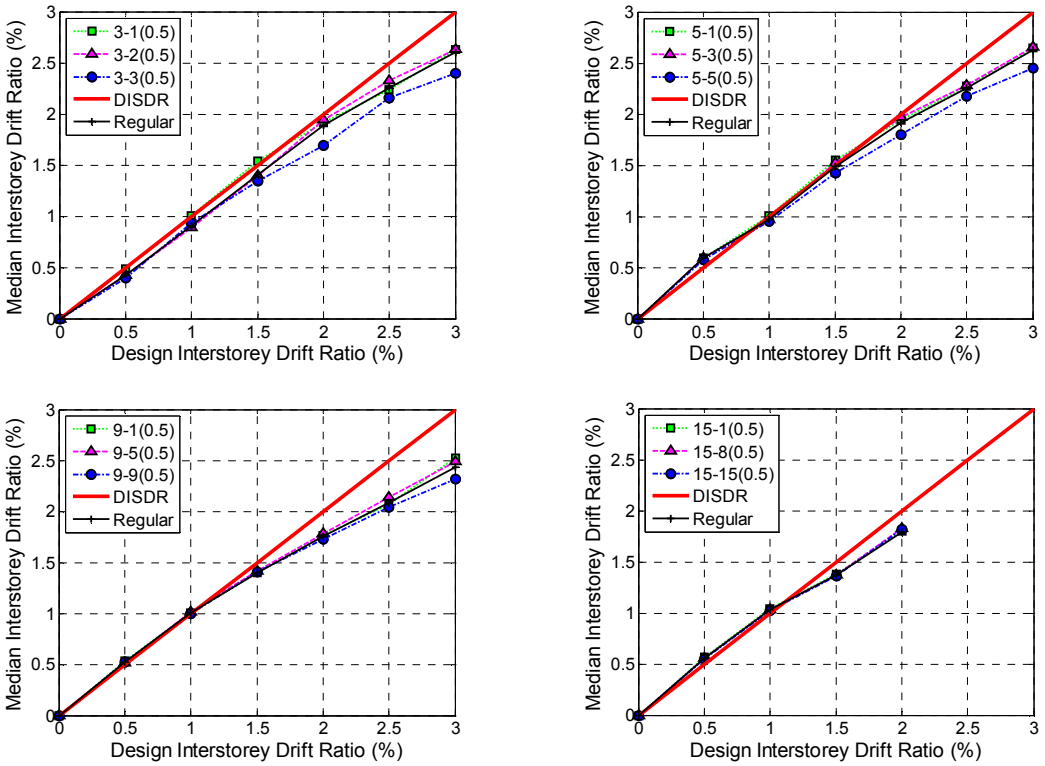

(2) Mass Ratio: 0.5

Figure G-2(a): Effect of magnitude and floor level of reduced floor mass for CS-VSTG model ($\mu = 2$, $Z = 0.4$) – Mass Ratios: 0.75 & 0.5.

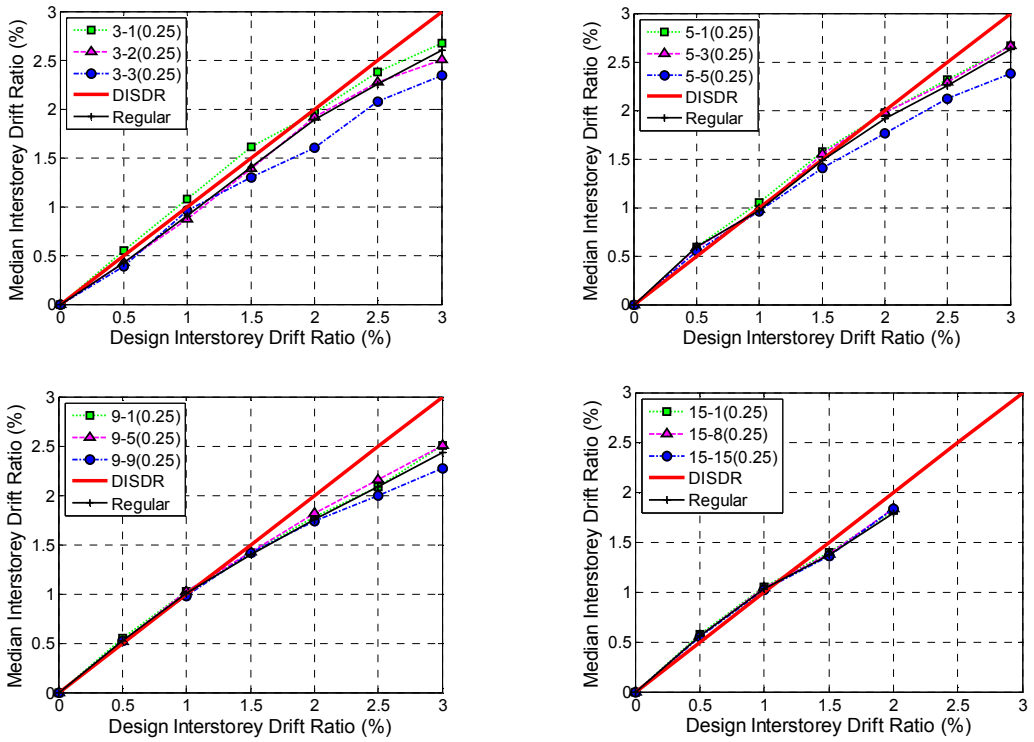

(3) Mass Ratio: 0.25

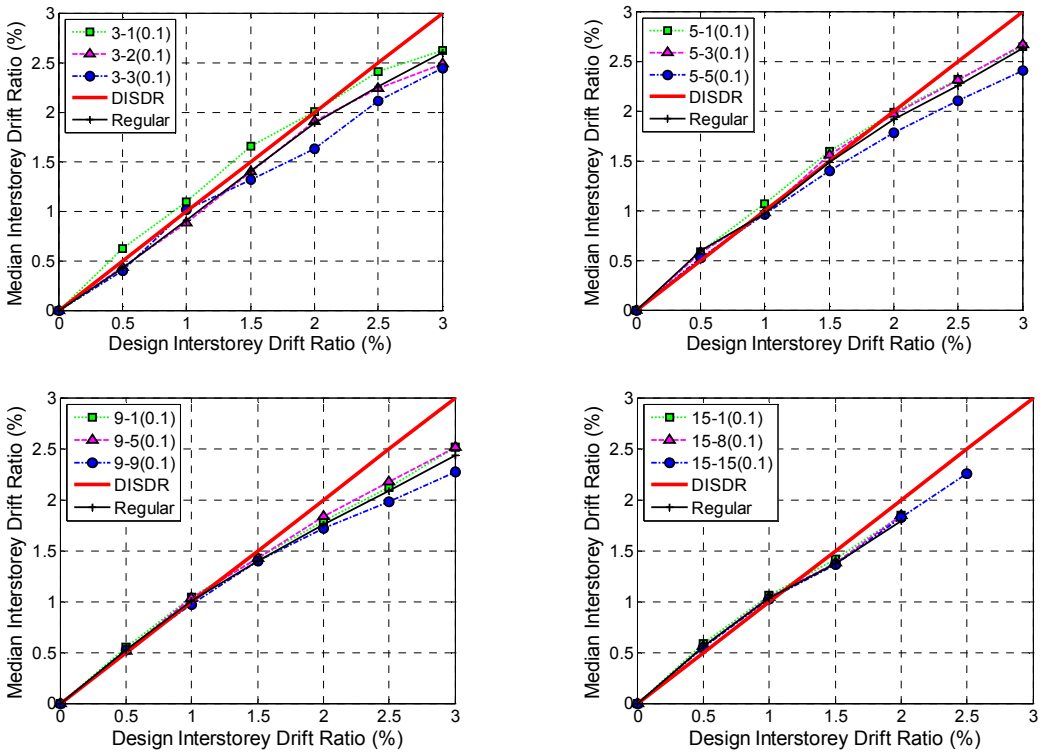

(4) Mass Ratio: 0.1

Figure G-2(b): Effect of magnitude and floor level of reduced floor mass for CS-VSTG model ($\mu = 2$, $Z = 0.4$) – Mass Ratios: 0.25 & 0.1.

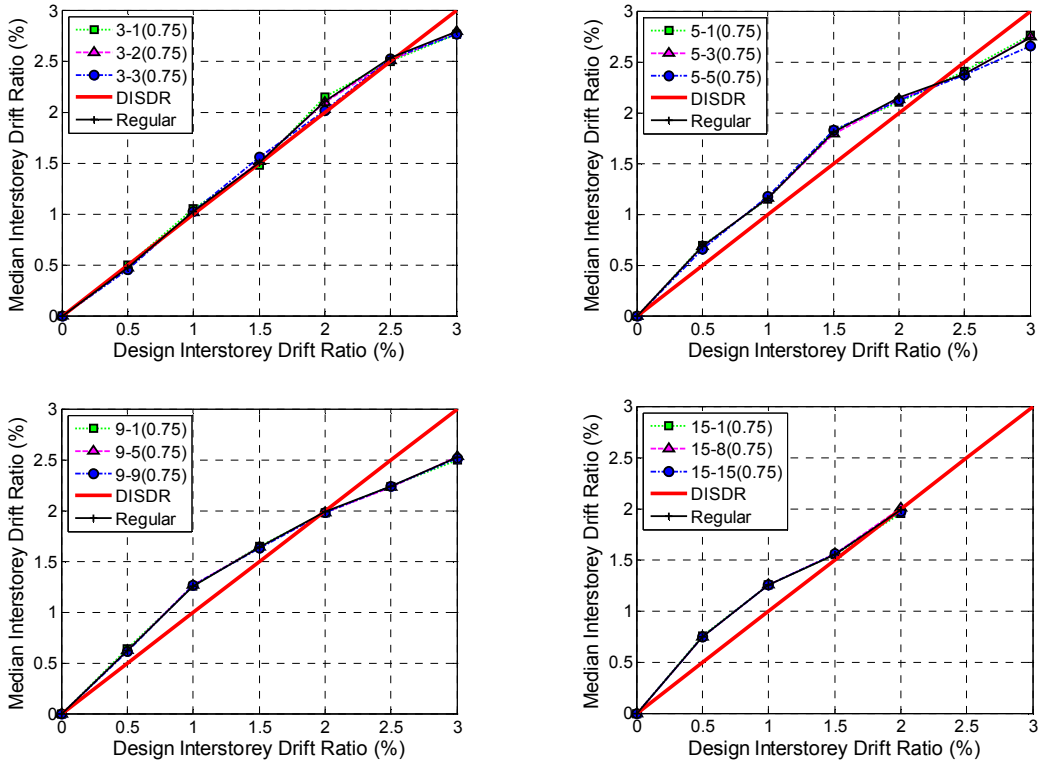

(1) Mass Ratio: 0.75

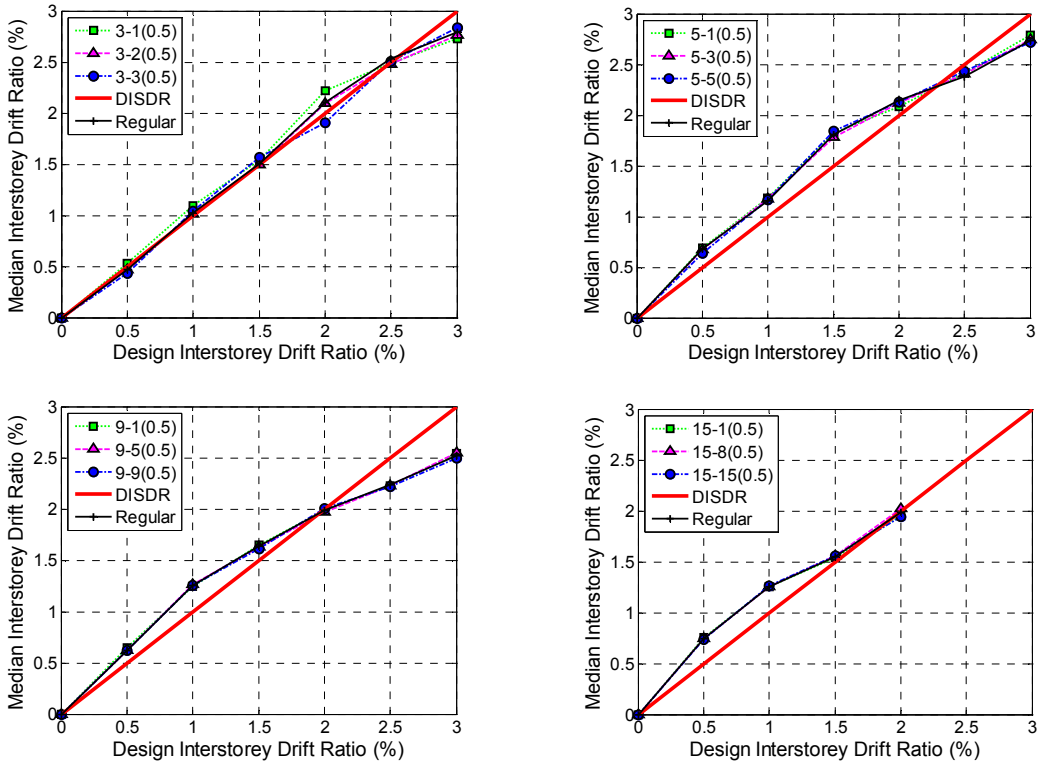

(2) Mass Ratio: 0.5

Figure G-3(a): Effect of magnitude and floor level of reduced floor mass for CS-CSTG model ($\mu = 2$, $Z = 0.4$) – Mass Ratios: 0.75 & 0.5.

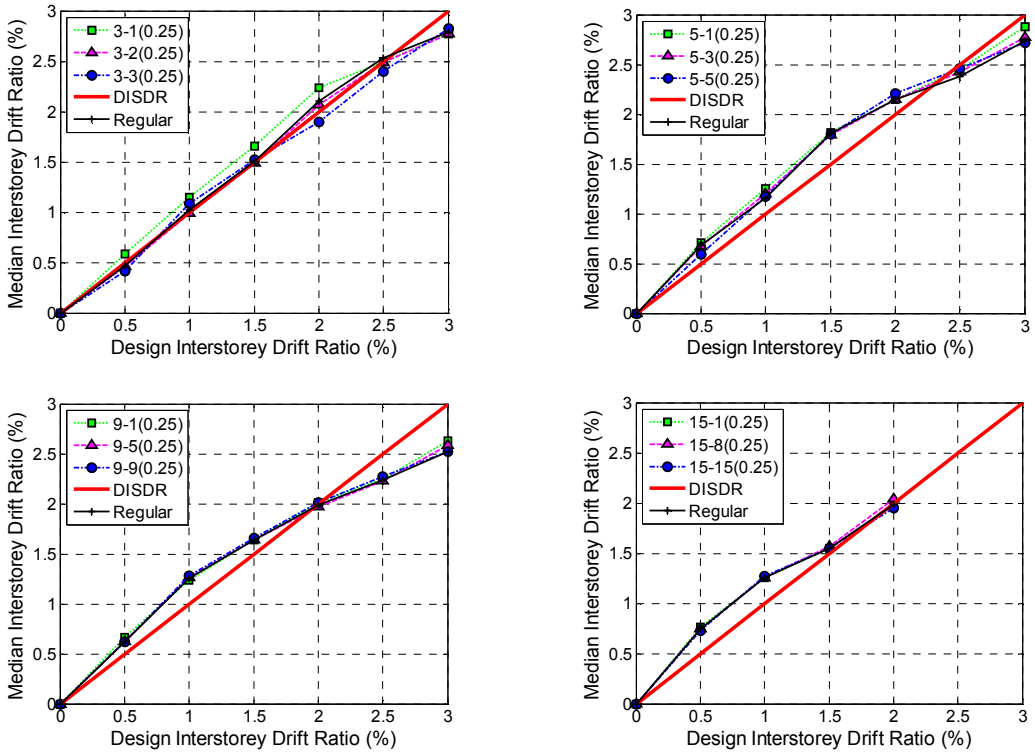

(3) Mass Ratio: 0.25

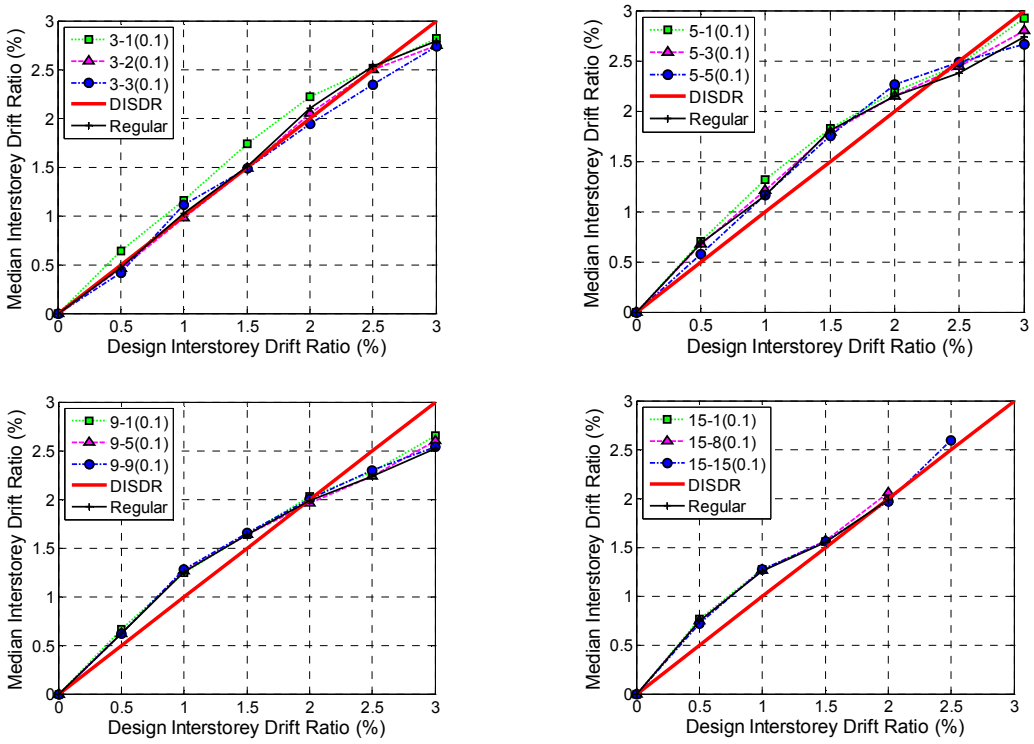

(4) Mass Ratio: 0.1

Figure G-3(b): Effect of magnitude and floor level of reduced floor mass for CS-CSTG model ($\mu = 2$, $Z = 0.4$) – Mass Ratios: 0.25 & 0.1.

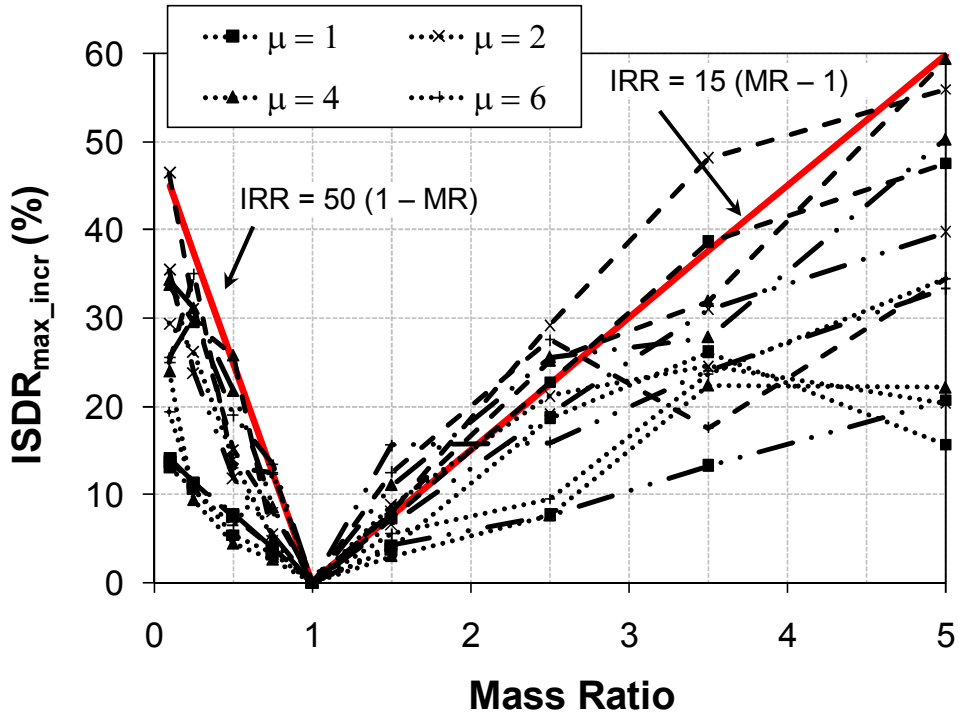

Figure G-4: Relationship between $ISDR_{max\_incr}$ and Mass Ratio.

(CISDR —— CS-CSTG —··—·· CS-VSTG - - - - -)

APPENDIX H: ALTERNATE IRREGULAR RESPONSE RATIO EXPRESSIONS FOR STRUCTURES WITH A MODIFIED STOREY HEIGHT

In Chapter 4, the effect of coupled stiffness-strength irregularity due to a modified storey height was explained for structures with realistic storey stiffness-strength relations. Based on the response of critical structures, a simple conservative equation (Equation (4-7)) was proposed to estimate the likely increase in response for a given interstorey height ratio, h_{rat}. This appendix shows alternate ways to obtain similar expressions for *Irregular Response Ratio* (*IRR*), from the results obtained in Chapter 4. The relationships between stiffness-strength modification factors (β_k - β_v) and interstorey height ratio for the groups of structures in Table 4-1, also shown in Figures H-1 and H-2, are used to obtain the *IRR* equations shown in Figures H-1 and H-2. Here, for a given stiffness modification factor, β_k, the likely increase to peak interstorey drift ratio can be determined for structures with different coupled stiffness-strength relationships.

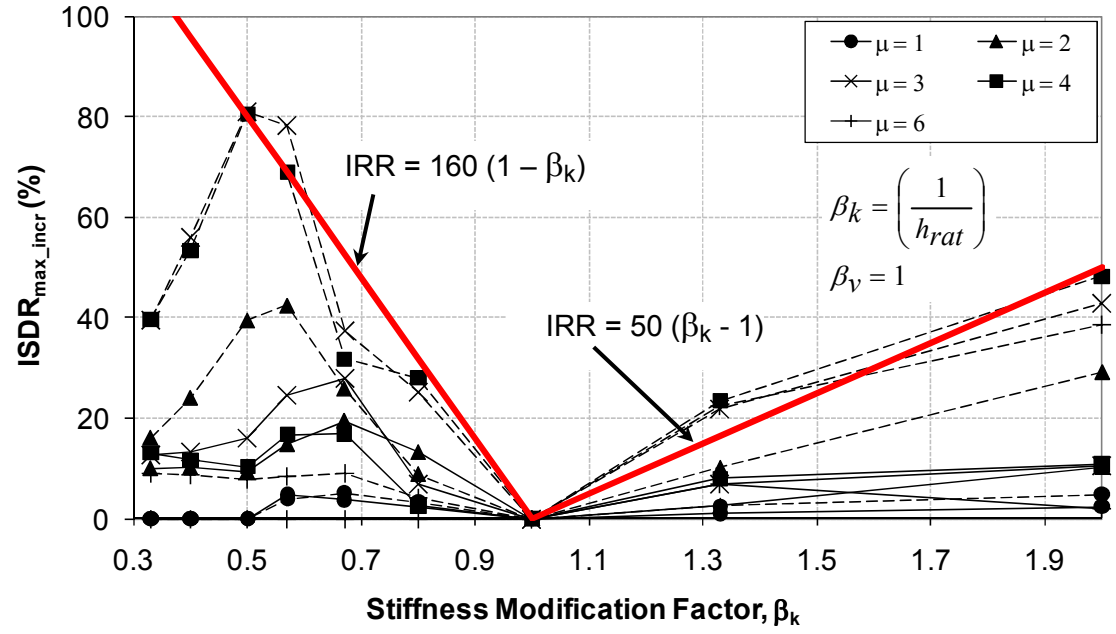

(1) Group 1

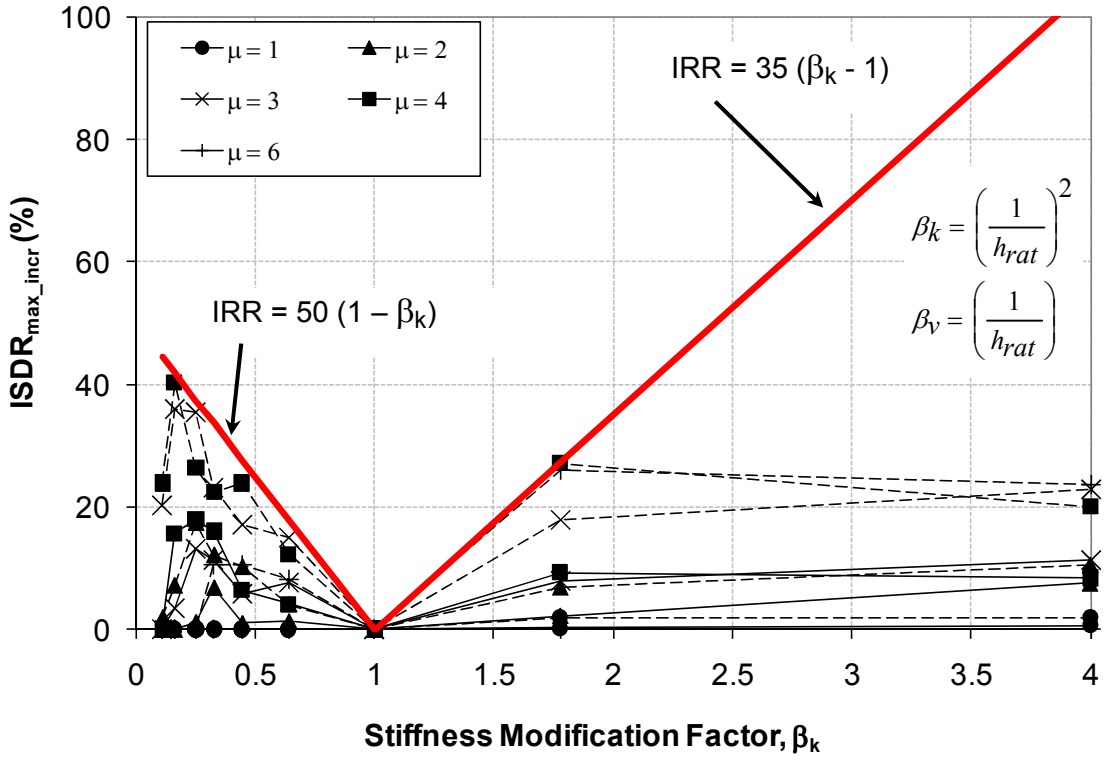

(2) Group 2

Figure H-1(a): Irregular Response Ratio as a function of Stiffness Modification Factor for Group 1 and Group 2 structures having a modified storey height.

(CISDR —— CS-CSTG - - - - -)

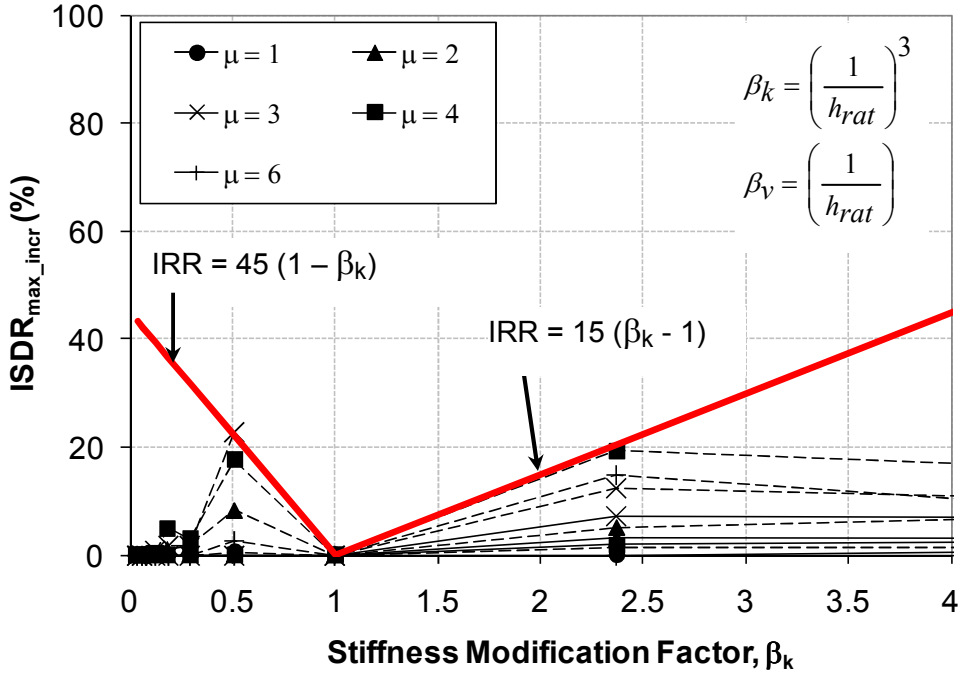

(1) Group 3

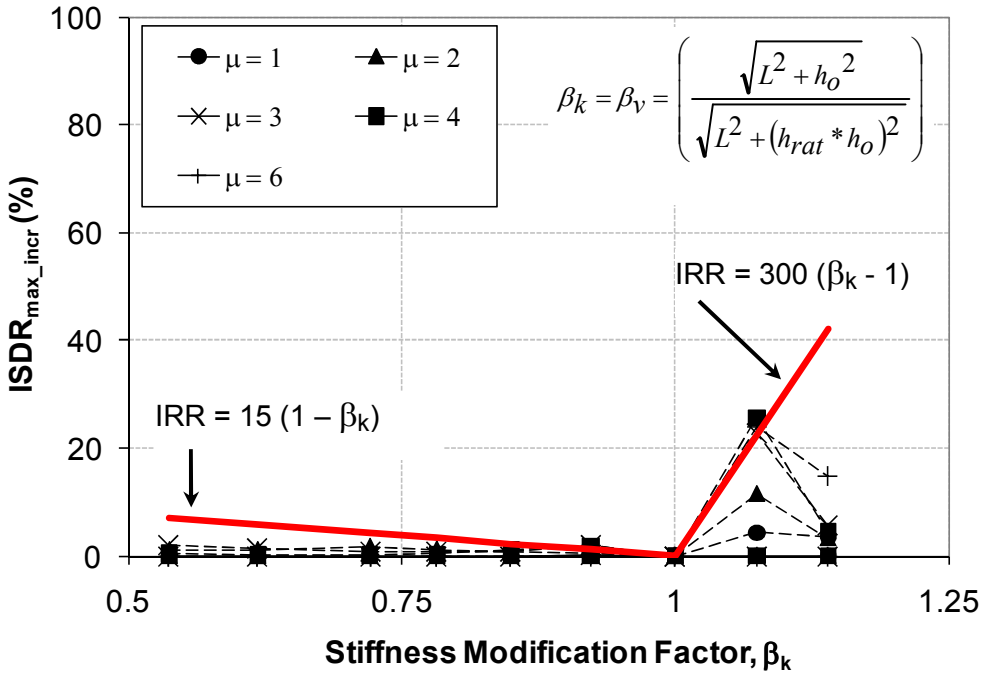

(2) Group 4

Figure H-1(b): Irregular Response Ratio as a function of Stiffness Modification Factor for Group 3 and Group 4 structures having a modified storey height.

(CISDR —— CS-CSTG - - - - -)

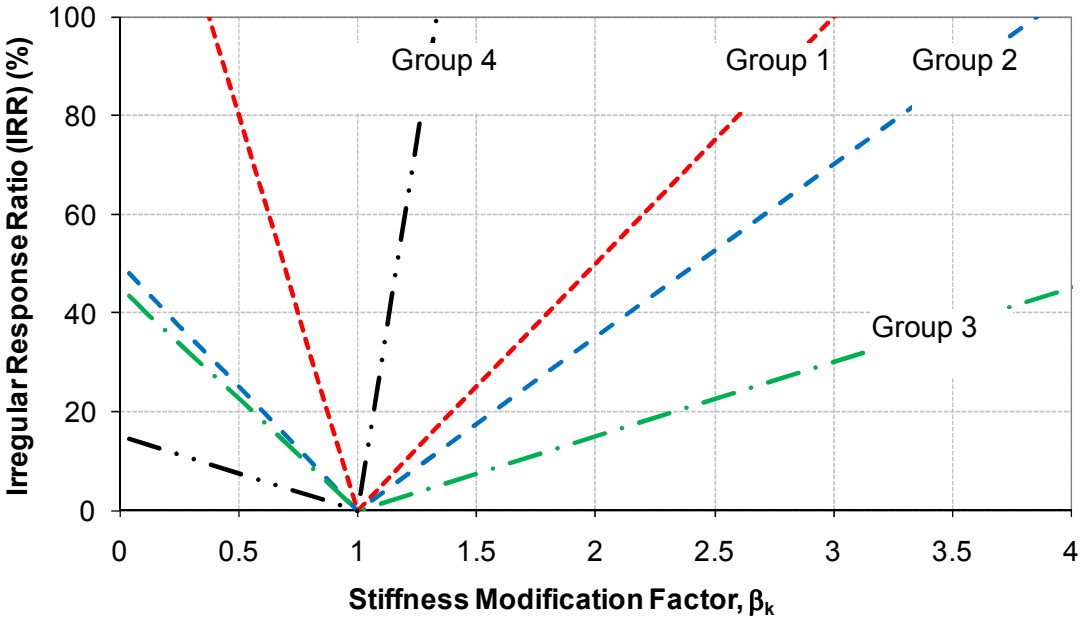

Figure H-2: Irregular Response Ratio for structures having a modified storey height.

APPENDIX I: USING BATCH MODE IN SAP2000 FOR PARAMETRIC ANALYSIS

SAP2000 can be used to carry out parametric analyses in the following way:

Stage A:

1. Open a new folder in the directory that you are working. Let us call this as "SAP_trial".
2. Double click on the SAP2000 icon to open SAP2000 GUI window.
3. Open a new file under the above defined "SAP_trial" directory.
4. Create the structural model that has to be analysed (see SAP2000 user manual). This model would act as the template structural model. A change to the parameters in this model can be done (explained later), which would produce multiple input files for parametric analysis. Do NOT run the analyses!
5. Choose the tables of input data and analysis result files that needs to be saved once analysis is complete. A name to the chosen set of tables should be given in :

   Define >> Named Sets >> Tables

6. The above action would open a new SAP window called "*Define Database Table Named Sets*". Choose the result cases whose output has to be saved. This can be chosen by clicking on "*Select Analysis Cases*.." under the "*Analysis Cases (Results)*". It may be time consuming (of course, it depends on your computer configuration and also the complexity of the structural model) to store the results of all the cases, so select the ones that are really needed. SAP2000 has the options of saving either the envelope (max and min) results or result at every time step can be saved. This can be chosen by clicking "*Enable All Options*" under "*Modify/Show Options*..". There is also an option for obtaining the interstorey drifts. This can be defined using: "*Define >> Generalized Displacements >> Add New Generalized Displacements*". An example of generalized displacement definition is shown below. Here, a positive and a negative unit scale factors (for U3) are used for finding the relative drifts between nodes 11 and 6. If there is a

need for interstorey drift ratio, the inverse of distance (say the interstorey height) has to be used as the scale factors.

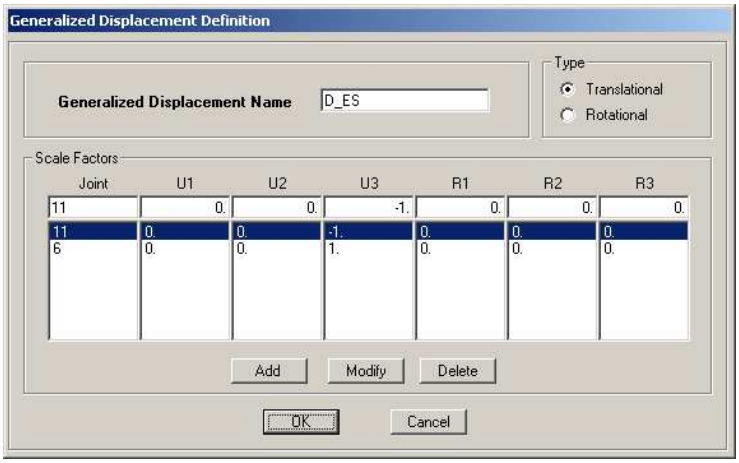

7. Click on "*Expose All Tables*" under "*Options*" to show all the available tables.

8. Check the boxes against each table that needs to be exported at the end of analysis. If generalised displacement function is used, add this table to the list. This is done by clicking on *Display >> Tables >> Joint output >> Displacements >> Joint Displacements – Generalised >> Set output selections >> Select Generalized Displacements >>* click on the named generalized displacement and click *OK*.

9. Assign a name for the set of tables chosen by clicking on "*Save Named Set..*" under "*Named Sets*". Click "*OK*".

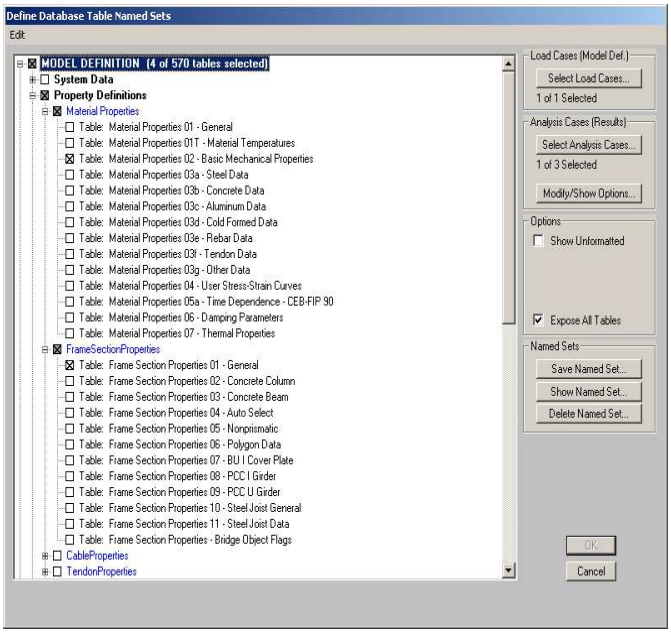

10. Use the *Analyze* menu >> *Set Analysis Options* command to specify that model definition and analysis results tables be automatically saved after an analysis has

been run for a model. This action opens a new SAP2000 window called "*Analysis Options*". Assign a name for the output file where the table containing data and analysis results would be stored. SAP2000 version 11.0.8 has options to save the file in .xls (Excel) or .mdb (Microsoft Access Database (default)) format.

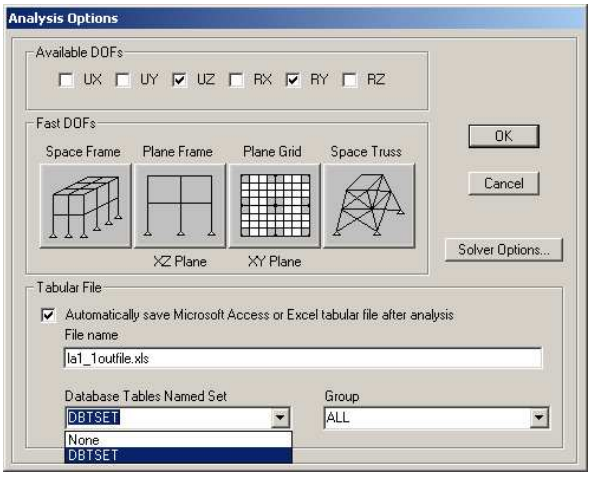

Note: .xls option may not work if the output file is too large (e.g., results of model with very small time-steps, high number of node results requested etc.). Newer version of SAP2000 (e.g., V14) may work better for saving the output in .xlsx format. .mdb option is good, but it would need the user to know how to deal with importing tables from this file for post-processing. Matlab can be used utilising the "*database*" toolbox. Alternatively, Matlab codes can be written to extract the table results from .mdb file onto Matlab workspace. Some information is available from:

www.mathworks.fr/matlabcentral/newsreader/view_thread/143522

Choose the database tables named set defined in Step A9 as shown above. Click "*OK*".

Save the structural model (*File >> Save*) by giving some file name. Let us call this la1_1. Again, do NOT run the analysis!

11. Open the folder "SAP_trial". Look for a file with a **$2K** extension. This file is the template model file that can be used to modify the parameters needed to define the structural models for parametric analyses. The file can be viewed using Notepad.

Stage B:

1. *Parametric Analyses Models* (**PAM**) can be created by simply modifying the template $2K file, and saving each file under a new $2K file name. If the number of PAM is less, the $2K files can be created easily by hand. For large numbers of

PAM, a program such as MATLAB can be used. The user has to know some basic file management techniques used in Matlab. This includes using functions such as "fopen", "fgetl" etc. in Matlab. The description and the syntax needed for generating PAM in Matlab in not explained here. The user is encouraged to learn from "Help" menu in MATLAB.

2. Change the required parameters in the template $2K file using Matlab to generate PAM $2K files. Save all the PAM files in a new folder. Let us name this folder as "SAP_PAM".

Stage C:

Approach A - A method to analyse structural models in a batch mode is given in SAP2000 help manual. It has the following steps.

Click the *File* menu >> *Batch File Control* command to access the Batch File Control form. Use the form to complete any of the following:

(a) Define a New Batch File

1. Access the Batch File Control form using the *File* menu > *Batch File Control* command.
2. Click the *Specify New Batch File Name* button. A Windows form for specifying the path and batch file name will appear. Select the path and type the batch file name into the *File* name edit box. Click the *Save* button and the batch file name will appear in the *Text Batch File Name* edit box near the top of the Batch File Control form.
3. Type the path and name of the model file to be included in the batch file in the *SAP2000 Filename (Full Path)* edit box near the middle of the form. Alternatively click the *Browse For SAP2000 Files* button to locate the files. When a file has been located, click on it and the path and filename will appear in the *SAP2000 Filename (Full Path)* edit box.
4. Click the *Add* button in the lower right area of the form to add the file to the list. The path and filename will appear in the display area in the middle of the form.

5. Click the "*Analysis Cases to Run*" drop-down list and choose to have SAP run *All analysis cases*, or only Selected cases. The cases are selected when the analysis is run.

6. Click the "*Options for Analysis Files*" drop-down list and choose from the following:

   Save All. SAP will save all of the analysis files generated when the analyses are run. Depending on the size of the model files, this option may require substantial file storage space.

   Save Recovery Only. SAP will save the minimum number of files needed to generate results. Use this option when file storage space is limited.

   Delete All. SAP will delete all of the analysis files generated when the analyses are run. Use this option when the *Analyze* menu >> *Set Analysis Options* command has been used to specify that model definition and analysis results tables be automatically saved after the analysis has been run. Use of the option will limit the space required for file storage.

(b)Save a Batch File Definition to a Text File

Save the batch file definition so that it can be recalled and run without redefining the list.

1. Define a new batch file as described above.
2. Click the *Save Current Batch File List* to *Text File* button.

(c) Open an Existing Batch Text File

1. Access the Batch File Control form using the *File* menu > > *Batch File Control* command.
2. Click the *Browse For Existing Batch Files* button. A Windows form for specifying the path and batch file name will appear. Select the path and the batch file name, which will appear in the *File name* edit box. Click the *Open* button and the batch file name will appear in the *Text Batch File Name* edit box near the top of the *Batch File Control* form.

3. As necessary use the following buttons to make changes to the list of model files:

   i. *Add* button. Follow Steps 3 and 4 of the *Define a New Batch File* explanation above to add a model file to the batch file definition.

   ii. *Modify* button. Highlight the model file name to be modified in the list in the display area in the middle of the form. Follow Steps 5 and 6 of the *Define a New Batch File* explanation above to change the analysis cases to be run and the management of the analysis files, respectively. Click the *Modify* button to complete the change(s).

   iii. *Delete* button. Highlight the model file name to be deleted in the list in the display area in the middle of the form. Click the *Delete* button.

   iv. *Change Filename Path* button. Click the *Change Filename Path* button to access the *Batch File Path* form.

(d) Run a Batch File

1. Define a batch file or open an existing batch text file as described above.
2. Use the Add, Modify, Delete and Change Filename Path buttons to make any necessary changes to the batch definition before running the batch file (see the Open an Existing Batch Text File explanation for more information about using these buttons).
3. Click the Run Models in Current Batch File List button to begin the batch run. That particular session of SAP2000 cannot be used while the batch file is running.
4. If the batch file has not been saved to a text file, SAP will prompt you to save it.
5. When the batch files are complete, the Status of Batch File Analyses form will appear, displaying a summary of the runs in the batch.

Done button. Click the Done button to close the form.

As seen above in Step a3, each \$2K file has to be imported in SAP2000 and the corresponding SAP file (.SDB) has to be provided **manually** in the batch file. This

method will be very tedious for large number of PAM. Another batch mode approach in SAP2000 is by utilising the command line function. This method is explained (www.wiki.csiberkeley.com/display/kb/Command+line) below.

Approach B –

The full command line includes the path to the SAP2000.exe program (*this may require copying all SAP license files into a new folder, say "SAP2000" in C (or other) drive*), the path to a SAP2000 data file plus four optional switches that control what happens in the program after the data file has been opened. An example of a full command line, including all possible switches, is as follows:

```
C:\SAP2000\SAP2000.EXE   C:\DATA\MYMODEL.SDB   /R  /D SCAO  /C  /K AO
```

SAP2000 can also be run through Matlab. Place the below code in each loop of analysis.

```
system('C:\SAP2000\SAP2000.EXE   C:\DATA\MYMODEL.SDB   /R  /D SCAO  /C  /K AO')
```

Following are explanations of each of the items in the example command line:

C:\SAP2000\SAP2000.EXE

The path to the SAP2000.exe program.

C:\DATA\MYMODEL.SDB

The path to the SAP2000 data file.

This item may have an extension of SDB, MDB, XLS, $2K or S2K. If the extension is SDB, the file is assumed to be a SAP2000 SDB file and the program will attempt to open it. If the extension is MDB, the file is assumed to be a Microsoft Access file and the program will attempt to import it. If the extension is XLS, the file is assumed to be a Microsoft Excel file and the program will attempt to import it. *If the extension is $2K or S2K, the file is assumed to be a SAP2000 text file and the program will attempt to import it*.

/R Pn Sn

The /R switch runs the analysis automatically after the data file has been successfully opened or imported.

The /R switch may be followed by Pn where n is 1 or 2. P1 forces the analysis to be run in the same process as SAP2000. P2 forces the analysis to run in a separate process from SAP2000.

The /R switch may also be followed by Sn where n is 1 or 2. S1 forces the analysis to use the standard solver. S2 forces the analysis to use the advanced solver.

/D SCAO

The /D switch alone automatically performs all possible types of design after the data file has been opened or imported and analysis results are available. If the /D switch is followed by S, steel frame design is performed. If it is followed by C, concrete frame design is performed. If it is followed by A, aluminium frame design is performed. If it is followed by O, coldformed frame design is performed. Specifying /D or /D SCAO starts all possible design.

/C

The /C switch closes SAP2000 after the analysis has been run and design has been completed.

/K AO

The /K switch alone deletes the files created when the analysis was run.

If the /K switch is followed by A, all analysis files except the log and out files are deleted. If it is followed by O, the log and output files are deleted. Specifying /K or /K AO causes the same files to be deleted.

The /K switch does not delete the Access database file that may be specified to be automatically saved after the analysis has been completed.

When a model is opened (or imported), run and designed from the command line, any Access database file specified to be automatically saved after the analysis has been completed is not saved until both the analysis and design have been completed. This allows the Access database file to include both analysis and design results.

Stage D:

Approach B from Step C is used here. Create a .bat file (batch file) by following the below steps:

1. Open a new Notepad file. Do not save the file yet.
2. Write the SAP command line commands in this file. Example of commands for running PAM files (la1_1, la2_1, la3_1, la4_1 and so on) is shown here.

```
C:\TEMP\SAP2000\Sap2000.exe  C:\TEMP\SAP_PAM\la1_1.$2k  /R /C /K A
C:\TEMP\SAP2000\Sap2000.exe  C:\TEMP\SAP_PAM\la2_1.$2k  /R /C /K A
C:\TEMP\SAP2000\Sap2000.exe  C:\TEMP\SAP_PAM\la3_1.$2k  /R /C /K A
C:\TEMP\SAP2000\Sap2000.exe  C:\TEMP\SAP_PAM\la4_1.$2k  /R /C /K A
…….
…….
```

3. Save the file in .bat format. Let us name this batch file as "SAP_CL.bat" as shown here. The created batch file can be viewed or edited by right clicking the file and clicking on "*Edit*".

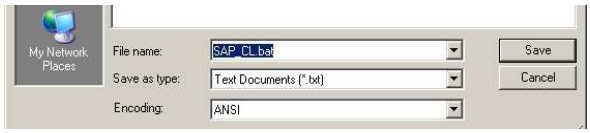

4. Run the batch file by double-clicking "SAP_CL.bat". Once all PAM are analysed, open the folder "SAP_PAM". The output files (e.g., la1_1outfile.xls, la2_1outfile.xls and so on) can then be accessed to obtain the results of analysed PAM. The information from these files can be used to plot graphs and interpret the results.

Note: A sample batch file developed for diaphragm flexibility study is shown below. Here, new folders are created to move the PAM files (.$2k), the SAP2000 log files, and the result file (.xls) into the appropriate named folder after each analysis. This batch file example is followed by a flow chart showing the steps used for this study.

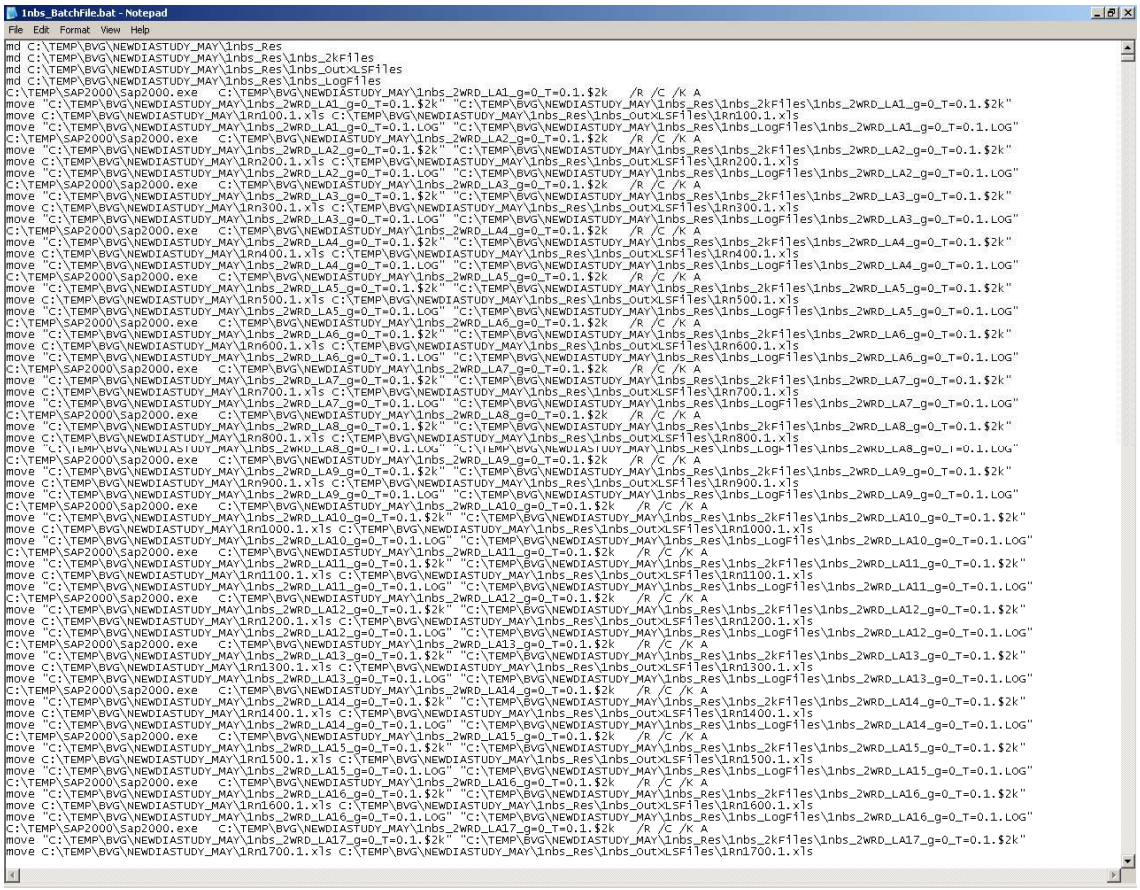

1nbs_BatchFile.bat - Notepad

File Edit Format View Help

```
md C:\TEMP\BVG\NEWDIASTUDY_MAY\1nbs_Res
md C:\TEMP\BVG\NEWDIASTUDY_MAY\1nbs_Res\1nbs_2kFiles
md C:\TEMP\BVG\NEWDIASTUDY_MAY\1nbs_Res\1nbs_OutXLSFiles
md C:\TEMP\BVG\NEWDIASTUDY_MAY\1nbs_Res\1nbs_LogFiles
C:\TEMP\SAP2000\Sap2000.exe   C:\TEMP\BVG\NEWDIASTUDY_MAY\1nbs_2WRD_LA1_g=0_T=0.1.$2k   /R /C /K A
move "C:\TEMP\BVG\NEWDIASTUDY_MAY\1nbs_2WRD_LA1_g=0_T=0.1.$2k" "C:\TEMP\BVG\NEWDIASTUDY_MAY\1nbs_Res\1nbs_2kFiles\1nbs_2WRD_LA1_g=0_T=0.1.$2k"
move C:\TEMP\BVG\NEWDIASTUDY_MAY\1Rn100.1.xls C:\TEMP\BVG\NEWDIASTUDY_MAY\1nbs_Res\1nbs_OutXLSFiles\1Rn100.1.xls
move "C:\TEMP\BVG\NEWDIASTUDY_MAY\1nbs_2WRD_LA1_g=0_T=0.1.LOG" "C:\TEMP\BVG\NEWDIASTUDY_MAY\1nbs_Res\1nbs_LogFiles\1nbs_2WRD_LA1_g=0_T=0.1.LOG"
C:\TEMP\SAP2000\Sap2000.exe   C:\TEMP\BVG\NEWDIASTUDY_MAY\1nbs_2WRD_LA2_g=0_T=0.1.$2k   /R /C /K A
move "C:\TEMP\BVG\NEWDIASTUDY_MAY\1nbs_2WRD_LA2_g=0_T=0.1.$2k" "C:\TEMP\BVG\NEWDIASTUDY_MAY\1nbs_Res\1nbs_2kFiles\1nbs_2WRD_LA2_g=0_T=0.1.$2k"
move C:\TEMP\BVG\NEWDIASTUDY_MAY\1Rn200.1.xls C:\TEMP\BVG\NEWDIASTUDY_MAY\1nbs_Res\1nbs_OutXLSFiles\1Rn200.1.xls
move "C:\TEMP\BVG\NEWDIASTUDY_MAY\1nbs_2WRD_LA2_g=0_T=0.1.LOG" "C:\TEMP\BVG\NEWDIASTUDY_MAY\1nbs_Res\1nbs_LogFiles\1nbs_2WRD_LA2_g=0_T=0.1.LOG"
C:\TEMP\SAP2000\Sap2000.exe   C:\TEMP\BVG\NEWDIASTUDY_MAY\1nbs_2WRD_LA3_g=0_T=0.1.$2k   /R /C /K A
move "C:\TEMP\BVG\NEWDIASTUDY_MAY\1nbs_2WRD_LA3_g=0_T=0.1.$2k" "C:\TEMP\BVG\NEWDIASTUDY_MAY\1nbs_Res\1nbs_2kFiles\1nbs_2WRD_LA3_g=0_T=0.1.$2k"
move C:\TEMP\BVG\NEWDIASTUDY_MAY\1Rn300.1.xls C:\TEMP\BVG\NEWDIASTUDY_MAY\1nbs_Res\1nbs_OutXLSFiles\1Rn300.1.xls
move "C:\TEMP\BVG\NEWDIASTUDY_MAY\1nbs_2WRD_LA3_g=0_T=0.1.LOG" "C:\TEMP\BVG\NEWDIASTUDY_MAY\1nbs_Res\1nbs_LogFiles\1nbs_2WRD_LA3_g=0_T=0.1.LOG"
C:\TEMP\SAP2000\Sap2000.exe   C:\TEMP\BVG\NEWDIASTUDY_MAY\1nbs_2WRD_LA4_g=0_T=0.1.$2k   /R /C /K A
move "C:\TEMP\BVG\NEWDIASTUDY_MAY\1nbs_2WRD_LA4_g=0_T=0.1.$2k" "C:\TEMP\BVG\NEWDIASTUDY_MAY\1nbs_Res\1nbs_2kFiles\1nbs_2WRD_LA4_g=0_T=0.1.$2k"
move C:\TEMP\BVG\NEWDIASTUDY_MAY\1Rn400.1.xls C:\TEMP\BVG\NEWDIASTUDY_MAY\1nbs_Res\1nbs_OutXLSFiles\1Rn400.1.xls
move "C:\TEMP\BVG\NEWDIASTUDY_MAY\1nbs_2WRD_LA4_g=0_T=0.1.LOG" "C:\TEMP\BVG\NEWDIASTUDY_MAY\1nbs_Res\1nbs_LogFiles\1nbs_2WRD_LA4_g=0_T=0.1.LOG"
C:\TEMP\SAP2000\Sap2000.exe   C:\TEMP\BVG\NEWDIASTUDY_MAY\1nbs_2WRD_LA5_g=0_T=0.1.$2k   /R /C /K A
move "C:\TEMP\BVG\NEWDIASTUDY_MAY\1nbs_2WRD_LA5_g=0_T=0.1.$2k" "C:\TEMP\BVG\NEWDIASTUDY_MAY\1nbs_Res\1nbs_2kFiles\1nbs_2WRD_LA5_g=0_T=0.1.$2k"
move C:\TEMP\BVG\NEWDIASTUDY_MAY\1Rn500.1.xls C:\TEMP\BVG\NEWDIASTUDY_MAY\1nbs_Res\1nbs_OutXLSFiles\1Rn500.1.xls
move "C:\TEMP\BVG\NEWDIASTUDY_MAY\1nbs_2WRD_LA5_g=0_T=0.1.LOG" "C:\TEMP\BVG\NEWDIASTUDY_MAY\1nbs_Res\1nbs_LogFiles\1nbs_2WRD_LA5_g=0_T=0.1.LOG"
C:\TEMP\SAP2000\Sap2000.exe   C:\TEMP\BVG\NEWDIASTUDY_MAY\1nbs_2WRD_LA6_g=0_T=0.1.$2k   /R /C /K A
move "C:\TEMP\BVG\NEWDIASTUDY_MAY\1nbs_2WRD_LA6_g=0_T=0.1.$2k" "C:\TEMP\BVG\NEWDIASTUDY_MAY\1nbs_Res\1nbs_2kFiles\1nbs_2WRD_LA6_g=0_T=0.1.$2k"
move C:\TEMP\BVG\NEWDIASTUDY_MAY\1Rn600.1.xls C:\TEMP\BVG\NEWDIASTUDY_MAY\1nbs_Res\1nbs_OutXLSFiles\1Rn600.1.xls
move "C:\TEMP\BVG\NEWDIASTUDY_MAY\1nbs_2WRD_LA6_g=0_T=0.1.LOG" "C:\TEMP\BVG\NEWDIASTUDY_MAY\1nbs_Res\1nbs_LogFiles\1nbs_2WRD_LA6_g=0_T=0.1.LOG"
C:\TEMP\SAP2000\Sap2000.exe   C:\TEMP\BVG\NEWDIASTUDY_MAY\1nbs_2WRD_LA7_g=0_T=0.1.$2k   /R /C /K A
move "C:\TEMP\BVG\NEWDIASTUDY_MAY\1nbs_2WRD_LA7_g=0_T=0.1.$2k" "C:\TEMP\BVG\NEWDIASTUDY_MAY\1nbs_Res\1nbs_2kFiles\1nbs_2WRD_LA7_g=0_T=0.1.$2k"
move C:\TEMP\BVG\NEWDIASTUDY_MAY\1Rn700.1.xls C:\TEMP\BVG\NEWDIASTUDY_MAY\1nbs_Res\1nbs_OutXLSFiles\1Rn700.1.xls
move "C:\TEMP\BVG\NEWDIASTUDY_MAY\1nbs_2WRD_LA7_g=0_T=0.1.LOG" "C:\TEMP\BVG\NEWDIASTUDY_MAY\1nbs_Res\1nbs_LogFiles\1nbs_2WRD_LA7_g=0_T=0.1.LOG"
C:\TEMP\SAP2000\Sap2000.exe   C:\TEMP\BVG\NEWDIASTUDY_MAY\1nbs_2WRD_LA8_g=0_T=0.1.$2k   /R /C /K A
move "C:\TEMP\BVG\NEWDIASTUDY_MAY\1nbs_2WRD_LA8_g=0_T=0.1.$2k" "C:\TEMP\BVG\NEWDIASTUDY_MAY\1nbs_Res\1nbs_2kFiles\1nbs_2WRD_LA8_g=0_T=0.1.$2k"
move C:\TEMP\BVG\NEWDIASTUDY_MAY\1Rn800.1.xls C:\TEMP\BVG\NEWDIASTUDY_MAY\1nbs_Res\1nbs_OutXLSFiles\1Rn800.1.xls
move "C:\TEMP\BVG\NEWDIASTUDY_MAY\1nbs_2WRD_LA8_g=0_T=0.1.LOG" "C:\TEMP\BVG\NEWDIASTUDY_MAY\1nbs_Res\1nbs_LogFiles\1nbs_2WRD_LA8_g=0_T=0.1.LOG"
C:\TEMP\SAP2000\Sap2000.exe   C:\TEMP\BVG\NEWDIASTUDY_MAY\1nbs_2WRD_LA9_g=0_T=0.1.$2k   /R /C /K A
move "C:\TEMP\BVG\NEWDIASTUDY_MAY\1nbs_2WRD_LA9_g=0_T=0.1.$2k" "C:\TEMP\BVG\NEWDIASTUDY_MAY\1nbs_Res\1nbs_2kFiles\1nbs_2WRD_LA9_g=0_T=0.1.$2k"
move C:\TEMP\BVG\NEWDIASTUDY_MAY\1Rn900.1.xls C:\TEMP\BVG\NEWDIASTUDY_MAY\1nbs_Res\1nbs_OutXLSFiles\1Rn900.1.xls
move "C:\TEMP\BVG\NEWDIASTUDY_MAY\1nbs_2WRD_LA9_g=0_T=0.1.LOG" "C:\TEMP\BVG\NEWDIASTUDY_MAY\1nbs_Res\1nbs_LogFiles\1nbs_2WRD_LA9_g=0_T=0.1.LOG"
C:\TEMP\SAP2000\Sap2000.exe   C:\TEMP\BVG\NEWDIASTUDY_MAY\1nbs_2WRD_LA10_g=0_T=0.1.$2k   /R /C /K A
move "C:\TEMP\BVG\NEWDIASTUDY_MAY\1nbs_2WRD_LA10_g=0_T=0.1.$2k" "C:\TEMP\BVG\NEWDIASTUDY_MAY\1nbs_Res\1nbs_2kFiles\1nbs_2WRD_LA10_g=0_T=0.1.$2k"
move C:\TEMP\BVG\NEWDIASTUDY_MAY\1Rn1000.1.xls C:\TEMP\BVG\NEWDIASTUDY_MAY\1nbs_Res\1nbs_OutXLSFiles\1Rn1000.1.xls
move "C:\TEMP\BVG\NEWDIASTUDY_MAY\1nbs_2WRD_LA10_g=0_T=0.1.LOG" "C:\TEMP\BVG\NEWDIASTUDY_MAY\1nbs_Res\1nbs_LogFiles\1nbs_2WRD_LA10_g=0_T=0.1.LOG"
C:\TEMP\SAP2000\Sap2000.exe   C:\TEMP\BVG\NEWDIASTUDY_MAY\1nbs_2WRD_LA11_g=0_T=0.1.$2k   /R /C /K A
move "C:\TEMP\BVG\NEWDIASTUDY_MAY\1nbs_2WRD_LA11_g=0_T=0.1.$2k" "C:\TEMP\BVG\NEWDIASTUDY_MAY\1nbs_Res\1nbs_2kFiles\1nbs_2WRD_LA11_g=0_T=0.1.$2k"
move C:\TEMP\BVG\NEWDIASTUDY_MAY\1Rn1100.1.xls C:\TEMP\BVG\NEWDIASTUDY_MAY\1nbs_Res\1nbs_OutXLSFiles\1Rn1100.1.xls
move "C:\TEMP\BVG\NEWDIASTUDY_MAY\1nbs_2WRD_LA11_g=0_T=0.1.LOG" "C:\TEMP\BVG\NEWDIASTUDY_MAY\1nbs_Res\1nbs_LogFiles\1nbs_2WRD_LA11_g=0_T=0.1.LOG"
C:\TEMP\SAP2000\Sap2000.exe   C:\TEMP\BVG\NEWDIASTUDY_MAY\1nbs_2WRD_LA12_g=0_T=0.1.$2k   /R /C /K A
move "C:\TEMP\BVG\NEWDIASTUDY_MAY\1nbs_2WRD_LA12_g=0_T=0.1.$2k" "C:\TEMP\BVG\NEWDIASTUDY_MAY\1nbs_Res\1nbs_2kFiles\1nbs_2WRD_LA12_g=0_T=0.1.$2k"
move C:\TEMP\BVG\NEWDIASTUDY_MAY\1Rn1200.1.xls C:\TEMP\BVG\NEWDIASTUDY_MAY\1nbs_Res\1nbs_OutXLSFiles\1Rn1200.1.xls
move "C:\TEMP\BVG\NEWDIASTUDY_MAY\1nbs_2WRD_LA12_g=0_T=0.1.LOG" "C:\TEMP\BVG\NEWDIASTUDY_MAY\1nbs_Res\1nbs_LogFiles\1nbs_2WRD_LA12_g=0_T=0.1.LOG"
C:\TEMP\SAP2000\Sap2000.exe   C:\TEMP\BVG\NEWDIASTUDY_MAY\1nbs_2WRD_LA13_g=0_T=0.1.$2k   /R /C /K A
move "C:\TEMP\BVG\NEWDIASTUDY_MAY\1nbs_2WRD_LA13_g=0_T=0.1.$2k" "C:\TEMP\BVG\NEWDIASTUDY_MAY\1nbs_Res\1nbs_2kFiles\1nbs_2WRD_LA13_g=0_T=0.1.$2k"
move C:\TEMP\BVG\NEWDIASTUDY_MAY\1Rn1300.1.xls C:\TEMP\BVG\NEWDIASTUDY_MAY\1nbs_Res\1nbs_OutXLSFiles\1Rn1300.1.xls
move "C:\TEMP\BVG\NEWDIASTUDY_MAY\1nbs_2WRD_LA13_g=0_T=0.1.LOG" "C:\TEMP\BVG\NEWDIASTUDY_MAY\1nbs_Res\1nbs_LogFiles\1nbs_2WRD_LA13_g=0_T=0.1.LOG"
C:\TEMP\SAP2000\Sap2000.exe   C:\TEMP\BVG\NEWDIASTUDY_MAY\1nbs_2WRD_LA14_g=0_T=0.1.$2k   /R /C /K A
move "C:\TEMP\BVG\NEWDIASTUDY_MAY\1nbs_2WRD_LA14_g=0_T=0.1.$2k" "C:\TEMP\BVG\NEWDIASTUDY_MAY\1nbs_Res\1nbs_2kFiles\1nbs_2WRD_LA14_g=0_T=0.1.$2k"
move C:\TEMP\BVG\NEWDIASTUDY_MAY\1Rn1400.1.xls C:\TEMP\BVG\NEWDIASTUDY_MAY\1nbs_Res\1nbs_OutXLSFiles\1Rn1400.1.xls
move "C:\TEMP\BVG\NEWDIASTUDY_MAY\1nbs_2WRD_LA14_g=0_T=0.1.LOG" "C:\TEMP\BVG\NEWDIASTUDY_MAY\1nbs_Res\1nbs_LogFiles\1nbs_2WRD_LA14_g=0_T=0.1.LOG"
C:\TEMP\SAP2000\Sap2000.exe   C:\TEMP\BVG\NEWDIASTUDY_MAY\1nbs_2WRD_LA15_g=0_T=0.1.$2k   /R /C /K A
move "C:\TEMP\BVG\NEWDIASTUDY_MAY\1nbs_2WRD_LA15_g=0_T=0.1.$2k" "C:\TEMP\BVG\NEWDIASTUDY_MAY\1nbs_Res\1nbs_2kFiles\1nbs_2WRD_LA15_g=0_T=0.1.$2k"
move C:\TEMP\BVG\NEWDIASTUDY_MAY\1Rn1500.1.xls C:\TEMP\BVG\NEWDIASTUDY_MAY\1nbs_Res\1nbs_OutXLSFiles\1Rn1500.1.xls
move "C:\TEMP\BVG\NEWDIASTUDY_MAY\1nbs_2WRD_LA15_g=0_T=0.1.LOG" "C:\TEMP\BVG\NEWDIASTUDY_MAY\1nbs_Res\1nbs_LogFiles\1nbs_2WRD_LA15_g=0_T=0.1.LOG"
C:\TEMP\SAP2000\Sap2000.exe   C:\TEMP\BVG\NEWDIASTUDY_MAY\1nbs_2WRD_LA16_g=0_T=0.1.$2k   /R /C /K A
move "C:\TEMP\BVG\NEWDIASTUDY_MAY\1nbs_2WRD_LA16_g=0_T=0.1.$2k" "C:\TEMP\BVG\NEWDIASTUDY_MAY\1nbs_Res\1nbs_2kFiles\1nbs_2WRD_LA16_g=0_T=0.1.$2k"
move C:\TEMP\BVG\NEWDIASTUDY_MAY\1Rn1600.1.xls C:\TEMP\BVG\NEWDIASTUDY_MAY\1nbs_Res\1nbs_OutXLSFiles\1Rn1600.1.xls
move "C:\TEMP\BVG\NEWDIASTUDY_MAY\1nbs_2WRD_LA16_g=0_T=0.1.LOG" "C:\TEMP\BVG\NEWDIASTUDY_MAY\1nbs_Res\1nbs_LogFiles\1nbs_2WRD_LA16_g=0_T=0.1.LOG"
C:\TEMP\SAP2000\Sap2000.exe   C:\TEMP\BVG\NEWDIASTUDY_MAY\1nbs_2WRD_LA17_g=0_T=0.1.$2k   /R /C /K A
move "C:\TEMP\BVG\NEWDIASTUDY_MAY\1nbs_2WRD_LA17_g=0_T=0.1.$2k" "C:\TEMP\BVG\NEWDIASTUDY_MAY\1nbs_Res\1nbs_2kFiles\1nbs_2WRD_LA17_g=0_T=0.1.$2k"
move C:\TEMP\BVG\NEWDIASTUDY_MAY\1Rn1700.1.xls C:\TEMP\BVG\NEWDIASTUDY_MAY\1nbs_Res\1nbs_OutXLSFiles\1Rn1700.1.xls
```

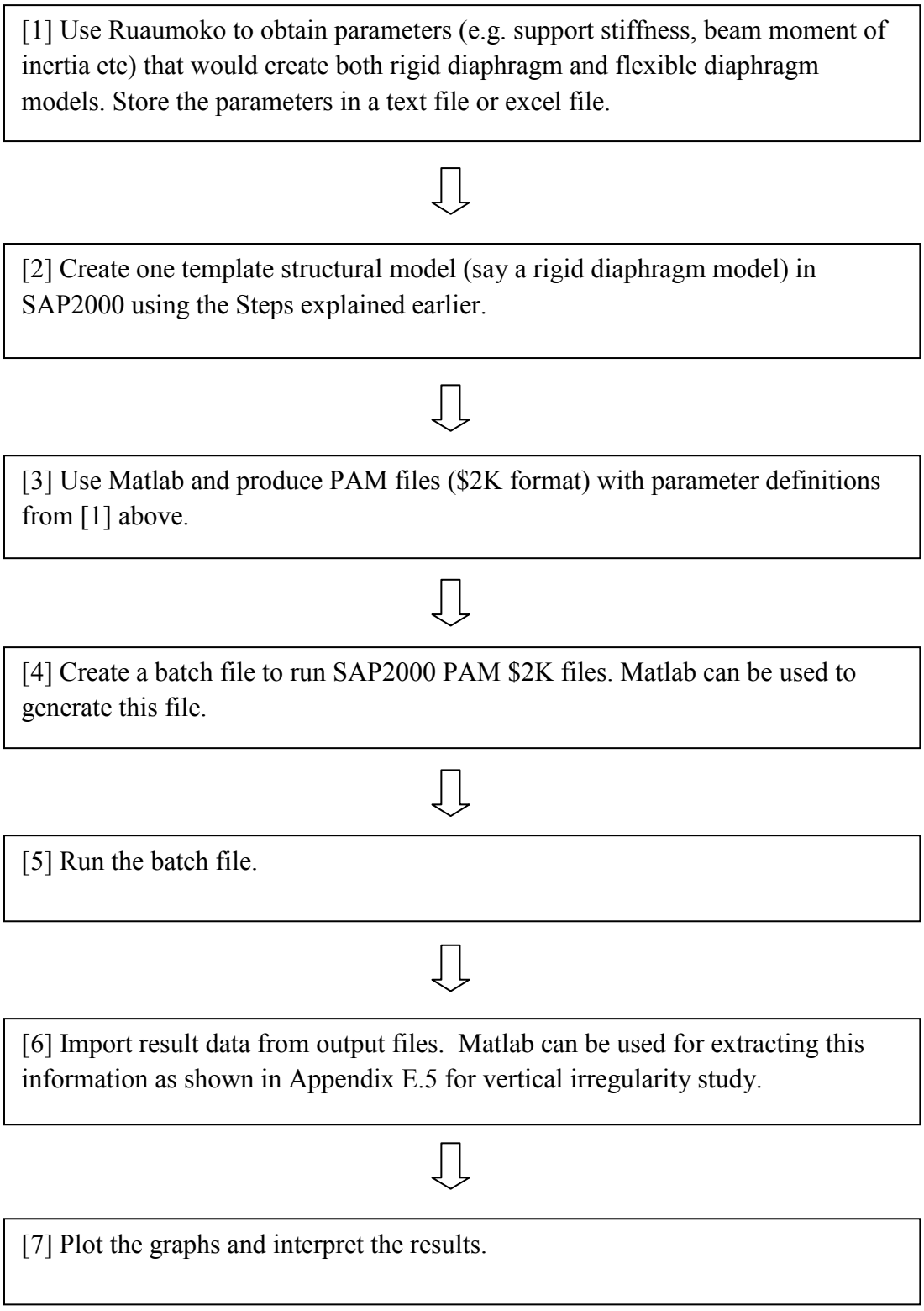

Figure I-1: Overview of steps used in for conducting diaphragm flexibility study in SAP2000.

APPENDIX J: SUPPLEMENTARY INFORMATION FOR DIAPHRAGM FLEXIBILITY STUDY

J.1 Idealising Diaphragm as a Simply Supported Beam

The three-dimensional continuous diaphragm between the lateral-force-resisting systems (LFR) in Figure J-1(a) is modelled as a simply supported beam as shown in Figure J-1(b) (Chopra [1]). For exact solution, the total diaphragm mass, M_d, given as the product of diaphragm mass per unit beam length, m_d, and the total length of the beam, L_d, should be lumped at infinite nodal points along the length of the beam. Such a multi-degree-of-freedom diaphragm (MDOF) would have infinite modes of vibration.

The beam deflection at a distance of x from the support of such MDOF system is given by Equation (J-1) as the product of the shape function, $\phi_i(x)$ corresponding to a particular mode i and the generalized co-ordinate, $q_i(t)$.

$$\delta_{di}(x,t) = \phi_i(x)\, q_i(t) \tag{J-1}$$

If the mode shapes are orthogonal, then the equation of motion (EOM) for the simply supported beam with distributed mass is given by Equation (J-2), where the generalised mass, M^*, the generalised stiffness, K^*, and the generalised excitation, L^*, are given respectively by Equations (J-3) through (J-5) [1]. Here, the equation is solved as a SDOF equation for each mode (with period, ω, and mode shape ϕ), i.

$$M_i^* \ddot{q}_i + K_i^* q_i = -L_i^* \ddot{u}_g \tag{J-2}$$

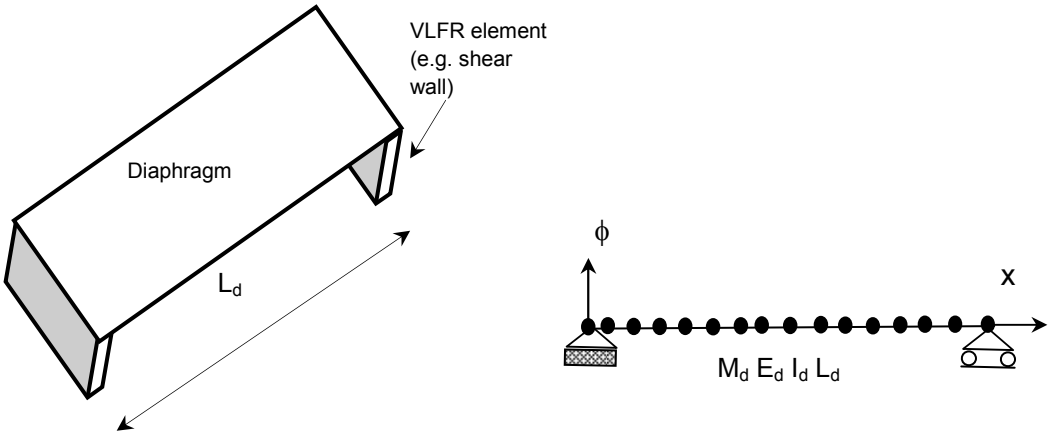

(a) Schematic of single-span one storey structure

(b) Diaphragm idealised as a simply supported beam – MDOF diaphragm

Figure J-1: Idealising three-dimensional diaphragm as a simply supported beam (not to scale).

$$M_i^* = \int_0^{L_d} m_d(x)[\phi_i(x)]^2\,dx \tag{J-3}$$

$$K_i^* = \int_0^{L_d} E_d I_d(x)[\phi_i''(x)]^2\,dx \tag{J-4}$$

$$L_i^* = \int_0^{L_d} m_d(x)\,\phi_i(x)\,dx \tag{J-5}$$

Dividing Equation (J-2) by M^* gives the below EOM, where the i^{th} mode participation factor, Γ_i, is given in Equation (J-7).

$$\ddot{q}_i + \frac{K_i^*}{M_i^*} q_i = -\left(\frac{L_i^*}{M_i^*}\right) \ddot{u}_g \tag{J-6}$$

$$\ddot{q}_i + \omega_i^2 q_i = -\Gamma_i \ddot{u}_g \tag{J-7}$$

For a simply supported beam with distributed mass, the mode shape and frequency for any mode, *i*, are given by Equations (J-8) and (J-9) respectively. These mode shapes have been normalized such that their maximum value is unity. Figure J-2 shows the first 6 modes of vibration.

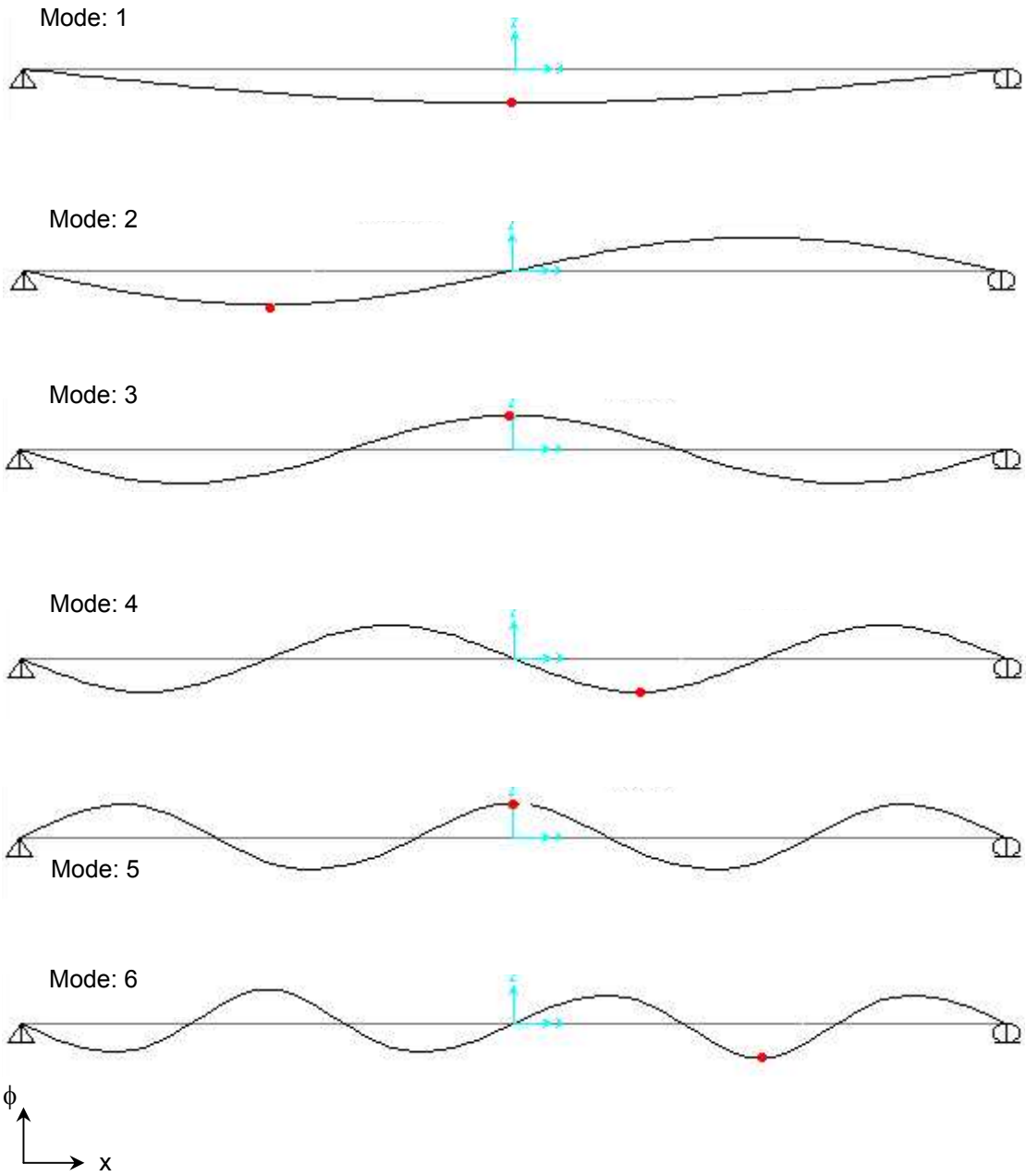

Figure J-2: Vibration mode shapes for a simply supported beam with distributed mass.

Substituting i = 1 in Equation (J-8) gives the fundamental mode shape for the continuous beam, shown in Figure J-2.

$$\phi_i(x) = Sin\left(\frac{i\pi x}{L_d}\right) \quad \text{where } i = 1, 2, 3\ldots\text{.vibration modes} \tag{J-8}$$

$$\omega_i = \sqrt{\frac{K_i^*}{M_i^*}} \tag{J-9}$$

$$\phi_1(x) = Sin\left(\frac{\pi x}{L_d}\right) \tag{J-10}$$

Substituting Equation (J-10) in Equations (J-3) through (J-5), the corresponding first mode generalised properties for the distributed system are found to be:

$$M_1^* = \left(\frac{m_d L_d}{2}\right) \tag{J-11}$$

$$K_1^* = \left(\frac{\pi^4 E_d I_d}{2 L_d^3}\right) \tag{J-12}$$

$$L_1^* = \left(\frac{2 m_d L_d}{\pi}\right) \tag{J-13}$$

Using Equations (J-11) and (J-12) in Equation (J-9), we get the fundamental natural period for the MDOF flexible diaphragm as given by Equation (J-16).

$$\omega^2_{id\_MDOF} = i^2\left(\frac{\pi}{L_d}\right)^4\left(\frac{E_d I_d}{m_d}\right) \tag{J-14}$$

$$\omega_{1d\_MDOF} = \left(\frac{\pi}{L_d}\right)^2\sqrt{\frac{E_d I_d}{m_d}} \tag{J-15}$$

$$T_{1d\_MDOF} = \sqrt{\frac{4\,m_d L_d^4}{E_d I_d\,\pi^2}} \tag{J-16}$$

From Equation (J-7), the participation factor for the first vibration mode, Γ_1, is given by Equation (J-18).

$$\Gamma_1 = \left(\frac{L_1^*}{M_1^*}\right) = \left(\frac{2\,m_d\,L_d}{\pi}\right) * \left(\frac{2}{m_d\,L_d}\right) \tag{J-17}$$

$$\Gamma_1 = \left(\frac{4}{\pi}\right) \tag{J-18}$$

The maximum deflection of the diaphragm from the first mode occurs at the mid-span of the beam. The peak value of the deflection for the fundamental mode is given by Equation (J-19) as the product of the corresponding participation factor and the spectral displacement, S_d.

$$q_{1\max} = \Gamma_1 * S_{d1} \tag{J-19}$$

Substituting Equation (J-19) in Equation (J-1), the maximum mid-span deflection due to the first mode is calculated as follows:

$$\delta_{d1\max\_MDOF} = \phi_1 (L_d / 2) * \Gamma_1 * S_{d1} \tag{J-20}$$

$$\delta_{d1\max\_MDOF} = \left(\frac{4}{\pi}\right) * S_{d1} \tag{J-21}$$

The bending moment, *BM*, and the shear force, *V*, are calculated by using the well-known relationships with the deflection function as:

$$\delta_{d1}(x,t) = \phi_1(x) * \Gamma_1 * S_{d1} \tag{J-22}$$

$$\delta_{d1}(x,t) = Sin\left(\frac{\pi x}{L_d}\right) * \left(\frac{4}{\pi}\right) * S_{d1} \qquad \text{(J-23)}$$

Differentiating Equation (J-23) twice with respect to the space variable, *x*, and multiplying the product with flexural rigidity, we get the first mode *BM* as:

$$BM_{1\_MDOF}(x) = -E_d I_d \left(\frac{4\pi}{L_d^{\,2}}\right) * S_{d1} * Sin\left(\frac{\pi x}{L_d}\right) \qquad \text{(J-24)}$$

The first mode shear force, V_1, at any distance *x* from the supports is obtained by differentiating the above bending moment equation with respect to *x*, to get Equation (J-25).

$$V_1(x) = -EI \left(\frac{4\pi^2}{L_d^{\,3}}\right) * S_{d1} * Cos\left(\frac{\pi x}{L_d}\right) \qquad \text{(J-25)}$$

For a simply supported beam with a uniform mass, the maximum shear force occurs at the supports; therefore substituting $x = 0$ in Equation (J-25), we get the shear force at the left simple support as:

$$V_1(0) = -E_d I_d \left(\frac{4\pi^2}{L_d^{\,3}}\right) * S_{d1} \qquad \text{(J-26)}$$

Since the beam is simply supported at the ends, the first mode total base shear, V_{1b_MDOF}, is given by Equation (J-27) as twice the shear force obtained from Equation (J-26).

$$V_{1b\_MDOF}(t) = \left(\frac{8\pi^2 E_d I_d}{L_d^3}\right) * S_{d1} \qquad \text{(J-27)}$$

J.2 Expression for Non-Dimensional Demand Parameter: δ_{total_ratio}

It was shown in Section 5.5.1 that the MDOF diaphragm in Figure J-1(b) can be easily be represented by an equivalent SDOF diaphragm. In 5.5.2, lumped mass models (Figure 5-13) were used to estimate the likely increase in the structural fundamental natural period and the total diaphragm mid-span displacement due to diaphragm flexibility. The following steps are involved in obtaining Equation (5-23).

Figure J-3 shows the in-plane displacement components for the lumped mass models of the one storey structure in Figure J-1(a).

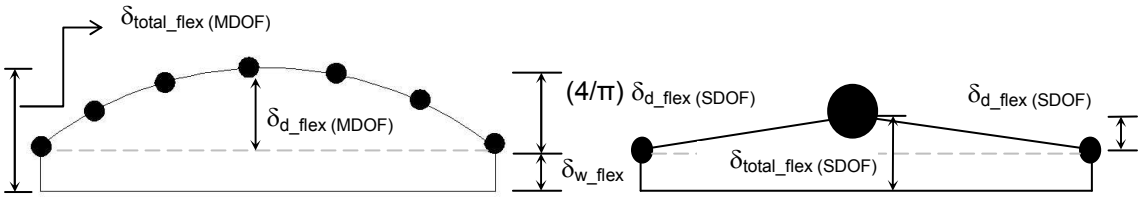

(a) MDOF flexible diaphragm (b) SDOF flexible diaphragm

Figure J-3: In-plane displacement components for a flexible diaphragm resting on end supports.

In this thesis, a rigid diaphragm is assumed to have negligible deformations compared to that of end supports, and therefore, the total in-plane displacement of a structure with a rigid diaphragm, δ_{total_rig}, equals the in-plane displacement of the wall alone, δ_{w_rig}. For a structure with a flexible diaphragm, as shown in Figure J-3, the total in-plane displacement of the structure is represented by $\delta_{total\_flex\ (MDOF)}$ for a MDOF flexible diaphragm and by $\delta_{total\_flex\ (SDOF)}$ for a SDOF flexible diaphragm. The in-plane displacement of the end walls supporting the flexible diaphragm is represented by δ_{w_flex}.

Recalling Equation (5-1) that defines the static flexibility ratio, γ_s;

$$\gamma_s = \frac{\delta_{d\_flex}}{\delta_{w\_flex}} \tag{J-28}$$

In the above Equation, the maximum in-plane displacement of the flexible diaphragm, δ_{d_flex}, is represented in Figure J-3 by $\delta_{d\_flex\ (MDOF)}$ for a MDOF flexible diaphragm and $\delta_{d\_flex\ (SDOF)}$ is used for a SDOF flexible diaphragm.

Applying Equation (J-28) to Figure J-3(a), the total in-plane displacement of the structure with a MDOF flexible diaphragm can be expressed by Equation (J-30).

$$\gamma_s = \left(\frac{\delta_{total\_flex(MDOF)} - \delta_{w\_flex}}{\delta_{w\_flex}} \right) = \left(\frac{\delta_{total\_flex(MDOF)}}{\delta_{w\_flex}} - 1 \right) \tag{J-29}$$

$$\delta_{total\_flex(MDOF)} = (\gamma_s + 1) * \delta_{w\_flex} \tag{J-30}$$

From Figure J-3(b),

$$\delta_{total\_flex(MDOF)} = \delta_{w\_flex} + \left(\frac{4}{\pi} \right) \delta_{d\_flex(SDOF)} \tag{J-31}$$

Equating (J-30) and (J-31);

$$(\gamma_s + 1 - 1) * \delta_{w\_flex} = \left(\frac{4}{\pi} \right) \delta_{d\_flex(SDOF)} \tag{J-32}$$

$$\delta_{w\_flex} = \left(\frac{4}{\pi} \right) \left(\frac{\delta_{d\_flex(SDOF)}}{\gamma_s} \right) \tag{J-33}$$

The total in-plane displacement of the structure with a SDOF flexible diaphragm, $\delta_{total\_flex\ (SDOF)}$, from Figure J-3(b) is given by Equation (J-34).

$$\delta_{total\_flex(SDOF)} = \delta_{w\_flex} + \delta_{d\_flex(SDOF)} \tag{J-34}$$

Using Equation (J-33) in (J-34);

$$\delta_{total\_flex(SDOF)} = \left(\frac{4}{\pi}\right)\left(\frac{\delta_{d\_flex(SDOF)}}{\gamma_s}\right) + \delta_{d\_flex(SDOF)} \quad \text{(J-35)}$$

Rearranging the above equation gives Equation (J-36) for in-plane displacement of the SDOF flexible diaphragm alone, $\delta_{d\_flex\ (SDOF)}$.

$$\delta_{d\_flex(SDOF)} = \left[\frac{\delta_{total\_flex(SDOF)}}{\left(1+\frac{4}{\pi\gamma_s}\right)}\right] \quad \text{(J-36)}$$

Equation (J-36) is used in Equation (J-33) and solved for the in-plane displacement of the end walls supporting the flexible diaphragm, δ_{w_flex}, giving Equation (J-38).

$$\delta_{w\_flex} = \left(\frac{4}{\pi\gamma}\right)\left[\frac{\delta_{total\_flex(SDOF)}}{\left(\frac{\pi\gamma+4}{\pi\gamma}\right)}\right] \quad \text{(J-37)}$$

$$= \left(\frac{4}{\pi\gamma+4}\right) * \delta_{total\_flex(SDOF)} \quad \text{(J-38)}$$

The change in total in-plane displacement at mid-span due to γ_s, δ_{total_ratio}, was calculated in Chapter 5 according to Equation (J-39);

$$\delta_{total\_ratio} = \frac{\delta_{total\_flex}}{\delta_{total\_rig}} \quad \text{(J-39)}$$

In the above equation, the total in-plane displacement at mid-span due to a flexible diaphragm, δ_{total_flex}, is equivalent to the total in-plane displacement at mid-span due to a MDOF flexible diaphragm, $\delta_{total\_flex\ (MDOF)}$ in Figure J-3(a). Substituting $\delta_{total\_rig} = \delta_{w\_rig}$ for a structure with a rigid diaphragm, Equation (J-39) is rearranged:

$$\delta_{total\_ratio} = \left(\frac{\delta_{w\_flex} + \delta_{d\_flex(MDOF)}}{\delta_{w\_rig}} \right) \qquad \text{(J-40)}$$

Applying Equation (J-28) above;

$$= \left(\frac{\delta_{w\_flex} + \gamma_s \, \delta_{w\_flex}}{\delta_{w\_rig}} \right) \qquad \text{(J-41)}$$

Using Equation (J-38) in the above equation, δ_{total_ratio} can be obtained. This is given by Equation (J-43), which is used in Section 5.5.2.

$$= \left(\frac{4}{\pi\gamma + 4} \right) (1 + \gamma_s) \left(\frac{\delta_{total\_flex(SDOF)}}{\delta_{w\_rig}} \right) \qquad \text{(J-42)}$$

$$\delta_{total\_ratio} = \left[\frac{4 + 4\gamma_{s_j}}{\pi\gamma_{s_j} + 4} \right] \left(\frac{\delta_{total\_flex(SDOF)}}{\delta_{w\_rig}} \right) \qquad \text{(J-43)}$$

J.3 Choice of Central Support Stiffness Factor, CSK_f

In Chapter 5, diaphragm flexibility effects were studied on structures having diaphragms supported on: (a) end supports; and (b) end supports and a mid-span support.

For diaphragms supported by two end walls and one central wall, the total support stiffness was divided between the supporting walls according to Equations (5-4b) and (5-4c), where CSK_f is defined as the central support stiffness factor. The sensitivity of this CSK_f factor in describing the diaphragm flexibility effects was investigated by applying the methodology described in Section 5.3.4 for one and five storey two-spanned structures considered in Chapter 5.

Figure J-4 shows the change in median peak total in-plane displacement at mid-span, δ_{total_ratio}, due to diaphragm flexibility, plotted against the central support stiffness factor for two spanned multi-storey structures having a mid-span pinned connection. For a very low diaphragm flexibility ratio, $\gamma_s = 0.1$, Figure J-4(a) shows that for both one storey structures (nbs = 1) and five storey structures (nbs = 5), the variation of δ_{total_ratio} is nearly constant at all CSK_f values. Increasing the diaphragm flexibility from $\gamma_s = 0.1$ to 2.5, increases δ_{total_ratio} for both structural heights. However, the 1 storey structures, rather than the 5 storey structures, show higher increases in δ_{total_ratio} due to diaphragm flexibility. The figure shows that when CSK_f is increased up to 2, δ_{total_ratio} increases, and for $CSK_f > 2$, the demand ratio decreases. The above trends in response for $\gamma_s = 2.5$ can again be observed for $\gamma_s = 5$ in Figure J-4(c). Here, it shows clearly that $CSK_f = 2$ produces the most change in response due to diaphragm flexibility. Therefore, this value of $CSK_f = 2$ was used for all analyses described in Chapter 5.

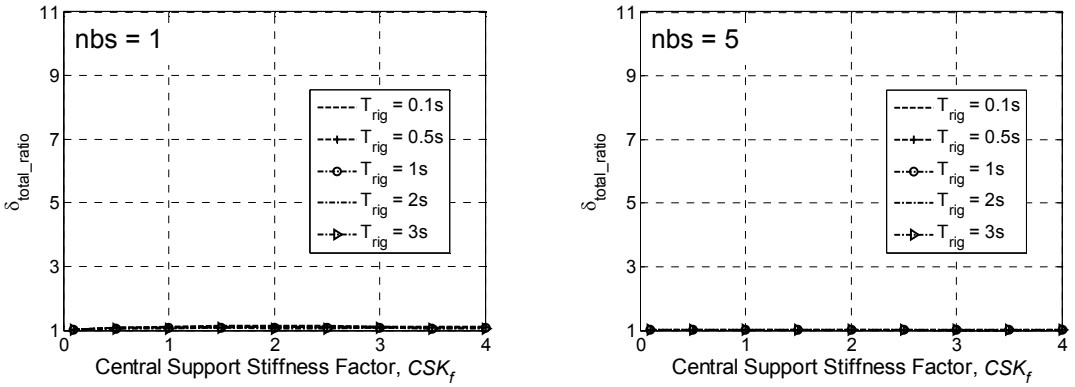

(a) $\gamma_s = 0.1$

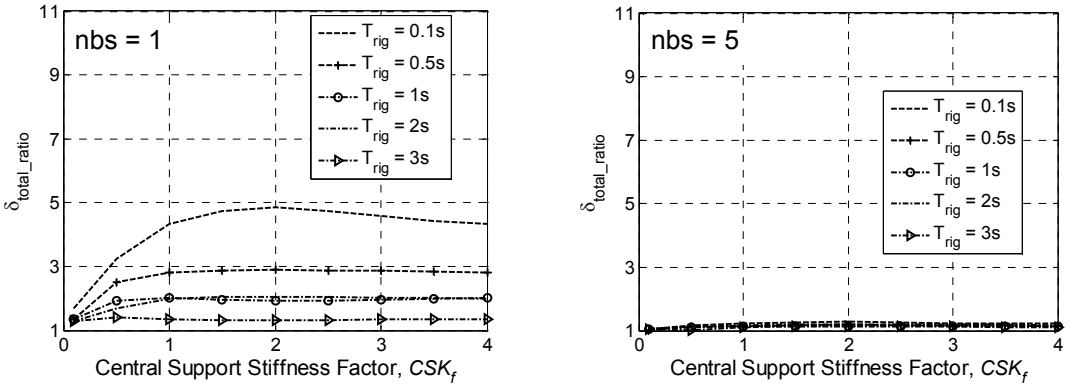

(b) $\gamma_s = 2.5$

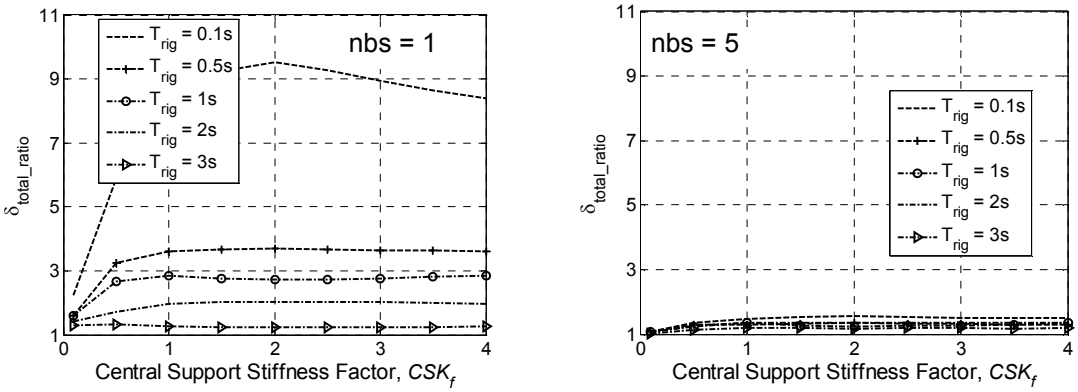

(c) $\gamma_s = 5$

Figure J-4: Sensitivity of central support stiffness factor on median peak total in-plane diaphragm displacements for 3WM-Pinned structures.

J.4 Over-Estimation of Design Base Shear Due To Rigid Diaphragm Assumption for Structures with Flexible Diaphragm

It was shown in Figure 5-4 that the fundamental natural period of structures with flexible diaphragms is higher than the natural period of structures with a rigid diaphragm. Ignoring diaphragm flexibility can therefore result in uneconomical designs due to overestimation of design base shears. For example, according to Figure 5-4(a), the fundamental natural period of a single span one storey structure (2WM) with γ_s = 2.5, is 1.68 times that due to a rigid diaphragm assumption for the same structure. The figure also shows that this increase in natural period is not sensitive to the chosen T_{rig}. Therefore, the likely over-estimation of the base shears can be calculated as shown in Figure J-5. Here, the base shears are calculated according to the NZS1170.5 [2] Equivalent Static (ES) method (see Appendix B) assuming that the one storey structures are located in Wellington.

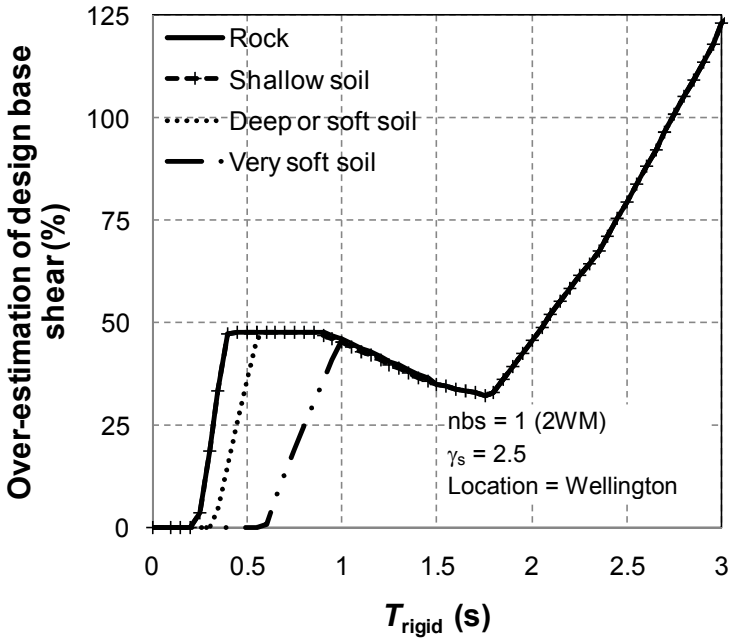

Figure J-5: Over-estimation of base shear calculation due to a rigid diaphragm assumption.

J.5 Influence of Shear Deformation on Response of Flexible Diaphragms

To determine the effect of shear deformations, Spooner [3] analysed diaphragms that were either modelled as an Euler-Bernoulli beam or as a Timoshenko beam. Here, flexural (Euler-Bernoulli) diaphragm approximation was modelled using a realistic elastic modulus and a very large shear modulus, and for the shear (Timoshenko) diaphragm approximation, a very large elastic modulus and a realistic shear modulus was used. His study showed that difference in response due to these two extreme beams modelling was minimal. For example, Figure J-6 shows that the change to median peak displacement due to diaphragm flexibility are generally very similar when diaphragms are modelled as an Euler-Bernoulli beam or as a Timoshenko beam model.

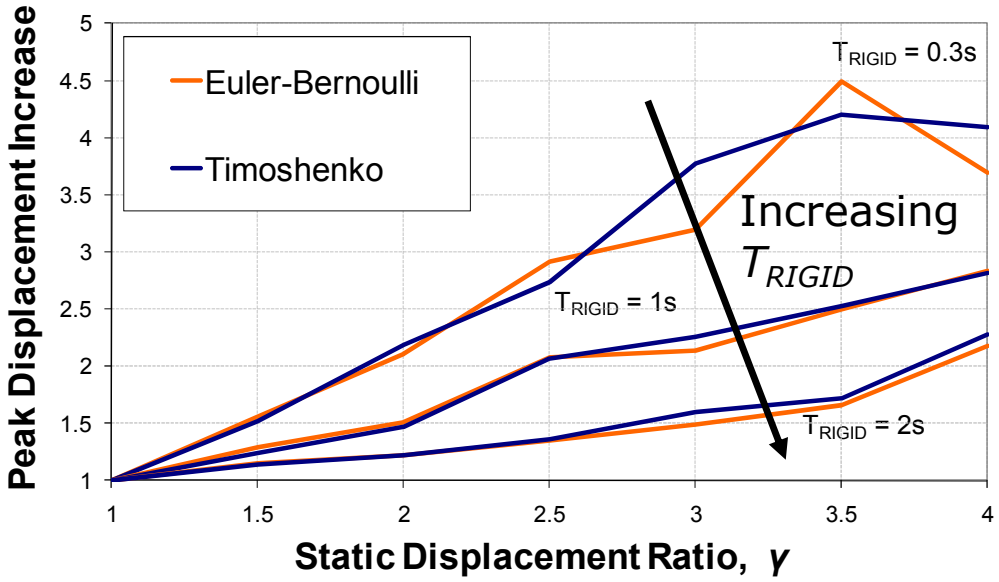

Figure J-6: Comparison of median peak displacement increase due to Timoshenko and Euler-Bernoulli beam models (from Spooner [3]).

J.6 Expression for Lateral Stiffness of Flexible Diaphragm, K_{d_flex} :

Recalling Equation (5-1) that defines static flexibility ratio, γ_s; where δ_{d_flex} is the lateral displacement of the flexible diaphragm, and δ_{w_flex} is the in-plane displacement of the supporting walls.

$$\gamma_s = \frac{\delta_{d\_flex}}{\delta_{w\_flex}} \tag{J-44}$$

$$\gamma_s = \frac{\delta_{d\_flex(MDOF)}}{\delta_{w\_flex}} \tag{J-45}$$

From Figure (J-3) and related discussion, the peak in-plane displacement of the MDOF flexible diaphragm, $\delta_{d\_flex(MDOF)}$, can be expressed by Equation (J-46).

$$\delta_{d\_flex(MDOF)} = \left(\frac{4}{\pi}\right) * \delta_{d\_flex(SDOF)} \tag{J-46}$$

Substituting Equation (J-46) in Equation (J-45) provides Equation (J-47) for static flexibility ratio:

$$\gamma_s = \frac{\left(\frac{4}{\pi}\right) * \delta_{d\_flex(SDOF)}}{\delta_{w\_flex}} \tag{J-47}$$

The first mode participatory mass ratio, α, is given by Equation (J-48) below, where M_d is the total diaphragm mass, and L^*_1 and M^*_1 are respectively the first mode generalised mass and excitation, given by Equations (J-13) and (J-11).

$$\alpha = \frac{\left(\frac{(L_1^*)^2}{M_1^*}\right)}{M_d} = \left(\frac{8}{\pi^2}\right) \tag{J-48}$$

For a certain force F on the structure, Equations (J-47) and (J-48) above are used to obtain the flexible diaphragm stiffness, K_{d_flex}. Here, K_{total_sup} is the total lateral stiffness of the supports.

$$\gamma_s = \frac{\left(\frac{4}{\pi}\right) * \left(\frac{8F}{\pi^2 K_{d\_flex}}\right)}{\left(\frac{F}{K_{total\_sup}}\right)} \tag{J-49}$$

$$K_{d\_flex} = \frac{32 K_{total\_sup}}{\pi^3 \gamma_s} \tag{J-50}$$

J.7 References

[1] Chopra AK. Dynamics of structures: Theory and Applications to Earthquake Engineering. New Jersey: Prentice Hall, 2000; 844 pp.

[2] SNZ. NZS 1170.5 Supp 1:2004, Structural Design Actions. Part 5: Earthquake actions – New Zealand – commentary. Standards New Zealand, Wellington, 2004.

[3] Spooner MS. Quantifying the dynamic response of flexible floor diaphragms. Third Professional Year Project, Department of Civil and Natural Resources Engineering, University of Canterbury, Christchurch, 2008

APPENDIX K: TIME-HISTORY ANALYSIS OPTIONS IN SAP2000

K.1 Choice of Time-History Type for Elastic and Inelastic Dynamic Time-History Analysis in SAP2000

This appendix provides a very brief description on the time-history analysis options available in SAP2000 [1] for conducting elastic and inelastic dynamic time-history analysis. Additional information can be found in SAP2000 manual.

K.1.1 Elastic Dynamic Time-History Analysis

SAP2000 has two options for conducting elastic dynamic time-history analyses: (1) Direct Integration, and (2) Modal Superposition. A direct integration time-history solves equations for the entire structure at each time step, as compared to the modal time-history analysis, which uses the method of mode superposition [2]. The direct integration results are very sensitive to the time-step size, requiring finer time-steps to obtain accurate results. This requirement makes the method less attractive for carrying out large parametric analyses. For modal time-history analysis though, closed-form integration of the modal equations is used to compute the response, assuming linear variation of time functions, between the input data time points. Therefore, numerical instability problems are not encountered. It is recommended that a time increment size equal to one-tenth of the time period of the highest mode is enough to capture the peak responses [1]. Also, past research works have shown that the modal time-history analysis method is highly efficient and accurate as compared to the direct-integration time-history analysis method (e.g., Marjanishvili and Agnew

[3], Wilson [4]). Therefore, this modal time-history analysis method has been used for all linear dynamic time-history analyses explained in diaphragm flexibility study.

K.1.2 Inelastic Dynamic Time-History Analysis

For non-linear dynamic time-history analysis, in addition to the direct-integration option, SAP2000 provides a non-linear modal analysis option. This latter method is also called as a *Fast Non-linear Analysis* method, and is an extension of *Fast Non-linear Analysis* method developed by Wilson [5-6]. It uses an iterative vector superposition algorithm that is extremely efficient for analysing structures with limited nonlinearities. For this method, only nonlinear material behaviour in link/support elements is considered; frame hinge and geometric nonlinearity is excluded. All inelastic dynamic time-history analyses explained in Chapter 5 was conducted using the Fast Non-linear Analysis method.

K.2 References

[1] CSI. Computers and Structures Inc. SAP2000 Advanced 11.0.8. Static and Dynamic Finite Element Analysis of Structures, Berkeley, 2007.

[2] Chopra AK. Dynamics of structures: Theory and Applications to Earthquake Engineering. New Jersey: Prentice Hall, 2000; 844 pp.

[3] Marjanishvili S, Agnew E. Comparison of various procedures for progressive collapse analysis. *Journal of Performance of Constructed Facilities* 2006. **20**(4): 365-374.

[4] Wilson EL. Three-dimensional static and dynamic analysis of structures, 3rd Edition, *Computers and Structures*, Inc., Berkeley, California, 2002.

[5] Ibrahimbegovic A, Wilson EL. Simple numerical algorithms for the mode superposition analysis of linear structural systems with non-proportional damping. *Computers and Structures* 1989. **33**(2): 523-531.

[6] Wilson EL. An efficient computational method for the base isolation and energy dissipation analysis of structural systems. ATC 17-1, *Proceedings of the Seminar on Seismic Isolation, Passive Energy Dissipation, and Active Control* 1993. Applied Technology Council, Redwood City, California, 2002.

APPENDIX L: ADDITIONAL PLOTS FROM MASS IRREGULARITY STUDY

L.1 Comparison between Inelastic Dynamic Time-History Analysis (IDTHA) and Code Responses

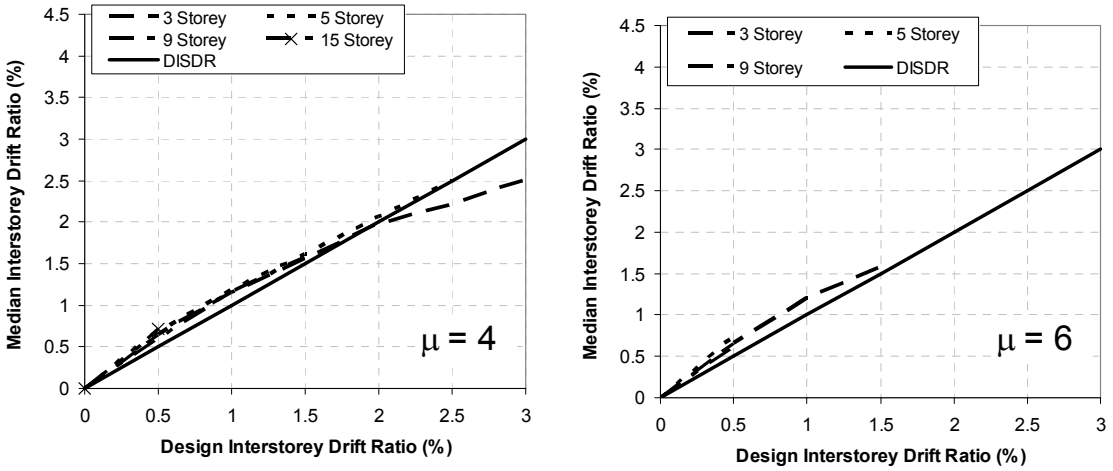

(a) CISDR design

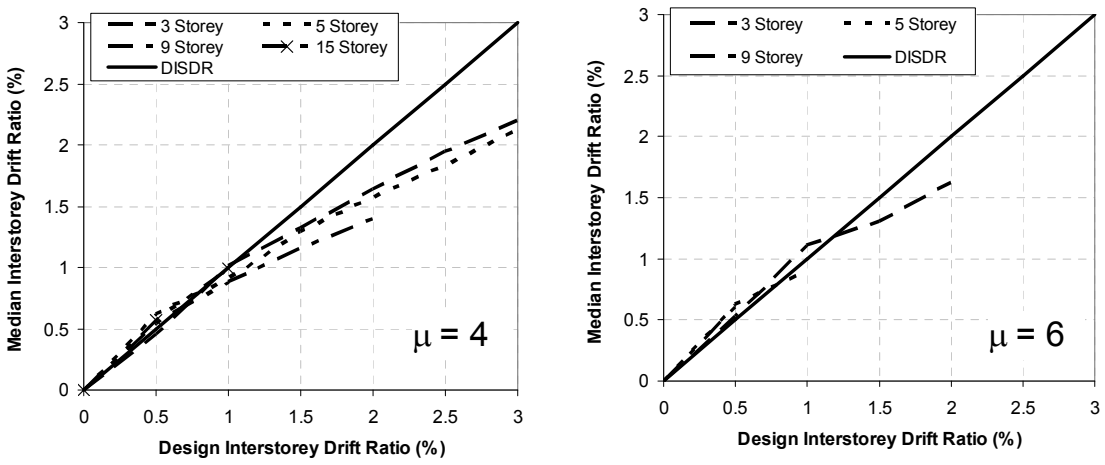

(b) CS-VSTG design

Figure L-1: Comparison between IDTHA and code response for regular models.

L.2 Effect of Magnitude and Floor Level of Mass Irregularity

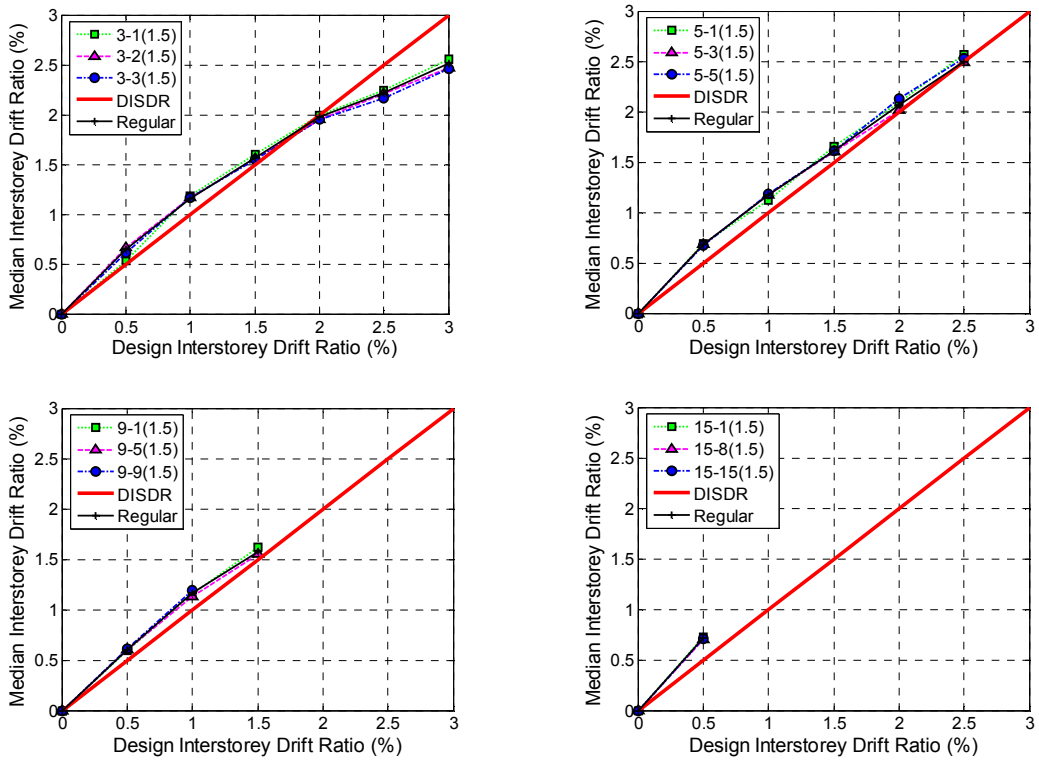

(1) Mass Ratio: 1.5

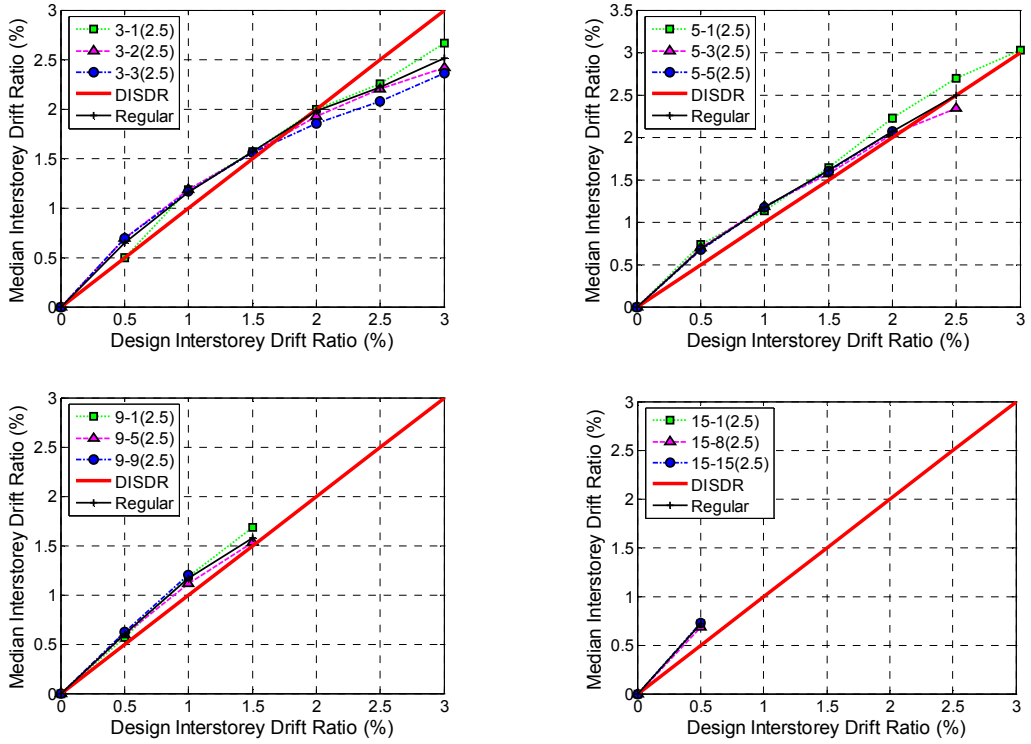

(2) Mass Ratio: 2.5

Figure L-2(a): Effect of magnitude and floor level of mass irregularity for CISDR model ($\mu = 4$, $Z = 0.4$) – Mass Ratios: 1.5 & 2.5.

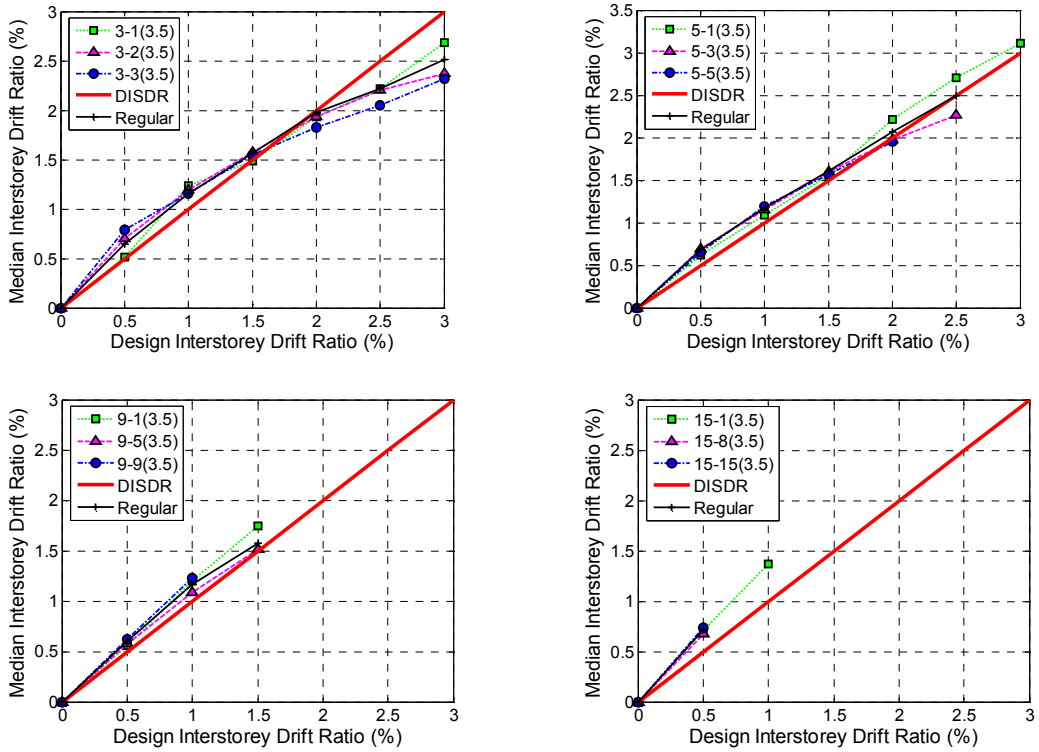

(1) Mass Ratio: 3.5

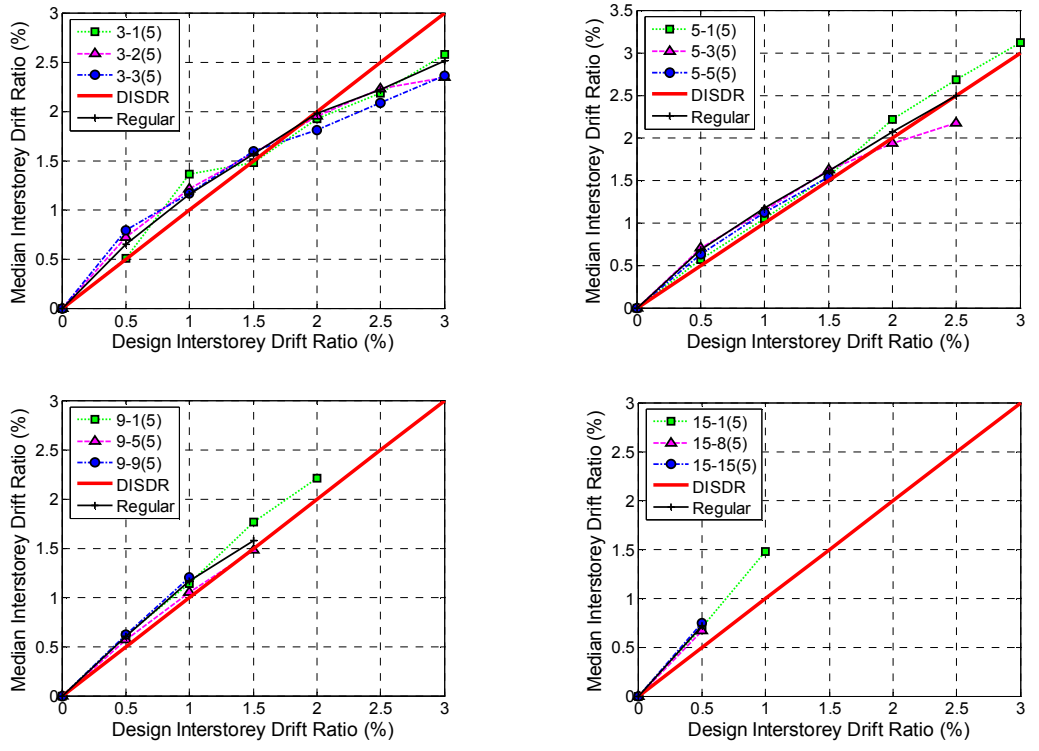

(2) Mass Ratio: 5

Figure L-2(b): Effect of magnitude and floor level of mass irregularity for CISDR model ($\mu = 4$, $Z = 0.4$) – Mass Ratios: 3.5 & 5.

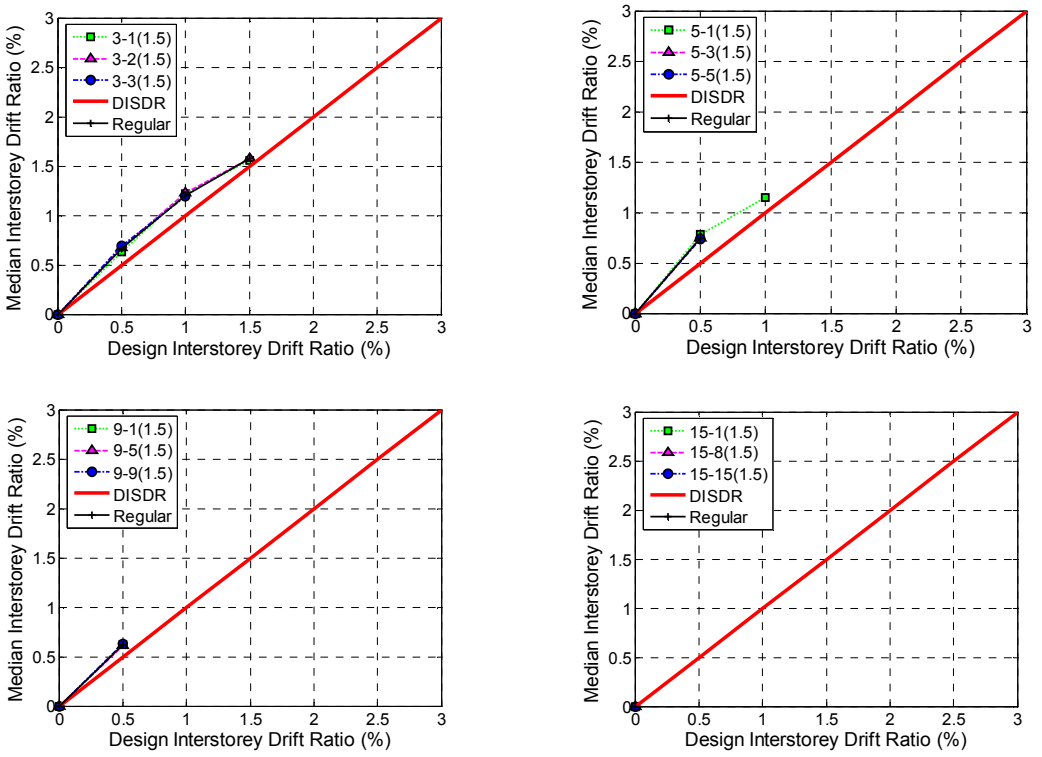

(1) Mass Ratio: 1.5

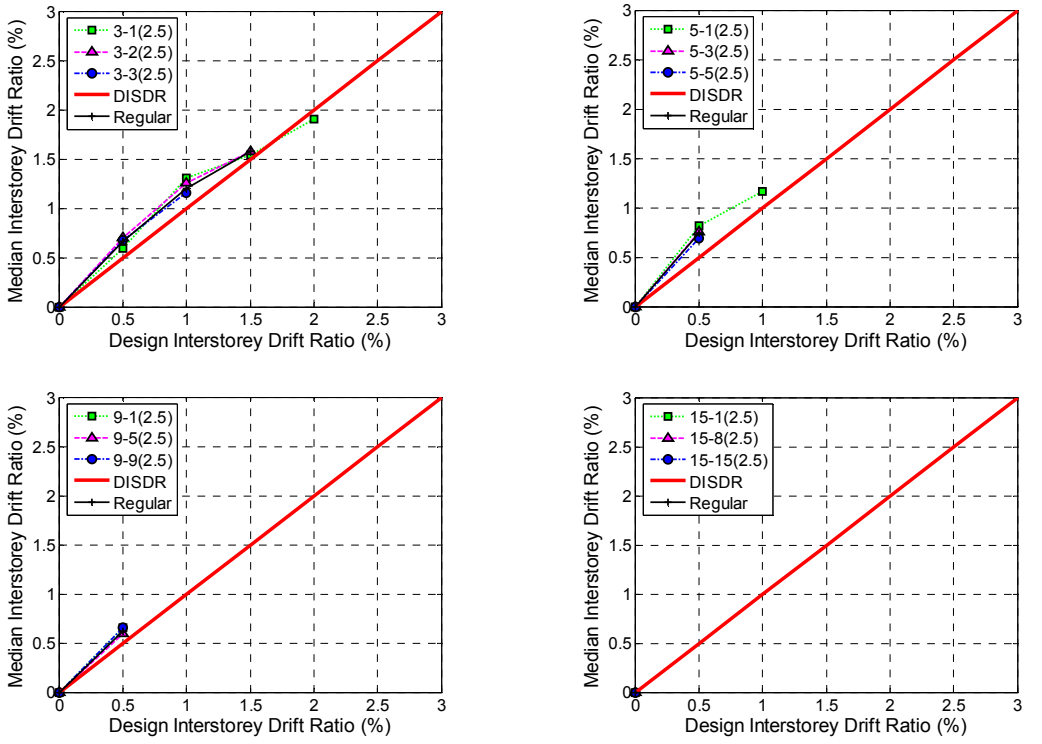

(2) Mass Ratio: 2.5

Figure L-3(a): Effect of magnitude and floor level of mass irregularity for CISDR model ($\mu = 6$, $Z = 0.4$) – Mass Ratios: 1.5 & 2.5.

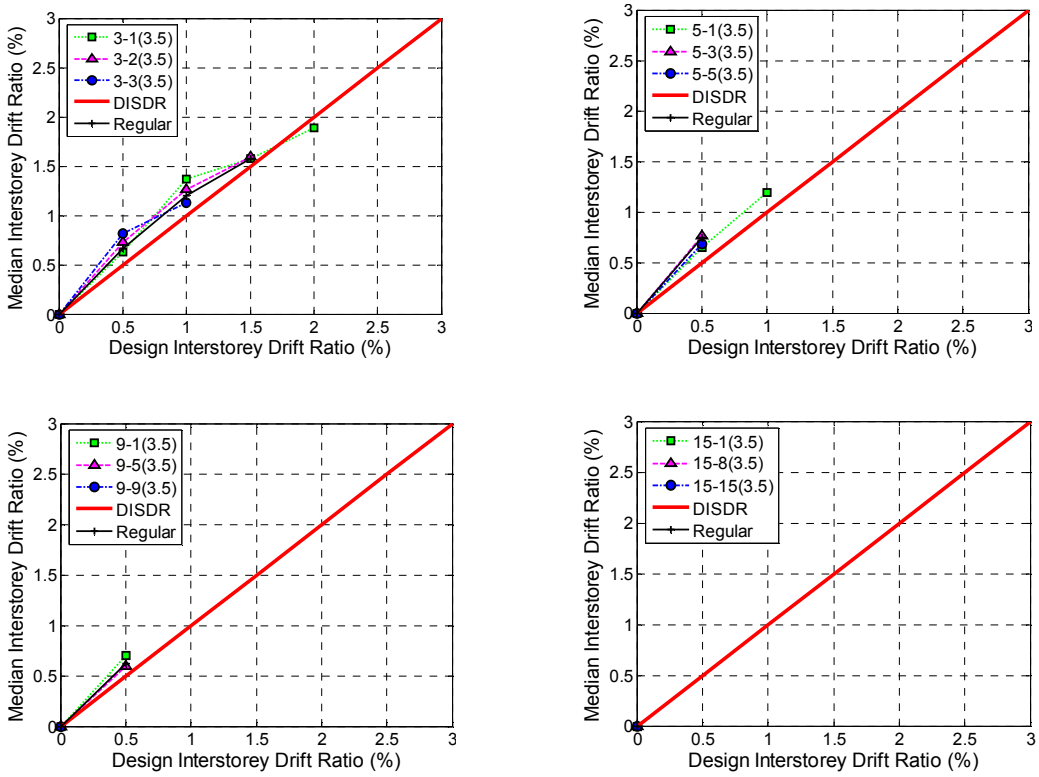

(1) Mass Ratio: 3.5

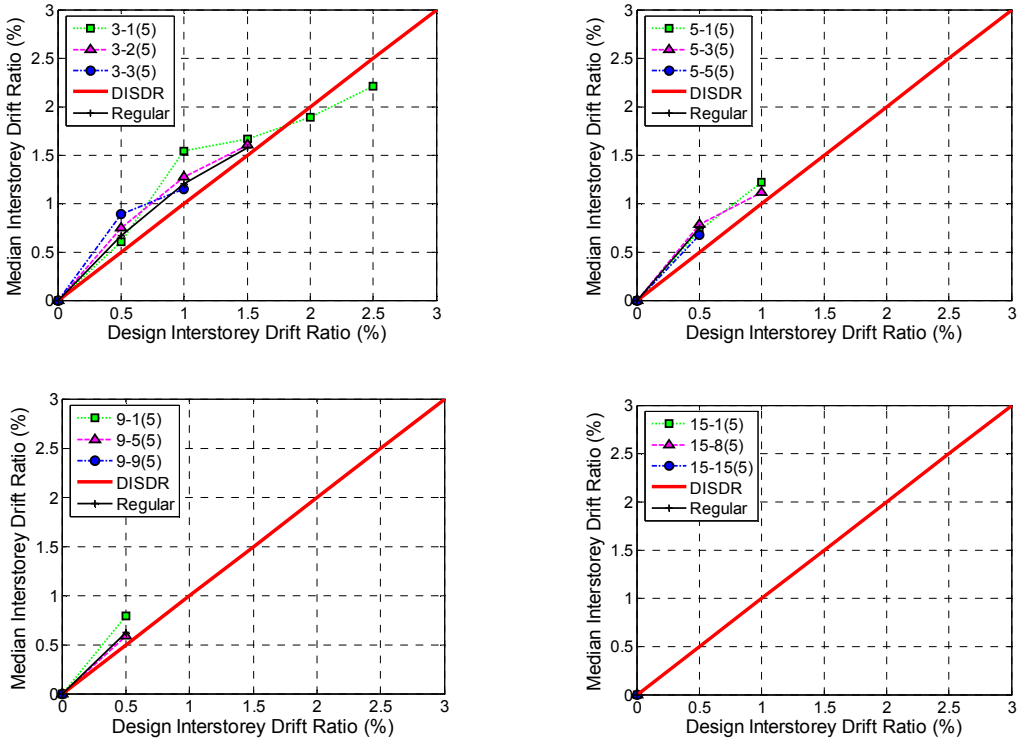

(2) Mass Ratio: 5

Figure L-3(b): Effect of magnitude and floor level of mass irregularity for CISDR model ($\mu = 6$, $Z = 0.4$) – Mass Ratios: 3.5 & 5.

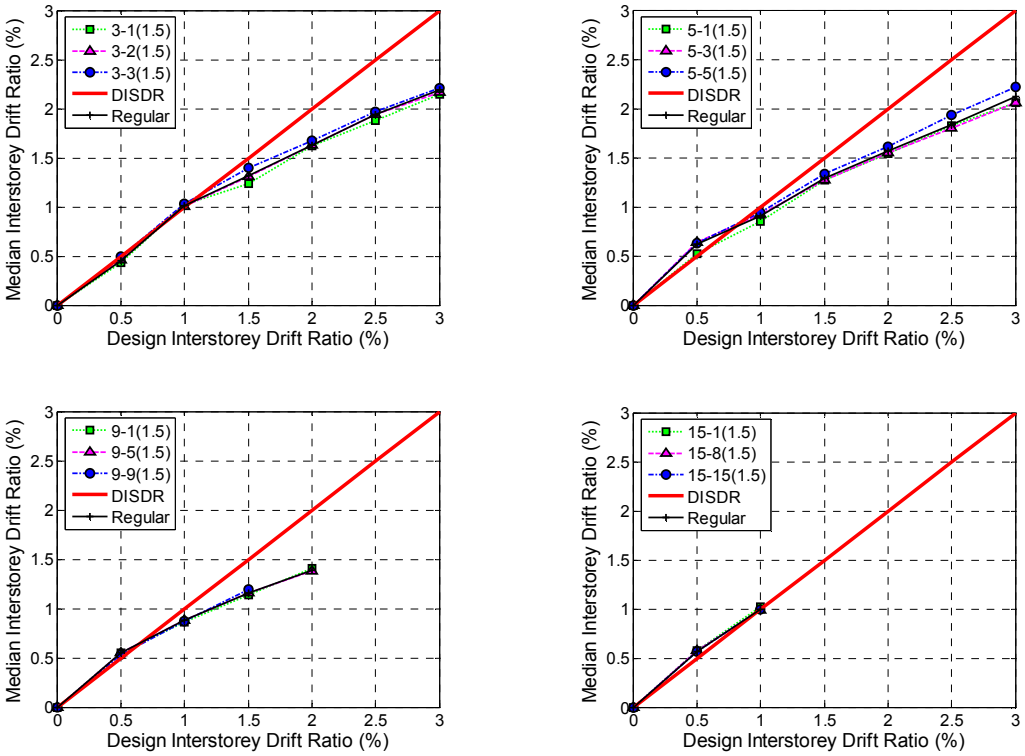

(1) Mass Ratio: 1.5

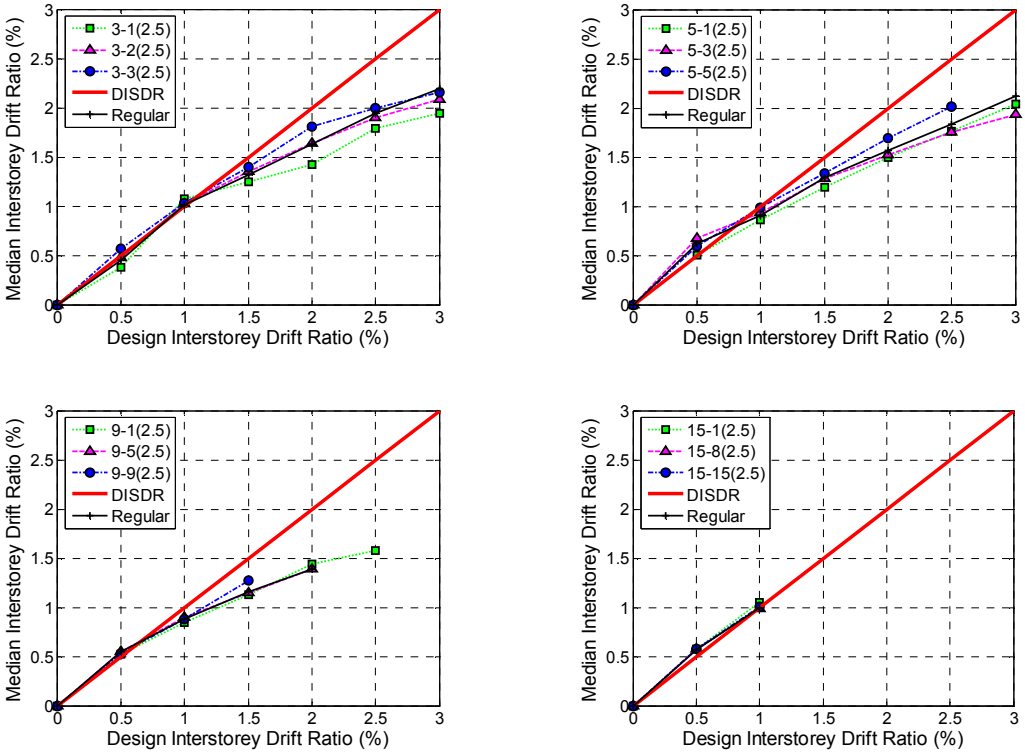

(2) Mass Ratio: 2.5

Figure L-4(a): Effect of magnitude and floor level of mass irregularity for CS-VSTG model ($\mu = 4$, $Z = 0.4$) – Mass Ratios: 1.5 & 2.5.

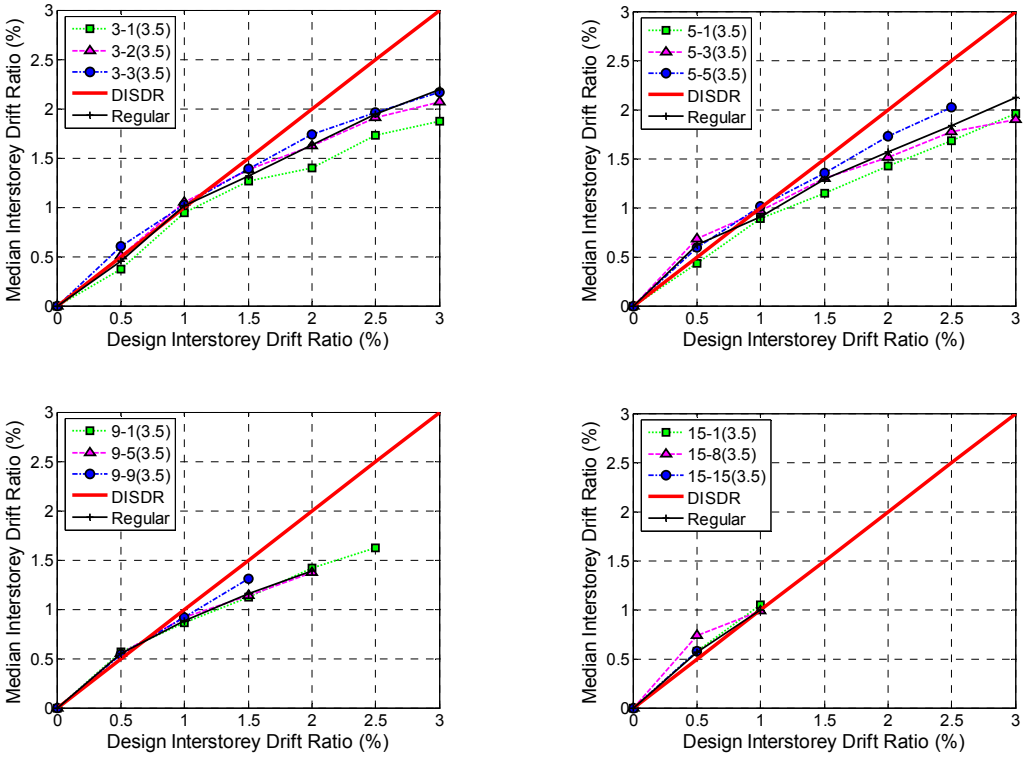

(1) Mass Ratio: 3.5

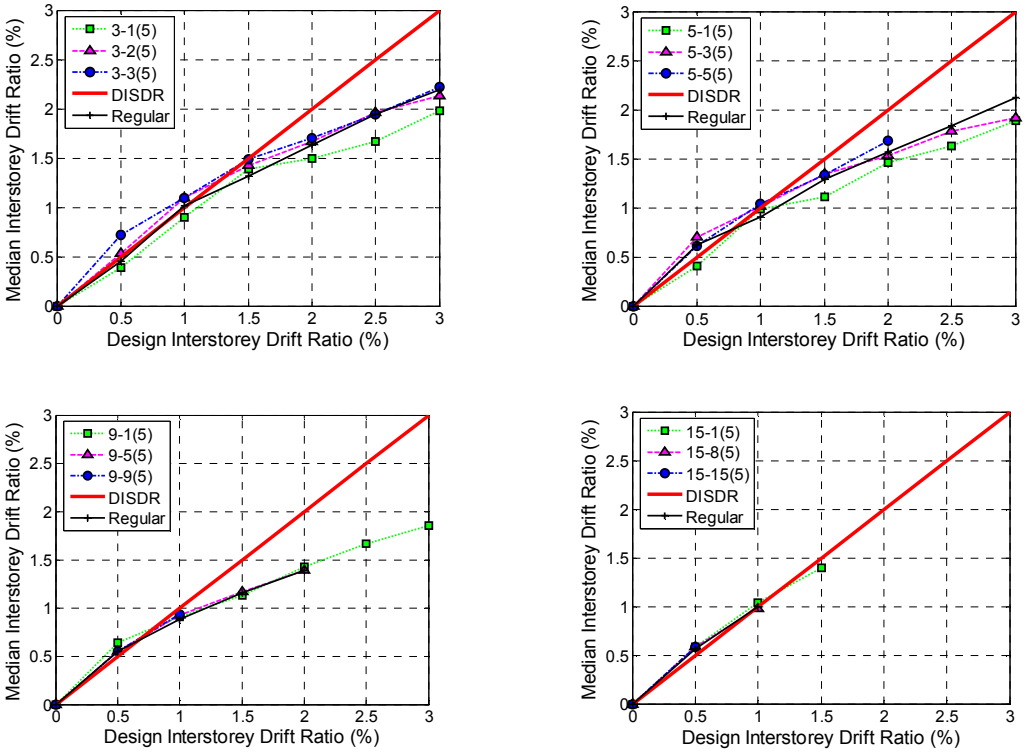

(2) Mass Ratio: 5

Figure L-4(b): Effect of magnitude and floor level of mass irregularity for CS-VSTG model ($\mu = 4$, $Z = 0.4$) – Mass Ratios: 3.5 & 5.

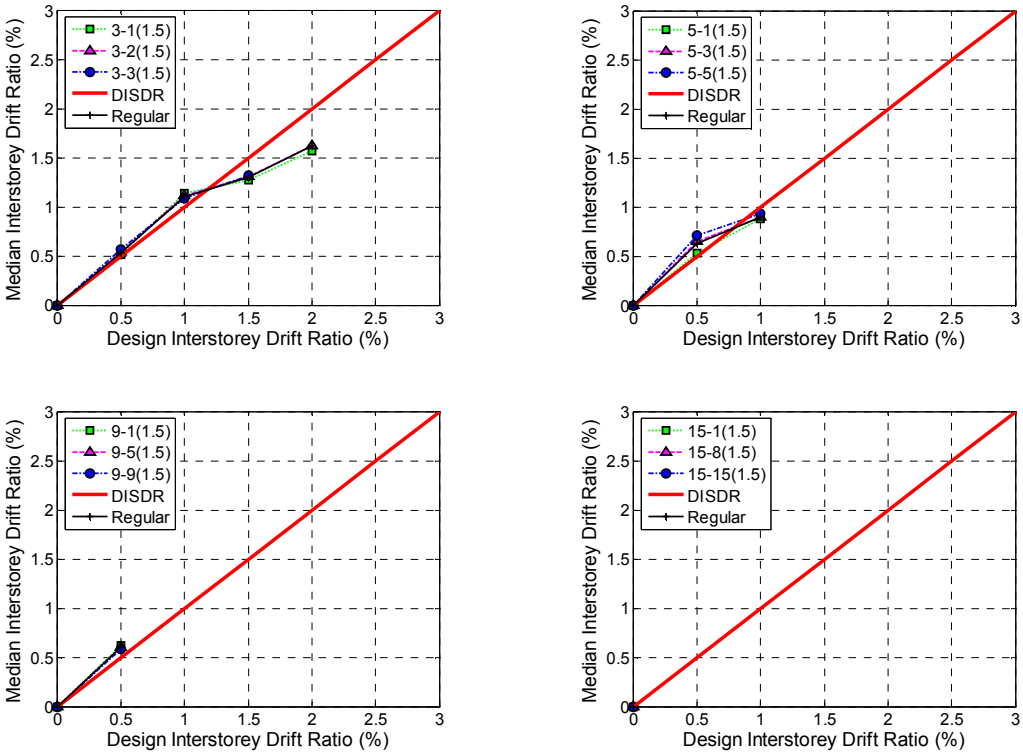

(1) Mass Ratio: 1.5

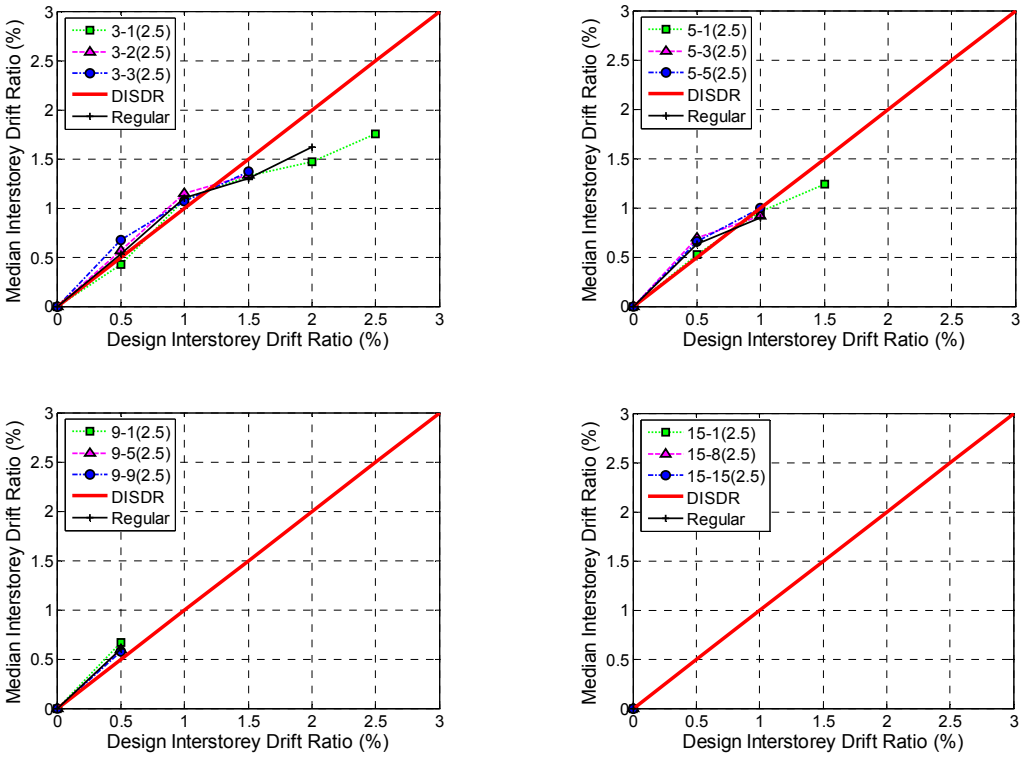

(2) Mass Ratio: 2.5

Figure L-5(a): Effect of magnitude and floor level of mass irregularity for CS-VSTG model ($\mu = 6$, $Z = 0.4$) – Mass Ratios: 1.5 & 2.5.

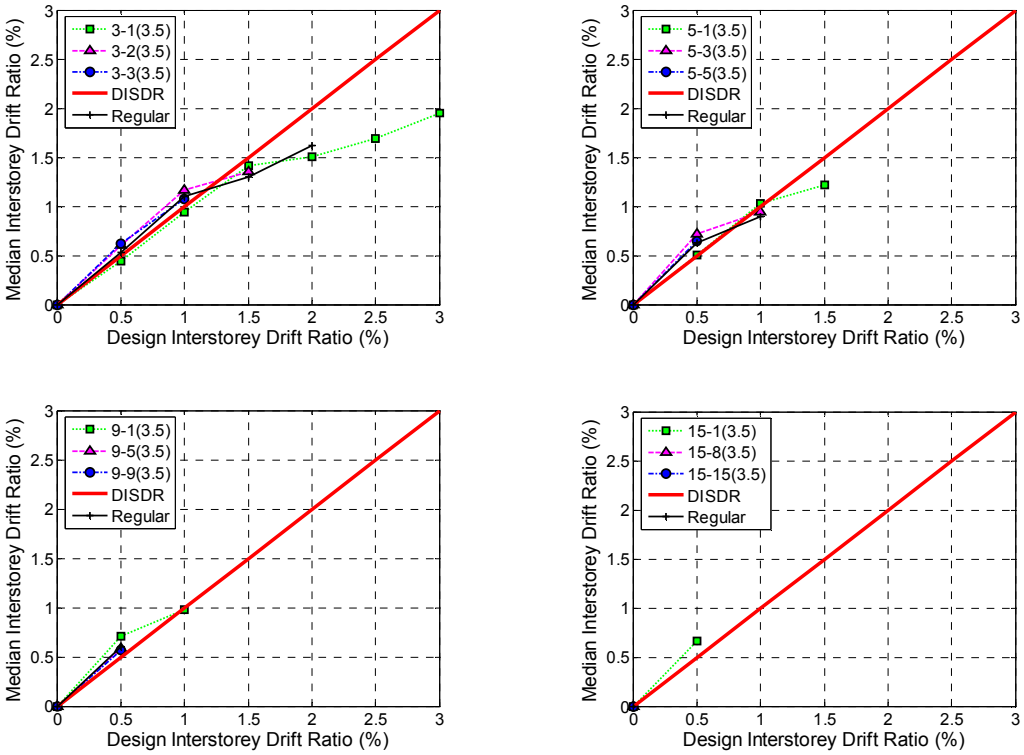

(1) Mass Ratio: 3.5

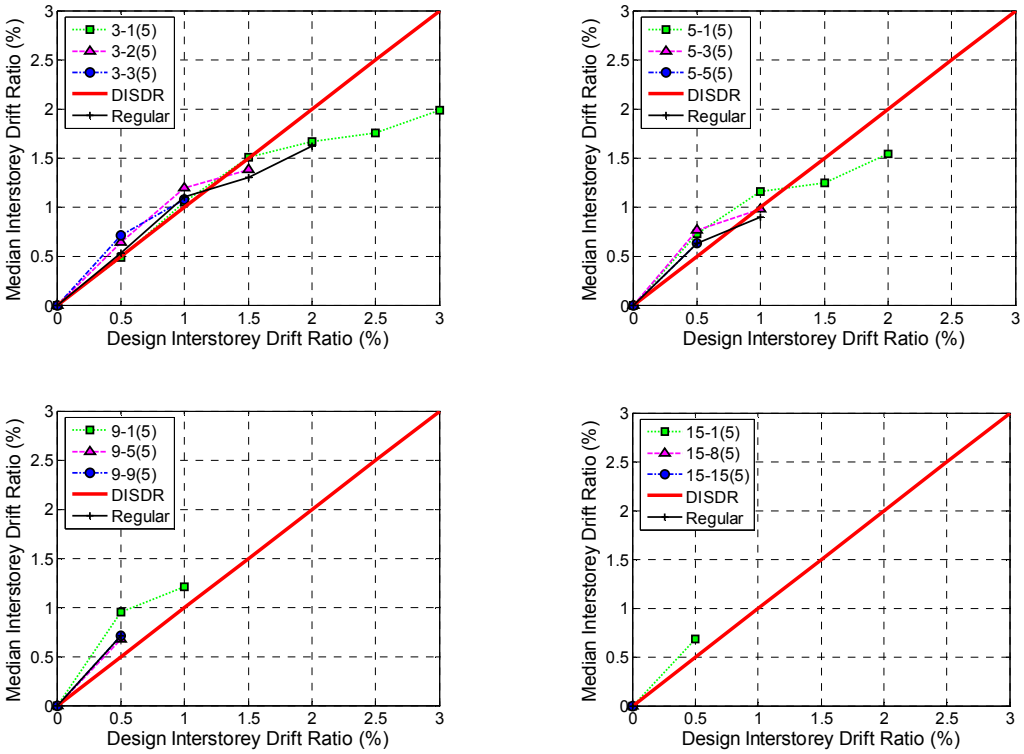

(2) Mass Ratio: 5

Figure L-5(b): Effect of magnitude and floor level of mass irregularity for CS-VSTG model ($\mu = 6$, $Z = 0.4$) – Mass Ratios: 3.5 & 5.

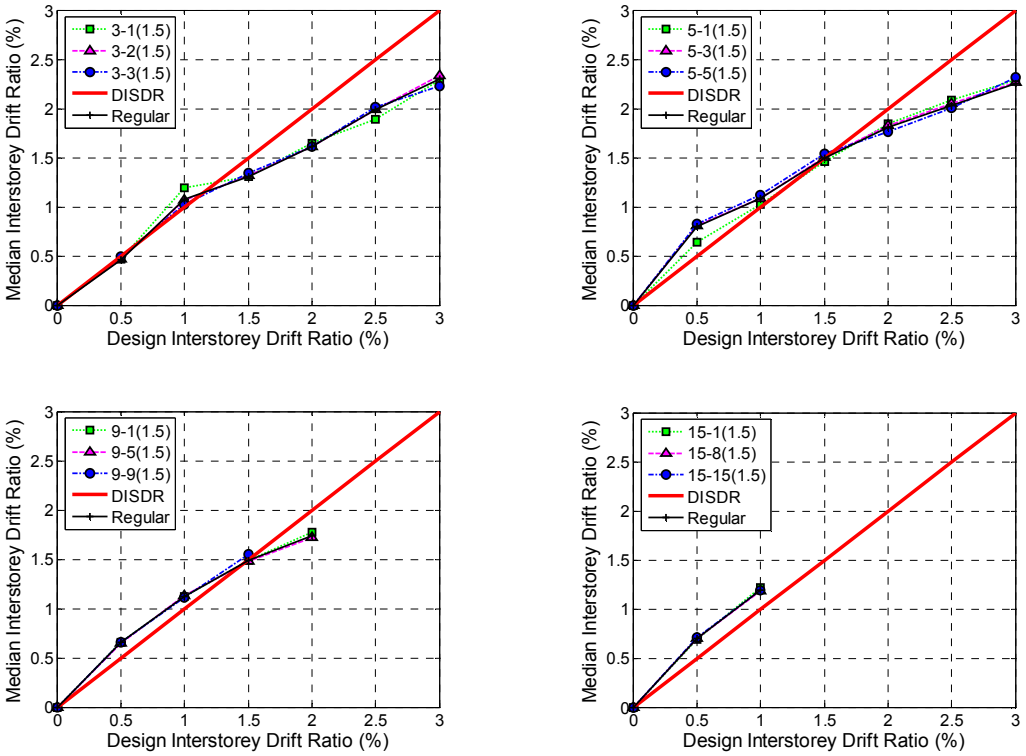

(1) Mass Ratio: 1.5

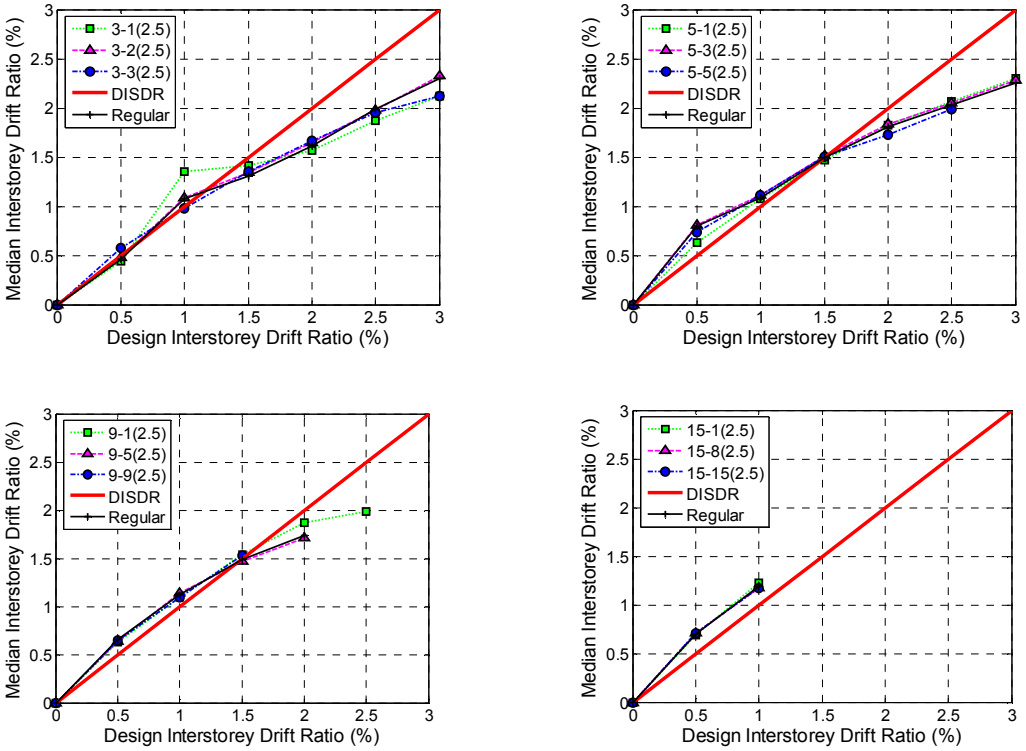

(2) Mass Ratio: 2.5

Figure L-6(a): Effect of magnitude and floor level of mass irregularity for CS-CSTG model ($\mu = 4$, $Z = 0.4$) – Mass Ratios: 1.5 & 2.5.

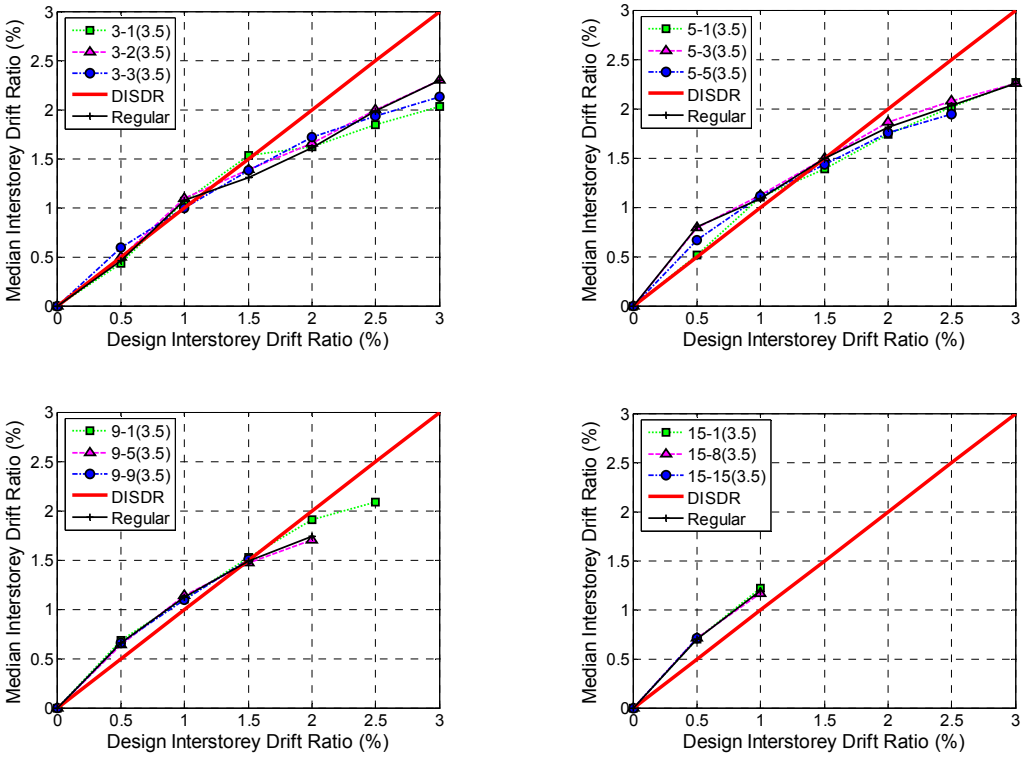

(1) Mass Ratio: 3.5

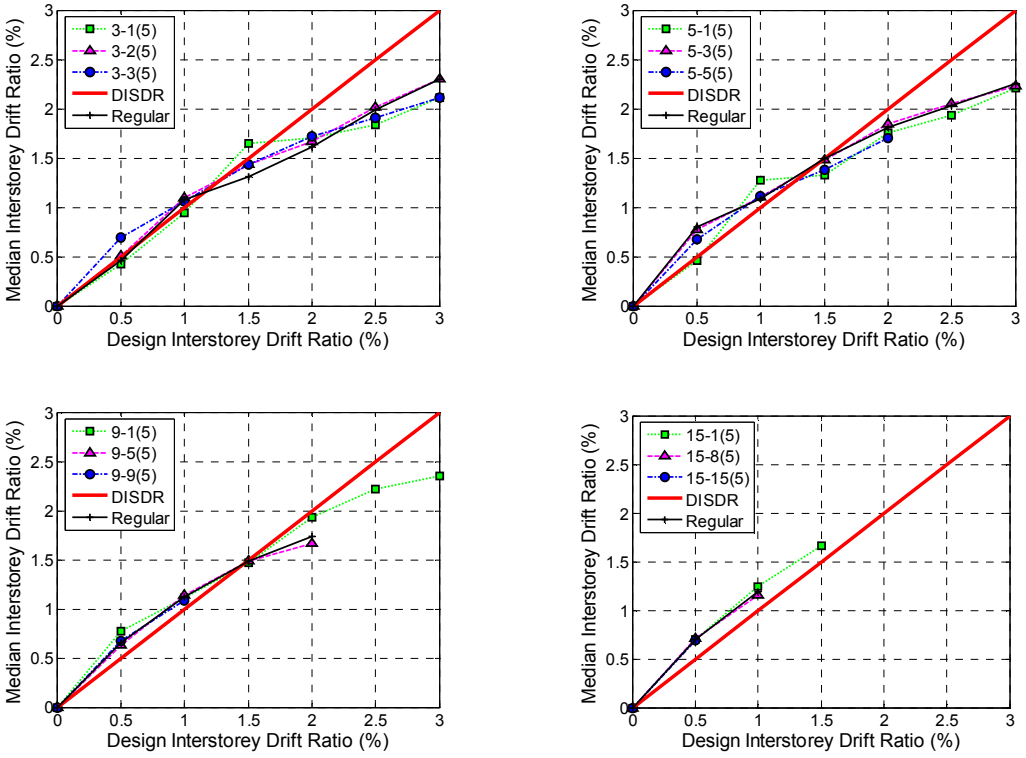

(2) Mass Ratio: 5

Figure L-6(b): Effect of magnitude and floor level of mass irregularity for CS-CSTG model ($\mu = 4$, $Z = 0.4$) – Mass Ratios: 3.5 & 5.

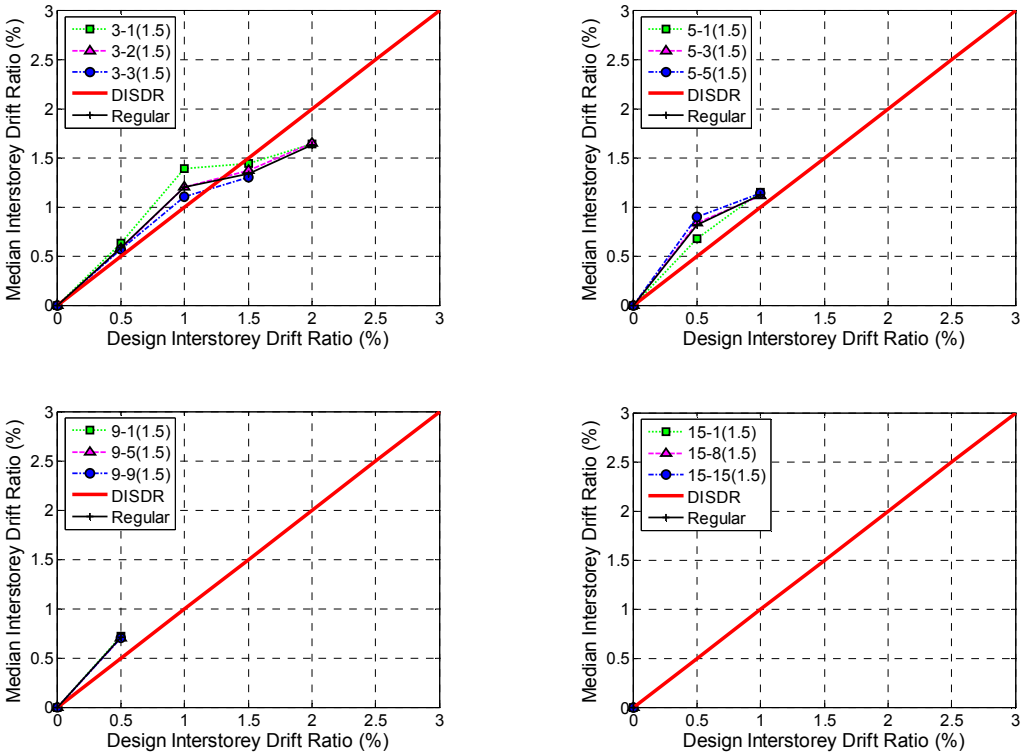

(1) Mass Ratio: 1.5

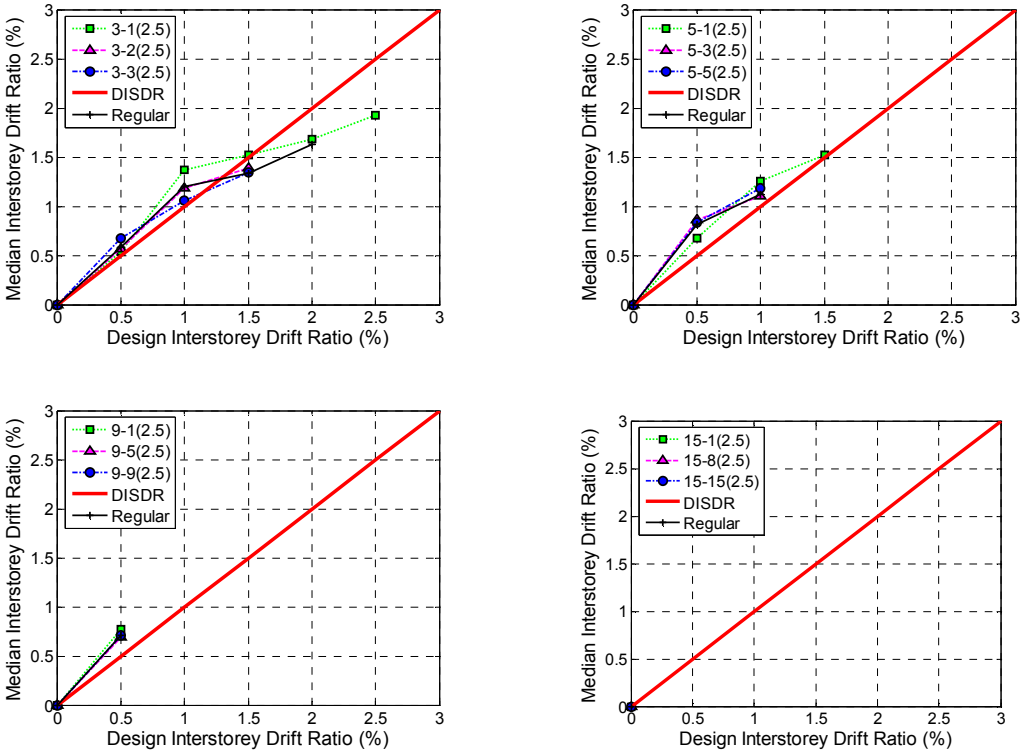

(2) Mass Ratio: 2.5

Figure L-7(a): Effect of magnitude and floor level of mass irregularity for CS-CSTG model ($\mu = 6$, $Z = 0.4$) – Mass Ratios: 1.5 & 2.5.

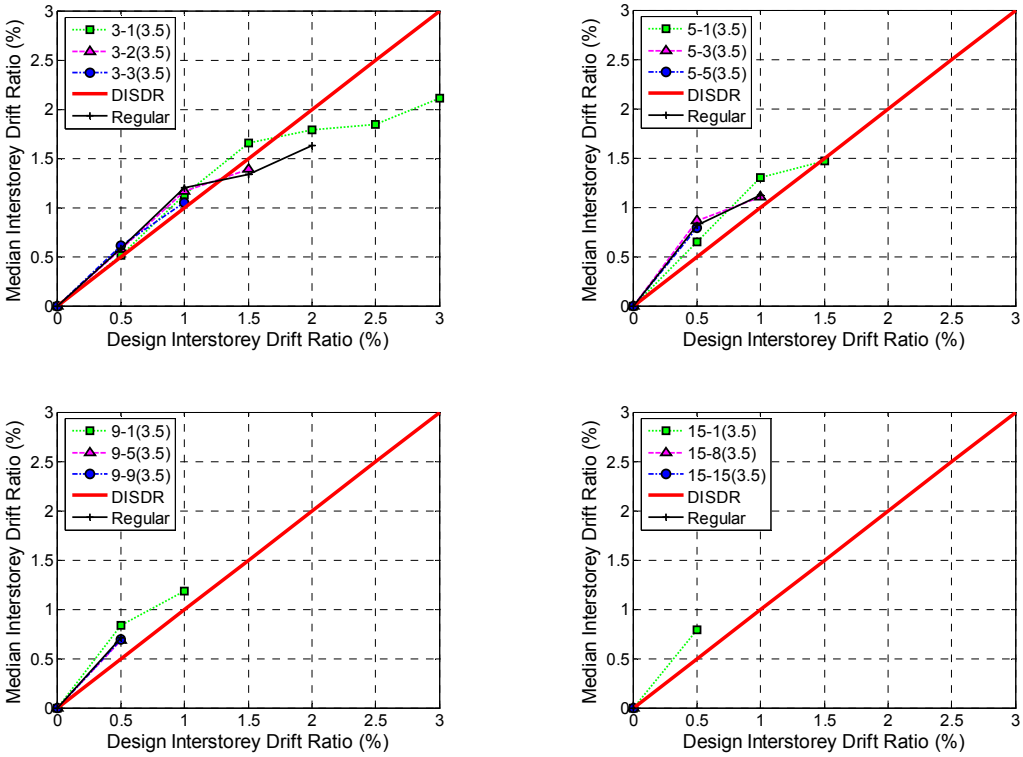

(1) Mass Ratio: 3.5

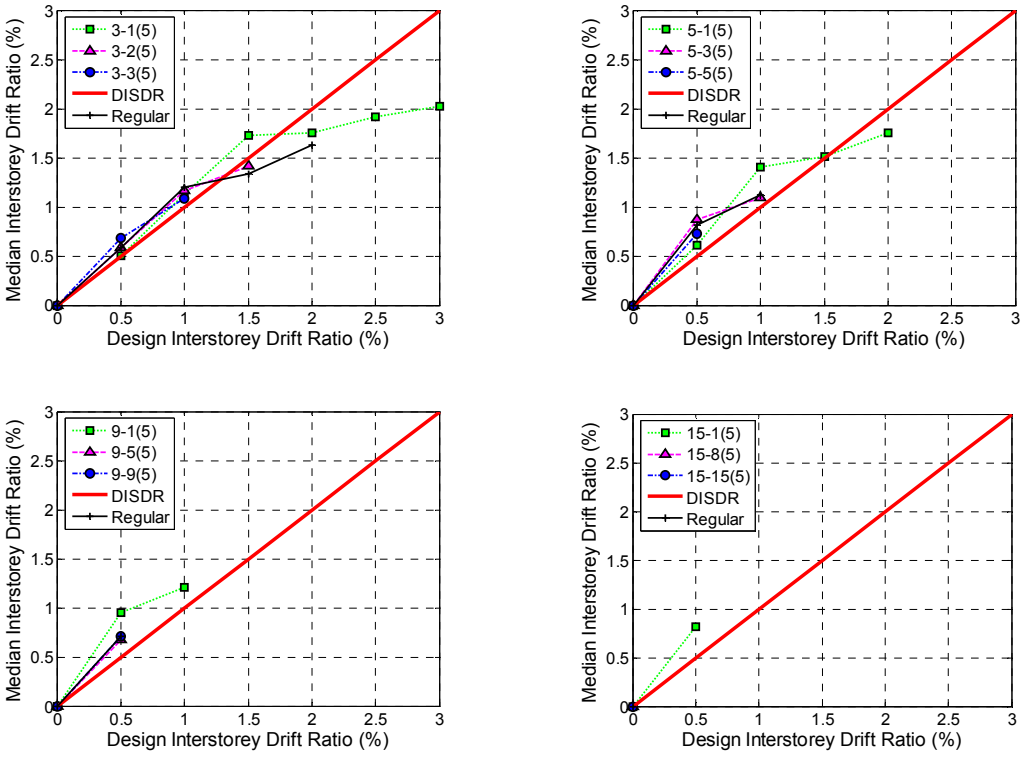

(2) Mass Ratio: 5

Figure L-7(b): Effect of magnitude and floor level of mass irregularity for CS-CSTG model ($\mu = 6$, $Z = 0.4$) – Mass Ratios: 3.5 & 5.

L.3 Statistics of Effect of Magnitude and Floor Level of Mass Irregularity

The effect of magnitude and floor level of mass irregularity was explained in Section 2.9.7 by comparing the median peak interstorey drift ratio (ISDR) of regular structures with the corresponding median peak ISDR of irregular structures. Using the median and dispersion of peak ISDR, the 16th percentile and the 84th percentile of peak ISDR were calculated for the record suite respectively according to Equations (L-2) and (L-2). In this section, representative statistics plots of effect of magnitude and floor level of mass irregularity for Wellington structures are shown in Figure L-8. It was shown in Section 2.9.7 that when irregular mass was introduced either at the first floor or at the topmost floor, it generally produced higher median peak ISDR than did the corresponding regular structures. Therefore, the following plots correspond to additional mass (represented by Mass Ratio, *MR*) introduced at these two critical floor levels of 3 and 9 (*nbs*) storey structures having CISDR or CS configurations In Figure L-8, it can be seen that the trend in median response difference between regular and irregular structures, is generally observed for the 16th and 84th percentile results, however with slightly higher change in peak demand due to irregularity observed for the later case as compared to the 50th percentile results.

$$1 + sigma\,level = \hat{x} \,/\, \exp\left[\sqrt{\frac{1}{(n-1)}\sum_{i=1}^{n}\left(\ln x_i - \ln \hat{x}\right)^2}\right] \qquad \text{(L-1)}$$

$$1 - sigma\,level = \hat{x} \cdot \exp\left[\sqrt{\frac{1}{(n-1)}\sum_{i=1}^{n}\left(\ln x_i - \ln \hat{x}\right)^2}\right] \qquad \text{(L-2)}$$

where x_i = response quantity due to i^{th} record; n = total number of earthquake records considered; and $\hat{x}$ = median peak ISDR.

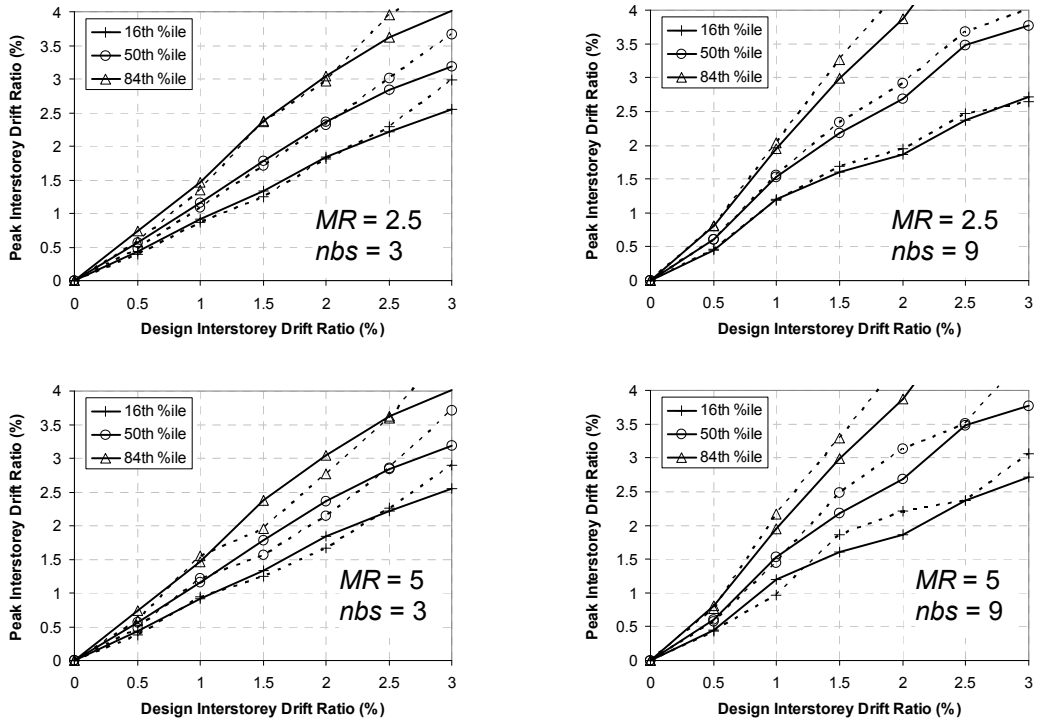

(1) Location of Mass Irregularity: First Floor

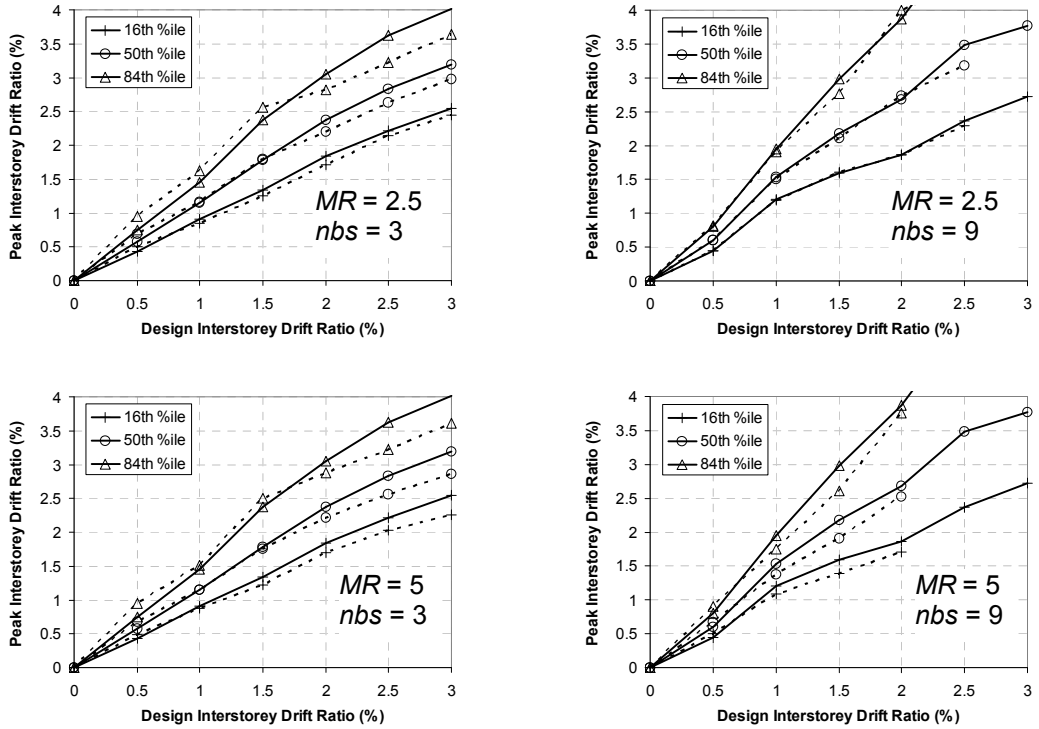

(2) Location of Mass Irregularity: Roof

Figure L-8(a): Statistics of effect of magnitude and floor level of mass irregularity for CISDR model ($\mu = 2$, $Z = 0.4$).

(Regular ——— Irregular - - - - - -)

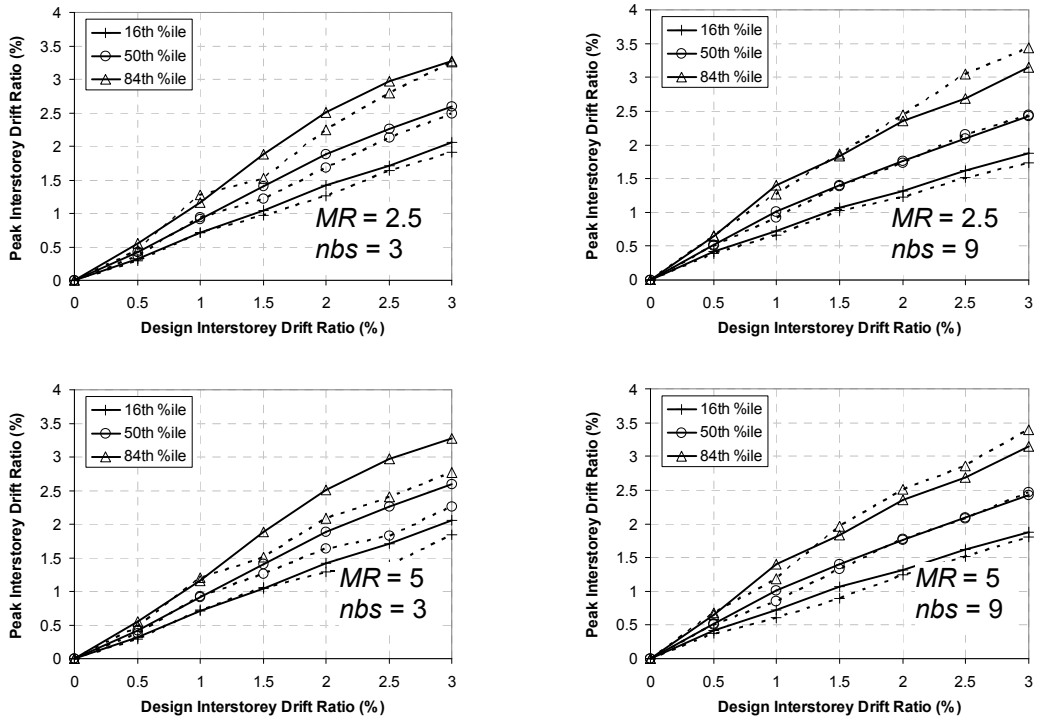

(1) Location of Mass Irregularity: First Floor

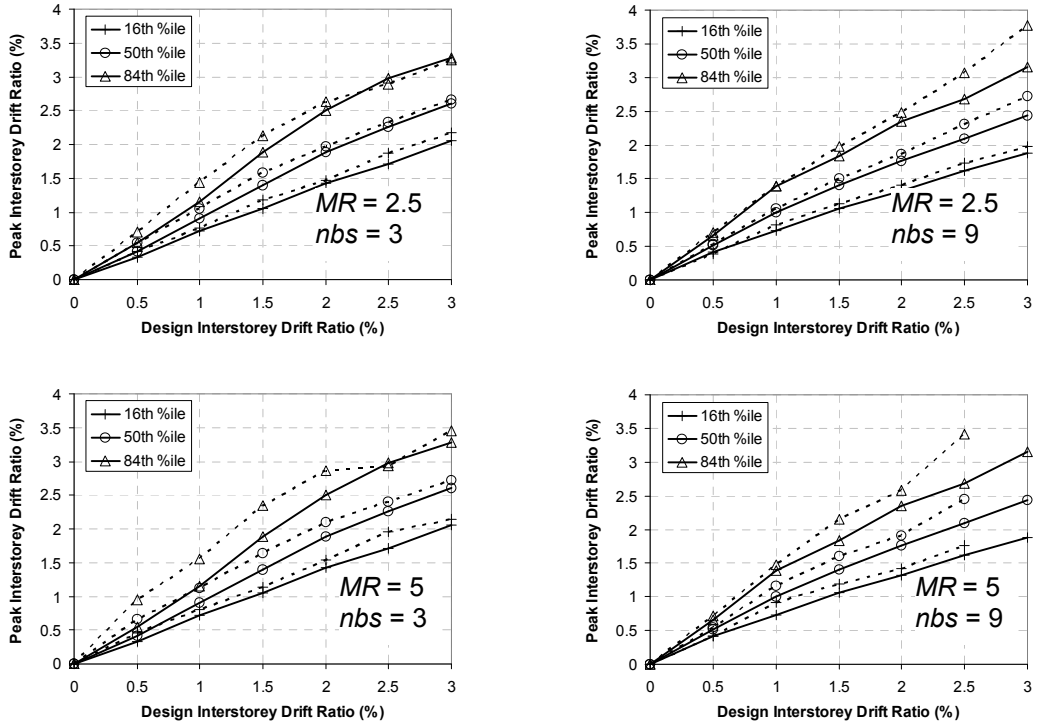

(2) Location of Mass Irregularity: Roof

Figure L-8(b): Statistics of effect of magnitude and floor level of mass irregularity for CS-VSTG model ($\mu = 2$, $Z = 0.4$).

(Regular—— Irregular - - - - - -)

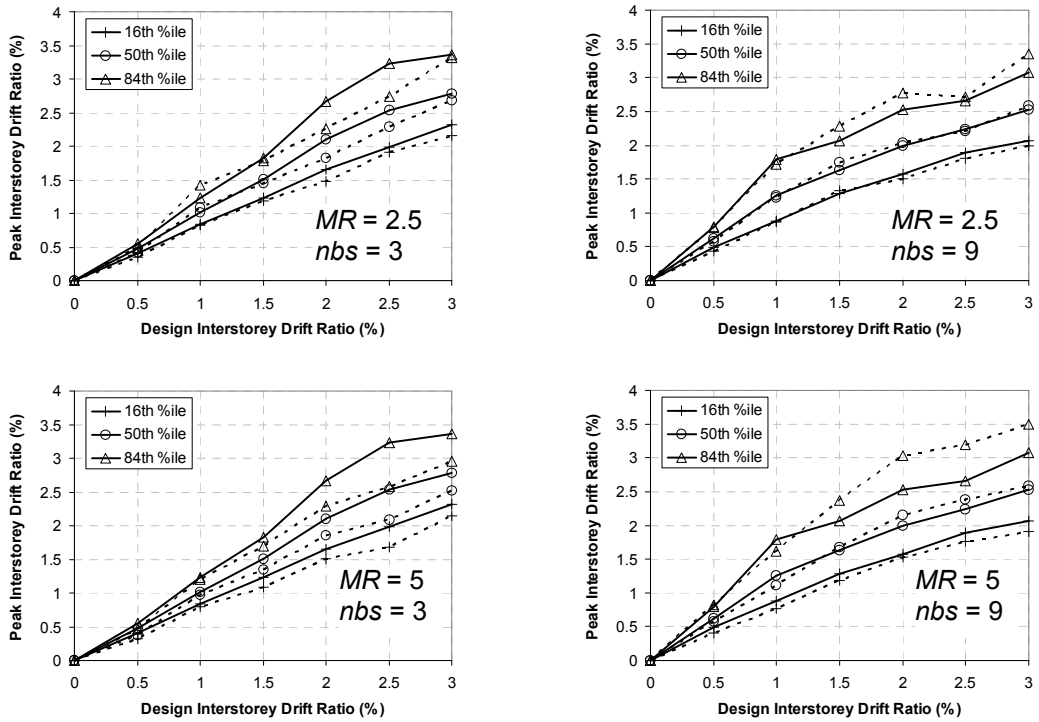

(1) Location of Mass Irregularity: First Floor

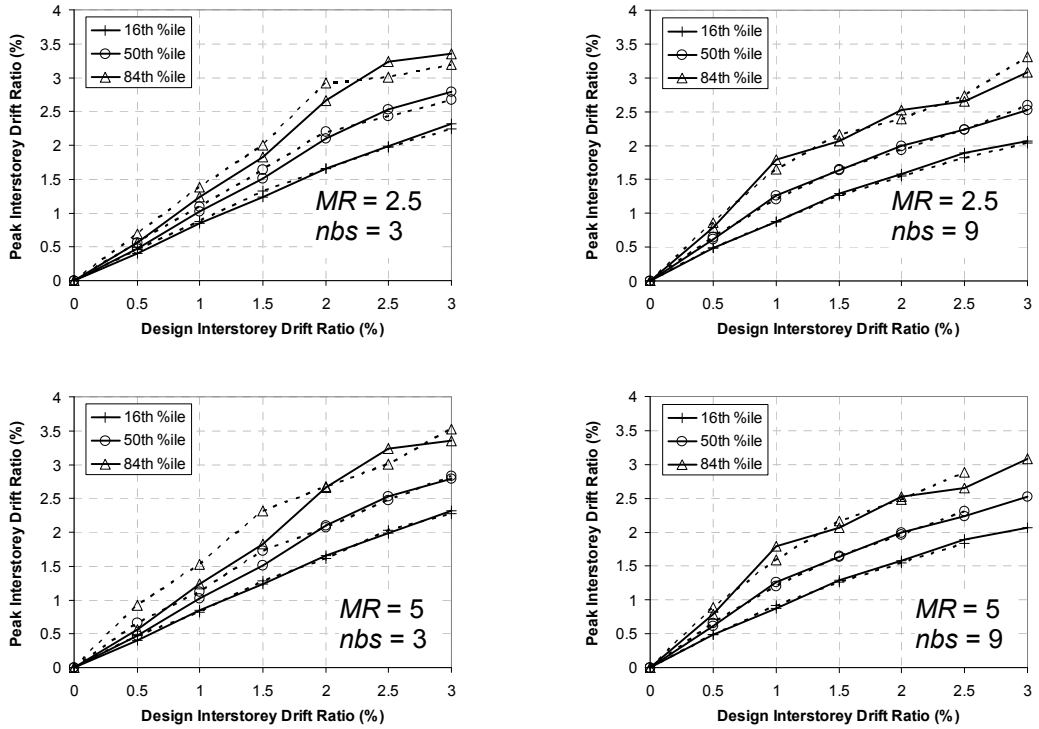

(2) Location of Mass Irregularity: Roof

Figure L-8(c): Statistics of effect of magnitude and floor level of mass irregularity for CS-CSTG model ($\mu = 2$, $Z = 0.4$).

(Regular——— Irregular - - - - - -)